Michael V. Sadovskii

Selected Works on Condensed Matter Theory

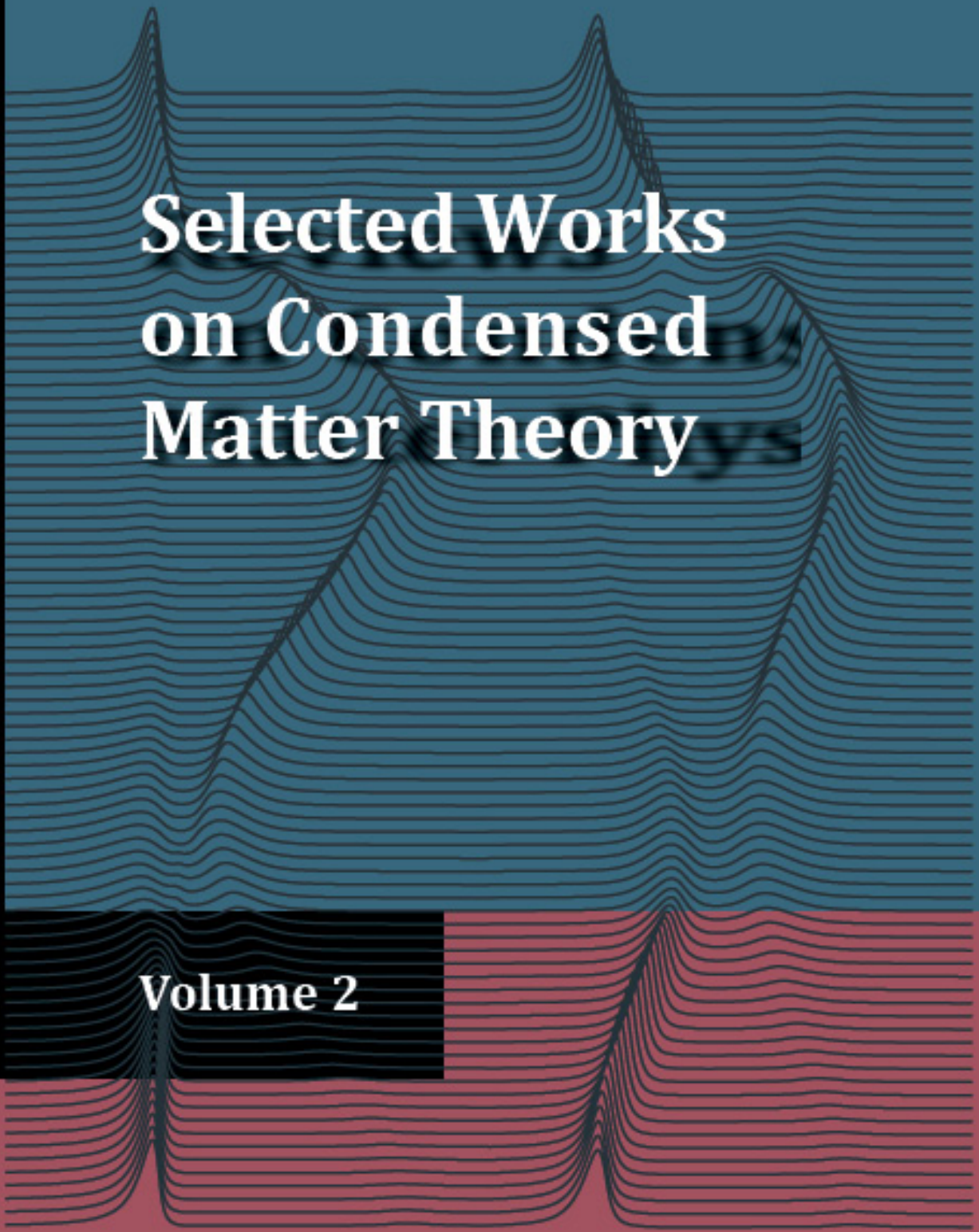

Volume 2

M.V. Sadovskii

Selected Works on Condensed Matter Theory

Volume 2

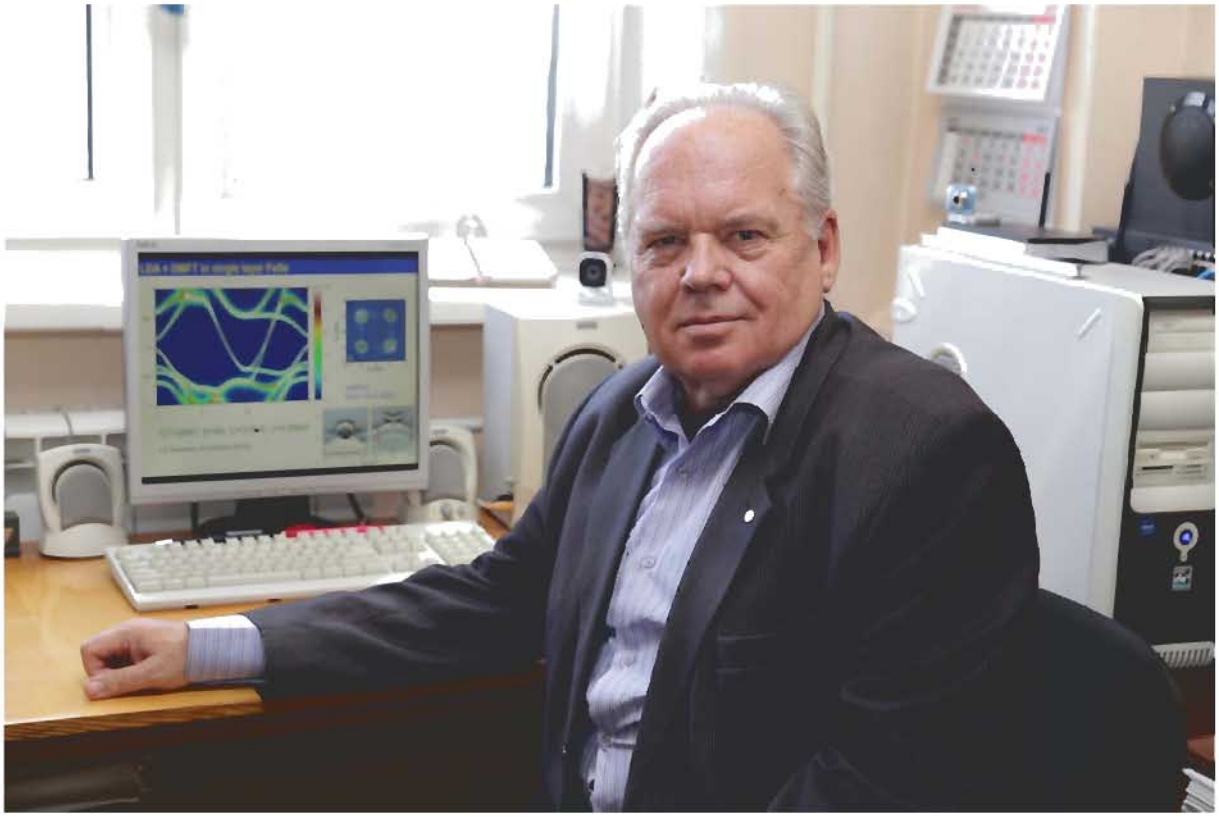

Contents:

46. E.Z. Kuchinskii, N.A. Kuleeva, M.V. Sadovskii. Ginzburg - Landau expansion in BCS-BEC crossover region of disordered attractive Hubbard model. Low Temperature Physics v. 43, No. 1 (2017)

47. E.Z. Kuchinskii, N.A. Kuleeva, M.V. Sadovskii. Ginzburg - Landau Expansion in Strongly Disordered Attractive Hubbard model. JETP v. 125, No. 1, 111-122 (2017)

48. E.Z. Kuchinskii, N.A. Kuleeva, M.V. Sadovskii. Temperature Dependence of the Upper Critical Field in Disordered Hubbard Model with Attraction. JETPcv. 125, No. 6, 1127-1156 (2017)

49. E.Z. Kuchinskii, N.A. Kuleeva, M.V. Sadovskii. Temperature Dependence of Paramagnetic Critical Magnetic Field of Disordered Attarctive Hubbard Model. JETP v. 127, No. 4, 753-760 (2018)

50. M.V. Sadovskii. Electron-Phonon Coupling in Eliashberg-McMillan Theory Beyond Adiabatic Approximation. JETP v. 128, No. 3, 455-463 (2019)

51. M.V. Sadovskii. Antiadiabatic Phonons, Coulomb Pseudopotential and Superconductivity in Eliashberg-McMillan Theory. JETP Letters v. 109, No. 3, 166-170 (2019)

52. M.V. Sadovskii. On Planckian limit for inelastic relaxation in metals. JETP Letters v. 111, No.3, 188-192 (2020)

53. M.V. Sadovskii. Superconducting Transition Temperature for Very Strong Coupling in the Antiadiabatic Limit of Eliashberg Equations. JETP Letters v. 113, No.9, 581-585 (2021)

54. E.Z. Kuchinskii, N.A. Kuleeva, D.I. Khomskii, M.V. Sadovskii. Hall effect in doped Mott insulator. JETP v. 136, No.3, 368-377 (2022)

55. E.Z. Kuchinskii, M.V. Sadovskii. Generalized Dynamical Keldysh Model. JETP, v. 166, No. 1(7), (2024)

56. M.V. Sadovskii. Upper Limit for the Superconducting Transition Temperature in Eliashberg-McMillan Theory. JETP Letters v. 120, No. 3, 205-207 (2024)

Journal of Experimental and Theoretical Physics, Vol. 95, No. 3, 2002, pp. 526–537.
Translated from Zhurnal Éksperimental'no i Teoreticheskoĭ Fiziki, Vol. 122, No. 3, 2002, pp. 610–623.

SOLIDS
Electronic Properties

Optical Conductivity in a 2D Model of the Pseudogap State

M. V. Sadovskiĭ * and N. A. Strigina**

Institute of Electrophysics, Ural Division, Russian Academy of Sciences, ul Komsomol'skaya 34, Yekaterinburg, 620016 Russia

**e-mail: sadovski@iep.uran.ru*

***e-mail: strigina@iep.uran.ru*

Received March 28, 2002

Abstract—A 2D model of the pseudogap state is considered on the basis of the scenario of strong electron scattering by short-range-order fluctuations of the "dielectric" (antiferromagnetic or charge density wave) type. A system of recurrence relations is constructed for a one-particle Green's function and the vertex part, describing the interaction of electrons with an external field. This system takes into account all Feynman diagrams for electron scattering at short-range-order fluctuations. The results of detailed calculations of optical conductivity are given for various geometries (topologies) of the Fermi surface, demonstrating both the effects of pseudogap formation in the electron spectrum and the localization effects. The obtained results are in qualitative agreement with experimental data for underdoped HTSC cuprates. © *2002 MAIK "Nauka/Interperiodica"*.

1. INTRODUCTION

One of the central problems in the physics of high-temperature copper-oxide superconductors (HTSC) is the description of the nature of the so-called pseudogap state [1, 2] existing in a wide region of the phase diagram. In our opinion [2], the preferable scenario for the pseudogap formation in HTSC oxides is based on the existence of strong scattering of charge carriers in this region at short-range-order fluctuations of the "dielectric" type (antiferromagnetic (AFM) fluctuations or charge-density wave (CDW) type fluctuations). This scattering is strong in the vicinity of the characteristic vector $\mathbf{Q} = (\pi/a, \pi/a)$ (a is the 2D lattice constant), corresponding to doubling of the period (antiferromagnetism vector) and is a precursor of the spectral rearrangement due to the establishment of the long-range AFM order. Accordingly, an essentially non-Fermi-liquid rearrangement of the electron spectrum occurs in this pretransition region of the phase diagram in certain regions of the momentum space in the vicinity of so-called hot spots on the Fermi surface [2], where its effective destruction takes place. A direct experimental verification of such a pattern of formation of a pseudogap was obtained in recent ARPES experiments on the system $Nd_{1.85}Ce_{0.15}CuO_4$ [3], in which the above-mentioned spectral rearrangement could be studied in the vicinity of hot spots.

In the framework of the above scenario of the pseudogap state formation, it is possible to construct a simplified "almost exactly" solvable model describing the main features of this state [2] and taking into account the contribution of all Feynman diagrams in the perturbation theory on the scattering by short-range-order (Gaussian) fluctuations with characteristic scattering momentum from the vicinity of $\mathbf{Q}$, determined by the corresponding correlation length ζ [4, 5]. This model is based on a generalization of the model of formation of a pseudogap in a 1D system due to developed short-range-order fluctuations of the CDW type (which was proposed earlier by one of the authors [6, 7]) to the 2D case. A simplified version of this 2D model (the model of hot patches) was used in [8–11] for describing the main properties of superconducting state formed against the background of a dielectric pseudogap.

In [4, 5], one-particle properties of the model under investigation (such as spectral density and the density of states) were mainly analyzed. A remarkable feature of this model is the possibility of summation of the entire series of Feynman diagrams also in the two-particle problem of calculation of the vertex part describing the response of the system to external perturbation (e.g., electromagnetic field) [6, 12, 13]. In the simplified version of the model of "hot patches" on the Fermi surface, the required calculations of optical conductivity in the 2D case were made in [14]. Here, we aim both at a detailed analysis of theoretical aspects of the calculation of two-particle properties in the framework of the general model [4, 5] and at the calculation of optical conductivity for various geometries (topologies) of the Fermi surface, emerging when a realistic form of the free electron spectrum is used.

2. MODEL OF HOT SPOTS

2.1. Description of the Model and "Almost Exact" Solution for One-Particle Green's Function

In the model of a "nearly antiferromagnetic" Fermi liquid, which is actively used for explaining the micro-

scopic mechanism of HTSC [15, 16], the effective interaction of electrons with short-range-order AFM spin fluctuations is introduced. This interaction is described by the dynamic spin susceptibility $\chi_{\mathbf{q}}(\omega)$ whose shape is determined from fitting to NMR data [16]:

$$V_{\text{eff}}(\mathbf{q}, \omega) = g^2\chi_{\mathbf{q}}(\omega) \approx \frac{g^2\xi^2}{1 + \xi^2(\mathbf{q} - \mathbf{Q})^2 - i\omega/\omega_{\text{sf}}}, \quad (1)$$

where g is the coupling constant, ξ is the correlation length of spin fluctuations, $\mathbf{Q} = (\pi/a, \pi/a)$ is the antiferromagnetic ordering vector in the dielectric phase, and ω_{sf} is the characteristic frequency of spin fluctuations. The dynamic susceptibility and, hence, the effective interaction (1) have peaks in the region $\mathbf{q} \sim \mathbf{Q}$; accordingly, two types of quasiparticles emerge in the system, i.e., hot particles, whose momenta lie in the vicinity of hot spots on the Fermi surface (Fig. 1), and cold particles, whose momenta lie in the vicinity of the regions on the Fermi surface surrounding the diagonals of the Brillouin zone [4]. As a matter of fact, quasiparticles from the regions of hot spots are strongly scattered with the momentum transfer of the order of $\mathbf{Q}$ due to their interaction with the spin fluctuations (1), while the same interaction for particles with momenta away from hot spots is quite weak.

Considering the region of rather high temperatures $\pi T \gg \omega_{sf}$, we can neglect the spin dynamics [4], confining our analysis of relation (1) to the static approximation. A considerable simplification of calculations, which makes it possible to analyze higher-order contribution of perturbation theory, can be obtained if we go over in relation (1) to a model interaction of the form [5]

$$V_{\text{eff}}(\mathbf{q}) = \Delta^2 \frac{2\xi^{-1}}{\xi^{-2} + (q_x - Q_x)^2} \frac{2\xi^{-1}}{\xi^{-2} + (q_y - Q_y)^2}, \quad (2)$$

where Δ is an effective parameter having the dimensions of energy. Following [4, 5], in the subsequent analysis we will treat Δ and ξ as phenomenological parameters (that can be determined experimentally). Expression (2) is qualitatively similar to the static limit (1) and differs from it quantitatively only slightly in the most interesting region $|\mathbf{q} - \mathbf{Q}| < \xi^{-1}$ determining scattering in the vicinity of hot spots.

We will take the spectrum of the "bare" (free) quasiparticles in the form [4]

$$\begin{aligned}\xi_{\mathbf{p}} &= -2t(\cos p_x a + \cos p_y a) \\ &\quad - 4t' \cos p_x a \cos p_y a - \mu,\end{aligned} \quad (3)$$

where t is the integral of transfer between the nearest neighbors, t' is the same for next-to-nearest neighbors in the square lattice, and μ is the chemical potential. This expression provides a satisfactory approximation to the results of band calculations for real HTSC systems. For example, for $YBa_2Cu_3O_{6+\delta}$, we have t = 0.25 eV and $t' = -0.45t$ [4]. The chemical potential μ is fixed by charge carrier concentrations. In this work, we consider various characteristic relations between parameters t and t' leading to different geometries (topologies) of the Fermi surface, aiming at an analysis of the general pattern, which is not necessarily associated with known specific systems.

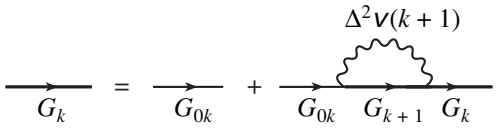

Fig. 1. Diagrammatic representation of recurrence relation for the Green's function.

In [5], a detailed analysis of contributions of all diagrams was carried out for the self-energy part $\Sigma(\varepsilon_n\mathbf{p})$ of an electron. It turns out that, in the case when the signs of the velocity components $v^x_{\mathbf{p}}$ and $v^x_{\mathbf{p}+\mathbf{Q}}$ (as well as of $v^y_{\mathbf{p}}$ and $v^y_{\mathbf{p}+\mathbf{Q}}$) coincide in hot spots on the Fermi surface, the Feynman integrals in a diagram of any order are determined only by the contributions from the poles of the Lorentzians in relation (2) and can easily be evaluated.[1] In this case, the contribution of an arbitrary diagram for the self-energy component of the Nth order in the interaction with fluctuations (2) has the form ($\varepsilon_n = (2n + 1)\pi T$)

$$\Sigma^{(N)}(\varepsilon_n\mathbf{p}) = \Delta^{2N} \prod_{j=1}^{2N-1} \frac{1}{i\varepsilon_n - \xi_j(\mathbf{p}) + in_j v_j \kappa}, \quad (4)$$

where $\xi_j(\mathbf{p}) = \xi_{\mathbf{p}+\mathbf{Q}}$ and $v_j = |v^x_{\mathbf{p}+\mathbf{Q}}| + |v^y_{\mathbf{p}+\mathbf{Q}}|$ for odd j, $\xi_j(\mathbf{p}) = \xi_{\mathbf{p}}$ and $v_j = |v^x_{\mathbf{p}}| + |v^y_{\mathbf{p}}|$ for even j, and $\kappa = \xi^{-1}$. Here, n_j is the number of interaction lines embracing the jth Green's function in the given diagram; for the sake of definiteness, we assume that $\varepsilon_n > 0$.

The conditions under which the above constraints are imposed on the velocities at the points on the Fermi surface connected by vector $\mathbf{Q}$ (hot spots) are analyzed in detail in [5], where examples of corresponding geometries of the Fermi surfaces realized for certain relations between parameters t and t' in Eq. (3) are considered. In these cases, expression (4) is virtually exact. In all remaining cases (for other relations between t and t'), expression (4) is used as a successful ansatz for an arbitrary-order contribution obtained by simple continuation of the spectrum in parameters t and t' to the region of interest. Even in the most unfavorable 1D case [7] corresponding to a square Fermi surface emerging from Eq. (3) for $t' = 0$ and $\mu = 0$, the use of this ansatz leads to results (e.g., for the density of states) very close quantitatively [17] to the results of the exact numerical

[1] A similar situation also emerges in the case when the velocities in the hot spots connected by vector $\mathbf{Q}$ are exactly perpendicular [4].

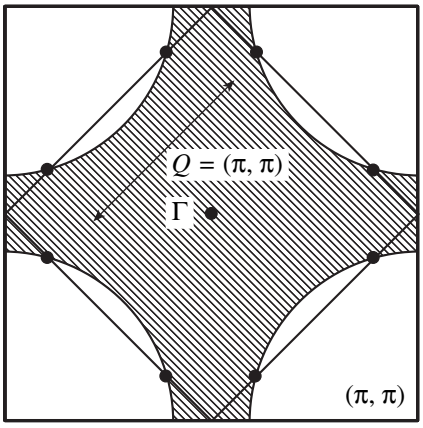

Fig. 2. Fermi surface with hot spots connected through the scattering vector of the order of $\mathbf{Q} = (\pi/a, \pi/a)$.

simulation of this problem [18]. In this sense, we are using the term "almost exact" solution.

When ansatz (4) is used, it is found that the contribution of any diagram with crossing interaction lines is equal to the contribution of a diagram of the same order without intersection of these lines [7]. For this reason, we can, in fact, take into account the contributions from diagrams without intersection of the interaction lines, taking into account the contribution from diagrams with intersection, with the help of additional combinatorial factors compared to the "initial" interaction vertices (or lines) [7]. As a result, we obtain the following recurrence relation (representation in the form of a continued fraction [7]) for a one-electron Green's function, which gives an effective logarithm for subsequent numerical calculations [5]:

$$G_k(\varepsilon_n\xi_\mathbf{p}) = \frac{1}{i\varepsilon_n - \xi_k(\mathbf{p}) + ikv_k\kappa - \Sigma_{k+1}(\varepsilon_n\xi_\mathbf{p})} \equiv \{G_{0k}^{-1}(\varepsilon_n\xi_\mathbf{p}) - \Sigma_{k+1}(\varepsilon_n\xi_\mathbf{p})\}^{-1}, \quad (5)$$

$$\Sigma_k(\varepsilon_n\xi_\mathbf{p}) = \Delta^2\frac{v(k)}{i\varepsilon_n - \xi_k(\mathbf{p}) + ikv_k\kappa - \Sigma_{k+1}(\varepsilon_n\xi_\mathbf{p})}. \quad (6)$$

Figure 2 is a graphical representation of this recurrence relation. The physical Green's function we are interested in is $G(\varepsilon_n\xi_\mathbf{p}) = G_{k=0}(\varepsilon_n\xi_\mathbf{p})$. In relation (5), we have also introduced the following auxiliary notation:

$$G_{0k}(\varepsilon_n\xi_\mathbf{p}) = \frac{1}{i\varepsilon_n - \xi_k(\mathbf{p}) + ikv_k\kappa}. \quad (7)$$

In the case of commensurate fluctuations with $\mathbf{Q} = (\pi/a, \pi/a)$ [7] under investigation, the combinatorial factor is given by

$$v(k) = k \quad (8)$$

if we disregard their spin structure (CDW-type fluctuations). If the spin structure of interactions is taken into account in the model of a nearly antiferromagnetic Fermi liquid (spin–fermion model [4]), the combinatorics of the diagrams becomes more complicated. In particular, the scattering with spin conservation gives a formally commensurate combinatorics, while scattering with spin flip is described by the diagrams for the incommensurate case ("charged" random field in the terminology used in [4]). As a result, the recurrence relation for the Green's function, as before, has the form (6), but the combinatorial factor $v(k)$ has the form [4]

$$v(k) = \begin{cases} \dfrac{k+2}{3} & \text{for odd } k \\ \dfrac{k}{3} & \text{for even } k. \end{cases} \quad (9)$$

In the subsequent analysis, we confine ourselves to cases (8) and (9); the details corresponding to incommensurate fluctuations of the CDW type can be found in [5–7].

The obtained solution for a one-particle Green's function is exact in the limit $\xi \longrightarrow \infty$, when a solution can be found in analytic form [4, 6]. This solution is exact in the trivial limit $\xi \longrightarrow 0$, when interaction (2) just vanishes for a fixed value of Δ. For all intermediate values of ξ, it gives a very good interpolation (see above) since it is virtually exact for certain geometries of the Fermi surface emerging for specific ranges of variation of the parameters of spectrum (3) [5].

Using relation (5), we can easily carry out numerical calculations of the one-electron spectral density and density of states:

$$A(E\mathbf{p}) = -\frac{1}{\pi}\mathrm{Im}G^R(E\mathbf{p}), \qquad N(E) = \sum_\mathbf{p} A(E\mathbf{p}). \quad (10)$$

In these relations, $G^R(E\mathbf{p})$ is the retarded Green's function obtained by the conventional analytical continuation of Eq. (5) from the Matsubara frequencies to the real axis E. The details of corresponding calculations and the discussion of the obtained results for the 2D model under investigation can be found in the publications [4, 5] mentioned above.

2.2. Recurrence Equations for the Vertex Part and Conductivity

In order to calculate the optical conductivity, we must calculate the vertex part describing the electromagnetic response of the system. This apex can be determined by the method proposed for an analogous one-dimensional model in [12, 13]. Any diagram for an irreducible vertex component can be obtained by inserting the external field lines into the corresponding diagram for the self-energy component [6]. Since our model can take into account only the diagrams for the self-energy component without intersection of the

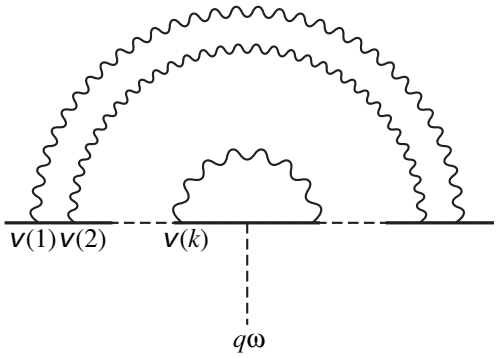

Fig. 3. General form of the higher order correction for the vertex part.

interaction lines with additional combinatorial factors $V(k)$ at initial vertices, it is sufficient to consider only diagrams of the type shown in Fig. 3 for calculating vertex corrections. This immediately gives a system of recurrence equations for the vertex parts, presented graphically in Fig. 4. In order to obtain the corresponding analytic expressions, we consider the simplest vertex correction shown in Fig. 5a. Carrying out calculations for $T = 0$ in the *RA* channel, we can easily obtain the corresponding contribution in the form

$$\begin{aligned}
&\mathcal{J}_1^{(1)RA}(\varepsilon\mathbf{p};\ \varepsilon+\omega,\ \mathbf{p}+\mathbf{q})\\
&= \sum_{\mathbf{K}} V_{\text{eff}}(\mathbf{k}) G_{00}^A(\varepsilon\xi_{\mathbf{p}-\mathbf{K}}) G_{00}^R(\varepsilon+\omega\xi_{\mathbf{p}-\mathbf{K}+\mathbf{q}})\\
&= \Delta^2\{G_{00}^A(\varepsilon,\ \xi_1(\mathbf{p})+iV_1\kappa)\\
&- G_{00}^R(\varepsilon+\omega,\ \xi_1(\mathbf{p}+\mathbf{q})-iV_1\kappa)\}\\
&\times\frac{1}{\omega+\xi_1(\mathbf{p})-\xi_1(\mathbf{p}+\mathbf{q})} \qquad (11)\\
&= \Delta^2 G_{00}^A(\varepsilon,\ \xi_1(\mathbf{p})+iV_1\kappa) G_{00}^R(\varepsilon+\omega,\ \xi_1(\mathbf{p}+\mathbf{q})-iV_1\kappa)\\
&\times\left\{1+\frac{2iV_1\kappa}{\omega+\xi_1(\mathbf{p})-\xi_1(\mathbf{p}+\mathbf{q})}\right\}\\
&\equiv \Delta^2 G_{01}^A(\varepsilon,\ \xi_{\mathbf{p}}) G_{01}^R(\varepsilon+\omega,\ \xi_{\mathbf{p}+\mathbf{q}})\\
&\times\left\{1+\frac{2iV_1\kappa}{\omega+\xi_1(\mathbf{p})-\xi_1(\mathbf{p}+\mathbf{q})}\right\},
\end{aligned}$$

where we have evaluated the integrals using the following identity valid for free-electron Green's functions:

$$\begin{aligned}
&G_{00}^A(\varepsilon\xi_p) G_{00}^R(\varepsilon+\omega\xi_{\mathbf{p}+\mathbf{q}})\\
&= \{G_{00}^A(\varepsilon\xi_{\mathbf{p}}) - G_{00}^R(\varepsilon+\omega\xi_{\mathbf{p}+\mathbf{q}})\}\frac{1}{\omega-\xi_{\mathbf{p}+\mathbf{q}}+\xi_{\mathbf{p}}}.
\end{aligned} \qquad (12)$$

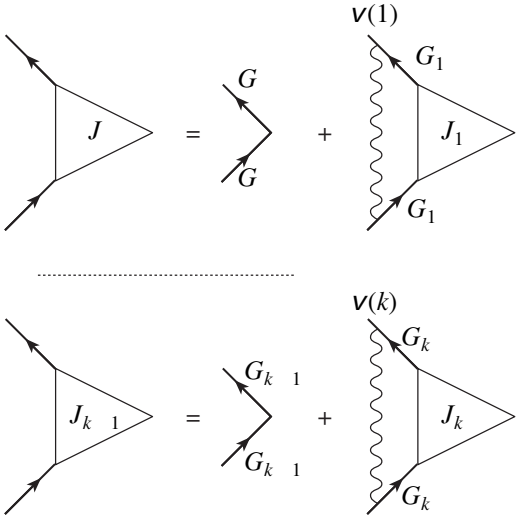

Fig. 4. Recurrence equations for the vertex part.

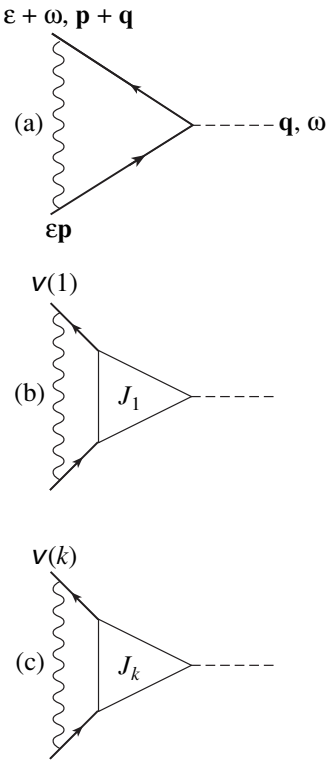

Fig. 5. Simplest corrections to vertex parts.

"Dressing" internal electron lines, we pass to the diagram in Fig. 5b. Using the identity

$$\begin{aligned}
&G^A(\varepsilon\xi_{\mathbf{p}}) G^R(\varepsilon+\omega\xi_{\mathbf{p}+\mathbf{q}}) = \{G^A(\varepsilon\xi_{\mathbf{p}}) - G^R(\varepsilon+\omega\xi_{\mathbf{p}+\mathbf{q}})\}\\
&\times\frac{1}{\omega-\xi_{\mathbf{p}+\mathbf{q}}+\xi_{\mathbf{p}}-\Sigma_1^R(\varepsilon+\omega\xi_{\mathbf{p}+\mathbf{q}})+\Sigma_1^A(\varepsilon\xi_{\mathbf{p}})},
\end{aligned} \qquad (13)$$

which is valid for exact Green functions, we can write the contribution of this diagram in the form

$$\mathcal{J}_1^{RA}(\varepsilon\mathbf{p};\ \varepsilon+\omega,\ \mathbf{p}+\mathbf{q})$$

$$= \Delta^2 v(1) G_1^A(\varepsilon, \xi_{\mathbf{p}}) G_1^R(\varepsilon+\omega, \xi_{\mathbf{p}+\mathbf{q}}) \left\{ 1 + \frac{2iv_1\kappa}{\omega - \xi_1(\mathbf{p}+\mathbf{q}) + \xi_1(\mathbf{p}) - \Sigma_2^R(\varepsilon+\omega\xi_{\mathbf{p}+\mathbf{q}}) + \Sigma_2^A(\varepsilon\xi_{\mathbf{p}})} \right\} \tag{14}$$

$$\times J_1^{RA}(\varepsilon\mathbf{p};\ \varepsilon+\omega,\ \mathbf{p}+\mathbf{q}).$$

Here, we have assumed that the line of interaction on the diagram for the vertex correction in Fig. 5b "transforms" the self-energy component $\Sigma_1^{R,A}$ of internal electron lines into $\Sigma_2^{R,A}$ in accordance with the approximation used above for the self-energy component (see Fig. 2).[2]

We can now easily write a similar expression for a general diagram shown in Fig. 5c:

$$\mathcal{J}_k^{RA}(\varepsilon\mathbf{p};\ \varepsilon+\omega,\ \mathbf{p}+\mathbf{q}) = \Delta^2 v(k) G_k^A(\varepsilon, \xi_{\mathbf{p}}) G_k^R(\varepsilon+\omega, \xi_{\mathbf{p}+\mathbf{q}})$$

$$\times \left\{ 1 + \frac{2iv_k\kappa k}{\omega - \xi_k(\mathbf{p}+\mathbf{q}) + \xi_k(\mathbf{p}) - \Sigma_{k+1}^R(\varepsilon+\omega\xi_{\mathbf{p}+\mathbf{q}}) + \Sigma_{k+1}^A(\varepsilon\xi_{\mathbf{p}})} \right\} J_k^{RA}(\varepsilon\mathbf{p};\ \varepsilon+\omega,\ \mathbf{p}+\mathbf{q}). \tag{15}$$

Accordingly, the fundamental recurrence relation for the vertex part in Fig. 4 can be written in the form

$$J_{k-1}^{RA}(\varepsilon\mathbf{p};\ \varepsilon+\omega,\ \mathbf{p}+\mathbf{q}) = 1 + \Delta^2 v(k) G_k^A(\varepsilon, \xi_{\mathbf{p}}) G_k^R(\varepsilon+\omega, \xi_{\mathbf{p}+\mathbf{q}})$$

$$\times \left\{ 1 + \frac{2iv_k\kappa k}{\omega - \xi_k(\mathbf{p}+\mathbf{q}) + \xi_k(\mathbf{p}) - \Sigma_{k+1}^R(\varepsilon+\omega\xi_{\mathbf{p}+\mathbf{q}}) + \Sigma_{k+1}^A(\varepsilon\xi_{\mathbf{p}})} \right\} J_k^{RA}(\varepsilon\mathbf{p};\ \varepsilon+\omega,\ \mathbf{p}+\mathbf{q}). \tag{16}$$

The physical apex $J^{RA}(\varepsilon\mathbf{p};\ \varepsilon+\omega,\ \mathbf{p}+\mathbf{q})$ is defined as $J_{k=0}^{RA}(\varepsilon\mathbf{p};\ \varepsilon+\omega,\ \mathbf{p}+\mathbf{q})$. The recurrence procedure (16) takes into account all diagrams in perturbation theory for the vertex component. As $\kappa \longrightarrow 0$ ($\xi \longrightarrow \infty$), Eq. (16) is reduced to the series studied in [6] (see also [4]), which can be summed exactly in analytic form. In our scheme of analysis, the standard ladder approximation corresponds to the case when all combinatorial factors $v(k)$ in Eq. (16) are assumed to be equal to unity [13].

The conductivity of the system can be expressed [19] in terms of the retarded density–density response function $\chi^R(q, \omega)$:

$$\sigma(\omega) = e^2 \lim_{q\to 0}\left(-\frac{i\omega}{q^2}\right)\chi^R(q, \omega), \tag{17}$$

where e is the electron charge and

$$\chi^R(q, \omega) = \omega\{\Phi^{RA}(0, q, \omega) - \Phi^{RA}(0, 0, \omega)\}, \tag{18}$$

while the two-particle Green's function $\Phi^{RA}(\varepsilon, q, \omega)$ is determined by the loop graph shown in Fig. 6.

Direct numerical calculations confirm that the recurrence procedure (16) satisfies the exact relation following (for $\omega \longrightarrow 0$) from the Ward identity [19]:

$$\Phi^{RA}(0, 0, \omega) = -N(E_F)/\omega, \tag{19}$$

where $N(E_F)$ is the density of states at the Fermi level $E_F = \mu$. This is the main argument in favor of the ansatz used in the derivation of Eqs. (14)–(16).

Ultimately, we can write conductivity in the symmetrized form convenient for numerical calculations:

$$\sigma(\omega) = \frac{e^2\omega^2}{\pi}\lim_{q\to 0}\frac{1}{q^2}\sum_{\mathbf{p}}\left\{ G^R\left(\frac{\omega}{2}, \mathbf{p}+\frac{\mathbf{q}}{2}\right)\right.$$

$$\times J^{RA}\left(\frac{\omega}{2}, \mathbf{p}+\frac{\mathbf{q}}{2}; -\frac{\omega}{2}, \mathbf{p}-\frac{\mathbf{q}}{2}\right) G^A\left(-\frac{\omega}{2}, \mathbf{p}-\frac{\mathbf{q}}{2}\right) \tag{20}$$

$$\left. - G^R\left(\frac{\omega}{2}, \mathbf{p}\right) J^{RA}\left(\frac{\omega}{2}, \mathbf{p}; -\frac{\omega}{2}, \mathbf{p}\right) G^A\left(-\frac{\omega}{2}, \mathbf{p}\right)\right\},$$

[2] A motivation for this notation is that it ensures the fulfillment of the Ward identity which will be discussed below.

where we have also taken into account the additional factor 2 associated with the summation over spin.

Numerical calculations were carried out directly by using formulas (20), (16), and (5), the recurrence procedure being terminated at a high "level" k, where all Σ_k and J_k were set equal to zero. Integration of Eq. (20) was carried out over the entire 2D Brillouin zone. The "bare" electron spectrum was taken in the form (3). Integration momenta are naturally reduced to dimensionless form with the help of lattice constant a, and all energies will be henceforth given in units of the transfer integral t. In this case, conductivity is measured in units of universal conductivity $\sigma_0 = e^2/\hbar = 2.5 \times 10^{-4}\ \Omega^{-1}$ of a 2D system, and the density of states is measured in units of $1/ta^2$.

3. RESULTS AND DISCUSSION

Optical conductivity and other parameters of the model under investigation were calculated for various values of parameters determining the spectrum (3) of free quasiparticles and for $\Delta = t$. Let us first consider the case when the Fermi surfaces are in the vicinity of half-filled band with $\mu = 0$ and $t' = 0$, which are presented in Fig. 7a for the first quadrant of the Brillouin zone. It is well known that, for $\mu = 0$ and $t' = 0$, the Fermi surface has the form of a square (complete nesting), so that the situation is equivalent to a certain extent to the 1D case considered in [6, 12, 13]. The results of calculations for the real part of optical conductivity in the 2D problem under investigation for the case of spin–fermion combinatorics of the diagrams and for various values of correlation length of the short-range AFM order (parameter $\kappa = \xi^{-1}$, where ξ is measured in units of the lattice constant a) are presented in Fig. 8. The form of conductivity is qualitatively quite similar to that obtained in [12, 13] in the 1D model (for the case of incommensurate CDW-type fluctuations). It is characterized by the presence of a well-defined peak due to pseudogap absorption (the corresponding curves for the density of states, demonstrating the presence of a pseudogap near the Fermi level, are shown in the inset to Fig. 8) for $\omega \sim 2\Delta$ and the presence of a maximum in the low-frequency region, which is associated with the localization of charge carriers in the static random field of AFM fluctuations. The localization nature of this maximum is confirmed by its conversion into the characteristic Drude peak (with a maximum at $\omega = 0$) for calculations in the ladder approximation, when the combinatorial factors $V(k) = 1$, which corresponds to the exclusion of the contribution from diagrams with crossed interaction lines which directly lead to 2D Anderson localization [19, 20]. The qualitative form of conductivity in this case is also quite similar to that obtained in [13]. The narrowing of the localization peak upon a decrease in the correlation length of fluctuations can be explained, according to [13], by a decrease in the effective interaction (2) upon a decrease in ξ (for a fixed value of Δ),

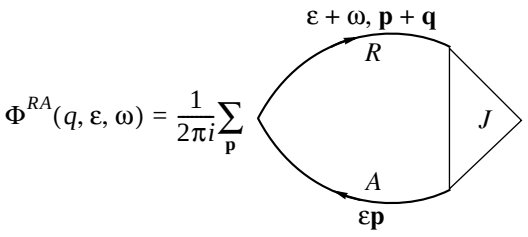

Fig. 6. Diagrammatic representation for the two-particle response function $\Phi^{RA}(q, \varepsilon, \omega)$.

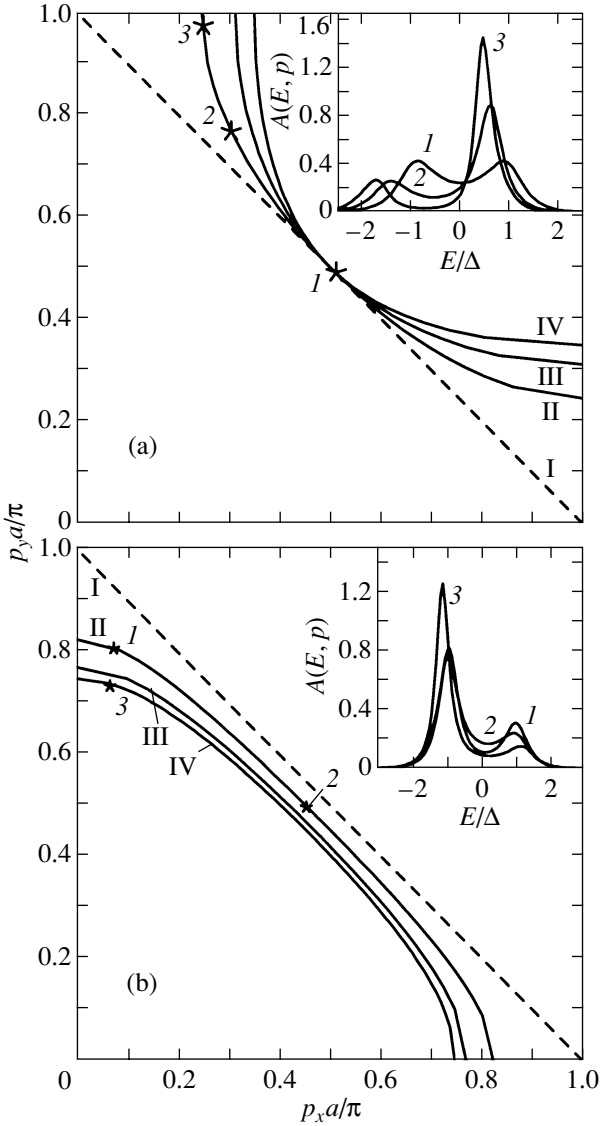

Fig. 7. Fermi surfaces for different values of parameter t' and chemical potential μ: (a) $\mu = 0$ and $t'/t = 0$ (I), –0.2 (II), –0.4 (III), and –0.6 (IV); (b) $t' = 0$ and $\mu/t = 0$ (I), –0.3 (II), –0.5 (III), and –0.6 (IV). The insets show the energy dependences of spectral density for the spin–fermion model for $\kappa a = 0.1$ at the points of the momentum space marked by asterisks.

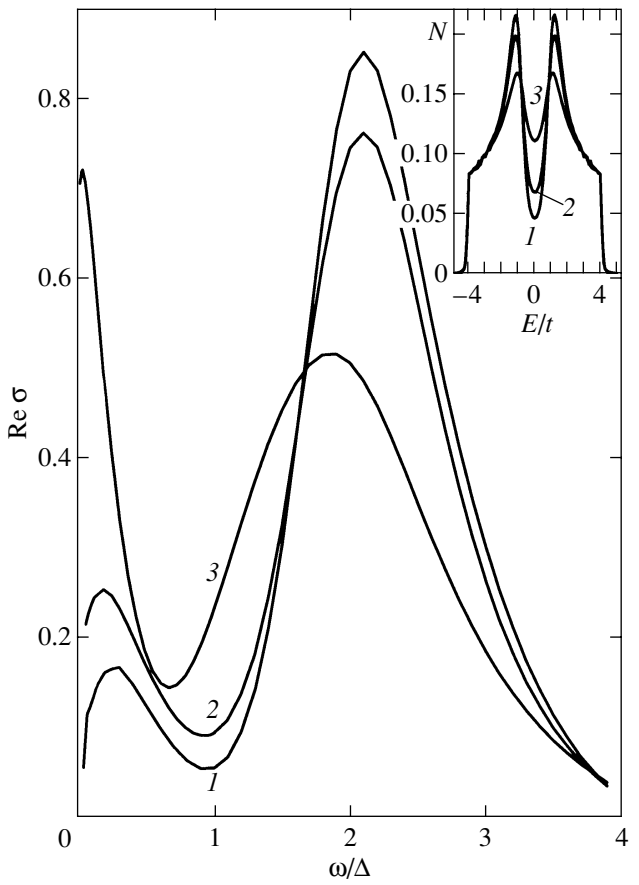

Fig. 8. Real part of optical conductivity in the spin–fermion model for a square Fermi surface ($\mu = 0$, $t' = 0$) for different values of the inverse short-range-order correlation length: $\kappa a = 0.1$ (*1*), 0.2 (*2*), and 0.5 (*3*). The inset shows the corresponding densities of states.

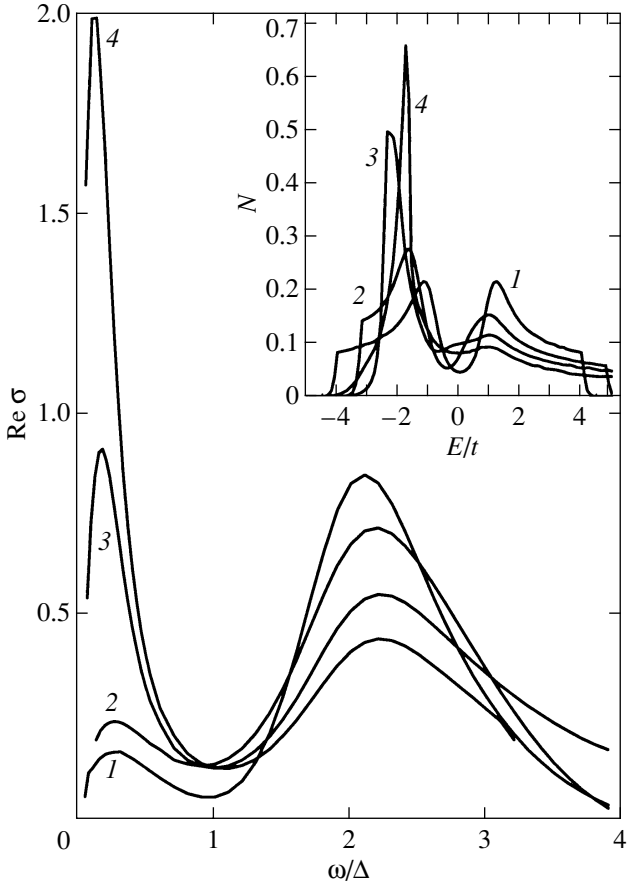

Fig. 9. Real part of optical conductivity in the spin–fermion model for $\mu = 0$ and $\kappa a = 0.1$ for various shapes of the Fermi surface obtained from the square surface taking into account the transfer integral: $t'/t = 0$ (*1*), –0.2 (*2*), –0.4 (*3*), and –0.6 (*4*). The inset shows the corresponding densities of states.

leading to a general decrease in scattering rate (including that at the cold part of the Fermi surface). It should be noted that the behavior of the density of states and optical conductivity determined here is in complete qualitative agreement with the results obtained for an analogous 2D model of the Peierls transition with the help of the quantum Monte Carlo method in a recent publication [21].

If we now include the transfer integral t' between the next-to-nearest neighbors in Eq. (3), assuming, as before, that $\mu = 0$, we arrive at shapes of the Fermi surface differing from a square and depicted in Fig. 7a. The inset to this figure shows the energy dependence of the spectral density (10) at several characteristic points on these Fermi surfaces. It can be seen that it displays a characteristic non-Fermi-liquid behavior of the type of that studied in [4, 5] practically at all points on the Fermi surface as long as the shape of this surface differs from a square not very strongly, in spite of the fact that a hot spot in the case under investigation lies strictly at the intersection of the Fermi surface with the diagonal of the Brillouin zone. The corresponding curves for the real part of optical conductivity are shown in Fig. 9; the inset to this figure depicts the shape of the corresponding densities of states. It can be seen that, as the situation differs more and more strongly from complete nesting, the pseudogap absorption peak decreases, while the localization peak increases in conformity with the general summation rule for conductivity. It should be noted, however, that the pseudogap absorption peak remains quite noticeable even when the pseudogap in the density of states is virtually imperceptible (curves *4* in Fig. 9).

Let us return to the case when $t' = 0$, but the value of μ is varied, so that we pass to the Fermi surfaces whose shape is quite close to the square shown in Fig. 7b. Strictly speaking, hot spots on the Fermi surface are absent altogether, but the spectral density shown in the inset to Fig. 7b preserves a typical pseudogap form. The corresponding dependences for the real part of optical conductivity are presented in Fig. 10.

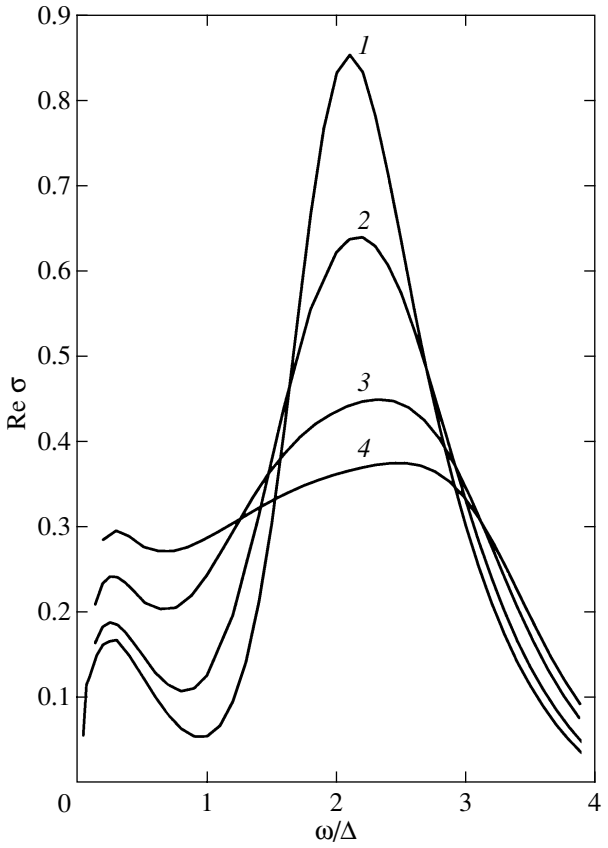

Fig. 10. Real part of optical conductivity in the spin–fermion model for different values of parameter t' and $\kappa a = 0.1$ for various shapes of the Fermi surface obtained from the square surface as a result of departure from half-filled band. The chemical potential corresponds to values of $\mu/t = 0$ (*1*), –0.3 (*2*), –0.5 (*3*), and –0.6 (*4*).

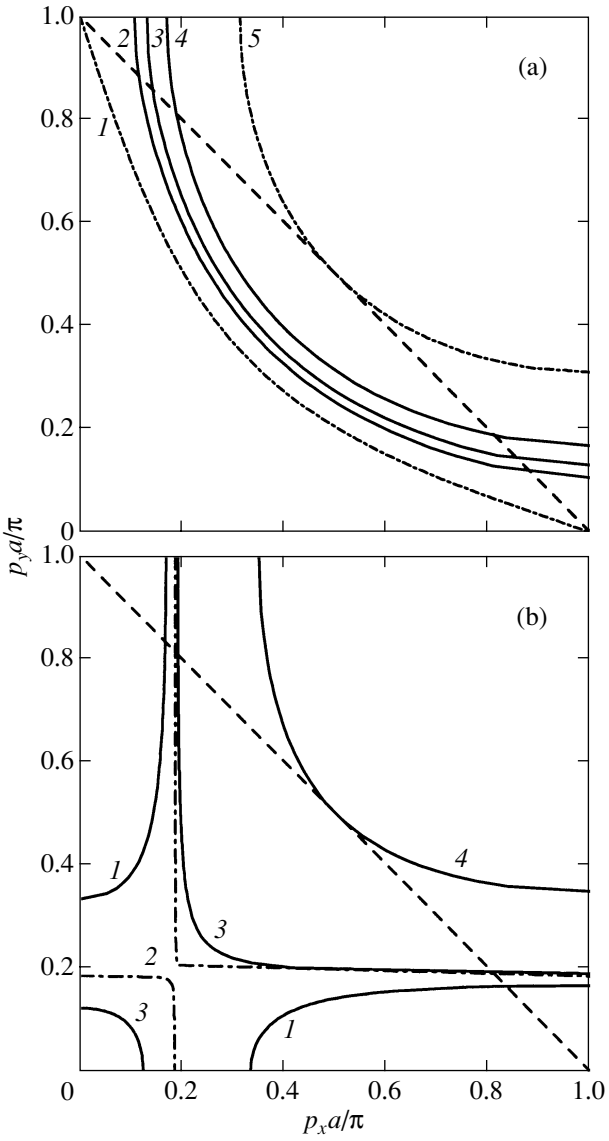

Fig. 11. Fermi surfaces for different values of parameter t' and chemical potential μ: (a) $t'/t = -0.4$ (which is typical of HTSC cuprates) and $\mu/t = -1.6$ (*1*), –1.4 (*2*), –1.3 (*3*), –1.1 (*4*), and 0 (*5*); hot spots exist for $-1.6 < \mu/t < 0$; (b) $t'/t = -0.6$ and $\mu/t = -1.8$ (*1*), –1.666 (*2*), –1.63 (*3*), and 0 (*4*). Hot spots exist for $\mu < 0$. Dashed lines mark the boundary of the magnetic Brillouin zone.

Let us now consider various geometries of the Fermi surface with hot spots shown in Fig. 11. Figures 12 and 13 depict the real part of optical conductivity, calculated (for different combinatorics of the diagrams) for two characteristic values $t' = -0.4t$ and $t' = -0.6t$ for the chemical potential $\mu = 0$, when hot spots are on the diagonal of the Brillouin zone (curve *5* in Fig. 11a and curve *4* in Fig. 11b). It can be seen that the pseudogap behavior of the conductivity persists even in the case when there is practically no pseudogap in the density of states (shown in the insets to Figs. 12, 13). The dashed curve in Fig. 12 shows the results of the ladder approximation, demonstrating the typical disappearance of 2D localization. Figure 13 illustrates the smearing of the pseudogap maximum of conductivity upon a decrease in the short-range-order correlation length.

For most high-temperature copper-oxides superconductors, the characteristic geometry of the Fermi surface is described by the case $t' = -0.4t$ and $\mu = -1.3t$ [4] (curve *3* in Fig. 11a). The results of calculation of optical conductivity for this case for different values of the inverse correlation length κ are presented in Fig. 14 (for the case of the spin–fermion combinatorics of diagrams). We have introduced additional weak scattering due to inelastic processes through the standard substitution $\omega \longrightarrow \omega + i\gamma$ [22], which leads to the emergence of a narrow Drude peak in the frequency range $\omega < \gamma$ (violation of 2D localization due to dephasing). It can easily be verified that, as the rate γ of inelastic scattering increases, the localization peak is smeared and is transformed into a conventional Drude peak in the low-frequency region. The pseudogap absorption peak becomes more pronounced upon an increase in correla-

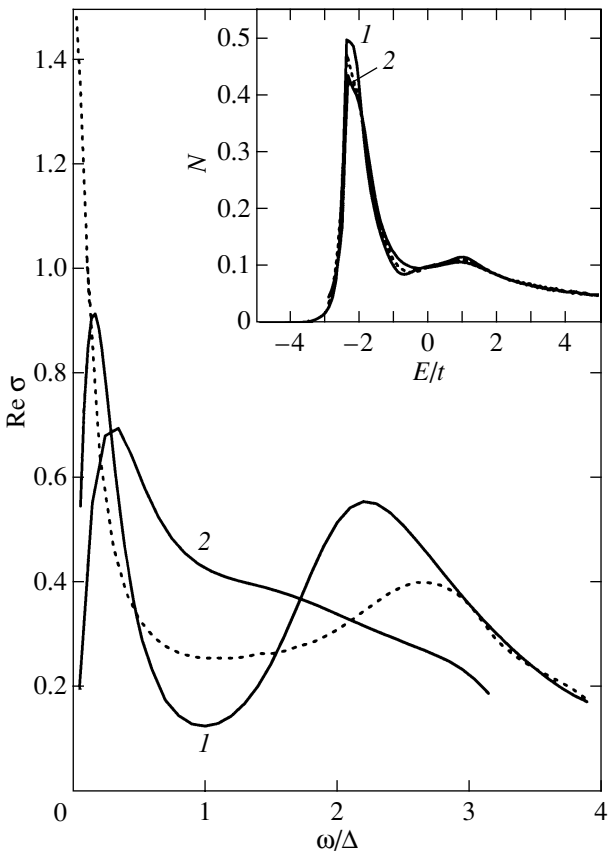

Fig. 12. Real part of optical conductivity for $t'/t = -0.4$, $\mu = 0$, and $\kappa a = 0.1$ for different combinatorics of diagrams: spin–fermion model (*1*) and commensurate case (*2*). The dotted curve corresponds to the ladder combinatorics. The inset shows the corresponding densities of states.

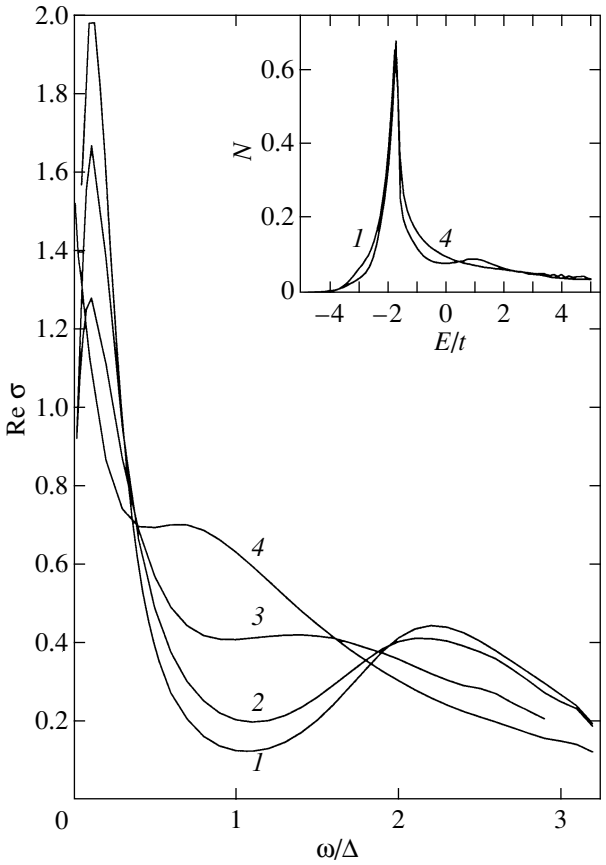

Fig. 13. Real part of optical conductivity in the spin–fermion model for $t'/t = -0.6$ and $\mu = 0$ for the values of inverse correlation length $\kappa a = 0.1$ (*1*), 0.2 (*2*), 0.5 (*3*) and 1.0 (*4*). The inset shows the densities of states corresponding to curves *1* and *4*.

tion length ξ (a decrease in parameter κ). Figure 15 shows the frequency dependences of the effective scattering rate $1/\tau(\omega)$ and effective mass $m^*(\omega)$, determined from the results of our calculations with the help of the generalized Drude formula, which is often used for experimental data fitting [1]:

$$\frac{1}{\tau(\omega)} = \frac{\omega_p^2}{4\pi}\mathrm{Re}\left(\frac{1}{\sigma(\omega)}\right), \tag{21}$$

$$\frac{m^*(\omega)}{m} = -\frac{1}{\omega}\frac{\omega_p^2}{4\pi}\mathrm{Im}\left(\frac{1}{\sigma(\omega)}\right). \tag{22}$$

Here, ω_p is the plasma frequency, and m is the free electron mass. It can be seen from Fig. 15 that the quantity $1/\tau(\omega)$ (which is expressed in units of $\omega_p^2\hbar/4\pi e^2$ in this figure) demonstrates a typical pseudogap behavior in the frequency range $\omega < 2\Delta$. It should be noted that the density of states in this case exhibits only a weakly pronounced pseudogap [5] (see the inset to Fig. 12). Figure 16 presents similar results for the same case (typical of HTSC oxides) obtained for a model with diagram combinatorics corresponding to commensurate fluctuations of the CDW type. It can be seen that the pseudogap absorption peak is virtually unnoticeable in this case.

It can be seen from Fig. 11b that, as the chemical potential changes from $\mu = 0$ to $\mu = -1.666t$, the Fermi surface acquires flat regions of increasing size and is transformed into a virtually cross-shaped surface for $\mu \approx 1.666t$. Such a Fermi surface was observed in ARPES experiments on the system $La_{1.28}Nd_{0.6}Sr_{0.12}CuO_4$ [23, 24]. In this case, the components of velocities at hot spots connected by the vector $\mathbf{Q} = (\pi/a, \pi/a)$ become orthogonal. For $\mu/t = -1.666\ldots$, the topology of the Fermi surface changes (Fig. 11b), and these components have the same sign in the entire region $\mu/t < -1.666\ldots$, which ensures exact fulfillment of our fundamental ansatz (4) for the contributions of higher order diagrams [5]. It is interesting to consider the results of calculations of optical conductivity in this region of variation of μ also. The corresponding results in the case of a commensurate (CDW) combinatorics

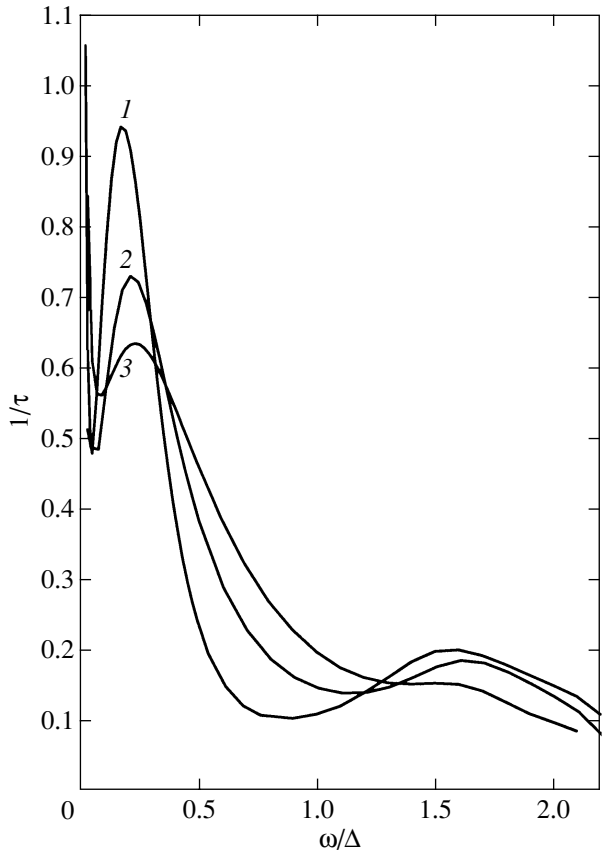

Fig. 14. Real part of optical conductivity in the spin–fermion model for $t'/t = -0.4$ and $\mu/t = -1.3$ for the values of inverse correlation length $\kappa a = 0.05$ (*1*), 0.1 (*2*), and 0.2 (*3*). The dephasing rate $\gamma/t = 0.005$.

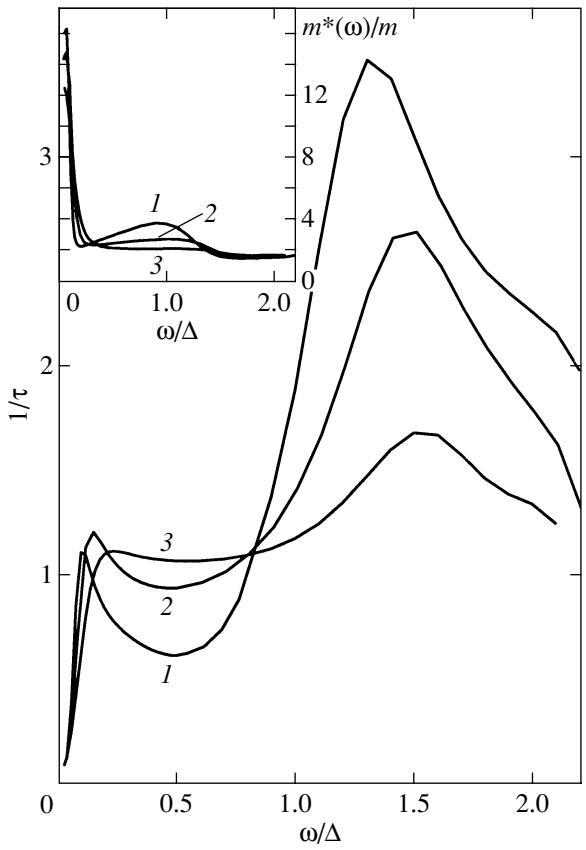

Fig. 15. Generalized scattering rate and effective mass for the case $t'/t = -0.4$ and $\mu/t = -1.3$ typical of high-temperature superconductors. The parameters of the generalized Drude model are obtained in the spin–fermion model for the values of inverse correlation length $\kappa a = 0.05$ (*1*), 0.1 (*2*), and 0.2 (*3*). The dephasing rate $\gamma/t = 0.005$.

are presented in Fig. 17, where the variation of the localization conductivity peak during the transition of chemical potential through the topological transition region can be traced. A low-intensity pseudogap absorption peak virtually remains unchanged. The inset to Fig. 17 shows the evolution of the localization peak taking into account inelastic scattering (parameter γ) for $\mu = -1.8t$. It can clearly be seen how a transition from the localization to the Drude behavior occurs due to dephasing processes. The obtained results show that the change in the Fermi surface topology itself does not lead to strong qualitative changes in optical conductivity in the framework of the model under investigation.

4. CONCLUSIONS

The above analysis demonstrates the variety of the results that can be obtained in the model under investigation for different geometries and topologies of the Fermi surface, emerging upon a change in the parameters of the "bare" quasiparticle spectrum (3). It is interesting to compare these results with those obtained earlier in the simplified model of hot patches on the Fermi surface [14]. Since the pseudogap anomalies in the hot-patches model are mainly determined by strong scattering precisely in these (flat) regions on the Fermi surface and by their relative size, the localization conductivity peak was virtually unnoticeable in this model, and the dominating role was played by the Drude peak associated with scattering from cold regions, which is determined by an auxiliary scattering rate γ (whose meaning is similar to the inelastic scattering rate introduced above). The above analysis of a more realistic model shows that the contribution of the localization peak may be quite noticeable and that it is this peak that can be transformed into a narrow Drude peak when dephasing processes are taken into account.

The main drawback of the model considered above is probably the disregard of the dynamics of short-range-order fluctuations. This approximation is justified, according to [4, 5], only at high temperatures, but the processes of inelastic scattering responsible for the dephasing and violation of localization become more significant just at such temperatures. Another draw-

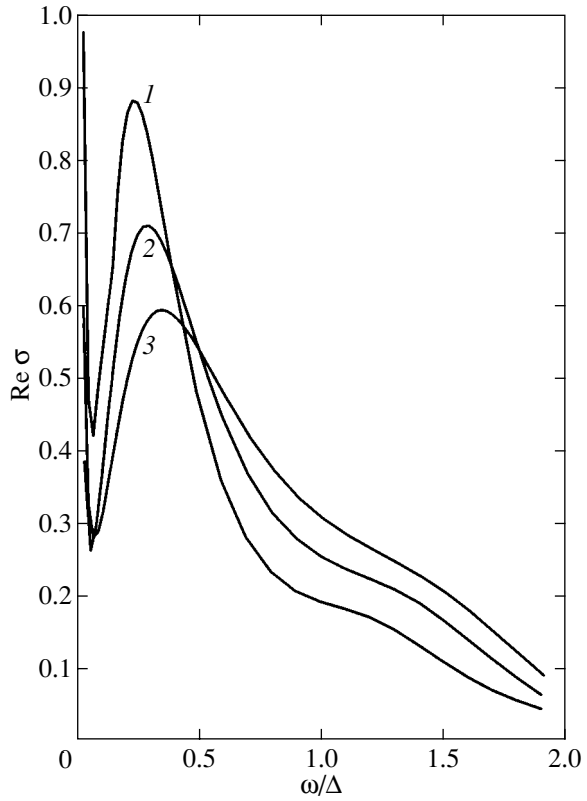

Fig. 16. Real part of optical conductivity in the commensurate case for $t'/t = -0.4$ and $\mu/t = -1.3$ for the values of inverse correlation length $\kappa a = 0.05$ (*1*), 0.1 (*2*), and 0.2 (*3*). The dephasing rate $\gamma/t = 0.005$.

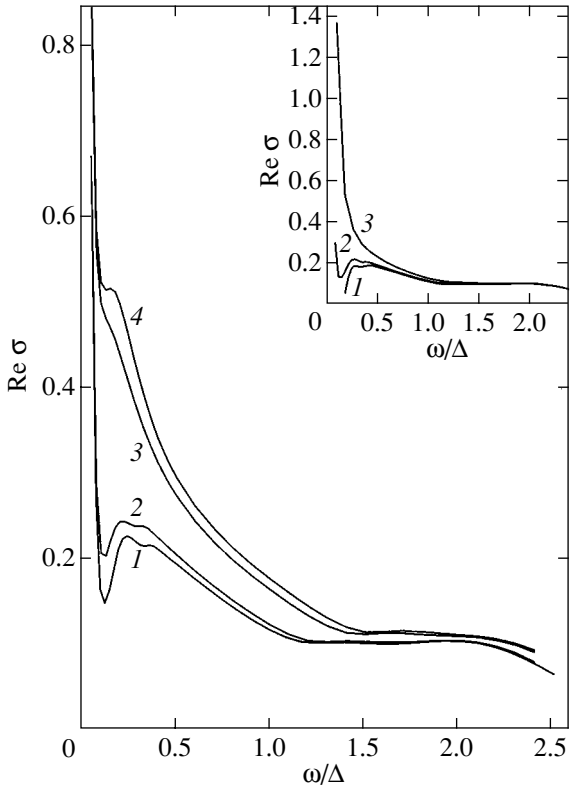

Fig. 17. Evolution of the real part of optical conductivity in the commensurate case for $t'/t = -0.6$ and $\kappa a = 0.2$ with a change in the chemical potential in the topological transition region. The curves correspond to values of $\mu/t = -1.79$ (*1*), -1.77 (*2*), -1.66 (*3*), and -1.63 (*4*). The dephasing rate $\gamma/t = 0.01$. The inset shows the real part of optical conductivity in the case when $\mu/t = -1.8$ for values of $\gamma/t = 0$ (*1*), 0.01 (*2*), and 0.05 (*3*).

back, as was noted repeatedly in [5, 7], is the confinement to the Gaussian approximation for fluctuation statistics, which can also be justified only for the region of high temperatures.

While considering a possible relation between the results obtained above and real experiments on HTSC cuprates, it should be borne in mind that no localization peak was observed in most of such experiments [1, 2], which can apparently be attributed to a noticeable role of inelastic processes (dephasing) at the high temperatures used in these experiments. Optical conductivity peaks in the low-frequency region, attributed to localization, were observed in disordered samples of the YBaCuO system in [25, 26]. Recent experiments on the NdCeCuO system [27, 28], in which such a peak was observed especially clearly, are worth mentioning. In particular, the qualitative behavior of optical conductivity observed in [28] for a series of NdCeCuO samples of various compositions (from underdoped to optimally doped) is in complete agreement with the behavior depicted in Fig. 14, which may be typical of HTSC cuprates (see above). Thus, in our opinion, the model of hot spots may claim at a realistic description of anomalies in the optical conductivity of high-temperature superconductors.

ACKNOWLEDGMENTS

The authors are grateful to É.Z. Kuchinski for numerous discussions.

This study was partly financed by the Russian Foundation for Basic Research (project no. 02-02-16031), CRDF no. REC-005, the Program of Fundamental Studies “Quantum Macrophysics” of the Presidium of the Russian Academy of Sciences, and under the project “Investigation of Collective and Quantum Effects in Condensed Media” of the Ministry of Industry and Science of the Russian Federation.

REFERENCES

1. T. Timusk and B. Statt, Rep. Prog. Phys. **62**, 61 (1999).
2. M. V. Sadovski , Usp. Fiz. Nauk **171**, 539 (2001).
3. N. P. Armitage, D. H. Lu, C. Kim, *et al.*, Phys. Rev. Lett. **87**, 147 003 (2001).
4. J. Schmalian, D. Pines, and B. Stojkovic, Phys. Rev. Lett. **80**, 3839 (1998); Phys. Rev. B **60**, 667 (1999).
5. É. Z. Kuchinski and M. V. Sadovski , Zh. Éksp. Teor. Fiz. **115**, 1765 (1999) [JETP **88**, 968 (1999)].

6. M. V. Sadovski , Zh. Éksp. Teor. Fiz. **66**, 1720 (1974) [Sov. Phys. JETP **39**, 845 (1974)]; Fiz. Tverd. Tela (Leningrad) **16**, 2504 (1974) [Sov. Phys. Solid State **16**, 1632 (1974)].
7. M. V. Sadovski , Zh. Éksp. Teor. Fiz. **77**, 2070 (1979) [Sov. Phys. JETP **50**, 989 (1979)].
8. A. I. Posazhennikova and M. V. Sadovski , Zh. Éksp. Teor. Fiz. **115**, 632 (1999) [JETP **88**, 347 (1999)].
9. É. Z. Kuchinski and M. V. Sadovski , Zh. Éksp. Teor. Fiz. **117**, 613 (2000) [JETP **90**, 535 (2000)].
10. É. Z. Kuchinski and M. V. Sadovski , Zh. Éksp. Teor. Fiz. **119**, 553 (2001) [JETP **92**, 480 (2001)].
11. É. Z. Kuchinski and M. V. Sadovski , Zh. Éksp. Teor. Fiz. **121**, 758 (2002) [JETP **94**, 654 (2002)].
12. M. V. Sadovski and A. A. Timofeev, Sverkhprovodimost: Fiz., Khim., Tekh. **4**, 11 (1991).
13. M. V. Sadovskii and A. A. Timofeev, J. Mosc. Phys. Soc. **1**, 391 (1991).
14. M. V. Sadovski , Pis'ma Zh. Éksp. Teor. Fiz. **69**, 447 (1999) [JETP Lett. **69**, 483 (1999)]; Physica C (Amsterdam) **341–348**, 939 (2000).
15. P. Monthoux, A. Balatsky, and D. Pines, Phys. Rev. B **46**, 14 803 (1992).
16. P. Monthoux and A. Balatsky, Phys. Rev. B **47**, 6069 (1993); Phys. Rev. B **48**, 4261 (1994).
17. M. V. Sadovskii, Physica C (Amsterdam) **341–348**, 811 (2000).
18. L. Bartosch and P. Kopietz, Phys. Rev. B **60**, 15 488 (1999).
19. D. Vollhardt and P. Wolfle, Phys. Rev. B **22**, 4666 (1980).
20. L. P. Gor'kov, A. I. Larkin, and D. E. Khmel'nitski , Pis'ma Zh. Éksp. Teor. Fiz. **30**, 248 (1979) [JETP Lett. **30**, 228 (1979)].
21. P. Monthoux and D. J. Scalapino, Phys. Rev. B **65**, 235 104 (2002).
22. A. A. Gogolin and G. T. Zimanyi, Solid State Commun. **46**, 469 (1983).
23. X. J. Zhou, P. Bogdanov, S. A. Kellar, *et al.*, Science **286**, 268 (1999).
24. A. Damascelli, D. H. Lu, and Z.-X. Shen, cond-mat/0107042.
25. D. N. Basov, A. V. Puchkov, R. A. Hughes, *et al.*, Phys. Rev. B **49**, 12 165 (1994).
26. D. N. Basov, B. Dabrowski, and T. Timusk, Phys. Rev. Lett. **81**, 2132 (1998).
27. E. J. Singley, D. N. Basov, K. Kurahashi, *et al.*, cond-mat/0103480.
28. Y. Onose, Y. Taguchi, K. Ishizaka, and Y. Tokura, Phys. Rev. Lett. **87**, 217 001 (2001).

Translated by N. Wadhwa

Journal of Experimental and Theoretical Physics, Vol. 98, No. 4, 2004, pp. 748–759.
Translated from Zhurnal Éksperimental'noĭ i Teoreticheskoĭ Fiziki, Vol. 125, No. 4, 2004, pp. 854–867.

SOLIDS
Electronic Properties

Superconductivity in the Pseudogap State in the Hot-Spot Model: Ginzburg–Landau Expansion

É. Z. Kuchinskiĭ, M. V. Sadovskiĭ, and N. A. Strigina

Institute of Electrophysics, Ural Division, Russian Academy of Sciences, Yekaterinburg, 620016 Russia

e-mail: kuchinsk@iep.uran.ru; sadovski@iep.uran.ru; strigina@iep.uran.ru

Received May 15, 2003

Abstract—Peculiarities of the superconducting state (*s* and *d* pairing) are considered in the model of the pseudogap state induced by short-range order fluctuations of the dielectric (AFM (SDW) or CDW) type, which is based on the model of the Fermi surface with "hot spots." A microscopic derivation of the Ginzburg–Landau expansion is given with allowance for all Feynman diagrams in perturbation theory in the electron interaction with short-range order fluctuations responsible for strong scattering in the vicinity of hot spots. The superconducting transition temperature is determined as a function of the effective pseudogap width and the correlation length of short-range order fluctuations. Similar dependences are derived for the main parameters of a superconductor in the vicinity of the superconducting transition temperature. It is shown, in particular, that the specific heat jump at the transition point is considerably suppressed upon a transition to the pseudogap region on the phase diagram. *© 2004 MAIK "Nauka/Interperiodica".*

1. INTRODUCTION

The pseudogap state observed in a wide region on the phase diagram of HTSC cuprates leads to numerous anomalies in the properties of these compounds both in the normal and in the superconducting state [1, 2]. In our opinion, the most feasible scenario for the formation of the pseudogap state in HTSC oxides is that [2] based on the existence of strong scattering of charge carriers under short-range order fluctuation of the "dielectric" type (antiferromagnetic AFM (SDW) or of the type of charge density waves (CDW)) in this region of the phase diagram. In the momentum space, this scattering occurs in the vicinity of the characteristic vector $\mathbf{Q} = (\pi/a, \pi/a)$ (a is the parameter of the 2D lattice), corresponding to period doubling (the antiferromagnetism vector) and is a predecessor of the spectrum rearrangement occurring during the establishment of the long-range AFM (SDW) order. Accordingly, an essentially non-Fermi-liquid rearrangement of the electron spectrum takes place in definite regions of the momentum space in the vicinity of the so-called hot spots at the Fermi surface [2]. In a number of recent experiments [3–5], precisely this scenario of pseudogap formation was convincingly confirmed. In the framework of the picture described above, it is possible to construct a simplified model of the pseudogap state, which describes the main features of this state [2] and takes into account the contribution from all Feynman diagrams in perturbation theory relative to scattering from (Gaussian) short-range order fluctuations with a characteristic scattering momentum from a neighborhood of vector $\mathbf{Q}$, which is determined by the corresponding correlation length ξ [6, 7].

Most of the previous theoretical publications were devoted to analysis of the models of the pseudogap state in the normal phase at $T > T_c$. In our earlier publications [8–11], we considered superconductivity using a simplified model of the pseudogap state, which is based on the assumption of the existence of hot (plane) regions at the Fermi surface. In the framework of this model, we constructed the Ginzburg–Landau expansion for various types of Cooper pairing [8, 10] and studied peculiarities of the superconducting state in the region of $T < T_c$ on the basis of analysis of the solutions to the Gor'kov equations [9–11]. It should be noted above all that we considered an extremely simplified model of Gaussian short-range order fluctuations with an infinitely large correlation length, for which an exact solution can be obtained for the pseudogap state [8, 9]. A more realistic case of finite correlation lengths was analyzed both for model [10] (under the assumption of self-averaging of the superconducting order parameter in short-range order fluctuations) and for an extremely simplified, exactly solvable model [11], in which the role of non-self-averaging effects could be analyzed [9, 11].

The present study aims at analyzing the basic properties of the superconducting state (for various types of pairing) arising against the background of a "dielectric" pseudogap in a more realistic model of hot spots at the Fermi surface. We will confine our analysis to a very close neighborhood of the superconducting transition temperature T_c based on the microscopic derivation of

the Ginzburg–Landau expansion, assuming that the superconducting order parameter is self-averaging, thus generalizing the approach proposed for the model of a hot region developed in [10].

2. HOT-SPOT MODEL AND PAIRING INTERACTION

In the model of an "almost antiferromagnetic" Fermi liquid, which is actively used for explaining the microscopic mechanism of HTSC [12, 13], the effective interaction of electrons with spin fluctuations is introduced. This interaction is described by the dynamic susceptibility characterized by the correlation length ξ of spin fluctuations (which must be determined from experiment), the vector $\mathbf{Q} = (\pi/a, \pi/a)$ of antiferromagnetic ordering in the dielectric phase, and the characteristic frequency ω_{sf} of spin fluctuations. This dynamic susceptibility and, hence, the effective interaction have peaks in the region of $\mathbf{q} \sim \mathbf{Q}$. Accordingly, two types of quasiparticles appear in the system: hot quasiparticles whose momenta lie in the vicinity of hot spots at the Fermi surface (Fig. 1) and cold quasiparticles whose momenta are in the vicinity of regions at the Fermi surface, surrounding the diagonals of the Brillouin zone [6]. As a matter of fact, quasiparticles from the neighborhoods of hot spots are strongly scattered over a vector on the order of $\mathbf{Q}$ due to their interaction with spin fluctuations, while this interaction for particles with momenta far away from hot spots is quite weak.

Considering the range of high temperatures $2\pi T \gg \omega_{sf}$, we can disregard the spin dynamics [6], confining our analysis to the static approximation. Computations can be considerably simplified and the contributions from higher orders of perturbation theory can be analyzed if we pass to the model interaction of electrons with spin (or charge) fluctuations of the form [7]

$$V_{\text{eff}}(\mathbf{q}) = W^2 \frac{2\xi^{-1}}{\xi^{-2} + (q_x - Q_x)^2} \frac{2\xi^{-1}}{\xi^{-2} + (q_y - Q_y)^2}, \quad (1)$$

where W is an effective parameter having the dimension of energy. Here, as in [6, 7], W and ξ are treated as phenomenological parameters (which are determined from experiment). Expression (1) is qualitatively similar to the static limit of the interaction considered in [12, 13] and quantitatively differs insignificantly from this limit in the most interesting region $|\mathbf{q} - \mathbf{Q}| < \xi^{-1}$, which determines scattering in the vicinity of hot spots, if the parameters appearing in this expression are appropriately defined. In fact, we are talking about the replacement of the actual interaction with dynamic short-range order fluctuations by the electron scattering from the static random (Gaussian) field of such fluctuations. The least justified assumption from the standpoint of physics is the one that concerns the static (and Gaussian) nature of fluctuations, which can be used only for quite high temperatures [6, 7]. At low temperatures (including those corresponding to the superconducting phase), the spin dynamics and the non-Gaussian nature of fluctuations may also become significant for the microscopy of Cooper pairing in the model of a nearly antiferromagnetic Fermi liquid [12, 13]. However, in our opinion, the static Gaussian approximation considered here might be sufficient for analyzing the qualitative effect of the pseudogap formation on superconductivity (in particular, in the vicinity of the superconducting transition temperature), which will be henceforth described by using the simple approach of the BCS theory and the Ginzburg–Landau phenomenology.

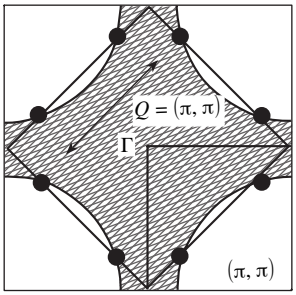

Fig. 1. Fermi surface with hot spots connected by a scattering momentum on the order of $\mathbf{Q} = (\pi/a, \pi/a)$.

The spectrum of the initial (free) quasiparticles will be taken in the form [6]

$$\xi_{\mathbf{p}} = -2t(\cos p_x a + \cos p_y a) - 4t' \cos p_x a \cos p_y a - \mu, \quad (2)$$

where t is the integral of transfer between the nearest neighbors, t' is the same for the next to nearest neighbors in a square lattice, a is the lattice parameter, and μ is the chemical potential. This expression provides a good approximation to the results of band calculations for real HTSC systems. For example, for $YBa_2Cu_3O_{6+\delta}$, we have $t = 0.25$ eV and $t' = -0.45t$ [6]. Chemical potential μ is determined by the carrier concentration.

In the limit of an infinitely large correlation length ($\xi \longrightarrow \infty$), the model of scattering from short-range order fluctuations of the type considered here has an exact solution [14]. For finite values of ξ, we can construct an approximate solution [7] generalizing the 1D approach proposed in [15]. In this case, it is possible to sum (approximately) the entire diagrammatic series for the one-particle electron Green function. As a result, the following recurrent procedure arises for the one-

where the generalized Cooper susceptibility is defined in Fig. 2 and is given by

$$\chi(\mathbf{q}; T) = -T\sum_{\varepsilon_n}\sum_{\mathbf{p},\mathbf{p}'} e(\mathbf{p})e(\mathbf{p}')\Phi_{\mathbf{p},\mathbf{p}'}(\varepsilon_n, -\varepsilon_n, \mathbf{q}); \quad (10)$$

here, $\Phi_{\mathbf{p},\mathbf{p}'}(\varepsilon_n, -\varepsilon_n, \mathbf{q})$ is a two-particle Green function in the Cooper channel, which takes into account the scattering from short-range order fluctuations.

We will first consider the case of charge fluctuations (CDW), where the interaction is independent of spin variables. For the s and d_{xy} pairing, the superconducting gap remains unchanged upon a transfer over $\mathbf{Q}$ (i.e., $e(\mathbf{p} + \mathbf{Q}) = e(\mathbf{p})$) and $e(\mathbf{p}') \approx e(\mathbf{p})$. In the case of anisotropic s and $d_{x^2-y^2}$ pairing, the superconducting gap reverses its sign upon a transfer over $\mathbf{Q}$ ($e(\mathbf{p} + \mathbf{Q}) = -e(\mathbf{p})$); consequently, $e(\mathbf{p}') \approx e(\mathbf{p})$ for $\mathbf{p}' \approx \mathbf{p}$ and $e(\mathbf{p}') \approx -e(\mathbf{p})$ for $\mathbf{p}' \approx \mathbf{p} + \mathbf{Q}$. Thus, for diagrams containing an even number of interaction lines connecting the upper (ε_n) and lower ($-\varepsilon_n$) electron lines, we have $\mathbf{p}' \approx \mathbf{p}$; Thus, we arrive at the same expression for the contribution to susceptibility as in the case of the s and d_{xy} pairing. On the other hand, for diagrams with an odd number of such interaction lines, we obtain an expression with the opposite sign for the contribution to susceptibility. This sign reversal can be attributed simply to the sign reversal for the interaction connecting the upper and lower electron lines of the loop in Fig. 2. In this case, we obtain for the generalized susceptibility the expression

$$\chi(\mathbf{q}; T) = -T\sum_{\varepsilon_n}\sum_{\mathbf{p}} G(\varepsilon_n\mathbf{p} + \mathbf{q})G(-\varepsilon_n, -\mathbf{p})e^2(\mathbf{p}) \times\Gamma^{\pm}(\varepsilon_n, -\varepsilon_n, \mathbf{q}), \quad (11)$$

where $\Gamma^{\pm}(\varepsilon_n, -\varepsilon_n, \mathbf{q})$ is the triangular vertex part taking into account the interaction with short-range order fluctuations, the superscript "$\pm$" allowing for the abovementioned difference in the signs of interactions connecting the upper and lower electron lines.

Let us now consider the scattering from spin fluctuations (AFM (SDW)). In this case, the line of interaction with the longitudinal spin component S^z, which embraces the vertex and changes the direction of the spin, should be supplemented with an additional factor of (–1) [6]. From this point of view, in the case of interaction with spin fluctuations, the types of pairing considered above "change places"[2] and the generalized Cooper susceptibility is determined by triangular vertex Γ^- for s and d_{xy} pairing and by triangular vertex Γ^+ for anisotropic s and $d_{x^2-y^2}$ pairing.

[2] This is due to the fact that the sign of the spin projection is reversed at the vertex of the interaction with the superconducting gap (we consider only the singlet pairing).

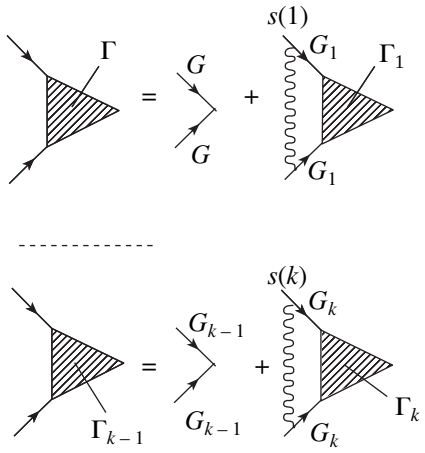

Fig. 3. Recurrence equations for the vertex part.

Thus, we must calculate the triangular vertices taking into account all diagrams (including cross diagrams) describing the interaction with dielectric fluctuations. The corresponding recurrence procedure for a 1D analog of our problem (and for real-valued frequencies, $T = 0$) was formulated for the first time in [18]. For the 2D model of the pseudogap with hot spots at the Fermi surface considered here, a generalization of this recurrence procedure is given in [19] in connection with optical conductivity calculations. The details of the corresponding derivation can also be found in [19]. A generalization to the case of Matsubara frequencies required for our problem can be carried out directly. For definiteness, we will henceforth assume, as before, that $\varepsilon_n > 0$. Ultimately, for a triangular vertex, we obtain the recurrence relation represented by the graphs in Fig. 3 (where the wavy line indicates the interaction with pseudogap fluctuations) and having the following analytic form:

$$\Gamma^{\pm}_{k-1}(\varepsilon_n, -\varepsilon_n, \mathbf{q}) = 1 \pm W^2 s(k) G_k \bar{G}_k \times\left\{1 + \frac{2ik v_k \kappa}{2i\varepsilon_n - \mathbf{v}_k\cdot\mathbf{q} - W^2 s(k+1)(G_{k+1} - \bar{G}_{k+1})}\right\} \times\Gamma^{\pm}_k(\varepsilon_n, -\varepsilon_n, \mathbf{q}); \quad (12)$$

here, $G_k = G_k(\varepsilon_n\mathbf{p} + \mathbf{q})$ and $\bar{G}_k = G_k(-\varepsilon_n, -\mathbf{p})$ are calculated in accordance with expression (3), v_k is defined by formula (5), and $\mathbf{v}_k$ have the form

$$\mathbf{v}_k = \begin{cases}\mathbf{v}(\mathbf{p} + \mathbf{Q}) \text{ for odd } k,\\ \mathbf{v}(\mathbf{p}) \text{ for even } k.\end{cases} \quad (13)$$

A "physical" vertex is defined as $\Gamma^{\pm}(\varepsilon_n, -\varepsilon_n, \mathbf{q}) \equiv \Gamma^{\pm}_0(\varepsilon_n, -\varepsilon_n, \mathbf{q})$.

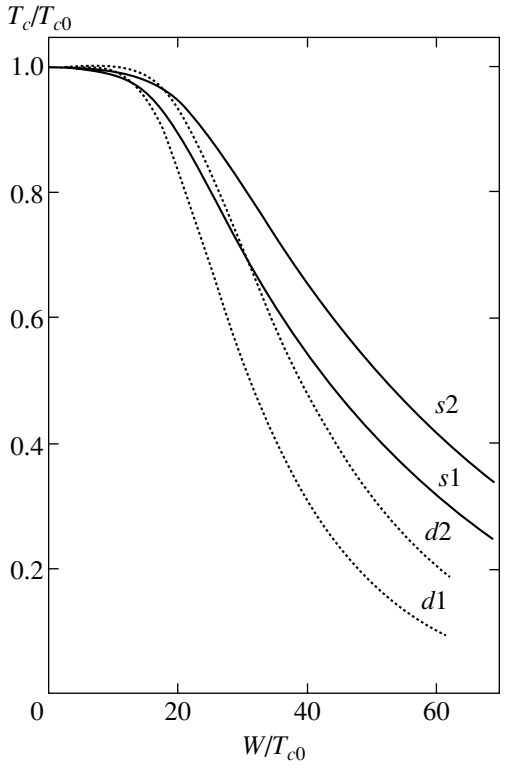

Fig. 4. Dependence of the superconducting transition temperature T_c/T_{c0} on effective pseudogap width W/T_{c0} for the s-type pairing and scattering from charge (CDW) fluctuations (curves $s1$ and $s2$) and for the $d_{x^2-y^2}$-type pairing and scattering from spin (AFM (SDW)) fluctuations (curves $d1$ and $d2$). The data are given for the following values of reciprocal correlation length: $\kappa a = 0.2$ ($s1$ and $d1$) and $\kappa a = 0.5$ ($s2$ and $d2$).

To determine T_c, we must consider the vertex for $\mathbf{q} = 0$. In this case, $\overline{G}_k = G_k^*$ and vertices Γ_k^+ and Γ_k^- become real-valued, which considerably simplifies procedures (12) For $\mathrm{Im}G_k$ and $\mathrm{Re}G_k$, we have the system of recurrence equations

$$\mathrm{Im}G_k = -\frac{\varepsilon_n + kv_k\kappa - W^2 s(k+1)\mathrm{Im}G_{k+1}}{D_k},$$
$$\mathrm{Re}G_k = -\frac{\xi_k(\mathbf{p}) + W^2 s(k+1)\mathrm{Re}G_{k+1}}{D_k}, \quad (14)$$

where $D_k = (\xi_k(\mathbf{p}) + W^2 s(k+1)\mathrm{Re}\,G_{k+1})^2 + (\varepsilon_n + kv_k\kappa - W^2 s(k+1)\mathrm{Im}\,G_{k+1})^2$ and the vertex part for $\mathbf{q} = 0$ can be determined from the equation

$$\Gamma_{k-1}^{\pm} = 1 \mp W^2 s(k)\frac{\mathrm{Im}G_k}{\varepsilon_n - W^2 s(k+1)\mathrm{Im}G_{k+1}}\Gamma_k^{\pm}. \quad (15)$$

Passing to numerical calculations, it is convenient to set the characteristic scale of energies (temperatures), which characterizes the superconducting state in our model in the absence of pseudogap fluctuations ($W = 0$). In this case, the equation for the corresponding superconducting transition temperature T_{c0} has the standard form for the BCS theory (in the general case of anisotropic pairing) and can be written as

$$1 = \frac{2VT}{\pi^2}\sum_{n=0}^{\overline{m}}\int_0^{\pi}dp_x\int_0^{\pi}dp_y\frac{e^2(\mathbf{p})}{\xi_{\mathbf{p}}^2 + \varepsilon_n^2}, \quad (16)$$

where $\overline{m} = [\omega_c/2\pi T_{c0}]$ is the dimensionless cutoff parameter for the sum over Matsubara frequencies. All calculations were made for a typical quasiparticle spectrum (2) in HTSC with $\mu = -1.3t$ and $t'/t = -0.4$. Choosing (quite arbitrarily) $\omega_c = 0.4t$ and $T_{c0} = 0.01t$, we can easily select the value of pairing parameter V in relation (16), which gives the same value of T_{c0} for various types of pairing enumerated in (8). In particular, we obtain $V/ta^2 = 1$ for the conventional isotropic s-type pairing and $V/ta^2 = 0.55$ for the $d_{x^2-y^2}$-type pairing. For the remaining types of pairing from relation (8), the values of the pairing constant for such a choice of parameters are found to be unrealistically high and we do not give the results of the corresponding calculations.[3]

Figures 4 and 5 show typical results of numerical calculations of the superconducting transition temperature T_c for a system with a pseudogap, which were obtained directly from relation (9) using the recurrence equations described above. It can be seen that pseudogap (dielectric) fluctuations considerably reduce the superconducting transition temperature in all cases. The $d_{x^2-y^2}$ pairing is suppressed much more rapidly than the isotropic s pairing. At the same time, a decrease in correlation length ξ (an increase in parameter κ) of pseudogap fluctuations facilitates an increase in T_c. These results are quite analogous to those obtained earlier in the model of hot regions [8, 10]. However, considerable differences also arise. It can be seen from Fig. 4 that the curve describing the dependence of T_c on pseudogap width W has a characteristic plateau in the region of $W < 10T_{c0}$ for s pairing and scattering from charge (CDW) fluctuations as well as for $d_{x^2-y^2}$ pairing and scattering from spin (AFM (SDW)) fluctuations[4] (i.e., in the cases when the upper sign in formulas (12) and (15) "operates", leading to sign-constant recurrence procedure for a vertex), while a consid-

[3] Of course, such a description on the basis of equations in the BCS theory with weak binding does not claim to be realistic in the cases of s and $d_{x^2-y^2}$ pairing considered here as well. We must just preset the characteristic scale of T_{c0} to express all temperatures in subsequent calculations in units of this temperature, assuming that a certain universality relative to this scale exists in the problem considered here.

[4] The latter case is realized, in all probability, in actual HTSC materials based on copper oxides.

erable suppression of T_c takes place on a scale of $W \sim 50T_{c0}$. Qualitative differences appear in the case of s pairing and scattering from spin (AFM (SDW)) fluctuations and in the case of $d_{x^2-y^2}$ pairing and scattering from charge fluctuations. Figure 5 shows that, in the latter case (when the lower sign in formulas (12) and (15) operates; i.e., an alternating procedure arises for a vertex), the rate of suppression of T_c is an order of magnitude higher. In the case of $d_{x^2-y^2}$ pairing, in the range of W/T_{c0} values corresponding to almost complete suppression of superconductivity, the accuracy of our calculations becomes considerably worse in view of the alternating nature of the recurrence procedure for the vertex part. In particular, a typical ambiguity of T_c may appear, which corresponds to possible existence of a narrow region of "recurrent" superconductivity on the phase diagram.[5] Such a behavior of T_c slightly resembles similar peculiarities emerging in superconductors with Kondo impurities [20]. Our calculations show, however, that the most probable scenario is the emergence of the critical value of parameter W/T_{c0}, for which superconductivity is completely suppressed. In this case, a region may appear, in which the transition to the superconducting state becomes a first-order phase transition analogously to the known situation in superconductors with a strong paramagnetic effect in an external magnetic field [21]. In any case, the effects arising in this case deserve a separate analysis. All results considered below correspond to the region of unambiguous behavior of T_c.

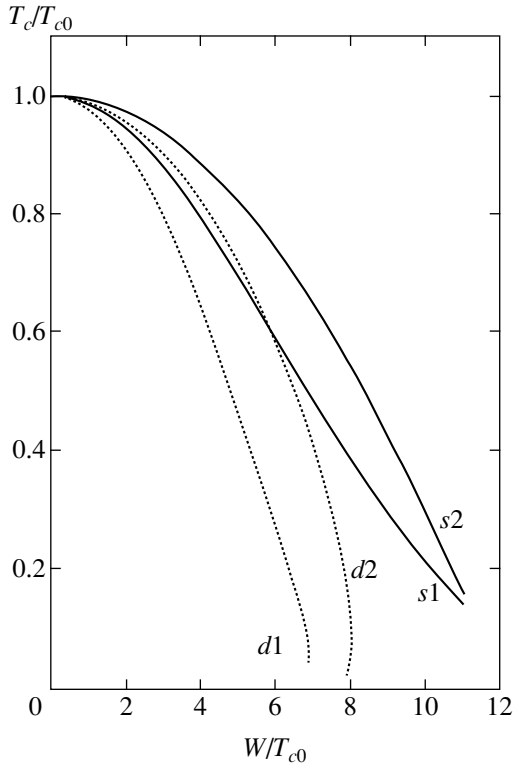

Fig. 5. Dependence of the superconducting transition temperature T_c/T_{c0} on effective pseudogap width W/T_{c0} for the s-type pairing and scattering from spin (AFM (SDW)) fluctuations (curves $s1$ and $s2$) and for the $d_{x^2-y^2}$-type pairing and scattering from charge (CDW) fluctuations (curves $d1$ and $d2$). The data are given for the following values of reciprocal correlation length: $\kappa a = 0.2$ ($s1$ and $d1$) and $\kappa a = 1.0$ ($s2$ and $d2$).

4. GINZBURG–LANDAU EXPANSION

In our earlier publication [8], the Ginzburg–Landau expansion was constructed in the exactly solvable model of a pseudogap with an infinitely large correlation length for short-range order fluctuations. Subsequently [10], these results were extended to the case of finite correlation lengths. In these publications, we considered, in fact, only charge fluctuations and used a simple model of the pseudogap state, which was based on the concept of hot (plane) regions existing at the Fermi surface. In this model, the sign of the superconducting gap remained unchanged upon a transfer over vector $\mathbf{Q}$ both for s and d pairing [10]. Here, we carry out the generalization to a more realistic case of the model of hot spots at the Fermi surface.

The Ginzburg–Landau expansion for the difference in the free energies of the superconducting and normal states can be written in the standard form

$$F_s - F_n = A|\Delta_{\mathbf{q}}|^2 + q^2 C|\Delta_{\mathbf{q}}|^2 + \frac{B}{2}|\Delta_{\mathbf{q}}|^4, \qquad (17)$$

where $\Delta_{\mathbf{q}}$ is the amplitude of the Fourier component of the order parameter, which can be written for various types of pairing in the form $\Delta(\mathbf{p}, \mathbf{q}) = \Delta_q e(\mathbf{p})$. Expansion (17) is determined by the graphs of the loop expansion for free energy in the field of order parameter fluctuations (shown by dashed lines) with a small wave vector $\mathbf{q}$ [8], which are represented in Fig. 6.

It is convenient to write the Ginzburg–Landau coefficients in the form

$$A = A_0 K_A, \quad C = C_0 K_C, \quad B = B_0 K_B, \qquad (18)$$

where A_0, C_0, and B_0 stand for the expressions for these coefficients in the absence of pseudogap fluctuations ($W = 0$), which are derived in the Appendix for an arbitrary spectrum ξ_p and various types of pairing,

$$A_0 = N_0(0)\frac{T - T_c}{T_c}\langle e^2(\mathbf{p})\rangle,$$

$$C_0 = N_0(0)\frac{7\zeta(3)}{32\pi^2 T_c^2}\langle |\mathbf{v}(\mathbf{p})|^2 e^2(\mathbf{p})\rangle, \qquad (19)$$

$$B_0 = N_0(0)\frac{7\zeta(3)}{8\pi^2 T_c^2}\langle e^4(\mathbf{p})\rangle,$$

[5] Such a peculiar behavior of T_c is manifested more strongly in the case of scattering from incommensurate pseudogap fluctuations.

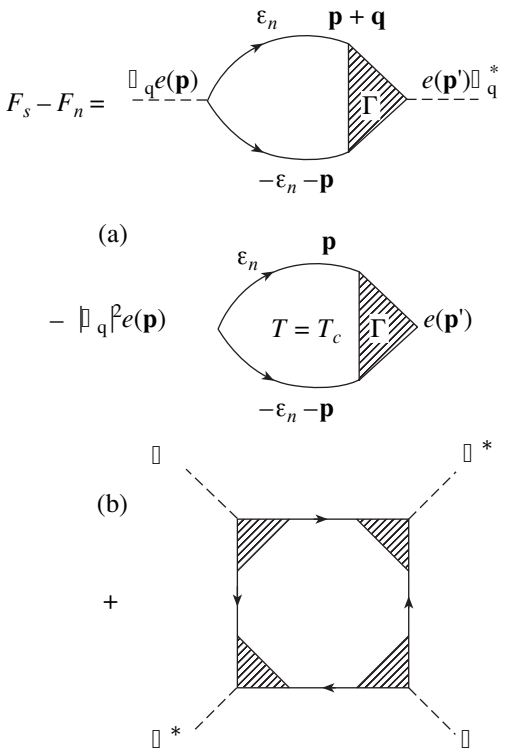

Fig. 6. Graphical form of the Ginzburg–Landau expansion.

angle brackets denote conventional averaging over the Fermi surface,

$$\langle \ldots \rangle = \frac{1}{N_0(0)} \sum_p \delta(\xi_\mathbf{p}) \ldots,$$

and $N_0(0)$ is the density of states for free electrons at the Fermi surface.

All peculiarities of the model in question, which are associated with the emergence of a pseudogap, are contained in dimensionless coefficients K_A, K_C, and K_B. In the absence of pseudogap fluctuations, all these coefficients are equal to unity.

It can be seen from Fig. 6a that coefficients K_A and K_C are completely determined by the generalized Cooper susceptibility [8, 10] $\chi(\mathbf{q}; T)$ depicted in Fig. 2:

$$K_A = \frac{\chi(0; T) - \chi(0; T_c)}{A_0}, \tag{20}$$

$$K_C = \lim_{q \to 0} \frac{\chi(\mathbf{q}; T_c) - \chi(0; T_c)}{q^2 C_0}. \tag{21}$$

It was shown above that the generalized susceptibility can be found from relation (11), where the triangular vertices are determined by recurrence procedures (12); this allows us to directly calculate coefficients K_A and K_C numerically.

The situation with coefficient B is more complicated in the general case. Calculations can be significantly simplified if we confine our analysis, as usual, to the case of $q = 0$ in the order of $|\Delta_q|^4$ and define coefficient B by the diagram show in Fig. 6b.Then we obtain the following expression for coefficient K_B:

$$K_B = \frac{T_c}{B_0} \sum_{\varepsilon_n} \sum_\mathbf{p} e^4(\mathbf{p}) \big(G(\varepsilon_n \mathbf{p}) G(-\varepsilon_n, -\mathbf{p})\big)^2 \times \big(\Gamma^{\pm}(\varepsilon_n, -\varepsilon_n, 0)\big)^4. \tag{22}$$

It should be noted from the very outset that this expression leads to a positive definite coefficient B. This follows from the fact that $G(-\varepsilon_n, -\mathbf{p}) = G^*(\varepsilon_n \mathbf{p})$ so that $G(\varepsilon_n \mathbf{p}) G(-\varepsilon_n, -\mathbf{p})$ is real-valued; accordingly, vertex part $\Gamma^{\pm}(\varepsilon_n, -\varepsilon_n, 0)$ defined by recurrence procedure (15) is also real.

5. PHYSICAL CHARACTERISTICS OF SUPERCONDUCTORS WITH A PSEUDOGAP

It is well known that the Ginzburg–Landau equations define two characteristic lengths of superconductor, viz., the coherence length and the magnetic field penetration depth.

For a given temperature, coherence length $\xi(T)$ gives the characteristic scale of inhomogeneities of order parameter Δ:

$$\xi^2(T) = -\frac{C}{A}. \tag{23}$$

In the absence of a pseudogap, we can write

$$\xi^2_{BCS}(T) = -\frac{C_0}{A_0}. \tag{24}$$

In our model, we have

$$\frac{\xi^2(T)}{\xi^2_{BCS}(T)} = \frac{K_C}{K_A}. \tag{25}$$

For the magnetic field penetration depth, we have

$$\lambda^2(T) = -\frac{c^2}{32\pi e^2} \frac{B}{AC}. \tag{26}$$

Analogously to relation (25), in the given model, we can write

$$\frac{\lambda(T)}{\lambda_{BCS}(T)} = \left(\frac{K_B}{K_A K_C}\right)^{1/2}. \tag{27}$$

In the vicinity of T_c, the upper critical field H_{c2} is

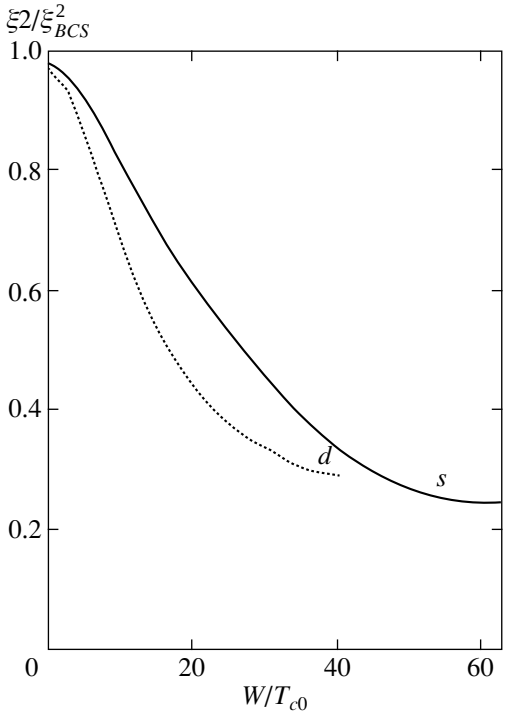

Fig. 7. Dependence of the squared coherence length ξ^2/ξ^2_{BCS} on effective pseudogap width W/T_{c0} for the *s*-type pairing and scattering from charge (CDW) fluctuations (solid curve) and for the $d_{x^2-y^2}$-type pairing and scattering from spin (AFM (SDW)) fluctuations (dotted curve). The data are given for the reciprocal correlation length $\kappa a = 0.2$.

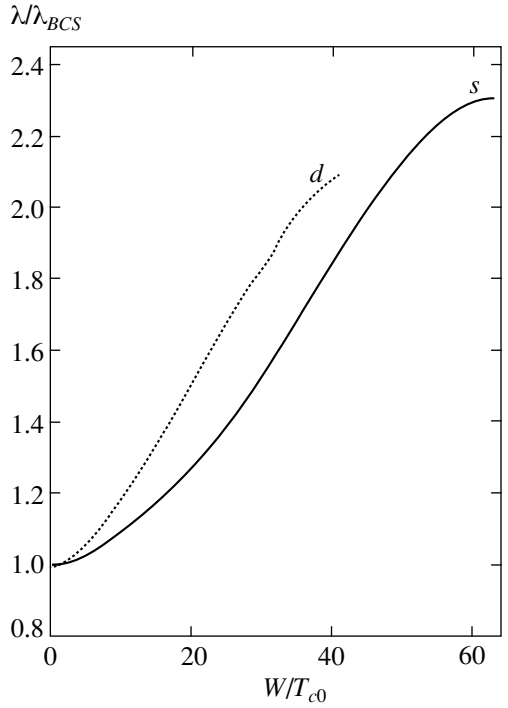

Fig. 8. Dependence of the penetration depth λ/λ_{BCS} on effective pseudogap width W/T_{c0} for the *s*-type pairing and scattering from charge (CDW) fluctuations (solid curve) and for the $d_{x^2-y^2}$-type pairing and scattering from spin (AFM (SDW)) fluctuations (dotted curve). The data are given for the reciprocal correlation length $\kappa a = 0.2$.

defined in terms of the Ginzburg–Landau coefficients as

$$H_{c2} = \frac{\varphi_0}{2\pi\xi^2(T)} = -\frac{\varphi_0}{2\pi}\frac{A}{C}, \tag{28}$$

where $\varphi_0 = c\pi/|e|$ is the magnetic flux quantum. Then the slope of the curve describing the upper critical field near T_c is given by

$$\left|\frac{dH_{c2}}{dT}\right|_{T_c} = \frac{16\pi\varphi_0\langle e^2(\mathbf{p})\rangle}{7\zeta(3)\langle|\mathbf{v}(\mathbf{p})|^2 e^2(\mathbf{p})\rangle}T_c\frac{K_A}{K_C}. \tag{29}$$

The specific heat discontinuity at the transition point has the form

$$(C_s - C_n)_{T_c} = \frac{T_c}{B}\left(\frac{A}{T - T_c}\right)^2, \tag{30}$$

where C_s and C_n are the specific heats of the superconducting and normal states, respectively. At temperature T_{c0} (in the absence of a pseudogap, $W = 0$), we have

$$(C_s - C_n)_{T_{c0}} = N(0)\frac{8\pi^2 T_{c0}\langle e^2(\mathbf{p})\rangle^2}{7\zeta(3)\langle e^4(\mathbf{p})\rangle}. \tag{31}$$

Then the relative specific heat discontinuity in the given model can be written as

$$\Delta C \equiv \frac{(C_s - C_n)_{T_c}}{(C_s - C_n)_{T_{c0}}} = \frac{T_c}{T_{c0}}\frac{K_A^2}{K_B}. \tag{32}$$

Coefficients K_A, K_B, and K_C were calculated numerically for the same typical parameters of the model as in the calculations of T_c described above. The numerical values of these coefficients as such are not very interesting and are not given here.[6] Figures 7–12 show the W/T_{c0} dependences of the corresponding physical quantities, defined by relations (23)–(32). In accordance with the situation with T_c described above, two qualitatively different modes of the behavior are also observed in this case depending on whether the behavior of the vertex part in the recurrence equations is sign-constant or alternating (the upper and lower signs in relation (12) and spin or charge fluctuations). The results of calculations of physical quantities for the first case (the *s*-type pairing and scattering from charge (CDW) fluctuations as well as the $d_{x^2-y^2}$-type pairing and scattering from spin (AFM (SDW)) fluctuations) are shown in Figs. 7–

[6] The typical dependences of these coefficients on parameter W/T_{c0} are functions rapidly decreasing from unity in the superconductivity range.

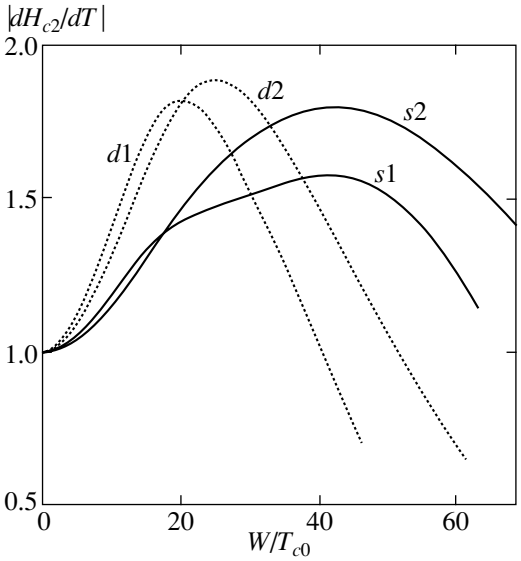

Fig. 9. Dependence of the derivative (slope) of the upper critical field on effective pseudogap width W/T_{c0} for the *s*-type pairing and scattering from charge (CDW) fluctuations (curves *s*1 and *s*2) and for the $d_{x^2-y^2}$-type pairing and scattering from spin (AFM (SDW)) fluctuations (curves *d*1 and *d*2). The data are given for the values of reciprocal correlation length $\kappa a = 0.2$ (*s*1 and *d*1) and $\kappa a = 0.5$ (*s*2 and *d*2) and are normalized to the value of the derivative in the absence of a pseudogap.

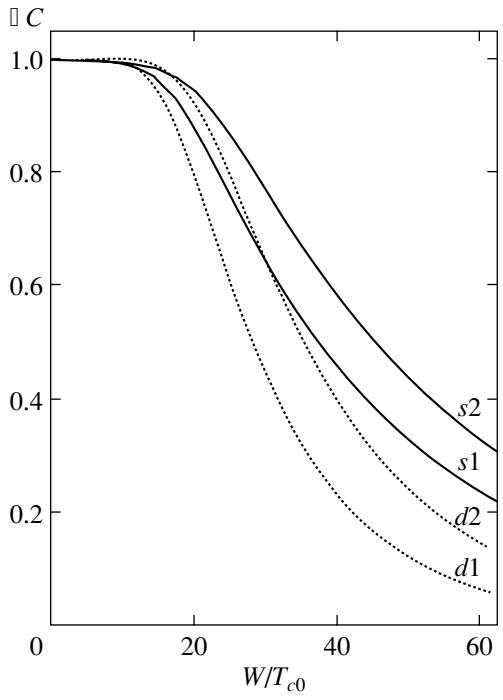

Fig. 10. Dependence of the specific heat discontinuity at the transition point on effective pseudogap width W/T_{c0} for the *s*-type pairing and scattering from charge (CDW) fluctuations (curves *s*1 and *s*2) and for the $d_{x^2-y^2}$-type pairing and scattering from spin (AFM (SDW)) fluctuations (curves *d*1 and *d*2). The data are given for the values of reciprocal correlation length $\kappa a = 0.2$ (*s*1 and *d*1) and $\kappa a = 0.5$ (*s*2 and *d*2).

10. It can be seen that, with increasing pseudogap width *W*, coherence length $\xi(T)$ decreases, while penetration depth $\lambda(T)$ increases as compared to the corresponding values in the BCS theory. Both these characteristic lengths exhibit a very weak dependence on parameter κ; for this reason, the results in Figs. 7 and 8 are given only for $\kappa a = 0.2$. The slope (derivative) of the upper critical field at $T = T_c$ first increases and then begins to decrease. The most typical is the decrease in the specific heat discontinuity as compared to the BCS value (see Fig. 10), which is in direct qualitative agreement with experimental data [22]. It should be noted that the specific heat discontinuity in our model also has a characteristic plateau in the region of $W/T_{c0} < 10$, which is similar to that noted above in the corresponding dependence of T_c.

The behavior of physical quantities in the case of the *s*-type pairing and scattering from spin (AFM (SDW)) fluctuations and the $d_{x^2-y^2}$-type pairing and scattering from charge (CDW) fluctuations is illustrated in Figs. 11 and 12. Data on the characteristic lengths are not shown since both coherence length $\xi(T)$ and penetration depth $\lambda(T)$ are virtually the same as the corresponding values in the BCS theory everywhere in the superconductivity range (except a small neighborhood of the region of ambiguity and vanishing of T_c, in which

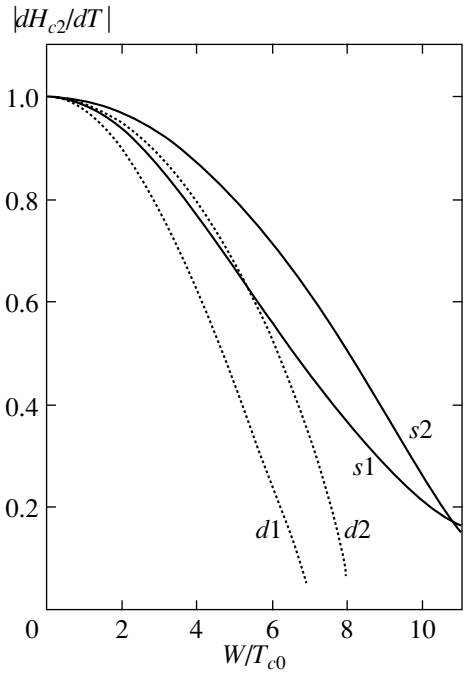

Fig. 11. Dependence of the derivative (slope) of the upper critical field on effective pseudogap width W/T_{c0} for the *s*-type pairing and scattering from spin (AFM (SDW)) fluctuations (curves *s*1 and *s*2) and for the $d_{x^2-y^2}$-type pairing and scattering from charge (CDW) fluctuations (curves *d*1 and *d*2). The data are given for the values of reciprocal correlation length $\kappa a = 0.2$ (*s*1 and *d*1) and $\kappa a = 1.0$ (*s*2 and *d*2) and normalized to the value of the derivative in the absence of a pseudogap.

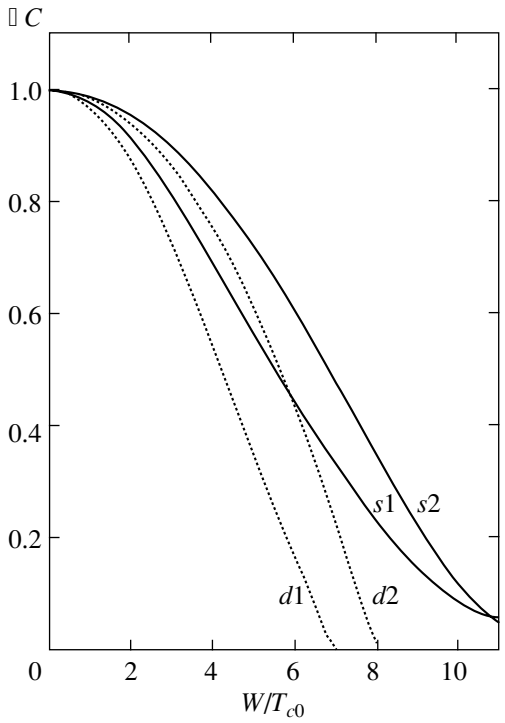

Fig. 12. Dependence of specific heat discontinuity at the transition point on the effective pseudogap width W/T_{c0} for s-type pairing and scattering from spin (AFM (CDW)) fluctuations (curves $s1$ and $s2$) and for $d_{x^2-y^2}$-type pairing and scattering from charge (CDW) fluctuations (curves $d1$ and $d2$). The data are given for the values of reciprocal correlation length $\kappa a = 0.2$ ($s1$ and $d1$) and $\kappa a = 1.0$ ($s2$ and $d2$).

these lengths sharply increase). As regards the derivative of the upper critical field and the specific heat discontinuity at the superconducting transition point, the values of these quantities decrease quite rapidly with increasing parameter W/T_{c0} apparently up to its critical value at which T_c is completely suppressed (or to the value at which a narrow region of the first-order transition is formed).

6. CONCLUSIONS

We have considered the peculiarities of the superconducting state emerging in the pseudogap state due to scattering of electrons from dielectric short-range order fluctuations in the model of hot spots at the Fermi surface. Our analysis was based on the microscopic derivation of the Ginzburg–Landau expansion taking into account all orders of perturbation theory in scattering from pseudogap fluctuations. The condensed phase of such a superconductor can be described on the basis of the corresponding analysis of the Gor'kov equations for a superconductor with a pseudogap (see [10]) and is the subject of special analysis.

The main result of this study is the demonstration of superconductivity suppression by pseudogap fluctuations of the CDW or AFM (SDW) type and the separation of two classes of qualitatively different models of such suppression depending on the sign-constant or alternating behavior of the vertex part in the recurrence equations (the upper or lower signs in expression (12) and spin or charge fluctuations). The version with scattering from spin fluctuations and pairing with the $d_{x^2-y^2}$-type symmetry is observed in high-T_c superconductors based on copper oxides; however, we are not aware of systems in which the peculiar behavior obtained above for the s-type pairing and scattering from spin (AFM (SDW)) fluctuations as well as for $d_{x^2-y^2}$-type pairing and scattering from charge (CDW) fluctuations is realized. The search for such systems is of considerable interest.

The most important question in the description of the pseudogap state of actual HTSC systems is the behavior of physical parameters upon a change in the carrier concentration. In our model, the concentration dependence must be expressed in terms of the corresponding dependence of effective width W of the pseudogap and correlation length ξ. Unfortunately, such dependences can be determined from experiment only indirectly and have been studied insufficiently [1, 2].[7] In a very rough approximation, we can state that correlation length ξ in a wide concentration range does not vary very strongly, while pseudogap width W linearly decreases with increasing charge carrier concentration from values on the order of 10^3 K in the vicinity of the dielectric phase region to values on the order of the superconducting transition temperature as we approach the optimal doping level, vanishing at slightly higher carrier concentrations (see Fig. 6 in review [2], which is based on Fig. 4 in [3], where the corresponding set of data is given for the YBCO system). Using this regularity, one can easily recalculate the above dependences on W to the corresponding dependences on the charge carrier concentration. In the extremely simplified version of our model with an infinitely large correlation length and the Fermi surface with complete nesting, such an analysis was carried out in a recent publication [23] under the assumption that the value of T_{c0} is also a linear function of the concentration. The typical form of the phase diagram for HTSC cuprates was completely reproduced qualitatively. At the same time, the obvious roughness of the model and the absence of reliable experimental data on the concentration dependences of W, ξ, and T_{c0} do not make it possible to treat the attempts at "improving" these qualitative conclusions very seriously.

In addition to the repeatedly mentioned disregard of the dynamics of short-range order fluctuations and the confinement to Gaussian fluctuations alone, it should be noted once again that the disadvantages of the model

[7] In addition, an analogous dependence of the value of T_{c0}, which is completely unknown, may turn out to be significant.

considered here also include the simplified analysis of the spin structure of interactions, which presumes that these interactions are of the Ising type. It would be interesting to also carry out a similar analysis for the general case of an interaction of the Heisenberg type.

ACKNOWLEDGMENTS

This study was partly supported by the Russian Foundation for Basic Research (project no. 02-02-16031); by the programs of fundamental studies in "Quantum Macrophysics" (the Presidium of the Russian Academy of Sciences) and "Strongly Correlated Electrons in Semiconductors, Metals, Superconductors, and Magnetic Materials" (Department of Physical Sciences, Russian Academy of Sciences); and by the project "Investigation of Collective and Quantum Effects in Condensed Media" (Ministry of Industry and Science of the Russian Federation).

APPENDIX

Ginzburg–Landau Coefficients for Anisotropic Pairing in the Absence of a Pseudogap

In the absence of fluctuations ($W = 0$), the generalized Cooper susceptibility, which is defined by the diagram in Fig. 2, assumes the form

$$\chi_0(\mathbf{q}; T) = -T\sum_{\varepsilon_n}\sum_{\mathbf{p}} e^2(\mathbf{p})\frac{1}{i\varepsilon_n - \xi_{\mathbf{p}+\mathbf{q}}}\frac{1}{-i\varepsilon_n - \xi_{\mathbf{p}}}. \quad \text{(A.1)}$$

For the susceptibility at $\mathbf{q} = 0$, which determines coefficient A_0, we obtain the expression

$$\begin{aligned}\chi_0(0; T) &= -T\sum_{\varepsilon_n}\sum_{\mathbf{p}} e^2(\mathbf{p})\frac{1}{\varepsilon_n^2 + \xi_{\mathbf{p}}^2}\\ &= -T\sum_{\varepsilon_n}\int_{-\infty}^{\infty} d\xi \frac{1}{\varepsilon_n^2 + \xi^2}\sum_{\mathbf{p}}\delta(\xi - \xi_{\mathbf{p}})e^2(\mathbf{p})\\ &\approx -N_0(0)T\sum_{\varepsilon_n}\int_{-\infty}^{\infty} d\xi \frac{1}{\varepsilon_n^2 + \xi^2}\frac{\Sigma_{\mathbf{p}}\delta(\xi_{\mathbf{p}})e^2(\mathbf{p})}{N_0(0)}\\ &= \chi_{BCS}(0; T)\langle e^2(\mathbf{p})\rangle,\end{aligned} \quad \text{(A.2)}$$

where the angle brackets denote averaging over the Fermi surface and the standard susceptibility $\chi_{BCS}(0; T)$ in the BCS model for isotropic s pairing is introduced.

As a result, coefficient A_0 assumes the form

$$A_0 = \chi_0(0; T) - \chi_0(0; T_c) = A_{BCS}\langle e^2(\mathbf{p})\rangle, \quad \text{(A.3)}$$

where

$$\begin{aligned}A_{BCS} &= \chi_{BCS}(0; T) - \chi_{BCS}(0; T_c)\\ &= N_0(0)\frac{T - T_c}{T_c}\end{aligned} \quad \text{(A.4)}$$

is the standard expression for coefficient A in the case of isotropic s pairing.

Coefficient C_0 of the Ginzburg–Landau expansion is defined by generalized susceptibility (A.1) for small values of $\mathbf{q}$:

$$C_0 = \lim_{q \to 0}\frac{\chi_0(\mathbf{q}; T_c) - \chi_0(0; T_c)}{q^2}. \quad \text{(A.5)}$$

Expanding expression (A.1) for $\chi_0(\mathbf{q}; T_c)$ into a series in small q, we obtain

$$\begin{aligned}\chi_0(\mathbf{q}; T_c) &= \chi_0(0; T_c)\\ &+ T_c\sum_{\varepsilon_n}\sum_{\mathbf{p}}\frac{3\varepsilon_n^2 - \xi_{\mathbf{p}}^2}{4(\varepsilon_n^2 + \xi_{\mathbf{p}}^2)^3}e^2(\mathbf{p})(\mathbf{v}(\mathbf{p})\mathbf{q})^2,\end{aligned} \quad \text{(A.6)}$$

so that we have for coefficient C_0 the expression

$$\begin{aligned}C_0 &= T_c\sum_{\varepsilon_n}\int_{-\infty}^{\infty} d\xi \frac{3\varepsilon_n^2 - \xi^2}{4(\varepsilon_n^2 + \xi^2)^3}\\ &\times\sum_{\mathbf{p}}\delta(\xi - \xi_{\mathbf{p}})e^2(\mathbf{p})|\mathbf{v}(\mathbf{p})|^2\cos^2\varphi\\ &\approx T_c\sum_{\varepsilon_n}\int_{-\infty}^{\infty} d\xi \frac{3\varepsilon_n^2 - \xi^2}{4(\varepsilon_n^2 + \xi^2)^3}\\ &\times\sum_{\mathbf{p}}\delta(\xi_{\mathbf{p}})e^2(\mathbf{p})|\mathbf{v}(\mathbf{p})|^2\cos^2\varphi\\ &= N_0(0)\frac{7\zeta(3)}{16\pi^2 T_c^2}\langle e^2(\mathbf{p})|\mathbf{v}(\mathbf{p})|^2\cos^2\varphi\rangle,\end{aligned} \quad \text{(A.7)}$$

where φ is the angle between vectors $\mathbf{v}(\mathbf{p})$ and $\mathbf{q}$ and

$$\zeta(3) = \sum_{n=1}^{\infty}\frac{1}{n^3} \approx 1.202.$$

For a square lattice, the Fermi surface and, hence, $|\mathbf{v}(\mathbf{p})|$ also possess a symmetry relative to rotation through angle $\pi/2$; the same symmetry is also inherent

in $e^2(\mathbf{p})$ for the types of pairing considered here. Consequently, we can easily find that

$$\begin{aligned}&\langle e^2(\mathbf{p})|\mathbf{v}(\mathbf{p})|^2\cos^2\varphi\rangle\\ &= \frac{1}{2}\langle e^2(\mathbf{p})|\mathbf{v}(\mathbf{p})|^2(1+\cos 2\varphi)\rangle\\ &= \frac{1}{2}\langle e^2(\mathbf{p})|\mathbf{v}(\mathbf{p})|^2\rangle,\end{aligned} \tag{A.8}$$

since quantity $\cos 2\varphi$ reverses its sign when vector $\mathbf{p}$ rotates through angle $\pi/2$. Indeed, the direction of velocity $\mathbf{v}(\mathbf{p})$ upon this rotation changes to the perpendicular direction; accordingly, $\cos 2\varphi \longrightarrow -\cos 2\varphi$. As a result, we obtain the isotropic expression for coefficient C_0,

$$C_0 = N_0(0)\frac{7\zeta(3)}{32\pi^2 T_c^2}\langle|\mathbf{v}(\mathbf{p})|^2 e^2(\mathbf{p})\rangle; \tag{A.9}$$

in the case of isotropic s pairing and a spherical Fermi surface, this expression acquires the standard form

$$C_{BCS} = N_0(0)\frac{7\zeta(3)v_F^2}{32\pi^2 T_c^2}. \tag{A.10}$$

In the absence of pseudogap fluctuations ($W = 0$) and for $\mathbf{q} = 0$, coefficient B defined by the diagram in Fig. 6b has the form

$$\begin{aligned}B_0 &= T_c\sum_{\varepsilon_n}\sum_{\mathbf{p}}\frac{1}{\left(\varepsilon_n^2+\xi_{\mathbf{p}}^2\right)^2}e^4(\mathbf{p})\\ &= T_c\sum_{\varepsilon_n}\int_{-\infty}^{\infty}d\xi\frac{1}{\left(\varepsilon_n^2+\xi^2\right)^2}\sum_{\mathbf{p}}\delta(\xi-\xi_{\mathbf{p}})e^4(\mathbf{p})\\ &\approx N_0(0)T_c\sum_{\varepsilon_n}\int_{-\infty}^{\infty}d\xi\frac{1}{\left(\varepsilon_n^2+\xi^2\right)^2}\frac{\Sigma_{\mathbf{p}}\delta(\xi_{\mathbf{p}})e^4(\mathbf{p})}{N_0(0)}\\ &= B_{BCS}\langle e^4(\mathbf{p})\rangle,\end{aligned} \tag{A.11}$$

where

$$B_{BCS} = N_0(0)\frac{7\zeta(3)}{8\pi^2 T_c^2} \tag{A.12}$$

is the standard expression for coefficient B in the case of isotropic s pairing.

REFERENCES

1. T. Timusk and B. Statt, Rep. Prog. Phys. **62**, 61 (1999).
2. M. V. Sadovskiĭ, Usp. Fiz. Nauk **171**, 539 (2001) [Phys. Usp. **44**, 515 (2001)].
3. J. L. Tallon and J. W. Loram, Physica C (Amsterdam) **349**, 53 (2000).
4. V. M. Krasnov, A. Yurgens, D. Winkler, *et al.*, Phys. Rev. Lett. **84**, 5860 (2000).
5. N. P. Armitage, D. H. Lu, C. Kim, *et al.*, Phys. Rev. Lett. **87**, 147003 (2001).
6. J. Schmalian, D. Pines, and B. Stojkovic, Phys. Rev. Lett. **80**, 3839 (1998); Phys. Rev. B **60**, 667 (1999).
7. É. Z. Kuchinskiĭ and M. V. Sadovskiĭ, Zh. Éksp. Teor. Fiz. **115**, 1765 (1999) [JETP **88**, 968 (1999)].
8. A. I. Posazhennikova and M. V. Sadovskiĭ, Zh. Éksp. Teor. Fiz. **115**, 632 (1999) [JETP **88**, 347 (1999)].
9. É. Z. Kuchinskiĭ and M. V. Sadovskiĭ, Zh. Éksp. Teor. Fiz. **117**, 613 (2000) [JETP **90**, 535 (2000)].
10. É. Z. Kuchinskiĭ and M. V. Sadovskiĭ, Zh. Éksp. Teor. Fiz. **119**, 553 (2001) [JETP **92**, 480 (2001)].
11. É. Z. Kuchinskiĭ and M. V. Sadovskiĭ, Zh. Éksp. Teor. Fiz. **121**, 758 (2002) [JETP **94**, 654 (2002)].
12. P. Monthoux, A. V. Balatsky, and D. Pines, Phys. Rev. B **46**, 14803 (1992).
13. P. Monthoux and D. Pines, Phys. Rev. B **47**, 6069 (1993); **49**, 4261 (1994).
14. M. V. Sadovskiĭ, Zh. Éksp. Teor. Fiz. **66**, 1720 (1974) [Sov. Phys. JETP **39**, 845 (1974)]; Fiz. Tverd. Tela (Leningrad) **16**, 2504 (1974) [Sov. Phys. Solid State **16**, 1632 (1974)].
15. M. V. Sadovskiĭ, Zh. Éksp. Teor. Fiz. **77**, 2070 (1979) [Sov. Phys. JETP **50**, 989 (1979)].
16. L. P. Gor'kov, Zh. Éksp. Teor. Fiz. **37**, 1407 (1959) [Sov. Phys. JETP **10**, 998 (1959)].
17. P. G. de Gennes, *Superconductivity of Metals and Alloys* (Benjamin, New York, 1966; Mir, Moscow, 1968).
18. M. V. Sadovskiĭ and A. A. Timofeev, Sverkhprovodimost: Fiz. Khim. Tekh. **4**, 11 (1991); J. Mosc. Phys. Soc. **1**, 391 (1991).
19. M. V. Sadovskiĭ and N. A. Strigina, Zh. Éksp. Teor. Fiz. **122**, 610 (2002) [JETP **95**, 526 (2002)].
20. E. Müller-Hartmann and J. Zittartz, Phys. Rev. Lett. **26**, 428 (1971).
21. D. St. James, G. Sarma, and E. J. Thomas, *Type II Superconductivity* (Pergamon Press, Oxford, 1969; Mir, Moscow, 1970).
22. J. W. Loram, K. A. Mirza, J. R. Cooper, *et al.*, J. Supercond. **7**, 243 (1994).
23. A. Posazhennikova and P. Coleman, Phys. Rev. B **67**, 165109 (2003).

Translated by N. Wadhwa

Journal of Experimental and Theoretical Physics, Vol. 99, No. 6, 2004, pp. 1264–1278.
Translated from Zhurnal Éksperimental'no i Teoreticheskoĭ Fiziki, Vol. 126, No. 6, 2004, pp. 1446–1464.

SOLIDS
Electronic Properties

Superconductivity in the Pseudogap State in the Hot Spot Model: The Influence of Impurities and the Phase Diagram

N. A. Kuleeva*, E. Z. Kuchinskii, and M. V. Sadovskii*****
Institute of Electrophysics, Russian Academy of Sciences, Ural Branch, Yekaterinburg, 620016 Russia
**e-mail: strigina@iep.uran.ru*
***e-mail: kuchinsk@iep.uran.ru*
****e-mail: sadovski@iep.uran.ru*
Received June 10, 2004

Abstract—We analyze the peculiarities of the superconducting state (*s*- and *d*-wave paring) in the model of the pseudogap state induced by Heisenberg antiferromagnetic short-range order spin fluctuations. The model is based on the pattern of strong scattering near hot spots at the Fermi surface. The analysis is based on the microscopic derivation of the Ginzburg–Landau expansion with the inclusion of all Feynman diagrams of perturbation theory for the interaction of an electron with short-range order fluctuations and in the ladder approximation for the scattering by normal (nonmagnetic) impurities. We determine the dependence of the critical superconducting transition temperature and other superconductor characteristics on the pseudogap parameters and the degree of impurity scattering. We show that the characteristic shape of the phase diagram for high-temperature superconductors can be explained in terms of the model under consideration. *© 2004 MAIK "Nauka/Interperiodica".*

1. INTRODUCTION

One of the most important problems in the physics of high-temperature superconductors (HTSCs) based on copper oxides is the theoretical description of the characteristic shape of their phase diagram [1]. Elucidating the nature of the pseudogap state that is observed over wide ranges of temperatures and carrier concentrations [2] and that undoubtedly plays the central role in shaping the properties of the normal and superconducting states of these systems arouses particular interest. Despite ongoing discussions, the pseudogap formation scenario based on the pattern of strong scattering of current carriers by antiferromagnetic[1] (AFM, SDW) short-range order spin fluctuations seems to be preferred [2, 3]. In the momentum space, this scattering takes place with the transfer of the wavevectors of order $\mathbf{Q} = (\pi/a, \pi/a)$ (a is the two-dimensional lattice constant) and leads to precursors of the rearrangement of the electron spectrum that arises when a long-range AFM order is established (the period doubles). This results in a non-Fermi liquid behavior (dielectrization) of the spectral characteristics near the so-called hot spots at the Fermi surface that emerge at the points of intersection of this surface with the boundaries of the "future" antiferromagnetic Brillouin zone [2].

A simplified model of the pseudogap behavior [4, 5] in which the scattering by real (dynamical) spin fluctuations was replaced (which is valid at fairly high temperatures) with a static Gaussian random field of pseudogap fluctuations with a characteristic wavevector from the vicinity of $\mathbf{Q}$ whose width is determined by the inverse correlation length of the short-range order $\kappa = \xi^{-1}$ has been intensively studied in terms of this approach. An overview of the works, as applied to the properties of the normal state and for simple models of the influence of pseudogap fluctuations on superconductivity, can be found in [2].

In our recent paper [6], based on the microscopic derivation of the Ginzburg–Landau expansion,[2] we have studied the influence of pseudogap fluctuations in the hot spot model on the basic characteristics of the superconducting state (*s*- and *d*-type pairing) that forms against the background of these fluctuations. We considered a slightly simplified version of the model where the Heisenberg spin fluctuations were replaced with Ising or spin-independent charge CDW fluctuations. These pseudogap fluctuations of a "dielectric" nature were shown to generally suppress conductivity, causing a decrease in superconducting transition temperature, a reduction in the jump in specific heat, and several other anomalies of the superconductor characteristics. We found two possible types of interaction between the superconducting order parameter and pseudogap fluctuations that lead to distinctly different scales of their influence on superconductivity.

The goal of this work is to generalize the approach proposed in [6] to the "realistic" case of Heisenberg

[1] The role of similar charge (CDW) fluctuations cannot be ruled out either.

[2] A similar analysis was performed in [7] on the basis of Gorkov's equations.

spin fluctuations and to calculate the influence of (nonmagnetic) impurities (disorder) on superconductivity in the pseudogap state. We show that the typical phase diagram for a HTSC can be semiquantitatively modeled in terms of the model under consideration.

2. THE HOT SPOT MODEL AND THE RECURRENCE PROCEDURE FOR CALCULATING THE GREEN FUNCTIONS AND THE VERTEX PARTS

The basic ideas of the hot spot model under consideration and the method for calculating the single-electron Green function were presented in detail in [4, 5]; the methods for determining the vertex parts of interest were described previously [6, 8]. Therefore, in this section, we provide only the basic equations and introduce the necessary notation by briefly describing the changes required to allow for the spin structure of the interaction in the Heisenberg model of antiferromagnetic fluctuations.

An effective interaction between electrons and spin fluctuations is introduced in the model of an "almost antiferromagnetic" Fermi liquid [4]. This interaction is described by the dynamical susceptibility characterized by the correlation length ξ of the spin fluctuations and their characteristic frequency ω_{sf} to be determined experimentally, which can depend significantly on the carrier concentration (and, for ξ, on the temperature). This dynamical susceptibility together with the effective interaction have (in momentum representation) a maximum in the vicinity of $\mathbf{Q} = (\pi/a, \pi/a)$, which gives rise to two types of quasi-particles: hot quasi-particles whose momenta lie near the points of the Fermi surface coupled by the scattering vector of order $\mathbf{Q}$ and cold quasi-particles whose momenta lie near the regions of the Fermi surface surrounding the diagonals of the Brillouin zone [2, 4, 5].

At high temperatures, $2\pi T \gg \omega_{sf}$, the spin dynamics may be disregarded [4]. The interaction with spin (pseudogap) fluctuations then reduces to the scattering of electrons by the corresponding static Gaussian random field. In this model, we can suggest a simplified form of the effective interaction (the correlator of the random fluctuation field) [4, 5] that allows full summation of the Feynman series of perturbation theory, which gives rise to the following recurrence procedure for determining the single-electron Green function:

$$G_k(\varepsilon_n, \mathbf{p}) = \frac{1}{i\varepsilon_n - \xi_k(\mathbf{p}) + ikv_k\kappa - \Sigma_k(\varepsilon_n, \mathbf{p})}, \quad (1)$$

$$\Sigma_k(\varepsilon_n, \mathbf{p}) = W^2 s(k+1) G_{k+1}(\varepsilon_n, \mathbf{p}). \quad (2)$$

This is shown in the form of a symbolic Dyson equation in Fig. 1a, where the following function is introduced:

$$G_{0k}(\varepsilon_n, \mathbf{p}) = \frac{1}{i\varepsilon_n - \xi_k(\mathbf{p}) + ikv_k\kappa}. \quad (3)$$

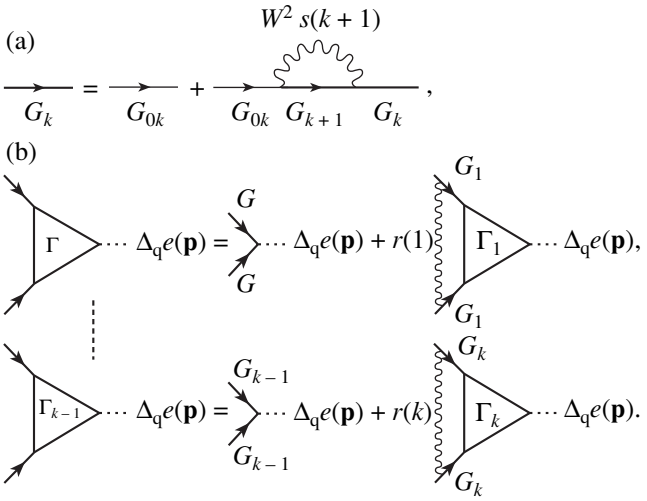

Fig. 1. Recurrence equations for (a) the Green function and (b) the triangular vertex.

Here, $\kappa = \xi^{-1}$ is the inverse correlation length of the pseudogap fluctuations; $\varepsilon_n = 2\pi T(n + 1/2)$ (to be specific, we assume that $\varepsilon_n > 0$);

$$\xi_k(\mathbf{p}) = \begin{cases} \xi_{\mathbf{p}+\mathbf{Q}} & \text{for odd } k, \\ \xi_{\mathbf{p}} & \text{for even } k; \end{cases} \quad (4)$$

$$v_k = \begin{cases} |v_x(\mathbf{p}+\mathbf{Q})| + |v_y(\mathbf{p}+\mathbf{Q})| & \text{for odd } k, \\ |v_x(\mathbf{p})| + |v_y(\mathbf{p})| & \text{for even } k; \end{cases} \quad (5)$$

$\mathbf{v}(\mathbf{p}) = \partial\xi_{\mathbf{p}}/\partial\mathbf{p}$ is the velocity of a free quasi-particle with the spectrum $\xi_{\mathbf{p}}$ that is taken in standard form [4]:

$$\xi_{\mathbf{p}} = -2t(\cos p_x a + \cos p_y a) - 4t' \cos p_x a \cos p_y a - \mu; \quad (6)$$

t and t' are the transfer integrals between the closest neighbors and between the second closest neighbors on the square lattice, respectively; a is the lattice constant; and μ is the chemical potential.

The parameter W has the dimensions of energy. It defines the effective pseudogap width and can be written in the model of Heisenberg spin fluctuations as [4]

$$W^2 = g^2 \frac{\langle \mathbf{S}_i^2 \rangle}{3} = g^2 \langle (n_{i\uparrow} - n_{i\downarrow})^2 \rangle, \quad (7)$$

where g is the coupling constant between electrons and spin fluctuations, $\langle \mathbf{S}_i^2 \rangle$ is the mean square of the spin at the lattice site, and $n_{i\uparrow}$ and $n_{i\downarrow}$ are the particle number operators at the site with the corresponding spin projections. Clearly, like the correlation length ξ, the parameter W in the semiphenomenological approach [4, 5] is

The choice of the sign in the recurrence procedure for the vertex part

Pairs	CDW fluctuations	SDW (Ising) fluctuations	SDW (Heisenberg) fluctuations
s	+	–	+
d	–	+	–

also a function of the carrier concentration (and temperature) to be determined experimentally.

The factor $s(k)$ is determined by the Feynman diagram combinatorics and is

$$s(k) = k \tag{8}$$

in the simplest case of commensurable short-range order charge (CDW) fluctuations, while for the most interesting case of Heisenberg spin (SDW) fluctuations [4],[3]

$$s(k) = \begin{cases} \dfrac{k+2}{3} & \text{for odd } k, \\ \dfrac{k}{3} & \text{for even } k. \end{cases} \tag{9}$$

The validity conditions for the approximation under consideration were discussed in detail in [4, 5].

A remarkable feature of the model under consideration is the possibility of full summation of the entire series of Feynman diagrams[4] for the vertex functions that describe the response of the system to an arbitrary external perturbation. This was considered in detail in [8]. Here, we immediately give the recurrence equations for the "triangular" vertices in the Cooper channel that arise in the corresponding analysis. These equations are similar to those derived in [6] and describe the response to an arbitrary fluctuation of the superconducting order (gap) parameter,

$$\Delta(\mathbf{p}, \mathbf{q}) = \Delta_{\mathbf{q}} e(\mathbf{p}), \tag{10}$$

where the symmetry factor that determines the type (symmetry) of pairing is taken in the form

$$e(\mathbf{p}) = \begin{cases} 1, & s\text{-wave paring}, \\ \cos(p_x a) - \cos(p_y a), & d_{x^2-y^2}\text{-type pairing}, \end{cases} \tag{11}$$

and it is implied that the pairing is singlet in spin. It is convenient to write the vertex of interest as

$$\Gamma(\varepsilon_n, -\varepsilon_n, \mathbf{p}, -\mathbf{p}+\mathbf{q}) \equiv \Gamma_{\mathbf{p}}(\varepsilon_n, -\varepsilon_n, \mathbf{q}) e(\mathbf{p}). \tag{12}$$

$\Gamma_{\mathbf{p}}(\varepsilon_n, -\varepsilon_n, \mathbf{q})$ is then defined by the recurrence procedure

$$\begin{aligned} &\Gamma_{\mathbf{p}k-1}(\varepsilon_n, -\varepsilon_n, \mathbf{q}) \\ &= 1 \pm W^2 r(k) G_k(\varepsilon_n, \mathbf{p}+\mathbf{q}) G_k(-\varepsilon_n, \mathbf{p}) \\ &\times \left[1 + \frac{2ik\kappa v_k}{G_k^{-1}(\varepsilon_n, \mathbf{p}+\mathbf{q}) - G_k^{-1}(-\varepsilon_n, \mathbf{p}) - 2ik\kappa v_k}\right] \\ &\times \Gamma_{\mathbf{p}k}(\varepsilon_n, -\varepsilon_n, \mathbf{q}), \end{aligned} \tag{13}$$

which is shown as graphs in Fig. 1b. The "physical" vertex corresponds to $\Gamma_{\mathbf{p}k=0}(\varepsilon_n, -\varepsilon_n, \mathbf{q})$. The additional combinatorial factor is $r(k) = s(k)$ for the simples case of charge (or Ising spin) pseudogap fluctuations considered in [6]. For the most interesting case of Heisenberg spin (SDW) fluctuations considered below, this factor is [4] (see also the Appendix)

$$r(k) = \begin{cases} k & \text{for even } k, \\ \dfrac{k+2}{9} & \text{for odd } k. \end{cases} \tag{14}$$

The choice of the sign of W^2 on the right-hand side of Eq. (13) depends on the symmetry of the superconducting order parameter and the type of pseudogap fluctuations [6] (for details, see the Appendix). The corresponding cases are listed in the table. In particular, we see from this table that in the most interesting case of *d*-type pairing and Heisenberg pseudogap fluctuations, we should take the minus, so the recurrence procedure for the vertex part becomes an alternating one. At the same time, for the case of *s*-wave paring and fluctuations of the same type, we should take the plus, and the recurrence procedure becomes a constant-sign one. It was shown in [6] (using other examples from the table) that this difference in the types of recurrence procedure leads to two qualitatively different behaviors of all basic superconductor characteristics.

3. THE INFLUENCE OF IMPURITIES

The influence of the scattering by normal (nonmagnetic) impurities can be easily taken into account in the self-consistent Born approximation by writing the Dyson equation shown graphically in Fig. 2a for the single-electron Green function. Compared to Fig. 1a, the standard contribution from the impurity scattering to the intrinsic-energy part [9] was added to this figure.

[3] The Feynman diagram combinatorics for the model of Heisenberg fluctuations is analyzed in detail in the Appendix.

[4] Including all of the diagrams with crossing interaction lines.

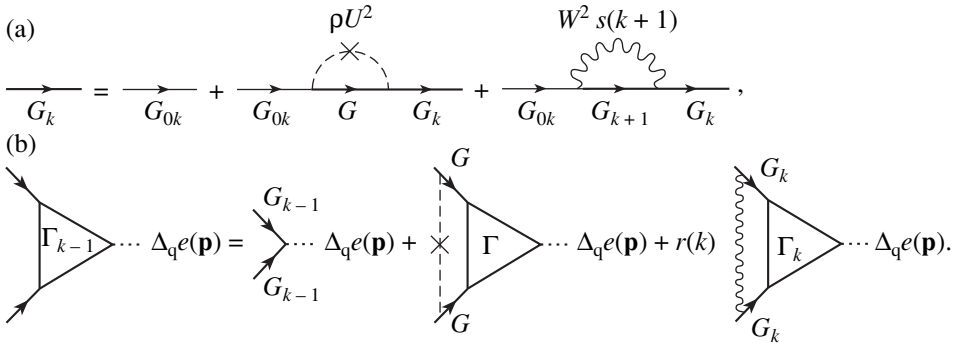

Fig. 2. Recurrence equations for (a) the Green function and (b) the triangular vertex including the impurity scattering

As a result, the recurrence equation for the Green function can be written as

$$G_k(\varepsilon_n, \mathbf{p}) = \left[G_{0k}^{-1}(\varepsilon_n, \mathbf{p}) - \rho U^2 \sum_{\mathbf{p}} G(\varepsilon_n, \mathbf{p}) - W^2 s(k+1) G_{k+1}(\varepsilon_n, \mathbf{p}) \right]^{-1}, \quad (15)$$

where ρ is the impurity concentration with a point potential U and the "impurity" intrinsic-energy part includes the full Green function $G(\varepsilon_n, \mathbf{q}) = G_{k=0}(\varepsilon_n, \mathbf{p})$, which must generally be determined in a self-consistent way by using the written procedure. The contribution from the real part of the Green function to this intrinsic-energy part typically reduces [9] to an insignificant renormalization of the chemical potential, so Eq. (15) takes the form

$$G_k(\varepsilon_n, \mathbf{p}) = \left[i\left(\varepsilon_n - \rho U^2 \sum_{\mathbf{p}} \mathrm{Im} G(\varepsilon_n, \mathbf{p}) + k v_k \kappa \right) - \xi_k(\mathbf{p}) - W^2 s(k+1) G_{k+1}(\varepsilon_n, \mathbf{p}) \right]^{-1}. \quad (16)$$

Therefore, compared to the impurity-free case, the following substitution (renormalization) actually takes place:

$$\varepsilon_n \longrightarrow \varepsilon_n - \rho U^2 \sum_{\mathbf{p}} \mathrm{Im} G(\varepsilon_n, \mathbf{p}) \equiv \varepsilon_n \eta_\epsilon, \quad (17)$$

$$\eta_\epsilon = 1 - \frac{\rho U^2}{\varepsilon_n} \sum_{\mathbf{p}} \mathrm{Im} G(\varepsilon_n, \mathbf{p}). \quad (18)$$

If no full self-consistent calculation is performed for the intrinsic-energy part of the impurity scattering, then we have in the simplest approximation

$$\varepsilon_n \longrightarrow \varepsilon_n - \rho U^2 \sum_{\mathbf{p}} \mathrm{Im} G_{00}(\varepsilon_n, \mathbf{p}) \equiv \varepsilon_n \eta_\epsilon = \varepsilon_n + \gamma_0 \mathrm{sgn} \varepsilon_n, \quad (19)$$

$$\eta_\epsilon = 1 + \frac{\gamma_0}{|\varepsilon_n|}, \quad (20)$$

where $\gamma_0 = \pi \rho U^2 N_0(0)$ is the standard Born impurity scattering frequency [9] ($N_0(0)$ is the density of state of the free electrons at the Fermi level).

For the triangular vertices of interest, the recurrence equation that includes the impurity scattering is shown as a graph in Fig. 2b. For the vertex that describes the interaction with the fluctuation of the superconducting order parameter (10) with *d*-wave symmetry (11), this equation simplifies significantly, because the contribution of the second diagram in the right-hand part of Fig. 2b is virtually equal to zero in view of the condition $\sum_{\mathbf{p}} e(\mathbf{p}) = 0$ (cf. the discussion of a similar situation in [10]). The recurrence equation for the vertex then has the form (13), where the expressions derived from (15) and (16), i.e., the "dressed" (by the impurity scattering) Green functions defined by Fig. 2a, should be used as $G_k(\pm\varepsilon_n, \mathbf{p})$. For the vertex that describes the interaction with the fluctuation of the order parameter with *s*-wave symmetry, we have the equation

$$\Gamma_{\mathbf{p}k-1}(\varepsilon_n, -\varepsilon_n, \mathbf{q}) = 1 + \rho U^2 \sum_{\mathbf{p}} G(\varepsilon_n, \mathbf{p}+\mathbf{q}) G(-\varepsilon_n, \mathbf{p}) \Gamma_{\mathbf{p}}(\varepsilon, -\varepsilon_n, \mathbf{q}) \pm W^2 r(k) G_k(\varepsilon_n, \mathbf{p}+\mathbf{q}) G_k(-\varepsilon_n, \mathbf{p}) \times \left\{ 1 + \frac{2ik\kappa v_k}{G_k^{-1}(\varepsilon_n, \mathbf{p}+\mathbf{q}) - G_k^{-1}(-\varepsilon_n, \mathbf{p}) - 2ik\kappa v_k} \right\} \times \Gamma_{\mathbf{p}k}(\varepsilon_n, -\varepsilon_n, \mathbf{q}), \quad (21)$$

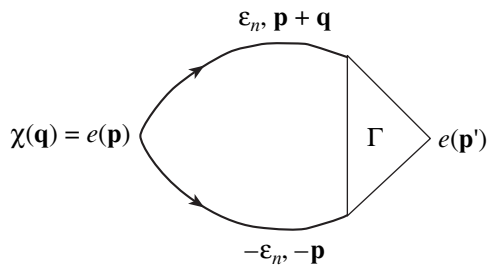

Fig. 3. Diagram for the generalized susceptibility $\chi(\mathbf{q})$ in the Cooper channel.

where expressions (15) and (16) should again be used as $G_k(\pm\varepsilon_n\mathbf{p})$ and the sign of W^2 is determined by the above rules. The difference between this vertex and the vertex of the interaction with *d*-wave symmetry fluctuations lies in the appearance of the second term on the right-hand side of Eq. (21), i.e., in the substitution

$$1 \longrightarrow \eta_\Gamma = 1 + \rho U^2 \sum_{\mathbf{p}} G(\varepsilon_n, \mathbf{p}+\mathbf{q}) \times G(-\varepsilon_n, \mathbf{p})\Gamma_{\mathbf{p}}(\varepsilon, -\varepsilon_n, \mathbf{q}). \quad (22)$$

Therefore, the self-consistent calculation procedure now looks as follows. Starting from the zero approximation $G = G_{00}$ and $\Gamma_{\mathbf{p}} = 1$, we then have in Eqs. (16) and (21)

$$\eta_\varepsilon = \eta_\Gamma = 1 - \frac{\rho U^2}{\varepsilon_n \sum_{\mathbf{p}} \mathrm{Im} G_{00}(\varepsilon_n, \mathbf{p})}.$$

We run the corresponding recurrence procedures (starting from a certain value of *k*) and determine the new values of $G = G_{k=0}$ and $\Gamma_{\mathbf{p}} = \Gamma_{k=0}$. We again calculate η_ε and η_Γ using (18) and (22), use these values in (16) and (21), and so on until convergence is achieved.

When considering the vertex of the *d*-wave symmetry, we should set $\eta_\Gamma = 1$ at all steps of our calculations. In this case, there is actually no particular need to perform full self-consistent impurity scattering calculation, because it leads to relatively small corrections to the results of non-self-consistent calculation using the simplest substitution (19) [7].

4. CALCULATING THE SUPERCONDUCTING TRANSITION TEMPERATURE AND THE GINZBURG–LANDAU COEFFICIENTS

The critical superconducting transition temperature is defined by the normal-phase Cooper instability equation

$$1 - V\chi(0; T) = 0, \quad (23)$$

where the generalized Cooper susceptibility is indicated by the graph in Fig. 3 and is

$$\chi(\mathbf{q}; T) = -T \sum_{\varepsilon_n} \sum_{\mathbf{p}} G(\varepsilon_n, \mathbf{p}+\mathbf{q}) \times G(-\varepsilon_n, -\mathbf{p}) e^2(\mathbf{p}) \Gamma_{\mathbf{p}}(\varepsilon_n, -\varepsilon_n, \mathbf{q}). \quad (24)$$

The pairing interaction constant *V*, which is nonzero in a layer $2\omega_c$ in width around the Fermi level, determines the seed transition temperature T_{c0} in the absence of pseudogap fluctuations by means of the standard BCS equation:[5]

$$1 = \frac{2VT}{\pi^2} \sum_{n=0}^{\bar{m}} \int_0^{\pi/a} dp_x \int_0^{\pi/a} dp_y \frac{e^2(\mathbf{p})}{\xi_{\mathbf{p}}^2 + \varepsilon_n^2}, \quad (25)$$

where $\bar{m} = [\omega_c/2\pi T_{c0}]$ is the dimensionless cutoff parameter of the Matsubara frequency sum. As in [6], all of our calculations were performed for the typical spectrum (6) of quasi-particles in HTSCs for various relations between *t*, *t*', and μ. By arbitrarily choosing $\omega_c = 0.4t$ and $T_{c0} = 0.01t$, we can easily find a value of the pairing parameter *V* in (25) that yields this value of T_{c0} for different types of pairing. In particular, we obtain $V/ta^2 = 1$ and $V/ta^2 = 0.55$ for *s*-type and $d_{x^2-y^2}$-type pairing, respectively.

The fact that the Cooper susceptibility at $q = 0$ is required to calculate T_c significantly simplifies the calculations [6]. In general, for example, knowledge of $\chi(q; T)$ at arbitrary (small) *q* is required to calculate the Ginzburg–Landau expansion coefficients.

The Ginzburg–Landau expansion for the difference between the free energy densities of the superconducting and normal states can be written in standard form:

$$F_s - F_n = A|\Delta_{\mathbf{q}}|^2 + q^2 C|\Delta_{\mathbf{q}}|^2 + \frac{B}{2}|\Delta_{\mathbf{q}}|^4; \quad (26)$$

it is defined by the loop expansion for the free energy in the fluctuation field of the order parameter (10).

It is convenient to normalize the Ginzburg–Landau coefficients *A*, *B*, and *C* to their values in the absence of pseudogap fluctuations by writing them as [6]

$$A = A_0 K_A, \quad C = C_0 K_C, \quad B = B_0 K_B, \quad (27)$$

[5] We do not discuss the microscopic nature of this interaction; it can be associated with the exchange by the same antiferromagnetic spin fluctuations, phonons, or a combination of the electron–phonon and spin–fluctuation interactions.

where

$$A_0 = N_0(0)\frac{T - T_c}{T_c}\langle e^2(\mathbf{p})\rangle,$$

$$C_0 = N_0(0)\frac{7\zeta(3)}{32\pi^2 T_c^2}\langle |\mathbf{v}(\mathbf{p})|^2 e^2(\mathbf{p})\rangle, \quad (28)$$

$$B_0 = N_0(0)\frac{7\zeta(3)}{8\pi^2 T_c^2}\langle e^4(\mathbf{p})\rangle;$$

the angular brackets denote an ordinary averaging over the Fermi surface:

$$\langle \ldots \rangle = \frac{1}{N_0(0)}\sum_p \delta(\xi_\mathbf{p})\ldots;$$

and $N_0(0)$ is the state density at the Fermi surface for free electrons.

We then obtain the following general expressions [6]:

$$K_A = \frac{\chi(0; T) - \chi(0; T_c)}{A_0}, \quad (29)$$

$$K_C = \lim_{q\to 0}\frac{\chi(\mathbf{q}; T_c) - \chi(0; T_c)}{q^2 C_0}, \quad (30)$$

$$K_b = \frac{T_c}{B_0}\sum_{\varepsilon_n}\sum_{\mathbf{p}} e^4(\mathbf{p})G^2(\varepsilon_n, \mathbf{p}) \times G^2(-\varepsilon_n, -\mathbf{p})\Gamma_\mathbf{p}^4(\varepsilon_n, -\varepsilon_n, 0), \quad (31)$$

which were used for our direct numerical calculations.

In the presence of impurities, all of the Green functions and the vertices appearing in these expressions should be calculated using Eqs. (16) and (21) written above.

Knowledge of the Ginzburg–Landau expansion coefficients allows all of the basic superconductor characteristics near the transition temperature T_c to be determined. The coherence length is defined as

$$\frac{\xi^2(T)}{\xi_{BCS}^2(T)} = \frac{K_C}{K_A}, \quad (32)$$

where $\xi_{BCS}(T)$ is the value of this length in the absence of a pseudogap. For the magnetic-field penetration depth, we have

$$\frac{\lambda(T)}{\lambda_{BCS}(T)} = \sqrt{\frac{K_B}{K_A K_C}}, \quad (33)$$

where this quantity was also normalized to its value of $\lambda_{BCS}(T)$ in the absence of pseudogap fluctuations.

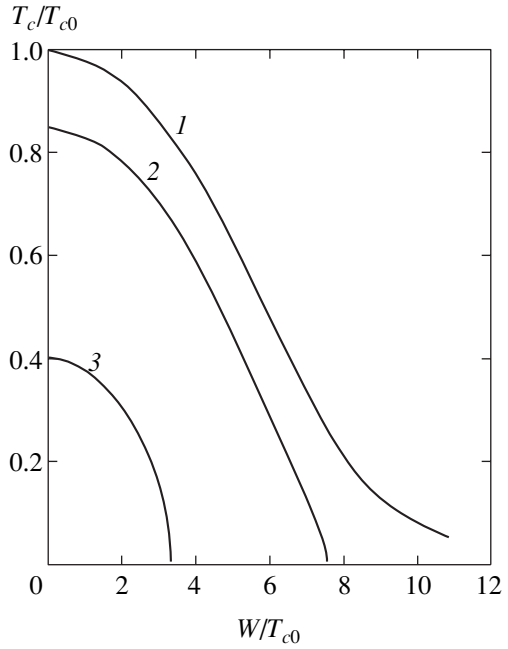

Fig. 4. T_c versus effective pseudogap width W for d-type pairing for three impurity scattering frequencies: γ_0/T_{c0} = 0 (*1*), 0.18 (*2*), and 0.64 (*3*). The inverse correlation length is $\kappa a = 0.2$.

The normalized slope of the upper critical field near T_c,

$$\left|\frac{dH_{c2}}{dT}\right|_{T_c} \Big/ \left|\frac{dH_{c2}}{dT}\right|_{T_{c0}} = \frac{T_c}{T_{c0}}\frac{K_A}{K_C}, \quad (34)$$

and the relative jump in specific heat at the transition point,

$$\Delta C = \frac{(C_s - C_n)_{T_c}}{(C_s - C_n)_{T_{c0}}} = \frac{T_c}{T_{c0}}\frac{K_A^2}{K_B}, \quad (35)$$

are determined in a similar way.

5. RESULTS OF CALCULATIONS

The results of calculations for the charge (CDW) and spin (SDW) Ising fluctuations of the short-range order were presented in [6]. Here, we focus on the analysis of the most important and interesting case of Heisenberg spin (SDW) fluctuations and on the discussion of the role of impurity scattering (disorder). Since the case of d-type pairing is of particular importance in the physics of HTSCs based on copper oxides, we pay slightly more attention to this case.

We performed all of the calculations in this section for the typical parameters of the initial electron spectrum $t'/t = -0.4$ and $\mu/t = -1.3$ and took $\kappa a = 0.2$ for the inverse correlation length. To save space, we do not present the results of our calculations for the dimen-

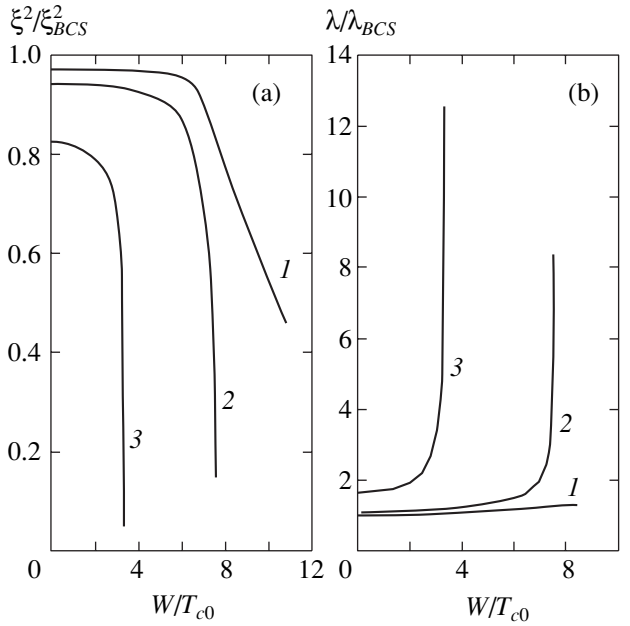

Fig. 5. Square of the coherence length (a) and magnetic-field penetration depth (b) versus effective pseudogap width W for d-type pairing for three impurity scattering frequencies: $\gamma_0/T_{c0} = 0$ (*1*), 0.18 (*2*), and 0.64 (*3*)

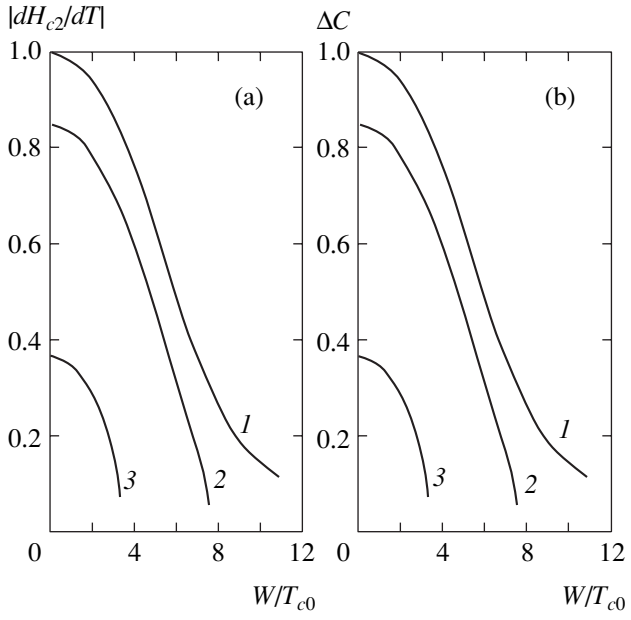

Fig. 6. Slope of the upper critical field and jump in specific heat at the transition point versus effective pseudogap width for d-type pairing for three impurity scattering frequencies: $\gamma_0/T_{c0} = 0$ (*1*), 0.18 (*2*), and 0.64 (*3*).

sionless Ginzburg–Landau expansion coefficients K_A, K_B, and K_C, but immediately show the typical dependences for the basic physical parameters.

When considering the dependences on the pseudogap width and the impurity scattering frequency γ_0, we give all of the characteristics normalized to their values, respectively, at $T = T_{c0}$ and $T = T_{c0}(W)$, i.e., at the seed transition temperature at a given W, but in the absence of impurity scattering ($\gamma_0 = 0$).

5.1. The d-Type Paring

In Fig. 4, the superconducting transition temperature T_c is plotted against the effective pseudogap width W for several impurity scattering frequencies. We see that pseudogap fluctuations lead to noticeable suppression of superconductivity; in the presence of finite disorder, a critical value of W at which T_c becomes zero arises. This suppression of T_c is naturally related to the partial dielectrization of the electron spectrum near hot spots [4, 5].

Similar dependences are shown in Fig. 5 for the coherence length and the magnetic-field penetration depth and in Fig. 6 for the slope of the temperature dependence of the upper critical field and the jump in specific heat at the transition point. The latter superconductor characteristics are rapidly suppressed by pseudogap fluctuations.

The dependence on the correlation length of the short-range order fluctuations is slower: in all cases, the increase in ξ (the decrease in parameter κ) enhances the pseudogap fluctuation effect.

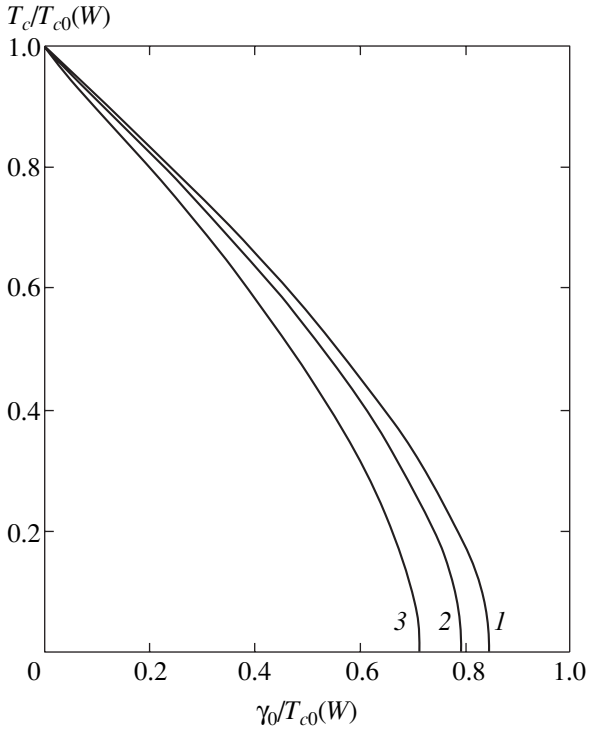

Fig. 7. T_c versus impurity scattering (disorder) frequency for d-type pairing for three effective pseudogap widths: $W/T_{c0} = 0$ (*1*), 2.8 (*2*), and 5.5 (*3*).

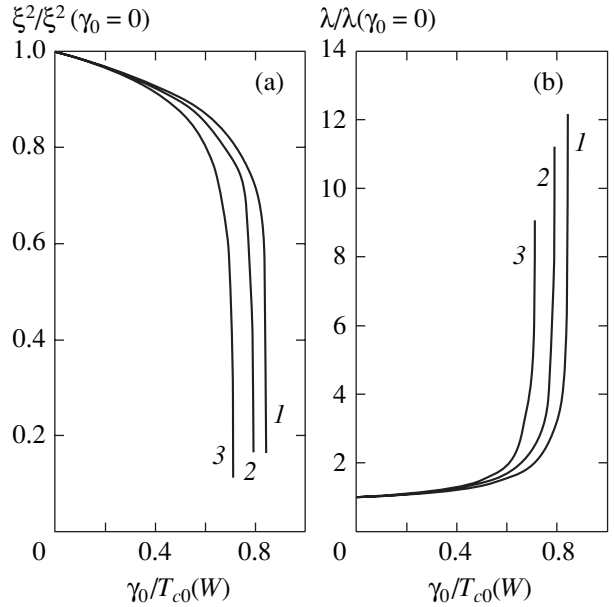

Fig. 8. Square of the coherence length (a) and magnetic-field penetration depth (b) versus impurity scattering frequency γ_0 for *d*-type pairing for three effective pseudogap widths: $W/T_{c0} = 0$ (*1*), 2.8 (*2*), and 5.5 (*3*).

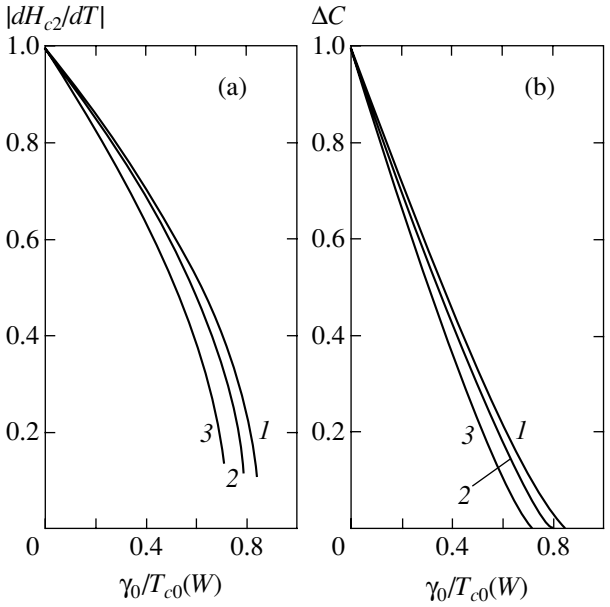

Fig. 9. Slope of the upper critical field and jump in specific heat at the transition point versus impurity scattering frequency γ_0 for *d*-type pairing for three effective pseudogap widths: $W/T_{c0} = 0$ (*1*), 2.8 (*2*), and 5.5 (*3*).

In Fig. 7, the superconducting transition temperature is plotted against the impurity scattering frequency γ_0 for several effective pseudogap widths. We see that, in the presence of pseudogap fluctuations, the suppression of T_c with growing disorder is appreciably faster that in their absence ($W = 0$) when the dependence $T_c(\gamma_0)$ for *d*-type paring is described by the standard Abrikosov–Gorkov curve [10, 11]. Similar dependences are shown in Fig. 8 for the coherence length and the penetration depth and in Fig. 9 for the slope of the $H_{c2}(T)$ curve and the jump in specific heat. We again see that impurity scattering (disorder) causes the last two parameters to rapidly decrease; i.e., it enhances the pseudogap fluctuation effect.

The derived dependences on the pseudogap parameters are qualitatively similar to those obtained in [6] for the case of charge (CDW) pseudogap fluctuations where, as in the case considered here, an alternating recurrence procedure arises for the vertex part. At the same time, certain quantitative differences associated with different diagram combinatorics also arise. The dependences on the impurity scattering (disorder) frequency have not been studied previously in this model.[6]

The dependences found are in qualitative agreement with most of the data from the experiments aimed at studying the superconductivity in the domain of existence of the pseudogap (the underdoped region in the cuprate phase diagram). Below, we show that the results obtained can be used to directly model the typical phase diagram for HTSC cuprates.

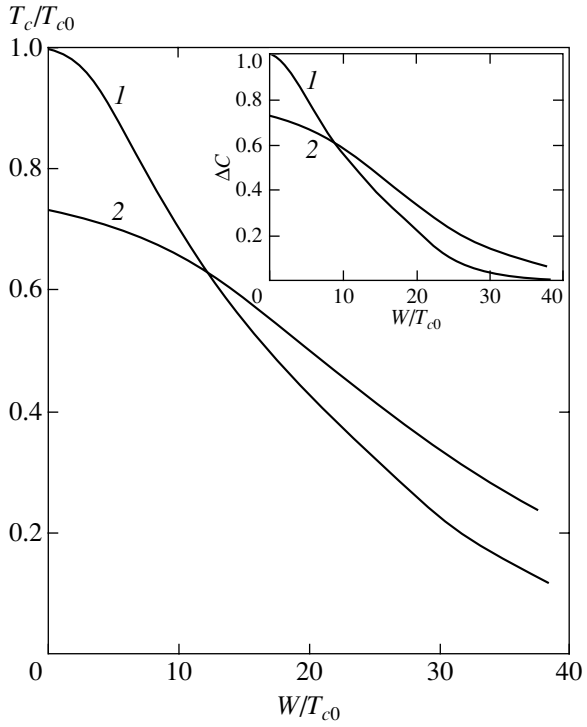

Fig. 10. T_c versus effective pseudogap width W for *s*-type pairing for two impurity scattering frequencies: $\gamma_0/T_{c0} = 0$ (*1*) and 20 (*2*). The inverse correlation length is $\kappa a = 0.2$. The insert shows the characteristic behavior of the jump in specific heat for similar parameters.

[6] The corresponding dependences of T_c were considered in [7] for the constant-sign recurrence procedure that arises in the case of Ising SDW fluctuations where the suppression of superconductivity is much slower.

5.2. The s-Type Pairing

The *s*-type pairing is mainly of interest in revealing the characteristic differences from the *d*-type pairing. There are virtually no experimental data on the *s*-type conductivity in systems with a pseudogap, although it may well be that the corresponding systems will be discovered in the future.

Our calculations indicate that pseudogap fluctuations suppress appreciably the superconducting transition temperature in this case as well (Fig. 10), although the scale length of these fluctuations required for significant suppression of superconductivity is much larger than that for the *d*-type pairing. This result has already been obtained in [6]. Note, however, that in the case of Heisenberg SDW fluctuations under consideration, there is no characteristic "shelf" on the $T_c(W)$ curve that is present in the case of scattering by CDW pseudogap fluctuations [6]. The jump in specific heat at the superconducting transition point is also significantly suppressed on the same scale of W, as shown in the insert to Fig. 10. The corresponding dependences for the coherence length and the penetration depth are similar to those obtained previously in [6] and are not given here. Figure 11 shows the calculated dependence of T_c on the impurity scattering (disorder) frequency. Apart from the relatively weak suppression of T_c by disorder related [7] to the state density smearing at the Fermi level, a weak effect of increase in T_c with γ_0 that is probably related to the smearing of the pseudogap in the state density by impurity scattering can also be observed.

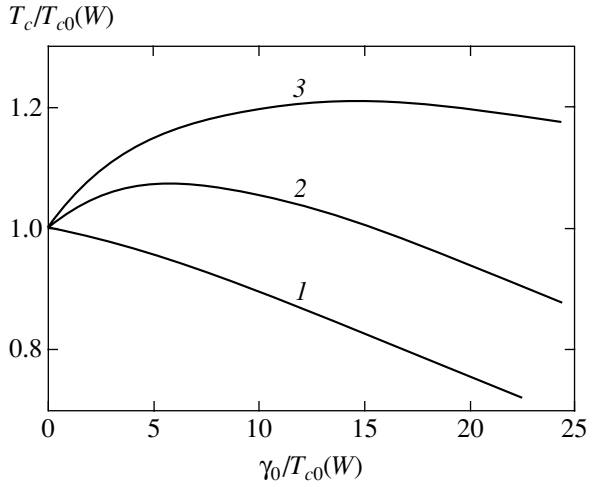

Fig. 11. Superconducting transition temperature T_c versus impurity scattering (disorder) frequency γ_0 for *s*-type pairing for three pseudogap widths: $W/T_{c0} = 0$ (*1*), 8 (*2*), and 15 (*3*).

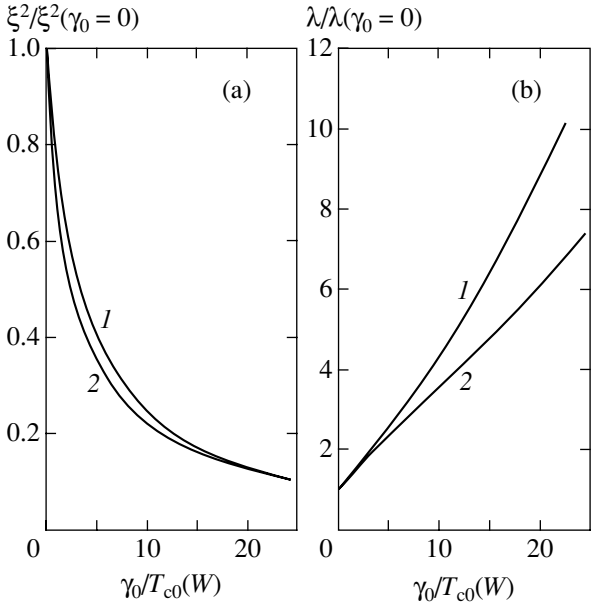

Fig. 12. Square of the coherence length (a) and magnetic-field penetration depth (b) versus impurity scattering (disorder) frequency γ_0 for *s*-type pairing for two effective pseudogap widths: $W/T_{c0} = 0$ (*1*) and 15 (*2*).

Figure 12 shows how impurity scattering (disorder) affects the coherence length and the magnetic-field penetration depth in the case of *s*-type pairing.

Finally, Fig. 13 shows how impurity scattering (disorder) affects the slope of the upper critical field and the jump in specific heat. The jump in specific heat is significantly suppressed by disorder, and the behavior of the slope of $H_{c2}(T)$ qualitatively differs from that in the case of *d*-type pairing: the growth of disorder causes this parameter to increase appreciably, as in the standard theory of "dirty" superconductors [20], while pseudogap fluctuations increase the slope of $H_{c2}(T)$. In the absence of pseudogap fluctuations, similar differences in the behavior of the slope of the $H_{c2}(T)$ curve for disorder have been pointed out [10].

6. MODELING THE PHASE DIAGRAM

The described model of the influence of pseudogap fluctuations on superconductivity allows the typical phase diagram for HTSC cuprates to be modeled.[7] Modeling of this kind, based on an extremely simplified version of our model, was originally attempted in [13]. The main idea is to identify the parameter W with the experimentally observed effective pseudogap width (the temperature of the crossover to the pseudogap region of the phase diagram), $E_g \approx T^*$, determined from many experiments [1–3]. This parameter is known to decrease almost linearly with increasing dopant (current carriers) concentration from values of ~10^3 K, becoming zero at a certain critical concentration $x_c \approx$

[7] We ignore the existence of a narrow region of antiferromagnetic ordering in the state of a Mott insulator that exists in the range of low dopant concentrations by restricting our analysis to the wide domain of existence of a "bad" metal.

0.19–0.22 that slightly exceeds the "optimal value" $x_{opt} \approx 0.15$–0.17 [1, 14]. Accordingly, we may take[8] a similar concentration dependence of our pseudogap width parameter $W(x)$. In this sense, the dependence $W(x)$ may be considered to be determined directly from experiments. The only parameter to be determined is then the concentration dependence of the seed superconducting transition temperature $T_{c0}(x)$ that would exist in the absence of pseudogap fluctuations. Its knowledge will allow the concentration behavior of the actual transition temperature $T_c(x)$ to be determined by solving the equations of our model. Unfortunately, as was pointed out in [6], the dependence $T_{c0}(x)$ is generally unknown and cannot be determined from experiments, remaining a fitting parameter of the theory.

Assuming, as was done in [13], that $T_{c0}(x)$ can be described by a linear function of x that becomes zero at $x = 0.3$ and choosing $T_{c0}(x = 0)$ to obtain the desired $T_c(x = x_{opt})$, we can calculate the form of the "observed" dependence $T_c(x)$. As an example, the results of such calculations for d-type pairing and the scattering by charge (CDW) pseudogap fluctuations [6] using a typical dependence $W(x)$ are shown in Fig. 14. We see that, even under such arbitrary assumptions, the hot spot model yields a dependence $T_c(x)$ close to the experimentally observed one. Similar calculations for the Ising model of the interaction with spin fluctuations (a constant-sign procedure for the vertex part [6]) indicate that reasonable values of $T_c(x)$ can be obtained only at nonrealistic values of $W(x)$ that are about an order of magnitude larger than the observed values.

In the BCS model for the seed temperature T_{c0} under consideration, the assumption of a noticeable concentration dependence of this parameter seems rather unrealistic.[9] Therefore, we assume that T_{c0} does not depend on the carrier concentration x at all, but take into account the fact that doping inevitably gives rise to impurity scattering (internal disorder), which can be described by the corresponding linear function $\gamma(x)$. Let us assume that this growth of disorder leads to total suppression of the d-type pairing at $x = 0.3$ in accordance with the standard Abrikosov–Gorkov dependence [11]. The phase diagram for a $La_{2-x}Sr_xCuO_4$ system calculated in our model for Heisenberg pseudogap fluctuations by taking into account the described role of impurity scattering is shown in Fig. 15. The parameters of the problem for this system used in our calculations are given in Fig. 15. The "experimental" values of $T_c(x)$ indicated in this figure (as well as in Fig. 14) by

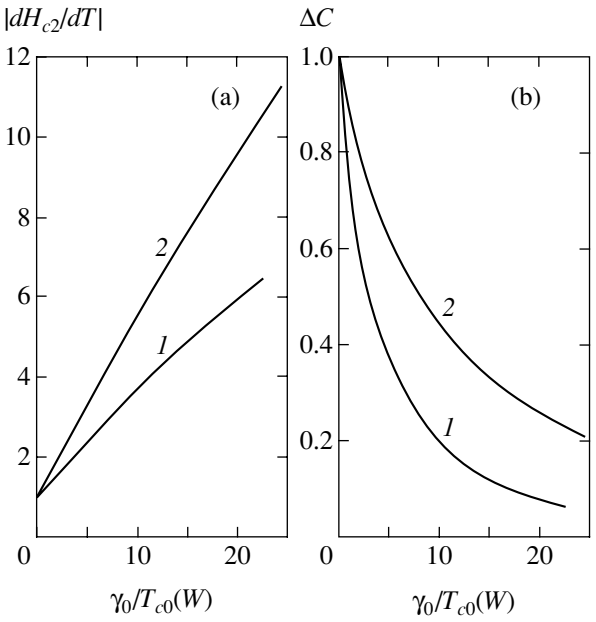

Fig. 13. Slope of the upper critical field and jump in specific heat at the transition point versus impurity scattering (disorder) frequency γ_0 for s-type pairing for two effective pseudogap widths: $W/T_{c0} = 0$ (*1*) and 15 (*2*).

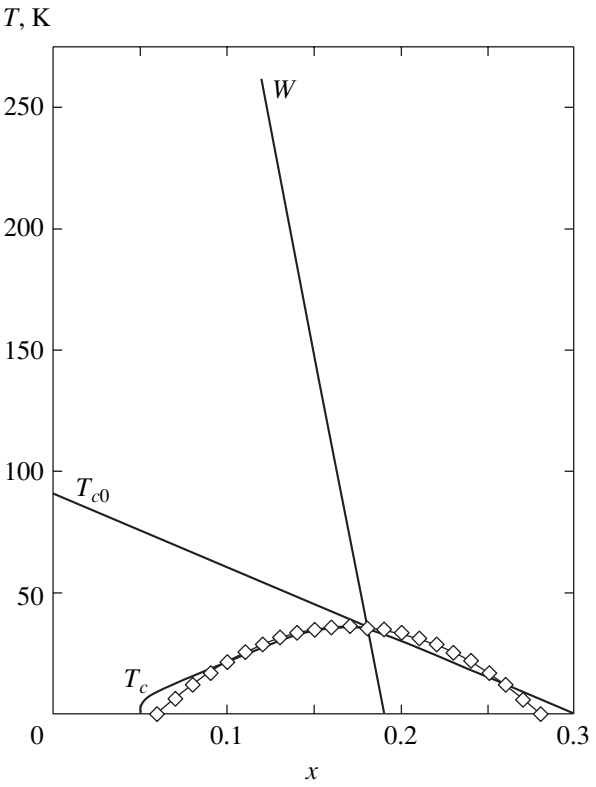

Fig. 14. Model phase diagram for the scattering by charge (CDW) pseudogap fluctuations (d-type pairing) and the seed superconducting transition temperature T_{c0} that is a linear function of the carrier concentration. The diamonds represent the "experimental" data; $W(x = 0) = 708$ K; $T_{c0}(x = 0) = 90$ K; $\kappa a = 0.2$; $T_c(x = 0.17) = 36$ K.

[8] Naturally, this identification can be made to the unknown proportionality factor of the order of unity.

[9] In this approach, the dependence $T_{c0}(x)$ may be attributable only to the corresponding relatively weak dependence of the state density at the Fermi level.

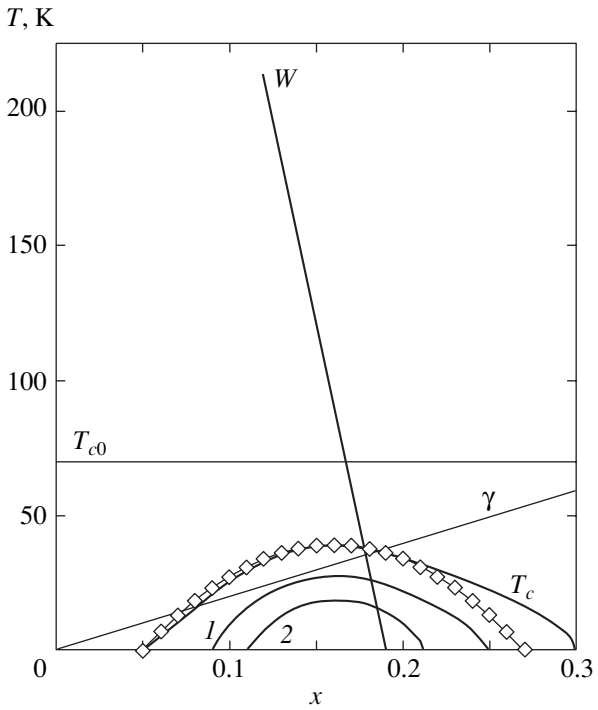

Fig. 15. Model phase diagram for the scattering by Heisenberg (SDW) pseudogap fluctuations (*d*-type pairing) and the seed superconducting transition temperature T_{c0} that does not depend on the carrier concentration with the inclusion of internal disorder $\gamma(x)$ that is linear in dopant concentration. The diamonds represent the "experimental" data; $\gamma_0 = 0.15T_{c0}$ (curve *1*), $\gamma_0 = 0.25T_{c0}$ (curve *2*); $W_m(x = 0) = 580$ K; $T_{c0} = 70$ K; $t'/t = -0.25$; $\mu/t = -0.8$; $\kappa a = 0.2$; $T_{\max}(x = 0.16) = 39$ K.

diamonds were obtained by using the empirical formula [14, 15]

$$\frac{T_c(x)}{T_c(x = x_{\text{opt}})} = 1 - 82.6(x - x_{\text{opt}})^2. \qquad (36)$$

This formula satisfactorily describes the concentration behavior of T_c for a number of HTSC cuprates. We see that our model gives an almost ideal description of the "experimental" data at reasonable values of $W(x)$ in the entire underdoped region. The description becomes poorer at the end of the overdoped region. It should be borne in mind, however, that formula (36) does not yield satisfactory results either; in addition, our superconductivity suppression model in the overdoped region is clearly very crude, and no special parameter fitting that would improve the agreement with the data in this region has been performed.

It is interesting to consider the behavior of the superconducting transition temperature T_c for additional disordering of the system for various compositions (carrier concentrations). There are many experimental works in which such disordering was achieved by doping [16, 17] or by fast neutron [18] and electron [19, 20] irradiation. The role of the additional disorder was discussed in the context of the existence of a pseudogap state only in [17].

In our model, this disordering can be simulated by introducing the additional impurity scattering parameter γ_0 that is added to the internal disorder parameter $\gamma(x)$. The calculated superconducting transition temperature for two values of this parameter is also shown in Fig. 15. We see that, in close agreement with the experiment [17], doping (disorder) causes the domain of existence of superconductivity to narrow rapidly. Also in close agreement with the conclusion drawn above from Fig. 7 and with the experimental data [17, 18], the suppression of superconductivity by disorder in the underdoped region (the pseudogap region) is much faster than that for the optimal composition. It might be expected that "normal" disorder, which clearly causes the pseudogap in the state density to slightly decrease, could lead to a certain "delay" of the decrease in T_c, but this effect is absent for *d*-type pairing.

However, the problem is that, in all cases, the decrease in T_c is faster than that implied by the standard Abrikosov–Gorkov curve for *d*-type pairing [11]. At the same time, attempts to properly process most of the experimental data on disordering in HTSC cuprates [16, 19, 20] lead to the conclusion that this decrease is actually much slower than that predicted by the Abrikosov–Gorkov dependence. This as yet unsolved problem is among the main problems in the theory of high-temperature superconductors [12]. One way to solve this problem may be associated with a consistent description of the role of disorder in superconductors located in the transition region from "loose" pairs of the BCS theory to "compact" pairs that emerge in the limit of strong coupling [21]. Another interesting possibility of explaining this delay of the decrease in T_c is related to the anisotropy of elastic impurity scattering considered in detail in [10, 22]. This effect can be included relatively easily in our calculations. It seems particularly interesting in connection with the established strong anisotropy of elastic scattering (with *d*-type symmetry) observed in ARPES experiments on a $Bi_2Sr_2CaCuO_{8+\delta}$ system [23, 24]. The corresponding scattering frequency varies over the range 20–60 meV [24], which is almost an order of magnitude higher than the maximum value of $\gamma(x)$ used in our calculations and points once again to the unusual stability of the *d*-type pairing in cuprates against static disorder. It should be noted that our model for the intrinsic-energy part of the electron actually describes a similar anisotropy of elastic scattering that corresponds to its increase near hot spots. However, no delay of the decrease in T_c was observed in our calculations.

The results show that, despite the obvious crudeness of our assumptions, the hot spot model gives a reasonable (occasionally even semiquantitative) description of the domain of existence of superconductivity on the

phase diagram for HTSC cuprates.[10] The significant uncertainty in the formation scenario for the concentration dependence of the seed superconducting transition temperature remains a major shortcoming in the approach.

7. CONCLUSIONS

Our analysis shows that the pseudogap state model based on the concept of hot spots can provide a fairly consistent description of the basic properties of the superconducting phase for HTSC cuprates and their phase diagram with a relatively small number of fitting parameters most of which can be determined from independent experiments.

It should be emphasized that our analysis was performed entirely under the standard assumption [12] about the self-averaging of the superconducting order (gap) parameter in the field of random impurities and pseudogap fluctuations. This assumption is generally justified for superconductors whose coherence length (the Cooper pair size) is much larger than other microscopic lengths in the system, such as the mean free path or the correlation length ξ of the pseudogap fluctuations. In the class of pseudogap state models under consideration, this is not necessarily the case, and significant non-self-averaging effects [25, 26] that lead to the qualitative picture of an inhomogeneous superconducting state with superconducting-phase drops existing at temperatures $T > T_c$ can arise. In principle, there are direct experimental data that confirm this picture of inhomogeneous superconductivity in HTSC cuprates [27–29]. Of course, we are far from asserting that these real experiments confirm the picture that has been theoretically developed by using simplified models in [25, 26]. Nevertheless, these results emphasize the importance of a consistent analysis of the non-self-averaging effects in relatively realistic pseudogap state models, such as the hot spot model considered above.[11]

ACKNOWLEDGMENTS

This work was supported in part by the Russian Foundation for Basic Research (project no. 02-02-16031), the Basic Research Programs of the Presidium of the Russian Academy of Sciences "Quantum Macrophysics" and the Department of Physical Sciences of the Russian Academy of Sciences "Strongly Correlated Electrons in Semiconductors, Metals, Superconductors, and Magnetic Materials," and the Project of the Ministry of Education and Science of Russia "Studies of Collective and Quantum Effects in Condensed Media."

[10] Above, we always implied hole-doped systems for which the dependence $T^*(x)$ is well established [1, 14]. The pseudogap state data for electron-doped systems are rather fragmentary.

[11] In principle, several experiments that are usually interpreted in favor of the superconducting nature of the pseudogap in HTSCs can also be understood in terms of the pattern of existence of superconducting drops.

APPENDIX

DIAGRAM COMBINATORICS IN THE MODEL OF HEISENBERG PSEUDOGAP FLUCTUATIONS

To analyze the diagram combinatorics, let us consider the limit of an infinite correlation length of spin fluctuations. In this case, the spin density by which an electron is scattered can be expressed as

$$\mathbf{S}_\mathbf{q} = \mathbf{S}\delta(\mathbf{q}-\mathbf{Q}), \tag{A.1}$$

and averaging over Gaussian spin fluctuations reduces to ordinary integration [4]:

$$\langle\ldots\rangle = \frac{g^3}{(2\pi)^{3/2}W^3}\int d\mathbf{S}\exp\left(-\frac{g^2\mathbf{S}^2}{2W^2}\right)\ldots. \tag{A.2}$$

Consequently, in this limit, we can first solve the problem of an electron in the coherent field of the spin density (A.1) and then perform averaging (A.2) over its fluctuations. For the subsequent analysis, it is convenient to introduce the fluctuating field $\boldsymbol{\delta} = (g/\sqrt{3})\mathbf{S}$, the potential by which an electron is scattered. Averaging (A.2) over the spin fluctuations then reduces to averaging over the fluctuations of this field:

$$\begin{aligned}\langle\ldots\rangle = {} & \sqrt{\frac{3}{2\pi W^2}}\int_{-\infty}^{\infty} d\delta_l \exp\left(-\frac{3\delta_l^2}{2W^2}\right)\frac{3}{2\pi W^2} \\ & \times \int_0^{2\pi} d\varphi \int_0^{\infty} d|\boldsymbol{\delta}_t||\boldsymbol{\delta}_t| \exp\left(-\frac{3|\delta_t|^2}{2W^2}\right)\ldots.\end{aligned} \tag{A.3}$$

Thus, there are two fluctuating fields by which free carriers are scattered: the real longitudinal field $\delta_l = (g/\sqrt{3})S_z$ and the complex transverse field $\boldsymbol{\delta}_t$ with amplitude $|\boldsymbol{\delta}_t|$ and phase φ that is associated with the two transverse components of the vector $\mathbf{S}$.

This averaging gives rise to a diagram technique with two types of effective interactions [4]: one is represented by the dashed line,

$$V_{\text{eff}1} = \frac{g^2}{3}\langle S_{z\mathbf{q}}S_{z-\mathbf{q}}\rangle = \pm\frac{W^2}{3}\delta(\mathbf{q}-\mathbf{Q}), \tag{A.4}$$

where the minus refers to the case of a change in spin projection under this line (e.g., when the dashed line encloses an odd number of spin flip operators S_+ and S_-); the other is represented by the wavy line,

$$V_{\text{eff}2} = \frac{g^2}{3}\langle S_{+\mathbf{q}}S_{--\mathbf{q}}\rangle = 2\frac{W^2}{3}\delta(\mathbf{q}-\mathbf{Q}). \tag{A.5}$$

The means $\langle S_+S_+\rangle$ and $\langle S_-S_-\rangle$ are equal to zero due to the phase averaging in (A.3).

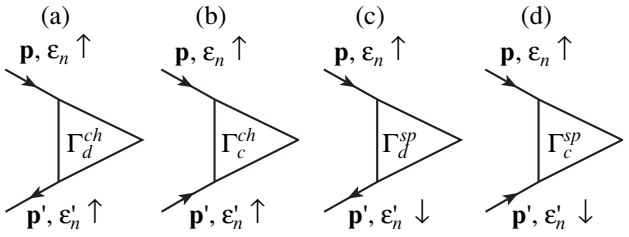

Fig. 16. Two-particles vertices with different diagram combinatorics.

Let us now solve the problem of an electron in the coherent field of the spin density (A.1). In this case, the matrix single-particle Green function has four independent components[12] that can be determined from the system of equations

$$\begin{aligned} G_{1\uparrow;\,1\uparrow} &= G_1 + G_1\delta_l G_{2\uparrow;\,1\uparrow} + G_1\delta_t G_{2\downarrow;\,1\uparrow}, \\ G_{2\uparrow;\,1\uparrow} &= G_2\delta_l G_{1\uparrow;\,1\uparrow} + G_2\delta_t G_{1\downarrow;\,1\uparrow}, \\ G_{2\downarrow;\,1\uparrow} &= -G_2\delta_l G_{1\downarrow;\,1\uparrow} + G_2\delta_t^* G_{1\uparrow;\,1\uparrow}, \\ G_{1\downarrow;\,1\uparrow} &= -G_1\delta_l G_{2\downarrow;\,1\uparrow} + G_1\delta_t^* G_{2\uparrow;\,1\uparrow}, \end{aligned} \tag{A.6}$$

where we use the short designations $(\varepsilon_n, \mathbf{p}) \longrightarrow 1$, $(\varepsilon_n, \mathbf{p} + \mathbf{Q}) \longrightarrow 2$ and

$$G_1 = \frac{1}{i\varepsilon_n - \xi_{\mathbf{p}}}, \quad G_2 = \frac{1}{i\varepsilon_n - \xi_{\mathbf{p}+\mathbf{Q}}}.$$

It thus follows that

$$\begin{aligned} G_{1\uparrow;\,1\uparrow} &= \frac{G_2^{-1}}{G_1^{-1}G_2^{-1} - |\boldsymbol{\delta}|^2}, \\ G_{2\uparrow;\,1\uparrow} &= \frac{\delta_l}{G_1^{-1}G_2^{-1} - |\boldsymbol{\delta}|^2}, \\ G_{1\downarrow;\,1\uparrow} &= 0, \quad G_{2\downarrow;\,1\uparrow} = \frac{\delta_t^*}{G_1^{-1}G_2^{-1} - |\boldsymbol{\delta}|^2}, \end{aligned} \tag{A.7}$$

where $|\boldsymbol{\delta}| = \sqrt{\delta_l^2 + |\boldsymbol{\delta}_t|^2}$ is the amplitude of the field $\boldsymbol{\delta}$.

In this case, the fluctuation-averaged single-particle Green function is

$$\begin{aligned} G = \langle G_{1\uparrow;\,1\uparrow}\rangle &= \sqrt{\frac{2}{\pi}}\left(\frac{3}{W^2}\right)^{3/2} \\ \times \int_0^\infty d|\boldsymbol{\delta}||\boldsymbol{\delta}|^2 &\exp\left(-\frac{3|\boldsymbol{\delta}|^2}{2W^2}\right)\frac{G_2^{-1}}{G_1^{-1}G_2^{-1} - |\boldsymbol{\delta}|^2}. \end{aligned} \tag{A.8}$$

[12]The components that differ from these by the change of sign of all spin projections can be obtained by the substitution $\delta_l \longrightarrow -\delta_l$ and $\delta_t \longleftrightarrow \delta_t^*$.

This integral representation can be easily written [4] as the continued fraction (1), (2) with $\kappa = 0$ and the combinatorial coefficients $s(k)$ defined by Eq. (9).

The combinatorial coefficients $r(k)$ for the two-particle vertices are slightly more difficult to determine. Four types of vertices (see Fig. 16) may be considered. For all four types of vertices, the recurrence procedure has the form (13), but the signs in the procedure and the combinatorial coefficients $r(k)$ can be different. Let us consider all vertices in the coherent field δ.

(1) The charge vertex (the spin projection is conserved at the vertex) in the diffusion channel (particle–hole), Fig. 16a:

$$\Gamma_d^{ch} = \sum_{i,\sigma} G_{1\uparrow;\,i\sigma}G_{i'\sigma;\,1'\uparrow} = \frac{(G_2G_{2'})^{-1} + |\boldsymbol{\delta}|^2}{d_\delta}, \tag{A.9}$$

where i and σ take on values of 1, 2 and $\uparrow$, $\downarrow$, and the designations $(\varepsilon_n', \mathbf{p}') \longrightarrow 1')$, $(\varepsilon_n', \mathbf{p}' + \mathbf{Q}) \longrightarrow 2')$, and $d_\delta = [(G_1G_2)^{-1} - |\boldsymbol{\delta}|^2][(G_{1'}G_{2'})^{-1} - |\boldsymbol{\delta}|^2]$ are used.

(2) The charge vertex in the Cooper channel (particle–particle),[13] Fig. 16b:

$$\Gamma_c^{ch} = \sum_{i,\sigma} G_{1\uparrow;\,i\sigma}G_{1'\uparrow;\,i'\sigma} = \frac{(G_2G_{2'})^{-1} + \delta_l^2}{d_\delta}. \tag{A.10}$$

(3) The spin vertex (the spin projection changes sign at the vertex) in the diffusion channel (particle–hole), Fig. 16c:

$$\Gamma_d^{sp} = \sum_{i,\sigma} G_{1\uparrow;\,i\sigma}G_{i'-\sigma;\,1'\downarrow} = \frac{(G_2G_{2'})^{-1} - \delta_l^2}{d_\delta}. \tag{A.11}$$

(4) The spin vertex in the Cooper channel (particle–particle), Fig. 16d:

$$\begin{aligned} \Gamma_c^{sp} &= \sum_{i,\sigma} G_{1\uparrow;\,i\sigma}G_{1'\downarrow;\,i'-\sigma} \\ &= \frac{(G_2G_{2'})^{-1} + (|\boldsymbol{\delta}_t|^2 - \delta_l^2)}{d_\delta}. \end{aligned} \tag{A.12}$$

The physical vertices can be obtained from these vertices with the coherent field δ by averaging (A.3) over the fluctuations of the corresponding field.

Thus, we see that the vertex Γ_d^{ch} is defined by Eq. (A.9), while all of the other vertices have the form[14]

$$\Gamma = \frac{(G_2G_{2'})^{-1} \pm |\boldsymbol{\delta}|^2/3}{d_\delta}, \tag{A.13}$$

[13] It emerges when the triplet pairing is described.

[14]This form is equivalent to (A.10)–(A.12) when averaged.

where the plus corresponds to the vertices Γ_c^{ch} and Γ_c^{sp}, and the minus corresponds to the vertex Γ_d^{sp}.

Obviously, $r(k) = s(k)$ for the vertex Γ_d^{ch}. Indeed, the expansion for the physical vertex $\langle \Gamma_d^{ch} \rangle$ can be obtained by inserting the corresponding free vertex in all the electron lines of an arbitrary diagram for the single-particle Green function. Inserting this vertex changes neither the direction of the electron line nor the spin projection; accordingly, the diagram combinatorics does not change either.

In the limit of an infinite correlation length, any skeleton diagram for the vertex differs from the ladder diagram of the same order with the interaction $(W^2/3)\delta(\mathbf{q} - \mathbf{Q})$ only by the sign and the factor 2^p, where p is the number of wavy lines. Thus, the sum of all skeleton diagrams of a given order may be replaced with the corresponding ladder diagram with the interaction $(W^2/3)\delta(\mathbf{q} - \mathbf{Q})$ multiplied by the combinatorial factor, which we call the number of skeleton diagrams of a given order.

The first term in Eqs. (A.9)–(A.12) is the same for all vertices and generates the numbers of skeleton diagrams of even (in W^2) order when averaged (since this term corresponds to the terms with $i = 1$ in these equations). Thus, the numbers of skeleton diagrams of even order are the same for all four vertices. The second term in these equations generates the numbers of diagrams of odd order (it corresponds to the terms with $i = 2$). Consequently, the numbers of skeleton diagrams of odd order for all three vertices defined by (A.13) are $\pm 1/3$ of the corresponding numbers of for the vertex Γ_d^{ch}. The minus corresponding to the vertex Γ_d^{sp} can be offset by changing the sign in the recurrence procedure for this vertex. Consequently, the sign of the second term in (A.13) determines the sign in the recurrence procedure (13) for these vertices, and the combinatorial coefficients $r(k)$ are the same for these three vertices.

The number of skeleton diagrams of order L is[15]

$$3^L \prod_{1 \le k \le L} r(k). \qquad \text{(A.14)}$$

Thus, we obtain

$$\prod_{1 \le k \le 2n} r(k) = \prod_{1 \le k \le 2n} s(k) \qquad \text{(A.15)}$$

for even $L = 2n + 1$ and

$$\prod_{1 \le k \le 2n+1} r(k) = \frac{1}{3} \prod_{1 \le k \le 2n+1} s(k) \qquad \text{(A.16)}$$

for odd $L = 2n + 1$; whence, given (9), follows (14).

In this paper, we were mainly interested in the vertex Γ_c^{sp}. The above analysis shows that a constant-sign procedure emerges for this vertex for the case of *s*-type paring where the symmetry factor $e(\mathbf{p})$, which must appear in the vertex, is equal to unity. In contrast, in the case of *d*-type paring where the superconducting gap when switching over to $\mathbf{Q}$ changes sign (i.e., $e(\mathbf{p}) = -e(\mathbf{p} + \mathbf{Q})$), the sign of the recurrence procedure must be reversed [6], and the procedure becomes an alternating one. For the Ising spin fluctuations considered in [6], the situation with the sign of the recurrence procedure for the vertex is reverse. This somewhat surprising result can be easily understood from Eq. (A.12) for the vertex Γ_c^{sp}. The two transverse components (i.e., the field δ_t) vanish in the Ising model, causing the sign of the second term in (A.12) and, hence, in the recurrence procedure to change.

[15] The factor 3^L emerges, because the recurrence procedure (13) and the combinatorial coefficients $r(k)$ correspond to the expansion in a power series of W^2, while the number of skeleton diagrams was determined for the expansion in a power series of $W^2/3$.

REFERENCES

1. J. L. Tallon and J. W. Loram, Physica C (Amsterdam) **349**, 53 (2000).
2. M. V. Sadovski , Usp. Fiz. Nauk **171**, 539 (2001) [Phys. Usp. **44**, 515 (2001)].
3. D. Pines, cond-mat/0404151.
4. J. Schmalian, D. Pines, and B. Stojkovic, Phys. Rev. B **60**, 667 (1999).
5. É. Z. Kuchinski and M. V. Sadovski , Zh. Éksp. Teor. Fiz. **115**, 1765 (1999) [JETP **88**, 968 (1999)].
6. É. Z. Kuchinski , M. V. Sadovski , and N. A. Strigina, Zh. Éksp. Teor. Fiz. **125**, 854 (2004) [JETP **98**, 748 (2004)].
7. N. A. Kuleeva and É. Z. Kuchinski , Fiz. Tverd. Tela (St. Petersburg) **46**, 1557 (2004) [Phys. Solid State **46**, 1604 (2004)].
8. M. V. Sadovski and N. A. Strigina, Zh. Éksp. Teor. Fiz. **122**, 610 (2002) [JETP **95**, 526 (2002)].
9. A. A. Abrikosov, L. P. Gor'kov, and I. E. Dzyaloshinski , *Methods of Quantum Field Theory in Statistical Physics* (Fizmatgiz, Moscow, 1962; Prentice Hall, Englewood Cliffs, N.J., 1963).
10. A. I. Posazhennikova and M. V. Sadovski , Pis'ma Zh. Éksp. Teor. Fiz. **63**, 347 (1996) [JETP Lett. **63**, 358 (1996)]; Zh. Éksp. Teor. Fiz. **112**, 2124 (1997) [JETP **85**, 1162 (1997)].
11. R. J. Radtke, K. Levin, H.-B. Schüttler, and M. R. Norman, Phys. Rev. B **48**, 653 (1993).
12. M. V. Sadovskii, *Superconductivity and Localization* (World Sci., Singapore, 2000).
13. A. Posazhennikova and P. Coleman, Phys. Rev. B **67**, 165109 (2003).

14. S. H. Naqib, J. R. Cooper, J. L. Tallon, *et al.*, cond-mat/0312443.
15. M. R. Presland, J. L. Tallon, R. G. Buckley, *et al.*, Physica C (Amsterdam) **176**, 95 (1991).
16. Y. Fukuzumi, K. Mizuhashi, K. Takenaka, and S. Uchida, Phys. Rev. Lett. **76**, 684 (1996).
17. J. L. Tallon, C. Bernhard, G. V. M. Williams, and J. W. Loram, Phys. Rev. Lett. **79**, 5294 (1997).
18. A. E. Kar'kin, S. A. Davydov, B. N. Goshchitski , *et al.*, Fiz. Met. Metalloved. **76**, 103 (1993).
19. S. K. Tolpygo, J.-Y. Lin, M. Gurvitch, *et al.*, Phys. Rev. B **53**, 12454 (1996); **53**, 12462 (1996).
20. F. Rullier-Albenque, H. Alloul, and R. Tourbot, Phys. Rev. Lett. **91**, 047001 (2003).
21. A. I. Posazhennikova and M. V. Sadovski , Pis'ma Zh. Éksp. Teor. Fiz. **65**, 258 (1997) [JETP Lett. **65**, 270 (1997)].
22. G. Haran and A. D. S. Nagy, Phys. Rev. B **54**, 15463 (1996).
23. T. Valla, A. V. Fedorov, P. D. Johnson, *et al.*, Phys. Rev. Lett. **85**, 828 (2000).
24. A. Kaminski, H. M. Fretwell, M. R. Norman, *et al.*, cond-mat/0404385.
25. É. Z. Kuchinski and M. V. Sadovski , Zh. Éksp. Teor. Fiz. **117**, 613 (2000) [JETP **90**, 535 (2000)].
26. É. Z. Kuchinski and M. V. Sadovski , Zh. Éksp. Teor. Fiz. **121**, 758 (2002) [JETP **94**, 654 (2002)].
27. S. H. Pan, J. P. O'Neil, R. L. Badzey, *et al.*, Nature **413**, 282 (2001).
28. K. McElroy, D.-H. Lee, J. E. Hoffman, *et al.*, cond-mat/0404005.
29. A. Fang, C. Howald, N. Kanenko, *et al.*, cond-mat/0404452.

Translated by V. Astakhov

JETP Letters, Vol. 82, No. 4, 2005, pp. 198–203. From Pis'ma v Zhurnal Éksperimental'noĭ i Teoreticheskoĭ Fiziki, Vol. 82, No. 4, 2005, pp. 217–222.

Destruction of the Fermi Surface Due to Pseudogap Fluctuations in Strongly Correlated Systems¶

E. Z. Kuchinskii, I. A. Nekrasov, and M. V. Sadovskii*

Institute of Electrophysics, Russian Academy of Sciences, Ural Division, Yekaterinburg, 620016 Russia

** e-mail: sadovski@iep.uran.ru*

Received June 9, 2005

We generalize the dynamical-mean field theory (DMFT) by including into the DMFT equations dependence on the correlation length of the pseudogap fluctuations via the additional (momentum dependent) self-energy $\Sigma_{\mathbf{k}}$. This self-energy describes nonlocal dynamical correlations induced by short-ranged collective SDW-like antiferromagnetic spin (or CDW-like charge) fluctuations. At high enough temperatures, these fluctuations can be viewed as a quenched Gaussian random field with finite correlation length. This generalized DMFT + $\Sigma_{\mathbf{k}}$ approach is used for the numerical solution of the weakly doped one-band Hubbard model with repulsive Coulomb interaction on a square lattice with nearest and next nearest neighbor hopping. The effective single impurity problem is solved by using a numerical renormalization group (NRG). Both types of strongly correlated metals, namely, (i) doped Mott insulator and (ii) the case of the bandwidth $W \lesssim U$ (U—value of local Coulomb interaction) are considered. By calculating profiles of the spectral densities for different parameters of the model, we demonstrate the qualitative picture of Fermi surface destruction and formation of Fermi arcs due to pseudogap fluctuations in qualitative agreement with the ARPES experiments. Blurring of the Fermi surface is enhanced with the growth of the Coulomb interaction. © *2005 Pleiades Publishing, Inc.*

PACS numbers: 71.10.Fd, 71.10.Hf, 71.27.+a, 71.30.+h, 74.72.–h

The pseudogap formation in the electronic spectrum of underdoped copper oxides [1, 2] is an especially striking anomaly of the normal state of high temperature superconductors. Despite continuing discussions on the nature of the pseudogap, we believe that the preferable scenario for its formation is most likely based on the model of strong scattering of the charge carriers by short-ranged antiferromagnetic (AFM, SDW) spin fluctuations [2, 3]. In momentum representation, this scattering transfers momenta of the order of $\mathbf{Q} = (\pi/a, \pi/a)$ (a—lattice constant of a two dimensional lattice). This leads to the formation of structures in the one-particle spectrum that are precursors of the changes in the spectra due to long-range AFM order (period doubling). As a result, we obtain non-Fermi liquidlike behavior (dielectrization) of the spectral density in the vicinity of the so-called hot spots on the Fermi surface appearing at intersections of the Fermi surface with the antiferromagnetic Brillouin zone boundary [2].

Within this spin-fluctuation scenario, a simplified model of the pseudogap state was studied [2, 4, 5] under the assumption that the scattering by dynamic spin fluctuations can be reduced for high enough temperatures to a static Gaussian random field (quenched disorder) of pseudogap fluctuations. These fluctuations are characterized by a scattering vector from the vicinity of $\mathbf{Q}$ with a width determined by the inverse correlation length of short-range order $\kappa = \xi^{-1}$ and by the appropriate energy scale Δ (typically of the order of the crossover temperature T^* to the pseudogap state [2]).

Undoped cuprates are antiferromagnetic Mott insulators with $U \gg W$ (U—value of the local Coulomb interaction, W—bandwidth of the noninteracting band), so that correlation effects are actually very important. It is thus clear that the electronic properties of underdoped (and, probably, also of optimally doped) cuprates are governed by strong electronic correlations too, so that these systems are typical strongly correlated metals. Two types of correlated metals can be distinguished: (i) the doped Mott insulator and (ii) the bandwidth controlled correlated metal $W \approx U$.

A state of the art tool to describe such correlated systems is the dynamical mean-field theory (DMFT) [6–10]. The characteristic features of correlated systems within the DMFT are the formation of incoherent structures (the so-called Hubbard bands) split by the Coulomb interaction U, and a quasiparticle (conduction) band near the Fermi level dynamically generated by the local correlations [6–10].

Unfortunately, the DMFT is not useful for the study of the antiferromagnetic scenario of pseudogap formation in strongly correlated metals. This is due to the basic approximation of the DMFT, which amounts to the complete neglect of nonlocal dynamical correlation effects [6–10]. As a result, within the standard DMFT approach, the Fermi surface of a quasiparticle band is not renormalized by interactions and just coincides

¶ The text was submitted by the authors in English.

with that of the bare quasiparticles [7]. Recently, we have formulated a semiphenomenological DMFT + $\Sigma_{\mathbf{k}}$ approach [11] allowing the introduction of a length scale (nonlocal correlations) into DMFT. Below, we present the basic points of this approach with application to the Fermi surface renormalization due to pseudogap fluctuations.

To include nonlocal effects while remaining within the usual impurity analogy of DMFT, we propose the following procedure. To be definite, let us consider a standard one-band Hubbard model. The major assumption of our approach is that the lattice and Matsubara time Fourier transform of the single-particle Green's function can be written as

$$G_{\mathbf{k}}(\omega) = \frac{1}{i\omega + \propto - \varepsilon(\mathbf{k}) - \Sigma(\omega) - \Sigma_{\mathbf{k}}(\omega)}, \quad (1)$$

where $\Sigma(\omega)$ is the local contribution to self-energy surviving in the DMFT ($\omega = \pi T(2n + 1)$), while $\Sigma_{\mathbf{k}}(\omega)$ is some momentum dependent part. We suppose that this last contribution is due to either electron interactions with some additional collective modes, order parameter fluctuations, or may be due to similar nonlocal contributions within the Hubbard model itself. To avoid possible confusion, we must stress that $\Sigma_{\mathbf{k}}(i\omega)$ can also contain a local (momentum independent) contribution that obviously vanishes in the limit of infinite dimensionality $d \longrightarrow \infty$ and is not taken into account within the standard DMFT. Due to this fact, there is no double counting problem within our approach for the Hubbard model. It is important to stress that the assumed additive form of self-energy $\Sigma(\omega) + \Sigma_{\mathbf{k}}(\omega)$ implicitly corresponds to the neglect of possible interference from these local (DMFT) and nonlocal contributions.

The self-consistency equations of our generalized DMFT + $\Sigma_{\mathbf{k}}$ approach are formulated as follows [11]:

(1) Start with some initial guess of the local self-energy $\Sigma(\omega)$; e.g., $\Sigma(\omega) = 0$.

(2) Construct $\Sigma_{\mathbf{k}}(\omega)$ within some (approximate) scheme taking into account the interactions with collective modes or order parameter fluctuations that in general can depend on $\Sigma(\omega)$ and $\propto$.

(3) Calculate the local Green's function

$$G_{ii}(\omega) = \frac{1}{N}\sum_{\mathbf{k}} \frac{1}{i\omega + \propto - \varepsilon(\mathbf{k}) - \Sigma(\omega) - \Sigma_{\mathbf{k}}(\omega)}. \quad (2)$$

(4) Define the Weiss field

$$\mathcal{G}_0^{-1}(\omega) = \Sigma(\omega) + G_{ii}^{-1}(\omega). \quad (3)$$

(5) Using some impurity solver to calculate the single-particle Green's function for the effective Anderson impurity problem defined by Grassmann integral

$$G_d(\tau - \tau') = \frac{1}{Z_{\text{eff}}}\int Dc_{i\sigma}^{+} Dc_{i\sigma} c_{i\sigma}(\tau) c_{i\sigma}^{+}(\tau') \exp(-S_{\text{eff}}), \quad (4)$$

with effective action for a fixed (impurity) i

$$S_{\text{eff}} = -\int_0^\beta d\tau_1 \int_0^\beta d\tau_2 c_{i\sigma}(\tau_1)\mathcal{G}_0^{-1}(\tau_1 - \tau_2) c_{i\sigma}^{+}(\tau_2) + \int_0^\beta d\tau U n_{i\uparrow}(\tau) n_{i\downarrow}(\tau), \quad (5)$$

$Z_{\text{eff}} = \int Dc_{i\sigma}^{+} Dc_{i\sigma} \exp(-S_{\text{eff}})$, and $\beta = T^{-1}$. This step produces a new set of values $G_d^{-1}(\omega)$.

(6) Define a new local self-energy

$$\Sigma(\omega) = \mathcal{G}_0^{-1}(\omega) - G_d^{-1}(\omega). \quad (6)$$

(7) Using this self-energy as the initial one in step 1, continue the procedure until (and if) convergency is reached to obtain

$$G_{ii}(\omega) = G_d(\omega). \quad (7)$$

Eventually, we get the desired Green's function in the form of (1), where $\Sigma(\omega)$ and $\Sigma_{\mathbf{k}}(\omega)$ are those appearing at the end of our iteration procedure.

For the momentum dependent part of the single-particle self-energy, we concentrate on the effects of scattering of electrons from collective short-range SDW-like antiferromagnetic spin (or CDW-like charge) fluctuations. To calculate $\Sigma_{\mathbf{k}}(\omega)$ for an electron moving in the quenched random field of (static) Gaussian spin (or charge) fluctuations with dominant scattering momentum transfers from the vicinity of some characteristic vector $\mathbf{Q}$ (the hot spots model [2]), we use the following recursion procedure proposed in [12, 4, 5], which takes into account all the Feynman diagrams describing the scattering of electrons by this random field:

$$\Sigma_{\mathbf{k}}(\omega) = \Sigma_{n=1}(\omega\mathbf{k}), \quad (8)$$

with

$$\Sigma_n(\omega\mathbf{k}) = \Delta^2 \frac{s(n)}{i\omega + \propto - \Sigma(\omega) - \varepsilon_n(\mathbf{k}) + in v_n \kappa - \Sigma_{n+1}(\omega\mathbf{k})}. \quad (9)$$

The quantity Δ characterizes the energy scale, and $\kappa = \xi^{-1}$ is the inverse correlation length of short range SDW (CDW) fluctuations; $\varepsilon_n(\mathbf{k}) = \varepsilon(\mathbf{k} + \mathbf{Q})$ and $v_n = |v_{\mathbf{k}+\mathbf{Q}}^x| + |v_{\mathbf{k}+\mathbf{Q}}^y|$ for odd n, while $\varepsilon_n(\mathbf{k}) = \varepsilon(\mathbf{k})$ and $v_n = |v_{\mathbf{k}}^x| + |v_{\mathbf{k}}^y|$ for even n. The velocity projections $v_{\mathbf{k}}^x$ and $v_{\mathbf{k}}^y$ are determined by the usual momentum derivatives of the bare electronic energy dispersion $\varepsilon(\mathbf{k})$. Finally, $s(n)$ represents a combinatorial factor with

$$s(n) = n \quad (10)$$

for the case of commensurate charge (CDW type) fluctuations with $\mathbf{Q} = (\pi/a, \pi/a)$ [12]. For incommensurate CDW fluctuations [12], one finds

$$s(n) = \begin{cases} \dfrac{n+1}{2} & \text{for odd } n \\ \dfrac{n}{2} & \text{for even } n. \end{cases} \quad (11)$$

If we take into account the (Heisenberg) spin structure of the interaction with spin fluctuations in nearly antiferromagnetic Fermi liquid (the spin-fermion (SF) model [4]), the combinatorics of the diagrams becomes more complicated and the factor $s(n)$ acquires the following form [4]:

$$s(n) = \begin{cases} \dfrac{n+2}{3} & \text{for odd } n \\ \dfrac{n}{3} & \text{for even } n. \end{cases} \quad (12)$$

Obviously, with this procedure, we introduce an important length scale ξ not present in standard DMFT. Physically, this scale mimics the effect of the short-range (SDW or CDW) correlations within the fermionic bath surrounding the effective Anderson impurity. Both the parameters Δ and ξ can, in principle, be calculated from the microscopic model at hand [11].

In the following, we will consider both Δ and especially ξ as some phenomenological parameters to be determined from experiments. This makes our approach somehow similar in spirit to the Landau approach to Fermi liquids.

In the following, we discuss a standard one-band Hubbard model on a square lattice. With the nearest (t) and next nearest (t') neighbor hopping integrals, the bare dispersion then reads

$$\varepsilon(\mathbf{k}) = -2t(\cos k_x a + \cos k_y a) - 4t' \cos k_x a \cos k_y a, \quad (13)$$

where a is the lattice constant. The correlations are introduced by a repulsive, local two-particle interaction U. We choose as the energy scale the nearest neighbor hopping integral t and as the length scale the lattice constant a. All the energies below are given in units of t.

For a square lattice, the bare bandwidth is $W = 8t$. To study a strongly correlated metallic state obtained as a doped Mott insulator, we use $U = 40t$ as the value for the Coulomb interaction and a filling $n = 0.8$ (hole doping). The correlated metal in the case of $W \gtrsim U$ is considered for the case of $U = 4t$ and the filling factor $n = 0.8$ (hole doping). For Δ, we choose rather typical values between $\Delta = 0.1t$ and $\Delta = 2t$ (actually, the approximate limiting values obtained in [11]), and, for the correlation length, we took $\xi = 10a$ (being motivated mainly by the experimental data for cuprates [2, 4]).

The DMFT maps the lattice problem onto an effective, self-consistent impurity defined by Eqs. (4), (5). In our work, we employed as an impurity solver the reliable method of a numerical renormalization group (NRG) [13, 14].

As already discussed in the Introduction, the characteristic feature of the strongly correlated metallic state is the coexistence of lower and upper Hubbard bands split by the value of U with a quasiparticle peak at the Fermi level.

Once we get a self-consistent solution of the DMFT + $\Sigma_{\mathbf{k}}$ equations with nonlocal fluctuations, we can compute the spectral functions $A(\omega, \mathbf{k})$ for real ω:

$$A(\omega, \mathbf{k}) = -\frac{1}{\pi}\mathrm{Im}\frac{1}{\omega + \propto - \varepsilon(\mathbf{k}) - \Sigma(\omega) - \Sigma_{\mathbf{k}}(\omega)}, \quad (14)$$

where the self-energy $\Sigma(\omega)$ and chemical potential $\propto$ are calculated self-consistently. The densities of states can be calculated by integrating (14) over the Brillouin zone.

Extensive calculations of the densities of states, spectral densities, and ARPES spectra for this model were performed in [11]. In the general case, a pseudogap appears in the density of states within the quasiparticle peak (correlated conduction band). The qualitative behavior of the pseudogap anomalies is similar to those for the case of $U = 0$ [2, 5]; e.g., a decrease of ξ makes the pseudogap less pronounced, while reducing Δ narrows the pseudogap and also makes it more shallow. For the doped Mott insulator, we find that the pseudogap is remarkably more pronounced for the SDW-like fluctuations than for the CDW-like fluctuations. Thus, below, we present mainly the results obtained using combinatorics (12) of the spin-fermion model.

As was noted above, within the standard DMFT approach, the Fermi surface is not renormalized by interactions and just coincides with that of the bare quasiparticles [7]. However, in the case of the nontrivial momentum dependence of the electron self-energy, important renormalization of the Fermi surface appears due to pseudogap formation [4]. There are a number of ways to define a Fermi surface in a strongly correlated system with pseudogap fluctuations. In the following, we use intensity plots (within the Brillouin zone) of the spectral density (14) taken at $\omega = 0$. These are readily measured by ARPES, and the appropriate peak positions define the Fermi surface in the usual Fermi liquid with ease.

In Figs. 1a–1c, we show such plots for the case of uncorrelated metal ($U = 0$) with pseudogap fluctuations obtained directly from the Green's function defined by the recursion procedure (8), (9). For comparison, in Fig. 1d, we show renormalized Fermi surfaces obtained for this model using a rather natural definition of the Fermi surface as defined by the solution of the equation

$$\omega - \varepsilon(\mathbf{k}) + \propto - \mathrm{Re}\Sigma(\omega) - \mathrm{Re}\Sigma_{\mathbf{k}}(\omega) = 0 \quad (15)$$

for $\omega = 0$, which was used, e.g., in [4]. It is seen that this last definition produces Fermi surfaces close to those defined by the intensity plots of the spectral density

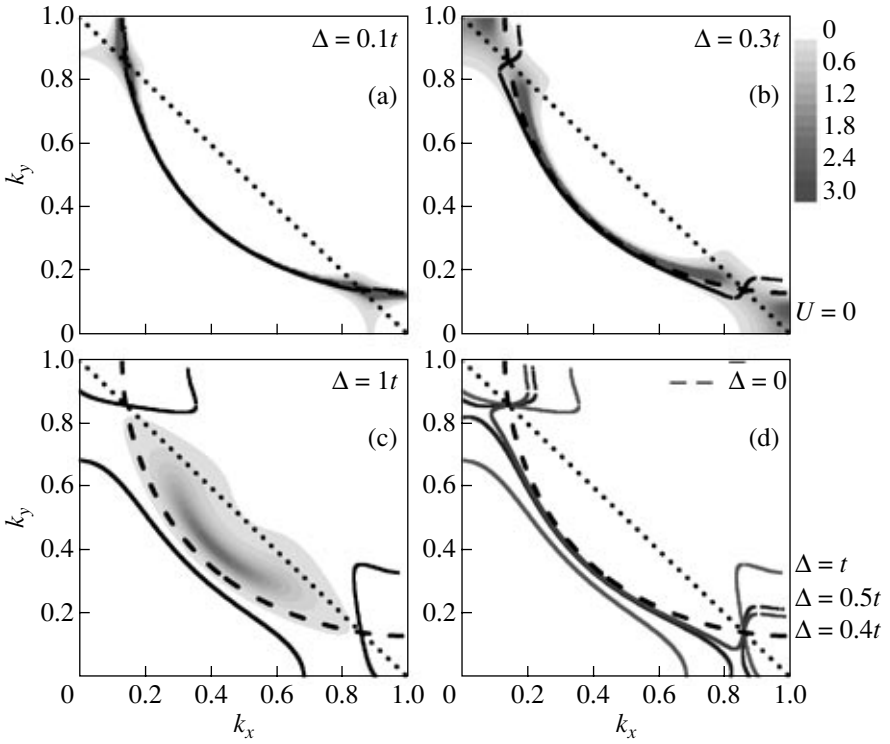

Fig. 1. Fermi surfaces obtained for the uncorrelated case of $U = 0$ and the filling factor $n = 0.8$. Shown are intensity plots of the spectral density (14) for $\omega = 0$. $\Delta =$ (a) $0.1t$; (b) $0.3t$; (c) t; (d) Fermi surfaces obtained solving Eq. (15). The dashed line denotes a bare Fermi surface.

only for small values of Δ, while, for larger values, we can see a rather unexpected topological transition. At the same time, the spectral density intensity plots clearly demonstrate destruction of the Fermi surface in the vicinity of the hot spots with Fermi arcs forming with the growth of Δ similar to those seen in the pioneering ARPES experiments of Norman *et al.* [15] and confirmed later in numerous works.

In Fig. 2, we show our results for the case of correlated metal with $U = 4t$, and, in Fig. 3, for the doped Mott insulator with $U = 40t$. Again, we see the qualitative behavior clearly demonstrating the destruction of the well defined Fermi surface in the strongly correlated metal with the growth of the pseudogap amplitude Δ. The role of finite U reduces to a lower intensity of spectral density in comparison with the case of $U = 0$ and leads to additional blurring, thus, making the hot spots less visible. Again, the destruction of the Fermi surface starts in the vicinity of the hot spots for small values of Δ, but, almost immediately, it disappears in the whole antinodal region of the Brillouin zone, while only Fermi arcs remain in the nodal region very close to the bare Fermi surface. These results give a natural explanation for the observed behavior and also for the fact that the existence of regions of hot spots was observed only in some rare cases [16].

For the case of the doped Mott insulator ($U = 40t$) shown in Fig. 3, we see that the Fermi surface is rather poorly defined for all the values of Δ, as the spectral density profiles are much more blurred than in the case of smaller values of U, thus, reflecting the important role of correlations.

It is interesting to note that, from Figs. 2 and 3, it is clearly seen that the natural definition of the Fermi surface from Eq. (15) is quite inadequate for correlated systems with finite U and nonlocal interactions (pseudogap fluctuations), thus, signifying the increased role of strong correlations.

To summarize, we propose a generalized DMFT + $\Sigma_{\mathbf{k}}$ approach that is meant to take into account the important effects due to nonlocal correlations in a systematic but, to some extent, phenomenological fashion. The main idea of this extension is to stay within the usual effective Anderson impurity analogy and introduce length scale dependence due to nonlocal correlation via the effective medium (bath) appearing in the standard DMFT. This becomes possible by incorporating scattering processes of fermions in the bath from nonlocal collective SDW-like antiferromagnetic spin (or CDW-like charge) fluctuations. Such a generalization of the DMFT allows one to overcome the well-known shortcoming of the **k** independence of the self-energy of the standard DMFT. It, in turn, opens the possibility to access the physics of low-dimensional strongly correlated systems where different types of spatial fluctuations (e.g., of some order parameter)

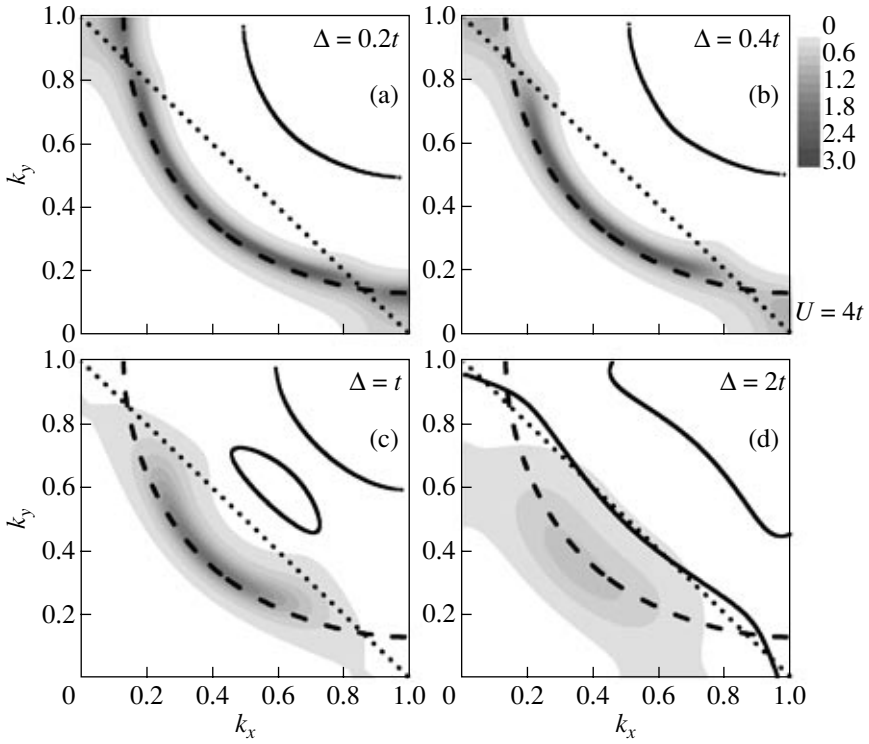

Fig. 2. Destruction of the Fermi surface as obtained from the DMFT + $\Sigma_{\mathbf{k}}$ calculations for $U = 4t$ and $n = 0.8$. The notations are the same as used in Fig. 1. Δ = (a) $0.2t$; (b) $0.4t$; (c) t; (d) $2t$. Black lines show the solution of Eq. (15).

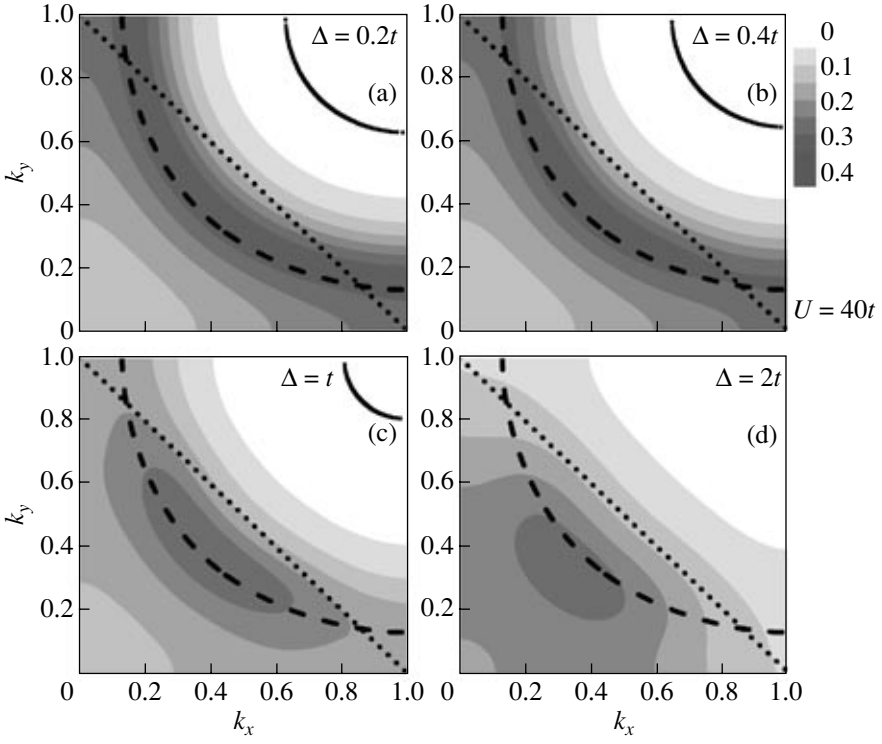

Fig. 3. Fermi surfaces obtained from the DMFT + $\Sigma_{\mathbf{k}}$ calculations for $U = 40t$ and $n = 0.8$. The other parameters and notations are the same as in Fig. 2.

become important in a nonperturbative way (at least with respect to the important local dynamical correlations). However, we must stress that our procedure in no way introduces any kind of systematic $1/d$ expansion, being only a qualitative method to include a length scale into DMFT.

In our present study, we addressed the problem of the Fermi surface renormalization (destruction) by pseudogap fluctuations in the strongly correlated metallic state. Our generalization of DMFT leads to nontrivial and, in our opinion, physically sensible **k** dependence of spectral functions, thus, leading to Fermi surface renormalization quite similar to that observed in ARPES experiments.

Similar results were obtained in recent years using the cluster mean-field theories [17]. The major advantage of our approach over these cluster mean-field theories is that we stay in an effective single-impurity representation. This means that our approach is computationally much less costly and therefore easily generalizable for the description of additional interactions.

We are grateful to Th. Pruschke for providing us with his NRG code and helpful discussions. This work was supported in part by the Russian Foundation for Basic Research (project nos. 05-02-16301, 05-02-17244); the program of the Presidium of the Russian Academy of Sciences (RAS) "Quantum Macrophysics"; and the program of the Division of Physical Sciences of the RAS "Strongly Correlated Electrons in Semiconductors, Metals, Superconductors, and Magnetic Materials." I.N. acknowledges support from the Dynasty Foundation, the International Centre for Fundamental Physics in Moscow "Program for Young Scientists 2005," and the Russian Science Support Foundation "Program for Young Candidates of the Russian Academy of Sciences 2005."

REFERENCES

1. T. Timusk and B. Statt, Rep. Prog. Phys. **62**, 61 (1999).
2. M. V. Sadovskii, Usp. Fiz. Nauk **171**, 539 (2001) [Phys. Usp. **44**, 515 (2001)].
3. D. Pines, cond-mat/0404151.
4. J. Schmalian, D. Pines, and B. Stojkovic, Phys. Rev. B **60**, 667 (1999).
5. E. Z. Kuchinskii and M. V. Sadovskii, Zh. Éksp. Teor. Fiz. **115**, 1765 (1999) [JETP **88**, 347 (1999)].
6. W. Metzner and D. Vollhardt, Phys. Rev. Lett. **62**, 324 (1989).
7. D. Vollhardt, in *Correlated Electron Systems*, Ed. by V. J. Emery (World Sci., Singapore, 1993), p. 57.
8. Th. Pruschke, M. Jarrell, and J. K. Freericks, Adv. Phys. **44**, 187 (1995).
9. A. Georges, G. Kotliar, W. Krauth, and M. J. Rozenberg, Rev. Mod. Phys. **68**, 13 (1996).
10. G. Kotliar and D. Vollhardt, Phys. Today **57** (3), 53 (2004).
11. M. V. Sadovskii, I. A. Nekrasov, E. Z. Kuchinskii, *et al.*, cond-mat/0502612.
12. M. V. Sadovskii, Zh. Éksp. Teor. Fiz. **77**, 2070 (1979) [Sov. Phys. JETP **50**, 989 (1979)].
13. K. G. Wilson, Rev. Mod. Phys. **47**, 773 (1975); H. R. Krishna-murthy, J. W. Wilkins, and K. G. Wilson, Phys. Rev. B **21**, 1003 (1980); Phys. Rev. B **21**, 1044 (1980); A. C. Hewson, *The Kondo Problem to Heavy Fermions* (Cambridge Univ. Press, Cambridge, 1993).
14. R. Bulla, A. C. Hewson, and Th. Pruschke, J. Phys.: Condens. Matter **10**, 8365 (1998); R. Bulla, Phys. Rev. Lett. **83**, 136 (1999).
15. M. R. Norman, M. Randeria, J. C. Campuzano, *et al.*, Nature **382**, 51 (1996).
16. N. P. Armitage, D. H. Lu, C. Kim, *et al.*, Phys. Rev. Lett. **87**, 147003 (2001).
17. Th. Maier, M. Jarrell, Th. Pruschke, and M. Hettler, Rev. Mod. Phys. (in press); cond-mat/0404055.

Pseudogaps in strongly correlated metals: A generalized dynamical mean-field theory approach

M. V. Sadovskii,[1] I. A. Nekrasov,[1,2] E. Z. Kuchinskii,[1] Th. Pruschke,[3] and V. I. Anisimov[2]
[1]*Institute for Electrophysics, Russian Academy of Sciences, Ekaterinburg, 620016, Russia*
[2]*Institute for Metal Physics, Russian Academy of Sciences, Ekaterinburg, 620219, Russia*
[3]*Institut für Theoretische Physik, Universität Göttingen, Germany*
(Received 4 March 2005; revised manuscript received 20 June 2005; published 6 October 2005)

We generalize the dynamical-mean field (DMFT) approximation by including into the DMFT equations some length scale ξ via a momentum dependent external self-energy $\Sigma_{\mathbf{k}}$. This external self-energy describes nonlocal dynamical correlations induced by the short-ranged collective spin density wave–like antiferromagnetic spin (or the charge density wave–like charge) fluctuations. At high enough temperatures these fluctuations can be viewed as a quenched Gaussian random field with a finite correlation length. This generalized DMFT+$\Sigma_{\mathbf{k}}$ approach is used for the numerical solution of the weakly doped one-band Hubbard model with repulsive Coulomb interaction on a square lattice with the nearest and the next nearest neighbor hopping. The effective single impurity problem in this generalized DMFT+$\Sigma_{\mathbf{k}}$ is solved by the numerical renormalization group. Both types of the strongly correlated metals, namely: (i) The doped Mott insulator and (ii) the case of the bandwidth $W \lesssim U$ (U—value of the local Coulomb interaction) are considered. The densities of states, the spectral functions, and the angle resolved photoemission spectra calculated within the DMFT+$\Sigma_{\mathbf{k}}$ show a pseudogap formation near the Fermi level of the quasiparticle band.

DOI: 10.1103/PhysRevB.72.155105 PACS number(s): 71.10.Fd, 71.10.Hf, 71.27.+a, 71.30.+h

I. INTRODUCTION

Among the numerous anomalies of the normal phase of high-temperature superconductors the observation of a pseudogap in the electronic spectrum of underdoped copper oxides[1,2] is especially interesting. Despite continuing discussions on the nature of the pseudogap, the preferable scenario for its formation is most likely based on the model of strong scattering of the charge carriers by a short-ranged antiferromagnetic (AFM) or spin density wave (SDW) spin fluctuations.[2,3] In a momentum representation, this scattering transfers momenta of the order of $\mathbf{Q}=(\pi/a,\pi/a)$ (a—lattice constant of a two-dimensional lattice). This leads to the formation of structures in the one-particle spectrum, which are precursors of the changes in the spectra due to the long-range AFM order (period doubling). As a result, we obtain non-Fermi-liquidlike behavior (dielectrization) of the spectral density in the vicinity of the so called hot spots on the Fermi surface, appearing at intersections of the Fermi surface with an antiferromagnetic Brillouin zone boundary (Umklapp surface).[2]

Within this spin-fluctuation scenario, a simplified model of the pseudogap state was studied[2,4,5] under the assumption that the scattering by dynamic spin fluctuations can be reduced for high enough temperatures to a static Gaussian random field (quenched disorder) of pseudogap fluctuations. These fluctuations are defined by a characteristic scattering vector from the vicinity of $\mathbf{Q}$, with a width determined by the inverse correlation length of a short-range order $\kappa=\xi^{-1}$, and by an appropriate energy scale Δ (typically of the order of the crossover temperature T^* to the pseudogap state[2]).

Undoped cuprates are antiferromagnetic Mott insulators with $U \gg W$ (U—value of the local Coulomb interaction, W—bandwidth of noninteracting band), so that correlation effects are very important. It is thus clear that the electronic properties of underdoped (and probably also optimally doped) cuprates are governed by strong electronic correlations also, so that these systems are typical strongly correlated metals. Two types of correlated metals can be distinguished: (i) the doped Mott insulator and (ii) the bandwidth controlled correlated metal $W \approx U$. Both types will be considered in this paper.

A state of the art tool to describe such correlated systems is the dynamical mean-field theory (DMFT).[6–10] The characteristic features of correlated systems within the DMFT are the formation of incoherent structures, the so-called Hubbard bands, split by the Coulomb interaction U, and a quasiparticle (conduction) band near the Fermi level dynamically generated by the local correlations.[6–10]

Unfortunately, the DMFT is not useful to the study of the antiferromagnetic scenario of the pseudogap formation in strongly correlated metals. This is due to the basic approximation of the DMFT, which amounts to the complete neglect of nonlocal dynamical correlation effects.

Besides the extended DMFT,[11] which locally includes a coupling to nonlocal dynamical fluctuations, a straightforward way to extend the DMFT are the so-called cluster mean-field theories.[12] Two variants of this approach are the dynamical cluster approximation (DCA) (Ref. 12) and the cellular DMFT (CDMFT).[13] In particular, the DCA has been applied to study the low-energy properties of the Hubbard model, systematically including short- to medium-ranged nonlocal correlations. Both improve on the cluster perturbation theory (CPT),[14,15] an attempt to use finite-size calculations to obtain approximate results for the thermodynamic limit.

However, these approaches have certain drawbacks from both the technical and the interpretation points of view. First, the effective quantum single impurity problem becomes rather complex. Thus, most computational methods available for the DMFT can be applied for the smallest clusters only,[12,16,17] i.e., include nearest-neighbor fluctuations only. For medium- to long-ranged correlations one is currently re-

stricted to the Quantum Monte-Carlo.[18,19] Since for cluster problems again a sign problem arises, one is restricted to relatively small values of the local Coulomb interaction and high temperatures. Second, the interpretation of electronic structures found has to be based on a reliable input from other, typically approximate, complementary techniques.

The aim of the present paper is to propose such an approach, which on the one hand retains the single-impurity description of the DMFT, viz a proper account for *local* correlations and the possibility of using very efficient impurity solvers like NRG;[20,21] on the other hand, we include nonlocal correlations on a nonperturbative model basis, which allows one to control characteristic scales and also types of nonlocal fluctuations. This latter point allows for a systematical study of the influence of a nonlocal fluctuation on the electronic properties and in particular provide valuable hints on the physical origin and the possible interpretation of results found in, e.g., more refined theoretical approaches.

The paper is organized as follows: In Sec. II we present a derivation of the self-consistent generalization we call DMFT+$\Sigma_{\mathbf{k}}$ which includes short-ranged dynamical correlations to some extent. Section III describes the construction of the **k**-dependent self-energy, and some computational details are presented in Sec. IV A. Results and discussion are given in the Sec. IV. Then the paper is ended with a summary (Sec. V) together with an overview of related recent approaches and results on a pseudogap issue.

II. INTRODUCING LENGTH SCALE INTO DMFT: DMFT+$\Sigma_{\mathbf{k}}$ APPROACH

The basic shortcoming of the traditional DMFT approach[6–10] is the neglect of the momentum dependence of the electron self-energy. This approximation, in principle, allows for an exact solution of the correlated electron systems fully preserving the local part of the dynamics introduced by electronic correlations. To include nonlocal effects, while remaining within the usual single impurity analogy, we propose the following procedure. To be definite, let us consider a standard one-band Hubbard model from now on. The extension to multi-orbital or multi-band models is straightforward. The major assumption of our approach is that the lattice and Matsubara time Fourier transformed of the single-particle Green function can be written as:

$$G_{\mathbf{k}}(i\omega) = \frac{1}{i\omega + \mu - \varepsilon(\mathbf{k}) - \Sigma(i\omega) - \Sigma_{\mathbf{k}}(i\omega)}, \quad \omega = \pi T(2n+1), \tag{1}$$

where $\Sigma(i\omega)$ is the *local* contribution to the self-energy, surviving in the DMFT, while $\Sigma_{\mathbf{k}}(i\omega)$ is a momentum dependent part. We suppose that this last contribution is due to either electron interactions with some additional collective modes or order parameter fluctuations, or may be due to a similar nonlocal contribution within the Hubbard model itself.

To avoid possible confusion, we must stress that $\Sigma_{\mathbf{k}}(i\omega)$ can, in principle, also contain local (momentum independent) contributions, which obviously *vanish* in the limit of an infinite dimensionality $d \to \infty$ and are not taken into account within the DMFT. Due to this fact there is no double counting of diagrams within our approach to the Hubbard model. This question does not arise at all if we consider $\Sigma_{\mathbf{k}}(i\omega)$ appearing due to some additional interaction. More important is that the assumed additive form of the self-energy $\Sigma(i\omega)+\Sigma_{\mathbf{k}}(i\omega)$ implicitly corresponds to the neglect of possible interference of these local (DMFT) and nonlocal contributions. Furthermore, both contributions to the total self-energy $\Sigma(i\omega)+\Sigma_{\mathbf{k}}(i\omega)$ individually obey causality by construction. Thus, the sum and finally the propagator (1) constructed from it are causal, too.

The self-consistency equations of our generalized DMFT+$\Sigma_{\mathbf{k}}$ approach are formulated as follows.

(1) Start with some initial guess of *local* self-energy $\Sigma(i\omega)$, e.g., $\Sigma(i\omega)=0$.

(2) Construct $\Sigma_{\mathbf{k}}(i\omega)$ within some (approximate) scheme, taking into account interactions with collective modes or order parameter fluctuations which in general can depend on $\Sigma(i\omega)$ and μ.

(3) Calculate the local Green function

$$G_{ii}(i\omega) = \frac{1}{N}\sum_{\mathbf{k}} \frac{1}{i\omega + \mu - \varepsilon(\mathbf{k}) - \Sigma(i\omega) - \Sigma_{\mathbf{k}}(i\omega)}. \tag{2}$$

(4) Define the "Weiss field"

$$\mathcal{G}_0^{-1}(i\omega) = \Sigma(i\omega) + G_{ii}^{-1}(i\omega). \tag{3}$$

(5) Use some "impurity solver" to calculate the single-particle Green function for the effective single Anderson impurity problem, defined by the Grassmanian integral

$$G_d(\tau - \tau') = \frac{1}{Z_{\text{eff}}} \int Dc_{i\sigma}^{\dagger} Dc_{i\sigma} c_{i\sigma}(\tau) c_{i\sigma}^{\dagger}(\tau') \exp(-S_{\text{eff}}) \tag{4}$$

with the effective action for a fixed site ("single impurity") i

$$S_{\text{eff}} = -\int_0^{\beta} d\tau_1 \int_0^{\beta} d\tau_2 \, c_{i\sigma}(\tau_1)\mathcal{G}_0^{-1}(\tau_1 - \tau_2)c_{i\sigma}^{\dagger}(\tau_2) + \int_0^{\beta} d\tau \, U n_{i\uparrow}(\tau) n_{i\downarrow}(\tau), \tag{5}$$

$Z_{\text{eff}} = \int Dc_{i\sigma}^{\dagger} Dc_{i\sigma} \exp(-S_{\text{eff}})$, and $\beta = T^{-1}$. This step produces a *new* set of values $G_d^{-1}(i\omega)$.

(6) Define a *new* local self-energy

$$\Sigma(i\omega) = \mathcal{G}_0^{-1}(i\omega) - G_d^{-1}(i\omega). \tag{6}$$

(7) Using this self-energy as an initial one in step (1), continue the procedure until (and if) convergency is reached to obtain

$$G_{ii}(i\omega) = G_d(i\omega). \tag{7}$$

Eventually, we get the desired Green function in the form of (1), where $\Sigma(i\omega)$ and $\Sigma_{\mathbf{k}}(i\omega)$ are those appearing at the end of our iteration procedure. A more detailed derivation of this scheme within a diagrammatic approach is given in Appendix A.

III. CONSTRUCTION OF k-DEPENDENT SELF-ENERGY

For the momentum dependent part of the single-particle self-energy we concentrate on the effects of the scattering of electrons from the collective short-range SDW–like antiferromagnetic spin [or charge density wave (CDW)–like charge] fluctuations. To calculate $\Sigma_{\mathbf{k}}(i\omega)$ for an electron moving in the quenched random field of (static) Gaussian spin (or charge) fluctuations with dominant scattering momentum transfers from the vicinity of some characteristic vector $\mathbf{Q}$ (hot spots model[2]), we use a slightly generalized version of the recursion procedure proposed in Refs. 4, 5, and 22 which takes into account *all* the Feynman diagrams describing the scattering of the electrons by this random field. This becomes possible due to a remarkable property of our simplified version of hot spots model that under certain conditions the contribution of an arbitrary diagram with intersecting interaction lines is actually equal to the contribution of some diagram of the same order without intersections of these lines.[5,22] Thus, in fact, we can limit ourselves to consideration of only diagrams without intersecting interaction lines, taking the contribution of diagrams with intersections into account with the help of additional combinatorial factors, which are attributed to "initial" vertices or just interaction lines.[22] As a result, we obtain the following recursion relation (continuous fraction representation[22]):

$$\Sigma_n(i\omega,\mathbf{k}) = \Delta^2 \frac{s(n)}{i\omega + \mu - \Sigma(i\omega) - \varepsilon_n(\mathbf{k}) + inv_n\kappa - \Sigma_{n+1}(i\omega,\mathbf{k})}. \tag{8}$$

The term $\Sigma_n(i\omega,\mathbf{k})$ of recurring sequence contains all contributions of diagrams with the number of interaction lines $\geqslant n$. Then

$$\Sigma_{\mathbf{k}}(i\omega) = \Sigma_{n=1}(i\omega,\mathbf{k}) \tag{9}$$

is actually the sum of all diagrammatic contributions. Since the convergence of this recursion procedure for $\Sigma_n(i\omega,\mathbf{k})$ is rather fast, one can set contributions for large enough n equal to zero and doing recursion backwards to $n=1$ to get the desired physical self-energy.[5]

The quantity Δ characterizes the energy scale and $\kappa=\xi^{-1}$ is the inverse correlation length of the short-range SDW (CDW) fluctuations, $\varepsilon_n(\mathbf{k})=\varepsilon(\mathbf{k}+\mathbf{Q})$ and $v_n=|v^x_{\mathbf{k}+\mathbf{Q}}|+|v^y_{\mathbf{k}+\mathbf{Q}}|$ for odd n while $\varepsilon_n(\mathbf{k})=\varepsilon(\mathbf{k})$ and $v_n=|v^x_{\mathbf{k}}|+|v^y_{\mathbf{k}}|$ for even n. The velocity projections $v^x_{\mathbf{k}}$ and $v^y_{\mathbf{k}}$ are determined by usual momentum derivatives of the "bare" electronic energy dispersion $\varepsilon(\mathbf{k})$. Finally, $s(n)$ represents a combinatorial factor with

$$s(n) = n \tag{10}$$

for the case of commensurate charge (CDW-type) fluctuations with $\mathbf{Q}=(\pi/a,\pi/a)$.[22] For the incommensurate CDW fluctuations[22] (when $\mathbf{Q}$ is not locked to the period of the reciprocal lattice) one finds

$$s(n) = \begin{cases} \dfrac{n+1}{2} & \text{for odd } n \\ \dfrac{n}{2} & \text{for even } n. \end{cases} \tag{11}$$

If we want to take into account the (Heisenberg) spin structure of interaction with spin fluctuations in nearly antiferromagnetic Fermi-liquid [spin-fermion (SF) model of Ref. 4, SDW-type fluctuations], the combinatorics of the diagrams becomes more complicated. Spin-conserving scattering processes obey commensurate combinatorics, while spin-flip scattering is described by the diagrams of incommensurate type (charged random field in terms of Ref. 4). In this model, the recursion relation for the single-particle Green function is again given by (8), but the combinatorial factor $s(n)$ now acquires the following form:[4]

$$s(n) = \begin{cases} \dfrac{n+2}{3} & \text{for odd } n \\ \dfrac{n}{3} & \text{for even } n. \end{cases} \tag{12}$$

Obviously, with this procedure we introduce an important length scale ξ not present in standard DMFT. Physically this scale mimics the effect of short-range (SDW or CDW) correlations within fermionic bath surrounding the effective single Anderson impurity of the DMFT. We expect that such a length scale will lead to a competition between local and nonlocal physics.

An important aspect of the theory is that both parameters Δ and ξ can, in principle, be calculated from the microscopic model at hand. For example, using the two-particle self-consistent approach of Ref. 23 with the approximations introduced in Refs. 4 and 5, one can derive within the standard Hubbard model the following microscopic expression for Δ:

$$\Delta^2 = \frac{1}{4}U^2\frac{\langle n_{i\uparrow}n_{i\downarrow}\rangle}{\langle n_{i\uparrow}\rangle\langle n_{i\downarrow}\rangle}[\langle n_{i\uparrow}\rangle + \langle n_{i\downarrow}\rangle - 2\langle n_{i\uparrow}n_{i\downarrow}\rangle] = U^2\frac{\langle n_{i\uparrow}n_{i\downarrow}\rangle}{n^2}\langle (n_{i\uparrow}-n_{i\downarrow})^2\rangle = U^2\frac{\langle n_{i\uparrow}n_{i\downarrow}\rangle}{n^2}\frac{1}{3}\langle \vec{S}_i^2\rangle, \tag{13}$$

where we consider only scattering from antiferromagnetic spin fluctuations. The different local quantities—spin fluctuation $\langle \vec{S}_i^2\rangle$, density n and double occupancy $\langle n_{i\uparrow}n_{i\downarrow}\rangle$—can easily be calculated within the standard DMFT.[9] A detailed derivation of (13) and the computational results for Δ obtained by the DMFT using the quantum Monte-Carlo (QMC) to solve the effective single impurity problem are presented in Appendix B. A corresponding microscopic expression for the correlation length ξ can also be derived within the two-particle self-consistent approach.[23] However, we expect those results for ξ to be less reliable, because this approach is valid only for relatively small (or medium) values of U/t. Thus, in the following, we will consider both Δ and especially ξ as some phenomenological parameters to be determined from the experiments.

IV. RESULTS AND DISCUSSION

A. Computation details

In the following, we want to discuss the results for a standard one-band Hubbard model on a square lattice. With the nearest (t) and next nearest (t') neighbor hopping integrals the dispersion then reads

$$\varepsilon(\mathbf{k}) = -2t(\cos k_x a + \cos k_y a) - 4t' \cos k_x a \cos k_y a, \tag{14}$$

where a is the lattice constant. The correlations are introduced by a repulsive local two-particle interaction U. We choose as an energy scale, the nearest neighbor hopping integral t and as a length scale, the lattice constant a.

For a square lattice the bare bandwidth is $W=8t$. To study a strongly correlated metallic state obtained as a doped Mott insulator we use $U=40t$ as a value for the Coulomb interaction and a filling $n=0.8$ (hole doping). The particular choice of the latter value for U is motivated by two aspects. First, this value of U leads to an insulating DMFT+$\Sigma_{\mathbf{k}}$, solution at half-filling. Second, the estimations of U for the stoichiometric La_2CuO_4 (high-T_C prototype compound) based on the constrained LDA (Ref. 24) calculations typically give U of the order of 10 eV,[25] which corresponds to $40t$ with our choice of parameters. The correlated metal in the case of $W \gtrsim U$ is realized via $U=4t$—a value used in various theoretical papers discussing the pseudogap state—and two fillings: half-filling ($n=1.0$) and $n=0.8$ (hole doping). As typical values for Δ we choose $\Delta=t$ and $\Delta=2t$ (actually as approximate limiting values—see Appendix B) and for the correlation length $\xi=2a$ and $\xi=10a$ (motivated mainly by the experimental data for cuprates[2,4]).

The DMFT maps the lattice problem onto an effective, self-consistent single impurity defined by Eqs. (4) and (5). In our work, we employ as "impurity solvers" two reliable numerically exact methods—quantum Monte-Carlo (QMC) (Ref. 18) and the numerical renormalization group (NRG).[20,21] The calculations were done for the case $t'=0$ and $t'/t=-0.4$ (more or less typical for cuprates) at two different temperatures $T=0.088t$ and $T=0.356t$ (for NRG computations).[40] QMC computations of double occupancies as functions of filling were done at temperatures $T=0.1t$ and $T=0.4t$.[41]

Below we present results only for most typical dependences and parameters, more data and figures can be found in Ref. 26.

B. Generalized DMFT+$\Sigma_{\mathbf{k}}$ approach: densities of states

Let us start the discussion of our results obtained within our generalized DMFT+$\Sigma_{\mathbf{k}}$ approach with the densities of states (DOS) for the case of the small (relative to bandwidth) Coulomb interaction $U=4t$ with and without pseudogap fluctuations. As already discussed in Sec. I, the characteristic feature of the strongly correlated metallic state is the coexistence of the lower and upper Hubbard bands split by the value of U with a quasiparticle peak at the Fermi level. Since at half-filling the bare DOS of the square lattice has a Van–Hove singularity at the Fermi level ($t'=0$) or close to it (in case of $t'/t=-0.4$) one cannot treat a peak on the Fermi level simply as a quasiparticle peak. In fact, there are two contributions to this peak; (i) the quasiparticle peak appearing in a strongly correlated metals due to many-body effects and (ii) the smoothed Van–Hove singularity from the bare DOS.[42] In Figs. 1 and 2 we show the corresponding DMFT (NRG) DOS without pseudogap fluctuations as black lines for both the bare dispersions $t'/t=-0.4$ (left panels) and for the $t'=0$ (right panels) for two different temperatures $T=0.356t$ (lower panels) and $T=0.088t$ (upper panels) with fillings $n=1.0$ and $n=0.8$, respectively. The remaining curves in Figs. 1 and 2 represent results for the DOS with nonlocal fluctuations switched on with the fluctuation amplitude $\Delta=2t$. For all sets of parameters, one can see that the introduction of nonlocal fluctuations into the calculation leads to the formation of pseudogap in the quasiparticle peak.

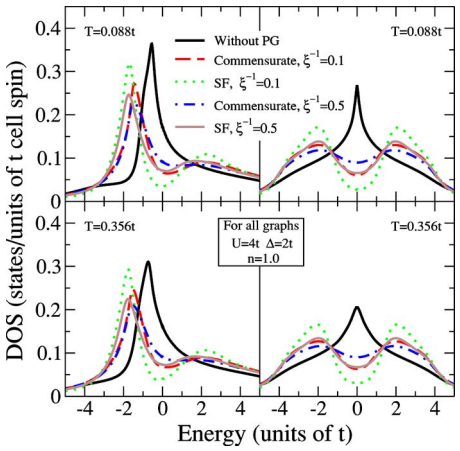

FIG. 1. (Color online) Comparison of DOS obtained from DMFT(NRG)+$\Sigma_{\mathbf{k}}$ calculations for different combinatorical factors (SF–spin-fermion model, commensurate), inverse correlation lengths (ξ^{-1}) in units of the lattice constant, temperatures (T), and the value of pseudogap potential $\Delta=2t$. The left column corresponds to $t'/t=-0.4$, the right column to $t'=0$. In all graphs the Coulomb interaction is $U=4t$ and $n=1$. The Fermi level corresponds to zero.

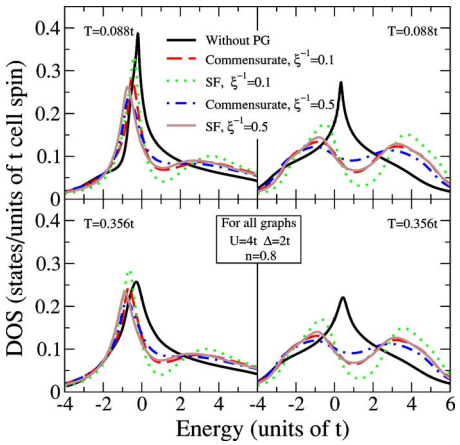

FIG. 2. (Color online) Comparison of DOS obtained from DMFT(NRG)+$\Sigma_{\mathbf{k}}$ calculations for a filling $n=0.8$, other parameters as in Fig. 1.

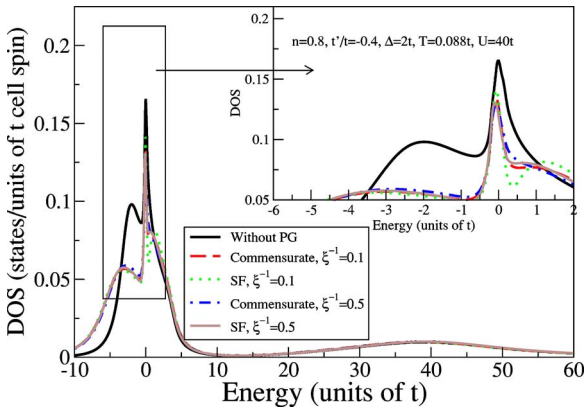

FIG. 3. (Color online) Comparison of DOS obtained from DMFT(NRG)+$\Sigma_{\mathbf{k}}$ calculations for $t'/t=-0.4$, $T=0.088t$, $U=40t$, $\Delta=2t$, and filling $n=0.8$.

The behavior of the pseudogaps in the DOS has some common features. For example, for $t'=0$ at half-filling (Fig. 1, right column) we find that the pseudogap is most pronounced. For $n=0.8$ (Fig. 2, right column) the picture is almost the same but slightly asymmetric. The width of the pseudogap (the distance between the peaks closest to the Fermi level) appears to be of the order of $\sim 2\Delta$ here. Decreasing the value of Δ from $2t$ to t leads to a pseudogap that is correspondingly twice smaller and in addition more shallow (see Ref. 26). When one uses the combinatorial factors corresponding to the spin-fermion model [Eq. (12)], we find that the pseudogap becomes more pronounced than in the case of commensurate charge fluctuations [combinatorial factors of Eq. (11)]. The influence of the correlation length ξ can be seen as expected. Changing from $\xi^{-1}=0.1$ to $\xi^{-1}=0.5$, i.e., decreasing the range of the nonlocal fluctuations, slightly washes out the pseudogap. Also, increasing the temperature from $T=0.088t$ to $T=0.356t$ leads to a general broadening of the structures in the DOS. These observations remain at least qualitatively valid for $t'/t=-0.4$ (Figs. 1 and 2, left columns) with an additional asymmetry due to the next-nearest neighbor hopping. Noteworthy is, however, the fact that for $t'/t=-0.4$ and $\xi^{-1}=0.5$ the pseudogap has almost disappeared for the temperatures studied here. Also a very remarkable point is the similarity of the results obtained with the generalized DMFT+$\Sigma_{\mathbf{k}}$ approach with $U=4t$ (smaller than the bandwidth W) to those obtained earlier without the Hubbard-like Coulomb interactions.[4,5]

Let us now consider the case of a doped Mott insulator. The model parameters are $t'/t=-0.4$ with filling $n=0.8$, but the Coulomb interaction strength is now set to $U=40t$. The characteristic features of the DOS for such a strongly correlated metal are a strong separation of the lower and upper Hubbard bands and a Fermi level crossing by the lower Hubbard band (for the non-half-filled case). Without nonlocal fluctuations the quasiparticle peak is again formed at the Fermi level; but now the upper Hubbard band is far to the right and does not touch the quasiparticle peak (as it was for the case of small Coulomb interactions). DOS without nonlocal fluctuations are again presented as black lines in Fig. 3. The results for the case $t'=0$ are presented elsewhere.[26]

With rather strong nonlocal fluctuations $\Delta=2t$, a pseudogap appears in the middle of the quasiparticle peak. In addition, we observe that the lower Hubbard band is slightly broadened by fluctuation effects. Qualitative behavior of the pseudogap anomalies is again similar to those described above for the case of $U=4t$, e.g., a decrease of ξ makes the pseudogap less pronounced, reducing Δ from $\Delta=2t$ to $\Delta=t$ narrows of the pseudogap and also makes it more shallow, etc. (see Ref. 26). Note that for the doped Mott-insulator we find that the pseudogap is remarkably more pronounced for the SDW-like fluctuations than for CDW-like fluctuations.

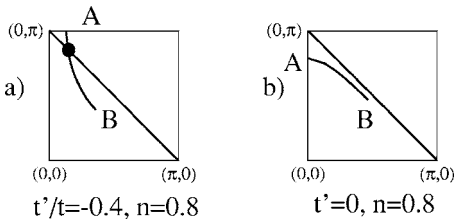

FIG. 4. One-eighth of the bare Fermi surfaces for the occupancy $n=0.8$ and different combinations (t,t') used for the calculation of spectral functions $A(\mathbf{k},\omega)$. The diagonal line corresponds to the Umklapp surface. The full circle marks the so-called hot spot.

There are, however, obvious differences of the case with $U=4t$. For example, the width of the pseudogap appears to be much smaller than 2Δ, being of the order of $\Delta/2$ instead (see Fig. 3). This effect we attribute to the fact that the quasiparticle peak itself is actually strongly narrowed now by the local correlations.

C. Generalized DMFT+$\Sigma_{\mathbf{k}}$ approach: spectral functions $A(\omega,\mathbf{k})$

In the previous subsections we discussed the densities of states obtained self-consistently by the DMFT+$\Sigma_{\mathbf{k}}$ approach. Once we get a self-consistent solution of the DMFT+$\Sigma_{\mathbf{k}}$ equations with nonlocal fluctuations we can, of course, also compute the spectral functions $A(\omega,\mathbf{k})$

$$A(\omega,\mathbf{k}) = -\frac{1}{\pi}\,\mathrm{Im}\,\frac{1}{\omega+\mu-\varepsilon(\mathbf{k})-\Sigma(\omega)-\Sigma_{\mathbf{k}}(\omega)}, \quad (15)$$

where the self-energy $\Sigma(\omega)$ and the chemical potential μ are calculated self-consistently as described in Sec. II. To plot $A(\omega,\mathbf{k})$ we choose $\mathbf{k}$ points along the bare Fermi surfaces for different types of lattice spectra and filling $n=0.8$. In Fig. 4 one can see corresponding shapes of these bare Fermi surfaces (presented are only $\frac{1}{8}$ th of the Fermi surfaces within the first quadrant of the first Brillouin zone).

A natural quantity to inspect is the self-energy $\Sigma(\mathbf{k},\omega+i\delta)$, shown in Fig. 5 for $t'/t=-0.4$, $n=0.8$, and $U=4t$ (left column) and $U=40t$ (right column). As a representative $\mathbf{k}$ points we chose the center of the first Brillouin zone (Γ), the hot-spot and cold-spot (point B in Fig. 4). The results were obtained with NRG at a temperature $T=0.088t$. The structures for $U=4t$ are rather broad, but reveal after a closer inspection features similar to the case $U=40t$. For the latter, the behavior at Γ and B is very different from the structures at the hot-spot. Namely, while for the former two $\mathbf{k}$ points $\mathrm{Im}\,\Sigma(\mathbf{k},\omega+i\delta)$ shows a nice parabolic maximum at the Fermi energy, the latter develops a minimum instead. Such a

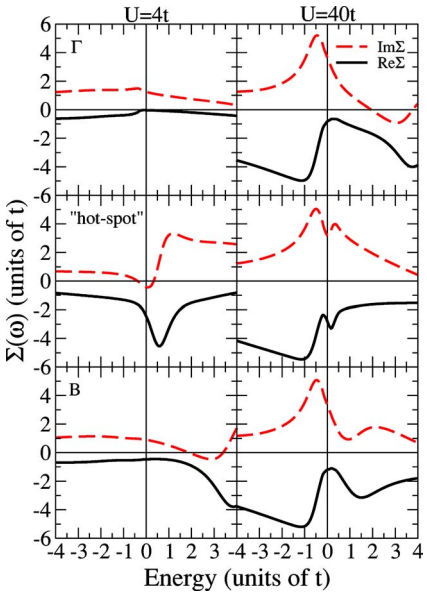

FIG. 5. (Color online) Real (dashed line) and imaginary (full line) parts of the self-energy $\Sigma(\mathbf{k},\omega)$ for $t/t'=-0.4$, $U=4t$ (left column), and $U=40t$ (right column) for characteristic $\mathbf{k}$ points: Γ, hot-spot (see Fig. 4) and cold-spot (point B in Fig. 4). For all graphs the filling is $n=0.8$, temperature $T=0.088t$, inverse correlation length $\xi^{-1}=0.1$, value of pseudogap potential $\Delta=2t$, and SF combinatorics.

structure in the self-energy will result in a rather evident (pseudo) gap in the spectral function at this $\mathbf{k}$ point and at weaker pseudogap behavior in the DOS. Its appearance is obviously due to the presence of the spin-fluctuations at the hot-spot. Note that similar features have been observed in numerically expensive cluster mean-field calculations,[27] too, with an interpretation as a spin fluctuation induced based on physical expectations. Our calculations, obtained at a minimum numerical expense, indeed show, that including short-ranged fluctuations will precisely produce these non-Fermi-liquid structures in the one-particle self-energy. This behavior is quite typical for the problem and was observed by other groups using different methods.[16,28–30] In several works the midgap peak in the pseudogap was obtained with an explanation of its origin by a particular shape of the self-energy close to the Fermi level.[28,29,31]

In the following we concentrate mainly on the case $U=4t$ and filling $n=0.8$ [Fermi surface of Fig. 4(a)]. The corresponding spectral functions $A(\omega,\mathbf{k})$ are depicted in Fig. 6. When $t'/t=-0.4$ (upper row), the spectral function close to the diagonal of the Brillouin zone (point B) has the typical Fermi-liquid behavior, consisting of a rather sharp peak close to the Fermi level. In the case of the SDW-like fluctuations this peak is shifted down in energy by about $-0.5t$ (left upper corner). In the vicinity of the hot-spot the shape of $A(\omega,\mathbf{k})$ is completely modified. Now $A(\omega,\mathbf{k})$ becomes double-peaked and non-Fermi-liquidlike. Directly at the hot-spot, $A(\omega,\mathbf{k})$ for SDW-like fluctuations has two equally intensive peaks situated symmetrically around the Fermi level and split from each other by $\sim 1.5\Delta$ Refs. 4 and 5. For the commensurate CDW-like fluctuations the spectral function in the hot-spot

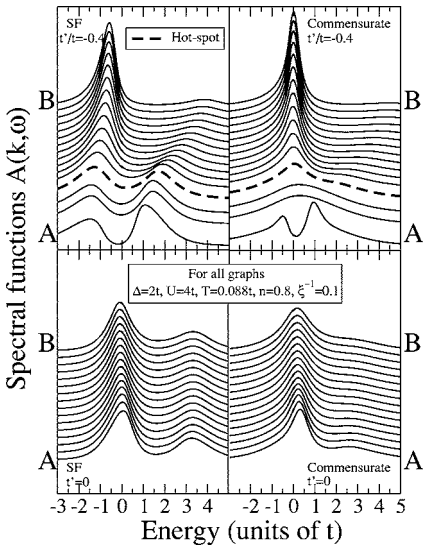

FIG. 6. Spectral functions $A(\mathbf{k},\omega)$ obtained from the DMFT(NRG)+$\Sigma_{\mathbf{k}}$ calculations along the directions shown in Fig. 4. Model parameters were chosen as $U=4t$, $n=0.8$, $\Delta=2t$, $\xi^{-1}=0.1$, and temperature $T=0.088t$. The hot-spot $\mathbf{k}$ point is marked as a fat dashed line. The Fermi level corresponds to zero.

region has one broad peak centered at the Fermi level with the width $\sim\Delta$. Such a merging of the two peaks at the hot spot for commensurate fluctuations was previously observed in Ref. 5. However, close to point **A** this type of fluctuations also produces a double-peak structure in the spectral function.

Spectral functions for the case of $U=4t$ at half-filling ($n=1$) and for $t'/t=-0.4$ are similar to those just discussed for $n=0.8$. However, the pseudogap is more pronounced in this case and remains open everywhere close to the Umklapp surface for SDW fluctuations.[26]

In the lower panel of Fig. 6 we show spectral functions for 20% hole doping ($n=0.8$) and the case of $t'=0$ [Fermi surface from Fig. 4(b)]. Since the Fermi surface now is close to the Umklapp surface, the pseudogap anomalies are rather strong and almost nondispersive along the Fermi surface. At half filling for $t'=0$ the Fermi surface actually coincides with the Umklapp surface (in case of perfect nesting the whole Fermi surface is the hot region). The spectral functions are now symmetric around the Fermi level. For SDW-like fluctuations there are two peaks split by $\sim 1.5\Delta$. Again, CDW-like fluctuations give just one peak centered at the Fermi level with width $\sim\Delta$.

For the case of a doped Mott insulator ($U=40t$, $n=0.8$), the spectral functions obtained by the DMFT+$\Sigma_{\mathbf{k}}$ approach are presented in Fig. 7. Qualitatively, the shapes of these spectral functions are similar to those shown in Fig. 6. As was pointed out above, the strong Coulomb correlations lead to a narrowing of the quasiparticle peak and a corresponding decrease of the pseudogap width. As is evident from Fig. 7 the structures connected to the pseudogap are now spread in an energy interval $\sim t$, while for $U=4t$ they are restricted to an interval $\sim 4t$ instead. One should also note that in contrast to $U=4t$ the spectral functions are now about four times less intensive, because part of the spectral weight is transferred to

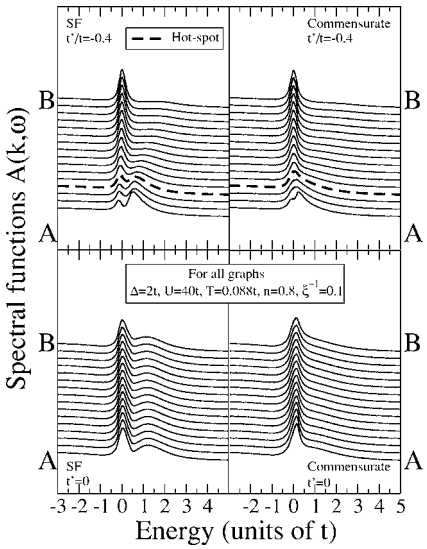

FIG. 7. Spectral functions $A(\mathbf{k},\omega)$ obtained from the DMFT(NRG)+$\Sigma_{\mathbf{k}}$ calculations for $U=40t$; other parameters as in Fig. 6.

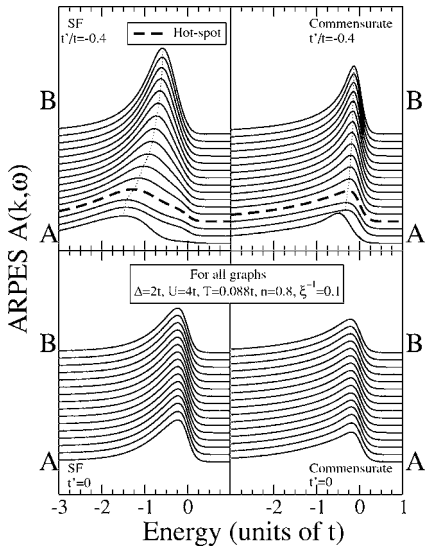

FIG. 9. ARPES spectra simulated by the multiplication of the spectral functions obtained from DMFT(NRG)+$\Sigma_{\mathbf{k}}$ calculations for $U=4t$ and $n=0.8$ in Fig. 6 with the Fermi function at $T=0.088t$ plotted along the lines in the first BZ as depicted by Fig. 4. All other parameters are the same as in Fig. 6.

the upper Hubbard band located at about $40t$ and is well separated from the quasiparticle peak now.

Using another quite common choice of $\mathbf{k}$ points we can compute $A(\omega,\mathbf{k})$ along high-symmetry directions in the first Brillouin zone: $\Gamma(0,0)-X(\pi,0)-M(\pi,\pi)-\Gamma(0,0)$. The spectral functions for these $\mathbf{k}$ points are collected in Fig. 8 for the case of SDW-like fluctuations. Characteristic curves for the doped Mott insulator are presented in Ref. 26. For all sets of parameters, one can see a characteristic double-peak pseudogap structure close to the X point. In the middle of the $M-\Gamma$ direction (so called "nodal" point) one can see the reminiscence of the AFM gap which has its biggest value here in the case of perfect antiferromagnetic ordering. Also in the nodal point "kinklike" behavior is observed caused by interactions between correlated electrons with short-range pseudogap fluctuations. A change of the filling leads mainly to a rigid shift of spectral functions with respect to the Fermi level.

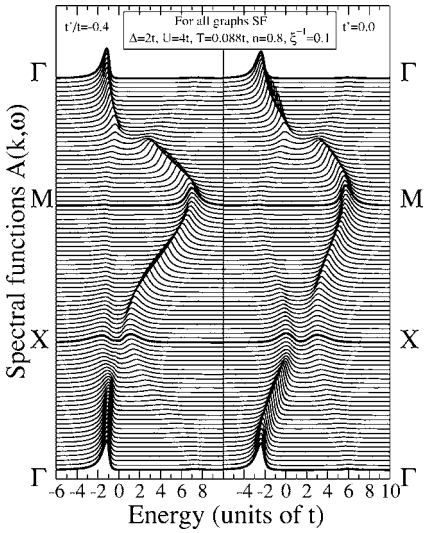

FIG. 8. Spectral functions $A(\mathbf{k},\omega)$ obtained from the DMFT(NRG)+$\Sigma_{\mathbf{k}}$ calculations along high-symmetry directions of the first Brillouin zone $\Gamma(0,0)-X(\pi,0)-M(\pi,\pi)-\Gamma(0,0)$, *SF* combinatorics (left row) and commensurate combinatorics (right column). Other parameters are $U=4t$, $n=0.8$, $\Delta=2t$, $\xi^{-1}=0.1$, and temperature $T=0.088t$. The Fermi level corresponds to zero.

With the spectral functions we are now, of course, in a position to calculate the angle resolved photoemission spectra (ARPES), which is the most direct experimental way to observe pseudogap in real compounds. For that purpose, we only need to multiply our results for the spectral functions with the Fermi function at temperature $T=0.088t$. A typical example of the resulting DMFT+$\Sigma_{\mathbf{k}}$ ARPES spectra are presented in Fig. 9. More figures of ARPES-like results obtained within the DMFT+$\Sigma_{\mathbf{k}}$ approach for a variety of parameters can be found in Ref. 26. One should note that for $t'/t=-0.4$ (upper panel of Fig. 9) as $\mathbf{k}$ goes from point A to point B the peak situated slightly below the Fermi level changes its position and moves down in energy. Simultaneously it becomes more broad and less intensive. The dotted line guides the motion of the peak maximum. Also at the hot spot and further to point B one can see some signs of the double-peak structure. Such behavior of the peak in the ARPES is rather reminiscent of those observed experimentally in underdoped cuprates.[2,4,32]

V. CONCLUSION

In summary, we propose a generalized DMFT+$\Sigma_{\mathbf{k}}$ approach, which is meant to take into account the important effects of nonlocal correlations (in principle of any type) in addition to the (essentially exact) treatment of local dynamical correaltions by the DMFT. In the standard DMFT the "bath" surrounding the effective single Anderson impurity is

spatially uniform since the DMFT self-energy is only energy dependent. The main idea of our extension is to introduce nonlocal correlations through the bath, i.e. to make it spatially nonuniform, while keeping standard DMFT self-consistency equations. Such a generalization of the DMFT allows us to supplement it with a **k**-dependent self-energy $\Sigma(\mathbf{k},\omega)$. It in turn opens the possibility of accessing the physics of low-dimensional strongly correlated systems, where different types of spatial fluctuations (e.g., of some order parameter) become important, in a nonperturbative way at least with respect to the important local dynamical correlations. However, we must stress that our procedure in no way introduces any kind of systematic $1/d$ expansion, being only a qualitative method to include a length scale into the DMFT. Nevertheless, we believe that such a technique can give valuable insight into the physical processes leading to the correlation induced **k**-dependent structures in single-particle properties.

In this work we model such effects for the two-dimensional Hubbard model by incorporating into the bath scattering of fermions from nonlocal collective SDW-like antiferromagnetic spin (or CDW-like charge) short-range fluctuations. The corresponding **k**-dependent self-energy $\Sigma(\mathbf{k},\omega)$ is obtained from a nonperturbative iterative scheme.[4,5] Such a choice of the $\Sigma(\mathbf{k},\omega)$ allows us to address the problem of pseudogap formation in the strongly correlated metallic state. We showed evidence that the pseudogap appears at the Fermi level within the quasiparticle peak, introducing a new small energy scale of the order of pseudogap potential value Δ in the DOS and more pronounced in spectral functions $A(\omega,\mathbf{k})$. Let us stress that our generalization of the DMFT leads to nontrivial and in our opinion physically sensible **k** dependence of spectral functions. It is significant that this particular choice of $\Sigma(\mathbf{k},\omega)$ (Refs. 4 and 5) does not cause difficulties to "double counting" problems within our combined DMFT$+\Sigma_{\mathbf{k}}$ approach. Also, the combination of diagrammatically correct techniques such as DMFT (Refs. 6–10) and the nonlocal self-energy ansatz of Refs. 4 and 5 preserves the correct analytical properties of the combined self-energy $\Sigma(i\omega)+\Sigma_{\mathbf{k}}(i\omega)$, as well as of the corresponding one-electron propagator (1).

Of course, our pseudogap observations are not entirely new. Similar results about pseudogap formation in the $2d$ Hubbard model were already obtained within cluster DMFT extensions, i.e., the dynamical cluster approximation (DCA) (Refs. 12 and 27) and the cellular DMFT (CDMFT),[16,17] CPT,[14,15,33] and two interacting Hubbard sites self-consistently embedded in a bath.[28] However, these methods have generic restrictions concerning the size of the cluster, temperature, or filling accessible and, in the case of the QMC, values of the local Coulomb energy. Recently, the EDMFT was also applied to demonstrate the pseudogap formation in the DOS due to dynamic Coulomb correlations.[34] Note, however, that within the EDMFT there is no way to obtain a **k** dependence in spectral functions beyond that originating from the bare electronic energy dispersion. Important progress was also made with the weak coupling approaches for the Hubbard model[35] and the functional renormalization group.[29,30] In several papers, pseudogap formation was described in the framework of the t-J model.[36] A more general scheme for the inclusion of nonlocal corrections was also formulated within the so called GW extension to the DMFT.[37,38]

While at a first glance the introduction of additional phenomenological parameters (correlation length ξ and pseudogap strength Δ) through the definition of $\Sigma(\mathbf{k},\omega)$ seems to take a step back with respect to the methods outlined above, it actually opens up the possibility to systematically distinguish between different types of nonlocal fluctuations and their effects and help to analyze experimental or theoretical data obtained within more advanced schemes in terms of intuitive physical pictures. Note, however, that in principle even the parameters ξ and Δ can be calculated from the original model.[23]

An essential advantage of the proposed combination of two nonperturbative methods [DMFT and $\Sigma(\mathbf{k},\omega)$ from Refs. 4 and 5] removes the restrictions on model parameters in, e.g., cluster mean-field theories. Our scheme works for any Coulomb interaction strength U, pseudogap strength Δ, correlation length ξ, filling n, and bare electron dispersion $\varepsilon(\mathbf{k})$ on a $2d$ square lattice for any set of **k** points. Although we presented only high-temperature data in this paper, the possibility of using Wilson's NRG to solve the effective impurity model also opens the possibiltiy of studying properties at $T=0$, which is currently impossible within the DCA or CDMFT for larger clusters. Moreover, the DMFT$+\Sigma_{\mathbf{k}}$ approach can be easily generalized to orbital degrees of freedom, phonons, impurities, etc.

As a further application of our generalized DMFT$+\Sigma_{\mathbf{k}}$ we would like to bring the reader's attention to Ref. 39, which deals with the problem of the Fermi surface destruction in high-T_c compounds because of pseudogap fluctuations.

ACKNOWLEDGMENTS

We are grateful to A. Kampf for useful discussions. This work was supported in part by the RFBR Grant Nos. 05-02-16301 (MS,EK,IN), 03-02-39024_a (VA,IN), 04-02-16096 (VA,IN), and 05-02-17244 (IN), the joint UrO-SO Project No. 22 (VA,IN), and programs of the Presidium of the Russian Academy of Sciences (RAS) and the Division of Physical Sciences of the RAS. I.N. acknowledges support from the Dynasty Foundation, International Centre for Fundamental Physics in Moscow program for young scientists 2005, Russian Science Support Foundation program for young Ph.D. of Russian Academy of Science 2005 and Grant of President of Russian Federation for young Ph.D. MK-2118.02.2005. One of us (T.P.) further acknowledges supercomputer support from the Norddeutsche Verbund für Hoch- und Höchstleistungsrechnen.

APPENDIX A: DERIVATION OF GENERALIZED DMFT$+\Sigma_{\mathbf{k}}$ APPROACH

In this Appendix we present a derivation of the generalized DMFT$+\Sigma_{\mathbf{k}}$ scheme for the Hubbard model

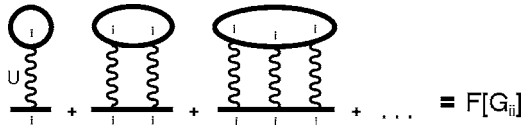

FIG. 10. Local skeleton diagrams for the DMFT self-energy Σ. Wavy lines represent the local (Hubbard) Coulomb interaction U; full lines denote the local Green function G_{ii}.

$$H = -\sum_{ij,\sigma} t_{ij} c_{i\sigma}^{\dagger} c_{j\sigma} + U \sum_{i} n_{i\uparrow} n_{i\downarrow}, \tag{A1}$$

using a diagrammatic approach. The single-particle Green function in Matsubara representation is as usual given by

$$G_{\mathbf{k}}(i\omega) = \frac{1}{i\omega + \mu - \varepsilon(\mathbf{k}) - \Sigma(i\omega, \mathbf{k})}. \tag{A2}$$

To establish the standard DMFT one invokes the limit of infinite dimensions $d \to \infty$. In this limit only local contributions to the electron self-energy survive,[7,9] i.e., $\Sigma_{ij} \to \delta_{ij} \Sigma_{ii}$ or, in reciprocal space, $\Sigma(i\omega, \mathbf{k}) \to \Sigma(i\omega)$.

In Fig. 10 we show examples of skeleton diagrams for the local self-energy, contributing in the limit of $d \to \infty$. The complete series of these and similar diagrams defines the local self-energy as a functional of the local Green function

$$\Sigma = F[G_{ii}], \tag{A3}$$

where

$$G_{ii}(i\omega) = \frac{1}{N} \sum_{\mathbf{k}} \frac{1}{i\omega + \mu - \varepsilon(\mathbf{k}) - \Sigma(i\omega)}. \tag{A4}$$

One then defines the Weiss field

$$\mathcal{G}_0^{-1}(i\omega) = \Sigma(i\omega) + G_{ii}^{-1}(i\omega) \tag{A5}$$

which is used to set up the effective single impurity problem with an effective action given by (5). In Dyson's equation, the Green function (4) for this effective single impurity problem can be written as

$$G_d(i\omega) = \frac{1}{\mathcal{G}_0^{-1}(i\omega) - \Sigma_d(i\omega)}, \tag{A6}$$

and the skeleton diagrams for self-energy Σ_d are just the same as shown in Fig. 10, with the replacement $G_{ii} \to G_d$. Thus we get

$$\Sigma_d = F[G_d], \tag{A7}$$

where F is the same functional as in (A3). The two equations (A6) and (A7) define both G_d and Σ_d for a given Weiss field $\mathcal{G}_0$. On the other hand, for the local Σ and G_{ii} of the initial (Hubbard) problem we have precisely the same pair of equations, (A3) and (A5), and $\mathcal{G}_0$ in both problems is just the same, so that

$$\Sigma = \Sigma_d; \quad G_{ii} = G_d. \tag{A8}$$

Thus, the task of finding the local self-energy of the $(d \to \infty)$ Hubbard model is eventually reduced to the calculation of the self-energy of an effective quantum single impurity problem defined by the effective action of Eq. (5).

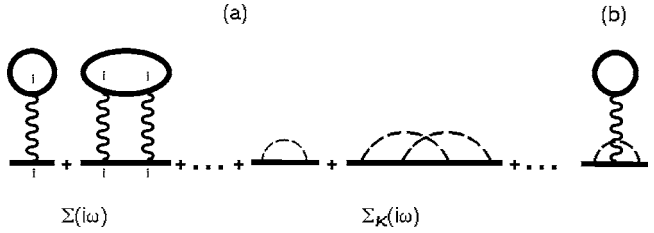

FIG. 11. Typical skeleton diagrams for the self-energy in the DMFT+$\Sigma_{\mathbf{k}}$ approach. The first two terms are DMFT self-energy diagrams; the middle two diagrams show contributions to the nonlocal part of the self-energy from spin fluctuations (see Sec. III) represented as dashed lines; the last diagram (b) is an example of the neglected diagram leading to the interference between the local and nonlocal parts.

Consider now the nonlocal contribution to the self-energy. If we neglect interference between local and nonlocal contributions [as given, e.g., by the diagram shown in Fig. 11(b)], the full self-energy is approximately determined by the sum of these two contributions. Skeleton diagrams for the nonlocal part of the self-energy, $\Sigma_{\mathbf{k}}(i\omega)$, are then those shown in Fig. 11(a), where the full line denotes the Green function $G_{\mathbf{k}}$ of Eq. (1), while dashed lines denote the interaction with static Gaussian spin (charge) fluctuations. These diagrams are just absent within the standard DMFT (as any contribution from Ornstein–Zernike type fluctuations vanish for $d \to \infty$), and no double counting problems arise at all.

The local contribution to the self-energy is again defined by the functional (A3) via the local Green function G_{ii}, which is now given by Eq. (2). Introducing again a Weiss field via (A5) and repeating all previous arguments, we again reduce the task of finding the local part of the self-energy to the solution of a single impurity problem with an effective action (5).

To determine the nonlocal contribution $\Sigma_{\mathbf{k}}(i\omega)$ we first introduce

$$\mathcal{G}_{0\mathbf{k}}(i\omega) = \frac{1}{G_{\mathbf{k}}^{-1}(i\omega) + \Sigma_{\mathbf{k}}(i\omega)} = \frac{1}{i\omega + \mu - \varepsilon(\mathbf{k}) - \Sigma(i\omega)} \tag{A9}$$

as the bare Green function for electron scattering by static Gaussian spin (charge) fluctuations. The assumed static nature of these fluctuations allows one to use the method of Refs. 4, 5, and 22 and the calculation of the nonlocal part of the self-energy $\Sigma_{\mathbf{k}}(i\omega)$ reduces to the recursion procedure defined by Eqs. (8) and (9). The choice of the bare Green function Eq. (A9) guarantees that the Green function dressed by fluctuations $G_{\mathbf{k}}^{-1}(i\omega) = \mathcal{G}_{0\mathbf{k}}^{-1}(i\omega) - \Sigma_{\mathbf{k}}(i\omega)$, which enters into the skeleton diagrams for $\Sigma_{\mathbf{k}}(i\omega)$, just coincides with the full Green functions $G_{\mathbf{k}}(i\omega)$.

Thus we obtain a fully self-consistent scheme to calculate both local (due to strong single-site correlations) and nonlocal (due to short-range fluctuations) contributions to electron self-energy.

APPENDIX B: Δ IN THE HUBBARD MODEL

In this Appendix we derive the explicit microscopic expression for pseudogap amplitude Δ given in Eq. (13).

Within the two-particle self-consistent approach of Ref. 23, valid for medium values of U, and neglecting charge fluctuations, we can write down an expression for the electron self-energy of the form used in Eq. (1), with

$$\Sigma_\sigma(i\omega) = Un_{-\sigma} \tag{B1}$$

as the lowest order local contribution due to the on-site Hubbard interaction, surviving in the limit of $d\to\infty$, and exactly accounted for in the DMFT (with all higher-order contributions). Nonlocal contribution to the self-energy (vanishing for $d\to\infty$ and not accounted within the DMFT) due to interaction with spin-fluctuations then leads to the expression

$$\Sigma_{\mathbf{k}}(i\omega) = \frac{U}{4}\frac{T}{N}\sum_m \sum_{\mathbf{q}} U_{sp}\chi_{sp}(\mathbf{q},\nu_m)G_0(\mathbf{k}+\mathbf{q}, i\omega + i\nu_m), \tag{B2}$$

where

$$U_{sp} = g_{\uparrow\downarrow}(0)U, \quad g_{\uparrow\downarrow}(0) = \frac{\langle n_{i\uparrow}n_{i\downarrow}\rangle}{\langle n_{i\uparrow}\rangle\langle n_{i\downarrow}\rangle} \tag{B3}$$

with $\langle n_\sigma^2\rangle = \langle n_\sigma\rangle$ and $\langle n_{i\uparrow}\rangle = \langle n_{i\downarrow}\rangle = \frac{1}{2}n$ in the paramagnetic phase. For the dynamic spin susceptibility $\chi_{sp}(\mathbf{q},\nu_m)$ we use the standard Ornstein–Zernike form,[23] similar to that used in the spin-fermion model,[4] which describes the enhanced scattering with momenta transfer close to the antiferromagnetic vector $\mathbf{Q}=(\pi/a,\pi/a)$. With these approximations, we can write down the following expression for the nonlocal contribution to the self-energy:[4,5]

$$\Sigma_{\mathbf{k}}(i\omega) = \frac{1}{4}UU_{sp}\frac{T}{N}\sum_m\sum_{\mathbf{q}}\chi_{sp}(\mathbf{q},\nu_m)\frac{1}{i\omega + i\nu_m + \mu - \varepsilon(\mathbf{k}+\mathbf{q})} \approx \frac{1}{4}UU_{sp}\frac{T}{N}\sum_m\sum_{\mathbf{q}}\chi_{sp}(\mathbf{q},\nu_m)\sum_{\mathbf{q}} S(\mathbf{q})\frac{1}{i\omega + \mu - \varepsilon(\mathbf{k}+\mathbf{q})}$$

$$\equiv \Delta^2\sum_{\mathbf{q}} S(\mathbf{q})\frac{1}{i\omega + \mu - \varepsilon(\mathbf{k}+\mathbf{q})} = \frac{\Delta^2}{i\omega + \mu - \varepsilon(\mathbf{p}+\mathbf{Q}) + i(|v^x_{\mathbf{p}+\mathbf{Q}}| + |v^y_{\mathbf{p}+\mathbf{Q}}|)\kappa\ \mathrm{sign}\ \omega}. \tag{B4}$$

Here we have introduced the static form factor (Ref. 5)

$$S(\mathbf{q}) = \frac{2\xi^{-1}}{(q_x - Q_x)^2 + \xi^{-2}}\frac{2\xi^{-1}}{(q_y - Q_y)^2 + \xi^{-2}} \tag{B5}$$

and the squared pseudogap amplitude

$$\Delta^2 = \frac{1}{4}UU_{sp}\frac{T}{N}\sum_m\sum_{\mathbf{q}}\chi_{sp}(\mathbf{q},\nu_m)$$

$$= \frac{1}{4}UU_{sp}[\langle n_{i\uparrow}\rangle + \langle n_{i\downarrow}\rangle - 2\langle n_{i\uparrow}n_{i\downarrow}\rangle] = \frac{1}{4}UU_{sp}\frac{1}{3}\langle\vec{S}_i^2\rangle, \tag{B6}$$

where we have used the exact sum rule for the susceptibility.[4,23] Taking into account Eq. (B3) we immediately obtain Eq. (13).

Actually, the approximations made in Eqs. (B4) and (B5) allow for an exact summation of the whole Feynman series for the electron interaction with spin fluctuations, replaced by the static Gaussian random field. Thus generalizing the one-loop approximation (B4) eventually leads to the basic recursion procedure given in Eqs. (9) and (8) and Refs. 4 and 5.

Using the DMFT(QMC) approach we computed occupancies $\langle n_{i\uparrow}\rangle$, $\langle n_{i\downarrow}\rangle$ and double occupancies $\langle n_{i\uparrow}n_{i\downarrow}\rangle$ required to calculate the pseudogap amplitude Δ of Eq. (B6). In Fig. 12 the corresponding values of Δ are presented. One can see that Δ grows when the filling goes to $n=1$. While U approaches $8t$ (the value of the bandwidth for a square lattice) Δ as a function of n grows monotonically. When U becomes larger than $W=8t$ (when a metal-insulator transition occurs) one can see a local minimum for $n=0.9$, which becomes more pronounced with further increase of U. For $t'/t=-0.4$ and both temperatures, the scatter of Δ values is smaller than for the case of $t'=0$. Also Δ has a rather weak temperature dependence. All values of Δ lie in the interval $\sim 0.75t \div 2t$. Therefore, for our computations we took only two characteristic values of $\Delta=t$ and $\Delta=2t$.

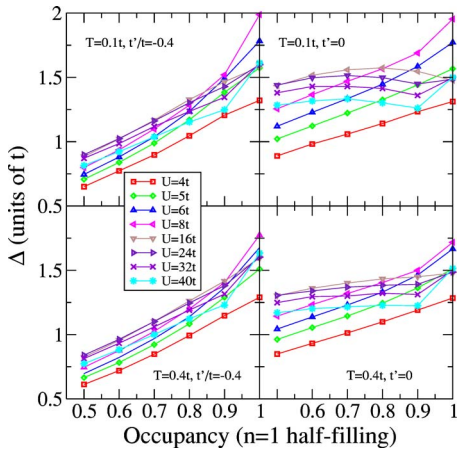

FIG. 12. (Color online) Filling dependence of the pseudogap potential Δ calculated with the DMFT(QMC) for the varying Coulomb interaction (U) and the temperature (T) on a two-dimensional square lattice with two sets of (t,t').

[1] T. Timusk and B. Statt, Rep. Prog. Phys. **62**, 61 (1999).
[2] M. V. Sadovskii, Usp. Fiz. Nauk **171**, 539 (2001) [Phys. Usp. **44**, 515 (2001)].
[3] D. Pines, ArXiv: cond-mat/0404151 (unpublished).
[4] J. Schmalian, D. Pines, and B. Stojkovic, Phys. Rev. Lett. **80**, 3839 (1998); Phys. Rev. B **60**, 667 (1999).
[5] E. Z. Kuchinskii and M. V. Sadovskii, Zh. Eksp. Teor. Fiz. **115**, 1765 (1999) [JETP **88**, 347 (1999)] [available as ArXiv: cond-mat/9808321 (unpublished)].
[6] W. Metzner and D. Vollhardt, Phys. Rev. Lett. **62**, 324 (1989).
[7] D. Vollhardt, in *Correlated Electron Systems*, edited by V. J. Emery (World Scientific, Singapore, 1993), p. 57.
[8] Th. Pruschke, M. Jarrell, and J. K. Freericks, Adv. Phys. **44**, 187 (1995).
[9] A. Georges, G. Kotliar, W. Krauth, and M. J. Rozenberg, Rev. Mod. Phys. **68**, 13 (1996).
[10] G. Kotliar and D. Vollhardt, Phys. Today **57**(3), 53 (2004).
[11] Q. Si and J. L. Smith, Phys. Rev. Lett. **77**, 3391 (1996).
[12] Th. Maier, M. Jarrell, Th. Pruschke, and M. Hettler, Rev. Mod. Phys. [in print, ArXiv: cond-mat/0404055 (unpublished)].
[13] G. Kotliar, S. Y. Savrasov, G. Palsson, and G. Biroli, Phys. Rev. Lett. **87**, 186401 (2001); for periodized version (PCDMFT), see M. Capone, M. Civelli, S. S. Kancharla, C. Castellani, and G. Kotliar, Phys. Rev. B **69**, 195105 (2004).
[14] C. Gros and R. Valenti, Ann. Phys. **3**, 460 (1994).
[15] D. Senechal, D. Perez, and M. Pioro-Ladriee, Phys. Rev. Lett. **84**, 522 (2000); D. Senechal, D. Perez, and D. Plouffe, Phys. Rev. B **66**, 075129 (2002).
[16] B. Kyung, S. S. Kancharla, D. Senechal, A.-M. S. Tremblay, M. Civelli, and G. Kotliar, ArXiv: cond-mat/0502565 (unpublished).
[17] M. Civelli, M. Capone, S. S. Kancharla, O. Parcollet, and G. Kotliar, Phys. Rev. Lett. **95**, 106402 (2005).
[18] J. E. Hirsch and R. M. Fye, Phys. Rev. Lett. **56**, 2521 (1986); M. Jarrell, Phys. Rev. Lett. **69**, 168 (1992); M. J. Rozenberg, X. Y. Zhang, and G. Kotliar, *ibid.* **69**, 1236 (1992); A. Georges and W. Krauth, *ibid.* **69**, 1240 (1992); M. Jarrell, in *Numerical Methods for Lattice Quantum Many-Body Problems*, edited by D. Scalapino (Addison Wesley, 1997). For a review of QMC for DMFT see Ref. 19.
[19] K. Held, I. A. Nekrasov, N. Blümer, V. I. Anisimov, and D. Vollhardt, Int. J. Mod. Phys. B **15**, 2611 (2001); K. Held, I. A. Nekrasov, G. Keller, V. Eyert, N. Blümer, A. K. McMahan, R. T. Scalettar, T. Pruschke, V. I. Anisimov, and D. Vollhardt, ArXiv: cond-mat/0112079 published in *Quantum Simulations of Complex Many-Body Systems: From Theory to Algorithms*, edited by J. Grotendorst, D. Marks, and A. Muramatsu, NIC Series Volume 10 (NIC Directors, Forschunszentrum Jülich, 2002) pp. 175–209.
[20] K. G. Wilson, Rev. Mod. Phys. **47**, 773 (1975); H. R. Krishnamurthy, J. W. Wilkins, and K. G. Wilson, Phys. Rev. B **21**, 1003 (1980); **21**, 1044 (1980); for a comprehensive introduction to NRG, see e.g., A. C. Hewson, in *The Kondo Problem to Heavy Fermions* (Cambridge University Press, Cambridge, 1993).
[21] R. Bulla, A. C. Hewson, and Th. Pruschke, J. Phys.: Condens. Matter **10**, 8365 (1998); R. Bulla, Phys. Rev. Lett. **83**, 136 (1999).
[22] M. V. Sadovskii, Zh. Eksp. Teor. Fiz. **77**, 2070 (1979) [Sov. Phys. JETP **50**, 989 (1979)].
[23] Y. M. Vilk and A.-M. S. Tremblay, J. Phys. I **7**, 1309 (1997).
[24] O. Gunnarsson, O. K. Andersen, O. Jepsen, and J. Zaanen, Phys. Rev. B **39**, 1708 (1989).
[25] M. T. Czyzyk and G. A. Sawatzky, Phys. Rev. B **49**, 14211 (1994).
[26] M. V. Sadovskii, I. A. Nekrasov, E. Z. Kuchinskii, Th. Prushke, and V. I. Anisimov, ArXiv: cond-mat/0502612 (unpublished).
[27] Th. A. Maier, Th. Pruschke, and M. Jarrell, Phys. Rev. B **66**, 075102 (2002).
[28] T. D. Stanescu and P. Phillips, Phys. Rev. Lett. **91**, 017002 (2003).
[29] A. A. Katanin and A. P. Kampf, Phys. Rev. Lett. **93**, 106406 (2004).
[30] D. Rohe and W. Metzner, Phys. Rev. B **71**, 115116 (2005).
[31] D. K. Sunko and S. Barisic, Eur. Phys. J. B **46**, 269 (2005).
[32] A. Kaminski, H. M. Fretwell, M. R. Norman, M. Randeria, S. Rosenkranz, U. Chatterjee, J. C. Campuzano, J. Mesot, T. Sato, T. Takahashi, T. Terashima, M. Takano, K. Kadowaki, Z. Z. Li, and H. Raffy, Phys. Rev. B **71**, 014517 (2005).
[33] D. Senechal and A.-M. S. Tremblay, Phys. Rev. Lett. **92**, 126401 (2004).
[34] K. Haule, A. Rosch, J. Kroha, and P. Wölfle, Phys. Rev. Lett. **89**, 236402 (2002); Phys. Rev. B **68**, 155119 (2003).
[35] B. Kyung, V. Hankevych, A.-M. Dare, and A.-M. S. Tremblay, Phys. Rev. Lett. **93**, 147004 (2004).
[36] P. Prelovsek and A. Ramsak, Phys. Rev. B **63**, 180506(R) (2001); P. Prelovsek and A. Ramsak, *ibid.* **72**, 012510 (2005).
[37] S. Biermann, F. Aryasetiawan, and A. Georges, Phys. Rev. Lett. **90**, 086402 (2003).
[38] P. Sun and G. Kotliar, Phys. Rev. Lett. **92**, 196402 (2004).
[39] E. Z. Kuchinskii, I. A. Nekrasov, and M. V. Sadovskii, JETP Lett. **82**, 198 (2005)[Pis'ma Zh. Eksp. Teor. Fiz. **82**, 217 (2005)].
[40] Discretization parameter $\Lambda=2$, the number of low energy states after the truncation 1000, cut off near Fermi energy 10^{-6}, broadening parameter $b=0.6$.
[41] Number warm-up sweeps 30000, the number of QMC sweeps 200 000, the number of imaginary time slices 40.
[42] We have checked that with the increase of Coulomb repulsion, the Van–Hove singularity *gradually* transforms into quasiparticle peak for $U=(6\div 8)t$.

ISSN 1063-7761, Journal of Experimental and Theoretical Physics, 2006, Vol. 103, No. 3, pp. 415–427. © Pleiades Publishing, Inc., 2006.

ELECTRONIC PROPERTIES OF SOLIDS

Non-Fermi-Liquid Behavior in the Fluctuating Gap Model: From the Pole to a Zero of the Green's Function¶

E. Z. Kuchinskii and M. V. Sadovskii

Institute for Electrophysics, Russian Academy of Sciences, Yekaterinburg, 620016 Russia

e-mail: sadovski@iep.uran.ru

Received February 17, 2006

Abstract—We analyze the non-Fermi-liquid (NFL) behavior of the fluctuating gap model (FGM) of pseudogap behavior in both one and two dimensions. A detailed discussion of quasiparticle renormalization (Z-factor) is given, demonstrating a kind of marginal Fermi-liquid or Luttinger-liquid behavior and topological stability of the bare Fermi surface (the Luttinger theorem). In the two-dimensional case, we discuss the effective picture of the Fermi surface destruction both in the hot spot model of dielectric (AFM, CDW) pseudogap fluctuations and for the qualitatively different case of superconducting d-wave fluctuations, reflecting the NFL spectral density behavior and similar to that observed in ARPES experiments on copper oxides.

PACS numbers: 71.10.Hf, 71.27.+a, 74.72.-h

DOI: 10.1134/S1063776106090111

1. INTRODUCTION

Pseudogap formation in the electronic spectrum of underdoped copper oxides is an especially striking anomaly of the normal state of high-temperature superconductors [1]. Discussions on the nature of the pseudogap state continue within two main scenarios—of superconducting fluctuations, leading to Cooper pair formation above T_c, or of other order-parameter fluctuations, in fact competing with superconductivity.

We believe that the preferable scenario for pseudogap formation is most likely based on the model of strong scattering of the charge carriers by short-range antiferromagnetic (AFM, SDW) spin fluctuations [1]. In the momentum representation, this scattering transfers momenta of the order of $\mathbf{Q} = (\pi/a, \pi/a)$ (where a is the lattice constant of a two-dimensional lattice). This leads to the formation of structures in the one-particle spectrum that are precursors of the changes in the spectra due to a long-range AFM order (period doubling).

Within this spin-fluctuation scenario, a simplified model of the pseudogap state was studied [1–3] under the assumption that the scattering by dynamic spin fluctuations can be reduced for high enough temperatures to a static Gaussian random field (quenched disorder) of pseudogap fluctuations. These fluctuations are defined by a characteristic scattering vector from the vicinity of $\mathbf{Q}$, with a width determined by the inverse correlation length of the short-range order, $\kappa = \xi^{-1}$. Actually, a similar model (formalism) can also be applied to the case of pseudogaps of a superconducting nature [3].

These models originated from the earlier one-dimensional model of pseudogap behavior [4, 5], the so-called fluctuating gap model (FGM), which is exactly solvable in the asymptotic limit of large correlation lengths of pseudogap fluctuations, $\kappa = \xi^{-1} \longrightarrow 0$ [4], and nearly exactly solvable in the case of finite κ, where we can take all Feynman diagrams of perturbation series into account, albeit using an approximate ansatz for higher-order contributions [5].

Non-Fermi-liquid behavior of the FGM model has already been discussed in one [4, 6–8] and two dimensions [1–3]. However, some interesting aspects of this model are still under discussion [9]. Below, we analyze different aspects of this anomalous behavior in both one-and two-dimensional versions, mainly in the case of AFM (SDW) or CDW pseudgap fluctuations, and also, more briefly, in the case of superconducting fluctuations, demonstrating a kind of marginal Fermi-liquid behavior and the qualitative picture of Fermi surface destruction and formation of Fermi arcs in two dimensions, similar to those observed in ARPES experiments on copper oxides.

¶ The text was submitted by the authors in English.

2. POSSIBLE TYPES OF GREEN FUNCTI ON RENORMALIZATION

We start with a qualitative discussion of possible manifestations of NFL behavior. The Green function of the interacting system of electrons is expressed via the Dyson equation (in the Matsubara representation, with $\varepsilon_n = (2n + 1)\pi T$ and $\xi_p = v_F(p - p_F)$) as[1]

$$G(\varepsilon_n, \xi_p) = \frac{1}{i\varepsilon_n - \xi_p - \Sigma(\varepsilon_n, \xi_p)}. \quad (1)$$

In what follows, we use a rather unusual definition of the renormalization (residue) Z-factor, introducing it as [9]:

$$G(\varepsilon_n, \xi_p) = Z(\varepsilon_n, \xi_p)G_0(\varepsilon_n, \xi_p) = \frac{Z(\varepsilon_n, \xi_p)}{i\varepsilon_n - \xi_p} \quad (2)$$

or

$$Z(\varepsilon_n, \xi_p) = \frac{i\varepsilon_n - \xi_p}{i\varepsilon_n - \xi_p - \Sigma(\varepsilon_n, \xi_p)} = (i\varepsilon_n - \xi_p)G(\varepsilon_n, \xi_p). \quad (3)$$

We note that $Z(\varepsilon_n, \xi_p)$ is in general complex and actually determines the full renormalization of the free-electron Green function $G_0(\varepsilon_n, \xi_p)$ due to interactions. At the same time, it is in some sense similar to the standard residue renormalization factor used in the Fermi-liquid theory.

We consider possible alternatives for the $Z(\varepsilon_n, \xi_p)$ behavior.

2.1. Fermi-Liquid Behavior

In a normal Fermi liquid, we can perform the usual expansion (close to the Fermi level and in obvious notation) assuming the absence of any singularities in $\Sigma(\varepsilon_n, \xi_p)$

$$\Sigma(\varepsilon_n, \xi_p) \approx \Sigma(0, 0) + i\varepsilon_n \frac{\partial\Sigma(\varepsilon_n, \xi_p)}{\partial(i\varepsilon_n)}\bigg|_0 + \xi_p \frac{\partial\Sigma(\varepsilon_n, \xi_p)}{\partial\xi_p}\bigg|_0 + \ldots. \quad (4)$$

In the absence of the static impurity scattering, $\Sigma(0, 0)$ is real and just renormalizes the chemical potential. We can then rewrite (1) as

$$G(\varepsilon) = \frac{1}{i\varepsilon_n\left\{1 - \frac{\partial\Sigma}{\partial(i\varepsilon_n)}\right\}_0 - \xi_p\left\{1 + \frac{\partial\Sigma}{\partial\xi_p}\right\}_0} \equiv \frac{\tilde{Z}}{i\varepsilon_n - \tilde{\xi}_p}, \quad (5)$$

where we have introduced the usual renormalized residue at the pole,

$$\tilde{Z} = \frac{1}{1 - \frac{\partial\Sigma}{\partial(i\varepsilon_n)}\Big|_0}, \quad \tilde{Z}^{-1} = 1 - \frac{\partial\Sigma}{\partial(i\varepsilon_n)}\bigg|_0, \quad (6)$$

and the spectrum of quasiparticles

$$\tilde{\xi}_p = \tilde{Z}\left(1 + \frac{\partial\Sigma}{\partial\xi_p}\right)_0 \xi_p. \quad (7)$$

The usual analytic continuation to real frequencies now yields the standard expressions of the normal Fermi-liquid theory [10, 11] with real $0 < \tilde{Z} < 1$, conserving the quasiparticle pole of the Green function.

In the special case where $\xi_p = 0$, i.e., at the Fermi surface, which is not renormalized by interactions in accordance with the Landau hypothesis and Luttinger theorem, we have

$$G(\varepsilon_n, \xi_p) = \frac{\tilde{Z}}{i\varepsilon_n}, \quad (8)$$

i.e., $\tilde{Z}$ coincides with the limit of $Z(\varepsilon_n \longrightarrow 0, \xi_p = 0)$ defined by (2) and (3), and we have the usual pole as $\varepsilon_n \longrightarrow 0$. Similarly, for $\varepsilon_n = 0$, we have $Z(\varepsilon_n = 0, \xi_p \longrightarrow 0) \sim \tilde{Z}$.

In general, this behavior is preserved not only in the case of $\Sigma(\varepsilon_n, \xi_p)$ possessing a regular expansion at small ε_n and ξ_p, but also for $\Sigma(\varepsilon_n, \xi_p) \sim \max(\varepsilon_n^\alpha, \xi_p^\alpha)$ with any $\alpha \geq 1$.

2.2. Impure Fermi Liquid

In the case of low concentration of random static impurities, we have $\Sigma(\varepsilon_n \longrightarrow 0, \xi_p \longrightarrow 0) \longrightarrow$ const, with $\mathrm{Re}\Sigma(0, 0)$ again giving a shift of the chemical potential, while $\mathrm{Im}\Sigma(0, 0) \sim \gamma$, where γ is the impurity scattering rate. For the Green function, we have

$$G(\varepsilon_n, \xi_p) = \frac{\tilde{Z}}{i\varepsilon_n - \tilde{\xi}_p + i\gamma\frac{\varepsilon_n}{|\varepsilon_n|}} \quad (9)$$

[1] Despite our use of the Matsubara representation, we treat ε_n as a continuous variable below.

and hence the renormalization factor defined by (3) is given by

$$Z(\varepsilon_n, \xi_p) = \tilde{Z}\frac{i\varepsilon_n - \xi_p}{i\varepsilon_n - \tilde{\xi}_p + i\gamma\dfrac{\varepsilon_n}{|\varepsilon_n|}}. \quad (10)$$

For $\xi_p = 0$, we have

$$Z(\varepsilon_n, \xi_p = 0) = \tilde{Z}\frac{i\varepsilon_n}{i\varepsilon_n + i\gamma\dfrac{\varepsilon_n}{|\varepsilon_n|}} \sim \frac{|\varepsilon_n|}{\gamma} \longrightarrow 0 \text{ as } |\varepsilon_n| \longrightarrow 0 \quad (11)$$

and for $|\varepsilon_n| \ll |\xi_p|$,

$$Z(\varepsilon_n \longrightarrow 0, \xi_p) = \tilde{Z}\frac{\xi_p}{\xi_p - i\gamma\dfrac{\varepsilon_n}{|\varepsilon_n|}} \sim \frac{\xi_p}{\gamma}\operatorname{sgn}\varepsilon_n \longrightarrow 0 \text{ as } \xi_p \longrightarrow 0, \quad (12)$$

i.e., impurity scattering leads to a Z-factor vanishing at the Fermi surface, just removing the usual Fermi-liquid pole singularity and producing a finite discontinuity of the Green function at $\varepsilon_n = 0$. This behavior is due to the loss of translational invariance of the Fermi liquid theory (momentum conservation) because of impurities. In fact, Green function (9) is obtained after averaging over the impurity position, which formally restores translational invariance, leading to a kind of (trivial) non-Fermi-liquid (NFL) behavior. We note that this behavior is observed for $|\varepsilon_n|, |\xi_p| \ll \gamma$, while in the opposite limit we obviously have a finite $Z(\varepsilon, \xi_p) \sim \tilde{Z}$.

2.3. Superconductors and Peierls and Excitonic Insulators

We now consider the case of an s-wave superconductor. The normal Gorkov Green function is given by

$$G(\varepsilon_n, \xi_p) = \frac{i\varepsilon_n + \xi_p}{(i\varepsilon_n)^2 - \xi_p^2 - |\Delta|^2}, \quad (13)$$

where Δ is the superconducting gap. The normal Green function also takes this form in an excitonic or Peierls insulator, where Δ denotes the appropriate insulating gap in the spectrum [11]. Then

$$Z(\varepsilon_n, \xi_p) = \frac{(i\varepsilon_n)^2 - (\xi_p)^2}{(i\varepsilon_n)^2 - \xi_p^2 - |\Delta|^2} \sim \frac{\max(\varepsilon_n^2, \xi_p^2)}{|\Delta|^2} \longrightarrow 0 \text{ for } \varepsilon_n, \xi_p \longrightarrow 0; \quad (14)$$

i.e., we have NFL behavior with the pole of the Green function at the Fermi surface replaced by a zero, due to the Fermi surface being closed by the superconducting (or insulating) gap.

Again, Fermi-liquid-type behavior with a finite Z-factor is restored for $|\varepsilon_n|, |\xi_p| \gg |\Delta|$.

But the complete description of the superconducting (excitonic, Peierls) phase is achieved only after the introduction of the anomalous Gorkov function. The excitation spectrum on both sides of the phase transition is determined by different Green functions with different topological properties [9].

2.4. Non-Fermi-Liquid Behavior Due to Interactions

Non-Fermi-liquid behavior of the Green function due to interactions may also occur in the case of the singular behavior $\Sigma(\varepsilon_n, \xi_p) \longrightarrow \infty$ as $\varepsilon_n \longrightarrow 0$ and $\xi_p \longrightarrow 0$, e.g., a power-like divergence[2] of $\Sigma(\varepsilon_n, \xi_p) \sim \max(\varepsilon_n^{-\alpha}, \xi_p^{-\alpha})$ with $\alpha > 0$. Obviously, $Z(\varepsilon_n \longrightarrow 0, \xi_p \longrightarrow 0) \longrightarrow 0$ in this case and we again have a zero of the Green function at the Fermi surface.

Another possibility is a singular behavior of derivatives of self-energy in (4), e.g., in the case where $\Sigma(\varepsilon_n, \xi_p) \sim \max(\varepsilon_n^{\alpha}, \xi_p^{\alpha})$ with $0 < \alpha < 1$, leading to the pole singularity of the Green function at the Fermi surface being weaker than usual.

Both types of behavior are realized within the Tomonaga–Luttinger model in one dimension [12], where the asymptotic behavior of $G(i\varepsilon_n, \xi_p)$ in the region of small $\xi_p \sim \varepsilon_n$ can be expressed as

$$G(\varepsilon_n \sim \xi_p) \sim \frac{1}{\varepsilon_n^{1-2\alpha'}}, \quad (15)$$

with $\alpha' < 1/2$. For $\alpha' > 1/2$,

$$G(\varepsilon_n \sim \xi_p) \sim A + B\varepsilon_n^{2\alpha'-1}. \quad (16)$$

For $3/2 > \alpha' > 1$,

$$G(\varepsilon_n \sim \xi_p) \sim A + B\varepsilon_n + C\varepsilon_n^{2\alpha'-1}, \quad (17)$$

etc., with the value of α' determined by the interaction strength.

A special case is given by the so-called marginal Fermi-liquid behavior assumed [13] for the interpretation of the electronic properties of CuO_2 planes of copper oxides. It is given by

$$\Sigma(\varepsilon_n, \xi_p) \sim \lambda i\varepsilon_n \ln\frac{\max(\varepsilon_n, \xi_p)}{\omega_c}, \quad (18)$$

[2] An additional logarithmic divergence can also be present here!

where λ is some dimensionless interaction constant and ω_c is a characteristic cutoff frequency. If we formally use (6) at finite ε_n, we obtain

$$\tilde{Z}(\varepsilon_n, \xi_p) \sim \frac{1}{1 - \lambda \ln \frac{\max(\varepsilon_n, \xi_p)}{\omega_c}}. \quad (19)$$

In this case, the residue at the pole of the Green function (Z-factor)[3] tends to zero at the Fermi surface itself, and, again, quasiparticles are simply not defined there at all! However, everywhere outside a narrow (logarithmic) region close to the Fermi surface, we have a more or less usual quasiparticle contribution: quasiparticles (close to the Fermi surface) are just marginally defined. At present, there are no generally accepted microscopic models of the marginal Fermi-liquid behavior in two dimensions.

3. FLUCTUATING GAP MODEL

The physical nature of the FGM was extensively discussed in the literature [1–8, 11]. The model based on the picture of an electron propagating in the (static!) Gaussian random field of (pseudogap) fluctuations, leading to scattering with the characteristic momentum transfer from a close vicinity of some fixed scattering vector $\mathbf{Q}$. These fluctuations are described by two basic parameters: the amplitude Δ and the correlation length (of short-range order) ξ^{-1}, determining the effective width $\kappa = \xi^{-1}$ of the scattering vector distribution.

In one dimension, the typical choice of the scattering vector is $Q = 2p_F$ (the fluctuation region of the Peierls transition) [4, 5], while in two dimensions, we usually mean the so-called hot spot model with $\mathbf{Q} = (\pi/a, \pi/a)$ [2, 3]. These models assume the dielectric (CDW, SDW) nature of pseudogap fluctuations, but essentially the same formalism can be used in the case of superconducting fluctuations [3].

The case of superconducting (s-wave) pseudogap fluctuations in higher dimensions is actually described by the same one-dimensional version of the FGM [3, 4, 9].

An attractive property of the models under discussion is the possibility of an exact solution achieved by the complete summation of the whole Feynman diagram series in the asymptotic limit of large correlation lengths $\xi \longrightarrow \infty$ [4, 6]. In the case of finite correlation lengths, we can also perform summation of all Feynman diagrams for the single-electron Green function, using an approximate ansatz for higher-order contributions in both one [5] and two dimensions [2, 3]. Similar methods of diagram summation can also be applied in calculations of the two-particle Green functions (vertex parts) [2–4, 7, 11, 14].

Our aim is to demonstrate that nearly all aspects of the NFL behavior discussed above can be nicely described within different variants of the FGM.

3.1. One Dimension

We limit ourselves here only to the case of incommensurate pseudogap (CDW) fluctuations [4, 5]. The commensurate case [6, 5] can be analyzed similarly. We note that the same expressions also apply in the case of superconducting (s-wave) fluctuations in all dimensions.

In the limit of the infinite correlation length of pseudogap fluctuations, we have the exact solution for a single-electron Green function [4, 11] given by

$$\begin{aligned} G(\varepsilon_n, \xi_p) &= \int_0^\infty d\zeta e^{-\zeta} \frac{i\varepsilon_n + \xi_p}{(i\varepsilon_n)^2 - \xi_p^2 - \zeta\Delta^2} \\ &= \frac{i\varepsilon_n + \xi_p}{\Delta^2} \exp\left(\frac{\varepsilon_n^2 + \xi_p^2}{\Delta^2}\right) \mathrm{Ei}\left(\frac{\varepsilon_n^2 + \xi_p^2}{\Delta^2}\right) \\ &\approx \frac{i\varepsilon_n + \xi_p}{\Delta^2} \ln\left(\gamma' \frac{\varepsilon_n^2 + \xi_p^2}{\Delta^2}\right) \\ &\text{as } \varepsilon_n \longrightarrow 0, \quad \xi_p \longrightarrow 0, \end{aligned} \quad (20)$$

where $\mathrm{Ei}(-x)$ denotes the integral exponential function and we use the asymptotic behavior $\mathrm{Ei}(-x) \sim \ln(\gamma' x)$ as $x \longrightarrow 0$ ($\ln\gamma' = 0.577$ is the Euler constant). Then, using (3), we immediately obtain

$$\begin{aligned} Z(\varepsilon_n, \xi_p) &= -\frac{\varepsilon_n^2 + \xi_p^2}{\Delta^2} \ln\left(\gamma' \frac{\varepsilon_n^2 + \xi_p^2}{\Delta^2}\right) \longrightarrow 0 \\ &\text{as } \varepsilon_n \longrightarrow 0, \quad \xi_p \longrightarrow 0. \end{aligned} \quad (21)$$

Precisely the same result is obtained if, for finite ε_n and ξ_p, we define

$$\tilde{Z}(\varepsilon_n, \xi_p) = \frac{1}{1 - \frac{\partial\Sigma(\varepsilon_n, \xi_p)}{\partial(i\varepsilon_n)}} \quad (22)$$

similarly to (6). We note that because $|\varepsilon_n| \ll \Delta$ and $|\xi_p| \ll \Delta$, we obviously have $Z > 0$, but the usual pole of the Green function at the Fermi surface (point) of the normal system is here transformed into a zero due to pseudogap fluctuations. Because of the topological stability [9], the singularity of the Green function at the

[3] We note that (19), strictly speaking, cannot give a correct definition of the residue, because standard expression (6) is defined only at the Fermi surface itself, where (19) simply does not exist. In what follows, we therefore prefer the rather unusual definition in (2).

Fermi surface is not destroyed: the zero is also a singularity (with the same topological charge) as the pole. But the FGM actually gives an explicit example of a kind of Luttinger or marginal Fermi liquid with a very strong renormalization of the singularity at the Fermi surface.

We consider the self-energy corresponding to Green functions (20):

$$\Sigma(\varepsilon_n, \xi_p) = i\varepsilon_n - \xi_p - \left[\int_0^\infty d\zeta e^{-\zeta} \frac{i\varepsilon_n + \xi_p}{(i\varepsilon_n)^2 - \xi_p^2 - \zeta\Delta^2}\right]^{-1}. \quad (23)$$

Taking $\xi_p = 0$ for simplicity and $\varepsilon_n \longrightarrow 0$, we obtain

$$\Sigma(\varepsilon_n \longrightarrow 0, \xi_p = 0) = \frac{1}{i\varepsilon_n}\left[\int_0^\infty d\zeta e^{-\zeta} \frac{1}{\varepsilon_n^2 + \zeta\Delta^2}\right]^{-1} \approx -\frac{\Delta^2}{i\varepsilon_n}\frac{1}{\ln\left(\gamma'\dfrac{\varepsilon_n^2}{\Delta^2}\right)} \longrightarrow \infty, \quad (24)$$

i.e., divergence of the type discussed above.

In the case of finite correlation lengths $\xi = \kappa^{-1}$ of pseudogap fluctuations, we use the continuous-fraction representation of the single-electron Green function derived in [5] to obtain the renormalization factor as ($\varepsilon_n > 0$)

$$Z(\varepsilon_n, \xi_p) = \cfrac{i\varepsilon_n - \xi_p}{i\varepsilon_n - \xi_p - \cfrac{\Delta^2}{i\varepsilon_n + \xi_p + iv_F\kappa - \cfrac{\Delta^2}{i\varepsilon_n - \xi_p + 2iv_F\kappa - \cfrac{2\Delta^2}{i\varepsilon_n + \xi_p + 3iv_F\kappa - \ldots}}}}, \quad (25)$$

which can be studied numerically.

In Fig. 1, we show typical dependences of the renormalization factor $Z(\varepsilon_n, \xi_p)$. In all cases, it tends to zero at the (bare) Fermi surface and the pole of the Green function disappears. Essentially, this strong renormalization starts on the scale of the pseudogap width; i.e., for $|\varepsilon_n| < \Delta$ and $|\xi_p| < \Delta$, reflecting a non-Fermi-liquid behavior due to pseudogap fluctuations.

However, the role of finite correlation lengths ξ (finite κ) is qualitatively similar to static impurity scattering,[4] and a more detailed calculation shows that the Z-factor behaves at small $\epsilon_n \ll v_F\kappa$ and $|\xi_p| \ll v_F\kappa$ (with $\varepsilon_n > 0$) as

$$Z(\epsilon_n, \xi_p) \approx \alpha\left(\frac{v_F\kappa}{\Delta}\right)\left(\frac{\epsilon_n + i\xi_p}{\Delta}\right) \longrightarrow 0 \quad \text{as } \varepsilon_n \longrightarrow 0, \quad \xi_p \longrightarrow 0, \quad (26)$$

with $\alpha(v_F\kappa/\Delta) \longrightarrow 0$ as $\kappa \longrightarrow 0$, as seen from Fig. 2. In terms of the Green function, this behavior corresponds to

$$G(\varepsilon_n, \xi_p) \approx \frac{1}{\Delta}\alpha\left(\frac{v_F\kappa}{\Delta}\right)\frac{\varepsilon_n + i\xi_p}{i\varepsilon_n - \xi_p} = -i\frac{1}{\Delta}\alpha\left(\frac{v_F\kappa}{\Delta}\right). \quad (27)$$

Therefore, for finite κ, the Green function has no zero at $\epsilon_n = 0$ and $\xi_p = 0$ and remains finite as in an impure system.

The vanishing of the renormalization factor $Z(\varepsilon_n, \xi_p)$ at the bare Fermi surface is in correspondence with the general topological stability arguments [9]: in the absence of static impurity-like scattering, the pole singularity of the Green function is replaced by a zero. In

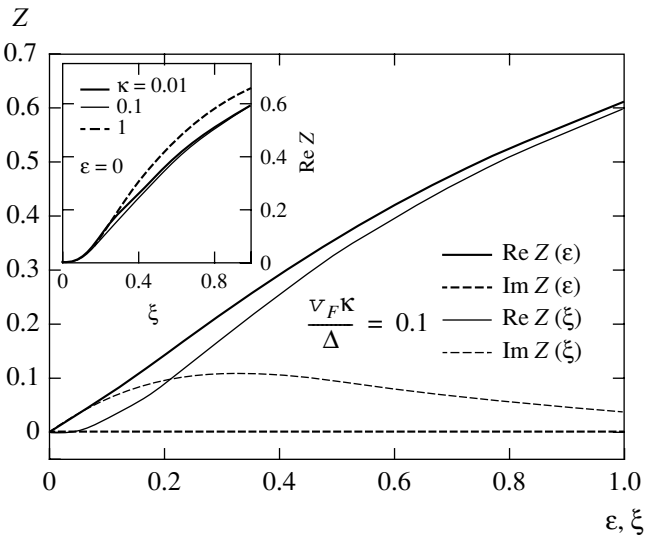

Fig. 1. Typical dependences of the $Z(\varepsilon_n, \xi_p)$ factor in the one-dimensional FGM with finite correlation lengths: dependences of $Z(\varepsilon_n = 0, \xi_p)$ and $Z(\varepsilon_n, \xi_p = 0)$ on ε_n and ξ_p for $v_F\kappa/\Delta = 0.1$. Inset: Dependences of $\mathrm{Re}\,Z(\varepsilon_n = 0, \xi_p)$ on ξ_p for different values of κ (in units of Δ/v_F). Both ε_n and ξ_p are given in units of Δ.

[4] This is due to our approximation of the static nature of pseudogap fluctuations.

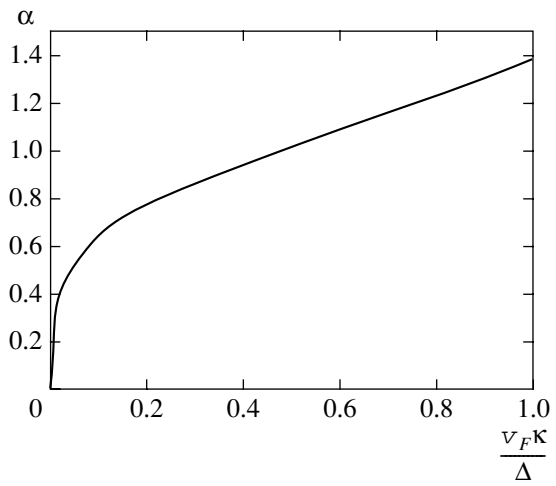

Fig. 2. Dependence of $\alpha(v_F\kappa/\Delta)$ on the inverse correlation length.

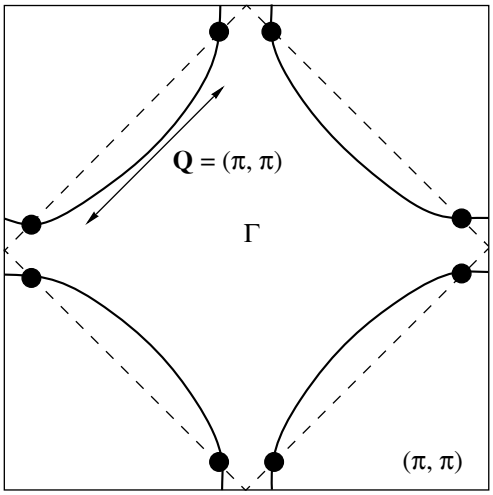

Fig. 3. Fermi surface in the Brillouin zone and the hot spot model. The magnetic zone appears, e.g., in the presence of antiferromagnetic long-range order. Hot spots correspond to intersections of the magnetic zone borders with the Fermi surface and are connected by a scattering vector on the order of $\mathbf{Q} = (\pi/a, \pi/a)$.

the presence of this additional scattering, this zero is replaced by a finite discontinuity, and the singularity therefore persists.

3.2. Hot Spot Model in Two Dimensions

In two dimensions, we introduce the so-called hot spot model. We consider a typical Fermi surface of electrons moving in the CuO_2 plane of copper oxides as shown in Fig. 3. If we neglect fine details, the observed (e.g., in ARPES experiments) Fermi surface (and also the spectrum of elementary excitations) in the CuO_2 plane is in the first approximation described by the usual tight-binding model,

$$\epsilon(\mathbf{p}) = -2t(\cos p_x a + \cos p_y a) - 4t'\cos p_x a \cos p_y a, \quad (28)$$

where t is the nearest-neighbor transfer integral, t' is the transfer integral between second-nearest neighbors, and a is the square lattice constant.

Phase transition to the antiferromagnetic state induces lattice period doubling and leads to the appearance of an antiferromagnetic Brillouin zone in inverse space, as is also shown in Fig. 3. If the spectrum of carriers is given by (28) with $t' = 0$ and we consider the half-filled case, the Fermi surface becomes just a square coinciding with the borders of the antiferromagnetic zone and we have a complete nesting: flat parts of the Fermi surface match each other after the translation by the vector of antiferromagnetic ordering $\mathbf{Q} = (\pm\pi/a, \pm\pi/a)$. In this case and for $T = 0$, the electron spectrum is unstable, the energy gap appears everywhere on the Fermi surface, and the system becomes an insulator due to the formation of an antiferromagnetic spin density wave (SDW).[5] In the case of the Fermi surface shown in Fig. 3, the appearance of the antiferromagnetic long-range order, in accordance with the general rules of band theory, leads to the appearance of discontinuities of isoenergetic surfaces (e.g., the Fermi surface) at crossing points with boundaries of a new (magnetic) Brillouin zone due to a gap opening at points connected by the vector $\mathbf{Q}$.

In the most part of the underdoped region of the cuprate phase diagram, the antiferromagnetic long-range order is absent, but a number of experiments support the existence of well-developed fluctuations of the antiferromagnetic short-range order that scatter electrons with the characteristic momentum transfer of the order of $\mathbf{Q}$. Similar effects may appear due to CDW fluctuations. These pseudogap fluctuations are again considered to be static and Gaussian, and characterized by two parameters: the amplitude Δ and correlation length $\xi = \kappa^{-1}$ [1]. In this case, we can obtain a rather complete solution for the single-electron Green function via summation of all Feynman diagrams of the perturbation series describing scattering by these fluctuations [1–3]. This solution is again exact in the limit as $\xi \longrightarrow \infty$ [2] and apparently very close to the exact solution in case of finite ξ [15]. Generalizations of this approach to two-particle properties (vertex parts) are also quite feasible.

We start again with an exact solution for $\xi \longrightarrow \infty$ (or $\kappa = 0$) [2]. We first introduce the (normal) Green func-

[5] Analogous dielectrization is also realized in the case of the formation of the similar charge density wave (CDW).

tion for the SDW (CDW) state with long-range order (see, e.g., [11]):

$$G(\varepsilon_n, \xi_{\mathbf{p}}) = \frac{i\varepsilon_n - \xi_{\mathbf{p}-\mathbf{Q}}}{(i\varepsilon_n - \xi_{\mathbf{p}})(i\varepsilon_n - \xi_{\mathbf{p}-\mathbf{Q}}) - W^2}, \quad (29)$$

where W denotes the amplitude of the SDW (CDW) periodic potential and $\xi_{\mathbf{p}} = \varepsilon(\mathbf{p}) - \mu$. Then we can write the appropriate Z factor as

$$Z(\varepsilon_n, \xi_{\mathbf{p}}) = \frac{(i\varepsilon_n - \xi_1)(i\varepsilon_n - \xi_2)}{(i\varepsilon_n - \xi_1)(i\varepsilon_n - \xi_2) - W^2}, \quad (30)$$

where we set $\xi_{\mathbf{p}} = \xi_1$ and $\xi_{\mathbf{p}-\mathbf{Q}} = \xi_2$ for brevity. In what follows, we are mainly interested in the limit as $\varepsilon_n \longrightarrow 0$ and $\xi_1 \longrightarrow 0$, i.e., in the vicinity of the bare Fermi surface. We note that $\xi_2 = 0$ defines the so-called shadow Fermi surface. We have $\xi_1 = \xi_2 = 0$ precisely at the hot spots. It is convenient to introduce the complex variable

$$z = (i\varepsilon_n - \xi_1)(i\varepsilon_n - \xi_2), \quad (31)$$

which becomes small as $\varepsilon_n, \xi_1, \xi_2 \longrightarrow 0$.

3.2.1. Incommensurate combinatorics. In the case of incommensurate (CDW) pseudogap fluctuations, an exact solution for the Green function of the FGM in the limit as $\xi \longrightarrow \infty$ takes a form similar to (20) [1, 2], and we obtain (averaging (30) with the Rayleigh distribution for W)

$$\begin{aligned} Z(z) &= \int_0^\infty dW \frac{2W}{\Delta^2} e^{-W^2/\Delta^2} \frac{z}{z - W^2} \\ &= \int_0^\infty \frac{d\zeta}{\Delta^2} e^{-\zeta/\Delta^2} \frac{z}{z-\zeta} = \frac{z}{\Delta^2} e^{-z/\Delta^2} \mathrm{Ei}\left(\frac{z}{\Delta^2}\right). \end{aligned} \quad (32)$$

Then, as $z \longrightarrow 0$ we obtain

$$Z(z \longrightarrow 0) \approx \frac{z}{\Delta^2}\left[\ln\left(\gamma' \frac{z}{\Delta^2}\right) - i\pi\right]. \quad (33)$$

At the bare Fermi surface, we have $\xi_1 = 0$, and we limit ourselves to $\varepsilon_n > 0$ in what follows. From (33), we can then easily find the limit behavior of $Z(z)$. Some of the results are as follows.

(1) For $\varepsilon_n \ll |\xi_2|$, we have

$$\mathrm{Re}Z(\varepsilon_n \ll |\xi_2|, \xi_1 = 0) \approx \frac{\pi}{2} \frac{\varepsilon_n |\xi_2|}{\Delta^2}, \quad (34)$$

i.e., the impure-like linear behavior in ε_n.

(2) For $\varepsilon_n \gg |\xi_2|$ (i.e., also at the hot spot, where $\xi_2 = 0$), we have

$$\begin{aligned} &\mathrm{Re}Z(\varepsilon_n \gg |\xi_2|, \xi_1 = 0) \\ &\approx -\frac{\varepsilon_n^2}{\Delta^2} \ln\left(\gamma' \frac{\varepsilon_n^2}{\Delta^2}\right) + \frac{1}{2} \frac{\xi_2^2}{\Delta^2}, \end{aligned} \quad (35)$$

i.e., for $\xi_2 = 0$, NFL behavior similar to the one-dimensional case.

We note that we always have $\mathrm{Im}Z = 0$ at $\xi_2 = 0$, i.e., at the shadow Fermi surface and in particular at the hot spot itself.

3.2.2. Spin-fermion combinatorics. We now consider the spin-fermion (Heisenberg) model for pseudogap (SDW) fluctuations [2]. In this case, we again obtain the FGM, but with the gap distribution different from the Rayleigh distribution; instead of (32), we have

$$\begin{aligned} Z(z) &= \frac{2}{\sqrt{2\pi}} \int_0^\infty dW \frac{W^2}{\left(\frac{\Delta^2}{3}\right)^{3/2}} \\ &\times \exp\left(-\frac{W^2}{2\left(\frac{\Delta^2}{3}\right)}\right) \frac{z}{z - W^2} \\ &= \frac{1}{\sqrt{2\pi}} \int_0^\infty d\zeta \frac{\sqrt{\zeta}}{\left(\frac{\Delta^2}{3}\right)^{3/2}} \exp\left(-\frac{\zeta}{2\left(\frac{\Delta^2}{3}\right)}\right) \frac{\zeta}{z - \zeta} \\ &= \frac{\Gamma(3/2)}{\sqrt{2\pi}} \frac{(-z)^{3/2}}{\left(\frac{\Delta^2}{3}\right)^{3/2}} \exp\left[-\frac{z}{2\left(\frac{\Delta^2}{3}\right)}\right] \\ &\times \Gamma\left(-\frac{1}{2}; -\frac{z}{2\left(\frac{\Delta^2}{3}\right)}\right). \end{aligned} \quad (36)$$

Hence, as $z \longrightarrow 0$, we obtain

$$\begin{aligned} Z(z) &\approx \frac{2\Gamma(3/2)}{\sqrt{\pi}} \\ &\times \left[-\frac{z}{2\left(\frac{\Delta^2}{3}\right)} + \Gamma\left(-\frac{1}{2}\right)\left(-\frac{z}{2\left(\frac{\Delta^2}{3}\right)}\right)^{3/2}\right]. \end{aligned} \quad (37)$$

On the bare Fermi surface ($\xi_p = 0$), we then have

$$Z(\varepsilon_n \longrightarrow 0, \xi_2, \zeta_1 = 0) = \frac{2\Gamma(3/2)}{\sqrt{\pi}} \times \left[-\frac{\varepsilon_n(\varepsilon_n + i\xi_2)}{2\left(\frac{\Delta^2}{3}\right)} + \Gamma\left(-\frac{1}{2}\right)\left(-\frac{\varepsilon_n(\varepsilon_n + i\xi_2)}{2\left(\frac{\Delta^2}{3}\right)} \right)^{3/2} \right]. \quad (38)$$

In particular, for $\xi_2 = 0$, we have $\mathrm{Im}Z = 0$ and

$$Z(\varepsilon_n \longrightarrow 0, \xi_2 = \xi_1 = 0) = \mathrm{Re}Z(\varepsilon_n \longrightarrow 0, \xi_2 = \xi_1 = 0) = \frac{\Gamma(3/2)}{\sqrt{\pi}} \frac{\varepsilon_n^2}{\left(\frac{\Delta^2}{3}\right)}, \quad (39)$$

and we thus obtain the quadratic NFL behavior of the Z factor. We again present some results on the limit behavior.

(1) For $\varepsilon_n \ll |\xi_2|$, we have

$$\mathrm{Re}Z(\varepsilon_n \ll |\xi_2|, \xi_1 = 0) = \frac{2\Gamma(3/2)}{\sqrt{\pi}} \times \left[\frac{\varepsilon_n^2}{2\left(\frac{\Delta^2}{3}\right)} + \sqrt{2\pi}\left(\frac{\varepsilon_n|\xi_2|}{2\left(\frac{\Delta^2}{3}\right)} \right)^{3/2} \right], \quad (40)$$

i.e., the NFL zero behavior.

(2) For $\varepsilon_n \gg |\xi_2|$ (i.e., also at the hot spot, where $\xi_2 = 0$) we have

$$\mathrm{Re}Z(\varepsilon_n \gg \xi_2, \xi_1 = 0) = \frac{\Gamma(3/2)}{\sqrt{\pi}} \frac{\varepsilon_n^2}{\left(\frac{\Delta^2}{3}\right)}, \quad (41)$$

which is again the NFL zero behavior.

In the general case of finite correlation lengths $\xi = \kappa^{-1}$, we have to perform numerical analysis using the recursive relations proposed in [2, 3]. We again use the basic definition of the Z factor in (3). To calculate the self-energy $\Sigma(\varepsilon_n, \xi_\mathbf{p})$ of an electron moving in the quenched random field of (static) Gaussian spin fluctuations with dominant scattering momentum transfers from the vicinity of the characteristic vector $\mathbf{Q}$, we use the recursive procedure [2, 3], in which all Feynman diagrams describing the scattering of electrons by this random field are taken into account. The sought self-energy is given by

$$\Sigma(\varepsilon_n, \xi_\mathbf{p}) = \Sigma_{k=1}(\varepsilon_n, \xi_\mathbf{p}) \quad (42)$$

with $\xi_\mathbf{p} = \epsilon(\mathbf{p}) - \mu$ (cf. (28)) and

$$\Sigma_k(\varepsilon_n, \xi_\mathbf{p}) = \Delta^2 \frac{s(k)}{i\varepsilon_n + \mu - \epsilon_k(\mathbf{p}) + in v_k \kappa - \Sigma_{k+1}(\varepsilon_n, \xi_\mathbf{p})}. \quad (43)$$

The quantity Δ again characterizes the energy scale of pseudogap fluctuations, and $\kappa = \xi^{-1}$ is the inverse correlation length of short-range SDW fluctuations, $\epsilon_k(\mathbf{p}) = \epsilon(\mathbf{p} + \mathbf{Q})$ and $v_k = \left|v^x_{\mathbf{p}+\mathbf{Q}}\right| + \left|v^y_{\mathbf{p}+\mathbf{Q}}\right|$ for odd k, while $\varepsilon_k(\mathbf{p}) = \varepsilon(\mathbf{p})$ and $v_k = \left|v^x_\mathbf{p}\right| + \left|v^y_\mathbf{p}\right|$ for even k. The velocity projections $v^x_\mathbf{p}$ and $v^y_\mathbf{p}$ are determined by the usual momentum derivatives of the bare electron energy dispersion $\epsilon(\mathbf{p})$ given by (28). Finally, $s(k)$ is a combinatorial factor, with

$$s(k) = k \quad (44)$$

for commensurate charge (CDW type) fluctuations with $\mathbf{Q} = (\pi/a, \pi/a)$ [5]. For incommensurate CDW fluctuations [5], we find

$$s(k) = \begin{cases} \frac{k+1}{2} & \text{for odd } k \\ \frac{k}{2} & \text{for even } k. \end{cases} \quad (45)$$

For the spin-fermion model in [2], the combinatorics of diagrams becomes more complicated. Spin-conserving scattering processes obey commensurate combinatorics, while spin-flip scattering is described by diagrams of the incommensurate type (charged random field in terms of [2]). In this model, the recursive relation for the single-particle Green function is again given by (43), but the combinatorial factor $s(n)$ acquires the form [2]

$$s(k) = \begin{cases} \frac{k+2}{3} & \text{for odd } k \\ \frac{k}{3} & \text{for even } k. \end{cases} \quad (46)$$

Below, we only present our results for the spin-fermion combinatorics, because in other cases, we obtain more or less similar behavior of the renormalization factors.

In Fig. 4, we show the results of numerical calculation of $\mathrm{Re}Z(\varepsilon_n, \xi_\mathbf{p} = 0)$ at different points taken at the bare Fermi surface, shown in the inset. For comparison, we show the data obtained in the limit of the infinite correlation length $\xi \longrightarrow \infty$ (or $\kappa = 0$, which is an exactly solvable case) and for finite $\kappa a = 0.01$ (i.e., $\xi = 100a$). It is clearly seen that in both cases, $\mathrm{Re}Z \sim 1$ at the nodal point D, except at very small values of ε_n, while in the vicinity of the hot spot (points A and C) and

also at the hot spot itself (point B), ReZ becomes small in a rather wide interval of $\varepsilon_n < \Delta$. This corresponds to an approximately Fermi-liquid behavior in the nodal region (the vicinity of the Brillouin zone diagonal), with a kind of marginal Fermi-liquid or Luttinger-liquid (NFL) behavior as we move to the vicinity of the hot spot.

For completeness, in Fig. 5, we show a similar comparison of the dependences of ImZ on ε_n at the same characteristic points on the Fermi surface and for the same parameters as in Fig. 4. It is only important to stress once again that we have Im$Z = 0$ only at the hot spot itself (point B), and therefore Z becomes real and shows a dependence on ε_n more or less equivalent to that proposed for marginal Fermi liquids (or Luttinger liquids).

In all cases, we observe the vanishing of the renormalization factor $Z(\varepsilon_n, \xi_p)$ at the bare Fermi surface. In the absence of static impurity-like scattering due to finite values of the correlation length $\xi = \kappa^{-1}$, the pole singularity of the Green function is replaced by a zero, reflecting the topological stability of the bare Fermi surface (the Luttinger theorem) [9]. In the presence of this scattering, the singularity of the Green function at the topologically stable bare Fermi surface remains in the form of a finite discontinuity.

3.3. Spectral Density and Fermi Surface Destruction in the Hot Spot Model

We return to (29) and perform the usual analytic continuation to real frequencies, $i\varepsilon_n \longrightarrow \varepsilon + i\delta$. We then obtain

$$G^R(\varepsilon, \xi_{\mathbf{p}}) = \frac{\varepsilon - \xi_2}{(\varepsilon + i\delta - \xi_1)(\varepsilon - \xi_2 + i\delta) - W^2} = \frac{\varepsilon - \xi_2}{(\varepsilon - \xi_1)(\varepsilon - \xi_2) - W^2 + i\delta(2\varepsilon - \xi_1 - \xi_2)} \quad (47)$$

and therefore the spectral density in the case of a long-range (CDW, SDW) order is given by

$$A_W(\varepsilon, \xi_{\mathbf{p}}) = -\frac{1}{\pi}\mathrm{Im}G^R(\varepsilon, \xi_{\mathbf{p}}) = (\varepsilon - \xi_2)\delta[(\varepsilon - \xi_1)(\varepsilon - \xi_2) - W^2]\,\mathrm{sgn}(2\varepsilon - \xi_1 - \xi_2). \quad (48)$$

Accordingly, for the FGM with the correlation length $\xi \longrightarrow \infty$, we have

$$A(\varepsilon, \xi_{\mathbf{p}}) = \int_0^\infty dW \mathcal{P}_W A_W(\varepsilon, \xi_{\mathbf{p}}), \quad (49)$$

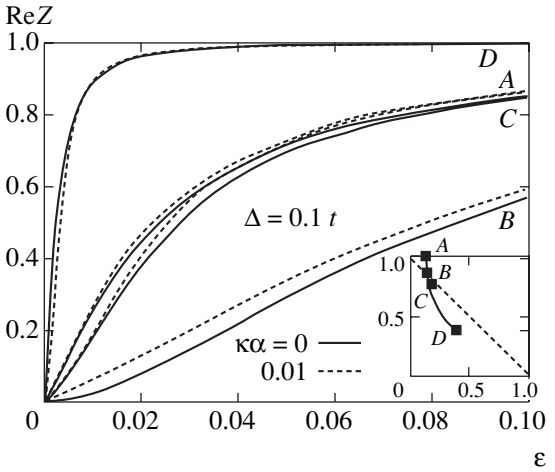

Fig. 4. Dependence of ReZ on ε_n (in units of t) at different points of the Fermi surface (corresponding to $t' = -0.4t$ and $\mu = -1.3t$) in the hot spot model (the spin-fermion combinatorics of diagrams) with correlation lengths of $\xi \longrightarrow \infty$ ($\kappa = 0$) and $\xi^{-1}a = \kappa a = 0.01$. The pseudogap amplitude is $\Delta = 0.1t$. Inset: The bare Fermi surface and the points where the calculations were performed.

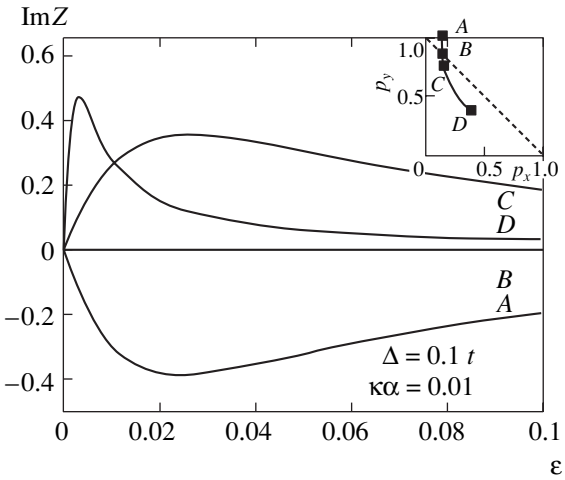

Fig. 5. Dependence of ImZ on ε_n (in units of the transfer integral t) at different points of the Fermi surface (corresponding to $t' = -0.4t$ and $\mu = -1.3t$) in the hot spot model with the finite correlation length $\xi^{-1}a = \kappa a = 0.01$ (the spin-fermion combinatorics of diagrams). The pseudogap amplitude is $\Delta = 0.1t$. Inset: the bare Fermi surface and the points where the calculations were performed.

where $\mathcal{P}_W$ is the distribution function of gap fluctuations, depending on the combinatorics of diagrams and leading to the following separate cases, already considered (or mentioned) above.

3.3.1. Incommensurate combinatorics. In the case of incommensurate CDW-like pseudogap fluctuations, we have

$$\mathcal{P}_W = \frac{2W}{\Delta^2}\exp\left(-\frac{W^2}{\Delta^2}\right), \quad (50)$$

which is the Rayleigh distribution [4, 11]. From (49), we then obtain

$$A(\varepsilon, \xi_{\mathbf{p}}) = \frac{\varepsilon - \xi_2}{\Delta^2}\exp\left(-\frac{(\varepsilon - \xi_1)(\varepsilon - \xi_2)}{\Delta^2}\right) \times \theta[(\varepsilon - \xi_1)(\varepsilon - \xi_2)]\,\mathrm{sgn}(2\varepsilon - \xi_1 - \xi_2). \quad (51)$$

For $\varepsilon = 0$, we have

$$A(\varepsilon = 0, \xi_{\mathbf{p}}) = \frac{\xi^2}{\Delta^2}\exp\left(-\frac{\xi_1\xi_2}{\Delta^2}\right)\theta[\xi_1, \xi_2]\,\mathrm{sgn}(\xi_1 + \xi_2). \quad (52)$$

For $\xi_1 \longrightarrow \pm 0$, we obtain

$$A(\varepsilon = 0, \xi_{\mathbf{p}} \longrightarrow \pm 0, \xi_2) = \pm\frac{\xi_2}{\Delta^2}\theta(\pm\xi_2), \quad (53)$$

and therefore $A(\varepsilon = 0, \xi_{\mathbf{p}})$ is nonzero within the Brillouin zone only in the space between the bare Fermi surface and the shadow Fermi surface. This qualitative result is confirmed below, for all other combinatorics, in the case of the pure FGM with $\xi^{-1} = \kappa = 0$.

3.3.2. Commensurate combinatorics. In the case of commensurate CDW-like pseudogap fluctuations, we have [6]

$$\mathcal{P}_W = \frac{1}{\sqrt{2\pi}\Delta}\exp\left(-\frac{W^2}{2\Delta^2}\right), \quad (54)$$

which is the Gaussian distribution. From (49), we then obtain

$$A(\varepsilon, \xi_{\mathbf{p}}) = \frac{1}{\sqrt{2\pi}\Delta}\frac{\varepsilon - \xi_2}{\sqrt{(\varepsilon - \xi_1)(\varepsilon - \xi_2)}} \times \exp\left(-\frac{(\varepsilon - \xi_1)(\varepsilon - \xi_2)}{2\Delta^2}\right) \times \theta[(\varepsilon - \xi_1)(\varepsilon - \xi_2)]\,\mathrm{sgn}(2\varepsilon - \xi_1 - \xi_2), \quad (55)$$

with the same qualitative conclusions as in the incommensurate case.

3.3.3. Spin-fermion combinatorics. In the case of SDW-like pseudogap fluctuations of the (Heisenberg) spin-fermion model [2], we have the gap distribution

$$\mathcal{P}_W = \frac{2}{\pi}\frac{W^2}{\left(\frac{\Delta^2}{3}\right)^{3/2}}\exp\left(-\frac{W^2}{2\left(\frac{\Delta^2}{3}\right)}\right). \quad (56)$$

From (49), we then obtain

$$A(\varepsilon, \xi_{\mathbf{p}}) = \frac{1}{\sqrt{2\pi}}\frac{\sqrt{(\varepsilon - \xi_1)(\varepsilon - \xi_2)}}{\left(\frac{\Delta^2}{3}\right)^{3/2}} \times \exp\left(-\frac{(\varepsilon - \xi_1)(\varepsilon - \xi_2)}{2\left(\frac{\Delta^2}{3}\right)}\right)\theta[(\varepsilon - \xi_1)(\varepsilon - \xi_2)] \times \mathrm{sgn}(2\varepsilon - \xi_1 - \xi_2), \quad (57)$$

again with the same qualitative conclusions as in the incommensurate case.

In the general case of finite correlation lengths $\xi = \kappa^{-1}$, spectral densities can be directly computed using analytic continuation of recursive relations (42) and (43) to real frequencies [2, 3].

Actually, two-dimensional contour plots of $A(\varepsilon = 0, \xi_{\mathbf{p}})$ (which directly correspond to ARPES intensity plots) can be used for a practical definition of the renormalized Fermi surface and provide a qualitative picture of its evolution in the FGM with changed model parameters.[6]

In Fig. 6, we show typical intensity plots of the spectral density $A(\varepsilon = 0, \xi_{\mathbf{p}})$ in the Brillouin zone for the hot spot model both in the case of the infinite correlation length $\xi^{-1} = \kappa = 0$ and for a finite (large!) correlation length $\xi^{-1}a = \kappa a = 0.01$ (for the spin-fermion combinatorics of diagrams; in other cases, the behavior is quite similar) and for different values of the pseudogap amplitude Δ. We see that these spectral density plots give a rather beautiful qualitative picture of the destruction of the Fermi surface in the vicinity of hot spots for small values of A, with formation of typical Fermi arcs as A increases, which qualitatively resembles typical ARPES data for copper oxides [16, 17].

3.4. Superconducting d-Wave Fluctuations

As noted above, the case of superconducting *s*-wave pseudogap fluctuations simply reduces to the one-dimensional FGM. Much more interesting is the case of superconducting *d*-wave fluctuations in two dimensions.

To obtain exact results in the case of the infinite correlation length $\xi^{-1} = \kappa = 0$, we have only to make simple replacements in the above expressions for the hot spot model with incommensurate combinatorics: $\xi_2 \longrightarrow -\xi_1 =$

[6] We note that for free electrons, $A(\varepsilon = 0, \xi_{\mathbf{p}}) = \delta(\xi_{\mathbf{p}})$, and therefore the appropriate intensity plot directly reproduces the bare Fermi surface.

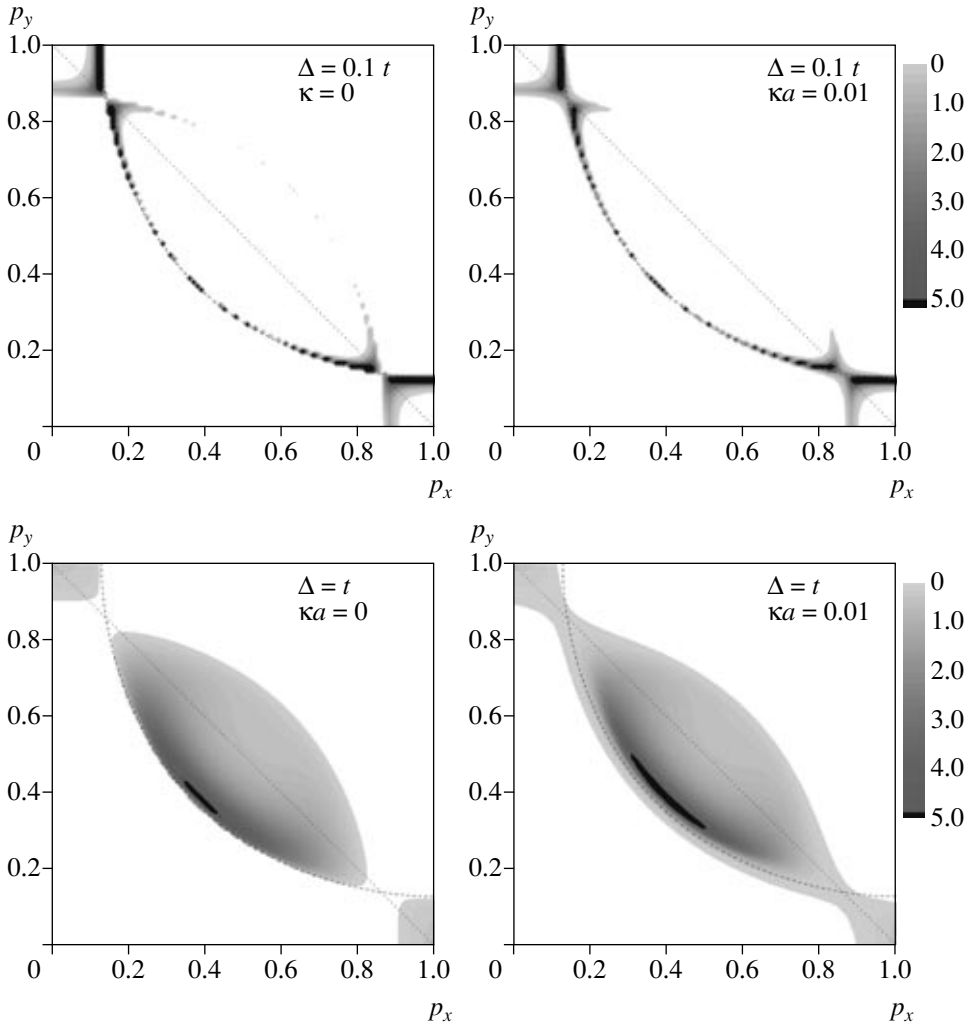

Fig. 6. Intensity plots of the spectral density $A(\varepsilon = 0, \xi_{\mathbf{p}})$ in the Brillouin zone for the hot spots model ($t' = -0.4t$ and $\mu = -1.3t$) in the case of infinite correlation length $\xi^{-1} = \kappa = 0$ and for a finite correlation length of $\xi^{-1}a = \kappa a = 0.01$ (the spin-fermion combinatorics of diagrams) with different values of the pseudogap amplitude. The bare Fermi surface is shown by the dashed line.

$-\xi_{\mathbf{p}}$ and $\Delta \longrightarrow \Delta_{\mathbf{p}}$, where $\Delta_{\mathbf{p}}$ defines the amplitude of fluctuations with the *d*-wave symmetry:

$$\Delta_{\mathbf{p}} = \frac{1}{2}\Delta[\cos(p_x a) - \cos(p_y a)], \tag{58}$$

where Δ now characterizes the energy scale of pseudogap fluctuations.

Equation (31) then reduces to $z = -(\varepsilon_n^2 + \xi_{\mathbf{p}}^2)$ and we immediately obtain an expression for the Z factor, similar to (21):

$$Z(\varepsilon_n, \xi_p) = -\frac{\varepsilon_n^2 + \xi_{\mathbf{p}}^2}{\Delta_{\mathbf{p}}^2}\exp\left(-\frac{\varepsilon_n^2 + \xi_{\mathbf{p}}^2}{\Delta_{\mathbf{p}}^2}\right)$$

$$\times \mathrm{Ei}\left(-\frac{\varepsilon_n^2 + \xi_{\mathbf{p}}^2}{\Delta_{\mathbf{p}}^2}\right) \approx -\frac{\varepsilon_n^2 + \xi_p^2}{\Delta_{\mathbf{p}}^2} \tag{59}$$

$$\times \ln\left(\gamma'\frac{\varepsilon_n^2 + \xi_p^2}{\Delta_{\mathbf{p}}^2}\right) \longrightarrow 0 \text{ as } \varepsilon_n \longrightarrow 0, \quad \xi_{\mathbf{p}} \longrightarrow 0,$$

again replacing the pole singularity by a zero at the bare Fermi surface, except for the nodal point at the diagonal of the Brillouin zone, where $\Delta_{\mathbf{p}} = 0$ (cf. (58)). Instead of (51), we obtain the spectral density as

$$A(\varepsilon, \xi_{\mathbf{p}}) = \frac{\varepsilon + \xi_{\mathbf{p}}}{\Delta_{\mathbf{p}}^2}\exp\left(-\frac{\varepsilon^2 - \xi_{\mathbf{p}}^2}{\Delta_{\mathbf{p}}^2}\right) \tag{60}$$

$$\times \theta(\varepsilon^2 - \xi_{\mathbf{p}}^2)\,\mathrm{sgn}\,\varepsilon,$$

which is nonzero only for $|\xi_{\mathbf{p}}| < \varepsilon$. As a result, at $\varepsilon = 0$, we have $A(\varepsilon = 0, \xi_{\mathbf{p}}) = 0$ for $\Delta_{\mathbf{p}} \neq 0$, and it is different from zero only at the intersection of the Brillouin zone

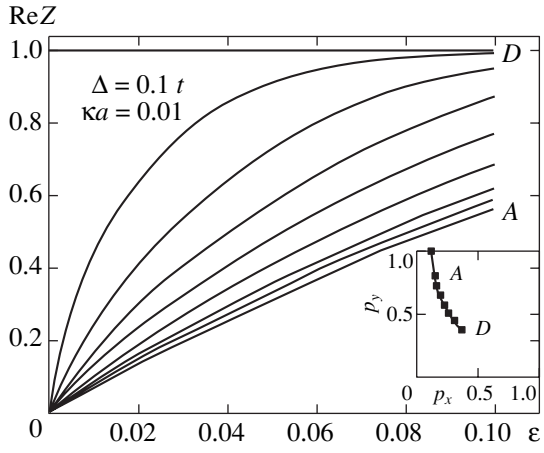

Fig. 7. The dependences of ReZ on ε_n (in units of t) at different points of the Fermi surface (corresponding to $t' = -0.4t$ and $\mu = -1.3t$) in the model of superconducting (d-wave) pseudpgap fluctuations with the correlation length $\xi^{-1}a = \kappa a = 0.01$. The pseudogap amplitude is $\Delta = 0.1t$. Inset: The bare Fermi surface and the points where the calculations were performed.

diagonal with the bare Fermi surface, where $\Delta_\mathbf{p}$ given by (58) is zero. At the Fermi surface itself, we have

$$A(\varepsilon, \xi_\mathbf{p} = 0) = \frac{|\varepsilon|}{\Delta_\mathbf{p}^2}\exp\left(-\frac{\varepsilon^2}{\Delta_\mathbf{p}^2}\right), \qquad (61)$$

with two maxima at $\varepsilon = \pm\Delta_\mathbf{p}/\sqrt{2}$.

Considering the general case of finite correlation lengths $\xi = \kappa^{-1}$, we again perform numerical analysis based on the recursive relations introduced for this problem in [3], using the basic definition of the Z factor in (3). To calculate the self-energy $\Sigma(\varepsilon_n, \xi_\mathbf{p})$ of an electron scattered by static fluctuations of the superconducting order parameter with the d-wave symmetry, we use the following relation (similar to (43)) slightly generalizing relations derived in [3]:

$$\Sigma_k(\varepsilon_n, \xi_\mathbf{p}) = \frac{\Delta_\mathbf{p}^2 s(k)}{i\varepsilon_n - (-1)^k\xi_\mathbf{p} + ik\kappa(|v_\mathbf{p}^x| + |v_\mathbf{p}^y|) - \Sigma_{k+1}(\varepsilon_n, \xi_\mathbf{p})}, \qquad (62)$$

where $s(k)$ is defined in (45).

In Fig. 7, we show the results for Re$Z(\varepsilon_n, \xi_\mathbf{p} = 0)$, again taken at different points of the bare Fermi surface, shown in the inset. The correlation length is $\xi = 100a$ ($\kappa a = 0.01$) and $\Delta = 0.1t$. It is clearly seen that Re$Z = 1$ precisely at the nodal point D (where $\Delta_\mathbf{p} = 0$), but at other points on the bare Fermi surface, ReZ is strongly renormalized in a rather wide intervals of $\varepsilon_n < |\Delta_\mathbf{p}|$, tending to zero as $\varepsilon_n \longrightarrow 0$. Thus we again obtain a kind of marginal Fermi liquid or Luttinger liquid (NFL), but qualitatively different from the case of hot spot model.

In Fig. 8, we also show typical intensity plots of the spectral density $A(\varepsilon = 0, \xi_\mathbf{p})$ in the Brillouin zone in the case of superconducting (d-wave) pseudogap fluctuations with the correlation length $\xi^{-1}a = \kappa a = 0.1$ and two different values of Δ. We see that these spectral density plots give a totally different picture of the destruction of the Fermi surface than the one given by the hot spot model, which also, in our opinion, differs significantly from most results of the ARPES measurements on cop-

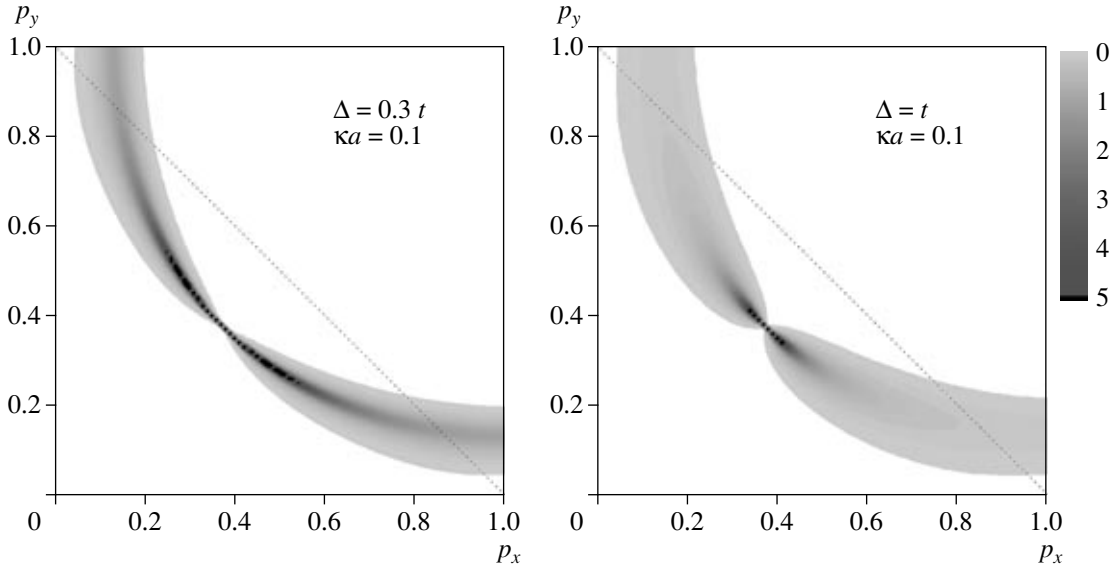

Fig. 8. Intensity plots of the spectral density $A(\varepsilon = 0, \xi_\mathbf{p})$ in the Brillouin zone ($t' = -0.4t$ and $\mu = -1.3t$) in the case of superconducting (d-wave) pseudogap fluctuations. The correlation length is $\xi^{-1}a = \kappa a = 0.1$ (with the spin-fermion combinatorics of diagrams) for two different values of the pseudogap amplitude $\Delta = 0.3t$ and $\Delta = t$.

per oxides. The Fermi surface is sharply defined only at one point (at the diagonal of the Brillouin zone), where $\Delta_{\mathbf{p}}$ given by (58) is precisely zero, and there are no sharply defined Fermi arcs formed close to this point. We observe only some more or less wide "dragonfly wings" formed around this point. We also note the absence of any signs of the shadow Fermi surface.

4. CONCLUSIONS

We analyzed the rather unusual (NFL) behavior of the fluctuating gap model of pseudogap behavior in both one and two dimensions. We studied the quasiparticle renormalization (Z factor) of the single-electron Green function, demonstrating a kind of marginal Fermi-liquid or Luttinger-liquid behavior (i.e., the absence of well-defined quasiparticles close to the Fermi surface) and also the topological stability of the bare Fermi surface (the Luttinger theorem). This reflects strong renormalization effects leading to the replacement of the usual pole singularity of the Green function in a Fermi liquid by a zero, thus effectively replacing the Fermi surface of poles by the Luttinger surface of zeroes [20]. In the presence of static impurity-like scattering due to the effects of finite correlation lengths of pseudogap fluctuations, this singularity is replaced by a finite discontinuity.

In the two-dimensional case, we discussed the effective picture of destruction of the Fermi surface both in the hot spot model of dielectric (AFM, CDW) pseudogap fluctuations and in the qualitatively different case of superconducting d-wave fluctuations, reflecting the NFL spectral density behavior and similar to that observed in ARPES experiments on copper oxides.

Intensity plots obtained in the case of AFM (CDW) fluctuations, in our opinion, are more similar to the ARPES intensity data obtained in experiments on copper oxides. We note that this effective picture was also directly generalized to the case of strongly correlated metals or doped Mott insulators [18] using the so-called DMFT + Σ_k approach in [19].

The authors are grateful to G.E. Volovik for his interest and very useful discussions, which, in fact, initiated this work.

This work was supported in part by the Russian Foundation for Basic Research (project no. 05-02-16301), the program "Quantum Macrophysics" of the Presidium of the Russian Academy of Sciences, and the program "Strongly Correlated Electrons in Semiconductors, Metals, Superconductors, and Magnetic Materials" of the Division of Physical Sciences of the Russian Academy of Sciences.

REFERENCES

1. M. V. Sadovskii, Usp. Fiz. Nauk **171**, 539 (2001) [Phys. Usp. **44**, 515 (2001)]; cond-mat/0408489.
2. J. Schmalian, D. Pines, and B. Stojkovic, Phys. Rev. B **60**, 667 (1999).
3. É. Z. Kuchinskiĭ and M. V. Sadovskiĭ, Zh. Éksp. Teor. Fiz. **115**, 1765 (1999) [JETP **88**, 968 (1999)].
4. M. V. Sadovskiĭ, Zh. Éksp. Teor. Fiz. **66**, 1720 (1974) [Sov. Phys. JETP **39**, 845 (1974)]; Fiz. Tverd. Tela (Leningrad) **16**, 2504 (1974) [Sov. Phys. Solid State **16**, 1632 (1974)].
5. M. V. Sadovskiĭ, Zh. Éksp. Teor. Fiz. **77**, 2070 (1979) [Sov. Phys. JETP **50**, 989 (1979)].
6. W. Wonneberger and R. Lautenschlager, J. Phys. C **9**, 2865 (1976).
7. M. V. Sadovskii and A. A. Timofeev, J. Mosc. Phys. Soc. **1**, 391 (1991).
8. R. H. McKenzie and D. Scarratt, Phys. Rev. **54**, R12709 (1996).
9. G. E. Volovik, cond-mat/0505089; cond-mat/0601372.
10. A. B. Migdal, *Theory of Finite Fermi Systems and Applications to Atomic Nuclei*, 2nd ed. (Nauka, Moscow, 1983; Interscience, New York, 1967).
11. M. V. Sadovskii, *Diagrammatics* (World Sci., Singapore, 2006).
12. I. E. Dzyaloshinskii and A. I. Larkin, Zh. Éksp. Teor. Fiz. **65**, 411 (1973) [Sov. Phys. JETP **38**, 202 (1974)].
13. C. M. Varma, P. B. Littlewood, S. Schmitt-Rink, et al., Phys. Rev. Lett. **63**, 1996 (1989).
14. M. V. Sadovskii and N. A. Strigina, Zh. Éksp. Teor. Fiz. **122**, 610 (2002) [JETP **95**, 526 (2002)].
15. M. V. Sadovskii, Physica C (Amsterdam) **341–348**, 811 (2000).
16. M. R. Norman, H. Ding, M. Randeria, et al., Nature **392**, 157 (1998).
17. A. A. Kordyuk, S. V. Borisenko, M. S. Golden, et al., Phys. Rev. B **66**, 014502 (2002).
18. E. Z. Kuchinskiĭ, I. A. Nekrasov, and M. V. Sadovskii, Pis'ma Zh. Eksp. Teor. Fiz. **82**, 217 (2005) [JETP Lett. **82**, 198 (2005)].
19. M. V. Sadovskii, I. A. Nekrasov, E. Z. Kuchinskii, et al., Phys. Rev. B **72**, 155105 (2005).
20. I. E. Dzyaloshinskii, Phys. Rev. B **68**, 085113 (2003).

Pseudogaps in strongly correlated metals: Optical conductivity within the generalized dynamical mean-field theory approach

E. Z. Kuchinskii, I. A. Nekrasov, and M. V. Sadovskii
Institute for Electrophysics, Russian Academy of Sciences, Ekaterinburg 620016, Russia
(Received 19 September 2006; revised manuscript received 24 October 2006; published 5 March 2007)

The optical conductivity of the weakly doped two-dimensional repulsive Hubbard model on the square lattice with the nearest and next-nearest hoppings is calculated within the generalized dynamical mean-field (DMFT+$\Sigma_{\mathbf{p}}$) approach, which includes correlation length scale ξ into the standard DMFT equations via the momentum dependent self-energy $\Sigma_{\mathbf{p}}$, with a full account of appropriate vertex corrections. This approach takes into consideration the nonlocal dynamical correlations induced, e.g., by short-ranged collective spin-density-wavelike antiferromagnetic spin fluctuations, which (at high enough temperatures) can be viewed as a quenched Gaussian random field with finite correlation length ξ. The DMFT effective single-impurity problem is solved by numerical renormalization group. We consider both the case of correlated metal with the bandwidth $W \lesssim U$ and that of doped Mott insulator with $U \gg W$ (U—the value of local Hubbard interaction). The optical conductivity calculated within DMFT+$\Sigma_{\mathbf{p}}$ demonstrates typical pseudogap behavior within the quasiparticle band, in qualitative agreement with experiments in copper oxide superconductors. For large values of U, pseudogap anomalies are effectively suppressed.

DOI: 10.1103/PhysRevB.75.115102 PACS number(s): 71.10.Fd, 71.10.Hf, 71.27.+a, 71.30.+h

I. INTRODUCTION

Pseudogap state is a major anomaly of the electronic properties of underdoped copper oxides[1,2]. We believe that the preferable "scenario" for its formation is most likely based on the model of strong scattering of electrons by short-ranged antiferromagnetic (AFM), spin-density-wave (SDW) spin fluctuations.[2] This scattering mainly transfers momenta of the order of $\mathbf{Q}=\left(\frac{\pi}{a},\frac{\pi}{a}\right)$ (a—the lattice constant of a two-dimensional lattice), leading to the formation of structures in the one-particle spectrum, which are precursors of the changes in the spectra due to long-range AFM order (period doubling) with non-Fermi-liquid-like behavior of the spectral density in the vicinity of the so-called hot spots on the Fermi surface, appearing at the intersections of the Fermi surface with antiferromagnetic Brillouin-zone boundary (umklapp surface).[2]

In recent years, a simplified model of the pseudogap state was studied[2–4] under the assumption that the scattering by dynamic spin fluctuations can be reduced for high enough temperatures to a static Gaussian random field (quenched disorder) of pseudogap fluctuations. These fluctuations are defined by characteristic scattering vectors of the order of $\mathbf{Q}$, with distribution width determined by the inverse correlation length of short-range order $\kappa=\xi^{-1}$ and by appropriate energy scale Δ (typically of the order of the crossover temperature T^* to the pseudogap state[2]).

It is also well known that undoped cuprates are antiferromagnetic Mott insulators with $U \gg W$ (U—the value of the local Hubbard interaction, W—the bandwidth of noninteracting band), so that correlation effects are very important and underdoped (and probably also optimally doped) cuprates are actually typical strongly correlated metals.

The cornerstone of the modern theory of strongly correlated systems is the dynamical mean-field theory (DMFT).[5–9] At the same time, standard DMFT is not appropriate for the "antiferromagnetic" scenario of pseudogap formation in strongly correlated metals due to the basic approximation of the DMFT, which completely neglects nonlocal dynamical correlation effects.

Different extensions of DMFT were proposed in recent years to cure this deficiency, such as extended DMFT (EDMFT),[10,11] which locally includes coupling to nonlocal dynamical fluctuations, and, most importantly, different versions of the so-called cluster mean-field theories, such as the dynamical cluster approximation[12] and cellular DMFT.[13] However, these approaches have certain drawbacks. First of all, the effective quantum single impurity problem becomes rather complex. Thus, majority of computational tools available for the DMFT can be used only for small enough clusters,[12] which include mostly nearest-neighbor fluctuations. It is especially difficult to apply these methods to the calculations of two-particle properties, e.g., optical conductivity.

Recently, we have proposed a generalized DMFT+$\Sigma_{\mathbf{p}}$ approach.[14–16] This approach, on the one hand, retains the single-impurity description of the DMFT, which properly accounts for *local* correlations, and the possibility to use impurity solvers such as numerical renormalization group (NRG).[25,26] On the other hand, this approach includes nonlocal correlations on a nonperturbative model basis, which allows us to control the characteristic scales and also the types of nonlocal fluctuations. This latter point allows us to systematically study the influence of nonlocal fluctuations on the electronic properties and, in particular, provides valuable hints on the physical origin and possible interpretation of the results. Within this approach, we have studied single-particle properties, such as pseudogap formation in the density of states of the quasiparticle band for both correlated metal and doped Mott insulator, evolution of the non-Fermi-liquid-like spectral density and angle-resolved photoemission spectra,[15] "destruction" of Fermi surfaces and formation of Fermi "arcs,"[14] as well as impurity scattering effects.[16] This formalism was also combined with modern local-density approxi-

mation (LDA)+DMFT calculations of the electronic structure of "realistic" correlated systems to formulate the LDA +DMFT+$\Sigma_{\mathbf{p}}$ approach, which was applied for the description of pseudogap behavior in $Bi_2Ca_2SrCu_2O_8$.[17]

In this paper, we develop our DMFT+$\Sigma_{\mathbf{p}}$ approach for the calculations of two-particle properties, such as (dynamic) optical conductivity, which is conveniently calculated within the standard DMFT.[7,8] We show that inclusion of nonlocal correlations (pseudogap fluctuations) with characteristic length scale ξ allows us to describe the pseudogap effects in longitudinal conductivity of the two-dimensional Hubbard plane.

The paper is organized as follows. In Sec. II we present a short description of our DMFT+$\Sigma_{\mathbf{p}}$ approach. In Sec. III we derive the basic DMFT+$\Sigma_{\mathbf{p}}$ expressions for dynamic (optical) conductivity, as well as formulate recurrence equations to calculate the **p**-dependent self-energy and appropriate vertex part, which take into account all the relevant Feynaman digrams of perturnbation series over pseudogap fluctuations. The computational details and basic results for optical conductivity are given in Sec. IV. We also compare our results with that of the standard DMFT. The paper ends with a summary, Sec. V, including a short overview of related experimental results.

II. BASICS OF THE DMFT+$\Sigma_{\mathbf{p}}$ APPROACH

As noted above, the basic shortcoming of the traditional DMFT approach[5–9] is the neglect of momentum dependence of the electron self-energy. To include nonlocal effects while remaining within the usual "single-impurity analogy," we have proposed[14–16] the following (DMFT+$\Sigma_{\mathbf{p}}$) approach. First of all, the Matsubara "time" Fourier-transformed single-particle Green's function of the Hubbard model is written in obvious notations as

$$G(i\varepsilon,\mathbf{p}) = \frac{1}{i\varepsilon + \mu - \varepsilon(\mathbf{p}) - \Sigma(i\varepsilon) - \Sigma_{\mathbf{p}}(i\varepsilon)},$$

$$\varepsilon = \pi T(2n+1), \tag{1}$$

where $\Sigma(i\varepsilon)$ is the local contribution to the self-energy of DMFT type (surviving in the limit of spatial dimensionality $d \to \infty$) while $\Sigma_{\mathbf{p}}(i\varepsilon)$ is some momentum dependent part. This last contribution can be due either to electron interactions with some "additional" collective modes or to order parameter fluctuations or may be induced by similar nonlocal contributions within the Hubbard model itself. No double-counting problem arises in this approach, as discussed in detail in Ref. 15. At the same time, our procedure does not represent any systematic $1/d$ expansion, as stressed in Refs. 14–16. The basic assumption here is the neglect of all interference processes of the local Hubbard interaction and nonlocal contributions owing to these additional scatterings (noncrossing approximation for appropriate diagrams),[15] as illustrated by the diagrams in Fig. 1.

The self-consistency equations of the generalized DMFT +$\Sigma_{\mathbf{p}}$ approach are formulated as follows:[14,15]

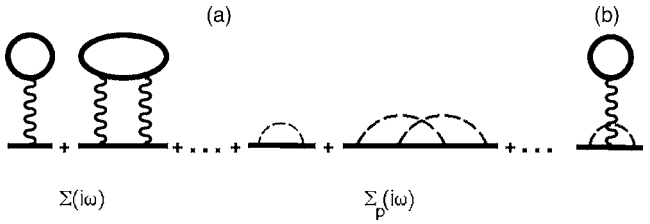

FIG. 1. Typical "skeleton" diagrams for the self-energy in the DMFT+$\Sigma_{\mathbf{p}}$ approach. The first two terms are examples of the DMFT self-energy diagrams, the middle two diagrams show some contributions to the nonlocal part of the self-energy (e.g., from spin fluctuations) represented as dashed lines, and the last diagram (b) is an example of the neglected diagrams leading to interference between the local and nonlocal parts.

(1) Start with some initial guess of local self-energy $\Sigma(i\varepsilon)$, e.g., $\Sigma(i\varepsilon)=0$.

(2) Construct $\Sigma_{\mathbf{p}}(i\varepsilon)$ within some (approximate) scheme, taking into account the interactions with collective modes or order parameter fluctuations, which, in general, can depend on $\Sigma(i\omega)$ and μ.

(3) Calculate the local Green's function,

$$G_{ii}(i\varepsilon) = \frac{1}{N}\sum_{\mathbf{p}} \frac{1}{i\varepsilon + \mu - \varepsilon(\mathbf{p}) - \Sigma(i\varepsilon) - \Sigma_{\mathbf{p}}(i\varepsilon)}. \tag{2}$$

(4) Define the "Weiss field"

$$\mathcal{G}_0^{-1}(i\varepsilon) = \Sigma(i\varepsilon) + G_{ii}^{-1}(i\varepsilon). \tag{3}$$

(5) Using some "impurity solver," calculate the single-particle Green's function $G_d(i\varepsilon)$ for the effective Anderson impurity problem, placed at lattice site i and defined by the effective action which is written, in obvious notations, as

$$S_{\text{eff}} = -\int_0^\beta d\tau_1 \int_0^\beta d\tau_2\, c_{i\sigma}(\tau_1)\mathcal{G}_0^{-1}(\tau_1-\tau_2)c_{i\sigma}^+(\tau_2) + \int_0^\beta d\tau\, U n_{i\uparrow}(\tau)n_{i\downarrow}(\tau). \tag{4}$$

(6) Define a *new* local self-energy,

$$\Sigma(i\omega) = \mathcal{G}_0^{-1}(i\omega) - G_d^{-1}(i\omega). \tag{5}$$

(7) Using this self-energy as the "initial" one in step (1), continue the procedure until (and if) convergency is reached to obtain

$$G_{ii}(i\varepsilon) = G_d(i\varepsilon). \tag{6}$$

Eventually, we get the desired Green's function in the form of Eq. (1), where $\Sigma(i\varepsilon)$ and $\Sigma_{\mathbf{p}}(i\varepsilon)$ are those appearing at the end of our iteration procedure.

III. OPTICAL CONDUCTIVITY IN DMFT+$\Sigma_{\mathbf{p}}$

A. Basic expressions for optical conductivity

To calculate dynamic conductivity, we use the general expression relating it to the retarded density-density correlation function $\chi^R(\omega,\mathbf{q})$ as follows:[18,19]

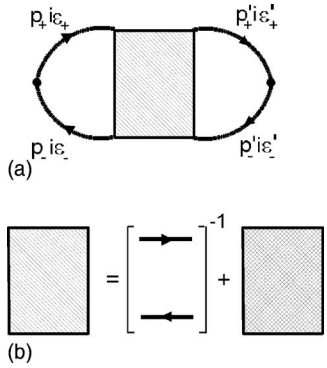

FIG. 2. Full polarization loop (a) with vertex part, which includes free-electron contribution in addition to the standard vertex, containing all interactions (b). Here, $\mathbf{p}_{\pm}=\mathbf{p}\pm\frac{\mathbf{q}}{2}$ and $\varepsilon_{\pm}=\varepsilon\pm\frac{\omega}{2}$.

$$\sigma(\omega)=-\lim_{q\to 0}\frac{ie^2\omega}{q^2}\chi^R(\omega,\mathbf{q}), \tag{7}$$

where e is the electronic charge.

Consider the full polarization loop graph in the Matsubara representation, as shown in Fig. 2(a), which is conveniently (with explicit frequency summation) written as

$$\Phi(i\omega,\mathbf{q})=\sum_{\varepsilon\varepsilon'}\Phi_{i\varepsilon i\varepsilon'}(i\omega,\mathbf{q})\equiv\sum_{\varepsilon}\Phi_{i\varepsilon}(i\omega,\mathbf{q}), \tag{8}$$

and contains all possible interactions of our model, described by the full vertex part of Fig. 2(b). Note that we use a slightly unusual definition of the vertex part to include the loop contribution without vertex corrections, which shortens further diagrammatic expressions. Retarded density-density correlation function is determined by appropriate analytic continuation of this loop and can be written as

$$\chi^R(\omega,\mathbf{q})=\int_{-\infty}^{\infty}\frac{d\varepsilon}{2\pi i}\{[f(\varepsilon_+)-f(\varepsilon_-)]\Phi_{\varepsilon}^{RA}(\mathbf{q},\omega)+f(\varepsilon_-)\Phi_{\varepsilon}^{RR}(\mathbf{q},\omega)-f(\varepsilon_+)\Phi_{\varepsilon}^{AA}(\mathbf{q},\omega)\}, \tag{9}$$

where $f(\varepsilon)$ is the Fermi distribution, $\varepsilon_{\pm}=\varepsilon\pm\frac{\omega}{2}$, and the two-particle loops $\Phi_{\varepsilon}^{RA}(\mathbf{q},\omega)$, $\Phi_{\varepsilon}^{RR}(\mathbf{q},\omega)$, $\Phi_{\varepsilon}^{AA}(\mathbf{q},\omega)$ are determined by appropriate analytic continuations ($i\varepsilon+i\omega\to\varepsilon+\omega+i\delta$, $i\varepsilon\to\varepsilon\pm i\delta$, and $\delta\to+0$) in Eq. (8). Then we can conveniently write the dynamic conductivity as

$$\sigma(\omega)=\lim_{q\to 0}\left(-\frac{e^2\omega}{2\pi q^2}\right)\int_{-\infty}^{\infty}d\varepsilon\{[f(\varepsilon_+)-f(\varepsilon_-)][\Phi_{\varepsilon}^{RA}(\mathbf{q},\omega)-\Phi_{\varepsilon}^{RA}(0,\omega)]+f(\varepsilon_-)[\Phi_{\varepsilon}^{RR}(\mathbf{q},\omega)-\Phi_{\varepsilon}^{RR}(0,\omega)]-f(\varepsilon_+)\times[\Phi_{\varepsilon}^{AA}(\mathbf{q},\omega)-\Phi_{\varepsilon}^{AA}(0,\omega)]\}, \tag{10}$$

where the total contribution of the additional terms with zero q can be shown (with the use of the general Ward identities[20]) to be zero.

To calculate $\Phi_{i\varepsilon i\varepsilon'}(i\omega,\mathbf{q})$ entering the sum over the Matsubara frequencies in Eq. (8) in the DMFT+$\Sigma_{\mathbf{p}}$ approximation, which neglects the interference between local Hubbard

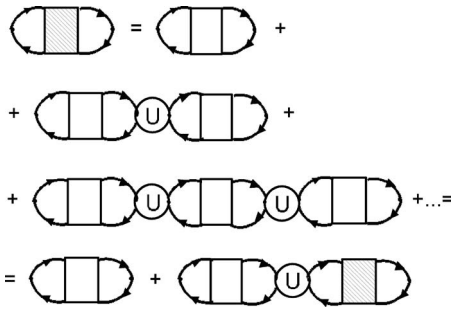

FIG. 3. Bethe-Salpeter equation for the polarization loop in the DMFT+$\Sigma_{\mathbf{p}}$ approach. The circles represent irreducible vertex part of DMFT, which contains only local interactions, surviving in the limit of $d\to\infty$. The unshaded rectangular vertex represents nonlocal interactions, e.g., with SDW (pseudogap) fluctuations, which is similarly defined to Fig. 2(b).

interaction and nonlocal contributions due to additional scatterings, e.g., by SDW pseudogap fluctuations,[15] we can write down the Bethe-Salpeter equation, as shown diagrammatically in Fig. 3, where we have introduced the irreducible (local) vertex $U_{i\varepsilon i\varepsilon'}(i\omega)$ of DMFT and "rectangular" vertex, defined as in Fig. 2(b) and containing all interactions with fluctuations. Analytically, this equation can be written as

$$\Phi_{i\varepsilon i\varepsilon'}(i\omega,\mathbf{q})=\Phi_{i\varepsilon}^0(i\omega,\mathbf{q})\delta_{\varepsilon\varepsilon'}+\Phi_{i\varepsilon}^0(i\omega,\mathbf{q})\sum_{\varepsilon''}U_{i\varepsilon i\varepsilon''}(i\omega)\Phi_{i\varepsilon'' i\varepsilon'}(i\omega,\mathbf{q}), \tag{11}$$

where $\Phi_{i\varepsilon}^0(i\omega,\mathbf{q})$ is the desired function calculated neglecting vertex corrections due to the Hubbard interaction (but taking into account all nonlocal interactions with fluctuations considered here to be static). Note that all q dependence here is determined by $\Phi_{i\varepsilon}^0(i\omega,\mathbf{q})$, as the vertex $U_{i\varepsilon i\varepsilon'}(i\omega)$ is local and q independent.

As clearly seen from Eq. (10), to calculate the conductivity, we need only to find the q^2 contribution to $\Phi(i\omega,\mathbf{q})$ defined in Eq. (8). This can be done in the following way. First of all, note that all the loops in Eq. (11) contain the q dependence starting from terms of the order of q^2. Then, we can take an arbitrary loop (cross section) in the expansion of Eq. (11) (see Fig. 3), calculating it up to terms of the order of q^2, and make a resummation of all the contributions to the right and to the left of this cross section (using the obvious left-right symmetry of diagram summation in the Bethe-Salpeter equation), putting $\mathbf{q}=0$ in all these graphs. This is equivalent to the simple q^2 differentiation of the expanded version of Eq. (11). This procedure immediately leads to the following relation for q^2 contribution to Eq. (8):

$$\phi(i\omega)\equiv\lim_{q\to 0}\frac{\Phi(i\omega,\mathbf{q})-\Phi(i\omega,0)}{q^2}=\sum_{\varepsilon}\gamma_{i\varepsilon}^2(i\omega,\mathbf{q}=0)\phi_{i\varepsilon}^0(i\omega), \tag{12}$$

where

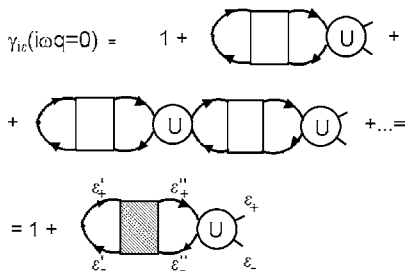

FIG. 4. Effective vertex $\gamma_{i\varepsilon}(i\omega,\mathbf{q}=0)$ used in the calculations of conductivity.

$$\phi^0_{i\varepsilon}(i\omega) \equiv \lim_{q\to 0} \frac{\Phi^0_{i\varepsilon}(i\omega,\mathbf{q}) - \Phi^0_{i\varepsilon}(i\omega,0)}{q^2}, \tag{13}$$

with $\Phi^0_{i\varepsilon}(i\omega,\mathbf{q})$ containing the vertex corrections only due to nonlocal (pseudogap) fluctuations, while the one-particle Green's functions in it are taken with self-energies due to both these fluctuations and local DMFT-like interaction, as in Eq. (1). The vertex $\gamma_{i\varepsilon}(i\omega,\mathbf{q}=0)$ is determined diagrammatically as shown in Fig. 4, or analytically,

$$\gamma_{i\varepsilon}(i\omega,\mathbf{q}=0) = 1 + \sum_{\varepsilon'\varepsilon''} U_{i\varepsilon i\varepsilon''}(i\omega)\Phi_{i\varepsilon'' i\varepsilon'}(i\omega,\mathbf{q}=0). \tag{14}$$

Now, using the Bethe-Salpeter equation (11), we can explicitly write

$$\gamma_{i\varepsilon}(i\omega,\mathbf{q}=0) = 1 + \sum_{\varepsilon'} \frac{\Phi_{i\varepsilon i\varepsilon'}(i\omega,\mathbf{q}=0) - \Phi^0_{i\varepsilon}(i\omega,\mathbf{q}=0)}{\Phi^0_{i\varepsilon}(i\omega,\mathbf{q}=0)} = \frac{\sum_{\varepsilon'} \Phi_{i\varepsilon i\varepsilon'}(i\omega,\mathbf{q}=0)}{\Phi^0_{i\varepsilon}(i\omega,\mathbf{q}=0)}. \tag{15}$$

For $\mathbf{q}=0$, we have the following Ward identity, which can be obtained by a direct generalization of the proof given in Refs. 18 and 20 (see the Appendix):

$$(-i\omega)\Phi_{i\varepsilon}(i\omega,\mathbf{q}=0) = (-i\omega)\sum_{\varepsilon'} \Phi_{i\varepsilon i\varepsilon'}(i\omega,\mathbf{q}=0) = \sum_{\mathbf{p}} G(i\varepsilon+i\omega,\mathbf{p}) - \sum_{\mathbf{p}} G(i\varepsilon,\mathbf{p}). \tag{16}$$

The denominator of Eq. (15) contains vertex corrections only from nonlocal correlations (e.g., pseudogap fluctuations), while Green's functions here are "dressed" *both* by these correlations and the local (DMFT) Hubbard interaction. Thus, we may consider the loop entering the denominator as dressed by (pseudogap) fluctuations only, but with "bare" Green's functions:

$$\tilde{G}_0(i\varepsilon,\mathbf{p}) = \frac{1}{i\varepsilon + \mu - \varepsilon(\mathbf{p}) - \Sigma(i\varepsilon)}, \tag{17}$$

where $\Sigma(i\varepsilon)$ is the local contribution to the self-energy from DMFT. For this problem, we have the following Ward identity, similar to Eq. (16) (see the Appendix):

$$\sum_{\mathbf{p}} G(i\varepsilon+i\omega,\mathbf{p}) - \sum_{\mathbf{p}} G(i\varepsilon,\mathbf{p}) = \Phi^0_{i\varepsilon}(i\omega,\mathbf{q}=0)\left[\Sigma(i\varepsilon+i\omega) - \Sigma(i\varepsilon) - i\omega\right] \equiv \Phi^0_{i\varepsilon}(i\omega,\mathbf{q}=0)\left[\Delta\Sigma(i\omega) - i\omega\right], \tag{18}$$

where we have introduced

$$\Delta\Sigma(i\omega) = \Sigma(i\varepsilon+i\omega) - \Sigma(i\varepsilon). \tag{19}$$

Thus, using Eqs. (16) and (18) in Eq. (15), we get the final expression for $\gamma_{i\varepsilon}(i\omega,\mathbf{q}=0)$ as follows:

$$\gamma_{i\varepsilon}(i\omega,\mathbf{q}=0) = 1 - \frac{\Delta\Sigma(i\omega)}{i\omega}. \tag{20}$$

Then, Eq. (12) reduces to

$$\phi(i\omega) = \sum_{\varepsilon} \phi^0_{i\varepsilon}(i\omega)\left[1 - \frac{\Delta\Sigma(i\omega)}{i\omega}\right]^2. \tag{21}$$

The analytic continuation to real frequencies is obvious, and using Eqs. (12) and (21) in Eq. (10), we can write the final expression for the real part of dynamic conductivity as

$$\mathrm{Re}\,\sigma(\omega) = \frac{e^2\omega}{2\pi}\int_{-\infty}^{\infty} d\varepsilon[f(\varepsilon_-) - f(\varepsilon_+)]\mathrm{Re} \times \left\{ \phi^{0RA}_{\varepsilon}(\omega)\left[1 - \frac{\Sigma^R(\varepsilon_+) - \Sigma^A(\varepsilon_-)}{\omega}\right]^2 - \phi^{0RR}_{\varepsilon}(\omega)\left[1 - \frac{\Sigma^R(\varepsilon_+) - \Sigma^R(\varepsilon_-)}{\omega}\right]^2 \right\}. \tag{22}$$

Thus we have achieved a great simplification of our problem. To calculate the optical conductivity in DMFT+$\Sigma_{\mathbf{p}}$, we only have to solve the single-particle problem as described by the DMFT+$\Sigma_{\mathbf{p}}$ procedure above to determine the self-consistent values of the local self-energies $\Sigma(\varepsilon_\pm)$, while the nontrivial contribution of nonlocal correlations is to be included via Eq. (13), which is to be calculated in some approximation, taking into account only the interaction with nonlocal (e.g., pseudogap) fluctuations, but using the bare Green's functions of the form Eq. (17), which include local self-energies already determined in the general DMFT+$\Sigma_{\mathbf{p}}$ procedure. Actually, Eq. (22) also provides an effective algorithm to calculate the dynamic conductivity in standard DMFT (neglecting any nonlocal correlations), as Eq. (13) is then easily calculated from a simple loop diagram, determined by two Green's functions and free *scalar* vertices. As usual, there is no need to calculate the vertex corrections within the DMFT itself, as was proven first by considering the loop with *vector* vertices.[7,8]

B. Recurrence relations for self-energy and vertex parts

As we are mainly interested in the pseudogap state of copper oxides, we shall further concentrate on the effects of scattering of electrons from collective short-range SDW-like antiferromagnetic spin fluctuations. In a kind of simplified approach, valid only for high enough temperatures,[3,4] we shall calculate $\Sigma_{\mathbf{p}}(i\omega)$ for an electron moving in the quenched random field of (static) Gaussian spin fluctuations, with dominant scattering momentum transfers from the vicinity of some characteristic vector $\mathbf{Q}$ (hot-spot model[2]), using (as we have done in Refs. 14–16) a slightly generalized version of the recurrence procedure proposed in Refs. 3, 4, and 21 (see also Ref. 19), which takes into account *all* Feynman diagrams describing the scattering of electrons by this random field. In general, the neglect of fluctuation dynamics overestimates pseudogap effects. Referring the reader to earlier papers for details,[3,4,14–16] here we just start with the main recurrence relation determining the self-energy as follows:

$$\Sigma_k(i\varepsilon,\mathbf{p}) = \Delta^2 \frac{s(k)}{i\varepsilon + \mu - \Sigma(i\varepsilon) - \varepsilon_k(\mathbf{p}) + inv_k\kappa - \Sigma_{k+1}(i\varepsilon,\mathbf{p})}. \tag{23}$$

Usually, one takes the value of Σ_{k+1} for large enough k equal to zero, and doing the recurrence backwards to $k=1$, we get the desired physical self-energy $\Sigma(i\varepsilon,\mathbf{p})=\Sigma_1(i\varepsilon,\mathbf{p})$.[4,19,21]

In Eq. (23), Δ characterizes the energy scale and $\kappa=\xi^{-1}$ is the inverse correlation length of short-range SDW fluctuations; $\varepsilon_k(\mathbf{p})=\varepsilon(\mathbf{p}+\mathbf{Q})$ and $v_k=|v^x_{\mathbf{p}+\mathbf{Q}}|+|v^y_{\mathbf{p}+\mathbf{Q}}|$ for odd k while $\varepsilon_k(\mathbf{p})=\varepsilon(\mathbf{p})$ and $v_k=|v^x_{\mathbf{p}}|+|v^y_{\mathbf{p}}|$ for even k. The velocity projections $v^x_{\mathbf{p}}$ and $v^y_{\mathbf{p}}$ are determined by the usual momentum derivatives of the bare electronic energy dispersion $\varepsilon(\mathbf{p})$. Finally, $s(k)$ represents a combinatorial factor, which is always assumed here to be that corresponding to the case of Heisenberg spin fluctuations in the "nearly antiferromagnetic Fermi liquid" (spin-fermion model of Ref. 3, SDW-type fluctuations):

$$s(k) = \begin{cases} \dfrac{k+2}{3} & \text{for odd } k, \\ \dfrac{k}{3} & \text{for even } k. \end{cases} \tag{24}$$

As was stressed in Refs. 15 and 16 this procedure introduces an important length scale ξ not present in standard DMFT, which mimics the effect of short-range (SDW) correlations within fermionic "bath" surrounding the DMFT effective single Anderson impurity.

An important aspect of the theory is that both parameters Δ and ξ can, in principle, be calculated from the microscopic model at hand,[15] but here we consider these as phenomenological parameters of the theory (i.e., to be determined from experiments).

Now, to calculate the optical conductivity, we need the knowledge of the basic block $\Phi^0_{i\varepsilon}(i\omega,\mathbf{q})$ entering Eq. (13), or, more precisely, appropriate functions analytically continued to real frequencies, $\Phi^{0RA}_{\varepsilon}(\omega,\mathbf{q})$ and $\Phi^{0RR}_{\varepsilon}(\omega,\mathbf{q})$, which in turn define $\phi^{0RA}_{\varepsilon}(\omega)$ and $\phi^{0RR}_{\varepsilon}(\omega)$ entering Eq. (22) and are defined by obvious relations similar to Eq. (13):

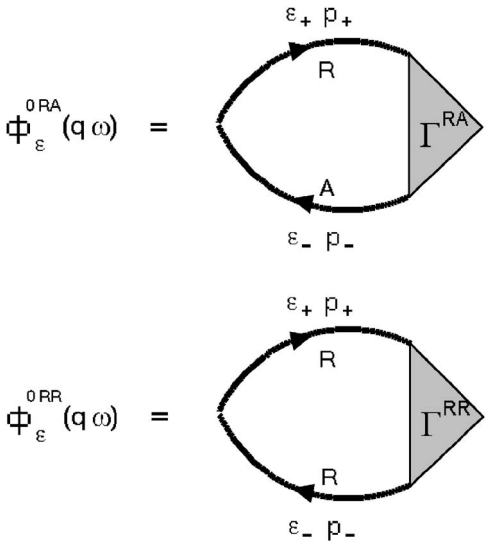

FIG. 5. Diagrammatic representation of $\Phi^{0RA}_{\varepsilon}(\omega,\mathbf{q})$.

$$\phi^{0RA}_{\varepsilon}(\omega) = \lim_{q\to 0} \frac{\Phi^{0RA}_{\varepsilon}(\omega,\mathbf{q}) - \Phi^{0RA}_{\varepsilon}(\omega,0)}{q^2}, \tag{25}$$

$$\phi^{0RR}_{\varepsilon}(\omega) = \lim_{q\to 0} \frac{\Phi^{0RR}_{\varepsilon}(\omega,\mathbf{q}) - \Phi^{0RR}_{\varepsilon}(\omega,0)}{q^2}. \tag{26}$$

By definition, we have

$$\Phi^{0RA}_{\varepsilon}(\omega,\mathbf{q}) = \sum_{\mathbf{p}} G^R(\varepsilon_+,\mathbf{p}_+)G^A(\varepsilon_-,\mathbf{p}_-)\Gamma^{RA}(\varepsilon_-,\mathbf{p}_-;\varepsilon_+,\mathbf{p}_+),$$

$$\Phi^{0RR}_{\varepsilon}(\omega,\mathbf{q}) = \sum_{\mathbf{p}} G^R(\varepsilon_+,\mathbf{p}_+)G^R(\varepsilon_-,\mathbf{p}_-)\Gamma^{RR}(\varepsilon_-,\mathbf{p}_-;\varepsilon_+,\mathbf{p}_+), \tag{27}$$

which are shown diagrammatically in Fig. 5. Here, Green's functions $G^R(\varepsilon_+,\mathbf{p}_+)$ and $G^A(\varepsilon_-,\mathbf{p}_-)$ are defined by an analytic continuation $(i\varepsilon\to\varepsilon\pm i\delta)$ of the Matsubara Green's functions (1) determined by the recurrence procedure [Eq. (23)], while vertices $\Gamma^{RA}(\varepsilon_-,\mathbf{p}_-;\varepsilon_+,\mathbf{p}_+)$ and $\Gamma^{RR}(\varepsilon_-,\mathbf{p}_-;\varepsilon_+,\mathbf{p}_+)$ containing all vertex corrections due to pseudogap fluctuations are given by the recurrence procedure, derived first (for one-dimensional case) in Ref. 22 (see also Ref. 19) and generalized for the two-dimensional problem in Ref. 23 (see also Ref. 3). The basic idea used here is that an arbitrary diagram for the vertex part can be obtained by an insertion of an "external field" line into the appropriate diagram for the self-energy.[22–24] In our model, we can limit ourselves only to diagrams with nonintersecting interaction lines with additional combinatorial factors $s(k)$ in initial interaction vertices.[3,4,21] Thus, all diagrams for the vertex part are, in fact, generated by simple ladder diagrams with addi-

tional $s(k)$ factors associated with interaction lines[22,23] (see also Ref. 19). Then we obtain the system of recurrence relations for the vertex part $\Gamma^{RA}(\varepsilon_-,\mathbf{p}_-;\varepsilon_+,\mathbf{p}_+)$, as shown by the diagrams of Fig. 6. Analytically, it has the following form,[23] where we now also included the contributions due to local (DMFT) self-energies, originating from the DMFT+$\Sigma_{\mathbf{p}}$ loop:

$$\Gamma^{RA}_{k-1}(\varepsilon_-,\mathbf{p}_-;\varepsilon_+,\mathbf{p}_+) = 1 + \Delta^2 s(k) G^A_k(\varepsilon_-,\mathbf{p}_-) G^R_k(\varepsilon_+,\mathbf{p}_+) \times \left\{ 1 + \frac{2iv_k\kappa k}{\omega - \varepsilon_k(\mathbf{p}_+) + \varepsilon_k(\mathbf{p}_-) - \Sigma^R(\varepsilon_+) + \Sigma^A(\varepsilon_-) - \Sigma^R_{k+1}(\varepsilon_+,\mathbf{p}_+) + \Sigma^A_{k+1}(\varepsilon_-,\mathbf{p}_-)} \right\} \Gamma^{RA}_k(\varepsilon_-,\mathbf{p}_-;\varepsilon_+,\mathbf{p}_+), \tag{28}$$

and

$$G^{R,A}_k(\varepsilon_\pm,\mathbf{p}_\pm) = \frac{1}{\varepsilon_\pm - \varepsilon_k(\mathbf{p}_\pm) \pm ikv_k\kappa - \Sigma^{R,A}(\varepsilon_\pm) - \Sigma^{R,A}_{k+1}(\varepsilon_\pm,\mathbf{p}_\pm)}. \tag{29}$$

The "physical" vertex $\Gamma^{RA}(\varepsilon_-,\mathbf{p}_-;\varepsilon_+,\mathbf{p}_+)$ is determined as $\Gamma^{RA}_{k=0}(\varepsilon_-,\mathbf{p}_-;\varepsilon_+,\mathbf{p}_+)$. The recurrence procedure [Eq. (28)] takes into account *all* perturbation theory diagrams for the vertex part. For $\kappa\to 0$ ($\xi\to\infty$), Eq. (28) reduces to the series studied in Ref. 24 (cf. also Ref. 3); which can be summed exactly in an analytic form. The standard "ladder" approximation in our scheme corresponds to the case of combinatorial factors $s(k)$ in Eq. (28) being equal to 1.[22]

The recurrence procedure for $\Gamma^{RR}(\varepsilon_-,\mathbf{p}_+;\varepsilon_+,\mathbf{p}_+)$ differs from Eq. (28) only by obvious replacements $A\to R$ and the whole expression in figure brackets in the right-hand side of Eq. (28) just replaced by 1:

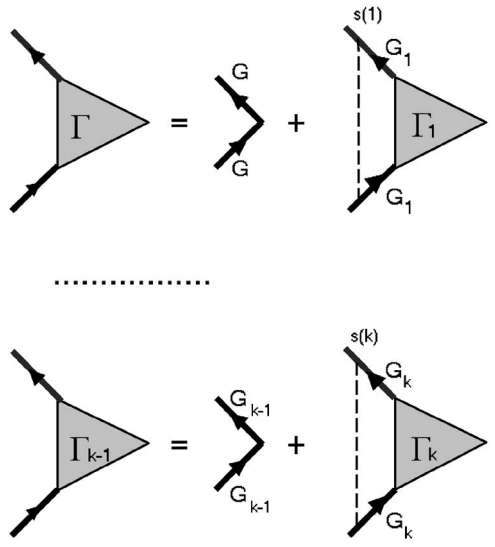

FIG. 6. Recurrence relations for the vertex part. Dashed lines denote Δ^2.

$$\Gamma^{RR}_{k-1}(\varepsilon_-,\mathbf{p}_-;\varepsilon_+,\mathbf{p}_+) = 1 + \Delta^2 s(k) G^R_k(\varepsilon_-,\mathbf{p}_-) G^R_k(\varepsilon_+,\mathbf{p}_+) \Gamma^{RR}_k(\varepsilon_-,\mathbf{p};\varepsilon_+,\mathbf{p}_+). \tag{30}$$

Note that the DMFT (Hubbard) interaction enters these equations only via local self-energies $\Sigma^{R,A}(\varepsilon_\pm)$ calculated self-consistently according to our DMFT+$\Sigma_{\mathbf{p}}$ procedure.

Equations (1), (23), (28), and (30), together with Eqs. (22), (25), and (26), provide us with the complete self-consistent procedure to calculate the optical conductivity of our model using the DMFT+$\Sigma_{\mathbf{p}}$ approach.

IV. RESULTS AND DISCUSSION

A. Generalities

In the following, we shall discuss our results for a standard one-band Hubbard model on a square lattice. The bare electronic dispersion in tight-binding approximation, with the account of the nearest- (t) and next-nearest- (t') neighbor hoppings, is given by

$$\varepsilon(\mathbf{p}) = -2t(\cos p_x a + \cos p_y a) - 4t' \cos p_x a \cos p_y a, \tag{31}$$

where a is the lattice constant. To be concrete, below we present the results for $t=0.25$ eV (more or less typical for cuprates) and $t'/t=-0.4$ (which gives Fermi surface similar to those observed in many cuprates).

For the square lattice, the bare bandwidth is $W=8t$. To study strongly correlated metallic state obtained as doped Mott insulator, we have used the value for the Hubbard interaction $U=40t$ and filling factors $n=1.0$ (half-filling) and $n=0.8$ (hole doping). For correlated metal with $W\gtrsim U$, we have taken typical values such as $U=4t$, $U=6t$, and $U=10t$ for $U\gtrsim W$. Calculations were performed for different fillings: half-filling ($n=1.0$) and for hole doping ($n=0.8,0.9$). For the typical values for Δ, we have chosen $\Delta=t$ and $\Delta=2t$ and for correlation length $\xi=2a$ and $\xi=10a$ (motivated mainly by the experimental data for cuprates[2,3]).

To solve an effective Anderson impurity problem of DMFT, we applied a reliable numerically exact method of numerical renormalization group (NRG),[25,26] which, actually,

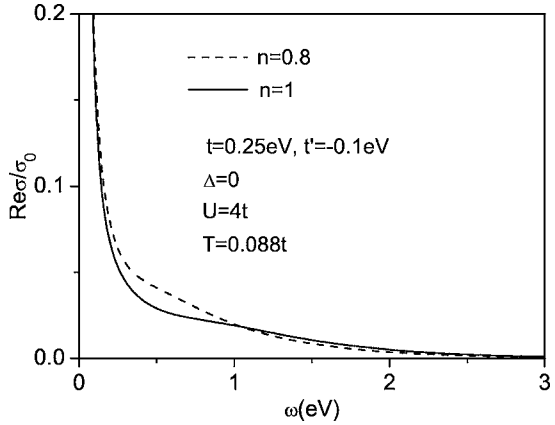

FIG. 7. Real part of the optical conductivity for correlated metal ($U=4t$, $t'=-0.4t$, and $t=0.25$ eV) in the DMFT approximation for two values of filling factor: $n=1$ and $n=0.8$. Temperature $T=0.088t$.

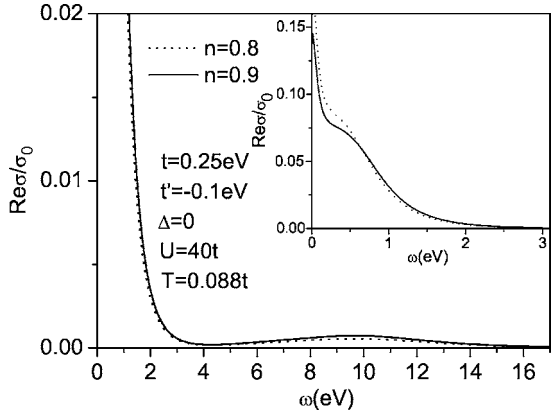

FIG. 8. Real part of the optical conductivity for doped Mott insulator ($U=40t$, $t'=-0.4t$, and $t=0.25$ eV) in the DMFT approximation. Filling factors are $n=0.8$ and $n=0.9$, and temperature $T=0.088t$. Small frequency behavior is shown in more detail in the inset.

allowed us to work with real frequencies from the very beginning, overcoming possible difficulties of performing analytical continuation numerically. Calculations were performed for two different temperatures: $T=0.088t$ and $T=0.356t$.

All necessary integrations were done directly, e.g., over the whole Brillouin zone (with the account of obvious symmetries) or wide enough frequency range. Integration momenta are made dimensionless in a natural way with the help of the lattice constant a. The conductivity is measured in units of the universal conductivity in two dimensions: $\sigma_0 = \frac{e^2}{\hbar} = 2.5 \times 10^{-4}\ \Omega^{-1}$.

B. Optical conductivity in standard DMFT

The optical conductivity was calculated for different combinations of the parameters of the model. Below, we present only a fraction of our results, which are, probably, most relevant for copper oxides. We shall start with presenting some typical results, obtained within our formalism in conventional DMFT approximation, neglecting pseudogap fluctuations, just to introduce the basic physical picture and demonstrate the effectiveness of our approach.

The characteristic feature of the strongly correlated metallic state is the coexistence of lower and upper Hubbard bands splitt by the value of $\sim U$ with a quasiparticle peak at the Fermi level.[7,8] For the case of a strongly correlated metal with $W \gtrsim U$, we observe almost no contribution from excitations to the upper Hubbard model in the optical conductivity, as can be seen in Fig. 7 [where we show the real part of conductivity Re $\sigma(\omega)$]. This contribution is almost completely masked by a typical Drude-like frequency behavior, with only slightly nonmonotonous behavior for $\omega \sim U$, which completely disappears as we increase the temperature.

The situation is different in doped Mott insulator with $U \gg W$. In Fig. 8, we clearly observe an additional maximum of optical absorption for $\omega \sim U$; however, at smaller frequencies, we again observe a typical Drude-like behavior, slightly nonmonotonous for small frequencies due to quasiparticle band formation (see the inset in Fig. 8).

These and similar results are more or less well known from the previous studies[7,8] and are quoted here only to demonstrate the consistency of our formalism and to prepare the reader for other results, showing pseudogap behavior.

C. Optical conductivity in DMFT+Σ_p

1. Correlated metal

Let us start the discussion of the results obtained within our generalized DMFT+Σ_p approach for the case of $W \gtrsim U$.

In Fig. 9, we show our DMFT+Σ_p results for the real part of the optical conductivity for correlated metal ($U=4t$) for two values of temperature, compared with similar data without pseudogap fluctuations (pure DMFT). We clearly observe the formation of typical pseudogap (absorption) anomaly on the "shoulder" of the Drude-like peak, which is partially "filled" with the growth of temperature. This behavior is quite similar to "midinfrared feature" that is observed in the

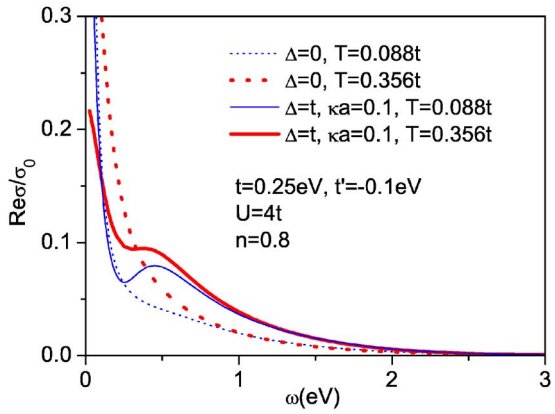

FIG. 9. (Color online) Real part of the optical conductivity for correlated metal ($U=4t$, $t'=-0.4t$, and $t=0.25$ eV) in the DMFT+Σ_p approximation for two different temperatures: $T=0.088t$ and $T=0.356t$. Pseudogap amplitude $\Delta=t$, correlation length $\xi=10a$, and filling factor $n=0.8$ electrons per atom.

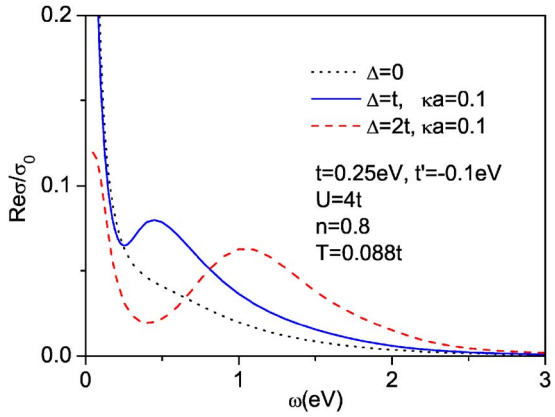

FIG. 10. (Color online) Real part of the optical conductivity for correlated metal ($U=4t$, $t'=-0.4t$, and $t=0.25$ eV) in the DMFT $+\Sigma_{\mathbf{p}}$ approximation—Δ dependence. Parameters are the same as in Fig. 9, but the data are for different values of $\Delta=0$, $\Delta=t$, and $\Delta=2t$, and temperature $T=0.088t$.

optical conductivity of cuprate superconductors.[27,28] In Fig. 10, we show the behavior of Re $\sigma(\omega)$ for different values of the pseudogap amplitude Δ. We see that the pseudogap anomaly naturally grows with the growth of Δ. Figure 11 illustrates the dependence of Re $\sigma(\omega)$ on the correlation length of pseudogap (AFM, SDW) fluctuations. Again, we observe the natural behavior—pseudogap anomaly is filled for shorter correlation lengths, i.e., as fluctuations become more short ranged. At last, in Fig. 12, we demonstrate the dependence of the pseudogap anomaly in the optical conductivity on the correlation strength, i.e., on the Hubbard interaction U. It is seen that the frequency range, where pseudogap anomaly is observed, becomes narrower as the correlation strength grows. This correlates with the general narrowing of the pseudogap anomaly and spectral densities with the growth of correlations, as observed in our previous work.[15,16] For large values of U, the pseudogap anomaly is practically suppressed. This is the main qualitative difference

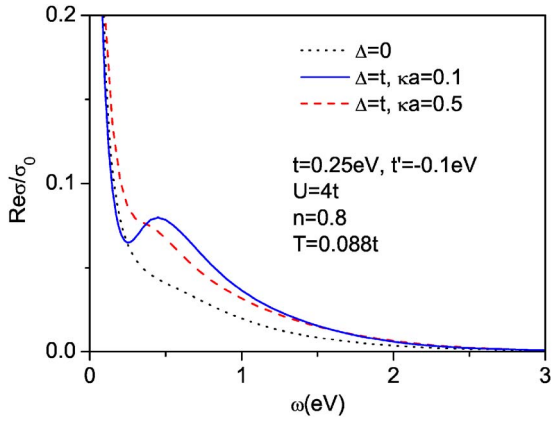

FIG. 11. (Color online) Real part of the optical conductivity for correlated metal ($U=4t$, $t'=-0.4t$, and $t=0.25$ eV) in the DMFT $+\Sigma_{\mathbf{p}}$ approximation—dependence on the correlation length. Parameters are the same as in Fig. 9, but in the data are for different values of the inverse correlation length $\kappa=\xi^{-1}$: $\kappa a=0.1$ and $\kappa a=0.5$, and temperature $T=0.088t$.

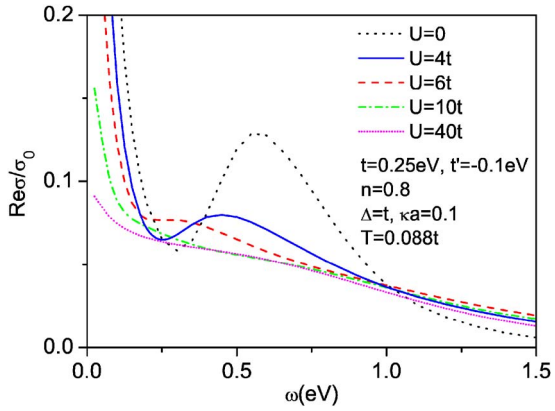

FIG. 12. (Color online) Real part of the optical conductivity for correlated metal in the DMFT+$\Sigma_{\mathbf{p}}$ approximation—U dependence. Parameters are the same as in Fig. 9, but the data are for different values of U: $U=0$, $U=4t$, $U=6t$, $U=10t$, and $U=40t$. Temperature $T=0.088t$.

of the results of the present approach compared to our earlier work[23] on the optical conductivity in the pseudogap state. Comparing the data of the present work for $U=0$ with similar data of Ref. 23, it should be noted that in this earlier work, we have performed calculations of dynamic conductivity only for $T=0$ and used simplified expressions, neglecting *RR*- and *AA*-loop contributions to conductivity, as well as small frequency expansion,[18] just to speed up the calculations. These simplifications lead to some quantitative differences with the results of the present work, where all calculations are done exactly using the general expression (22), though qualitatively the frequency behavior of conductivity is the same.

2. Doped Mott insulator

Now, we shall discuss our results for the case of doped Mott insulator with $U \gg W$. This case has no direct relevance to copper oxides, but is interesting from the general point of view and we present some of our results.

The real part of the optical conductivity for the case of $U=40t$ is shown in Figs. 13 and 14.

In Fig. 13, we show Re $\sigma(\omega)$ several values of the pseudogap amplitude Δ for the doped Mott insulator in the DMFT+$\Sigma_{\mathbf{p}}$ approach. Obviously enough, pseudogap fluctuations lead to significant changes of the optical conductivity only for relatively small frequencies of the order of Δ, while for high frequencies (e.g., of the order of U, where the upper Hubbard band contributes), we do not observe pseudogap effects (see the inset in Fig. 13). For small frequencies, we observe pseudogap suppression of the Drude-like peak, with only a shallow anomaly for $\omega \sim \Delta$, which just disappears for smaller values of Δ or shorter correlation lengths.

In Fig. 14, we show similar data for the special case of $t'=0$ and $n=1$, i.e., at half-filling (Mott insulator) for different values of the inverse correlation length $\kappa=\xi^{-1}$. The conductivity at small frequencies is determined only by thermal excitations, and pseudogap fluctuations suppress it significantly. Shorter correlation lengths obviously lead to larger values of conductivity at small frequencies. Transitions to the

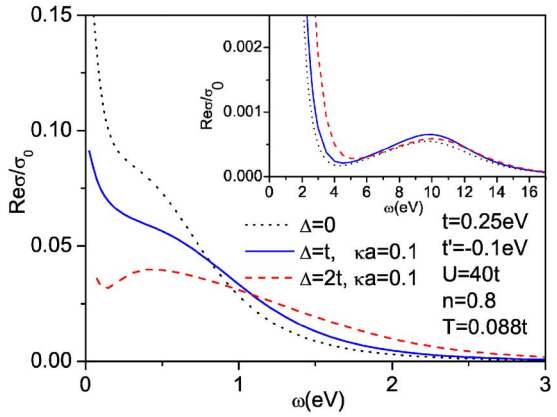

FIG. 13. (Color online) Real part of the optical conductivity for doped Mott insulator ($U=40t$, $t'=-0.4t$, and $t=0.25$ eV) in the DMFT+$\Sigma_{\mathbf{p}}$ approximation for different values of $\Delta=0$, $\Delta=t$, and $\Delta=2t$, and temperature $T=0.088t$. Correlation length $\xi=10a$, and filling factor $n=0.8$. Inset: conductivity in a wide frequency interval, including transitions to the upper Hubbard band.

upper Hubbard band are not affected by these fluctuations at all.

V. CONCLUSION

The present work is the direct continuation of our previous work,[14–16] where we have proposed a generalized DMFT+$\Sigma_{\mathbf{p}}$ approach, which is meant to take into account the important effects of nonlocal correlations (in principle, of any type) in addition to the (essentially exact) treatment of local dynamical correlations by DMFT. Here, we used a generalized DMFT+$\Sigma_{\mathbf{p}}$ approach to calculate the dynamic (optical) conductivity of the two-dimensional Hubbard model with pseudogap fluctuations. Our results demonstrate that pseudogap anomalies observed in optical conductivity of copper oxides can, in principle, be explained by this model. The main advantage in comparison to the previous work[23] is our ability now to study the role of strong electronic correlations, which are decisive in the formation of electronic structure of systems such as copper oxides. In fact, we have demonstrated an important suppression of pseudogap anomaly in optical conductivity with the growth of correlation strength.

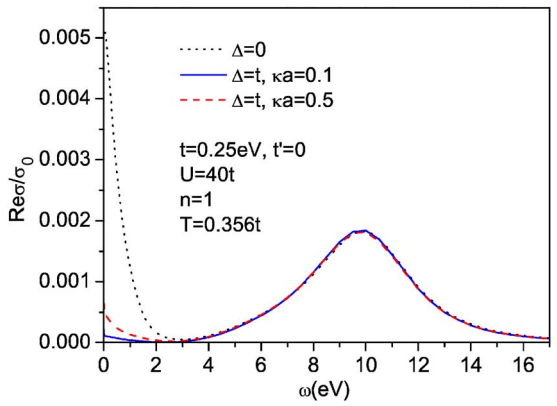

FIG. 14. (Color online) Real part of the optical conductivity for doped Mott insulator ($U=40t$, $t=0.25$ eV, and $t'=0$) in the DMFT+$\Sigma_{\mathbf{p}}$ approximation for different values of the inverse correlation length $\kappa=\xi^{-1}$: $\kappa a=0.1$ and $\kappa a=0.5$, temperature $T=0.356t$, and filling $n=1$.

As we already noted in Ref. 15, qualitatively similar results on pseudogap formation in single-particle characteristics for the two-dimensional Hubbard model were also obtained within cluster extensions of DMFT.[12,13] However, these methods have generic restrictions concerning the size of the cluster and up to now have not been not widely applied to calculations of two-particle properties, such as general response functions, and, in particular, to calculations of the dynamic (optical) conductivity.

Our approach is free of these limitations, though at the price of introduction of additional (semi)phenomenological parameters (correlation length ξ and pseudogap amplitude Δ). It is much less time consuming; thus its advantage for the calculations of two-particle response functions is obvious. It also opens the possibility of systematic comparison of different types of nonlocal fluctuations and their effects on electronic properties, providing a more intuitive way to analyze experiments or theoretical data obtained within more advanced schemes. Again, note that, in principle, both ξ and Δ can be calculated from the original model.[15] Our scheme works for any Coulomb interaction strength U, pseudogap strength Δ, correlation length ξ, filling n, and bare electron dispersion $\varepsilon(\mathbf{k})$.

The present formalism can be easily generalized in the framework of our recently proposed LDA+DMFT+$\Sigma_{\mathbf{p}}$ approach, which will allow us to perform calculations of pseudogap anomalies of the optical conductivity for realistic models. It can also be easily generalized to orbital degrees of freedom, phonons, impurities, etc.

ACKNOWLEDGMENTS

We are grateful to Th. Pruschke for providing us with his effective NRG code. This work was supported in part by RFBR Grants No. 05-02-16301 (M.V.S., E.Z.K., and I.A.N.), No. 05-02-17244 (I.A.N.), No. 06-02-90537 (I.A.N.), by the joint UrO-SO project (E.Z.K. and I.A.N.), and by the programs of the Presidium of the Russian Academy of Sciences (RAS) "Quantum macrophysics" and of the Division of Physical Sciences of the RAS "Strongly correlated electrons in semiconductors, metals, superconductors, and magnetic materials." I.A.N. acknowledges the support from the Dynasty Foundation and International Center for Fundamental Physics in Moscow program for young scientists and also from the grant of the President of the Russian Federation for young Ph.D. MK-2118.2005.02.

VI. APPENDIX: WARD IDENTITIES

In this appendix, we present the derivation of Ward identities used in the main text. Let us start with the general expression for the variation of the electron self-energy due to an arbitrary variation of the complete Green's function, which is valid for any interacting Fermi system:[29]

$$\Delta\Sigma_p = \sum_{p'} U_{pp'}(q)\Delta G_{p'}, \tag{A1}$$

where $U_{pp'}(q)$ is an irreducible vertex in particle-hole channel, and we use four-dimensional notations $p=(i\varepsilon,\mathbf{p})$, $q=(i\omega,\mathbf{q})$, etc. In the following, we take

$$\Delta\Sigma_p = \Sigma_+ - \Sigma_- \equiv \Sigma(i\varepsilon_+,\mathbf{p}_+) - \Sigma(i\varepsilon_-,\mathbf{p}_-), \tag{A2}$$

and (in the same notations)

$$\Delta G_p = G_+ - G_- = (G_+G_-)_p\left[\Delta\Sigma_p - \Delta(G_0^{-1})_p\right], \tag{A3}$$

where $\Delta(G_0^{-1})_p = G_{0+}^{-1} - G_{0-}^{-1}$, and the last expression was obtained using the standard Dyson equation.

Note the similarity of Eq. (A1) to the Ward identity for noninteracting electrons in the impure system derived in Ref. 18.

Now, substituting the last expression in Eq. (A3), we get

$$\Delta\Sigma_p = \sum_{p'} U_{pp'}(q)(G_+G_-)_{p'}\left[\Delta\Sigma_{p'} - \Delta(G_0^{-1})_{p'}\right]. \tag{A4}$$

Iterating this equation, we obtain

$$\Delta\Sigma_p = \sum_{p'} U_{pp'}(G_+G_-)_{p'}[-\Delta(G_0^{-1})_{p'}] + \sum_{p''p'} U_{pp''}(G_+G_-)_{p''}U_{p''p'}(G_+G_-)_{p'}[-\Delta(G_0^{-1})_{p'}] + \cdots. \tag{A5}$$

Multiplying both sides of Eq. (A5) by $(G_+G_-)_p$ and adding

$$\sum_{p'} (G_+G_-)_p\delta_{pp'}[-\Delta(G_0^{-1})_{p'}] = (G_+G_-)_p[-\Delta(G_0^{-1})_p],$$

we have

$$\begin{aligned}(G_+G_-)_p&\left[\Delta\Sigma_p - \Delta(G_0^{-1})_p\right] \\ &= \sum_{p'}\Bigg[(G_+G_-)_p\delta_{pp'} + (G_+G_-)_pU_{pp'}(G_+G_-)_{p'} + (G_+G_-)_p \\ &\quad\times\sum_{p''} U_{pp''}(G_+G_-)_{p''}U_{p''p'}(G_+G_-)_{p'} + \cdots\Bigg][-\Delta(G_0^{-1})] \\ &= \sum_p \Phi_{pp'}(q)[-\Delta(G_0^{-1})_{p'}],\end{aligned} \tag{A6}$$

where $\Phi_{pp'}(q)$ is the complete two-particle Green's function determined by the following Bethe-Salpeter equation:[29]

$$\Phi_{pp'}(q) = (G_+G_-)_p\delta_{pp'} + (G_+G_-)_p\sum_{p'} U_{pp'}\Phi_{pp'}(q). \tag{A7}$$

Finally, we obtain

$$\Delta G_p = \sum_{p'} \Phi_{pp'}(q)[-\Delta(G_0^{-1})_{p'}], \tag{A8}$$

which is the general form of our Ward identity.

Summing both sides of Eq. (A8) over $\mathbf{p}$ and taking $\mathbf{q}=0$, we obtain the identity (16) used above. Similarly, taking the bare Green's function (17), we obtain Eq. (18).

[1] T. Timusk and B. Statt, Rep. Prog. Phys. **62**, 61 (1999).
[2] M. V. Sadovskii, Usp. Fiz. Nauk **171**, 539 (2001) [Phys. Usp. **44**, 515 (2001)].
[3] J. Schmalian, D. Pines, and B. Stojkovič, Phys. Rev. Lett. **80**, 3839 (1998); Phys. Rev. B **60**, 667 (1999).
[4] E. Z. Kuchinskii and M. V. Sadovskii, Zh. Eksp. Teor. Fiz. **115**, 1765 (1999) [JETP **88**, 347 (1999)].
[5] W. Metzner and D. Vollhardt, Phys. Rev. Lett. **62**, 324 (1989).
[6] D. Vollhardt, in *Correlated Electron Systems*, edited by V. J. Emery (World Scientific, Singapore, 1993), p. 57.
[7] Th. Pruschke, M. Jarrell, and J. K. Freericks, Adv. Phys. **44**, 187 (1995).
[8] A. Georges, G. Kotliar, W. Krauth, and M. J. Rozenberg, Rev. Mod. Phys. **68**, 13 (1996).
[9] G. Kotliar and D. Vollhardt, Phys. Today **57**(3), 53 (2004).
[10] Q. Si and J. L. Smith, Phys. Rev. Lett. **77**, 3391 (1996).
[11] EDMFT approach to pseudogap formation can be found in K. Haule, A. Rosch, J. Kroha, and P. Wölfle, Phys. Rev. Lett. **89**, 236402 (2002); Phys. Rev. B **68**, 155119 (2003).
[12] Th. Maier, M. Jarrell, Th. Pruschke, and M. Hettler, Rev. Mod. Phys. **77**, 1027 (2005).
[13] G. Kotliar, S. Y. Savrasov, G. Palsson, and G. Biroli, Phys. Rev. Lett. **87**, 186401 (2001); M. Capone, M. Civelli, S. S. Kancharla, C. Castellani, and G. Kotliar, Phys. Rev. B **69**, 195105 (2004).
[14] E. Z. Kuchinskii, I. A. Nekrasov, and M. V. Sadovskii, Pis'ma Zh. Eksp. Teor. Fiz. **82**, 217 (2005) [JETP Lett. **82**, 198 (2005)].
[15] M. V. Sadovskii, I. A. Nekrasov, E. Z. Kuchinskii, Th. Pruschke, and V. I. Anisimov, Phys. Rev. B **72**, 155105 (2005).
[16] E. Z. Kuchinskii, I. A. Nekrasov, and M. V. Sadovskii, Fiz. Nizk. Temp. **32**, 528 (2006) [Low Temp. Phys. **32**, 398 (2006)].
[17] E. Z. Kuchinskii, I. A. Nekrasov, Z. V. Pchelkina, and M. V. Sadovskii, cond-mat/0606651 (to be published).
[18] D. Vollhardt and P. Wölfle, Phys. Rev. B **22**, 4666 (1980).
[19] M. V. Sadovskii, *Diagrammatics* (World Scientific, Singapore, 2006).
[20] V. Janiš, J. Kolorenč, and V. Špička, Eur. Phys. J. B **35**, 77 (2003).
[21] M. V. Sadovskii, Zh. Eksp. Teor. Fiz. **77**, 2070 (1979) [Sov. Phys. JETP **50**, 989 (1979)].
[22] M. V. Sadovskii and A. A. Timofeev, J. Mosc. Phys. Soc. **1**, 391 (1991).
[23] M. V. Sadovskii and N. A. Strigina, Zh. Eksp. Teor. Fiz. **122**, 610 (2002) [JETP **95**, 526 (2002)].
[24] M. V. Sadovskii, Zh. Eksp. Teor. Fiz. **66**, 1720 (1974) [Sov. Phys. JETP **39**, 845 (1974)].
[25] K. G. Wilson, Rev. Mod. Phys. **47**, 773 (1975); H. R. Krishnamurthy, J. W. Wilkins, and K. G. Wilson, Phys. Rev. B **21**, 1003

(1980); **21**, 1044 (1980); A. C. Hewson, *The Kondo Problem to Heavy Fermions* (Cambridge University Press, Cambridge, 1993).

[26] R. Bulla, A. C. Hewson, and Th. Pruschke, J. Phys.: Condens. Matter **10**, 8365 (1998); R. Bulla, Phys. Rev. Lett. **83**, 136 (1999).

[27] D. N. Basov and T. Timusk, Rev. Mod. Phys. **77**, 721 (2005).

[28] J. Hwang, T. Timusk, and G. D. Gu, cond-mat/0607653 (to be published).

[29] A. B. Migdal, *Theory of Finite Fermi Systems and Applications to Atomic Nuclei* (Interscience Publishers, New York, 1967).

ISSN 1063-7761, Journal of Experimental and Theoretical Physics, 2008, Vol. 106, No. 3, pp. 581–596. © Pleiades Publishing, Inc., 2008.

ELECTRONIC PROPERTIES OF SOLIDS

Mott–Hubbard Transition and Anderson Localization: A Generalized Dynamical Mean-Field Theory Approach[1]

E. Z. Kuchinskii, I. A. Nekrasov, and M. V. Sadovskii

Institute for Electrophysics, Russian Academy of Sciences, Yekaterinburg, 620016 Russia

e-mail: sadovski@iep.uran.ru

Received October 4, 2007

Abstract—The DOS, the dynamic (optical) conductivity, and the phase diagram of a strongly correlated and strongly disordered paramagnetic Anderson–Hubbard model are analyzed within the generalized dynamical mean field theory (DMFT + Σ approximation). Strong correlations are taken into account by the DMFT, and disorder is taken into account via an appropriate generalization of the self-consistent theory of localization. The DMFT effective single-impurity problem is solved by a numerical renormalization group (NRG); we consider the three-dimensional system with a semielliptic DOS. The correlated metal, Mott insulator, and correlated Anderson insulator phases are identified via the evolution of the DOS and dynamic conductivity, demonstrating both the Mott–Hubbard and Anderson metal–insulator transition and allowing the construction of the complete zero-temperature phase diagram of the Anderson–Hubbard model. Rather unusual is the possibility of a disorder-induced Mott insulator-to-metal transition.

PACS numbers: 71.10.Fd, 71.27.+a, 71.30.+h

DOI: 10.1134/S1063776108030187

1. INTRODUCTION

The importance of the electronic interaction and randomness for the properties of condensed matter is well known [1]. Both Coulomb correlations and disorder are driving forces of metal–insulator transitions (MITs) connected with the localization and derealization of particles. In particular, the Mott–Hubbard MIT is caused by electronic repulsion [2], while the Anderson MIT is due to random scattering of noninteracting particles [3]. Actually, disorder and interaction effects are known to compete in many subtle ways [1, 4]; this problem becomes much more complicated in the case of strong electron correlations and strong disorder, determining the physical mechanisms of the Mott–Anderson MIT [1].

The cornerstone of the modern theory of strongly correlated systems is the dynamic mean-field theory (DMFT) [5–8], constituting a nonperturbative theoretical framework for the investigation of correlated lattice electrons with a local interaction. In this approach, the effect of local disorder can be taken into account through the standard average density of states (DOS) [9] in the absence of interactions, leading to the well-known coherent potential approximation [10], which does not describe the physics of Anderson localization. To overcome this deficiency, Dobrosavljević and Kotliar [11] formulated a variant of the DMFT where the geometrically averaged local DOS was computed from solutions of the self-consistent stochastic DMFT equations. Subsequently, Dobrosavljević et al. [12] incorporated the geometrically averaged local DOS into the self-consistency cycle and derived a mean-field theory of Anderson localization that reproduced many of the expected features of the disorder-driven MIT for noninteracting electrons. This approach was extended in [13] to include Hubbard correlations via DMFT, which led to a highly nontrivial phase diagram of the Anderson–Hubbard model with the correlated metal, Mott insulator, and correlated Anderson insulator phases. The main deficiency of these approaches, however, is the inability to directly calculate measurable physical properties, such as conductivity, which is of major importance and defines the MIT itself.

At the same time, the well-developed approach of the self-consistent theory of Anderson localization, based on solving the equations for the generalized diffusion coefficient, demonstrated its efficiency in the noninteracting case a long time ago [14–19]; several attempts to include interaction effects into this approach were made with some promising results [17, 20]. However, until recently, there have been no attempts to incorporate this approach into the modern theory of strongly correlated electronic systems. Here, we undertake such research, studying the Mott–Hubbard and Anderson MITs via direct calculations of both the average DOS and the dynamic (optical) conductivity.

Our approach is based on the recently proposed generalized DMFT + Σ approximation [21–24], which, on the one hand, retains the single-impurity description of the DMFT, with a proper account for local Hubbard-

[1] The text was submitted by the authors in English.

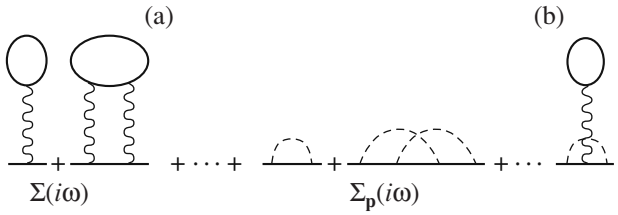

Fig. 1. Typical "skeleton" diagrams for the self-energy in the DMFT + Σ approach. (a) The first two terms are examples of DMFT self-energy diagrams; the middle two diagrams show contributions due to random impurity scattering, represented by dashed lines. The last diagram (b) is an example of a neglected diagram leading to interference between the local Hubbard interaction and impurity scattering.

like correlations and the possibility of using impurity solvers like NRG [25–27], and on the other hand, allows including additional (either local or nonlocal) interactions (fluctuations) on a nonperturbative model basis.

Within this approach, we have already studied both single- and two-particle properties of the two-dimensional Hubbard model, concentrating mainly on the problem of pseudogap formation in the DOS of the quasiparticle band in both correlated metals and doped Mott insulators, in application to superconducting cuprates. We analyzed the evolution of non-Fermi-liquid-like spectral density and ARPES spectra [22], "destruction" of Fermi surfaces and formation of Fermi "arcs" [21], as well as pseudogap anomalies of optical conductivity [24]. Briefly, we also considered impurity scattering effects [23].

In this paper, we apply our DMFT + Σ approach for calculations of the DOS, dynamic conductivity, and phase diagram of the strongly correlated and strongly disordered three-dimensional paramagnetic Anderson–Hubbard model. Strong correlations are again taken into account by DMFT, while disorder is taken into account via the appropriate generalization of the self-consistent theory of localization.

This paper is organized as follows. In Section 2, we briefly describe our generalized DMFT + Σ approximation with application to the disordered Hubbard model. In Section 3, we present basic DMFT + Σ expressions for dynamic (optical) conductivity and formulate the appropriate self-consistent equations for the generalized diffusion coefficient. Computational details and results for the DOS and dynamic conductivity are given in Section 4, where we also analyze the phase diagram of the strongly disordered Hubbard model within our approach. The paper ends with a short summary Section 5 including a discussion of some related problems.

2. BASICS OF THE DMFT + Σ APPROACH

Our aim is to consider the nonmagnetic disordered Anderson–Hubbard model (mainly) at half-filling for arbitrary interaction and disorder strengths. The Mott–Hubbard and Anderson MITs are investigated on an equal footing. The Hamiltonian of the model is written as

$$H = -t\sum_{\langle ij\rangle\sigma} a^{\dagger}_{i\sigma}a_{j\sigma} + \sum_{i\sigma}\epsilon_i n_{i\sigma} + U\sum_i n_{i\uparrow}n_{i\downarrow}, \qquad (1)$$

where $t > 0$ is the amplitude for hopping between nearest neighbors, U is the on-site repulsion, $n_{i\sigma} = a^{\dagger}_{i\sigma}a_{i\sigma}$ is the local electron number operator, $a_{i\sigma}$ ($a^{\dagger}_{i\sigma}$) is the annihilation (creation) operator of an electron with spin σ, and the local ionic energies ϵ_i at different lattice sites are considered independent random variables. To simplify the diagrammatics in what follows, we assume the Gaussian probability distribution for ϵ_i:

$$\mathcal{P}(\epsilon_i) = \frac{1}{\sqrt{2\pi}\Delta}\exp\left(-\frac{\epsilon_i^2}{2\Delta^2}\right), \qquad (2)$$

where the parameter Δ is a measure of the disorder strength, and a Gaussian (white noise) random field of energy level ϵ_i at lattice sites produces impurity scattering, leading to the standard diagram technique for calculating the averaged Green functions [19].

The DMFT + Σ approach was initially proposed [21–23] as a simple method to include nonlocal fluctuations of essentially arbitrary nature into the standard DMFT. In fact, it can be used to include any additional interaction into DMFT as follows. Working at finite temperatures T, we write the Matsubara-"time," Fourier-transformed, single-particle Green function of the Hubbard model as

$$G(i\varepsilon, \mathbf{p}) = \frac{1}{i\varepsilon + \mu - \epsilon(\mathbf{p}) - \Sigma(i\varepsilon) - \Sigma_{\mathbf{p}}(i\varepsilon)}, \qquad (3)$$
$$\varepsilon = \pi T(2n+1),$$

where $\epsilon(\mathbf{p})$ is the single-particle spectrum corresponding to the free part of (1); μ is the chemical potential fixed by the electron concentration; $\Sigma(i\varepsilon)$ is the local contribution to self-energy due to the Hubbard interaction, of DMFT type (surviving in the limit of spatial dimensionality $d \longrightarrow \infty$); and $\Sigma_{\mathbf{p}}(i\varepsilon)$ is some additional (in general, momentum-dependent) self-energy part. This last contribution can be caused, e.g., by electron interactions with certain "additional" collective modes or order parameter fluctuations within the Hubbard model itself. But it can actually be due to any other interactions (fluctuations) outside the standard Hubbard model, e.g., due to phonons or random impurity scattering, when it is in fact local (momentum independent). The last interaction is the main subject of our interest in the present paper. The basic assumption here is the neglect of all interference processes of the local Hubbard interaction and "external" contributions due to these additional scatterings (noncrossing approximation for appropriate diagrams) [22], as illustrated by diagrams in Fig. 1.

The self-consistency equations of the generalized DMFT + Σ approach are formulated as follows [21, 22].

(1) Start with some initial guess for the local self-energy $\Sigma(i\varepsilon)$, e.g., $\Sigma(i\varepsilon) = 0$.

(2) Construct $\Sigma_{\mathbf{p}}(i\varepsilon)$ within some (approximate) scheme, accounting for interactions with an external interaction (impurity scattering in our case), which can in general depend on $\Sigma(i\omega)$ and μ.

(3) Calculate the local Green function

$$G_{ii}(i\varepsilon) = \frac{1}{N}\sum_{\mathbf{p}}\frac{1}{i\varepsilon + \mu - \epsilon(\mathbf{p}) - \Sigma(i\varepsilon) - \Sigma_{\mathbf{p}}(i\varepsilon)}. \quad (4)$$

(4) Define the "Weiss field"

$$\mathcal{G}_0^{-1}(i\varepsilon) = \Sigma(i\varepsilon) + G_{ii}^{-1}(i\varepsilon). \quad (5)$$

(5) Using some "impurity solver," calculate the single-particle Green function $G_d(i\varepsilon)$ for the effective Anderson impurity problem, placed at a lattice site i and defined by the effective action that in the obvious notation is written as

$$S_{\text{eff}} = -\int_0^\beta d\tau_1 \int_0^\beta d\tau_2 c_{i\sigma}(\tau_1)\mathcal{G}_0^{-1}(\tau_1 - \tau_2)c_{i\sigma}^+(\tau_2) + \int_0^\beta d\tau U n_{i\uparrow}(\tau)n_{i\downarrow}(\tau). \quad (6)$$

In what follows, we use NRG [25–27] for the "impurity solver," which allows us to deal also with real frequencies, thus avoiding the complicated problem of analytic continuation from Matsubara frequencies.

(6) Define the new local self-energy

$$\Sigma(i\omega) = \mathcal{G}_0^{-1}(i\omega) - G_d^{-1}(i\omega). \quad (7)$$

(7) Using this self-energy as the "initial" one in step 1, continue the procedure until (and if) convergence is reached, to obtain

$$G_{ii}(i\varepsilon) = G_d(i\varepsilon). \quad (8)$$

Eventually, we obtain the desired Green function in form (3), with $\Sigma(i\varepsilon)$ and $\Sigma_{\mathbf{p}}(i\varepsilon)$ appearing at the end of our iteration procedure.

For $\Sigma_{\mathbf{p}}(i\varepsilon)$ in the random impurity problem, we use the simplest possible one-loop contribution, given by the third diagram in Fig. 1a neglecting "crossing" diagrams like the fourth one in Fig. 1a, i.e., just the self-consistent Born approximation [19], which in the case of Gaussian disorder (2) leads to the usual expression

$$\Sigma_{\mathbf{p}}(i\varepsilon) = \Delta^2\sum_{\mathbf{p}} G(i\varepsilon, \mathbf{p}) \equiv \Sigma_{\text{imp}}(i\varepsilon) \quad (9)$$

which is actually **p**-independent (local).

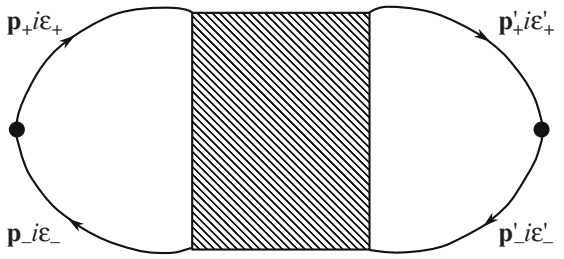

Fig. 2. Full polarization loop with the vertex part describing all interactions and impurity scatterings in the particle–hole channel. The loop without vertex corrections is included implicitly. Here, $\mathbf{p}_\pm = \mathbf{p} \pm \mathbf{q}/2$ and $\varepsilon_\pm = \varepsilon \pm \omega/2$.

3. DYNAMIC CONDUCTIVITY IN THE DMFT + Σ APPROACH

3.1. Basic Expressions for Optical Conductivity

Physically, it is clear that calculations of the dynamic conductivity are the most direct way to study MITs, because its frequency dependence along with the static value at zero frequency of an external field makes it possible to clearly distinguish between metallic and insulating phases (at zero temperature $T = 0$).

To calculate the dynamic conductivity, we use the general expression relating it to the retarded density-density correlation function $\chi^R(\omega, \mathbf{q})$ [14, 19]:

$$\sigma(\omega) = -\lim_{q\to 0}\frac{ie^2\omega}{q^2}\chi^R(\omega, \mathbf{q}), \quad (10)$$

where e is the electron charge.

We next outline the derivation presented in detail in [24] for the pseudogap problem, with necessary modifications for the present case. We consider the full polarization loop graph in the Matsubara representation shown in Fig. 2, which is conveniently (with explicit frequency summation) written as

$$\Phi(i\omega, \mathbf{q}) = \sum_{\varepsilon\varepsilon'}\Phi_{i\varepsilon i\varepsilon'}(i\omega, \mathbf{q}) \equiv \sum_{\varepsilon}\Phi_{i\varepsilon}(i\omega, \mathbf{q}) \quad (11)$$

and contains all possible interactions of our model, described by the full shaded vertex part. Actually, we implicitly assume here that the simple-loop contribution without vertex corrections is also included in Fig. 2, which shortens further diagrammatic expressions [24]. The retarded density–density correlation function is determined by an appropriate analytic continuation of this loop and can be written as [14]

$$\chi^R(\omega, \mathbf{q}) = \int_{-\infty}^{\infty}\frac{d\varepsilon}{2\pi i}\{[f(\varepsilon_+) - f(\varepsilon_-)]\Phi_\varepsilon^{RA}(\mathbf{q}, \omega) + f(\varepsilon_-)\Phi_\varepsilon^{RR}(\mathbf{q}, \omega) - f(\varepsilon_+)\Phi_\varepsilon^{AA}(\mathbf{q}, \omega)\}, \quad (12)$$

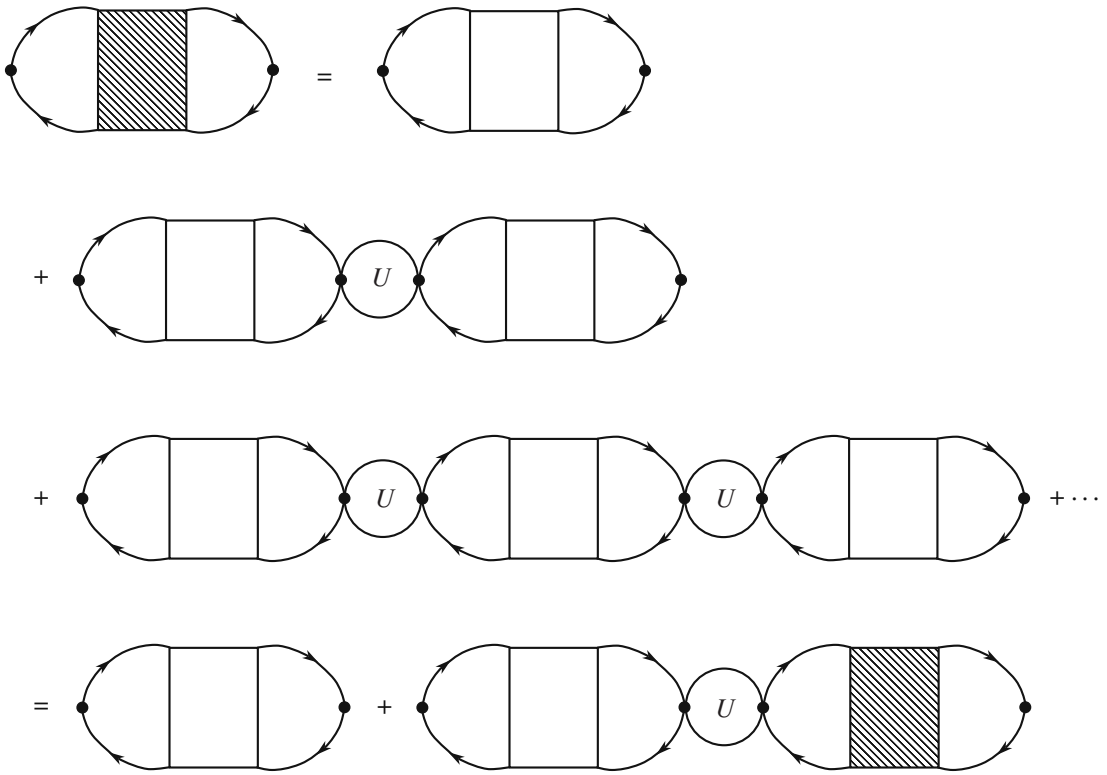

Fig. 3. Bethe–Salpeter equation for the polarization loop in the DMFT + Σ approach. A circle represents the irreducible vertex part in the particle–hole channel of the DMFT approach, which contains only local Hubbard interactions. An unshaded rectangular vertex represents corrections from impurity scattering only, implicitly including the case of free particle–hole propagation.

where $f(\varepsilon)$ is the Fermi distribution, $\varepsilon_\pm = \varepsilon \pm \frac{\omega}{2}$, and two-particle loops $\Phi_\varepsilon^{RA}(\mathbf{q}, \omega)$, $\Phi_\varepsilon^{RR}(\mathbf{q}, \omega)$, and $\Phi_\varepsilon^{AA}(\mathbf{q}, \omega)$ are determined by the appropriate analytic continuations ($i\varepsilon + i\omega \longrightarrow \varepsilon + \omega + i\delta$, $i\varepsilon \longrightarrow \varepsilon \pm i\delta$, and $\delta \longrightarrow +0$) in (11). Then we can write the dynamic (optical) conductivity as

$$\begin{aligned}\sigma(\omega) = \lim_{q\to 0}\left(-\frac{e^2\omega}{2\pi q^2}\right)\int_{-\infty}^{\infty} d\varepsilon\{[f(\varepsilon_+) - f(\varepsilon_-)]\\ \times[\Phi_\varepsilon^{RA}(\mathbf{q}, \omega) - \Phi_\varepsilon^{RA}(0, \omega)]\\ + f(\varepsilon_-)[\Phi_\varepsilon^{RR}(\mathbf{q}, \omega) - \Phi_\varepsilon^{RR}(0, \omega)]\\ - f(\varepsilon_+)[\Phi_\varepsilon^{AA}(\mathbf{q}, \omega) - \Phi_\varepsilon^{AA}(0, \omega)]\},\end{aligned} \tag{13}$$

where the total contribution of additional terms with zero q can be shown (with the use of general Ward identities) to be zero.

In the DMFT + Σ approximation, which neglects interference between the local Hubbard interaction and impurity scattering, we calculate $\Phi_{i\varepsilon i\varepsilon'}(i\omega, \mathbf{q})$ entering the sum over Matsubara frequencies in (11) by writing the Bethe–Salpeter equation, shown diagrammatically in Fig. 3, where we introduce the irreducible (local) DMFT vertex $U_{i\varepsilon i\varepsilon'}(i\omega)$ and the "rectangular" vertex containing all interactions with impurities. Analytically, this equation can be written as

$$\begin{aligned}\Phi_{i\varepsilon i\varepsilon'}(i\omega, \mathbf{q}) = \Phi^0_{i\varepsilon}(i\omega, \mathbf{q})\delta_{\varepsilon\varepsilon'}\\ + \Phi^0_{i\varepsilon}(i\omega, \mathbf{q})\sum_{\varepsilon''} U_{i\varepsilon i\varepsilon''}(i\omega)\Phi_{i\varepsilon'' i\varepsilon'}(i\omega, \mathbf{q}),\end{aligned} \tag{14}$$

where $\Phi^0_{i\varepsilon}(i\omega, \mathbf{q})$ is the sought function calculated neglecting vertex corrections due to the Hubbard interaction (but taking all interactions due to impurity scattering into account). We note that all the q-dependence is here determined by $\Phi^0_{i\varepsilon}(i\omega, \mathbf{q})$ because the vertex $U_{i\varepsilon i\varepsilon'}(i\omega)$ is local and q-independent.

As we noted in [24], it is clear from (13) that calculation of the conductivity requires only the knowledge of the q^2-contribution to $\Phi(i\omega, \mathbf{q})$. This can be easily found as follows. First, we note that all the loops in (14) contain a q-dependence starting from terms of the order q^2. Then we can take an arbitrary loop (cros section) in the expansion of (14) (see Fig. 3), calculate it up to terms of the order q^2, and re-sum all contributions to the right and to the left of this cross section, setting $q = 0$ in all these graphs. This is equivalent to simple q^2-differentiation of the expanded version of Eq. (14). This pro-

cedure immediately leads to the following relation for the q^2-contribution to (11):

$$\phi(i\omega) \equiv \lim_{q\to 0}\frac{\Phi(i\omega, \mathbf{q}) - \Phi(i\omega, 0)}{q^2} = \sum_{\varepsilon}\gamma^2_{i\varepsilon}(i\omega, \mathbf{q}=0)\phi^0_{i\varepsilon}(i\omega) \quad (15)$$

with

$$\phi^0_{i\varepsilon}(i\omega) \equiv \lim_{q\to 0}\frac{\Phi^0_{i\varepsilon}(i\omega, \mathbf{q}) - \Phi^0_{i\varepsilon}(i\omega, 0)}{q^2}, \quad (16)$$

where $\Phi^0_{i\varepsilon}(i\omega, \mathbf{q})$ contains vertex corrections due only to impurity scattering, while the one-particle Green functions entering it are taken with self-energies due to both impurity scattering and the local DMFT-like interaction, as in Eq. (3). The vertex $\gamma_{i\varepsilon}(i\omega, \mathbf{q} = 0)$ is determined diagrammatically as shown in Fig. 4, or analytically as

$$\gamma_{i\varepsilon}(i\omega, \mathbf{q}=0) = 1 + \sum_{\varepsilon'\varepsilon''}U_{i\varepsilon i\varepsilon''}(i\omega)\Phi_{i\varepsilon''i\varepsilon'}(i\omega, \mathbf{q}=0). \quad (17)$$

Next, using Bethe–Salpeter Eq. (14), we can explicitly write

$$\gamma_{i\varepsilon}(i\omega, \mathbf{q}=0) = 1 + \sum_{\varepsilon'}\frac{\Phi_{i\varepsilon i\varepsilon'}(i\omega, \mathbf{q}=0) - \Phi^0_{i\varepsilon}(i\omega, \mathbf{q}=0)}{\Phi^0_{i\varepsilon}(i\omega, \mathbf{q}=0)} = \frac{\sum_{\varepsilon'}\Phi_{i\varepsilon i\varepsilon'}(i\omega, \mathbf{q}=0)}{\Phi^0_{i\varepsilon}(i\omega, \mathbf{q}=0)}. \quad (18)$$

At $\mathbf{q} = 0$, we have the following Ward identity, which can be obtained by direct generalization of the proof given in [14, 28] (see the details in the Appendix of [24]):

$$(-i\omega)\Phi_{i\varepsilon}(i\omega, \mathbf{q}=0) = (-i\omega)\sum_{\varepsilon'}\Phi_{i\varepsilon i\varepsilon'}(i\omega, \mathbf{q}=0) = \sum_{\mathbf{p}}G(i\varepsilon + i\omega, \mathbf{p}) - \sum_{\mathbf{p}}G(i\varepsilon, \mathbf{p}). \quad (19)$$

The denominator of (18) contains vertex corrections only from impurity scattering, while the Green functions here are dressed by both impurities and the local (DMFT) Hubbard interaction. We can therefore regard the loop entering the denominator as dressed by impurities only, but with the "bare" Green functions:

$$\tilde{G}_0(i\varepsilon, \mathbf{p}) = \frac{1}{i\varepsilon + \mu - \epsilon(\mathbf{p}) - \Sigma(i\varepsilon)}, \quad (20)$$

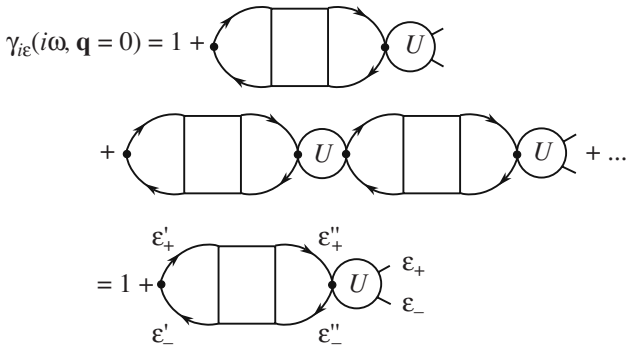

Fig. 4. Effective vertex $\gamma_{i\epsilon}(i\omega, \mathbf{q} = 0)$ used in calculations of conductivity.

where $\Sigma(i\varepsilon)$ is the local contribution to self-energy from the DMFT. For this problem, we have a Ward identity similar to (19) (see the Appendix in [24]),

$$\sum_{\mathbf{p}}G(i\varepsilon + i\omega, \mathbf{p}) - \sum_{\mathbf{p}}G(i\varepsilon, \mathbf{p}) = \Phi^0_{i\varepsilon}(i\omega, \mathbf{q}=0)[\Sigma(i\varepsilon + i\omega) - \Sigma(i\varepsilon) - i\omega] \equiv \Phi_{i\varepsilon}(i\omega, \mathbf{q}=0)[\Delta\Sigma(i\omega) - i\omega], \quad (21)$$

where we set

$$\Delta\Sigma(i\omega) = \Sigma(i\varepsilon + i\omega) - \Sigma(i\varepsilon). \quad (22)$$

Thus, using (19) and (21) in (18), we obtain the final expression for $\gamma_{i\varepsilon}(i\omega, \mathbf{q} = 0)$ as

$$\gamma_{i\varepsilon}(i\omega, \mathbf{q}=0) = 1 - \frac{\Delta\Sigma(i\omega)}{i\omega}. \quad (23)$$

Then (15) reduces to

$$\phi(i\omega) = \sum_{\varepsilon}\phi^0_{i\varepsilon}(i\omega)\left[1 - \frac{\Delta\Sigma(i\omega)}{i\omega}\right]^2. \quad (24)$$

Analytic continuation to real frequencies is obvious; using (15) and (24) in (13), we can write the final expression for the real part of dynamic (optical) conductivity as

$$\mathrm{Re}\sigma(\omega) = \frac{e^2\omega}{2\pi}\int_{-\infty}^{\infty}d\varepsilon[f(\varepsilon_-) - f(\varepsilon_+)] \times \mathrm{Re}\left\{\phi^{0RA}_{\varepsilon}(\omega)\left[1 - \frac{\Sigma^R(\varepsilon_+) - \Sigma^A(\varepsilon_-)}{\omega}\right]^2 - \phi^{0RR}_{\varepsilon}(\omega)\left[1 - \frac{\Sigma^R(\varepsilon_+) - \Sigma^R(\varepsilon_-)}{\omega}\right]^2\right\}. \quad (25)$$

Thus, we have greatly simplified our problem. To calculate the dynamic conductivity in the DMFT + Σ approximation, we only have to solve a single-particle

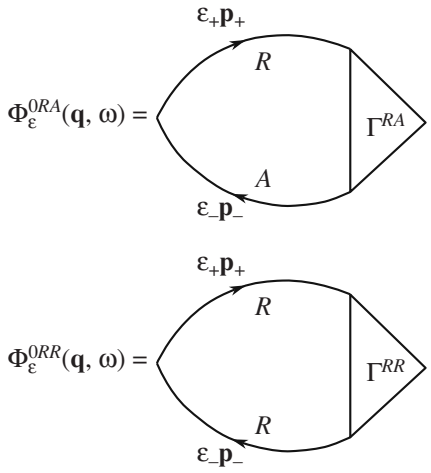

Fig. 5. Diagram representation of $\Phi_\varepsilon^{0RA}(\omega, \mathbf{q})$ and $\Phi_\varepsilon^{0RR}(\omega, \mathbf{q})$.

problem as described by the DMFT + Σ procedure above to determine self-consistent values of local self-energies $\Sigma(\varepsilon_\pm)$, while the nontrivial contribution of impurity scattering are to be included via (16), which is to be calculated in some approximation, taking only interaction with impurities (random scattering) into account, but using the bare Green functions of form (20), which include local self-energies that have already been determined via the general DMFT + Σ procedure. Actually, (25) also provides an effective algorithm to calculate dynamic conductivity in the standard DMFT (neglecting impurity scattering), because (16) is then easily calculated from a simple loop diagram, determined by two Green functions and free scalar vertices. As usual, there is no need to calculate vertex corrections within the DMFT itself, as was first proved considering the loop with vector vertices [7, 8]. Obviously, Eq. (25) effectively interpolates between the case of strong correlations without disorder and the case of pure disorder, without Hubbard correlations, which is of major interest to us. In what follows, we see that calculations based on Eq. (25) give a reasonable overall picture of MIT in the Anderson–Hubbard model.

3.2. Self-Consistent Equations for the Generalized Diffusion Coefficient and Conductivity

To calculate the optical conductivity, we need to know the basic block $\Phi_{i\varepsilon}^0(i\omega, \mathbf{q})$ entering (16) or, more precisely, the appropriate functions analytically continued to real frequencies: $\Phi_\varepsilon^{0RA}(\omega, \mathbf{q})$ and $\Phi_\varepsilon^{0RR}(\omega, \mathbf{q})$, which in turn define $\phi_\varepsilon^{0RA}(\omega)$ and $\phi_\varepsilon^{0RR}(\omega)$ entering (25) and are defined by obvious relations similar to (16):

$$\phi_\varepsilon^{0RA}(\omega) = \lim_{q\to 0}\frac{\Phi_\varepsilon^{0RA}(\omega, \mathbf{q}) - \Phi_\varepsilon^{0RA}(\omega, 0)}{q^2}, \quad (26)$$

$$\phi_\varepsilon^{0RR}(\omega) = \lim_{q\to 0}\frac{\Phi_\varepsilon^{0RR}(\omega, \mathbf{q}) - \Phi_\varepsilon^{0RR}(\omega, 0)}{q^2}. \quad (27)$$

By definition, we have (with $\mathbf{p}_\pm = \mathbf{p} \pm \mathbf{q}/2$)

$$\begin{aligned}\Phi_\varepsilon^{0RA}(\omega, \mathbf{q}) &= \sum_{\mathbf{p}} G^R(\varepsilon_+, \mathbf{p}_+)G^A(\varepsilon_-, \mathbf{p}_-)\\ &\times \Gamma^{RA}(\varepsilon_-, \mathbf{p}_-; \varepsilon_+, \mathbf{p}_+),\\ \Phi_\varepsilon^{0RR}(\omega, \mathbf{q}) &= \sum_{\mathbf{p}} G^R(\varepsilon_+, \mathbf{p}_+)G^R(\varepsilon_-, \mathbf{p}_-)\\ &\times \Gamma^{RR}(\varepsilon_-, \mathbf{p}_-; \varepsilon_+, \mathbf{p}_+),\end{aligned} \quad (28)$$

shown diagrammatically in Fig. 5. Here, the Green functions $G^R(\varepsilon_+, \mathbf{p}_+)$ and $G^A(\varepsilon_-, \mathbf{p}_-)$ are defined by analytic continuation ($i\varepsilon \longrightarrow \varepsilon \pm i\delta$) of Matsubara Green functions (3) determined via our DMFT + Σ algorithm (4)–(9), while the vertices $\Gamma^{RA}(\varepsilon_-, \mathbf{p}_-; \varepsilon_+, \mathbf{p}_+)$ and $\Gamma^{RR}(\varepsilon_-, \mathbf{p}_-; \varepsilon_+, \mathbf{p}_+)$ contain all vertex corrections due to impurity scattering.

The most important block $\Phi_\varepsilon^{0RA}(\omega, \mathbf{q})$ can be calculated using the basic approach of the self-consistent theory of localization [14–19] with appropriate extensions, taking the role of the local Hubbard interaction into account using the DMFT + Σ approach. The only important difference from the standard approach is that the self-consistent theory equations are derived using

$$G^{R,A}(\varepsilon, \mathbf{p}) = \frac{1}{\varepsilon + \mu - \epsilon(\mathbf{p}) - \Sigma^{R,A}(\varepsilon) - \Sigma_{\text{imp}}^{R,A}(\varepsilon)}, \quad (29)$$

which contains DMFT contributions $\Sigma^{R,A}(\varepsilon)$ in addition to the impurity scattering contained in

$$\begin{aligned}\Sigma_{\text{imp}}^{R,A}(\varepsilon) &= \Delta^2\sum_{\mathbf{p}} G^{R,A}(\varepsilon, \mathbf{p})\\ &= \text{Re}\Sigma_{\text{imp}}(\varepsilon) \pm i\gamma(\varepsilon),\end{aligned} \quad (30)$$

where $\gamma(\varepsilon) = \pi\Delta^2 N(\varepsilon)$ and $N(\varepsilon)$ is the DOS renormalized by the Hubbard interaction, given in the DMFT + Σ approach by the usual expression

$$N(\varepsilon) = -\frac{1}{\pi}\sum_{\mathbf{p}} \text{Im}G^R(\varepsilon, \mathbf{p}). \quad (31)$$

Following all the usual steps of the standard derivation [14–19], we obtain the diffusion-like (at small ω and q) contribution to $\Phi_\varepsilon^{0RA}(\omega, \mathbf{q})$ as

$$\Phi_\varepsilon^{0RA}(\mathbf{q}, \tilde{\omega}) = \frac{2\pi i N(\varepsilon)}{\tilde{\omega} + iD(\omega)q^2}, \quad (32)$$

where an important difference from the single-particle case is contained in

$$\begin{aligned}\tilde{\omega} &= \varepsilon_+ - \varepsilon_- - \Sigma^R(\varepsilon_+) + \Sigma^A(\varepsilon_-) \\ &= \omega - \Sigma^R(\varepsilon_+) + \Sigma^A(\varepsilon_-) \equiv \omega - \Delta\Sigma^{RA}(\omega),\end{aligned} \tag{33}$$

which replaces the usual ω term in the denominator of the standard expression for $\Phi_\varepsilon^{0RA}(\omega, \mathbf{q})$. On general grounds, it is clear that in the metallic phase as $\omega \longrightarrow 0$, we have $\Delta\Sigma^{RA}(\omega = 0) = 2i\mathrm{Im}\Sigma(\varepsilon) \sim \max\{T^2, \varepsilon^2\}$, reflecting the Fermi-liquid behavior of DMFT (conserved by elastic impurity scattering). At finite T, this leads to the usual phase decoherence due to electron–electron scattering [1, 4]. The generalized diffusion coefficient $D(\omega)$ should be determined by solving the basic self-consistency equation introduced below.

Using (32) in (26), we easily obtain

$$\phi_\varepsilon^{0RA}(\omega) = \frac{2\pi N(\varepsilon)D(\omega)}{\omega^2\left(1 - \dfrac{\Delta\Sigma^{RA}(\omega)}{\omega}\right)^2}. \tag{34}$$

Then using (34) in (25) with $\omega \longrightarrow 0$ and $T = 0$, we obtain just the usual Einstein relation for the static conductivity:

$$\sigma(0) = e^2 N(0) D(0). \tag{35}$$

All contributions form the Hubbard interaction are reduced to renormalization of the DOS at the Fermi level and of the diffusion coefficient $D(0)$.

It follows that (25) reduces to

$$\begin{aligned}\mathrm{Re}\sigma(\omega) &= \frac{e^2\omega}{2\pi}\int_{-\infty}^{\infty} d\varepsilon[f(\varepsilon_-) - f(\varepsilon_+)] \\ &\times \mathrm{Re}\left\{\frac{2\pi N(\varepsilon)D(\omega)}{\omega^2} - \phi_\varepsilon^{0RR}(\omega)\left[1 - \frac{\Delta\Sigma^{RR}(\omega)}{\omega}\right]^2\right\},\end{aligned} \tag{36}$$

where the second term can actually be neglected at small ω, or just calculated from (27) with $\Phi_\varepsilon^{0RR}(\omega, \mathbf{q})$ given by the usual "ladder" approximation (A.10).

We now formulate our basic self-consistent equation determining the generalized diffusion coefficient $D(\omega)$. We again follow all the usual steps of the self-consistent theory of localization (for details see Appendix A), taking into account the form of our single-particle Green function (29) and not restricting analysis to the small-ω limit. We can then write the generalized diffusion coefficient as

$$D(\omega) = \frac{\langle v\rangle^2}{d}\frac{i}{\tilde{\omega} + M(\omega)}, \tag{37}$$

where d is the spatial dimensionality, the average velocity $\langle v\rangle$ is defined in (A.6) (to a good approximation, it is just the Fermi velocity), and the relaxation kernel $M(\omega)$ satisfies the self-consistency equation, similar to that derived in [14–19] using "maximally crossed" diagrams for the irreducible impurity scattering vertex (built with Green functions (29)):

$$\begin{aligned}M(\omega) &= -\Delta\Sigma_{\mathrm{imp}}^{RA}(\omega) \\ &+ \Delta^4\sum_{\mathbf{p}}(\Delta G_{\mathbf{p}})^2\sum_{\mathbf{q}}\frac{1}{\tilde{\omega} + iD(\omega)q^2}\end{aligned} \tag{38}$$

with

$$\Delta G_{\mathbf{p}} = G^R(\varepsilon_+, \mathbf{p}) - G^A(\varepsilon_-, \mathbf{p}), \tag{39}$$

and $\Delta\Sigma_{\mathrm{imp}}^{RA}(\omega) = \Sigma_{\mathrm{imp}}^R(\varepsilon_+) - \Sigma_{\mathrm{imp}}^A(\varepsilon_-)$ is due to impurity scattering. It is important to stress once again that there are no contributions to this equation due to vertex corrections determined by the local Hubbard interaction. Using definition (37), we can rewrite Eq. (38) as a self-consistent equation for the generalized diffusion coefficient itself:

$$\begin{aligned}D(\omega) &= i\frac{\langle v\rangle^2}{d}\left\{\tilde{\omega} - \Delta\Sigma_{\mathrm{imp}}^{RA}(\omega)\right. \\ &\left. + \Delta^4\sum_{\mathbf{p}}(\Delta G_{\mathbf{p}})^2\sum_{\mathbf{q}}\frac{1}{\tilde{\omega} + iD(\omega)q^2}\right\}^{-1}\end{aligned} \tag{40}$$

which should be solved in conjunction with our DMFT + Σ loop (3)–(9). Due to the limitations of diffusion approximation, summation over q in (40) should be restricted to

$$q < k_0 = \min\{l^{-1}, p_{\mathrm{F}}\}, \tag{41}$$

where $l = \langle v\rangle/2\gamma(0)$ is the elastic mean-free path and p_{F} is the Fermi momentum [17, 19].

Solving (40) for different sets of parameters of our model and using it in (36) with regular contributions from (A.10), we can calculate the dynamic (optical) conductivity in different phases of the Anderson–Hubbard model.

4. RESULTS AND DISCUSSION

We performed extensive numerical calculations for a simplified version of the three-dimensional Anderson–Hubbard model on a cubic lattice with the semielliptic DOS of the bare band with a width of $W = 2D$:

$$N_0(\varepsilon) = \frac{2}{\pi D^2}\sqrt{D^2 - \varepsilon^2}. \tag{42}$$

The DOS is always given in units of the number of states per energy interval, per lattice cell volume a^3 (a is lattice spacing), and per spin. Some related technical details are given in Appendix B.

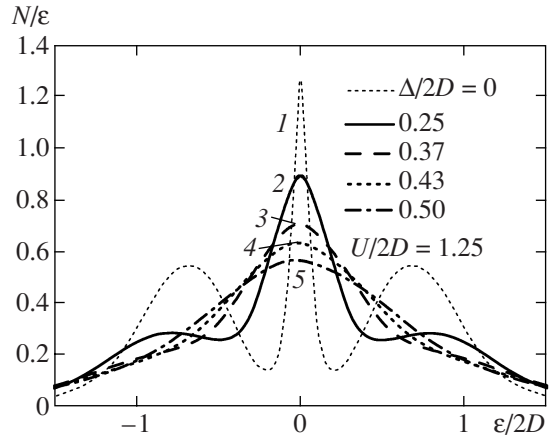

Fig. 6. Density of states of the half-filled Anderson–Hubbard model for different degrees of disorder Δ, and $U = 2.5D$, typical for a correlated metal.

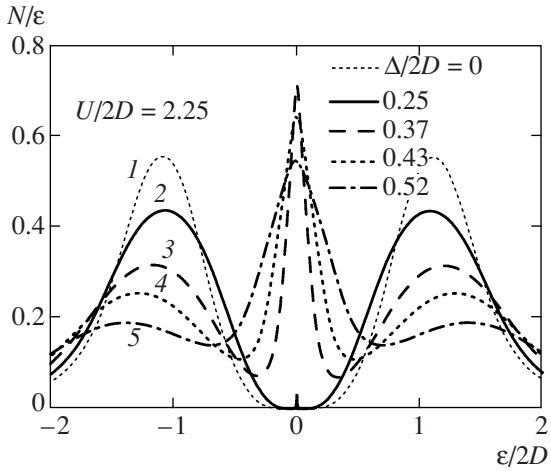

Fig. 7. Density of states of the half-filled Anderson–Hubbard model for different degrees of disorder Δ and $U = 4.5D$, typical for a Mott insulator.

We mostly concentrate on the half-filled case, although some results for finite dopings are also presented. The Fermi level is always placed at zero energy.

As the impurity solver of DMFT, we used the reliable numerically exact method of a numerical renormalization group (NRG) [25–27]. Calculations were performed for temperatures $T \sim 0.001D$, which effectively makes temperature effects in the DOS and conductivity negligible. The discretization parameter of the NRG was always $\Lambda = 2$, the number of low energy states after truncation was 1000, the cutoff was near the Fermi energy [1–6], and the broadening parameter $b = 0.6$.

We present only a fraction of the most typical results in what follows.

4.1. Evolution of the DOS

Within the standard DMFT approach, the DOS of the half-filled Hubbard model has a typical three-peak structure: a narrow quasiparticle band (central peak) develops at the Fermi level, with wider upper and lower Hubbard bands forming at $\varepsilon \sim \pm U/2$. The quasiparticle band narrows further with an increase in U in the metallic phase, vanishing at the critical value $U_{c2} \approx 1.5W$, signifying the Mott–Hubbard MIT with a gap opening at the Fermi level [7, 8, 27].

In Fig. 6, we present our DMFT + Σ results for the DOS, obtained for $U = 2.5D = 1.25W$, typical for a correlated metal without disorder, for different degrees of disorder Δ, including rather large values, actually transforming the correlated metal to a correlated Anderson insulator (see Section 4.2.). As may be expected, we observe typical widening and damping of the DOS by disorder.

More unexpected are the results obtained for values of U typical for a Mott insulator without disorder, as shown in Fig. 7 for $U = 4.5D = 2.25W$. We see the restoration of the central peak (quasiparticle band) in the DOS as disorder increases, transforming the Mott insulator to either a correlated metal or a correlated Anderson insulator. Similar behavior of the DOS was recently obtained in [13], but in our calculations the presence of distinct Hubbard bands was already observed for rather large values of disorder, with no signs of vanishing of the Hubbard structure of the DOS, which was observed in [13]. This is probably due to the very simple nature of our approximation for the DOS under disordering, although we must stress that this difference may also be due to another model of disorder used in [13] (a flat distribution of ϵ_i in (1) instead of our Gaussian case (2)). Although unimportant, in general, for the physics of the Anderson transition, the type of disorder may be significant for the DOS behavior.

It is well known that the hysteresis behavior of the DOS is obtained for the Mott–Hubbard transition if DMFT calculations are performed with U decreasing from the insulating phase [8, 27]. The Mott insulator phase survives for values of U well inside the correlated metal phase, obtained with an increase in U. The metallic phase is restored at $U_{c1} \approx 1.0W$. The values of U in the interval $U_{c1} < U < U_{c2}$ are usually considered as belonging to the coexistence region of the metallic and (Mott) insulating phases, with the metallic phase being thermodynamically more stable [8, 27, 29].

In Fig. 8, we present our typical data for the DOS with different disorder for the same value of $U = 2.5D = 1.25W$ as in Fig. 6, but for the hysteresis region, obtained by decreasing U from the Mott insulator phase. We again observe the restoration of the central peak (quasiparticle band) in the DOS under disordering. We also note the peculiar form of the DOS around the Fermi level during this transition: a narrow energy gap is conserved until it is closed by disorder, and a central peak is formed from two symmetrical maxima in the DOS merging into the quasiparticle band. This

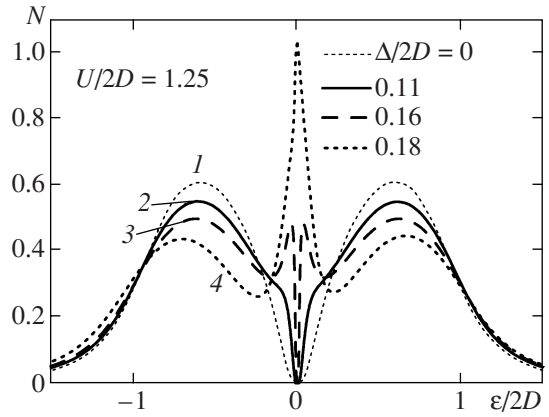

Fig. 8. Restoration of the quasiparticle band by disorder in the coexistence (hysteresis) region for $U = 2.5D$, obtained from a Mott insulator with decreasing U.

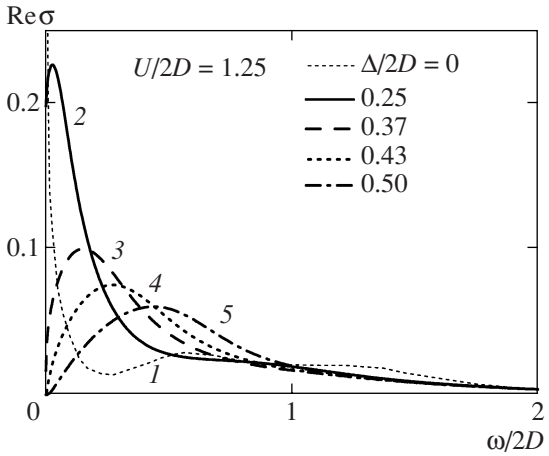

Fig. 9. Real part of dynamic conductivity for the half-filled Anderson–Hubbard model for different degrees of disorder Δ, and $U = 2.5D$, typical for a correlated metal. Lines *1* and *2* are for the metallic phase, line *3* corresponds to the mobility edge (Anderson transition), and lines *4* and *5* correspond to a correlated Anderson insulator.

resembles similar behavior observed in the periodic Anderson model [8]. This effect was apparently unnoticed in previous calculations of the DOS in the coexistence region [27] (in the absence of disorder); in our case, it was obtained mainly due to our use of a very fine mesh of values of the disorder parameter Δ.

The physical reason for the rather unexpected restoration of the central (quasiparticle) peak in the DOS is in fact clear. The controlling parameter for its appearance or disappearance in DMFT is actually the ratio of the Hubbard interaction U and the bare bandwidth $W = 2D$. Under disordering, we obtain the new effective bandwidth W_{eff} (in the absence of the Hubbard interaction), which increases with disorder, while the semielliptic form of the DOS, with well-defined band edges, is preserved in self-consistent Born approximation (9). This leads to a decrease in the ratio U/W_{eff}, which induces the reappearance of the quasiparticle band in our model. This is illustrated in more detail in Section 4.3, where our DOS calculations within the DMFT + Σ approach for a wide range of parameters are used to study the phase diagram of the Anderson–Hubbard model.

4.2. Dynamic Conductivity: Mott–Hubbard and Anderson Transitions

The real part of dynamic (optical) conductivity was calculated for different combinations of the parameters of our model directly from Eqs. (36), (A.9), (A.10), and (40) using the results of DMFT + Σ loop (3)–(9) as an input. The conductivity values are given below in natural units of $e^2/\hbar a$ (a is the lattice spacing).

In the absence of disorder, evidently, we reproduce the results of the standard DMFT approach [7, 8] with the dynamic conductivity characterized in general by the usual (metallic) Drude-like peak at zero frequency and a wide absorption maximum at $\omega \sim U$, corresponding to transitions to the upper Hubbard band. With an increase in U, the Drude peak decreases and vanishes at the Mott transition, when only transitions through the Mott–Hubbard gap contribute. Introduction of disorder leads to qualitative changes in the frequency dependence of conductivity. In what follows, we mainly show the results obtained for the same values of U and Δ that were used above to illustrate the DOS behavior.

In Fig. 9, we present the real part of dynamic (optical) conductivity for the half-filled Anderson–Hubbard model for different degrees of disorder Δ, and $U = 2.5D$, typical for a correlated metal. Transitions to the upper Hubbard band at $\omega \sim U$ are practically unobservable in these data, but it can clearly be seen that the metallic Drude peak at zero frequency is widened and suppressed, gradually transformed into a peak at finite frequencies due to effects of Anderson localization. The Anderson transition occurs at $\Delta_c \approx 0.74D = 0.37W$ (which corresponds to curve *3* in all our graphs, including those for DOS). We note that this value is actually dependent on the value of cutoff (41), which is defined up to a constant on the order of unity [17, 19]. Naive expectations might lead to the conclusion that a narrow quasiparticle band at the Fermi level, which forms in the general case of a highly correlated metal, may be localized much more easily than the typical conduction band. We see, however, that these expectations are wrong and that this band is localized only at strong enough disorder $\Delta_c \sim D$, just as for the whole conduction band of the width $\sim W$.

This is in accordance with the previous analysis of localization in a two-band model [30].

More important is the fact that in the DMFT + Σ approximation, the value of Δ_c is independent of U because all interaction effects enter Eq. (40) only via $\Delta\Sigma^{RA}(\omega) \longrightarrow 0$ as $\omega \longrightarrow 0$ (at $T = 0$) and hence interaction drops out at $\omega = 0$. This is actually the main defi-

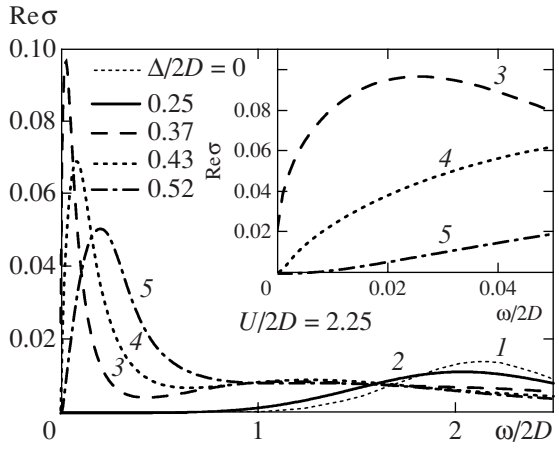

Fig. 10. Real part of dynamic conductivity of the half-filled Anderson–Hubbard model for different degrees of disorder Δ and $U = 4.5D$, typical for a Mott insulator. Lines *1* and *2* correspond to a Mott insulator, line *3* corresponds to the mobility edge (Anderson transition), and lines *4* and *5* are for a correlated Anderson insulator. Inset: the region of low frequencies magnified.

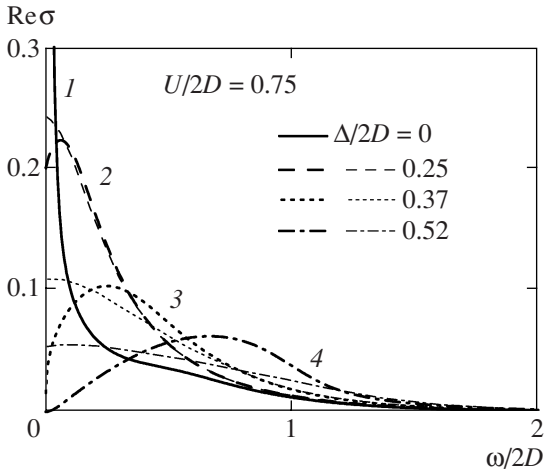

Fig. 11. Real part of dynamic conductivity of the half-filled Anderson–Hubbard model for different degrees of disorder Δ and $U = 1.5D$, comparison of the self-consistent theory (bold curves) with the ladder approximation (thin curves).

ciency of our approximation, occurring because we neglect interference effects between the interaction and disorder scattering. An important role of these interference effects has been known for a long time [1, 4]. However, despite the neglect of these effects, we are able to produce a physically sound interpolation between the two main limits of interest, the pure Anderson transition due to disorder and the Mott–Hubbard transition due to strong correlations. We thus consider it a reasonable first step to the future complete theory of MIT in strongly correlated disordered systems.

In Fig. 10, we present the real part of dynamic (optical) conductivity for different degrees of disorder Δ, and $U = 4.5D$ typical for a Mott–Hubbard insulator. In the inset, we show our data for small frequencies, which allow clear distinction of different types of conductivity behavior, especially close to the Anderson transition or in the Mott insulator phase. In this figure, we clearly see the contribution of transitions to the upper Hubbard band at $\omega \sim U$. More importantly, we observe that an increase in disorder produces finite conductivity within the frequency range of the Mott–Hubbard gap, which correlates to the appearance of the quasiparticle band (central peak) in the DOS within this gap, as shown in Fig. 7. In the general case, this conductivity is metallic (finite in the static limit $\omega = 0$) for $\Delta < \Delta_c$; for $\Delta > \Delta_c$, at small frequencies, we obtain $\mathrm{Re}\sigma(\omega) \sim \omega^2$, which is typical of an Anderson insulator [14–19]. We note that due to a finite internal accuracy of NRG numerics, small but finite spurious contributions to $\mathrm{Im}\Sigma^{R,A}(\varepsilon = 0)$ always appear [27] and formally increase with U. These contributions are all but irrelevant in calculating the conductivity in the metallic state. However, in an Anderson insulator, these spurious terms contribute via $\tilde{\omega}$ in Eq. (40) and lead to unphysical finite dephasing effects at $\omega = 0$ (or $T = 0$), which can simulate a small finite static conductivity. To exclude these spurious effects, we had to make appropriate subtractions in our data for $\mathrm{Im}\Sigma^{R,A}(\varepsilon)$ at $\varepsilon = 0$.

Rather unusual is the appearance of a low-frequency peak in $\mathrm{Re}\sigma(\omega)$ even in the metallic phase. It occurs because of weak localization effects, as can be clearly seen from Fig. 11, where we compare the real part of dynamic conductivity for different degrees of disorder Δ and $U = 1.5D$, obtained via our self-consistent approach (taking localization effects into account via "maximally crossed" diagrams) with that obtained using the ladder approximation for $\Phi_\varepsilon^{0RA}(\omega, \mathbf{q})$ (similar to (A.10)), which neglects all localization effects. It is clearly seen that in this simple approximation, we just obtain the usual Drude-like peak at $\omega = 0$, while accounting for localization effects produces a peak in $\mathrm{Re}\sigma(\omega)$ at low (finite) frequencies. The metallic state is defined [2] by the finite value of zero temperature conductivity at $\omega = 0$.

Up to now, we have presented only conductivity data obtained with an increase in U from the metallic to the (Mott) insulating phase. As U decreases from the Mott insulator phase, a hysteresis of conductivity is observed in the coexistence region, defined (in the absence of disorder, $\Delta = 0$) by $U_{c1} < U < U_{c2}$. Typical data are shown in Fig. 12, where we present the real part of dynamic conductivity for different degrees of disorder Δ and $U = 2.5D$, obtained from the Mott insulator phase with decreasing U, which should be compared with the data in Fig. 9. Transition to the metallic state via the closure of a narrow gap, "inside" a much wider Mott–Hubbard gap, is clearly seen, which correlates with the DOS data in Fig. 8.

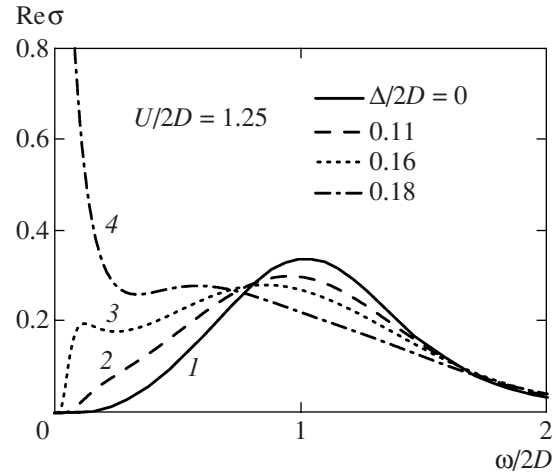

Fig. 12. Real part of dynamic conductivity of the half-filled Anderson–Hubbard model for different degrees of disorder Δ and $U = 2.5D$, obtained from a Mott insulator with decreasing U.

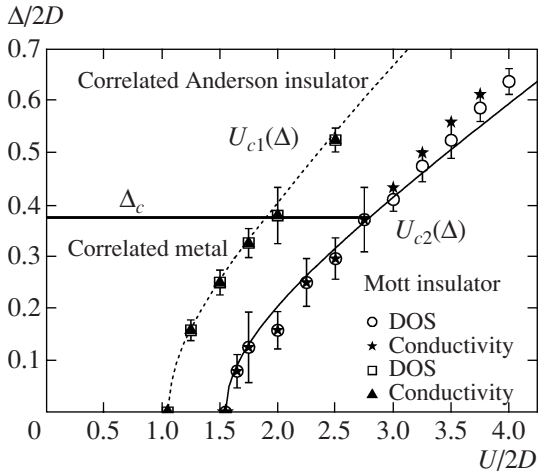

Fig. 13. Zero-temperature phase diagram of the paramagnetic Anderson–Hubbard model. Boundaries of the Mott insulator phase $U_{c1,\,c2}(\Delta)$ are shown as obtained from Eq. (45); different symbols show values calculated from either the DOS or the conductivity behavior. The dotted line defines the boundary of the coexistence region obtained with decreasing U from the Mott insulator phase. The Anderson transition line is given by the calculated value of $\Delta_c = 0.37$.

4.3. Phase Diagram of the Half-Filled Anderson–Hubbard Model

The phase diagram of a half-filled Anderson–Hubbard model was studied in [13] using the approach based on direct DMFT calculations for a set of random realizations of site energies ϵ_i in (1) with subsequent averaging to obtain both the standard average DOS and the geometrically averaged local DOS, which was used to determine the transition to the Anderson insulator phase. Here, we present our results for the zero-temperature phase diagram of the half-filled paramagnetic Anderson–Hubbard model, obtained from extensive calculations of both the average DOS and dynamic (optical) conductivity in the DMFT + Σ approximation. We note that conductivity calculations are the most direct way to distinguish between metallic and insulating phases [2].

Our phase diagram in the disorder–correlation (Δ, U)-plane is shown in Fig. 13. The Anderson transition line $\Delta_c \approx 0.37W = 0.74D$ was determined as the value of disorder for which the static conductivity becomes zero at $T = 0$. The Mott–Hubbard transition can be determined either via the disappearance of the central peak (quasiparticle band) in the DOS or from the conductivity, e.g., from the closure of the gap in dynamic conductivity in the insulating phase, or from vanishing of the static conductivity in the metallic region. All these methods were used, and the corresponding results are shown for comparison in Fig. 13.

We have already stressed that the DMFT + Σ approximation gives the universal (U-independent) value of Δ_c. This is due to neglect of the interference between disorder scattering and Hubbard interaction, and it leads to the main (over)simplification of our phase diagram, compared with that obtained in [13]. We note that direct comparison of our critical disorder value with those of [13] is complicated by different types of random site–energy distributions used here (Gaussian) and in [13] (rectangular). As a rule of thumb (cf. the second reference in [16]), our Gaussian value of Δ_c should be multiplied by $\sqrt{12}$ to obtain the critical disorder value for the rectangular distribution. This gives $\Delta_c \approx 1.28$, in rather good agreement with the value of $\Delta_c(U = 0) \approx 1.35W$ in [13], justifying our choice of cutoff in (41).

The influence of disorder scattering on the Mott–Hubbard transition is highly nontrivial and in some respects is in qualitative agreement with the results in [13]. The main difference is that our data indicate the survival of Hubbard band structures in the DOS even in the limit of rather large disorder, while it was claimed in [13] that these disappear. Also we obtain the coexistence region, which smoothly widens with an increase in disorder and does not disappear at a critical point, as in [13]. The borders of our coexistence region, which in fact define the boundaries of the Mott insulator phase obtained with increasing or decreasing U, are determined by the lines $U_{c1}(\Delta)$ and $U_{c2}(\Delta)$ shown in Fig. 13, which are obtained from the simple equation

$$\frac{U_{c1,\,c2}(\Delta)}{W_{\text{eff}}} = \frac{U_{c1,\,c2}}{W} \tag{43}$$

with

$$W_{\text{eff}} = W\sqrt{1 + 16\frac{\Delta^2}{W^2}}, \tag{44}$$

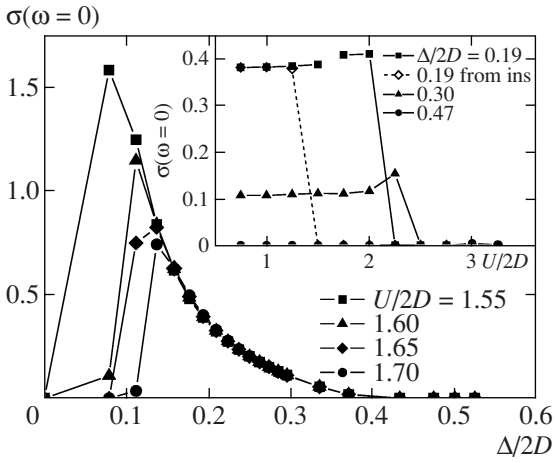

Fig. 14. Disorder dependence of static conductivity, obtained for several values of U and showing disorder-induced Mott-insulator-to-metal transition. Inset: the static conductivity dependence on U close to the Mott transition, including a typical hysteresis behavior obtained with U decreasing from the Mott insulator phase.

which is the effective bandwidth in the presence of disorder, calculated for $U = 0$ in self-consistent Born approximation (9). Thus, the boundaries of the coexistence region are given by

$$U_{c1,c2}(\Delta) = U_{c1,c2}\sqrt{1 + 16\frac{\Delta^2}{W^2}}, \qquad (45)$$

which are explicitly shown in Fig. 13 by dotted and solid lines, defining the boundaries of the Mott insulator phase. Numerical results for the disappearance of the quasiparticle band (central peak) in the DOS, as well as points following from a qualitative change in the conductivity behavior, are shown in Fig. 13 by different symbols demonstrating very good agreement with these lines, confirming the ratio in (43) as the controlling parameter of the Mott transition in the presence of disorder.

The most striking result of our analysis (also qualitatively demonstrated in [13]) is the possibility of the metallic state being restored from the Mott–Hubbard insulator with an increase in disorder. This is clear from the phase diagram and is nicely demonstrated by our data for (static) conductivity shown in Fig. 14 for several values of $U > U_{c2}$ and disorder values $\Delta < \Delta_c$. In the inset to Fig. 14, we also illustrate the static conductivity hysteresis observed in the coexistence region of the phase diagram, obtained with U decreasing from the Mott insulator phase.

4.4. Doped Mott Insulator

All results presented above were obtained in the half-filled case. Here, we briefly consider deviations from half-filling. In the metallic phase, doping from half-filling does not produce any qualitative changes in the conductivity behavior, which only demonstrates the Anderson transition with an increase in disorder. We therefore concentrate on the case of a doped Mott insulator. Strictly speaking, in the non-half-filled case, we never obtain a Mott–Hubbard insulator in the DMFT method at all. In Fig. 15, we show the DOS of the Anderson–Hubbard model with an electron concentration of $n = 0.8$ for different degrees of disorder Δ and $U = 6.0D$, representing a typical case of the doped Mott insulator. The quasiparticle band overlaps with the lower Hubbard band and is smeared by disorder, which is precisely the expected behavior in the metallic state. Nothing spectacular happens to conductivity either,

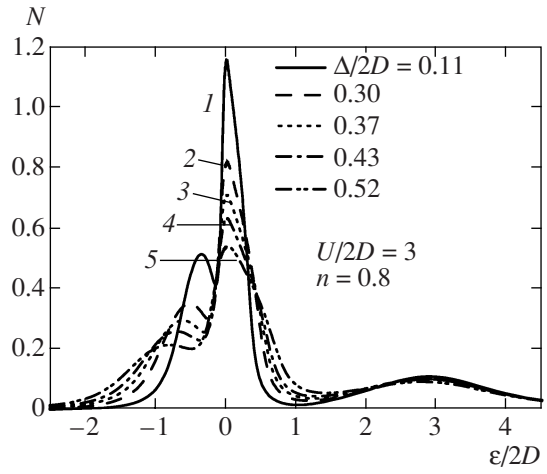

Fig. 15. Density of states of the Anderson–Hubbard model with the electron concentration $n = 0.8$ for different degrees of disorder Δ and $U = 6.0D$, representing the doped Mott insulator.

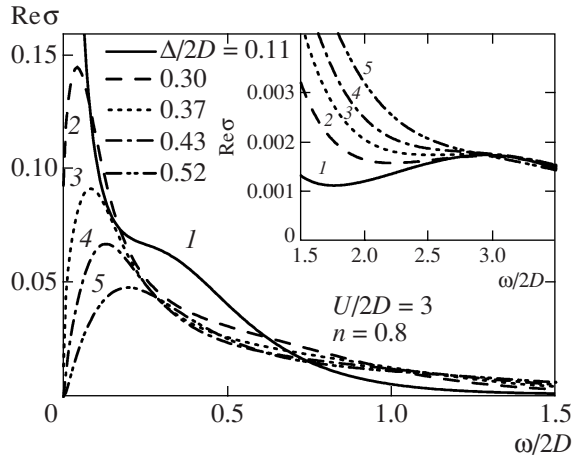

Fig. 16. Real part of dynamic conductivity of the Anderson–Hubbard model with the electron concentration $n = 0.8$ for different degrees of disorder Δ and $U = 6.0D$ representing the doped Mott insulator. Inset: high-frequency behavior with signs of transition to the upper Hubbard band.

which is shown for the same set of parameters in Fig. 16. It shows the typical behavior associated with the disorder-induced Anderson MIT. Small signs of transitions to the upper Hubbard band can be seen for $\omega \sim U$ (see the inset to Fig. 16). Therefore, a doped Mott insulator with disorder is qualitatively quite similar to the disordered correlated metal discussed above.

5. CONCLUSIONS

We used the generalized DMFT + Σ approach to calculate the basic properties of the disordered Hubbard model. The main advantage of our method is its ability to provide a relatively simple interpolation scheme between rather well understood cases of a strongly correlated system (DMFT and Mott–Hubbard MIT) and of a strongly disordered metal without Hubbard correlations, undergoing an Anderson MIT. Apparently, this interpolation scheme captures the main qualitative features of the Anderson–Hubbard model, such as the general behavior of the DOS and dynamic (optical) conductivity. The overall picture of the zero-temperature phase diagram is also quite reasonable and is in satisfactory agreement with the results of more elaborate numerical work [13]. Actually, our DMFT + Σ approach is much less time-consuming than more direct numerical approaches, such as that in [13], and in fact allows one to calculate all basic (measurable) physical characteristics of the Anderson–Hubbard model.

The main shortcoming of our approach is its neglect of interference effects of disorder scattering and Hubbard interaction, which leads to the independence of the Anderson MIT critical disorder Δ_c from the interaction U. The importance of interference effects has been known for a long time [1, 4], but its consideration was only partially successful in the case of weak correlations. At the same time, the neglect of these interference effects is the major approximation of the DMFT + Σ method, allowing the derivation of a rather simple and physical interpolation scheme and an analysis of the strong-correlation limit. Attempts to include interference effects in our scheme have been postponed for future study.

Another simplification is, of course, our assumption of a nonmagnetic (paramagnetic) ground state of the Anderson–Hubbard model. The importance of magnetic (spin) effects in strongly correlated systems is well known, as is the problem of competition of ground states with different types of magnetic ordering [8]. The importance of disorder in studying the interplay of these possible ground states is also quite evident. These may also be the subject of our future work.

Despite these shortcomings, our results seem very promising, especially concerning the influence of strong disorder on the Mott–Hubbard MIT and the overall form of the phase diagram at zero temperature. The changes in the phase diagram at finite temperatures will be the subject of further studies. Nontrivial predictions of our approach, such as the general behavior of dynamic (optical) conductivity and, especially, the prediction of a disorder-induced Mott-insulator-to-metal transition can be the subject of direct experimental verification.

ACKNOWLEDGMENTS

We are grateful to Th. Pruschke for providing us with his effective NRG code. This work was supported in part by the Russian Foundation for Basic Research (project nos. 05-02-16301 (M.S., E.K., I.N.), 05-02-17244 (I.N.), 06-02-90537 (I.N.)), by the joint UrO-SO project (E.K, I.N), and programs of the Presidium of the Russian Academy of Sciences (RAS) "Quantum Macrophysics" and of the Division of Physical Sciences of the RAS "Strongly Correlated Electrons in Semiconductors, Metals, Superconductors, and Magnetic Materials." I.N. acknowledges support from the Dynasty Foundation; the program for young scientists, International Center for Fundamental Physics in Moscow; and from a grant of the President of the Russian Federation for young PhD candidates, MK-2118.2005.02.

APPENDIX A

Equation for Relaxation Kernel

We follow the standard approach of the self-consistent theory of localization [14–19], taking the DMFT contributions $\Sigma^{R,A}(\varepsilon)$ into account in single-particle Green functions (29) and not restricting ourselves to the usual limit of small ω.

We consider the Bethe–Salpeter equation relating the full two-particle Green function $\Phi^{0RA}_{\mathbf{pp}'}(\omega, \mathbf{q})$ to the irreducible vertex $U^{0RA}_{\mathbf{pp}'}(\omega, \mathbf{q})$, accounting only for impurity scattering in vertices, but built upon Green functions given by (29). This equation can be written as a generalized kinetic equation in the form [14–19]

$$(\tilde{\omega} - \epsilon(\mathbf{p}) - \Delta\Sigma^{RA}_{\mathrm{imp}}(\omega))\Phi^{0RA}_{\mathbf{pp}'}(\omega, \mathbf{q}) = -\Delta G_{\mathbf{p}} \times \left(\delta_{\mathbf{pp}'} + \sum_{\mathbf{p}_1} U^{0RA}_{\mathbf{pp}_1}(\omega, \mathbf{q})\Phi^{0RA}_{\mathbf{p}_1\mathbf{p}'}(\omega, \mathbf{q})\right), \quad \text{(A.1)}$$

where $\Delta G_{\mathbf{p}} = G^R(\varepsilon_+, \mathbf{p}_+) - G^A(\varepsilon_-, \mathbf{p}_-)$. The main difference with a similar equation in [14–19] is the replacement $\omega \longrightarrow \tilde{\omega}$.

We sum both sides of (A.1) and of the same equation multiplied by $\hat{\mathbf{p}} \cdot \hat{\mathbf{q}}$ (where $\hat{\mathbf{p}} = \mathbf{p}/|\mathbf{p}|$ and $\hat{\mathbf{q}} = \mathbf{q}/|\mathbf{q}|$ are appropriate unit vectors) over $\mathbf{p}$ and $\mathbf{p}'$, with the exact Ward identity [14]

$$\Delta\Sigma^{RA}_{\mathrm{imp}}(\omega) = \sum_{\mathbf{p}'} U^{0RA}_{\mathbf{pp}'}(\omega, \mathbf{q})\Delta G_{\mathbf{p}'} \quad \text{(A.2)}$$

taken into account and with the approximate representation (cf. [14])

$$\sum_{\mathbf{p}'}\Phi^{0RA}_{\mathbf{pp}'}(\omega,\mathbf{q}) \approx \frac{\Delta G_{\mathbf{p}}}{\sum_{\mathbf{p}}\Delta G_{\mathbf{p}}}\Phi^{0RA}_{\varepsilon}(\omega,\mathbf{q}) + \frac{\Delta G_{\mathbf{p}}(\hat{\mathbf{p}}\cdot\hat{\mathbf{q}})}{\sum_{\mathbf{p}}\Delta G_{\mathbf{p}}(\hat{\mathbf{p}}\cdot\hat{\mathbf{q}})^2}\Phi^{0RA}_{1\varepsilon}(\omega,\mathbf{q}), \tag{A.3}$$

where $\Phi^{0RA}_{\varepsilon}(\omega,\mathbf{q}) = \sum_{\mathbf{pp}'}\Phi^{0RA}_{\mathbf{pp}'}(\omega,\mathbf{q})$ is our loop (28) and $\Phi^{0RA}_{1\varepsilon}(\omega,\mathbf{q}) = \sum_{\mathbf{pp}'}(\hat{\mathbf{p}}\cdot\hat{\mathbf{q}})\Phi^{0RA}_{\mathbf{pp}'}(\omega,\mathbf{q})$. An important difference from a similar representation in [14–19] is that (A.3) is not limited to small ω.

Now (as $q \longrightarrow 0$), we obtain the closed system of equations for both $\Phi^{0RA}_{\varepsilon}(\omega,\mathbf{q})$ and $\Phi^{0RA}_{1\varepsilon}(\omega,\mathbf{q})$

$$\begin{aligned}\tilde{\omega}\Phi^{0RA}_{\varepsilon}(\omega,\mathbf{q}) - \langle v\rangle q\Phi^{0RA}_{1\varepsilon}(\omega,\mathbf{q}) &= -\sum_{\mathbf{p}}\Delta G_{\mathbf{p}},\\ (\tilde{\omega}+M(\omega))\Phi^{0RA}_{1\varepsilon}(\omega,\mathbf{q}) - \frac{\langle v\rangle}{d}q\Phi^{0RA}_{1\varepsilon}(\omega,\mathbf{q}) &= 0,\end{aligned} \tag{A.4}$$

where the relaxation kernel is given by

$$M(\omega) = -\Delta\Sigma^{RA}_{\mathrm{imp}}(\omega) + d\frac{\sum_{\mathbf{pp}'}(\hat{\mathbf{p}}\cdot\hat{\mathbf{q}})\Delta G_{\mathbf{p}}U^{0RA}_{\mathbf{pp}'}(\omega,\mathbf{q})\Delta G_{\mathbf{p}'}(\hat{\mathbf{p}}'\cdot\hat{\mathbf{q}})}{\sum_{\mathbf{p}}\Delta G_{\mathbf{p}}}, \tag{A.5}$$

with the average speed $\langle v\rangle$ determined as

$$\langle v\rangle = \frac{\sum_{\mathbf{p}}|\mathbf{v}_{\mathbf{p}}|\Delta G_{\mathbf{p}}}{\sum_{\mathbf{p}}\Delta G_{\mathbf{p}}}; \quad \mathbf{v}_{\mathbf{p}} = \frac{\partial\epsilon(\mathbf{p})}{\partial\mathbf{p}}. \tag{A.6}$$

From (A.4), we immediately find that

$$\Phi^{0RA}_{\varepsilon}(\mathbf{q},\tilde{\omega}) = \frac{-\sum_{\mathbf{p}}\Delta G_{\mathbf{p}}}{\tilde{\omega}+iD(\omega)q^2} \tag{A.7}$$

which for small ω reduces to (32) with the generalized diffusion coefficient given by (37).

Using an approximation of maximally crossed diagrams for the irreducible vertex $U^{0RA}_{\mathbf{pp}'}(\omega,\mathbf{q})$ and introducing the standard self-consistency procedure in [14–19] (i.e., replacing the Drude diffusion coefficient in the Cooperon contribution to the irreducible vertex with the generalized one determined by (37)), we obtain our expression (38) for the relaxation kernel from (A.5).

Our Eq. (40) for the generalized diffusion coefficient (which is complex in general) reduces precisely to the usual transcendental equation. It was solved by iterations for each value of $\tilde{\omega}$, taking into account that for $d = 3$ and the cutoff given by (41), the sum entering (40) reduces to

$$\begin{aligned}\sum_{\mathbf{q}}\frac{1}{\tilde{\omega}+iD(\omega)q^2} &= \frac{1}{2\pi^2}\frac{k_0^3}{iD(\omega)k_0^2}\\ \times\int_0^1\frac{y^2dy}{y^2+\dfrac{\tilde{\omega}}{iD(\omega)k_0^2}} &= \frac{1}{2\pi^2}\frac{k_0^3}{iD(\omega)k_0^2}\\ \times\left\{1-\left(\frac{\tilde{\omega}}{iD(\omega)k_0^2}\right)^{1/2}\right.&\\ \left.\times\arctan\left(\left(\frac{iD(\omega)k_0^2}{\tilde{\omega}}\right)^{1/2}\right)\right\}.&\end{aligned} \tag{A.8}$$

For finite frequencies ω, we use $\Phi^{0RA}_{\varepsilon}(\mathbf{q},\tilde{\omega})$ given by (A.7), and hence expression (25) for the dynamic conductivity should be rewritten as

$$\mathrm{Re}\sigma(\omega) = \frac{e^2\omega}{2\pi}\int_{-\infty}^{\infty}d\varepsilon[f(\varepsilon_-)-f(\varepsilon_+)] \times\mathrm{Re}\left\{\frac{i\sum_{\mathbf{p}}\Delta G_{\mathbf{p}}D(\omega)}{\omega^2}-\phi^{0RR}_{\varepsilon}(\omega)\left[1-\frac{\Delta\Sigma^{RR}(\omega)}{\omega}\right]^2\right\}. \tag{A.9}$$

The second term was here taken in the ladder approximation:

$$\Phi^{0RR}_{\varepsilon}(\omega,\mathbf{q}) = \frac{\sum_{\mathbf{p}}G^R(\varepsilon_+,\mathbf{p}_+)G^R(\varepsilon_-,\mathbf{p}_-)}{1-\Delta^2\sum_{\mathbf{p}}G^R(\varepsilon_+,\mathbf{p}_+)G^R(\varepsilon_-,\mathbf{p}_-)}. \tag{A.10}$$

This contribution (nonsingular at small ω) is irrelevant for the conductivity as $\omega \longrightarrow 0$, but leads to finite corrections with increasing ω. Equation (A.9) is our final result, which was analyzed numerically in a wide range of frequencies (for small ω), it reduces to (36)).

APPENDIX B

Bare Electron Dispersion and Velocity

We consider the bare energy band with semielliptic DOS (42). Assuming an isotropic electron spectrum $\epsilon(\mathbf{p}) = \epsilon(|\mathbf{p}|) \equiv \epsilon(p)$ and equating the number of states in a spherical layer of momentum space to the number of states in the energy interval $[\epsilon, \epsilon + d\epsilon]$, we obtain a differential equation determining the energy dispersion $\epsilon(p)$:

$$\frac{4\pi p^2 dp}{(2\pi)^3} = N_0(\epsilon)d\epsilon. \quad \text{(B.1)}$$

For a quadratic energy dispersion $\epsilon(p)$ close to the lower band edge, we obtain the initial condition for Eq. (B.1) as $p \longrightarrow 0$ and $\epsilon \longrightarrow -D$. Then we obtain

$$p = \left[6\pi\left(\pi - \varphi + \frac{1}{2}\sin(2\varphi)\right)\right]^{1/3} \quad \text{(B.2)}$$

with $\varphi = \arccos(\epsilon/D)$ and the momentum in units of the inverse lattice spacing. Equation (B.2) implicitly defines a "bare" energy dispersion $\epsilon(p)$ for the electronic part of the spectrum $\epsilon \in [-D, 0]$.

For a half-filled band, we easily determine the Fermi momentum as

$$p_F = p(\epsilon = 0) = (3\pi^2)^{1/3}. \quad \text{(B.3)}$$

We also need the electron speed $|\mathbf{v}_\mathbf{p}| = |\partial\epsilon(\mathbf{p})/\partial\mathbf{p}| = \partial\epsilon(p)/\partial p$, which enters expression (A.6) for the average speed. From (B.1), we obtain

$$|\mathbf{v}_\mathbf{p}| = \frac{d\epsilon}{dp} = \frac{p^2}{2\pi^2}\frac{1}{N_0(\epsilon)}, \quad \text{(B.4)}$$

where p is given by Eq. (B.2).

To obtain a quadratic dispersion for hole part of the spectrum ($\epsilon \in [0, D]$) close to the upper band edge ($\epsilon \longrightarrow D$), we introduce the hole momentum $\tilde{p} = 2p_F - p$ and write

$$\frac{4\pi\tilde{p}^2 d\tilde{p}}{(2\pi)^3} = -N_0(\epsilon)d\epsilon \quad \text{(B.5)}$$

similarly to (B.1). Letting $\tilde{p} \longrightarrow 0$ at the upper band edge $\epsilon \longrightarrow 0$, we obtain

$$\tilde{p} = \left[6\pi\left(\varphi - \frac{1}{2}\sin(2\varphi)\right)\right]^{1/3}. \quad \text{(B.6)}$$

We then obtain the speed at the hole part of the spectrum as

$$|\mathbf{v}_\mathbf{p}| = \frac{d\epsilon}{dp} = -\frac{d\epsilon}{d\tilde{p}} = \frac{\tilde{p}^2}{2\pi^2}\frac{1}{N_0(\epsilon)}. \quad \text{(B.7)}$$

Equations (B.4) and (B.7) determine the energy dependence of $|\mathbf{v}_\mathbf{p}|$. It is easily seen that the speed is even in energy and becomes zero at the band edges. These expressions allow passing from momentum summation (e.g., in Eq. (A.6)) to energy integration.

Note added in proof. Further numerical work has shown that the tendency of $U_{c2}(\Delta)$ data points in Fig. 13 to deviate upwards from the "universal" curve given by Eq. (45) increases for large values of U, with these data points approaching the $U_{c1}(\Delta)$ curve. However, up to $U/2D \sim 10$, we do not observe the "critical point" discovered in Ref. [13].

December 27, 2007

REFERENCES

1. P. A. Lee and T. V. Ramakrishnan, Rev. Mod. Phys. **57**, 287 (1985); D. Belitz and T. R. Kirkpatrick, Rev. Mod. Phys. **66**, 261 (1994).
2. N. F. Mott, Proc. Phys. Soc., London, Sect. A **62**, 416 (1949); *Metal–Insulator Transitions*, 2nd ed. (Taylor and Francis, London, 1990).
3. P. W. Anderson, Phys. Rev. **109**, 1492 (1958).
4. A. M. Finkelshteĭn, Zh. Éksp. Teor. Fiz. **84** (1), 168 (1983) [Sov. Phys. JETP **57** (1), 97 (1983)]; C. Castellani, C. Di Castro, P. A. Lee, and M. Ma, Phys. Rev. B: Condens. Matter **30**, 527 (1984).
5. W. Metzner and D. Vollhardt, Phys. Rev. Lett. **62**, 324 (1989).
6. D. Vollhardt, in *Correlated Electron Systems*, Ed. by V. J. Emery (World Sci., Singapore, 1993), p. 57.
7. Th. Pruschke, M. Jarrell, and J. K. Freericks, Adv. Phys. **44**, 187 (1995).
8. A. Georges, G. Kotliar, W. Krauth, and M. J. Rozenberg, Rev. Mod. Phys. **68**, 13 (1996).
9. M. Ulmke, V. Janiš, and D. Vollhardt, Phys. Rev. B: Condens. Matter **51**, 10411 (1995).
10. R. Vlaming and D. Vollhardt, Phys. Rev. B: Condens. Matter **45**, 4637 (1992).
11. V. Dobrosavljević and G. Kotliar, Phys. Rev. Lett. **78**, 3943 (1997).
12. V. Dobrosavljević, A. A. Pastor, and B. K. Nikolić, Europhys. Lett. **62**, 76 (2003).
13. K. Byczuk, W. Hofstetter, and D. Vollhardt, Phys. Rev. Lett. **94**, 056404 (2005).
14. D. Vollhardt and P. Wölfle, Phys. Rev. B: Condens. Matter **22**, 4666 (1980); Phys. Rev. Lett. **48**, 699 (1982).
15. P. Wölfle and D. Vollhardt, in *Anderson Localization*, Vol. 39: *Springer Series in Solid State Physics*, Ed. by Y. Nagaoka and H. Fukuyama (Springer-Verlag, Berlin, 1982), p. 26.
16. A. V. Myasnikov and M. V. Sadovskii, Fiz. Tverd. Tela (Leningrad) **24** (12), 3569 (1982) [Sov. Phys. Solid State **24** (12), 2033 (1982)]; E. A. Kotov and M. V. Sadovskii, Z. Phys. B: Condens. Matter **51**, 17 (1983).
17. M. V. Sadovskii, in *Soviet Scientific Reviews: Physics Reviews*, Ed. by I. M. Khalatnikov (Academic, New York, 1986), Vol. 7, p. 1.
18. D. Vollhardt and P. Wölfle, in *Electronic Phase Transitions*, Ed. by W. Hanke and Yu. V. Kopaev (North-Holland, Amsterdam, 1992), p. 1.

19. M. V. Sadovskii, *Diagrammatics* (World Sci., Singapore, 2006).
20. É. Z. Kuchinskii, M. V. Sadovskii, V. G. Suvorov, and M. A. Érkabaev, Zh. Éksp. Teor. Fiz. **107** (6), 2027 (1995) [JETP **80** (6), 1122 (1995)]; É. Z. Kuchinskii and M. A. Érkabaev, Fiz. Tverd. Tela (St. Petersburg) **39** (3), 412 (1997) [Phys. Solid State **39** (3), 357 (1997)].
21. E. Z. Kuchinskii, I. A. Nekrasov, and M. V. Sadovskii, Pis'ma Zh. Éksp. Teor. Fiz. **82** (4), 217 (2005) [JETP Lett. **82** (4), 198 (2005)].
22. M. V. Sadovskii, I. A. Nekrasov, E. Z. Kuchinskii, et al., Phys. Rev. B: Condens. Matter **72**, 155105 (2005).
23. E. Z. Kuchinskii, I. A. Nekrasov, and M. V. Sadovskii, Fiz. Nizk. Temp. (Kharkov) **32** (4), 528 (2006) [Low Temp. Phys. **32** (4), 398 (2006)].
24. E. Z. Kuchinskii, I. A. Nekrasov, and M. V. Sadovskii, Phys. Rev. B: Condens. Matter **75**, 115102 (2007).
25. K. G. Wilson, Rev. Mod. Phys. **47**, 773 (1975); H. R. Krishna-Murthy, J. W. Wilkins, and K. G. Wilson, Phys. Rev. B: Condens. Matter **21**, 1003 (1980); Phys. Rev. B: Condens. Matter **21**, 1044 (1980); A. C. Hewson, *The Kondo Problem to Heavy Fermions* (Cambridge University Press, Cambridge, 1993).
26. R. Bulla, A. C. Hewson and Th. Pruschke, J. Phys.: Condens. Matter **10**, 8365 (1998).
27. R. Bulla, Phys. Rev. Lett. **83**, 136 (1999); R. Bulla, T. A. Costi, and D. Vollhardt, Phys. Rev. B: Condens. Matter **64**, 045103 (2001).
28. A. B. Migdal, *Theory of Finite Fermi Systems and Applications to Atomic Nuclei* (Interscience, New York, 1967).
29. N. Blümer, *Mott–Hubbard Metal–Insulator Transition and Optical Conductivity* (Shaker, München, 2002).
30. M. A. Erkabaev and M. V. Sadovskii, J. Moscow Phys. Soc. **2**, 233 (1992).

ISSN 1063-7761, Journal of Experimental and Theoretical Physics, 2008, Vol. 107, No. 2, pp. 281–287. © Pleiades Publishing, Inc., 2008.

ELECTRONIC PROPERTIES OF SOLIDS

The Optical Sum Rule in Strongly Correlated Systems[1]

E. Z. Kuchinskii, N. A. Kuleeva, I. A. Nekrasov, and M. V. Sadovskii

Institute for Electrophysics, Russian Academy of Sciences, Ural Branch, Ekaterinburg, 620016 Russia

e-mail: sadovski@iep.uran.ru

Received March 27, 2008

Abstract—We discuss the problem of a possible "violation" of the optical sum rule in the normal (nonsuperconducting) state of strongly correlated electronic systems, using our recently proposed DMFT + Σ approach applied to two typical models: the "hot spot" model of the pseudogap state and the disordered Anderson–Hubbard model. We explicitly demonstrate that the general Kubo single-band sum rule is satisfied for both models, but the optical integral itself is in general dependent on temperature and characteristic parameters, such as the pseudogap width, correlation strength, and disorder scattering, leading to an effective "violation" of the optical sum rule, which may be observed in experiments.

PACS numbers: 74.25.Gz, 71.10.Fd, 71.10.Hf, 71.27.+a, 71.30.+h, 74.72.-h

DOI: 10.1134/S1063776108080128

1. INTRODUCTION

Many years ago, Kubo [1] proved the general sum rule for the diagonal dynamic (frequency-dependent) conductivity $\sigma(\omega)$, which holds for any system of charged particles irrespective of interactions, temperature, or statistics. This sum rule is usually written as

$$\frac{2}{\pi}\int_0^\infty \mathrm{Re}\sigma(\omega)d\omega = \sum_r \frac{n_r e_r^2}{m_r}, \qquad (1)$$

where r specifies the type of charged particles and n_r and e_r are the respective densities and charges.

For the system of electrons in a solid, Eq. (1) takes the form

$$\int_0^\infty \mathrm{Re}\sigma(\omega)d\omega = \frac{\omega_{\mathrm{pl}}^2}{8}, \qquad (2)$$

where n is the density of electrons and $\omega_{\mathrm{pl}}^2 = 4\pi ne^2/m$ is the plasma frequency.

In any real experiment, however, we are not dealing with an infinite range of frequencies. If we consider electrons in a crystal and limit ourself to the electrons in a particular (e.g., conduction) band, neglecting interband transitions, the general sum rule (2) reduces to Kubo's single-band sum rule [1, 2]:

$$W = \int_0^{\omega_c} \mathrm{Re}\sigma(\omega)d\omega = f(\omega_c)\frac{\pi e^2}{2}\sum_{\mathbf{p}} \frac{\partial^2 \varepsilon_p}{\partial p_x^2} n_p, \qquad (3)$$

where ε_p is the bare dispersion defined by the effective single-band Hamiltonian and n_p is the momentum distribution function (occupation number), which is in general defined by the interacting retarded electron Green's function $G^R(\varepsilon, \mathbf{p})$ [3, 4]:

$$n_p = -\frac{1}{\pi}\int_{-\infty}^{\infty} d\varepsilon n(\varepsilon)\mathrm{Im}G^R(\varepsilon, \mathbf{p}), \qquad (4)$$

where $n(\varepsilon)$ is the usual Fermi distribution. In Eq. (3), ω_c represents an ultraviolet cutoff, a frequency that is assumed to be larger than the bandwidth of the low-energy band but smaller than the gap to other bands. The function $f(\omega_c)$ accounts for the cutoff dependence, which arises from the presence of the Drude spectral weight beyond ω_c [5]; this function is equal to unity if we formally set ω_c to infinity and ignore the interband transitions.

Although the general sum rule is certainly preserved, the optical integral $W(\omega_c, T)$ is not a conserved quantity because both $f(\omega_c)$ [5] and n_p [4, 6] depend on the temperature T and the details of interactions [3]. This dependence of W on T and other parameters of the system under study has been termed sum rule violation. It was actively studied experimentally, especially in cuprates, where pronounced anomalies were observed in both the c axis and in-plane conductivity, in normal as well as superconducting states [8–13].

The finite cutoff effects were extensively studied in several theoretical papers on the T dependence of the optical integral [4, 5, 7]. In [5, 7], the effect of the cutoff was considered in the context of electrons coupled to phonons. In a simple Drude model,

[1] The text was submitted by the authors in English.

$$\sigma(\omega) = \frac{\omega_{pl}^2}{4\pi}/\left(\frac{1}{\tau} - i\omega\right)$$

and the sum rule can only be violated due to the presence of $f(\omega_c)$. Integrating over ω and expanding for $\omega_c\tau \gg 1$, we can see that

$$f(\omega_c) = \left(1 - \frac{2}{\pi}\frac{1}{\omega_c\tau}\right). \quad (5)$$

For the infinite cutoff, $f(\omega_c) = 1$ and $W = \omega_{pl}^2/8$, but for a finite cutoff, $f(\omega_c)$ contains a term proportional to $1/\omega_c\tau$. If $1/\tau$ changes with T, then we obtain a sum rule violation even if ω_{pl} is independent of T [5, 7]. Other aspects of the cutoff dependence were recently discussed in detail in [2].

In this paper, we neglect the cutoff effects in the optical integral from the outset. Our goal is to study the dependence of W on T and a number of interaction parameters that determine the electron properties of strongly correlated systems, such as cuprates. In this context, we discuss the problem of a possible violation of the optical sum rule in the normal (nonsuperconducting) state of strongly correlated electronic systems, using our recently proposed DMFT + Σ approach [14–16] applied to dynamic conductivity in two typical models of such systems: the hot spot model of the pseudogap state [19] and the disordered Anderson–Hubbard model [20]. Our goal is to check the consistency of the DMFT + Σ approach applied to calculations of optical conductivity as well as to demonstrate rather important dependences of the optical integral W not only on T but also on such important characteristics as the pseudogap width, disorder, and correlation strength, which makes the (single-band) sum rule violation rather ubiquitous in strongly correlated systems, even if the cutoff effects are neglected.

2. OPTICAL SUM RULE IN THE GENERALIZED DMFT + Σ APPROACH

A characteristic feature of the general sum rule expressed by Eqs. (3) and (4) is that the integral W over frequency in the left-hand side is calculated based on a two-particle property (the dynamic conductivity, which is determined by the two-particle Green's function, with appropriate vertex corrections in general), but the right-hand side is determined by single-particle characteristics, such as the bare dispersion and occupation number (4) (determined by a single-particle Green's function). Thus, checking the validity of this sum rule, we are in fact thoroughly checking the consistency of any theoretical approach used in our model calculations.

Our generalized DMFT + Σ approach [14–16], supplementing the standard DMFT [17, 18] with an additional "external" self-energy Σ (due to any kind of interaction outside the scope of the DMFT, which is exact only in infinitely many dimensions), provides an effective method to calculate both single-particle and two-particle properties [19, 20]. A consistency check for this new approach is obviously of great interest in itself. We also see in what follows that it gives a kind of a new insight into the sum rule violation problem.

2.1. Pseudogap State: Hot Spot Model

Pseudogap phenomena in strongly correlated systems have a substantial spatial length scale dependence [21]. To merge pseudogap physics and strong electron correlations, we have generalized the DMFT [17, 18] by including the dependence on the correlation length of pseudogap fluctuations via an additional (momentum-dependent) self-energy $\Sigma_{\mathbf{p}}(\varepsilon)$. This self-energy $\Sigma_{\mathbf{p}}(\varepsilon)$ describes nonlocal dynamic correlations induced either by short-ranged collective SDW-like antiferromagnetic spin or CDW-like charge fluctuations [22, 23].

To calculate $\Sigma_{\mathbf{p}}(\varepsilon)$ in the two-dimensional hot spot model [21] for an electron moving in the random field of pseudogap fluctuations (considered to be static and Gaussian) with dominant scattering momentum transfers on the order of the characteristic vector $\mathbf{Q} = (\pi/a, \pi/a)$ (where a is the lattice spacing), we used [15, 16] the recursion procedure proposed in [22, 23], which is controlled by the two main physical characteristics of the pseudogap state: the pseudogap amplitude Δ, which characterizes the energy scale of the pseudogap, and the inverse correlation length $\kappa = \xi^{-1}$ of short-range SDW (CDW) fluctuations. Both parameters Δ and ξ, determining pseudogap behavior can, in principle, be calculated from the relevant microscopic model [15].

The weakly doped one-band Hubbard model with a repulsive Coulomb interaction U on a square lattice with nearest and next-to-nearest neighbor hopping was numerically investigated within this generalized DMFT + Σ self-consistent approach, as described in detail in [14–16].

Briefly, the DMFT+ Σ self-consistent loop is as follows. First, we guess some initial local (DMFT) electron self-energy $\Sigma(\varepsilon)$. Second, we compute the $\mathbf{p}$-dependent external self-energy $\Sigma_{\mathbf{p}}(\varepsilon)$, which is in general a functional of $\Sigma(\varepsilon)$. Then, neglecting interference effects between the self-energies (which is in fact the major assumption of our approach), we can set up and solve the lattice problem of DMFT [17, 18]. Finally, we define an effective Anderson single-impurity problem, which is to be solved by any "impurity solver" (we mostly use the numerical renormalization group, NRG) to close the DMFT + Σ equations.

The additive form of self-energy is in fact an advantage to our approach [14–16]. It allows preserving the set of self-consistent equations of the standard DMFT [17, 18]. However, there are two distinctions from the conventional DMFT. During each DMFT iteration, we recalculate the corresponding $\mathbf{p}$-dependent self-energy

$\Sigma_{\mathbf{p}}(\mu, \varepsilon, [\Sigma(\omega)])$ via an approximate scheme, taking interactions with collective modes or order parameter fluctuations into account, and the local Green's function $G_{ii}(i\omega)$ is "dressed" by $\Sigma_{\mathbf{p}}(\varepsilon)$ at each step. When the input and output Green's functions (or self-energies) converge to each other (with prescribed accuracy), we consider the solution self-consistent. Physically, this corresponds to accounting for some external (e.g., pseudogap) fluctuations, characterized by an important length scale ξ, in the fermionic "bath" surrounding the effective Anderson impurity of the usual DMFT. The cases of strongly correlated metals and doped Mott insulators were considered in [15, 16]. Energy dispersions, quasiparticle damping, spectral functions, and ARPES spectra calculated within the DMFT + Σ scheme all show a pseudogap effect close to the Fermi level of the quasiparticle band.

In [19], this DMFT + Σ procedure was generalized to calculate two-particle properties, such as the dynamic conductivity, using the previously developed recursion procedure for vertex corrections due to pseudogap fluctuations [24], producing typical pseudogap anomalies of the optical conductivity and a dependence of these anomalies on the correlation strength U. Below, we use the approach in [19] to investigate the sum rule in the hot spot model.

To calculate the optical integral W, we just used the conductivity data in [19] (extended to a wider frequency range needed to calculate W), while the right-hand side of (3) was recalculated using recursion relations for $\Sigma_{\mathbf{p}}(\varepsilon)$ and the whole self-consistency DMFT + Σ loop. All calculations were performed for a tight-binding "bare" spectrum on the square lattice, with the nearest-neighbor transfer integral t and the next-to-nearest-neighbor transfer integral t'.

In Fig. 1, we present our typical data for the real part of the conductivity (with $t' = -0.4t$, $t = 0.25$ eV, a band filling of $n = 0.8$, and a temperature of $T = 0.089t$) for different values of Hubbard interaction $U = 4t$, $6t$, $10t$, $40t$ and a fixed pseudogap amplitude $\Delta = t$ (at the correlation length $\xi = 10a$). It is obvious from these data that the optical integral W is different for all of these curves; its value actually decreases with an increase in U (along with damping of pseudogap anomalies [19]). However, the single band optical sum rule in (3) is satisfied within our numerical accuracy, as can be seen from Table 1. The small "deficiency" in the values of W in Table 1 is naturally due to a finite frequency integration interval over the conductivity data in Fig. 1.

In Fig. 2, we show the real part of the optical conductivity for a doped Mott insulator (at a fixed $U = 40t$, $t' = -0.4t$, $t = 0.25$ eV, and the band filling $n = 0.8$, $T = 0.089t$) for different values of the pseudogap amplitude $\Delta = 0$, $\Delta = t$, and $\Delta = 2t$. The correlation length is again $\xi = 10a$ and the band filling factor $n = 0.8$. The "violation" of the sum rule here is especially striking: the optical integral obviously decreases with an increase in

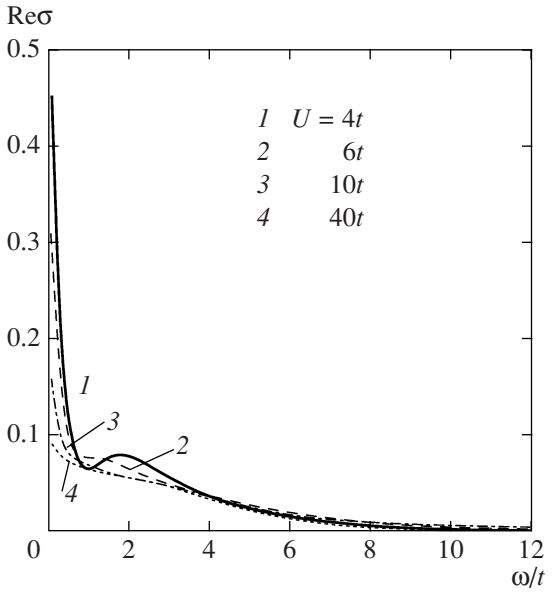

Fig. 1. Real part of the optical conductivity for a strongly correlated system in the pseudogap state ($t' = -0.4t$, $t = 0.25$ eV, and $T = 0.089t$) in the DMFT + $\Sigma_{\mathbf{p}}$ approximation, the U dependence. Band filling $n = 0.8$, pseudogap amplitude $\Delta = t$, correlation length $\xi = 10a$. Conductivity is given in units of $\sigma_0 = e^2/\hbar$.

Δ. However, again, the single-band optical sum rule in (3) is strictly valid, as can be seen from Table 2.

To study the details of the sum rule "violation," i.e., the dependence of the optical integral W on the parameters of the model, we performed extensive calculations of the appropriate dependences of the right-hand side of Eq. (3) and the optical integral W on the temperature T, doping, the pseudogap amplitude Δ, the correlation length of pseudogap fluctuations $\xi = \kappa^{-1}$, and the correlation strength U. Some of the results are presented in Figs. 3–5.

A typical dependence of the (normalized) optical integral on the correlation strength U is shown in Fig. 3 for two values of Δ. We can see a rather significant decrease in W with an increase in U. As regards the correlation length dependence, which is shown in the inset

Table 1. Single-band optical sum rule check in the hot spot model, the U dependence. The optical integral is given in units of $e^2t/\hbar$

U	$\frac{\pi e^2}{2}\sum_{\mathbf{p}}\frac{\partial^2\varepsilon_p}{\partial p_x^2}n_p$	$W = \int_0^\infty \mathrm{Re}\sigma(\omega)d\omega$
$4t$	0.456	0.408
$6t$	0.419	0.387
$10t$	0.371	0.359
$40t$	0.323	0.306

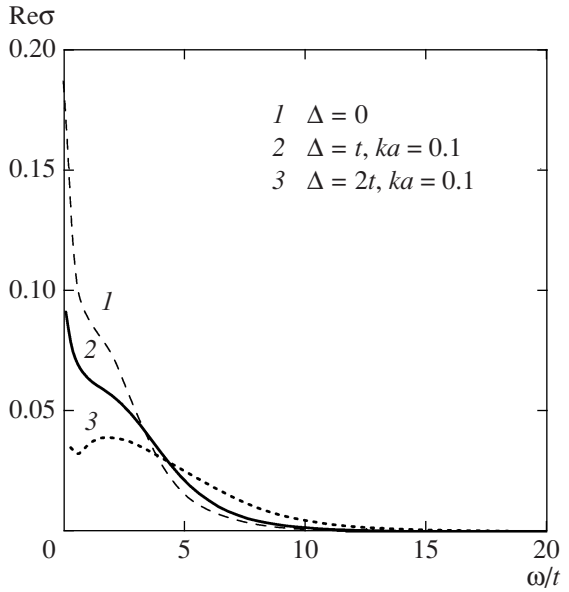

Fig. 2. Real part of the optical conductivity for a doped Mott insulator ($U = 40t$, $t' = -0.4t$, $t = 0.25$ eV, and $T = 0.089t$) in the DMFT + $\Sigma_{\mathbf{p}}$ approximation for different values of the pseudogap amplitude $\Delta = 0$, $\Delta = t$, and $\Delta = 2t$. Correlation length $\xi = 10a$, band filling factor $n = 0.8$.

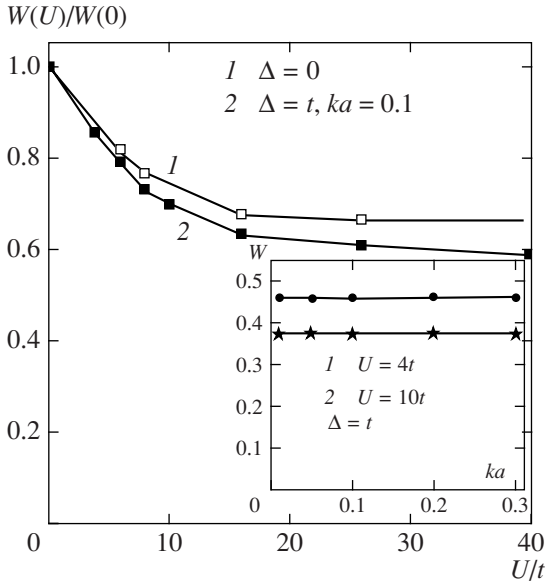

Fig. 3. Dependence of the normalized optical integral on the correlation strength U in the pseudogap state ($T = 0.089t$, $t = 0.25$ eV, $t' = -0.1$ eV, $n = 0.8$). Inset: the correlation length dependence of the optical integral in units of $e^2t/\hbar$.

to Fig. 3, it was found to be very weak (practically negligible) in the whole region of realistic values of Δ, and we therefore do not discuss it further. The dependence of W on the pseudogap amplitude Δ (for several values of U) is shown in Fig. 4. A typical doping dependence, which reflects just the dependence of the square of the plasma frequency ω_{pl}^2 on doping, is given in Fig. 5. In all other cases, the change of the relevant parameters of the model leads to a rather significant decrease in the values of W. As regards the temperature dependence (shown in the inset to Fig. 5), it is rather weak, quadratic in T and quite similar to that found in Refs. [4].

Basically, these results show that the value of the optical integral depends on all the major parameters of the model and, in this sense, its value is not universal and hence the optical sum rule is significantly "violated" if we restrict ourself to a single-band contribution.

Table 2. Single-band optical sum rule check in the hot spot model, the Δ dependence. The optical integral is given in units of $e^2t/\hbar$

Δ	$\frac{\pi e^2}{2}\sum_{\mathbf{p}}\frac{\partial^2\varepsilon_p}{\partial p_x^2}n_p$	$W = \int_0^\infty \text{Re}\sigma(\omega)d\omega$
0	0.366	0.36
t	0.314	0.304
$2t$	0.264	0.252

2.2. Disordered Anderson–Hubbard Model

In [20], we used the DMFT + Σ approximation to calculate the density of states, the optical conductivity, and the phase diagram of a strongly correlated and strongly disordered paramagnetic Anderson–Hubbard model, with a Gaussian site disorder. Strong correlations were taken into account by the DMFT, while disorder was taken into account via the appropriate generalization of the self-consistent theory of localization [25–28]. We considered the three-dimensional system with a semi-elliptic density of states. The correlated metal, Mott insulator, and correlated Anderson insulator phases were identified via the evolution of the density of states and dynamic conductivity, demonstrating both Mott–Hubbard and Anderson metal–insulator transitions and allowing the construction of the complete zero-temperature phase diagram of the Anderson–Hubbard model.

For the "external" self-energy entering the DMFT + Σ loop, we used the simplest possible approximation (neglecting "crossing" diagrams for disorder scattering), i.e., just the self-consistent Born approximation, which in the case of Gaussian site-energy disorder takes the usual form

$$\Sigma(\varepsilon) = \Delta^2\sum_{\mathbf{p}} G(\varepsilon, \mathbf{p}), \qquad (6)$$

where Δ now denotes the amplitude of site disorder.

Calculations of the optical conductivity are considerably simplified [20] because there are no contribu-

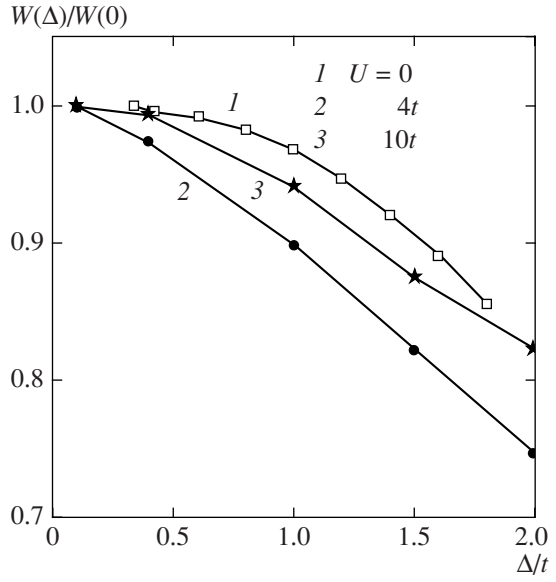

Fig. 4. Dependence of the normalized optical integral on the pseudogap amplitude Δ ($T = 0.011t$, $t = 0.25$ eV, $t' = -0.1$ eV, $n = 0.8$, $\kappa a = 0.1$).

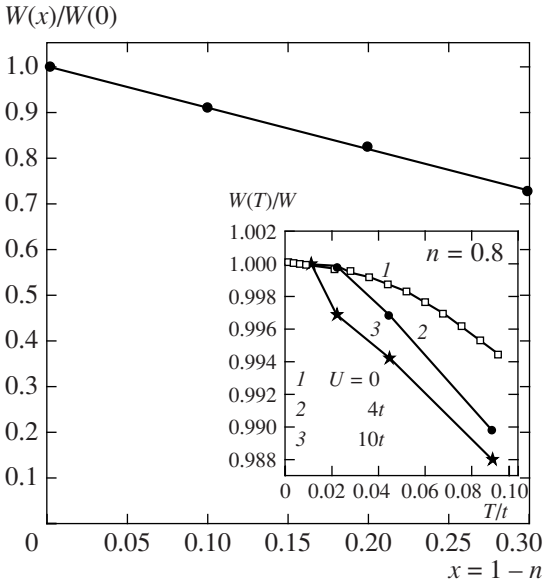

Fig. 5. Dependence of the normalized optical integral on hole doping in the pseudogap state. Inset: temperature dependence ($T = 0.011t$, $U = 4t$, $\Delta = t$, $t = 0.25$ eV, $t' = -0.1$ eV, $\kappa a = 0.1$).

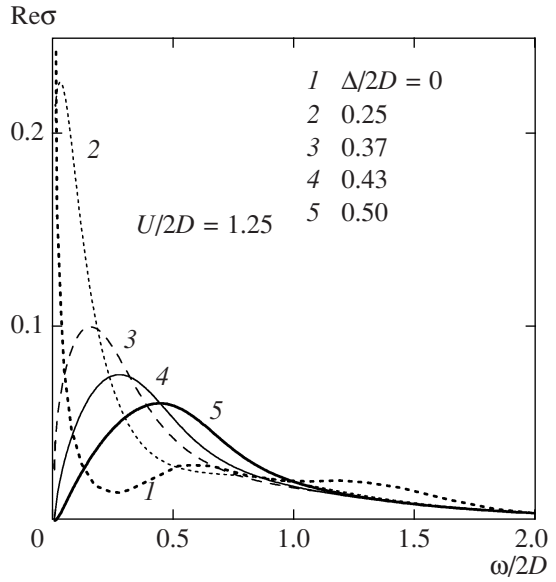

Fig. 6. Real part of the dynamic conductivity for the half-filled Anderson–Hubbard model for different degrees of disorder Δ and $U = 2.5D$ typical for a correlated metal. Lines *1* and *2* are for the metallic phase, line *3* corresponds to the mobility edge (Anderson transition), and lines *4* and *5* correspond to the correlated Anderson insulator. The conductivity is in units of $e^2/\hbar a$.

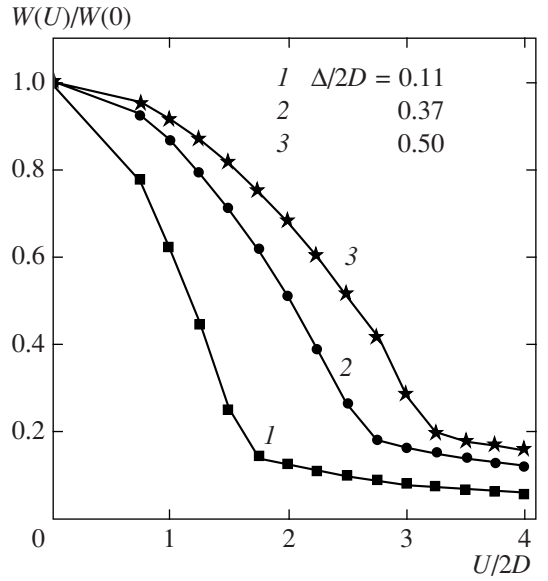

Fig. 7. Dependence of the normalized optical integral on the correlation strength in the Anderson–Hubbard model for different degrees of disorder Δ (*1* and *2*, strongly disordered metal; *3*, correlated Anderson insulator).

tions to conductivity due to vertex corrections determined by a local Hubbard interaction. The conductivity is essentially determined by the generalized diffusion coefficient, which is obtained from the appropriate generalization of the self-consistency equation in [25–28], which is to be solved in conjunction with the DMFT + Σ loop.

In Fig. 6, we show typical results for the real part of the dynamic conductivity of a correlated metal described by the half-filled Anderson–Hubbard model (with the bandwidth $2D$) for different degrees of disorder Δ and $U = 2.5D$; the results demonstrate a continuous transition to the correlated Anderson insulator as disorder increases.

Table 3. Single-band optical sum rule check in the Anderson–Hubbard model, the Δ dependence. The optical integral is in units of $2e^2D/\hbar a$

$\Delta/2D$	$\frac{\pi e^2}{2}\sum_{\mathbf{p}}\frac{\partial^2\varepsilon_p}{\partial p_x^2}n_p$	$W = \int_0^\infty \mathrm{Re}\sigma(\omega)d\omega$
0	0.063	0.064
0.25	0.068	0.07
0.37	0.06	0.056
0.5	0.049	0.05

Again, the direct check shows that the single-band optical sum rule in (3) is satisfied within our numerical accuracy, as can be seen from Table 3. At the same time, the optical integral W itself obviously changes with disorder.

Again, to study the details of this sum rule violation, i.e., the dependence of W on the parameters of the Anderson–Hubbard model, we performed detailed calculations of its dependences on the temperature T, the disorder amplitude Δ, and the correlation strength U. Some of the results are presented in Figs. 7–9.

In Fig. 7, we show the dependence of the normalized optical integral on U for different degrees of disorder (for both a strongly disordered metal and a correlated Anderson insulator). It is seen that in all cases, an increase in the correlation strength leads to a rather sharp decrease in W in the metallic state; this decrease is much slower in the Mott insulator.

In Fig. 8, we present similar dependences on the disorder strength Δ. In the metallic state, the optical integral generally decreases as disorder increases, but the opposite behavior is observed if we start from the Mott insulator (obtained either with an increase in U from the metallic state or for a reduced U in the hysteresis region of the phase diagram [20]). We note the absence of any significant changes in the immediate vicinity of the critical disorder $\Delta_c/2D = 0.37$, corresponding to the Anderson metal–insulator transition. At the same time, we note that the most significant increase in the optical integral occurs as the system transforms into the disorder-induced metallic state obtained from the Mott insulator, as observed in [20].

In Fig. 9, we show the temperature dependence of the normalized optical integral for different degrees of disorder. In the Anderson–Hubbard model, it appears to be significantly stronger than in the hot spot model (see above) and decreases as disorder increases. Moreover, in a relatively weakly correlated state, the situation is qualitatively the same: the optical integral decreases as T increases, but in a disordered Mott insulator, the integral increases, as can be seen from line *3* in the inset to Fig. 9.

Again, as in the case of the pseudogap hot spot model, these results for the Anderson–Hubbard model clearly demonstrate that the value of the optical integral is not universal and depends on all the major parame-

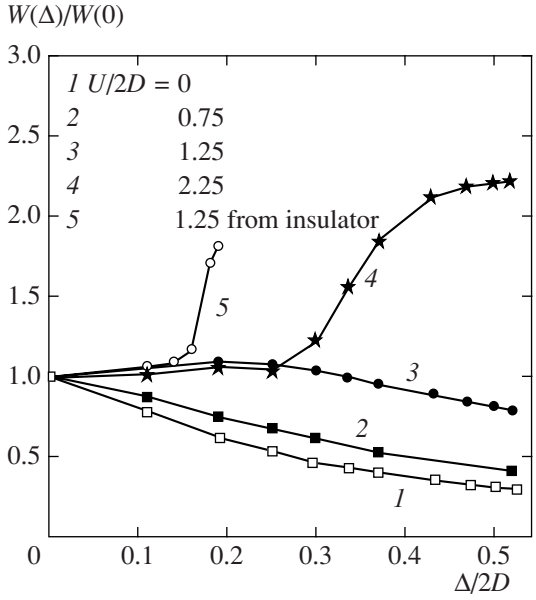

Fig. 8. Disorder dependence of the normalized optical integral in the Anderson–Hubbard model for different values of Hubbard interaction U. Lines *1, 2, 3*—correlated metal, transforming into Anderson insulator. Line *4*—Mott insulator state obtained with the growth of U from correlated metal. Line *5*—Mott insulator obtained with diminishing U in the hysteresis region of the phase diagram.

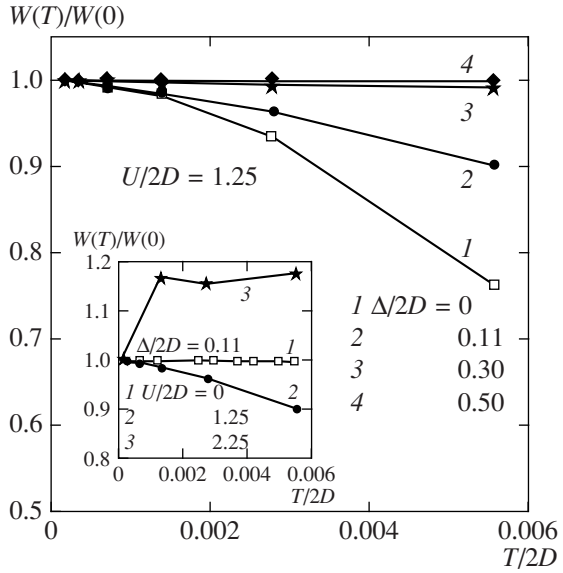

Fig. 9. Temperature dependence of the normalized optical integral in the Anderson–Hubbard model for different degrees of disorder. Inset: a similar dependence at a fixed disorder but for different values of the Hubbard interaction U; line *3* here corresponds to a disordered Mott insulator.

ters of the model; therefore the single-band optical sum rule is strongly violated.

3. CONCLUSIONS

Based on the DMFT + Σ approach, we have studied the single-band optical sum rule for two typical strongly correlated systems, which are outside the scope of the standard DMFT scheme: (i) the hot spot model of the pseudogap state, which takes into account important nonlocal correlations due to AFM(CDW) short-range order fluctuations and (ii) the Anderson–Hubbard model, which includes strong disorder effects leading to the disorder-induced metal–insulator (Anderson) transition alongside with the Mott transition.

We have explicitly demonstrated that the single-band optical sum rule in (3) is satisfied for both models, confirming the self-consistency of the DMFT + Σ approach for calculation of two-particle properties.

However, the optical integral

$$W = 2\int_0^\infty \mathrm{Re}\sigma(\omega)d\omega$$

entering single-band sum rule (3) is nonuniversal and depends on the parameters of the model under consideration. Most of the previous studies addressed its (relatively weak) temperature dependence. Here, we have analyzed dependences on the essential parameters of our models, showing that these may lead to rather strong violations of the optical sum rule. Because most of the parameters under discussion can be varied in different kinds of experiments, these dependences should be taken into account in the analysis of optical experiments on strongly correlated systems.

ACKNOWLEDGMENTS

We thank Th. Pruschke for providing us with the NRG code. This work is supported by Russian Foundation for Basic Research (project nos. 08-02-00021 and 08-02-00712) and the RAS programs "Quantum Macrophysics" and "Strongly Correlated Electrons in Semiconductors, Metals, Superconductors, and Magnetic Materials." I.N. is also supported a Grant of the President of Russian Federation (MK.2242.2007.2) and the Russian Science Support Foundation.

REFERENCES

1. R. Kubo, J. Phys. Soc. Jpn. **12**, 570 (1957).
2. M. R. Norman, A. V. Chubukov, E. van Heumen, et al., Phys. Rev. B: Condens. Matter **76**, 220509(R) (2007).
3. M. R. Norman and C. Pepin, Phys. Rev. B: Condens. Matter **66**, 100506(R) (2002).
4. A. Toschi, M. Capone, M. Ortolani, et al., Phys. Rev. B: Condens. Matter **77**, 014518 (2008).
5. A. E. Karakozov, E. G. Maksimov, and O. V. Dolgov, Solid State Commun. **124**, 119 (2002); A. E. Karakozov and E. G. Maksimov, Solid State Commun. **139**, 80 (2006).
6. M. R. Norman, M. Randeria, B. Janko, and J. C. Campuzano, Phys. Rev. B: Condens. Matter **61**, 14742 (2000).
7. A. E. Karakozov and E. G. Maksimov, Zh. Éksp. Teor. Fiz. **132** (4), 852 (2007) [JETP **105** (4), 745 (2007)].
8. D. N. Basov, S. I. Woods, A. S. Katz, et al., Science (Washington) **283**, 49 (1999).
9. H. J. A. Molegraaf, C. Presura, D. van der Marel, et al., Science (Washington) **295**, 2239 (2002).
10. A. F. Santander-Syro, R. P. S. M. Lobo, N. Bontemps, et al., Phys. Rev. B: Condens. Matter **70**, 134504 (2004).
11. F. Carbone, A. B. Kuzmenko, H. J. A. Molegraaf, et al., Rev. B: Condens. Matter **74**, 024502 (2006).
12. E. van Heumen, R. Lortz, A. B. Kuzmenko, et al., Phys. Rev. B: Condens. Matter **75**, 054522 (2007).
13. D. N. Basov and T. Timusk, Rev. Mod. Phys. **77**, 721 (2005).
14. E. Z. Kuchinskii, I. A. Nekrasov, and M. V. Sadovskii, Pis'ma Zh. Éksp. Teor. Fiz. **82** (4), 217 (2005) [JETP Lett. **82** (4), 198 (2005)].
15. M. V. Sadovskii, I. A. Nekrasov, E. Z. Kuchinskii, et al., Phys. Rev. B: Condens. Matter **72**, 155105 (2005).
16. E. Z. Kuchinskii, I. A. Nekrasov, and M. V. Sadovskii, Fiz. Nizk. Temp. (Kharkov) **32** (4–5), 528 (2006) [Low Temp. Phys. **32** (4–5), 528 (2006)].
17. Th. Pruschke, M. Jarrell, and J. K. Freericks, Adv. Phys. **44**, 187 (1995).
18. A. Georges, G. Kotliar, W. Krauth, and M. J. Rozenberg, Rev. Mod. Phys. **68**, 13 (1996).
19. E. Z. Kuchinskii, I. A. Nekrasov, and M. V. Sadovskii, Phys. Rev. B: Condens. Matter **75** 115102 (2007).
20. E. Z. Kuchinskii, I. A. Nekrasov, and M. V. Sadovskii, Zh. Éksp. Teor. Fiz. **133** (3), 670 (2008) [JETP **106** (3), 581 (2008)].
21. M. V. Sadovskii, Usp. Fiz. Nauk **171**, 539 (2001) [Phys.—Usp. **44**, 515 (2001)].
22. J. Schmalian, D. Pines, and B. Stojkovic, Phys. Rev. B: Condens. Matter **60**, 667 (1999).
23. É. Z. Kuchinskiĭ and M. V. Sadovskiĭ, Zh. Éksp. Teor. Fiz. **115** (5), 1765 (1999) [JETP **88** (5), 968 (1999)].
24. M. V. Sadovskiĭ and N. A. Strigina, Zh. Éksp. Teor. Fiz. **122** (3), 610 (2002) [JETP **95** (3), 526 (2002)].
25. D. Vollhardt and P. Wöle, Phys. Rev. B: Condens. Matter **22**, 4666 (1980); Phys. Rev. Lett. **48**, 699 (1982).
26. P. Wöle and D. Vollhardt, in *Anderson Localization*, Ed. by Y. Nagaoka and H. Fukuyama, in *Springer Series in Solid State Sciences* (Springer, Berlin, 1982), Vol. 39, p. 26.
27. A. V. Myasnikov and M. V. Sadovskiĭ, Fiz. Tverd. Tela **24** (12), 3569 (1982) [Sov. Phys. Solid State **24** (12), 2033 (1982)]; E. A. Kotov and M. V. Sadovskii, Z. Phys. B: Condens. Matter **51**, 17 (1983).
28. M. V. Sadovskii, in *Soviet Scientific Reviews—Physics Reviews*, Ed. by I. M. Khalatnikov (Harwood, New York, 1986), Vol. 7, p. 1.

ISSN 0021-3640, JETP Letters, 2008, Vol. 88, No. 2, pp. 144–149. © Pleiades Publishing, Ltd., 2008.

Electronic Structure of Prototype AFe_2As_2 and ReOFeAs High-Temperature Superconductors: A Comparison¶

I. A. Nekrasov[a], Z. V. Pchelkina[b], and M. V. Sadovskii[a]

[a] *Institute for Electrophysics, Russian Academy of Sciences, Ural Division, Yekaterinburg, 620016 Russia*

[b] *Institute for Metal Physics, Russian Academy of Sciences, Ural Division, GSP-170, Yekaterinburg, 620041 Russia*

Received June 17, 2008

We have performed ab initio LDA calculations of the electronic structure of newly discovered prototype high-temperature superconductors AFe_2As_2 (A = Ba, Sr) and compared it with the previously calculated electronic spectra of ReOFeAs (Re = La, Ce, Pr, Nd, Sm). In all cases, we obtain almost identical densities of states in a rather wide energy interval (up to 1 eV) around the Fermi level. Energy dispersions are also very similar and almost two dimensional in this energy interval, leading to the same basic (minimal) model of the electronic spectra, determined mainly by Fe *d* orbitals of the FeAs layers. The other constituents, such as A ions or rare-earth Re (or oxygen states) are more or less irrelevant for superconductivity. LDA Fermi surfaces for AFe_2As_2 are also very similar to that of ReOFeAs. This makes the more simple AFe_2As_2 a generic system to study the high-temperature superconductivity in FeAs-layered compounds.

PACS numbers: 71.20.-b, 74.25.Jb, 74.70.-b

DOI: 10.1134/S0021364008140166

The recent discovery of the new superconductor $LaO_{1-x}F_xFeAs$ with the transition temperature T_c up to 26 K [1–4] and even higher values of T_c = 41–55 K in $CeO_{1-x}F_xFeAs$ [5], $SmO_{1-x}F_xFeAs$ [6], $NdO_{1-x}F_xFeAs$, and $PrO_{1-x}F_xFeAs$ [7, 8] was recently followed by the discovery of high-temperature superconductivity with T_c up to 38 K in potassium-doped ternary iron arsenides $BaFe_2As_2$ [9] and $SrFe_2As_2$ [10], with the further synthesis of superconducting AFe_2As_2 (A = K, Cs, K/Sr, Cs/Sr) [11]. Relatively large single crystals of superconducting $Ba_{1-x}K_xFe_2As_2$ were also grown [12], providing a major breakthrough in the studies of anisotropic electronic properties of FeAs-layered superconductors.

The LDA electronic structure of LaOFeAs were calculated in a number of papers (see, e.g., [13, 14, 15]) producing results that are qualitatively similar to that first obtained for LaOFeP [16]. We have performed LDA calculations for the whole series of ReOFeAs (R = La, Ce, Pr, Nd, Sm) [17], demonstrating a very weak (or absent) dependence of the electronic spectrum on the type of the rare-earth ion Re in a rather wide energy interval (~2 eV) around the Fermi level.

First, the LDA results for the density of states (DOS) of $BaFe_2As_2$ were recently presented in [18, 19]. Here, we present the results of our ab initio calculations of an electronic structure of the newly discovered prototype high-temperature superconductors AFe_2As_2 (A = Ba, Sr) with the aim of comparing it with the previously discussed ReOFeAs series. We present the LDA DOS, energy dispersions, and Fermi surfaces of these compounds and briefly discuss the possible conclusions with respect to the minimal model of the electronic spectrum and superconductivity. Since all of the results are quite similar for both A = Ba and A = Sr, as well as for the whole Re series, below we present the data mainly for A = Ba and Re = La.

Crystal structure data for $BaFe_2As_2$ and LaOFeAs compounds. Atomic positions for $BaFe_2As_2$ are Ba (0, 0, 0), Fe (0.5, 0, 0.25), As (0, 0, z) and for LaOFeAs are La (0.25, 0.25, z_{La}), Fe (0.75, 0.25, 0.5), As (0.25, 0.25, z_{As}), O (0.75, 0.25, 0)

Parameter	$BaFe_2As_2$	LaOFeAs
Group	*I*4/*mmm*	*P*4/*nmm*
a, Å	3.9090(1)	4.03533(4)
c, Å	13.2122(4)	8.74090(9)
z_{La}	–	0.14154(5)
z_{As}	0.3538(1)	0.6512(2)
Source	[9]	[1]
Ba–As, Å	3.372(1) × 8	–
La–As, Å	–	3.380 × 4
Fe–As, Å	2.388(1) × 4	2.412 × 4
Fe–Fe, Å	2.764(1) × 4	2.853 × 4
As–Fe–As	109.9(1)°	113.6°
	109.3(1)°	107.5°

¶The text was submitted by the authors in English.

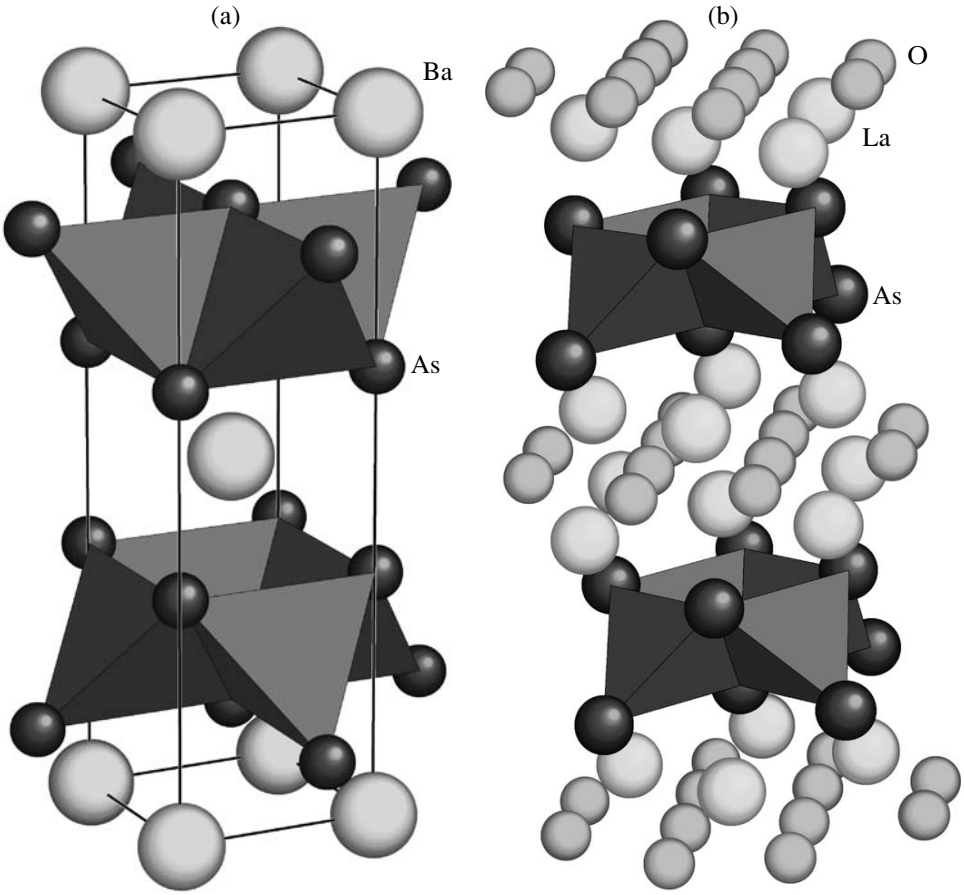

Fig. 1. Crystal structure of $BaFe_2As_2$ and LaOFeAs. FeAs tetrahedra form two-dimensional layers (violet) sandwiched by Ba ion (cyan) or LaO (yellow and green) layers.

Both $BaFe_2As_2$ and LaOFeAs crystallize in a tetragonal structure with the space group *I*4/*mmm* and *P*4/*nmm*, respectively. Both compounds are formed from $(FeAs)^-$ layers alternating with $Ba^{2+}_{0.5}$ or $(LaO)^+$. Fe^{2+} ions are surrounded by four As ions forming a tetrahedron. The crystal structures of $BaFe_2As_2$ and LaOFeAs are shown in Fig. 1. The quasi two-dimensional character of both compounds makes them similar to the well-studied class of superconducting copper oxides. At 140 K, $BaFe_2As_2$ undergoes a structural phase transition from the tetragonal (*I*4/*mmm*) to orthorhombic (*Fmmm*) space group [20]. The same transition takes place for the LaOFeAs system at 150 K: *P*4/*nmm* (tetragonal) $\longrightarrow$ *Cmma* (orthorhombic) [21]. The crystallographic data for the tetragonal phase of two compounds are shown in the table. It can be seen that for $BaFe_2As_2$ compound the Fe–As distance is smaller than for LaOFeAs. Therefore, one would expect a more considerable Fe-*d*-As-*p* hybridization for the $BaFe_2As_2$ system in comparison with LaOFeAs and, as a result, a wider Fe-*d* bandwidth. The distance between the nearest Fe atoms within FeAs layers is also significantly smaller in $BaFe_2As_2$ as compared with the LaOFeAs system. After the phase transition of the $BaFe_2As_2$ system to the orthorhombic structure, the four equal Fe–Fe distances break into two bond pairs with lengths of 2.808 and 2.877 Å.

Moreover, the two As–Fe–As angles are quite different in the case of the LaOFeAs system (113.6° and 107.5°) and have very close values (~109°) for $BaFe_2As_2$. Such differences in the nearest surrounding of Fe ions should evoke distinctions in the electronic structure of these two compounds.

The electronic structure of $BaFe_2As_2$ and LaOFeAs was calculated within the local density approximation (LDA) by using the basis of the linearized muffin-tin orbitals (LMTO) [22]. For $BaFe_2As_2$, we used the structure data for a K-doped system and temperature T = 20 K [9]. The LDA calculated total and partial densities of states for the $BaFe_2As_2$ and LaOFeAs are shown in Fig. 2. In the lower panel of Fig. 2, we show the magnified behavior of the total DOS around the Fermi level for three different systems under discussion. In all cases, the DOS is almost flat. It is well known that the DOS of two-dimensional (nearly free) electrons is a constant defined just by the renormalized electron

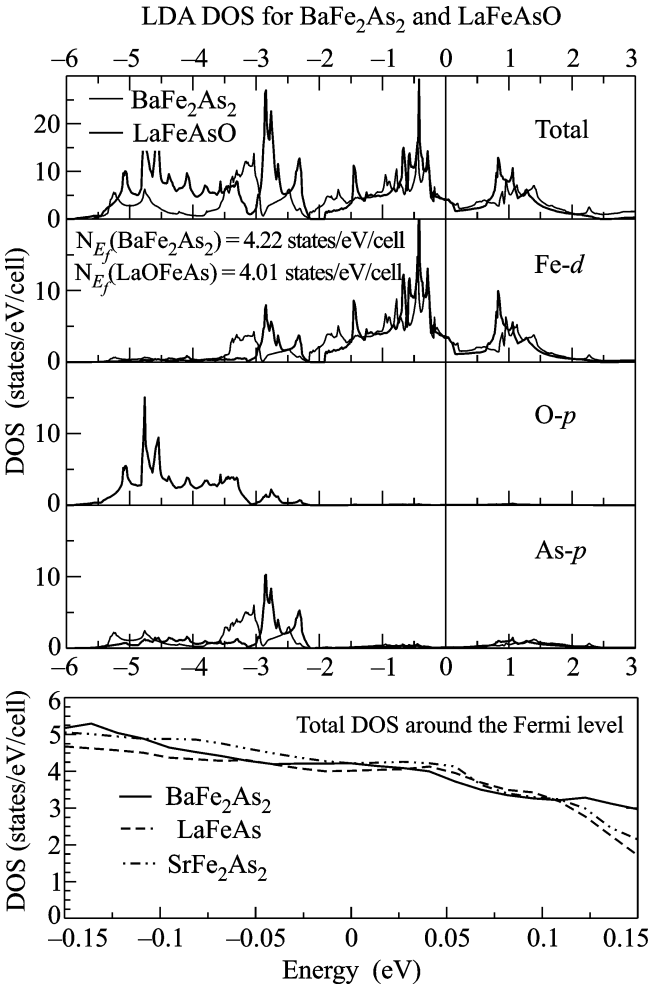

Fig. 2. Total and partial LDA DOS for $BaFe_2As_2$ (black lines) and LaOFeAs (light lines) compounds. The lower panel presents the total DOS for different FeAs systems in the vicinity of the Fermi level. The Fermi level corresponds to zero.

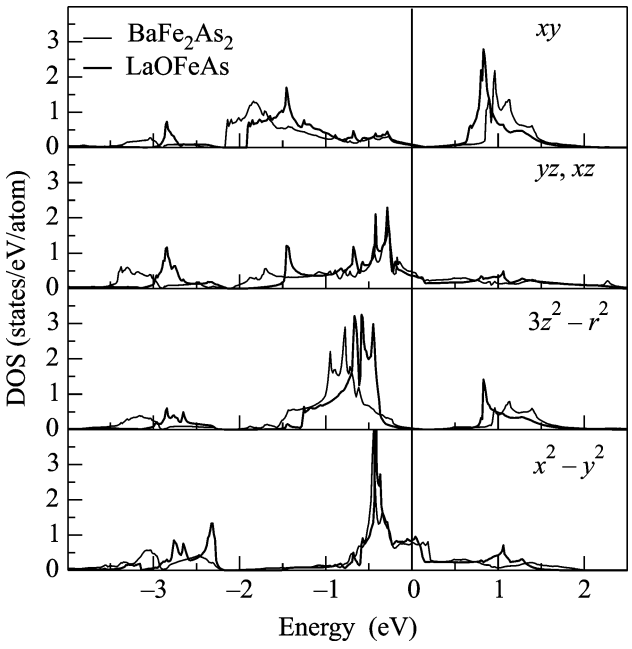

Fig. 3. Orbital projected Fe-d DOS for $BaFe_2As_2$ (black lines) and LaOFeAs (light lines) compounds. The Fermi level corresponds to zero.

mass. Thus, our results support the two-dimensional nature of these compounds.

The orbital projected Fe-d DOS for two compounds is shown in Fig. 3. The values of the density of states at the Fermi level are very similar in both compounds. The 0.3 eV wider Fe-d bandwidth in the case of $BaFe_2As_2$ in comparison with LaOFeAs arises from the shorter Fe–As bonds and, hence, a stronger Fe-d-As-p hybridization for this system. The partial As-p DOS is split into two parts in the case of the Ba system. One can see that, for both systems, three Fe-d orbitals of the t_{2g} symmetry—xz, yz, $x^2 - y^2$—mainly contribute to the bands crossing the Fermi level. We call here the $x^2 - y^2$ (a basically rotated xy orbital) as one of t_{2g} orbitals following the established earlier terminology for ReOFeAs systems.

Energy bands along the high-symmetry directions of the Brillouin zone are shown in Fig. 4. The bands around the Fermi level for both compounds are primarily formed by Fe-d states. In the LaOFeAs system, the As-p states are also hybridized with O-p states and the corresponding bands are separated from the Fe-d ones. On the contrary, in $BaFe_2As_2$, the Fe-d and As-p bands are entangled. The lower two panels of Fig. 4 compare the band dispersions for both systems close to the Fermi level. Here, only the (k_x, k_y) dispersion is shown. Taking into account the different notations of the high-symmetry points for these two different crystal structures, one can find that these dispersions are pretty similar to each other. There are three hole-like bands around the Γ point and two electron bands around the X point. Thus, one can define a minimal model of "bare" electronic bands to treat, e.g., superconductivity, similar to that discussed in [23]. Let us mention that, along the $X - M$ direction in LaOFeAs, there are two degenerate bands.

In Fig. 5, the relative onsite energies of the hybridized Fe-3d and As-4p states are presented. A bird's eye view tells us that this picture for both $BaFe_2As_2$ (left) and LaOFeAs (right) is rather similar. There are two groups of states—antibonding (mostly Fe-3d) and bonding (mostly As-4p) states. However, there are some fine differences. First of all, for $BaFe_2As_2$, the hybridization between the Fe-3d-z^2 and As-4$p_z$orbitals is about 0.4 eV weaker. This leads to a swap of the energy positions of the Fe-3d-z^2 and x^2 orbitals and, similarly, for the corresponding As-4p orbitals. Secondly, the Fe-d-t_{2g} orbitals are degenerate for $BaFe_2As_2$ in contrast to LaOFeAs.

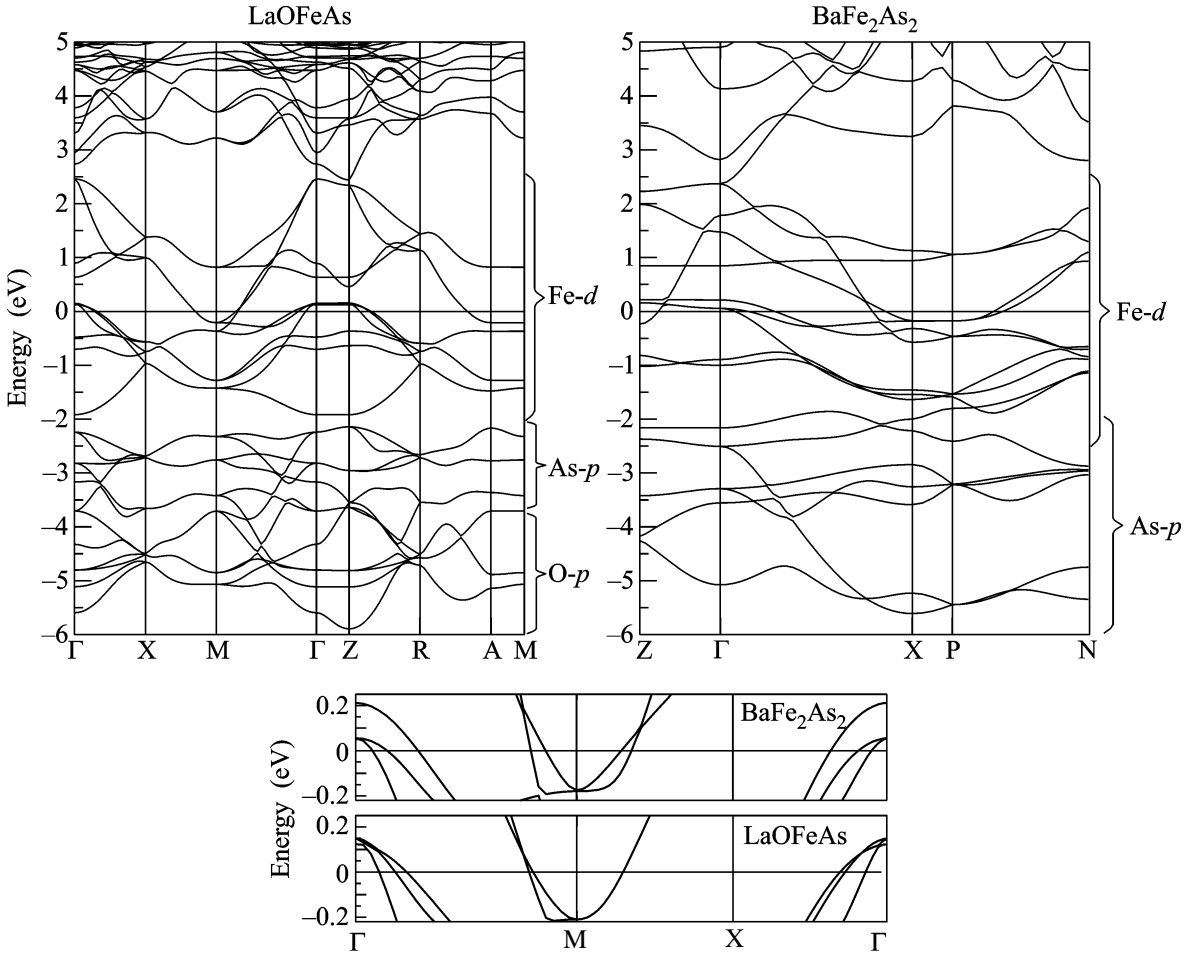

Fig. 4. Energy bands for LaOFeAs (left) and $BaFe_2As_2$ (right) compounds. The lower two panels present the (k_x, k_y) dispersions for $BaFe_2As_2$ and LaOFeAs systems in the vicinity of the Fermi level. The Fermi level corresponds to zero.

Neglecting the small difference, the overall picture of the energy spectrum in the vicinity of the Fermi level is very similar for both compounds and is determined mainly by the Fe-*d* states of the FeAs layers, making the states of the A ions or rare-earth Re more or less irrelevant for superconductivity. Thus, the superconductivity of FeAs-layered compounds may be studied within the minimal model, taking into account only the essential Fe-*d* bands close to the Fermi level. The variants of such a model proposed, e.g., in [23, 24], for the LaOFeAs system may also be used for AFe_2As_2 with only a slight modification of the model parameters, such as the transfer integrals.

The role of the electronic correlations remains disputable at the moment. In general, it can be expected to be rather important due to the large values of Hubbard and Hund interactions on Fe. However, the LDA + DMFT calculations from [25, 26] have produced rather contradictory claims. Obviously, this problem requires further studies. Assuming that the correlations in these compounds are most likely in the intermediate range,

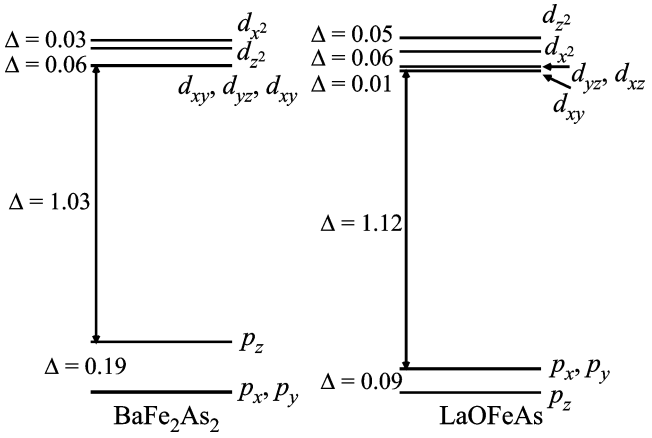

Fig. 5. Relative onsite energies of the hybridized Fe-3*d* and As-4*p* states obtained from the LDA dispersions for $BaFe_2As_2$ (left) and LaOFeAs (right). Δ stands for the corresponding energy distances in eV.

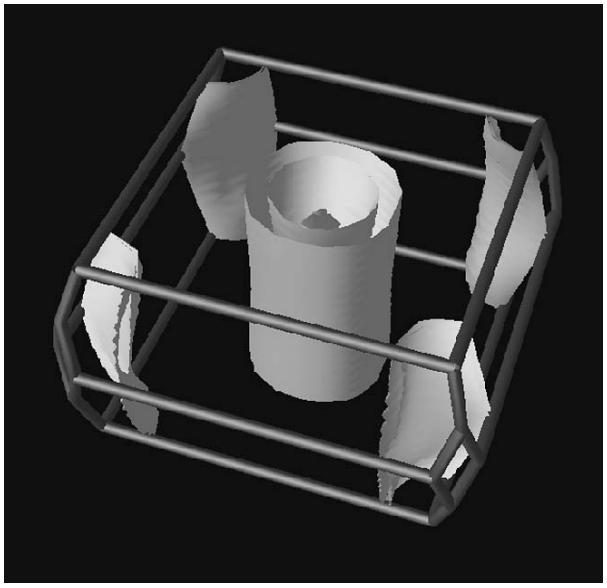

Fig. 6. Fermi surface of $BaFe_2As_2$.

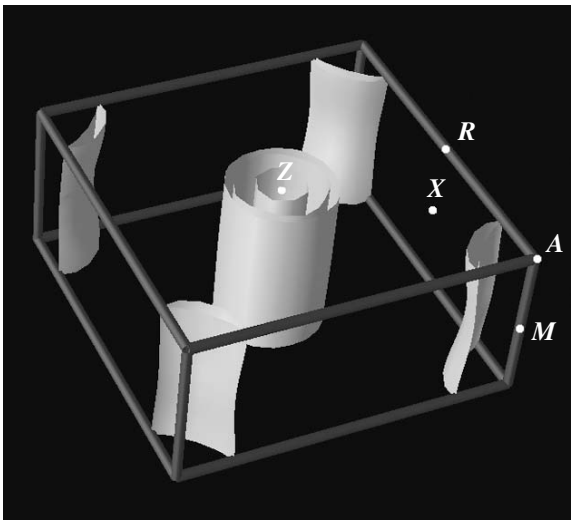

Fig. 7. Fermi surface of LaOFeAs shown in the first Brillouin zone centered at Γ point.

we may hope that the standard LDA approach used here is reliable enough.

The Fermi surfaces obtained from the LDA calculations for $BaFe_2As_2$ and LaOFeAs are shown in Figs. 6 and 7, respectively. There are five sheets of the Fermi surface for both compounds. Qualitatively, the Fermi surfaces are similar to that reported for LaOFeAs in [13] (see also [15]). There are three hole cylinders in the middle of the Brillouin zones and two electron sheets at the corners of the Brillouin zone. The smallest of the hole cylinders is usually neglected in the analysis of the superconducting pairings [23, 27] and the analysis is restricted to the smallest two [27] or four bands [23] models, reproducing two-hole and two-electron cylinders.

The tetragonal-to-orthorhombic phase transition taking place in undoped compounds is usually attributed to the SDW formation due to the nesting properties of the electron and hole Fermi surfaces [15, 24] or due to the excitonic instability in the triplet channel [23]. The difficulties of calculating the magnetic state of LaOFeAs related to the apparently itinerant nature of magnetism were recently discussed in [28].

In conclusion, we have presented the results of the LDA calculations of a new prototype high-temperature superconductor AFe_2As_2 (A = Ba, Sr) and compared it with the previously discussed ReOFeAs series, demonstrating the essential similarity of the electronic states close to the Fermi level and the most important for superconductivity. These states are formed mainly by the Fe orbitals in the two-dimensional FeAs layer, which is the basic structural motif, where the superconducting state is formed. Thus, the rather simple AFe_2As_2 system may be considered generic for the studies of a high-temperature superconductivity in the whole class of FeAs-layered compounds.

We are grateful to L.P. Gor'kov for useful discussions. This work was supported by the Russian Foundation for Basic Research (project nos. 08-02-00021 and 08-02-00712), the Russian Academy of Sciences ("Quantum Macrophysics" and "Strongly Correlated Electrons in Semiconductors, Metals, Superconductors, and Magnetic Materials" programs), the Council of the President of the Russian Federation for Support of Young Scientists and Leading Scientific Schools (project no. NSh-1929.2008.2), and by the Ural Division and Siberian Branch, Russian Academy of Sciences. The work of I.A.N. was supported by the Council of the President of the Russian Federation for Support of Young Scientists and Leading Scientific Schools (project no. MK-2242.2007.2) and the Russian Science Support Foundation. The work of Z.V.P. was supported by the Council of the President of the Russian Federation for Support of Young Scientists and Leading Scientific Schools (project no. MK-3227.2008.2) and the Dynasty Foundation.

REFERENCES

1. Y. Kamihara, T. Watanabe, M. Hirano, and H. Hosono, J. Am. Chem. Soc. **130**, 3296 (2008).
2. G. F. Chen, Z. Li, G. Zhou, et al., arXiv: 0803.0128.
3. X. Zhu, H. Yang, L. Fang, et al., arXiv: 0803.1288v1.
4. A. S. Sefat, M. A. McGuire, B. C. Sales, et al., arXiv:0803.2528.
5. G. F. Chen, Z. Li, D. Wu, et al., arXiv: 0803.3790.
6. X. H. Chen, T. Wu, G. Wu, et al., arXiv: 0803.3603.
7. Z.-A. Ren, J. Yang, W. Lu, et al., arXiv: 0803.4234.
8. Z.-A. Ren, J. Yang, W. Lu, et al., arXiv: 0803.4283.
9. M. Rotter, M. Tegel, and D. Johrendt, arXiv: 0805.4630.

10. G. F. Chen, Z. Li, G. Li, et al., arXiv: 0806.1209.
11. K. Sasmal, B. Lv, B. Lorenz, et al., arXiv: 0806.1301.
12. N. Ni, S. L. Bud'ko, A. Kreyssig, et al., arXiv: 0806.1874.
13. D. J. Singh and M. H. Du, Phys. Rev. Lett. **100**, 237003 (2008); arXiv:0803.0429.
14. L. Boeri, O. V. Dolgov, and A. A. Golubov, arXiv:0803.2703v1.
15. I. I. Mazin, D. J. Singh, M. D. Johannes, and M. H. Du, arXiv: 0803.2740v1.
16. S. Lebègue, Phys. Rev. B **75**, 035110 (2007).
17. I. A. Nekrasov, Z. V. Pchelkina, and M. V. Sadovskii, Pis'ma Zh. Éksp. Teor. Fiz. **87**, 647 (2008) [JETP Lett. **87**, (2008)]; arXiv: 0804.1239.
18. I. R. Shein and A. L. Ivanovskii, arXiv: 0806.0750.
19. C. Krellner, N. Caroca-Canales, A. Jesche, et al., arXiv:0806.1043.
20. M. Rotter, M. Tegel, and D. Johrendt, arXiv: 0805.4021.
21. T. Nomura, S. W. Kim, Y. Kamihara, et al., arXiv:0804.3569.
22. O. K. Andersen, Phys. Rev. B **12**, 3060 (1975); O. Gunnarsson, O. Jepsen, and O. K. Andersen, Phys. Rev. B **27**, 7144 (1983); O. K. Andersen and O. Jepsen. Phys. Rev. Lett. **53**, 2571 (1984).
23. V. Barzykin and L. P. Gorkov, arXiv: 0806.1993, JETP Lett. (in press).
24. S. Raghu, Xiao-Liang Qi, Chao-Xing Liu, et al., arXiv:0804.1113.
25. K. Haule, J. H. Singh, and G. Kotliar, Phys. Rev. Lett. **100**, 226402 (2008); arXiv: 0803.1279.
26. A. O. Shorikov, M. A. Korotin, S. V. Streltsov, et al., arXiv: 0804.3283.
27. Xiao-Liang Qi, S. Raghu, Chao-Xing Liu, et al., arXiv:0804.4332.
28. I. I. Mazin, M. D. Johannes, L. Boeri, et al., arXiv:0806.1869.

Pis'ma v ZhETF, vol. 88, iss. 3, pp. 224 – 228

Reconstruction of the Fermi surface in the pseudogap state of cuprates

E. Z. Kuchinskii, M. V. Sadovskii[1)]

Institute for Electrophysics, Ural Branch RAS, 620016 Ekaterinburg, Russia

Submitted 24 June 2008

Reconstruction of the Fermi surface of high-temperature superconducting cuprates in the pseudogap state is analyzed within nearly exactly solvable model of the pseudogap state, induced by short-range order fluctuations of antiferromagnetic (AFM), spin density wave (SDW), or similar charge density wave (CDW)) order parameter, competing with superconductivity. We explicitly demonstrate the evolution from "Fermi arcs" (on the "large" Fermi surface) observed in ARPES experiments at relatively high temperatures (when both the amplitude and phase of density waves fluctuate randomly) towards formation of typical "small" electron and hole "pockets", which are apparently observed in de Haas – van Alfen and Hall resistance oscillation experiments at low temperatures (when only the phase of density waves fluctuate, and correlation length of the short-range order is large enough). A qualitative criterion for quantum oscillations in high magnetic fields to be observable in the pseudogap state is formulated in terms of cyclotron frequency, correlation length of fluctuations and Fermi velocity.

PACS: 71.10.Hf, 74.72.–h

Pseudogap state of underdoped copper oxides [1 – 4] is probably the main anomaly of the normal state of high temperature superconductors. Especially striking is the observation of "Fermi arcs" in ARPES experiments, i.e. parts on the "large" Fermi surface around the diagonal of the Brillouin zone (BZ) with more or less well defined quasiparticles, while the parts of the Fermi surface close to BZ boundaries are almost completely "destroyed" [5 – 7].

However, the recent observation of quantum oscillation effects in Hall resistance [8], Shubnikov – de Haas [9] and de Haas – van Alfen (dHvA) oscillations [9, 10] in the underdoped YBCO cuprates, producing evidence for rather "small" hole or electron [11] pockets of the Fermi surface, seemed to contradict the well established ARPES data on the Fermi surface of cuprates.

Qualitatvive explanation of this apparent contradiction was given in Ref. [12] within very simplified model of hole-like Fermi surface evolution under the effect of short-range AFM fluctuations. Here we present an exactly solvable model of such an evolution, which is able to describe continuous transformation of "large" ARPES Fermi surface with typical "Fermi arcs" at high-enough temperatures into a collection of "small" hole-like and electron-like "pockets", which form due to electron interaction with fluctuations of SDW (CDW) short-range order at low temperatures (in the absence of any kind of AFM (or charge) long-range order). We also formulate a qualitative criterion for observability of quantum oscillation effects in high-magnetic field in this, rather unusual, situation.

[1)] e-mail: sadovski@iep.uran.ru

We believe that the preferable "scenario" for pseudogap formation can be most likely based on the picture of strong scattering of the charge carriers by short–ranged antiferromagnetic (AFM, SDW) spin fluctuations [2, 3], i.e. fluctuations of the order parameter competing with superconductivity. In momentum representation this scattering transfers momenta of the order of $\mathbf{Q} = (\pi/a, \pi/a)$ (a – lattice constant of two dimensional lattice). This leads to the formation of structures in the one-particle spectrum, which are precursors of the changes in the spectra due to long–range AFM order (period doubling). As a result we obtain non–Fermi liquid like behavior of the spectral density in the vicinity of the so called "hot spots" on the Fermi surface, appearing at intersections of the Fermi surface with antiferromagnetic Brillouin zone boundary [2, 3], which in the low temperarure (large correlation length of the short-range order) can lead to a significant Fermi surface reconstruction, similar to that appearing in the case of AFM long-range order.

Within this approach we have already demonstrated [13, 14] the formation of "Fermi arcs" at high-enough temperatures, when AFM fluctuations can be effectively considered as static and Gaussian [15, 16]. Here we present an exactly solvable model, quite similar to that analyzed qualitatively in Ref. [12], which is capable to describe a crossover from "Fermi arc" picture at high temperatures (typical for most of ARPES experiments) to that of small "pockets" at low temperatures (typical for quantum oscillation experiments).

We shall consider a two – dimensional generalization of an exactly solvable model proposed in one – dimen-

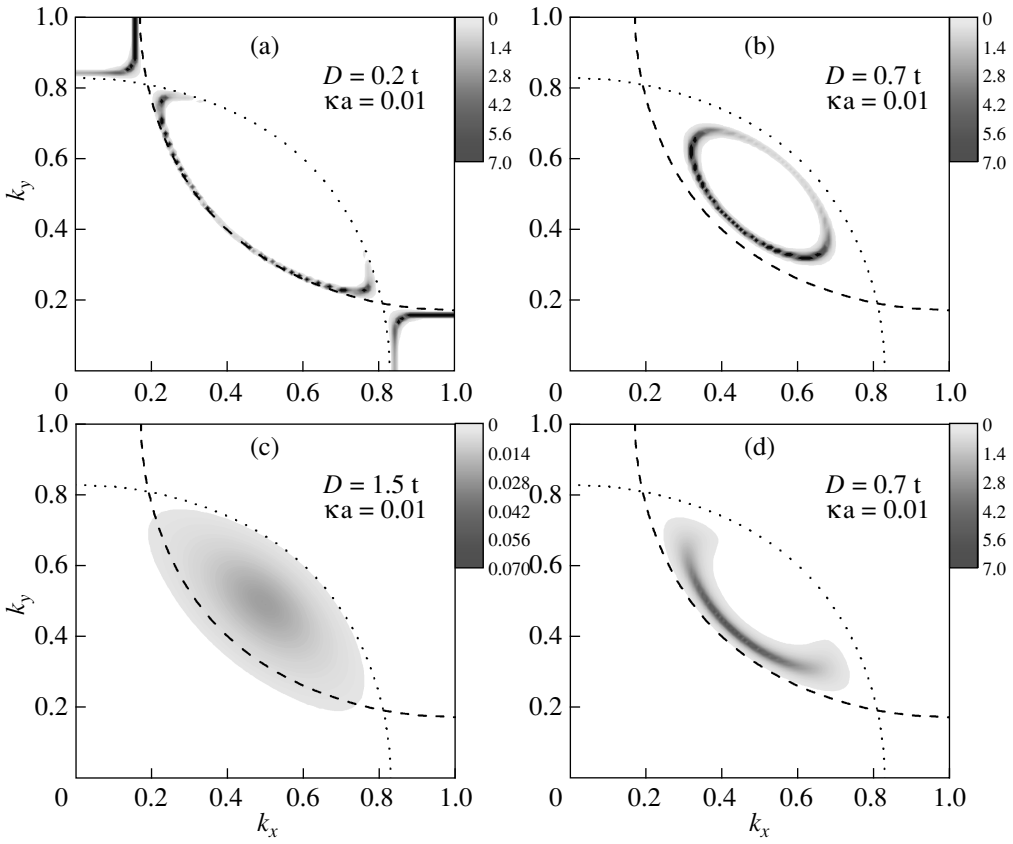

Fig.1. Reconstruction of the Fermi surface in the low temperature (large correlation length) regime of pseudogap fluctuations ($n = 0.9$, $t'/t = -0.4$. Shown are intensity plots of spectral density for $\varepsilon = 0$: (a) – $D = 0.2t$, $\kappa a = 0.01$; (b) – $D = 0.7t$, $\kappa a = 0.01$; (c) – $D = 1.5t$, $\kappa a = 0.01$; (d) – $D = 0.7t$, $\kappa a = 0.1$. Dashed line denotes "bare" Fermi surface, dotted line – shadow Fermi surface

sion in Ref. [17] (and also analyzed in a simplified two-dimensional approach in Ref. [18]), which is physically equivalent to the model of Ref. [12], but can produce a complete picture of Fermi surface reconstruction and formation of both hole and electron "pockets".

We consider electrons in two-dimensional square lattice with nearest (t) and next nearest (t') neighbour hopping integrals, which leads to the usual "bare" dispersion:

$$\varepsilon(\mathbf{k}) = -2t(\cos k_x a + \cos k_y a) - 4t' \cos k_x a \cos k_y a - \mu, \quad (1)$$

where a is the lattice constant, μ – chemical potential, and assume that these electrons are scattered by the following (static) random field, imitating AFM(SDW) (or similar CDW) short-range order:

$$V(\mathbf{l}) = D \exp(i\mathbf{Q}\mathbf{l} - i\mathbf{q}\mathbf{l}) + D^* \exp(-i\mathbf{Q}\mathbf{l} + i\mathbf{q}\mathbf{l}), \quad (2)$$

where $\mathbf{l} = (n_x a, n_y a)$ numerates lattice sites and $D = |D|e^{i\phi}$ denotes the complex amplitude of fluctuating SDW (or CDW) order parameter, while $\mathbf{q} = (q_x, q_y)$ is a small deviation from the dominating scattering vector $\mathbf{Q} = (Q_x, Q_y) = (\frac{\pi}{a}, \frac{\pi}{a})$.

Generalizing the approach of Refs. [17, 18] (compare with Ref. [12]) we consider a specific model of disorder, where both q_x and q_y are random and distributed according to:

$$\mathcal{P}(q_x, q_y) = \frac{1}{\pi^2} \frac{\kappa}{q_x^2 + \kappa^2} \frac{\kappa}{q_y^2 + \kappa^2}, \quad (3)$$

where $\kappa = \xi^{-1}$ is determined by the inverse correlation length of short-range order. Phase ϕ is also considred to be random and distributed uniformly on the interval $[0, 2\pi]$.

Factorized form of (3) is not very important physically, but allows for an analytic solution for the Green' function which takes the form [18]:

$$G_D(\varepsilon, \mathbf{k}) = \frac{\varepsilon - \varepsilon(\mathbf{k} + \mathbf{Q}) + iv\kappa}{(\varepsilon - \varepsilon(\mathbf{k}))(\varepsilon - \varepsilon(\mathbf{k} + \mathbf{Q}) + iv\kappa) - |D|^2}, \quad (4)$$

$$v = |v_x(\mathbf{k} + \mathbf{Q})| + |v_y(\mathbf{k} + \mathbf{Q})|, \; v_{x,y}(\mathbf{k}) = \frac{\partial \varepsilon(\mathbf{k})}{\partial k_{x,y}}.$$

Spectral density $A(\varepsilon,\mathbf{k}) = -\frac{1}{\pi}\mathrm{Im}\,G_D(\varepsilon,\mathbf{k})$ at the Fermi level ($\varepsilon = 0$), is shown in Fig.1, and demonstrate the formation of small "pockets" instead of large "bare" Fermi surface. Here and in the following we have assumed rather typical (for cuprates) values of $t'/t = -0.4$ and doping $n = 0.9$ (10% hole doping), corresponding to $\mu = -1.08t$.

The poles of the Green's function (4), determining the quasiparticle dispersion and damping the limit of large enough correlation length ($v\kappa \ll t$, low temperature), are given by:

$$\tilde{E}^{(\pm)} = E^{(\pm)}_{\mathbf{k}} - i\frac{v\kappa}{2}\left(1 \mp \frac{\varepsilon^{(-)}_{\mathbf{k}}}{E_{\mathbf{k}}}\right), \qquad (5)$$

with $\varepsilon^{(\pm)}_{\mathbf{k}} = \frac{1}{2}[\varepsilon(\mathbf{k}) \pm \varepsilon(\mathbf{k}+\mathbf{Q})]$, $E_{\mathbf{k}} = \sqrt{\varepsilon^{(-)2}_{\mathbf{k}} + |D|^2}$, and

$$E^{(\pm)}_{\mathbf{k}} = \varepsilon^{(+)}_{\mathbf{k}} \pm \sqrt{\varepsilon^{(-)2}_{\mathbf{k}} + |D|^2} \qquad (6)$$

which is just the same as dispersion in the case of the presence of long-range AFM order. Equation $E^{(-)}_{\mathbf{k}} = 0$ determines the hole "pocket" of the Fermi surface, around the point $(\frac{\pi}{2a}, \frac{\pi}{2a})$ in the Brillouin zone, while $E^{(+)}_{\mathbf{k}} = 0$ defines the electronic "pockets", centered around $(\frac{\pi}{a}, 0)$ and $(0, \frac{\pi}{a})$, as shown in Fig.1a.

Quasiparticle damping as given by the imaginary part of (5) is, in fact, changing rather drastically as particle moves around the "pocket" of the Fermi surface. Being practically zero in the nearest to point $\Gamma = (0,0)$ nodal (i.e. on the diagonal of the Brillouin zone) point of this trajectory on the hole "pocket", it becomes of the order of $\approx v^n_F\kappa$ in the far (from Γ) nodal point. Here we have introduced $v^n_F = |v_x(\mathbf{k}|) + |v_y(\mathbf{k})||_{\varepsilon(\mathbf{k})=0, k_x=k_y}$ – particle velocity at the nodal point of the "bare" Fermi surface. On the trajectory around the electronic "pocket" quasiparticle damping changes from nearly zero near the crossing points of the "bare" Fermi surface with Brillouin zone boundary up to $\approx v^a_F\kappa$ at points close to the similar crossing points of the "shadow" Fermi surface. Here $v^a_F = |v_x(\mathbf{k}|) + |v_y(\mathbf{k})||_{\varepsilon(\mathbf{k})=0, k_x=\frac{\pi}{a}}$ is the velocity in the antinodal point of "bare" Fermi surface.

Of course, the complete theory of quantum (Shubnikov – de Haas or de Haas – van Alfen) oscillations for such peculiar situation can be rather complicated. However, a rough qualitative criterion for the observability of quantum oscillations in our model can be easily formulated as follows. Effective width of spectral densities in our model, which determines smearing of the Fermi surfaces, can be roughly compared to impurity scattering contribution to Dingle temperature and estimated as $\tau^{-1} \sim < v_F > /\xi$, where $< v_F >$ is the velocity averaged over the Fermi surface. In fact it gives a kind of the upper boundary to pseudogap scattering rate in our model. Then our criterion takes the obvious form:

$$\omega_H \frac{\xi}{< v_F >} \sim \frac{\omega_H}{t}\frac{\xi}{a} \gg 1, \qquad (7)$$

where ω_H is the usual cyclotron frequency.

As the most unfavourable estimate (overestimating the effective damping) we take:

$$< v_F >= \begin{cases} v^n_F \text{ for hole "pocket"} \\ v^a_F \text{ for electronic "pocket"} \end{cases}. \qquad (8)$$

Experimentally oscillations become observable in magnetic fields larger than 50 T [8–11]. Taking the large correlation length $\xi = 100\,a$ and magnetic field H =50T we get $\omega_H\tau \approx 0.8$ for hole "pocket" and $\omega_H\tau \approx 1.3$ for electronic "pockets" in our model. Thus we need rather large values of correlation length $\xi \sim 50 - 100\,a$ for oscillations to be observable. However, this value may be smaller in the case of cyclotron mass larger than the mass of the free electron used in the above estimates.

From Luttinger theorem it follows that the number of electrons per cell is given by $n = 2a^2\frac{S_{fs}}{\pi^2}$, where S_{fs} is the area of the "bare" Fermi surface ($\varepsilon(\mathbf{k}) = 0$) in the quarter of the Brillouin zone. Similarly, we can determine this concentration as $n = 2a^2\frac{S_{sh}}{\pi^2}$ calculating the area S_{sh} of the "shadow" Fermi surface ($\varepsilon(\mathbf{k}+\mathbf{Q}) = 0$)

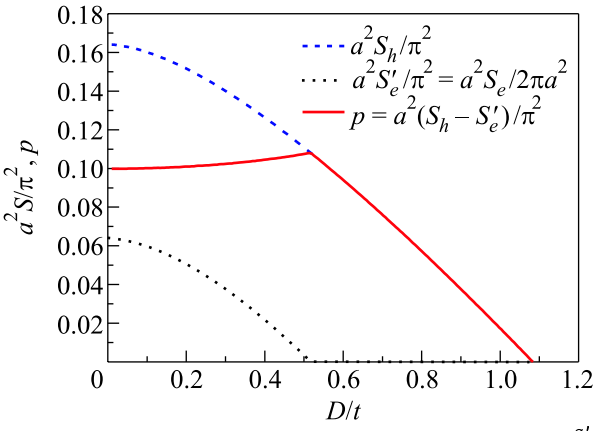

Fig.2. The area of hole ($a^2\frac{S_h}{\pi^2}$) and electronic ($a^2\frac{S'_e}{\pi^2}$) "pockets" in the quarter of Brillouin zone and "doping" $p = a^2\frac{(S_h - S'_e)}{\pi^2}$ as fuctions of the pseudogap amplitude D/t ($n = 0.9$ ($\mu = -1.08t$), $t'/t = -0.4$)

around the point $M(\frac{\pi}{a}, \frac{\pi}{a})$. Obviously $S_{sh} = S_{fs}$. Then, in the limit of $|D| \to 0$, for hole doping we get [19, 20]:

$$p = 1 - n = a^2\frac{S_h - S'_e}{\pi^2} = a^2\frac{S_h - S_e/2}{\pi^2}, \qquad (9)$$

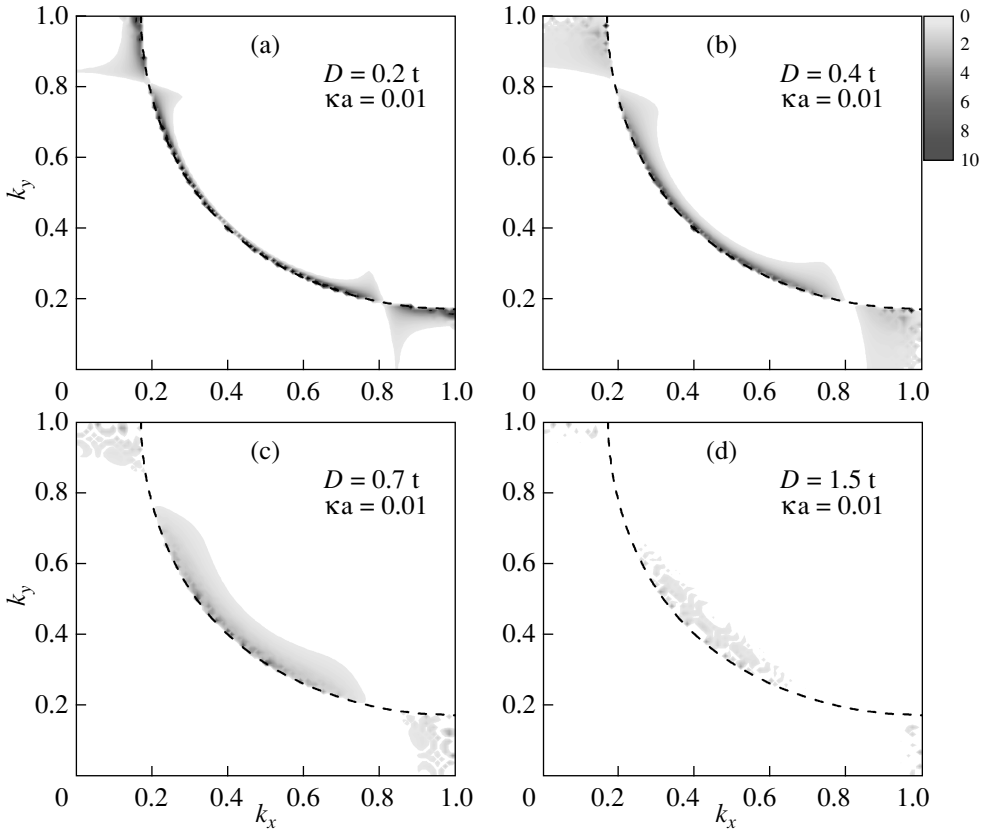

Fig.3. Formation of the Fermi "arcs" in the high-temperature regime of pseudogap fluctuations ($n = 0.9$, $t'/t = -0.4$, $\kappa a = 0.01$). Shown are intensity plots of spectral density for $\varepsilon = 0$. (a) – $\Delta = 0.2t$; (b) – $\Delta = 0.4t$; (c) – $\Delta = 0.7t$; (d) – $\Delta = 1.5t$; Dashed line denotes "bare" Fermi surface

where S_h is the area of hole "pocket" and S'_e is the area of the parts of electronic pocket inside the quarter of the Brillouin zone (which is a half of the total area of electronic "pocket" S_e).

However, these expressions are valid only for $|D| \to$ $\to 0$. With the growth of the pseudogap amplitude $|D|$ the area of both hole and electronic "pockets" diminish (as can be seen from Fig.1 and Fig.2). In the presence of electronic "pocket" this suppression of the area of both "pockets" compensate each other, leaving the doping given by Eq. (9) almost unchanged (Fig.2). After the disappearance of electronic "pocket", taking place at $|D| = \mu - 4t' = 0.52t$ (i.e. when $E^{(+)}_{\mathbf{k}=(\pi/a,0)} = 0$), there is no way to compensate the suppression of the area the hole "pockets" with the growth of $|D|$ and the number of carriers, determined by (9), will also be suppressed, going to zero with the disappearance of the hole "pocket", taking place at $|D| = -\mu = 1.08t$ (which is defined by $E^{(-)}_{\mathbf{k}=(\pi/2a,\pi/2a)} = 0$) and dielectric (AFM) gap "closes" the whole Fermi surface (Fig.1c). Thus, the doping calculated according to Eq. (9) in the case of large enough pseudogap amplitude (in the absence of electronic "pocket") will be significantly underestimated.

Experimentally, only one frequency of quantum oscillations $F \approx 540T$ was observed in YBCO [9]. Assuming it corresponds to the presence of only the hole "pocket", we obtain for the area of this "pocket" $a^2 S_h/\pi^2 = 0.078$, which, according to Fig.2 corresponds to $|D| \approx 0.7t$.

Green's function (4) describes the "low temperature" regime of pseudogap fluctuations, when the amplitude fluctuations of the random field (2) are "frozen out". In the "high temperature" regime both the phase and the amplitude $|D|$ of (2) are fluctuating. Assuming these fluctuations Gaussian we take the probability distribution of amplitude fluctuations given by Rayleigh distribution [18]:

$$\mathcal{P}_D(|D|) = \frac{2|D|}{\Delta^2} exp\left(-\frac{|D|^2}{\Delta^2}\right). \qquad (10)$$

Then the averaged Green's function takes the form:

$$G_\Delta(\varepsilon, \mathbf{k}) = \int_0^\infty d|D| \mathcal{P}_D(|D|) G_D(\varepsilon, \mathbf{k}). \qquad (11)$$

Profiles of the spectral density at the Fermi level ($\varepsilon = 0$), corresponding to (11) and different values of the pseudogap width Δ are shown in Fig.3. The growth of the pseudogap width leads to the "destruction" of the Fermi surface close to Brillouin zone boundaries and formation of typical Fermi "arcs", qualitatively (and quantitatively) similar to that obtained in our previous work [13, 14] and in accordance with the results of ARPES experiments, which are typically done at much higher temperatures, than experiments on quantum fluctuations.

This work is supported by RFBR grant # 08-02-00021 and RAS programs "Quantum macrophysics" and "Strongly correlated electrons in semiconductors, metals, superconductors and magnetic materials". MVS is gratefully acknowledges a discussion with L. Taillefer at GRC'07 Conference on Superconductivity, which stimulated his interest in this problem.

1. T. Timusk and B. Statt, Rep. Progr. Phys, **62**, 61 (1999).
2. M. V. Sadovskii, Usp. Fiz. Nauk **171**, 539 (2001) [Physics – Uspekhi **44**, 515 (2001)].
3. M. V. Sadovskii, *Models of the pseudogap state in high-temperature superconductors*. In *"Strings, branes, lattices, networks, pseudogaps and dust"*, Scientific World, Moscow, 2007, p. 357 (in Russian); arXiv: cond-mat/0408489.
4. M. R. Norman, D. Pines, and C. Kallin, Adv. Phys. **54**, 715 (2007)
5. M. R. Norman, H. Ding, J. C. Campuzano et al., Nature **392**, 157 (1998).
6. A. Damascelli, Z. Hussain, and Z.-X. Shen. Rev. Mod. Phys. **75**, 473 (2003).
7. J. C. Campuzano, M. R. Norman, and M. Randeria. In *"Physics of Superconductors"*, Vol. II, Ed. K. H. Bennemann and J. B. Ketterson, Springer, Berlin 2004, p. 167.
8. N. Doiron-Leyraud, C. Proust, D. LeBoeuf et al., Nature **447**, 565 (2007).
9. A. F. Bangura, J. D. Fletcher, A. Carrington et al., Phys. Rev. Lett. **100**, 047004 (2008).
10. C. Jaudet, D. Vignolles, A. Audouard et al., Phys. Rev. Lett. **100**, 187005 (2008).
11. D. LeBoeuf, N. Doiron-Leyraud, J. Levallois et al., Nature **450**, 533 (2007).
12. N. Harrison, R. D. McDonald, and J. Singleton, Phys. Rev. Lett. **99**, 206406 (2007).
13. E. Z. Kuchinskii, I. A. Nekrasov, and M. V. Sadovskii, Pisma Zh. Eksp. Teor. Fiz. **82**, 217 (2005) [JETP Lett. **82**, 198 (2005)].
14. E. Z. Kuchinskii and M. V. Sadovskii, Zh. Eksp. Teor. Fiz. **130**, 477 (2006) [JETP **103**, 415 (2006)].
15. E. Z. Kuchinskii and M. V. Sadovskii, Zh. Eksp. Teor. Fiz. **115**, 1765 (1999) [JETP **88**, 347 (1999)].
16. J. Schmalian, D. Pines, and B. Stojkovic, Phys. Rev. B **60**, 667 (1999).
17. L. Bartosch and P. Kopietz, Eur. J. Phys. B **17**, 555 (2000).
18. E. Z. Kuchinskii and M. V. Sadovskii, Zh. Eksp. Teor. Fiz. **121**, 758 (2002) [JETP **94**, 654 (2002)].
19. S. Chakravarty and H.-Y. Kee. arXiv: 0710.0608.
20. T. Morinari. arXiv: 0805.1977.

Pis'ma v ZhETF, vol. 89, iss. 3, pp. 176 – 180

Multiple bands – a key to high-temperature superconductivity in iron arsenides?

E. Z. Kuchinskii[1)], *M. V. Sadovskii*[1)]

Institute for Electrophysics, Ural Division RAS, 620016 Ekaterinburg, Russia

Submitted 11 Januar 2009

In the framework of four-band model of superconductivity in iron arsenides proposed by Barzykin and Gor'kov we analyze the gap ratios on hole – like and electron – like Fermi – surface cylinders. It is shown that experimentally observed (ARPES) gap ratios can be obtained only within rather strict limits on the values of pairing coupling constants. The difference of T_c values in 1111 and 122 systems is reasonably explained by the relative values of partial densities of states. The multiple bands electronic structure of these systems leads to a significant enhancement of effective pairing coupling constant determining T_c, so that high enough T_c values can be achieved even for the case of rather small intraband and interband pairing interactions.

PACS: 74.20.-z, 74.20.Fg, 74.20.Mn, 74.20.Rp

The discovery of high-temperature superconductivity in layered FeAs compounds stimulated active experimental and theoretical studies of these new superconductors [1]. The main anomaly of these systems is their multiple bands nature. Electronic structure in a narrow enough energy interval around the Fermi level is formed almost only from the d – states of Fe. In fact, electronic spectrum of iron arsenides was calculated in a number of papers [2 – 6]. The Fermi surface consists of several hole – like and electron – like cylinders and on each of these its "own" superconducting gap can be formed. In the energy interval relevant to superconductivity electronic spectrum is especially simple [7 – 9]. It was used by Barzykin and Gor'kov to formulate a simple (analytic) model of superconducting state of new superconductors [10].

Schematically, the simplified electronic spectrum and Fermi surfaces of these systems are shown in Fig.1 [10]. There are two hole – like Fermi surface cylinders surrounding the Γ point and two electronic pockets around X and Y points in extended Brillouin zone.

Let Δ_i be a superconducting order – parameter (gap) on the i-th sheet of the Fermi surface. The value of Δ_i is determined by self – consistency equation for the anomalous Gor'kov Green's function.

Pairing BCS-like interaction can be represented by a matrix:

$$V = \begin{pmatrix} u & w & t & t \\ w & u' & t & t \\ t & t & \lambda & \mu \\ t & t & \mu & \lambda \end{pmatrix} \qquad (1)$$

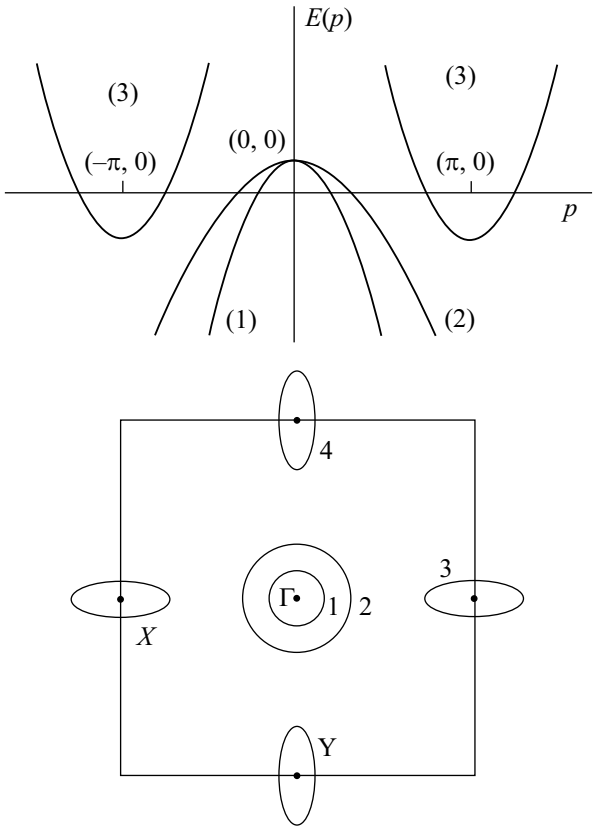

Fig.1. Schematic electronic spectrum and Fermi surfaces of FeAs superconductor in the extended band picture. There are two hole-like cylinders around point Γ, while electron-like cylinders are around X (Y) points [10]

where matrix elements $V^{i,j}$ define intraband and interband pairing coupling constants. For example, $\lambda = V^{eX,eX} = V^{eY,eY}$ determines pairing interactions on the same electronic pocket at point X or Y, $\mu = V^{eX,eY}$

[1)] e-mail: kuchinsk@iep.uran.ru; sadovski@iep.uran.ru

connects electrons of different pockets at these points, $u = V^{h1,h1}$, $u' = V^{h2,h2}$ and $w = V^{h1,h2}$ characterize BCS interactions within two hole – like pockets – the small one ($h1$) and the large one ($h2$), as well as between these pockets, while $t = V^{h,eX} = V^{h,eY}$ couple electrons at points X and Γ. In Ref. [10] it was assumed that $u = u' = w$. This assumption seems to be too strong and below we analyze the general case.

Superconducting critical temperature T_c is determined by an effective pairing coupling constant g_{eff}:

$$T_c = \frac{2\gamma\omega_c}{\pi} e^{-1/g_{\text{eff}}}, \tag{2}$$

where ω_c is the usual cut – off frequency in Cooper channel (assumed to be the same for all types of couplings under consideration – a simplification!), while g_{eff} in this model is defined by the solution of the system of linearized gap equations:

$$g_{\text{eff}}\Delta_i = \sum_j g_{ij}\Delta_j, \tag{3}$$

where

$$g_{ij} \equiv -V^{i,j}\nu_j, \quad g_{\text{eff}}^{-1} = \ln\frac{2\gamma}{\pi}\frac{\omega_c}{T_c}. \tag{4}$$

The matrix of dimensionless coupling constants g_{ij} is determined by matrix elements of (1) and partial densities of states on different Fermi surface cylinders – ν_j is density of states per single spin projection on the j-th cylinder.

From symmetry it is clear that $\nu_3 = \nu_4$ and the system (3) possesses solutions of two types [10]:

1) solution corresponding to $d_{x^2-y^2}$ symmetry, when gaps on different pockets at points X and Y differ by sign, while gaps on hole-like pockets are just zero:

$$\Delta_1 = \Delta_2 = 0, \quad \Delta_3 = -\Delta_4 = \Delta, \tag{5}$$

and

$$g_{\text{eff}} = (\mu - \lambda)\nu_3. \tag{6}$$

2)solutions corresponding to the so called $s^{\pm}$ pairing [3], for which gaps on the cylinders at points X and Y are equal to each other: $\Delta_3 = \Delta_4$, while gaps on Fermi surfaces surrounding the point Γ are of different sign in case of repulsive interaction between electron-like and hole-like pockets ($t > 0$), and of the same sign for the case of $t < 0$.

As in this case we have $\Delta_3 = \Delta_4$ and $\nu_3 = \nu_4$, two equations in (3) just coincide and instead of (1), (4) we are dealing with 3×3 matrix of coupling constants of the following form:

$$-\hat{g} = \begin{pmatrix} u\nu_1 & w\nu_2 & 2t\nu_3 \\ w\nu_1 & u'\nu_2 & 2t\nu_3 \\ t\nu_1 & t\nu_2 & 2\bar{\lambda}\nu_3 \end{pmatrix}, \tag{7}$$

where $\bar{\lambda} = (\lambda + \mu)/2$ and (3) reduces to the standard problem of finding eigenvalues and eigenvectors for the matrix of dimensionless couplings g_{ij} (7), which has three solutions, determined by cubic secular equation:

$$\text{Det}(g_{ij} - g_{eff}\delta_{ij}) = 0. \tag{8}$$

Physical solution corresponds to a maximal positive value of g_{eff}, which determines the highest value of T_c.

Under the simple assumption of Ref. [10], when $u = u' = w$, situation simplifies further, as in (3) only two independent equations remain, so that we have 2×2 matrix of coupling constants and (8) reduces to a quadratic equation. Then we easily obtain [10]:

$$\Delta_1 = \Delta_2 = \kappa\Delta, \quad \Delta_3 = \Delta_4 = \Delta, \tag{9}$$

where $\kappa^{-1} = -(g_{\text{eff}} + u(\nu_1 + \nu_2))/t\nu_3$, and maximal effective pairing constant is given by:

$$2g_{\text{eff}} = -u(\nu_1 + \nu_2) - 2\bar{\lambda}\nu_3 + \\ + \sqrt{(u(\nu_1 + \nu_2) - 2\bar{\lambda}\nu_3)^2 + 8t^2\nu_3(\nu_1 + \nu_2)}. \tag{10}$$

Possibility of $s^{\pm}$-pairing in FeAs compounds was first noted in Ref. [3]. This kind of solution qualitatively agrees with ARPES data of Refs. [11–13], except the result $\Delta_1 = \Delta_2$ (9), which contradicts the established experimental fact – the gap on the small hole-like cylinder Δ_1 is approximately twice as large as the gap Δ_2 on the large cylinder. In fact, this contradiction is basically due to an unnecessary limitation to the case of $u = u' = w$ used in Ref. [10].

The system of linearized gap equations determines their ratios on different sheets of the Fermi surface for temperatures $T \to T_c$. In general case, the temperature dependence of gaps is determined by the generalized BCS equations:

$$\Delta_i = \sum_j g_{ij}\Delta_j \int_0^{\omega_c} d\xi \frac{\text{th}\dfrac{\sqrt{\xi^2 + \Delta_j^2}}{2T}}{\sqrt{\xi^2 + \Delta_j^2}}. \tag{11}$$

For $T \to 0$ these equations take the form:

$$\Delta_i = \sum_j g_{ij}\Delta_j F\left(\frac{\Delta_j}{\omega_c}\right), \tag{12}$$

where we have introduced $F(x) = \ln\left(\frac{1+\sqrt{1+x^2}}{|x|}\right)$.

Below we present the results of numerical studies of Eqs. (3) and (12) for typical values of parameters (couplings).

Let us denote the pairing coupling constant on a small hole-like cylinder as $g = g_{11}$. In the following we take $g = 0.2$, which allows us to remain within the limits of weak coupling approximation.

The ratio of partial densities of states for different Fermi surface cylinders in quasi-two-dimensional case can be approximated by effective mass ratio on the same cylinders. These can be estimated from the data for electronic dispersions in symmetric directions in the Brillouin zone, obtained in LDA calculations [7–9]. For REOFeAs series (RE=La,Ce,Nd,Pr,Sm...) (1111) and for $BaFe_2As_2$ (122) from these data we get:

$$\begin{array}{lll} \dfrac{\nu_2}{\nu_1} \approx 1.18, & \dfrac{\nu_3}{\nu_1} \approx 0.64, & \text{for 1111,} \\ \dfrac{\nu_2}{\nu_1} \approx 1.26, & \dfrac{\nu_3}{\nu_1} \approx 0.34, & \text{for 122.} \end{array} \qquad (13)$$

We suppose that pairing interactions on hole-like cylinders and between them, as well as on electron-like cylinders and between them, are most probably determined by electron-phonon interaction, the relevance of which is clearly demonstrated by rather strong isotope effect, observed in Ref. [14]. At the same time, interband pairing interaction between hole-like and electron-like cylinders is probably due to antiferromagnetic fluctuations and is repulsive ($t > 0$). It should be noted that parameter t from coupling constants matrix (7) enters Eq. (8), determining g_{eff}, only via t^2, i.e. independent of sign. Thus its sign does not change the value of an effective pairing coupling constant and that of T_c. Repulsion between quasiparticles on hole-like and electron-like cylinders does not suppress, but actually enhances superconductivity leading to the increase of g_{eff}. Also the sign change of t does not change the absolute values of gaps on different cylinders, though the repulsion between electron-like and hole-like cylinders ($t > 0$) leads to different signs of gaps at these cylinders, while for the case of $t < 0$ both gaps acquire the same sign.

Despite rather large number of free parameters of the model it is not easy to obtain the observable (in ARPES experiments of Refs. [11–13]) values of the ratios $|\Delta_2/\Delta_1| \approx 0.5$ and $|\Delta_3/\Delta_1| \approx 1$. In fact it requires small enough attraction (or even repulsion, $u' > 0$) on the "large" hole-like cylinder (cf. Fig.2). In the following we assume the ratios of pairing coupling constants as $w/u = 1$, $t/u = -1$, $\bar{\lambda}/u = 1$, which guarantees us the ratio $|\Delta_3/\Delta_1| = 1$ for any values of u' and arbitrary ratios of partial densities of states at different cylinders. Another choice of pairing couplings producing $|\Delta_3/\Delta_1| = 1$ is also possible, but in general we need larger repulsion on "large" hole-like cylinder to get $|\Delta_2/\Delta_1| \approx 0.5$. In Fig.2 we show the dependences of the gap ratios at $T = 0$ on u'/u, obtained from (12), using the partial density of states ratios on different cylinders (13), characteristic for (1111) and (122) systems. The gap ratios for $T \to T_c$ differ from the values obtained at $T = 0$ rather insignificantly.

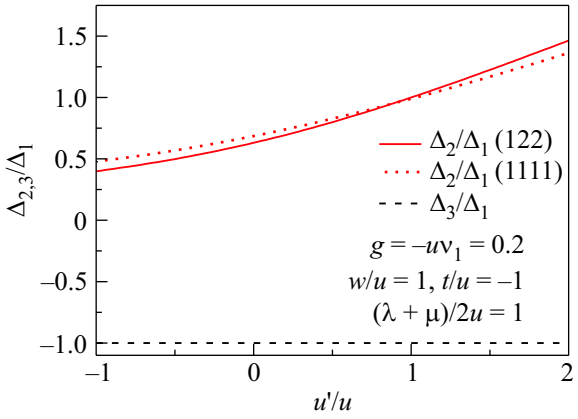

Fig.2. Dependence of gap ratios on different pockets of the Fermi surface on u'/u for $g = 0.2$, $w/u = 1$, $t/u = -1$, $\bar{\lambda}/u = 1$ and partial density of states ratios given by (13)

In Ref. [15] a two-band model with two hole-like cylinders was analyzed, assuming that only interband coupling exists, i.e. the coupling constants matrix has the form:

$$-g_{ij} = \begin{pmatrix} 0 & w\nu_2 \\ w\nu_1 & 0 \end{pmatrix}. \qquad (14)$$

Under this assumption the gap ratio on hole-like cylinders is given by:

$$\frac{\Delta_2}{\Delta_1} = \sqrt{\frac{\nu_1}{\nu_2}} \qquad (15)$$

so that for characteristic for $BaFe_2As_2$ value of $\nu_2/\nu_1 \approx \approx 1.26$ we obtain $\Delta_1/\Delta_2 \approx 1.12$, which is significantly lower than the experimentally observed value of [11] $\Delta_1/\Delta_2 \approx 2$.

Four-band model somehow similar to that considered above was analyzed in Ref. [16], where temperature dependences of gaps (with proper ratios) on different sheets of the Fermi surface were calculated along with the temperature dependence of superfluid electron density. However, in this work no analysis was made of the important role of multiple bands structure for the increase of T_c, which we shall discuss shortly.

In Fig.3 we show the dependence of an effective pairing coupling constant and superconducting critical temperature on u'/u for both classes of FeAs systems (1111 and 122). It is clearly seen that the effective coupling

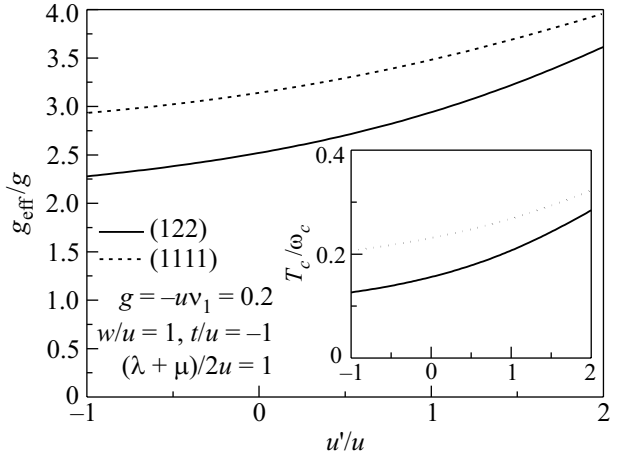

Fig.3. Dependence of effective pairing coupling constant on u'/u for $g = 0.2$, $w/u = 1$, $t/u = -1$, $\bar{\lambda}/u = 1$ and partial density of states ratios on different Fermi surface pockets given by (13). At the insert – similar dependence of the critical temperature

constant $g_{\rm eff}$ is significantly larger than the pairing constant g on the small hole-like cylinder. It can be said that coupling constants from different cylinders effectively produce "additive" effect. In fact this can lead to high enough values of T_c even for relatively small values of intraband [2] and interband pairing constants. Actually, using this type of estimates we can convince ourselves that the critical temperature for superconducting transition with $d_{x^2-y^2}$ gap symmetry, which is determined by an effective pairing constant given by (6), is always smaller (for typical values of parameters) than the critical temperature for $s^{\pm}$ pairing.

To clarify the reasons for the growth of effective pairing coupling it is helpful to analyze the most simple case, when all pairing interactions (both intraband and interband) in (1) are just the same (and equal e.g. to u), and all partial densities of states on all four Fermi surface pockets are also the same (and equal e.g. to ν_1). In this case we obtain $g_{\rm eff} = 4g = -4u\nu_1$, which simply corresponds to the fact that now the total density of states at the Fermi level is four times partial. However, in real situation the growth of an effective pairing constant does not reduce to this simple summation of partial densities of states. In particular, the effective pairing coupling may be much larger than the simple sum of intraband (diagonal) dimensionless coupling constants, e.g. in case of significant interband pairing interaction, which can be present in iron arsenides, where the pairing interaction between electron-like and hole-like cylinders is most probably attributed to antiferromagnetic fluctuations.

It can be estimated that with the same values of interaction constants in (1) the critical temperature in 1111-type systems is typically larger than in 122 just due to the difference of partial densities of states as given in (13) (cf. insert in Fig.3). For example, in case of $u'/u = 0$ (with the values of parameters for 122-system we get the ratio of gaps $\Delta_2/\Delta_1 \approx 0.6$) the calculated ratio of critical temperatures of 122 and 1111 systems $T_c(122)/T_c(1111) = 0.67$ is very close to the observed ration of maximal critical temperatures obtained for these systems: 38 K/55 K≈ 0.69. Thus the typical difference of T_c's for both classes of new superconductors can be attributed to the different values of partial densities of states on corresponding Fermi surface cylinders, despite the fact that total densities of states at the Fermi level in these systems are practically the same [7 – 9]. Of course, the accuracy obtained should not be taken too seriously, as in real systems rather strong renormalization effects of electronic spectrum (effective masses, bandwidths etc.) in comparison with the results of LDA calculations are definitely present (and observed in ARPES experiments), e.g. due to moderate or probably even strong enough Coulomb correlations [1]. The main conclusion following from our analysis is the simple fact that the value of T_c in multiple bands systems is determined by the relations between partial densities of states on different sheets of the Fermi surface, not by the total density of states at the Fermi level as in the standard BCS model.

It should be noted that for the first time (though only implicitly) the role of multiple bands structure of electronic spectrum as the reason for the increase of superconducting T_c was apparently discussed in relation to superconductivity in multivalley doped semiconductors [17, 18]. In these works the important role of interband electron-phonon pairing mechanism was also stressed. It was noted that such processes with large momentum transfer, leading to reduced screening, may be most relevant for the increase of T_c. This fact can be also important for new superconductors besides the abovementioned role of pairing due to spin fluctuations.

Direct experimental confirmation of the role of multiple bands in new superconductors follows from ARPES measurements on extremely (hole) overdoped system KFe_2As_2 with T_c=3 K [19] and similar heavily (electron) overdoped $BaFe_{1.7}Co_{0.3}As_2$ [20], where superconductivity is just absent. From these measurements it is clearly seen how the disappearance of electronic pockets in the first system and hole-like pockets in the second one leads to strong suppression or even the complete disappearance of T_c.

To conclude, on Fig.4 we show the dependence of $2\Delta/T_c$ ratio on different sheets of the Fermi surface on the ratio of coupling constants u'/u. Here it is important to note that the value of this characteristic

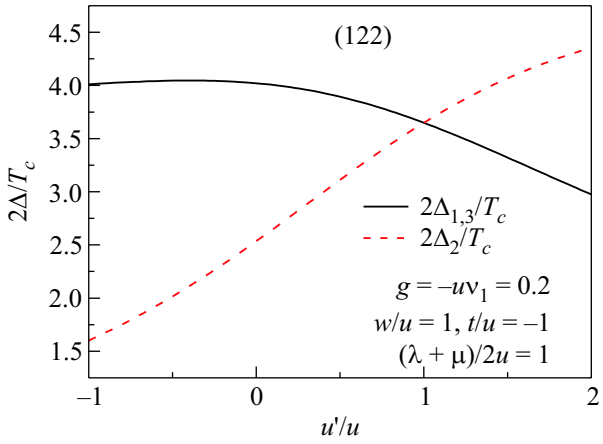

Fig.4. Dependence of $2\Delta/T_c$ ratio on u'/u for 122 – system with $g = 0.2$, $w/u = 1$, $t/u = -1$, $\bar{\lambda}/u = 1$ and partial densities of states ratios on different Fermi surface sheets, as given in (13)

ratio can be significantly different from the standard BCS value $2\Delta/T_c \approx 3.5$. However, the values shown in Fig.4 are much lower than the ratios observed in ARPES experiments [11–13], where the typical values are $2\Delta_{1,3}/T_c \approx 7.5$ and $2\Delta_2/T_c \approx 3.7$, which is apparently due to the strong coupling effects important in real systems. Our analysis was limited to the standard BCS-like weak coupling approach. Strong coupling Eliashberg-type analysis of multiple bands effects for new superconductors is yet to be done. Preliminary results on gap ratios in the strong coupling limit for the simple two-band model were derived in Ref. [15].

Authors are grateful to L.P. Gor'kov and E.G. Maksimov for stimulating discussions.

This work is partly supported by RFBR grant # 08-02-00021 and was performed within the framework of programs of fundamental research of the Russian Academy of Sciences (RAS) "Quantum physics of condensed matter" and of the Physics Division of RAS "Strongly correlated electrons in solid states".

1. M. V. Sadovskii, Uspekhi Fiz. Nauk **178**, 1243 (2008); Physics Uspekhi **51**, No. 12 (2008); arXiv: 0812.0302
2. L. Boeri, O. V. Dolgov, and A. A. Golubov, Phys. Rev. Lett. **101**, 026403 (2008); arXiv: 0803.2703v1.
3. I. I. Mazin, D. J. Singh, M. D. Johannes, and M. H. Du, Phys. Rev. Lett. **101**, 057003 (2008); arXiv: 0803.2740.
4. G. Xu, W. Ming, Y. Yao et al., Europhys. Lett. **82**, 67002 (2008); arXiv: 0803.
5. I. R. Shein and A. L. Ivanovskii, Pis'ma v ZhETF **88**, 115 (2008); arXiv: 0806.0750.
6. D. J. Singh, Phys. Rev. B **78**, 094511 (2008); arXiv: 0807.2643.
7. I. A. Nekrasov, Z. V. Pchelkina, and M. V. Sadovskii, Pis'ma v ZhETF **87**, 647 (2008); JETP Lett. **87**, 620 (2008); arXiv: 0804.1239.
8. I. A. Nekrasov, Z. V. Pchelkina, and M. V. Sadovskii, Pis'ma ZhETF **88**, 155 (2008); JETP Lett. **88**, 144 (2008); arXiv: 0806.2630.
9. I. A. Nekrasov, Z. V. Pchelkina, and M. V. Sadovskii, Pis'ma v ZhETF **88**, 621 (2008); JETP Lett. **88**, 543 (2008); arXiv: 0807.1010.
10. V. Barzykin and L. P. Gorkov, Pis'ma v ZhETF **88**, 142 (2008); arXiv: 0806.1993.
11. H. Ding, P. Richard, K. Nakayama et al., Europhys. Lett. **83**, 47001 (2008); arXiv: 0807.0419.
12. L. Eray, D. Qian, D. Hsiech et al., arXiv: 0808.2185.
13. D. V. Evtushinsky, D. S. Inosov, V. B. Zabolotnyy et al., arXiv: 0809.4455.
14. R. H. Liu, T. Wu, G. Wu et al., arXiv: 0810.2694.
15. O. V. Dolgov, I. I. Mazin, D. Parker, and A. A. Golubov, arXiv: 0810.1476.
16. L. Benfatto, M. Capone, S. Caprara et al., Phys. Rev. B **78**, 140502 (2008); arXiv: 0807.4408.
17. V. L. Gurevich, A. I. Larkin, and Yu. A. Firsov, Fiz. Tverd. Tela (Leningrad) **4**, 185 (1962).
18. M. L. Cohen. In "Superconductivity" (Ed. R. D. Parks), Marcel Dekker, New York, 1969.
19. T. Sato, K. Nakayama, Y. Sekiba et al., arXiv: 0810.3047.
20. Y. Sekiba, T. Sato, K. Nakayama et al., arXiv: 0812.4111.

ISSN 0021-3640, JETP Letters, 2010, Vol. 91, No. 10, pp. 518–522. © Pleiades Publishing, Inc., 2010.

Anion Height Dependence of T_c and the Density of States in Iron-Based Superconductors¶

E. Z. Kuchinskii, I. A. Nekrasov, and M. V. Sadovskii

Institute for Electrophysics, Ural Branch, Russian Academy of Sciences, Yekaterinburg, 620016 Russia

e-mail: kuchinsk@iep.uran.ru, nekrasov@iep.uran.ru, sadovski@iep.uran.ru

Received April 7, 2010

Systematic ab initio LDA calculations were performed for all the typical representatives of recently discovered class of iron-based high-temperature superconductors: REOFe(As,P) (RE = La, Ce, Nd, Sm, Tb), Ba_2Fe_2As, (Sr,Ca)FFeAs, $Sr_4Sc_2O_6Fe_2P_2$, LiFeAs and Fe(Se,Te). Non-monotonic behavior of total density of states at the Fermi level is observed as a function of anion height relative to Fe layer with maximum at about $\Delta z_a \sim 1.37$ Å, attributed to changing Fe–As (P, Se, Te) hybridization. This leads to a similar dependence of superconducting transition temperature T_c as observed in the experiments. The fit of this dependence to elementary BCS theory produces semiquantitative agreement with experimental data for T_c for the whole class of iron-based superconductors. The similar fit to Allen–Dynes formula underestimates T_c in the vicinity of the maximum, signifying the possible importance of non-phonon pairing in this region. These results unambiguously demonstrate that the main effect of T_c variation between different types of iron-based superconductors is due to the corresponding variation of the density of states at the Fermi level.

DOI: 10.1134/S0021364010100061

Recent discovery of the new class of iron-based high-temperature superconductors [1] has ignited almost unprecedented stream of experimental and theoretical studies (for the review of an early work see [2, 3]). Despite the immense progress in understanding of these systems, the nature (mechanism) of superconducting pairing, as well as the reasons for high values of superconducting temperature T_c, are still under debate. Mizuguhci et al. [4] have recently established an interesting anion height dependence of T_c for the typical representatives of Fe-based superconductors, demonstrating almost symmetric curve with a peak around $\Delta z_a \sim 1.37$ Å. Below we present an explanation of this dependence, attributing it to the effect of the appropriate variation of the total density of states at the Fermi level within standard BCS-like approach.

The main representatives of the class of iron-based superconductors (pnictides, chalcogenides) known at the moment are:

(i) Doped RE111 (RE = La, Ce, Pr, Nd, Sm, Tb, Dy) with T_c about 25–55 K, with most typical representatives such as $LaO_{1-x}F_xFeAs$ [1, 5–12] and $LaO_{1-x}F_xFeP$ [13] with much lower $T_c = 6.6$ K.

(ii) Doped A122 (A = Ba, Sr), such as $Ba_{1-x}K_xFe_2As_2$ [14–17] and T_c about 38 K.

(iii) $Li_{1-x}FeAs$ with $T_c = 18$ K [18, 19].

(iv) (Sr, Ca, Eu)FFeAs [20–22] with $T_c = 36$ K [23].

(v) $Sr_4(Sc,V)_2O_6Fe_2(P,As)_2$ with $T_c = 17$ K [24].

(vi) $FeSe_x$, $FeSe_{1-x}Te_x$ with T_c up to 14 K [25].

There is now a plenty of papers on LDA (local density approximation) calculation of the band structure of La111 [30–32], LaOFeP [33], RE111 series [26], $BaFe_2As_2$ [27, 34, 35], LiFeAs [28, 36], (Sr, Ca)FFeAs [29, 37], Sr42622 [38] and Fe(S, Se, Te) [39]. Below we present some of the results of our continued work on LDA electronic structure, along the lines of [26–29], covering all typical representatives of the whole class of iron-based superconductors and taking into account some new structural data.

Iron-based high-T_c superconductors in general have tetragonal structure with the space group $P4/nmm$ (RE1111, LiFeAs, Sr42622, Fe(Te, Se), SrFFeAs) and the space group $I4/mmm$ (Ba122). For the $P4/nmm$ systems Fe ions occupy positions (2b) (0.75, 0.25, 0.5), and anion ions A = P, As, Se, Te—(2c) (0.25, 0.25, z_a) and for Ba122 Fe(4d) (0.5, 0, 0.25), As(4e) (0, 0, z_a). Corresponding experimental lattice parameters and atomic coordinates (used in this work) are collected in Table 1.

Physically important electronic bands (those which cross the Fermi level) are formed by antibonding Fe($3d$)-A(p) states of FeA_4 tetrahedron layer. Here A denotes different types of anions: P, As, Se, Te. To calculate electronic structure of compounds listed in Table 1 linearized muffin-tin orbitals method

¶The article is published in the original.

Table 1. Experimental crystallographic data for iron-based superconductors

System	Δz_a, Å	a, Å	c, Å	z_{Re}	z_a	$\angle a$–Fe–a
LaOFeP	1.140	3.9636	8.5122	0.1487	0.6339	104.4
$Sr_4Sc_2O_6Fe_2P_2$	1.200	4.0160	15.5430	–	0.5772	105.2
LaOFeAs	1.320	4.0353	8.7409	0.1415	0.6512	107.5
CeOFeAs	1.354	3.9959	8.6522	0.1480	0.6565	108.4
SmOFeAs	1.357	3.9270	8.4413	0.1420	0.6608	108.8
NdOFeAs	1.367	3.9476	8.5446	0.1440	0.6600	110.5
TbOFeAs	1.373	3.8530	8.2990	0.1447	0.6654	109.7
SrFFeAs	1.369	4.0110	8.9650	0.1598	0.6527	108.6
$BaFe_2As_2$	1.371	3.9090	13.2122	–	0.3538	109.3
CaFFeAs	1.417	3.8780	8.5920	0.1505	0.6649	110.4
LiFeAs	1.505	3.7914	6.3642	0.8459	0.2635	112.7
Fe(Se, Te)	1.630	3.8215	6.2695	–	0.2599	111.5

(LMTO) [40] with default settings was employed (except for Re111 systems, where Re-4f states were taken as a pseudocore states). Obtained results are in good agreement with other LDA calculations by other authors.

Motivated by the results of [4] we present here our LDA calculated total density of states $N(E_F)$ as a function of anion height Δz_a with respect to Fe layer. Corresponding dependence is plotted in the figure with circles. We can see that $N(E_F)$ has an interesting behavior with clear maximum at about $\Delta z_a \sim 1.37$ Å (see also Table 2). Such nonmonotonic behavior can be explained by hybridization effects. Namely, as a governing structural parameter characterizing hybridization strength one can chose a-Fe-a angle—an angle between anions (a) and Fe within the same tetrahedron. The value of the angle corresponding to the strongest hybridization is 109.45°, i.e., for an ideal anion tetrahedron with Fe in the very center of it. Other crystal structure parameters which might be marked as important here such as Fe–Fe, Fe–a or a–a distances are not changed very much from system to system and do not have any transparent dependence of Δz_a. The values of these distances are about following 2.8, 2.4 and 3.85 Å with slight lowering for LaOFeP, LiFeAs and Fe(Te,Se) compounds.

From Table 1 one can see that compounds with highest $N(E_F)$ values have the a-Fe-a angle very close to this value. Decrease or increase of this angle leads to $N(E_F)$ drop from this maximum value. This comes from partial DOS behavior. The strongest hybridization corresponds to the strongest bonding-antibonding splitting. Since antibonding band DOS grows monotonically with binding energy [26–29] stronger hybridization will lead to higher values of $N(E_F)$. With lowering of hybridization bonding-antibonding splitting goes down together with $N(E_F)$.

The Δz_a dependence of $N(E_F)$ inevitably leads to the corresponding dependence of superconducting critical temperature T_c. To estimate this we, first of all, use the elementary BCS expression: $T_c = 1.14\omega_D e^{-1/\lambda}$, where ω_D is the characteristic frequency of collective excitations involved in pairing interaction (phonons, spin fluctuations, etc.), and $\lambda = gN(E_F)/2$ is the dimension-less pairing interaction constant (g is the appropriate dimensional coupling constant). In the following we take $\omega_D = 350$ K in rough accord with neutron scattering experiments on phonon density of states for La111 [41] and Ba122 [42] systems. We fix g to fit the experimental value of T_c for Ba122 system since this system possesses probably most stable value

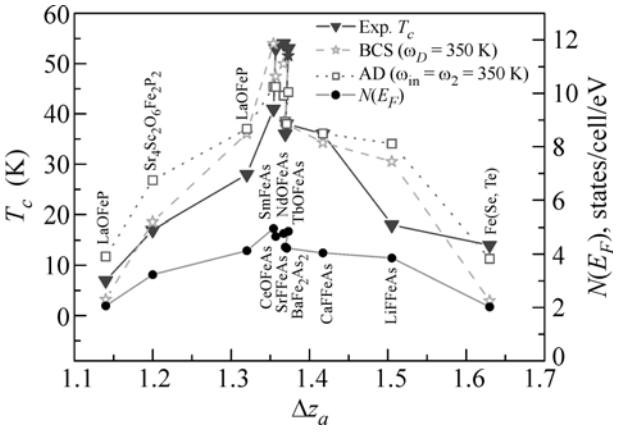

(Circles, right scale) Total LDA density of states $N(E_F)$, (left scale) superconducting transition temperatures T_c obtained from the (stars) simple BCS and (squares) Allen–Dynes (AD) expressions, and (triangles) experimental T_c values versus the anion height Δz_a over the Fe layer for a number of iron-based high temperature superconductors.

Table 2. Total LDA density of states $N(E_F)$, calculated and experimental T_c for iron-based superconductors

System	Δz_a, Å	$N(E_F)$, states/cell/eV	T_c^{BCS}, K	T_c^{AD}, K	T_c^{Exp}, K
LaOFeP	1.140	2.06	3.2	12	6.6
$Sr_4Sc_2O_6Fe_2P_2$	1.200	3.24	19	27	17
LaOFeAs	1.320	4.13	36	37	28
CeOFeAs	1.354	4.96	54	43	41
SmOFeAs	1.357	4.66	48	37	53
NdOFeAs	1.367	4.78	50	44	54
TbOFeAs	1.373	4.85	52	45	53
SrFFeAs	1.369	4.26	38	39	36
$BaFe_2As_2$	1.371	4.22	38	38	38
CaFFeAs	1.417	4.04	34	36	36
LiFeAs	1.505	3.86	31	34	18
Fe(Se, Te)	1.630	2.02	3	11	14

of T_c (about 38 K) with respect to the way of sample preparation and doping. Thus we obtain the value of dimensionless coupling constant $\lambda = 0.43$. Then just fixing the value of g as for Ba122 we obtain T_c values for all other systems, taking into account the appropriate change of the density of states. Rather surprisingly we observe almost quantitative agreement with experimental data on T_c (see triangles in figure and Table 2). Note that we can even obtain the right order of T_c values for 1111 systems with different rare-earth elements as due to rather small difference of corresponding densities of states, which were not obtained in our previous work [26], where we just fixed Δz_a to the only known at that time experimental value for LaOFeAs. However, the calculated value of T_c for LaOFeAs system is still rather higher than most typical experimental value of 26–28 K. At the same time, the samples of this system obtained via high pressure synthesis [43] demonstrated much higher values of $T_c \sim 41$ K, which is pretty closer to our calculated values. Also the notable deviation of our calculated T_c for LiFeAs system may be attributed both to the crudeness of our model (e.g., our use of a single value of ω_D for all compounds), as well as to probable experimental uncertainties of T_c in this system.

In principle, for the number of systems under consideration we can obtain even better results if we use the multiple band BCS-like approach, along the lines of [44]. However, to reduce the number of free parameters, the multiple band model fit requires additional information on the relations between energy gaps on different Fermi surface sheets (cylinders), which at present is only available for some of 122 systems.

It is well known that the elementary BCS-like expression for T_c has a tendency to overestimate the role of the density of states at the Fermi level. As an alternative we try the same approach estimating superconducting critical temperature T_c using Allen–Dynes interpolation formula (which is probably the best semi-analytic expression for T_c in case of electron-phonon pairing mechanism, including the strong coupling region) [45]:

$$T_c = \frac{f_1 f_2 \omega_{ln}}{1.20} \exp\left(-\frac{1.04(1+\lambda)}{\lambda - \mu^* - 0.62\lambda\mu^*}\right), \qquad (1)$$

where

$$f_1 = [1 + (\lambda/\Lambda_1)^{3/2}]^{1/3}, \quad \Lambda_1 = 2.46(1 + 3.8\mu^*),$$

$$f_2 = 1 + \frac{(\bar{\omega}_2/\omega_{ln} - 1)\lambda^2}{\lambda^2 + \Lambda_2^2},$$

$$\Lambda_2 = 1.82(1 + 6.3\mu^*)(\bar{\omega}_2/\omega_{ln}),$$

and $\bar{\omega}_2 = \langle\omega^2\rangle^{1/2}$, ω_{ln} are square root average and average logarithm of phonon frequency. Assuming for simplicity $\omega_{ln} \approx \bar{\omega}_2 = 350$ K, and taking the optimistic value of Coulomb pseudopotential $\mu^* = 0$, we repeat our previous analysis, fixing first $\lambda = 0.97$ for Ba122 and then changing only the density of states as obtained in our calculations for all other systems. The results for T_c obtained in this way from Allen–Dynes expression (1) are shown in figure by squares (see also Table 2).

We can see that Allen–Dynes expression produces a kind of a lower bound T_c estimate, with obvious deficit in T_c values in the vicinity of maximum. This deficit may signify the importance of non phonon pairing mechanism to obtain maximal values of T_c in FeAs superconductors. However, our main conclusion on important correlation of T_c with the values of the density of states at the Fermi level remains intact.

In fact we do not adhere at the moment to any specific pairing mechanism. Main objection to electron–phonon pairing in iron-based superconductors comes from microscopic calculations, e.g., those of [31]. At the same time, there are experiments on isotope effect [46, 47], which support the importance of this mechanism, though the other isotope experiments [48] produce quite opposite picture.

Our choice of characteristic phonon frequencies in the pre-exponential factor of BCS and Allen–Dynes expressions for T_c is used only as a kind of an estimate. What is important to us, is the well known fact that the dimensionless pairing constant is proportional to the total density of states in almost any BCS-like model of superconducting pairing, with some additional modifications in the case of multiple band models [44].

In conclusion, our results show unambiguous correlation of the values of superconducting T_c and those of the total density of electronic states at the Fermi level for the whole class of iron-based superconductors, thus supporting the usual BCS-like pairing mechanism in these systems.

This work is supported in part by the Russian Foundation for Basic Research (project no. 08-02-00021), by the Russian Academy of Sciences (project no. 09-II-2-1009, program "Quantum Physics of Condensed Matter"), and by the Branch of Physical Sciences, Russian Academy of Sciences (project no. 09-T-2-1011, program "Strongly Correlated Electrons in Solids"). I.A.N. acknowledges the support of the Council of the President of the Russian Federation for Support of Young Scientists and Leading Scientific Schools (project no. MK-614.2009.2); the Ural and Siberian Branches, Russian Academy of Sciences (interdisciplinary project); and the Russian Science Support Foundation.

REFERENCES

1. Y. Kamihara, T. Watanabe, M. Hirano, and H. Hosono, J. Am. Chem. Soc. **130**, 3296 (2008).
2. M. V. Sadovskii, Usp. Fiz. Nauk **178**, 1243 (2008) [Phys. Usp. **51**, 1243 (2008)]; arXiv: 0812.0302.
3. K. Ishida, Y. Nakai, and H. Hosono, J. Phys. Soc. Jpn. **78**, 062001 (2009).
4. Y. Mizuguhci, Y. Hara, K. Deguchi, et al., arXiv:1001.1801.
5. G. F. Chen, Z. Li, G. Zhou, et al., Phys. Rev. Lett. **101**, 057007 (2008).
6. X. Zhu, H. Yang, L. Fang, et al., Supercond. Sci. Technol. **21**, 105001 (2008).
7. A. S. Sefat, M. A. McGuire, B. C. Sales, et al., Phys. Rev. B **77**, 174503 (2008).
8. G. F. Chen, Z. Li, D. Wu, et al., Phys. Rev. Lett. **100**, 247002 (2008).
9. X. H. Chen, T. Wu, G. Wu, et al., Nature **453**, 761 (2008).
10. Z.-A. Ren, J. Yang, W. Lu, et al., Europhys. Lett. **82**, 57002 (2008).
11. Z.-A. Ren, J. Yang, W. Lu, et al., Mater. Res. Innovat. **12**, 105 (2008).
12. J.-W. G. Bos, G. B. S. Penny, J. A. Rodgers, et al., Chem. Commun. **31**, 3634 (2008).
13. Y. Kamihara, H. Hiramatsu, M. Hirano, et al., J. Am. Chem. Soc. **128**, 10012 (2006).
14. M. Rotter, M. Tegel, and D. Johrendt, Phys. Rev. Lett. **101**, 107006 (2008).
15. G. F. Chen, Z. Li, G. Li, et al., Chin. Phys. Lett. **25**, 3403 (2008).
16. K. Sasmal, Bing Lv, B. Lorenz, et al., Phys. Rev. Lett. **101**, 107007 (2008).
17. N. Ni, S. L. Bud'ko, A. Kreyssig, et al., Phys. Rev. B **78**, 014507 (2008).
18. J. H. Tapp, Z. Tang, Bing Lv, et al., Phys. Rev. B **78**, 060505(R) (2008).
19. X. C. Wang, Q. Q. Liu, Y. X. Lv, et al., Solid State Commun. **148**, 538 (2008).
20. M. Tegel, S. Johansson, V. Weiss, et al., Europhys. Lett. **84**, 67007 (2008).
21. F. Han, X. Zhu, G. Mu, et al., Phys. Rev. B **78**, 180503 (2008).
22. S. Matsuishi, Y. Inoue, T. Nomura, et al., J. Phys. Soc. Jpn. **77**, 113709 (2008); J. Am. Chem. Soc. **130**, 14428 (2008).
23. X. Zhu, F. Han, P. Cheng, et al., Europhys. Lett. **85**, 17011 (2009).
24. H. Ogino, Y. Katsura, S. Horii, et al., Supercond. Sci. Technol. **22**, 085001 (2009); Y. L. Xie, R. H. Liu, T. Wu, et al., Europhys. Lett. **86**, 57007 (2009); G. F. Chen, T. L. Xia, P. Zheng, et al., Supercond. Sci. Technol. **22**, 072001 (2009).
25. F. C. Hsu, J. Y. Luo, K. W. Yeh, et al., Proc. Nat. Acad. Sci. **105**, 14262 (2008).
26. I. A. Nekrasov, Z. V. Pchelkina, and M. V. Sadovskii, Pis'ma Zh. Eksp. Teor. Fiz. **87**, 647 (2008) [JETP Lett. **87**, 560 (2008)]; arXiv: 0804.1239.
27. I. A. Nekrasov, Z. V. Pchelkina, and M. V. Sadovskii, Pis'ma Zh. Eksp. Teor. Fiz. **88**, 155 (2008) [JETP Lett. **88**, 144 (2008)]; arXiv:0806.2630.
28. I. A. Nekrasov, Z. V. Pchelkina, and M. V. Sadovskii, Pis'ma Zh. Eksp. Teor. Fiz. **88**, 621 (2008) [JETP Lett. **88**, 543 (2008)]; arXiv:0807.1010.
29. I. A. Nekrasov, Z. V. Pchelkina, and M. V. Sadovskii, Pis'ma Zh. Eksp. Teor. Fiz. **88**, 777 (2008) [JETP Lett. **88**, 679 (2008)]; arXiv:0810.3377.
30. D. J. Singh and M. H. Du, Phys. Rev. Lett. **100**, 237003 (2008).
31. L. Boeri, O. V. Dolgov, and A. A. Golubov, Phys. Rev. Lett. **101**, 026403 (2008).
32. I. I. Mazin, D. J. Singh, M. D. Johannes, and M. H. Du, Phys. Rev. Lett. **101**, 057003 (2008).
33. S. Lebégue, Phys. Rev. B **75**, 035110 (2007).
34. I. R. Shein and A. L. Ivanovskii, Pis'ma Zh. Eksp. Teor. Fiz. **88**, 115 (2008) [JETP Lett. **88**, 107 (2008)]; arXiv: 0806.0750.
35. C. Krellner, N. Caroca-Canales, A. Jesche, et al., Phys. Rev. B **78**, 100504(R) (2008).

36. I. R. Shein and A. L. Ivanovskii, Pis'ma Zh. Eksp. Teor. Fiz. **88**, 377 (2008) [JETP Lett. **88**, 329 (2008)].
37. I. R. Shein and A. L. Ivanovskii, Pis'ma Zh. Eksp. Teor. Fiz. **88**, 781 (2008) [JETP Lett. **88**, 683 (2008)]; arXiv:0810.4581.
38. I. R. Shein and A. L. Ivanovskii, Phys. Rev. B **79**, 245115 (2009); J. Supercond Nov. Magn. Lett. **22**, 613 (2009).
39. A. Subedi, L. Zhang, D. J. Singh, and M. H. Du, Phys. Rev. B **78**, 134514 (2008).
40. O. K. Andersen, Phys. Rev. B **12**, 3060 (1975); O. Gunnarsson, O. Jepsen, and O. K. Andersen, Phys. Rev. B **27**, 7144 (1983); O. K. Andersen and O. Jepsen, Phys. Rev. Lett. **53**, 2571 (1984).
41. A. D. Christianson, M. D. Lumsden, O. Delaire, et al., Phys. Rev. Lett. **101**, 157004 (2008).
42. R. Mittal, Y. Su, S. Sols, et al., Phys. Rev. B **78**, 104514 (2008); arXiv: 0807.3172.
43. W. Lu, X.-L. Shen, J. Yang, et al., Solid State Commun. **148**, 168 (2008); arXiv:0804.3725.
44. E. Z. Kuchinskii and M. V. Sadovskii, Pis'ma Zh. Eksp. Teor. Fiz. **89**, 176 (2009) [JETP Lett. **89**, 156 (2009)]; arXiv: 0901.0164; Physica C, doi; 10.1016/j.physc.2009.08.005.
45. P. B. Allen and R. C. Dynes, Phys. Rev. B **12**, 905 (1975).
46. R. H. Liu, T. Wu, H. Chen, et al., Nature **459**, 64 (2009); arXiv:0810.2694.
47. R. Khasanov, M. Bendele, K. Conder, et al., arXiv:1002.2510.
48. P. M. Shirage, K. Kihou, K. Miyazawa, et al., Phys. Rev. Lett. **103**, 257003 (2009); arXiv:0903.3515.

ISSN 1063-7761, Journal of Experimental and Theoretical Physics, 2015, Vol. 120, No. 6, pp. 1055–1063. © Pleiades Publishing, Inc., 2015.

ELECTRONIC PROPERTIES OF SOLID

Attractive Hubbard Model with Disorder and the Generalized Anderson Theorem[1]

E. Z. Kuchinskii[a,*], N. A. Kuleeva[a,], and M. V. Sadovskii[a,b,***]**

[a] *Institute for Electrophysics, Ural Branch, Russian Academy of Sciences, Yekaterinburg, 620016 Russia*

[b] *Institute for Metal Physics, Ural Branch, Russian Academy of Sciences, Yekaterinburg, 620290 Russia*

**e-mail: kuchinsk@iep.uran.ru*

***e-mail: strigina@iep.uran.ru*

****e-mail: sadovski@iep.uran.ru*

Received November 6, 2014

Abstract—Using the generalized DMFT+Σ approach, we study the influence of disorder on single-particle properties of the normal phase and the superconducting transition temperature in the attractive Hubbard model. A wide range of attractive potentials U is studied, from the weak coupling region, where both the instability of the normal phase and superconductivity are well described by the BCS model, to the strong-coupling region, where the superconducting transition is due to Bose–Einstein condensation (BEC) of compact Cooper pairs, formed at temperatures much higher than the superconducting transition temperature. We study two typical models of the conduction band with semi-elliptic and flat densities of states, respectively appropriate for three-dimensional and two-dimensional systems. For the semi-elliptic density of states, the disorder influence on all single-particle properties (e.g., density of states) is universal for an arbitrary strength of electronic correlations and disorder and is due to only the general disorder widening of the conduction band. In the case of a flat density of states, universality is absent in the general case, but still the disorder influence is mainly due to band widening, and the universal behavior is restored for large enough disorder. Using the combination of DMFT+Σ and Nozieres–Schmitt-Rink approximations, we study the disorder influence on the superconducting transition temperature T_c for a range of characteristic values of U and disorder, including the BCS–BEC crossover region and the limit of strong-coupling. Disorder can either suppress T_c (in the weak-coupling region) or significantly increase T_c (in the strong-coupling region). However, in all cases, the generalized Anderson theorem is valid and all changes of the superconducting critical temperature are essentially due to only the general disorder widening of the conduction band.

DOI: 10.1134/S1063776115050143

1. INTRODUCTION

The problem of strong-coupling superconductivity has been studied for a long time, starting with the pioneering papers by Eagles and Leggett [1, 2]. Significant progress here was achieved by Nozieres and Schmitt-Rink [3], who suggested an effective method to study the transition temperature crossover from weak-coupling BCS-like behavior to the Bose–Einstein condensation (BEC) scenario in the strong-coupling region. Recent progress in experimental studies of quantum gases in magnetic and optical dipole traps, as well as in optical lattices, with controllable parameters, such as the density and interaction strength (see reviews [4, 5]), has increased the interest in superconductivity (superfluidity of fermions) with strong pairing interaction, including the region of the BCS–BEC crossover. One of the simplest models allowing the study of the BCS–BEC crossover is the Hubbard model with an attractive on-site interaction. The most successive approach to the solution of the Hubbard model, both in the case of repulsive interaction and for the studies of BCS–BEC crossover in the case of attraction, is the dynamical mean field theory (DMFT) [6–8]. The attractive Hubbard model was studied within the DMFT in a number of recent papers [9–13]. However, up to now there have been only a few studies of the disorder influence on the properties of normal and superconducting phases in this model, especially in the region of the BCS–BEC crossover. Disorder effects in this region were analyzed qualitatively in [14], where it was argued that the Anderson theorem remains valid in the BCS–BEC crossover region in the case of s-wave pairing. A diagrammatic approach to (weak) disorder effects on the superconducting transition temperature and the properties of the normal phase in the crossover region was developed recently in [15].

In recent years, we have developed a generalized DMFT+Σ approach to the Hubbard model [16–19], which is very convenient for the studies of different external interactions with respect to those taken into account in the DMFT, such as pseudogap fluctuations

[1] The article is published in the original.

[16–19], disorder [20, 21], electron–phonon interaction [22], etc. This approach is also well suited to the analysis of two-particle properties, such as optical (dynamic) conductivity [20, 23]. In [13], we used this approximation to calculate single-particle properties of the normal phase and optical conductivity in the attractive Hubbard model. In a recent paper [24], the DMFT+Σ approach was used by us to study the disorder influence on the superconducting transition temperature, which was calculated in the Nozieres–Schmitt-Rink approximation. In that paper, for the semi-elliptic density of states of the "bare" conduction band, which is adequate for three-dimensional systems, we numerically demonstrated the validity of the generalized Anderson theorem according to which all changes in the critical temperature are controlled only by the general widening of the conduction band by disorder.

In this paper, we present an analytic proof of such universal influence of disorder (in the DMFT+Σ approximation) on single-particle characteristics and the superconducting transition temperature for the semi-elliptic density of states and also investigate disorder effects in the case of the "bare" band with a flat density of states, qualitatively appropriate for two-dimensional systems. We show that for the flat band model, the universal dependence of single-particle properties and the superconducting transition temperature is also realized for the case of sufficiently strong disorder.

2. DISORDERED HUBBARD MODEL WITHIN THE DMFT+Σ APPROACH

We consider the disordered nonmagnetic Hubbard model with attractive interaction with the Hamiltonian

$$H = -t\sum_{\langle ij\rangle\sigma} a^{\dagger}_{i\sigma}a_{j\sigma} + \sum_{i\sigma}\epsilon_i n_{i\sigma} - U\sum_i n_{i\uparrow}n_{i\downarrow}, \qquad (1)$$

where $t > 0$ is the transfer integral between nearest neighbors on the lattice, U represents Hubbard-like on site attraction, $a_{i\sigma}(a^{\dagger}_{i\sigma})$ is the annihilation (creation) operator of an electron with spin σ, $n_{i\sigma} = a^{\dagger}_{i\sigma}a_{i\sigma}$ is the particle number operator on a lattice site i, while local on-site energies are assumed to be random variables (independent on the lattice sites). For the standard "impurity" diagram technique to be valid, we take the Gaussian distribution of energy levels ϵ_i:

$$\mathcal{P}(\epsilon_i) = \frac{1}{\sqrt{2\pi}\Delta}\exp\left(-\frac{\epsilon_i^2}{2\Delta^2}\right). \qquad (2)$$

The parameter Δ is a measure of the disorder strength, while the Gaussian random field of random on-site energy levels, which are independent on different sites ("white noise" correlation) induces "impurity" scattering, which is analyzed using the standard formalism of averaged Green's functions [25].

The generalized DMFT+Σ approach [16–19] extends the standard dynamical mean field theory (DMFT) [6–8] taking into account an additional "external" self-energy part $\Sigma_{\mathbf{p}}(\varepsilon)$ (in the general case, momentum dependent), which is due to some additional interaction outside the DMFT, and gives an effective method to calculate both single-particle and two-particle properties [20, 23]. The success of this generalized approach is based on the choice of the single-particle Green's function in the form

$$G(\varepsilon, \mathbf{p}) = \frac{1}{\varepsilon + \mu - \varepsilon(\mathbf{p}) - \Sigma(\varepsilon) - \Sigma_{\mathbf{p}}(\varepsilon)}, \qquad (3)$$

where $\varepsilon(\mathbf{p})$ is the "bare" electron dispersion, while the complete self-energy is assumed to be an additive sum of the local DMFT self-energy and some "external" self-energy $\Sigma_{\mathbf{p}}(\varepsilon)$, due to the neglect of the interference of Hubbard and "external" interactions. This allows the conservation of the standard form of self-consistent equations of the standard DMFT [6–8]. At the same time, at each step of DMFT iterations, we consistently recalculate the "external" self-energy $\Sigma_{\mathbf{p}}(\varepsilon)$ using an appropriate approximate scheme, corresponding to the form of the additional interaction, while the local Green's function is also "dressed" by $\Sigma_{\mathbf{p}}(\varepsilon)$ at each step of the standard DMFT procedure.

For the "external" self-energy entering the DMFT+Σ cycle for the problem of random scattering by disorder, we use the simplest self-consistent Born approximation, neglecting diagrams with crossing "impurity" lines, which gives

$$\Sigma_{\mathbf{p}}(\varepsilon) \longrightarrow \tilde{\Sigma}(\varepsilon) = \Delta^2\sum_{\mathbf{p}} G(\varepsilon, \mathbf{p}), \qquad (4)$$

where $G(\varepsilon, \mathbf{p})$ is the single-electron Green's function (3) and Δ is the amplitude of site disorder.

To solve the effective single-Anderson-impurity problem of DMFT, we use the numerical renormalization group approach (NRG) [26].

In what follows, we consider two models of the "bare" conduction band. The first is the band with a semi-elliptic density of states (per unit cell and single spin projection)

$$N_0(\varepsilon) = \frac{2}{\pi D^2}\sqrt{D^2 - \varepsilon^2}, \qquad (5)$$

where D is the band half-width. This model is appropriate for a three-dimensional system. The second model is the one with the flat density of states, appropriate for the two-dimensional case:

$$N_0(\varepsilon) = \begin{cases} \dfrac{1}{2D} & |\varepsilon| \le D, \\ 0 & |\varepsilon| > D. \end{cases} \qquad (6)$$

In principle, for two-dimensional systems, we should take the presence of the weak (logarithmic) Van Hove singularity in the density of states into account. However, this singularity is already effectively suppressed by rather small disorder, and hence the simple model in Eq. (6) is quite sufficient for our aims.

All calculations in this paper are done for a quarter-filled band (the number of electrons per lattice site is $n = 0.5$).

The superconducting transition temperature in the attractive model was analyzed in a number of papers [9, 10, 12], both from the condition of instability of the normal phase [9] (divergence of the Cooper susceptibility) and from the condition of the superconducting order parameter going to zero [10, 12]. In recent paper [13], we determined the critical temperature from the condition of instability of the normal phase, reflected in the instability of the DMFT iteration procedure. The results obtained in this way in fact coincide with those in [9, 10, 12]. Also, to calculate T_c in [13], we used the approach due to Nozieres and Schmitt-Rink [3], which allows the correct (though approximate) description of T_c in the BCS–BEC crossover region. In a later paper [24], we used the combination of Nozieres and Schmitt-Rink and DMFT+Σ approximations for detailed numerical studies of the disorder dependence of T_c and the number of local pairs in the model with the semi-elliptic density of states.

3. DISORDER INFLUENCE ON SINGLE-PARTICLE PROPERTIES FOR THE SEMI-ELLIPTIC DENSITY OF STATES

In this section, we analytically demonstrate that in the DMFT+Σ approximation, the disorder influence on single-particle properties of the disordered Hubbard model (both attractive or repulsive) with a semi-elliptic "bare" conduction band is completely described by effects of general band widening by disorder scattering.

In the system of self-consistent DMFT+Σ equations [17, 19, 20], information on the "bare" band and disorder scattering enter only at the stage of calculations of the local Green's function

$$G_{ii} = \sum_{\mathbf{p}} G(\varepsilon, \mathbf{p}), \tag{7}$$

where the full Green's function $G(\varepsilon, \mathbf{p})$ is determined by Eq. (3), while the self-energy due to disorder, in the self-consistent Born approximation, is defined by Eq. (4). Then the local Green's function takes the form

$$\begin{aligned} G_{ii} &= \int_{-D}^{D} d\varepsilon' \frac{N_0(\varepsilon')}{\varepsilon + \mu - \varepsilon' - \Sigma(\varepsilon) - \Delta^2 G_{ii}} \\ &= \int_{-D}^{D} d\varepsilon' \frac{N_0(\varepsilon')}{E_t - \varepsilon'}, \end{aligned} \tag{8}$$

where we introduce the notation $E_t = \varepsilon + \mu - \Sigma(\varepsilon) - \Delta^2 G_{ii}$. In the case of semi-elliptic density of states (5), this integral is easily calculated in analytic form, and hence the local Green's function is written as

$$G_{ii} = 2\frac{E_t - \sqrt{E_t^2 - D^2}}{D^2}. \tag{9}$$

It can be easily seen that Eq. (9) represents one of the roots of the quadratic equation

$$G_{ii}^{-1} = E_t - \frac{D^2}{4} G_{ii}, \tag{10}$$

corresponding to the correct limit of $G_{ii} \longrightarrow E_t^{-1}$ for an infinitely narrow band ($D \longrightarrow 0$). Then

$$\begin{aligned} G_{ii}^{-1} &= \varepsilon + \mu - \Sigma(\varepsilon) - \Delta^2 G_{ii} - \frac{D^2}{4} G_{ii} \\ &= \varepsilon + \mu - \Sigma(\varepsilon) - \frac{D_{\text{eff}}^2}{4} G_{ii}, \end{aligned} \tag{11}$$

where we introduce D_{eff} as the effective half-width of the band (in the absence of electronic correlations, i.e., for $U = 0$) widened by disorder scattering:

$$D_{\text{eff}} = D\sqrt{1 + 4\frac{\Delta^2}{D^2}}. \tag{12}$$

Equation (10) was obtained from (8), and hence comparing (11) and (10), we obtain:

$$G_{ii} = \int_{-D_{\text{eff}}}^{D_{\text{eff}}} d\varepsilon' \frac{\tilde{N}_0(\varepsilon')}{\varepsilon + \mu - \varepsilon' - \Sigma(\varepsilon)}, \tag{13}$$

where

$$\tilde{N}_0(\varepsilon) = \frac{2}{\pi D_{\text{eff}}^2}\sqrt{D_{\text{eff}}^2 - \varepsilon^2} \tag{14}$$

represents the density of states in the absence of the interaction U "dressed" by disorder. This density of states remains semi-elliptic in the presence of disorder, and therefore all effects of disorder scattering on single-particle properties of the disordered Hubbard model in the DMFT+Σ approximation reduce to only disorder widening of the conduction band, i.e., to the replacement $D \longrightarrow D_{\text{eff}}$.

4. DISORDER INFLUENCE ON THE SUPERCONDUCTING TRANSITION TEMPERATURE

The superconducting transition temperature T_c is not a single-particle characteristic of the system. The Cooper instability determining T_c is related to the divergence of a two-particle loop in the Cooper channel. In the weak-coupling limit, when superconductivity is due to the appearance of Cooper pairs at T_c, disorder only slightly influences superconductivity with the *s*-wave pairing [27, 28]. The so-called Anderson theorem is valid and changes of T_c are connected only with the relatively small changes of the density of states by disorder. The standard derivation of the Anderson theorem [27, 28] uses the formalism of exact eigenstates of an electron in the random field of impurities. Here, we present another derivation of the Anderson theorem, using the exact Ward identity, which allows us to derive the equation for T_c, which is then used to calculate T_c in the Nozieres–Schmitt-Rink approximation in a disordered system.

In general, the Nozieres–Schmitt-Rink approach [3] assumes that corrections due to strong pairing attraction significantly change the chemical potential of the system, while possible corrections due to this interaction to the Cooper instability condition can be neglected, and we can therefore always use the weak-coupling (ladder) approximation. In that approximation, the Cooper instability condition in the disordered Hubbard model takes the form

$$1 = U\chi_0(q = 0, \omega_m = 0), \tag{15}$$

where

$$\chi_0(q = 0, \omega_m = 0) = T\sum_n \sum_{\mathbf{pp'}} \Phi_{\mathbf{pp'}}(\varepsilon_n) \tag{16}$$

represents the two-particle loop (susceptibility) in the Cooper channel "dressed" only by disorder scattering, and $\Phi_{\mathbf{pp'}}(\varepsilon_n)$ is the averaged two-particle Green's function in the Cooper channel ($\omega_m = 2\pi m T$ and $\varepsilon_n = \pi T(2n + 1)$ are the usual boson and fermion Matsubara frequencies).

To obtain $\sum_{\mathbf{pp'}} \Phi_{\mathbf{pp'}}(\varepsilon_n)$, we use the exact Ward identity, derived by us in [23]:

$$G(\varepsilon_n, \mathbf{p}) - G(-\varepsilon_n, -\mathbf{p}) = -\sum_{\mathbf{p'}} \Phi_{\mathbf{pp'}}(\varepsilon_n) \times (G_0^{-1}(\varepsilon_n, \mathbf{p'}) - G_0^{-1}(-\varepsilon_n, -\mathbf{p'})). \tag{17}$$

Here, $G(\varepsilon_n, \mathbf{p})$ is the impurity-averaged single-particle Green's function (not containing Hubbard interaction corrections!). Using the obvious symmetry $\varepsilon(\mathbf{p}) = \varepsilon(-\mathbf{p})$ and $G(\varepsilon_n, -\mathbf{p}) = G(\varepsilon_n, \mathbf{p})$, we obtain from the Ward identity (17) that

$$\sum_{\mathbf{pp'}} \Phi_{\mathbf{pp'}}(\varepsilon_n) = -\frac{\sum_{\mathbf{p}} G(\varepsilon_n, \mathbf{p}) - \sum_{\mathbf{p}} G(-\varepsilon_n, \mathbf{p})}{2i\varepsilon_n}, \tag{18}$$

and hence for Cooper susceptibility (16) we have

$$\chi_0(q = 0, \omega_m = 0) = -T\sum_n \frac{\sum_{\mathbf{p}} G(\varepsilon_n, \mathbf{p}) - \sum_{\mathbf{p}} G(-\varepsilon_n, \mathbf{p})}{2i\varepsilon_n} = -T\sum_n \frac{\sum_{\mathbf{p}} G(\varepsilon_n, \mathbf{p})}{i\varepsilon_n}. \tag{19}$$

Performing the standard summation over Matsubara frequencies [25], we obtain

$$\chi_0(q = 0, \omega_m = 0) = -\frac{1}{4\pi i}\int_{-\infty}^{\infty} d\varepsilon \times \frac{\sum_{\mathbf{p}} G^R(\varepsilon, \mathbf{p}) - \sum_{\mathbf{p}} G^A(\varepsilon, \mathbf{p})}{\varepsilon} \tanh\frac{\varepsilon}{2T} = \int_{-\infty}^{\infty} d\varepsilon \frac{\tilde{N}(\varepsilon)}{2\varepsilon}\tanh\frac{\varepsilon}{2T}, \tag{20}$$

where $\tilde{N}(\varepsilon)$ is the density of states ($U = 0$) "dressed" by disorder scattering. In Eq. (20), the energy ε is referenced to the chemical potential, and if we reference it to the center of the conduction band, we have to replace $\varepsilon \longrightarrow \varepsilon - \mu$, such that Cooper instability condition (15) leads to the following equation for T_c:

$$1 = \frac{U}{2}\int_{-\infty}^{\infty} d\varepsilon \tilde{N}_0(\varepsilon)\frac{\tanh((\varepsilon - \mu)/2T_c)}{\varepsilon - \mu}, \tag{21}$$

where $\tilde{N}_0(\varepsilon)$ is again the density of states (calculated at $U = 0$) "dressed" by disorder scattering. At the same time, the chemical potential of the system at different values of U and Δ should be determined from DMFT+Σ calculations, i.e., from the standard equation for the number of electrons (band filling) determined by the Green's function in Eq. (3), which allows us to find T_c for the wide range of model parameters, including the BCS–BEC crossover and strong-coupling regions, as well as for different levels of disorder. This reflects the physical meaning of the Nozieres–Schmitt-Rink approximation: in the weak-coupling region, the transition temperature is controlled by Cooper instability equation (21), while in the limit of strong-coupling, it is determined as the BEC temperature controlled by the chemical potential. Thus, the joint solution of Eq. (21) and the equa-

tion for the chemical potential guarantees the correct interpolation for T_c through the BCS–BEC crossover region. This approach gives the results for the critical temperature that are quantitatively close to the exact results obtained by direct numerical DMFT calculations [13], but demands much less numerical effort.

We stress that we have used the exact Ward identity, which also allows using Eq. (21) in the region of strong disorder, when the effects of Anderson localization may become relevant. Equation (21) demonstrates that the critical temperature depends on disorder only through the disorder dependence of the density of states $\tilde{N}(\varepsilon)$, which is the main statement of the Anderson theorem. In the framework of the Nozieres–Schmitt-Rink approach, Eq. (21) is also preserved in the strong-coupling region, when the critical temperature is determined by the BEC condition for compact Cooper pairs. In this case, the chemical potential μ entering Eq. (21) may significantly depend on disorder. However, in the DMFT+Σ approximation, this dependence of the chemical potential (as well as of any other single-particle characteristic) in the model with a semi-elliptic density of states is only due to disorder widening of the conduction band. Thus, in both the BCS–BEC crossover and strong-coupling regions, the generalized Anderson theorem actually remains valid. Accordingly, in the model of a semi-elliptic band, Eq. (21) leads to a universal dependence of T_c on disorder, due to the change $D \longrightarrow D_{\text{eff}}$. Such universality is fully confirmed by numerical calculations of T_c in this model, performed in [24] (cf. also the results presented below).

5. MAIN RESULTS

We now discuss the main results of our numerical calculations, explicitly demonstrating the universal behavior of single-particle properties and the superconducting transition temperature with disorder. We see below that all disorder effects are effectively controlled, in fact, only by the growth of the half-width of conduction band, which for a semi-elliptic density of states is given by Eq. (12). In the case of the band with a flat density of states, the growth of disorder changes the shape of the density of states, making it semi-elliptic in the limit of sufficiently strong disorder, while the effective half-width of the band is given by (cf. Appendix A)

$$\frac{D_{\text{eff}}}{D} = \sqrt{1+\frac{\Delta^2}{D^2}} + \frac{1}{2}\frac{\Delta^2}{D^2}\ln\left(\frac{\sqrt{1+\Delta^2/D^2}+1}{\sqrt{1+\Delta^2/D^2}-1}\right). \quad (22)$$

As an example of the most important single-particle property, we take the density of states. In Fig. 1, we show the evolution of the density of states with disorder in the model of a semi-elliptic band [13]. We can see that the growth of disorder smears the density of states and widens the band. This smearing somehow

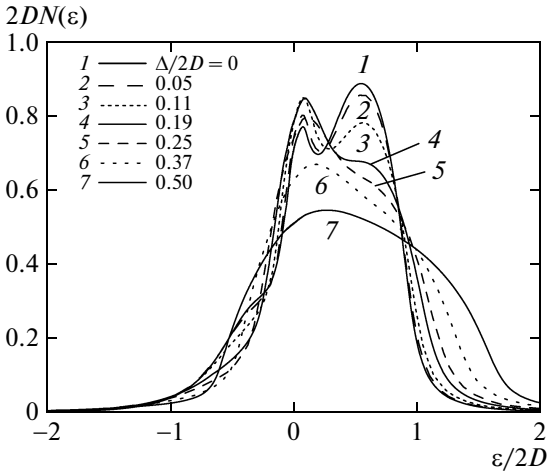

Fig. 1. Dependence of the density of states on disorder in the model with a semi-elliptic band, $|U|/2D = 0.8$, $I/2D = 0.05$.

masks the peculiarities of the density of states due to correlation effects. In particular, both the quasiparticle peak and the lower and upper Hubbard bands, observed in Fig. 1 in the absence of disorder, are completely destroyed in the limit of strong enough disorder. However, we can easily convince ourselves that this evolution is only due to the general widening of the band due to disorder (cf. Eqs. (12) and (22)), because all the data for the density of states belong to the same universal curve replotted in appropriate new variables, with all energies (and temperature) normalized by the effective bandwidth by replacing $D \longrightarrow D_{\text{eff}}$, as shown in Fig. 2a, in complete agreement with the general results obtained above. For the conduction band with a flat density of states, there is no complete universality, as can be seen from Fig. 2b for low enough values of disorder. However, for large enough disorder, the dashed curve shown in Fig. 2b practically coincides with the universal curve for the density of states shown in Fig. 2a. This reflects the simple fact that at large disorder, the flat density of states effectively transforms into a semi-elliptic one (cf. Appendix A).

Going now to the analysis of the superconducting transition temperature, in Fig. 3 we present the dependence of T_c (normalized by the critical temperature in the absence of disorder, $T_{c0} = T_c(\Delta = 0)$) on disorder for different values of the pairing interaction U for both models of the initial "bare" density of states, semi-elliptic (Fig. 3a) and flat (Fig. 3b). Qualitatively, the evolution of T_c with disorder is the same for both models. We can see that in the weak-coupling limit ($U/2D \ll 1$), disorder slightly suppresses T_c (curves *1*). At intermediate couplings ($U/2D \sim 1$), weak disorder increases T_c, while the further increase in disorder suppresses the critical temperature (curves *3*). In the strong-coupling region ($U/2D \gg 1$), the growth of disorder leads to a significant increase in the critical tem-

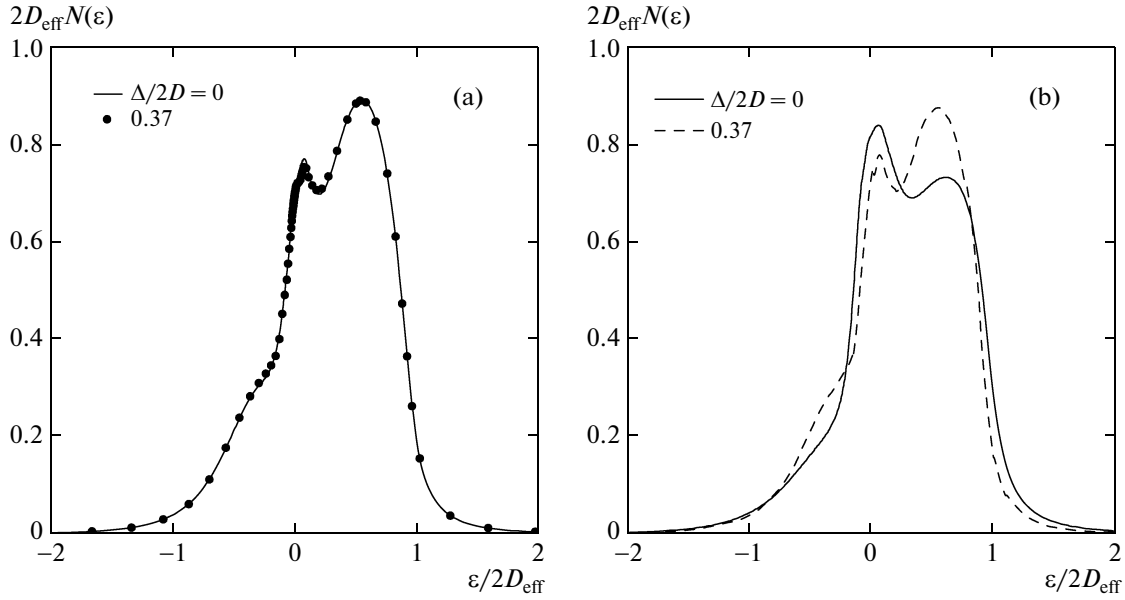

Fig. 2. Universal dependence of the density of states on disorder: (a) the model of a semi-elliptic "bare" density of states; (b) the model of a flat "bare" density of states.

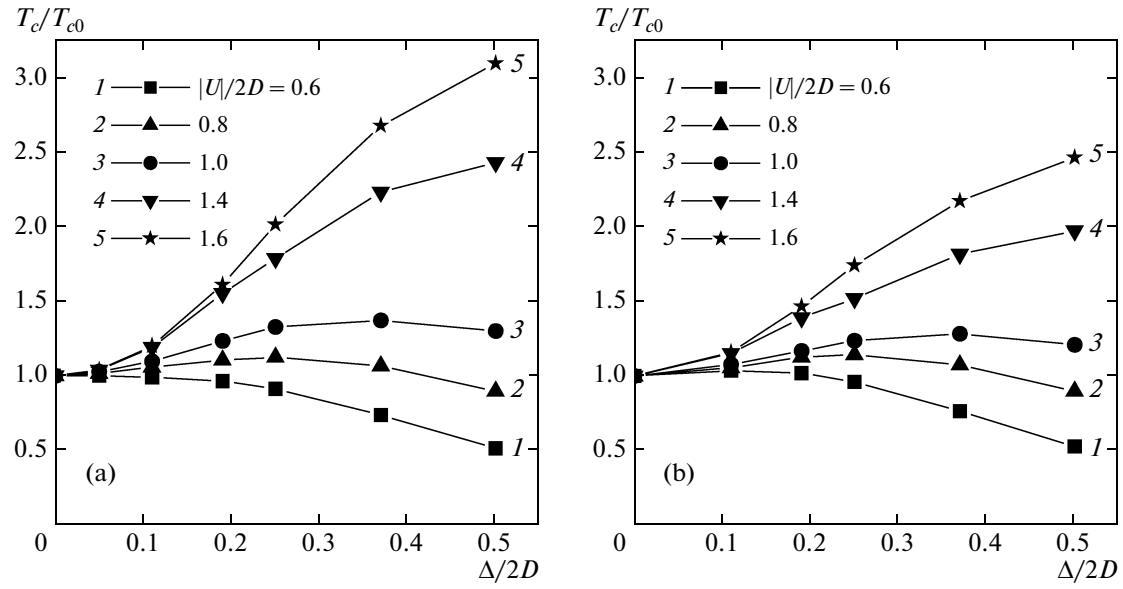

Fig. 3. Dependence of the superconducting transition temperature on disorder for different values of the Hubbard attraction U: (a) semi-elliptic band; (b) flat band.

perature (curves *5*). However, we can easily see that such a complicated dependence of T_c on disorder is completely determined by the disorder widening of the "bare" ($U = 0$) conduction band, demonstrating the validity of the generalized Anderson theorem for all values of U. In Fig. 4, the curve with octagons shows the dependence of the critical temperature $T_c/2D$ on the coupling strength $U/2D$ in the absence of disorder ($\Delta = 0$) for both models of "bare" conduction bands, semi-elliptic (Fig. 4a) and flat (Fig. 4b). We can see that in both models, in the weak-coupling region, the superconducting transition temperature is well described by the BCS model (in Fig. 4a), the dashed curve represents the result of the BCS model, with T_c defined by Eq. (21), with the chemical potential independent of U and determined by the quarter-filling of the "bare" band), while in the strong-coupling region, the critical temperature is determined by the BEC

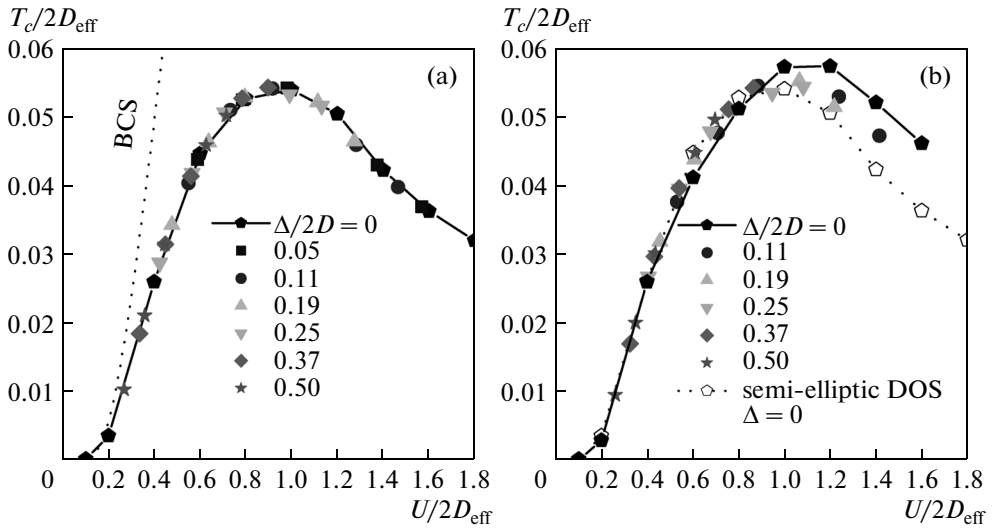

Fig. 4. Universal dependence of the superconducting critical temperature on the Hubbard attraction U for different disorder levels: (a) semi-elliptic band; the dotted curve represents the BCS dependence in the absence of disorder; (b) flat band; the dotted line represents a similar dependence for the semi-elliptic band for $\Delta = 0$.

condition for Cooper pairs and decreases as t^2/U as U increases (inversely proportional to the effective mass of the pair), passing through the maximum at $U/2D_{\text{eff}} \sim 1$. The other symbols in Fig. 4a show the results for T_c obtained by a combination of the DMFT+Σ and Nozieres–Schmitt-Rink approximations for a semi-elliptic "bare" band. We can see that all data (expressed in normalized units of $U/2D_{\text{eff}}$ and $T_c/2D_{\text{eff}}$) ideally fit the universal curve obtained in the absence of disorder. For a flat "bare" band, results of our calculations are shown in Fig. 4b and we do not observe the complete universality: data points, corresponding to different degrees of disorder, somehow deviate from the curve obtained in the absence of disorder. However, with the increase in disorder, the form of the band becomes close to semi-elliptic and our data points move towards the universal curve obtained for the semi-elliptic case and shown by the dashed curve in Fig. 4b, thus confirming the validity of the generalized Anderson theorem.

6. CONCLUSION

In this paper, in the framework of the DMFT+Σ generalization of dynamical mean field theory, we have studied the disorder influence on single-particle properties (e.g., the density of states) and the superconducting transition temperature in the attractive Hubbard model. Calculations were done for a wide range of attractive interactions U, from the weak-coupling region $U/2D_{\text{eff}} \ll 1$, where both instability of the normal phase and superconductivity are well described by the BCS model, to the strong-coupling limit $U/2D_{\text{eff}} \gg 1$, where the superconducting transition is determined by Bose–Einstein condensation of compact Cooper pairs forming at temperatures much higher than the superconducting transition temperature. We have shown analytically that for the conduction band with a semi-elliptic density of states, which is a good approximation in the three-dimensional case, disorder influences all single-particle properties in a universal way: all changes of these properties are only due to the disorder widening of the band. In the model of the conduction band with a flat density of states, which is appropriate for two-dimensional systems, there is no universality in the region of weak disorder. However, the main effects are again due to the general widening of the band and complete universality is restored for high enough disorder, when the density of states effectively becomes semi-elliptic.

To study the superconducting transition temperature, we have used the combination of the DMFT+Σ approach and the Nozieres–Schmitt-Rink approximation. For both models of the conduction band, disordering the density of states may either suppress the critical temperature T_c (in the region of weak coupling) or significantly increase it (in the strong-coupling region). However, in all these cases, we have actually proved the validity of the generalized Anderson theorem, and hence all changes of the transition temperature are in fact controlled only by the effects of general disorder widening of the conduction band. In the case of the initial semi-elliptic band, the disorder influence on T_c is completely universal, while in the case of the initial flat band, such universality is absent at weak disorder, but is completely restored for high enough disorder levels.

Finally, we present some additional comments on the methods and approximations used. Both the DMFT+Σ and Nozieres–Schmitt-Rink approaches represent certain approximate interpolation schemes, strictly valid only in the corresponding limit cases

(e.g., small disorder or small (large) U). However, both schemes demonstrate their effectiveness also in the case of intermediate values of U and intermediate (or even strong) disorder. Actually, the effectiveness of the Nozieres–Schmitt-Rink approximation (neglecting U corrections in the Cooper channel) was verified by comparison with the direct DMFT calculations [13]. The use of DMFT+Σ to analyze the disorder effects in the repulsive Hubbard model was shown to produce reasonable results for the phase diagram, compared to exact numerical simulations of disorder in DMFT, including the region of large disorder (the Anderson localized phase) [19–21]. However, the role of the approximations made in DMFT+Σ, such as the neglect of the interference of disorder scattering and correlation effects, deserves further studies.

ACKNOWLEDGMENTS

This paper is supported by the Russian Science Foundation, grant no. 14-12-00502.

APPENDIX A

For the band with a flat density of states (at $U = 0$ and $\Delta = 0$), disorder leads both to widening of the band and to a change of the form of the density of states. Taking the density of states in the form given by Eqs. (6), we calculate the local Green's function as

$$G_{ii} = \frac{1}{2D}\int_{-D}^{D} d\varepsilon' \frac{1}{\varepsilon - \varepsilon' - \Delta^2 G_{ii}} = \frac{1}{2D}\ln\left(\frac{\varepsilon - \Delta^2 G_{ii} + D}{\varepsilon - \Delta^2 G_{ii} - D}\right), \quad \text{(A1)}$$

where the energy ε is referenced to the middle of the "bare" band. We introduce the auxiliary notation $G_{ii} = R - iI$. At the band edges, $I \longrightarrow 0$, and therefore expanding the r.h.s. of Eq. (A.1) up to linear terms in I, we obtain

$$R - iI \approx \frac{1}{2D}\ln\left(\frac{\varepsilon - \Delta^2 R + D}{\varepsilon - \Delta^2 R - D}\right) - iI\frac{\Delta^2}{(\varepsilon - \Delta^2 R)^2 - D^2}. \quad \text{(A2)}$$

Equating the real parts in (A.2), we obtain

$$R = \frac{1}{2D}\ln\left(\frac{\varepsilon - \Delta^2 R + D}{\varepsilon - \Delta^2 R - D}\right).$$

Similarly, equating the imaginary parts at the band edges, we obtain $\varepsilon - \Delta^2 R = \pm\sqrt{D^2 + \Delta^2}$, and substituting this expression into the logarithm in the preceding expression, we find R and the band edge positions at

$$\varepsilon = \pm\left(\sqrt{D^2 + \Delta^2} + \frac{\Delta^2}{2D}\ln\left(\frac{\sqrt{D^2 + \Delta^2} + D}{\sqrt{D^2 + \Delta^2} - D}\right)\right). \quad \text{(A3)}$$

Thus, the half-width of the band D_{eff} widened by disorder in this model is determined by Eq. (22) used above.

We note that although the Born approximation for disorder scattering that we use is formally valid only for small disorder $\Delta \ll D$, the effects of Anderson localization at large disorder $\Delta \sim D$ do not qualitatively change the density of states [27], and hence the Born approximation gives qualitatively correct results also in the region of large disorder. Actually, this approximation neglects only the appearance of exponentially small "tails" in the density of states, outside the "mean field" band edges [27] and gives more or less correct results inside such a band.

At large enough disorder, almost any "bare" band width $2D$ and an arbitrary density of states $N_0(\varepsilon)$ acquires a semi-elliptic density of states. In the limit of very large disorder $\Delta \gg D$, almost in the whole band, widened by disorder, we have $|\varepsilon - \Delta^2 R| \gg D$ and in the expression for the local Green's function we can neglect the ε'-dependence in the denominator of the integrand:

$$R - iI = G_{ii} = \int_{-\infty}^{\infty} d\varepsilon' \frac{N_0(\varepsilon')}{\varepsilon - \varepsilon' - \Delta^2 G_{ii}} \approx \frac{1}{\varepsilon - \Delta^2 R + i\Delta^2 I}. \quad \text{(A4)}$$

Then we immediately obtain

$$\varepsilon - \Delta^2 R = \frac{\varepsilon}{2}, \quad I = \frac{1}{2\Delta^2}\sqrt{4\Delta^2 - \varepsilon^2} \quad \text{(A5)}$$

whence the density of states "dressed" by disorder

$$N(\varepsilon) = -\frac{1}{\pi}\text{Im}G_{ii} = \frac{I}{\pi} = \frac{2}{\pi(2\Delta)^2}\sqrt{(2\Delta)^2 - \varepsilon^2} \quad \text{(A6)}$$

becomes semi-elliptic, Eq. (5), with the half-width $D_{\text{eff}} = 2\Delta$. Thus, at strong enough disorder, any "bare" band becomes semi-elliptic, restoring the universal dependence of single-particle properties on disorder discussed above. In this sense, the model of the "bare" band with a semi-elliptic density of states is most appropriate for the studies of the effects of strong disorder.

REFERENCES

1. D. M. Eagles, Phys. Rev. **186**, 456 (1969).
2. A. J. Leggett, in: *Modern Trends in the Theory of Condensed Matter*, Ed. by A. Pekalski and J. Przystawa (Springer-Verlag, Berlin, 1980).
3. P. Nozieres and S. Schmitt-Rink, J. Low Temp. Phys. **59**, 195 (1985).

4. I. Bloch, J. Dalibard, and W. Zwerger, Rev. Mod. Phys. **80**, 885 (2008).
5. L. P. Pitaevskii, Phys.—Usp. **49** (4), 333 (2006).
6. Th. Pruschke, M. Jarrell, and J. K. Freericks, Adv. Phys. **44**, 187 (1995).
7. A. Georges, G. Kotliar, W. Krauth, and M. J. Rozenberg, Rev. Mod. Phys. **68**, 13 (1996).
8. D. Vollhardt, in *Lectures on the Physics of Strongly Correlated Systems XIV*, Ed. by A. Avella and F. Mancini (American Institute of Physics, Melville, New York, 2010), AIP Conf. Proc. **1297**, 339; D. Vollhardt, arXiv:1004.5069.
9. M. Keller, W. Metzner, and U. Schollwock, Phys. Rev. Lett. **86**, 4612 (2001); M. Keller, W. Metzner, and U. Schollwock, arXiv:cond-mat/0101047.
10. A. Toschi, P. Barone, M. Capone, and C. Castellani, New J. Phys. **7**, 7 (2005); A. Toschi, P. Barone, M. Capone, and C. Castellani, arXiv:cond-mat/0411637v1.
11. J. Bauer, A. C. Hewson, and N. Dupis, Phys. Rev. B: Condens. Matter **79**, 214518 (2009); J. Bauer, A. C. Hewson, and N. Dupis, arXiv:0901.1760v2.
12. A. Koga and P. Werner, Phys. Rev. A: At., Mol., Opt. Phys. **84**, 023638 (2011); A. Koga and P. Werner, arXiv:1106.4559v1.
13. N. A. Kuleeva, E. Z. Kuchinskii, and M. V. Sadovskii, J. Exp. Theor. Phys. **119** (2), 264 (2014); N. A. Kuleeva, E. Z. Kuchinskii, and M. V. Sadovskii, arXiv:1401.2295.
14. A. I. Posazhennikova and M. V. Sadovskii, JETP Lett. **65** (3), 270 (1997).
15. F. Palestini and G. C. Strinati, Phys. Rev. B: Condens. Matter **88**, 174504 (2013); F. Palestini and G. C. Strinati, arXiv:1311.2761.
16. E. Z. Kuchinskii, I. A. Nekrasov, and M. V. Sadovskii, JETP Lett. **82** (4), 198 (2005); E. Z. Kuchinskii, I. A. Nekrasov, and M. V. Sadovskii, arXiv:cond-mat/0506215.
17. M. V. Sadovskii, I. A. Nekrasov, E. Z. Kuchinskii, Th. Prushke, and V. I. Anisimov, Phys. Rev. B: Condens. Matter **72**, 155105 (2005); M. V. Sadovskii, I. A. Nekrasov, E. Z. Kuchinskii, Th. Prushke, and V. I. Anisimov, arXiv:cond-mat/0508585.
18. E. Z. Kuchinskii, I. A. Nekrasov, and M. V. Sadovskii, Low Temp. Phys. **32** (4), 398 (2006); E. Z. Kuchinskii, I. A. Nekrasov, and M. V. Sadovskii, arXiv:cond-mat/0510376.
19. E. Z. Kuchinskii, I. A. Nekrasov, and M. V. Sadovskii, Phys.—Usp. **55** (4), 325 (2012); E. Z. Kuchinskii, I. A. Nekrasov, and M. V. Sadovskii, arXiv:1109.2305.
20. E. Z. Kuchinskii, I. A. Nekrasov, and M. V. Sadovskii, J. Exp. Theor. Phys. **106** (3), 581 (2008); E. Z. Kuchinskii, I. A. Nekrasov, and M. V. Sadovskii, arXiv:0706.2618.
21. E. Z. Kuchinskii, N. A. Kuleeva, I. A. Nekrasov, and M. V. Sadovskii, J. Exp. Theor. Phys. **110** (2), 325 (2010); E. Z. Kuchinskii, N. A. Kuleeva, I. A. Nekrasov, and M. V. Sadovskii, arXiv:0908.3747.
22. E. Z. Kuchinskii, I. A. Nekrasov, and M. V. Sadovskii, Phys. Rev. B: Condens. Matter **80**, 115124 (2009); E. Z. Kuchinskii, I. A. Nekrasov, and M. V. Sadovskii, arXiv:0906.3865.
23. E. Z. Kuchinskii, I. A. Nekrasov, and M. V. Sadovskii, Phys. Rev. B: Condens. Matter **75**, 115102 (2007); E. Z. Kuchinskii, I. A. Nekrasov, and M. V. Sadovskii, arXiv:cond-mat/0609404.
24. E. Z. Kuchinskii, N. A. Kuleeva, and M. V. Sadovskii, JETP Lett. **100** (3), 192 (2014); E. Z. Kuchinskii, N. A. Kuleeva, and M. V. Sadovskii, arXiv:1406.5603.
25. A. A. Abrikosov, L. P. Gor'kov, and I. E. Dzyaloshinskii, *Quantum Field Theoretical Methods in Statistical Physics* (Pergamon, Oxford, 1965); M. V. Sadovskii, *Diagrammatics* (World Scientific, Singapore, 2006).
26. R. Bulla, T. A. Costi, and T. Pruschke, Rev. Mod. Phys. **60**, 395 (2008).
27. M. V. Sadovskii, *Superconductivity and Localization* (World Scientific, Singapore, 2000).
28. P. G. De Gennes, *Superconductivity of Metals and Alloys* (W. A. Benjamin, New York, 1966).

ISSN 1063-7761, Journal of Experimental and Theoretical Physics, 2016, Vol. 122, No. 2, pp. 375–383. © Pleiades Publishing, Inc., 2016.

ELECTRONIC PROPERTIES OF SOLID

Attractive Hubbard Model: Homogeneous Ginzburg–Landau Expansion and Disorder[1]

E. Z. Kuchinskii[a], N. A. Kuleeva[a], and M. V. Sadovskii[a, b]

[a] *Institute for Electrophysics, Ural Branch, Russian Academy of Sciences, Yekaterinburg, 620016 Russia*

[b] *Mikheev Institute for Metal Physics, Ural Branch, Russian Academy of Sciences, Yekaterinburg, 620290 Russia*

e-mail: kuchinsk@iep.uran.ru; sadovski@iep.uran.ru

Received July 28, 2015

Abstract—We derive a Ginzburg–Landau (GL) expansion in the disordered attractive Hubbard model within the combined Nozieres–Schmitt-Rink and DMFT+Σ approximation. Restricting ourselves to the homogeneous expansion, we analyze the disorder dependence of GL expansion coefficients for a wide range of attractive potentials U, from the weak BCS coupling region to the strong-coupling limit, where superconductivity is described by Bose–Einstein condensation (BEC) of preformed Cooper pairs. We show that for the a semi-elliptic "bare" density of states of the conduction band, the disorder influence on the GL coefficients A and B before quadratic and quartic terms of the order parameter, as well as on the specific heat discontinuity at the superconducting transition, is of a universal nature at any strength of the attractive interaction and is related only to the general widening of the conduction band by disorder. In general, disorder growth increases the values of the coefficients A and B, leading either to a suppression of the specific heat discontinuity (in the weak-coupling limit), or to its significant growth (in the strong-coupling region). However, this behavior actually confirms the validity of the generalized Anderson theorem, because the disorder dependence of the superconducting transition temperature T_c, is also controlled only by disorder widening of the conduction band (density of states).

DOI: 10.1134/S1063776116020072

1. INTRODUCTION

The problem of superconductivity in the BCS–BEC crossover region (and up to the strong coupling limit) has a long history, starting with early works by Leggett and Nozieres and Schmitt-Rink [1, 2]. Probably the simplest model to study this crossover is the Hubbard model with attractive interaction. The most successive approach to the studies of the Hubbard model (both repulsive and attractive) is the dynamical mean field theory (DMFT) [3–5]. The attractive Hubbard model was already studied within DMFT in a number of papers [6–10]. However, up to now there are only a few works where disorder effects were taken into account, either in normal or in superconducting phase of this model. Qualitative analysis of disorder effects on the critical temperature T_c in the BCS–BEC crossover region was presented in [11], which claimed the validity of the Anderson theorem in this region in the case of s-wave pairing. A diagram analysis of disorder effects on T_c and the properties of the normal state in the crossover region were recently presented in [12].

We have developed the generalized DMFT+Σ approach to the Hubbard model [13–16], which is quite convenient for including various "external" interactions, such as disorder scattering [17, 18]. This approach is also well suited to the studies of two-particle properties, such as dynamic (optical) conductivity [17, 19]. In recent paper [10], we used this approach to analyze the single-particle properties of the normal phase and optical conductivity in the attractive Hubbard model. Subsequently, the DMFT+Σ approximation was combined with the Nozieres–Schmitt-Rink approach to study the influence of disorder on the superconducting critical temperature T_c in the BCS-BEC crossover and strong-coupling regions [20, 21], demonstrating the validity of the generalized Anderson theorem. Disorder effects on T_c are essentially due to only the general widening of the conduction band by random scattering. This was demonstrated exactly (for the whole range of attractive interactions) in the case of a semi-elliptic density of states of the conduction band (three-dimensional case) at any disorder level and is also valid in the case of a flat band (two-dimensional case) in the limit of strong enough disorder.

The Ginzburg–Landau (GL) expansion in the BCS–BEC crossover region was derived in a number of papers [22–24], but no effects of disorder scattering on the GL expansion coefficients were considered. Here, we derive the microscopic coefficients of a

[1] The article is published in the original.

(homogeneous) GL expansion for the attractive Hubbard model and study disorder effects on these coefficients including the BCS–BEC and strong-coupling regions, as well as on the specific heat discontinuity at the superconducting transition, demonstrating a certain universality of disorder behavior of these characteristics.

2. DISORDERED HUBBARD MODEL IN THE DMFT+Σ APPROACH

We consider the disordered attractive Hubbard model with the Hamiltonian

$$H = -t\sum_{\langle ij\rangle\sigma} a^{\dagger}_{i\sigma}a_{j\sigma} + \sum_{i\sigma}\epsilon_i n_{i\sigma} - U\sum_i n_{i\uparrow}n_{i\downarrow}, \qquad (1)$$

where $t > 0$ is a transfer integral between the nearest neighbors and U is the onsite Hubbard attraction, $n_{i\sigma} = a^{\dagger}_{i\sigma}a_{i\sigma}$ is electron number operator at site i, and $a_{i\sigma}$ ($a^{\dagger}_{i\sigma}$) is the annihilation (creation) operator of an electron with spin σ. Local energy levels ϵ_i are assumed to be independent random variables on different lattice sites. We assume the Gaussian distribution of ϵ_i at each site for the validity of the standard "impurity" scattering diagram technique [25]:

$$\mathcal{P}(\epsilon_i) = \frac{1}{\sqrt{2\pi}\Delta}\exp\left(-\frac{\epsilon_i^2}{2\Delta^2}\right). \qquad (2)$$

Here, Δ is the measure of disorder scattering.

The generalized DMFT+Σ approach [13–16] supplies the standard DMFT [3–5] with an additional "external" self-energy (in general, momentum dependent) due to any interaction outside the DMFT, which provides an effective method to calculate both single- and two-particle properties [17, 19]. The additive form of the total self-energy preserves the structure of the self-consistent DMFT equations [3–5]. The "external" self-energy is recalculated at each step of the standard DMFT iteration scheme, using some approximations corresponding to the form of the additional interaction, while the local Green's function (central for DMFT) is also "dressed" by the additional interaction.

For the disordered Hubbard model, we take the "external" self-energy entering the DMFT+Σ loop in the simplest form of a self-consistent Born approximation, neglecting the "crossing" diagrams due to disorder scattering:

$$\tilde{\Sigma}(\varepsilon) = \Delta^2\sum_{\mathbf{p}} G(\varepsilon, \mathbf{p}), \qquad (3)$$

where $G(\varepsilon, \mathbf{p})$ is the complete single-particle Green's function.

To solve the effective Anderson impurity model of DMFT, we here use the effective algorithm of the numerical renormalization group (NRG) [26].

In what follows, we consider the model of a "bare" conduction band with the semi-elliptic density of states (per unit cell and spin projection)

$$N_0(\varepsilon) = \frac{2}{\pi D^2}\sqrt{D^2 - \varepsilon^2}, \qquad (4)$$

where D determines the half-width of the conduction band. This is a good approximation in the three-dimensional case.

In [21], we have shown analytically that in the DMFT+Σ approach, within these approximations, all the disorder influence on the single-particle properties reduces to the simple effect of band widening by disorder scattering, $D \to D_{\text{eff}}$, where D_{eff} is the effective band half-width in the presence of disorder (in the absence of correlations, i.e., for $U = 0$):

$$D_{\text{eff}} = D\sqrt{1 + 4\frac{\Delta^2}{D^2}}, \qquad (5)$$

and the conduction band density of states (in the absence of U) "dressed" by disorder is given by

$$\tilde{N}_0(\varepsilon) = \frac{2}{\pi D_{\text{eff}}^2}\sqrt{D_{\text{eff}}^2 - \varepsilon^2}, \qquad (6)$$

preserving its semi-elliptic form.

For other models of the "bare" conduction band density of states, besides band widening, disorder scattering changes the form of the density of states, and hence the complete universality of disorder influence of single-particle properties, strictly speaking, is absent. But in the limit of strong enough disorder, the "bare" band density effectively becomes elliptic for any reasonable model, and the universality is thus restored [21].

All calculation below were performed for the quarter-filled band ($n = 0.5$ per lattice site).

3. GINZBURG–LANDAU EXPANSION

The critical temperature of the superconducting transition T_c in the attractive Hubbard model was analyzed using direct DMFT calculations in a number of papers [6, 7, 9]. In [10], we determined T_c from the instability condition of the normal phase (instability of the DMFT iteration procedure). The results obtained in this way were in good agreement with the results in [6, 7, 9]. Additionally, in [10], we calculated T_c using the approximate Nozieres–Schmitt-Rink approach in combination with DMFT (used to calculate the chemical potential of the system), demonstrating that being much less time consuming, it provides a semi-quantitative description of the T_c behavior in the BCS–BEC crossover region, in good agreement with direct DMFT calculations. In [20, 21], the combined Nozieres–Schmitt-Rink approach was used to study the detailed dependence of T_c on disorder. Below, we use this combined approach to derive the GL expan-

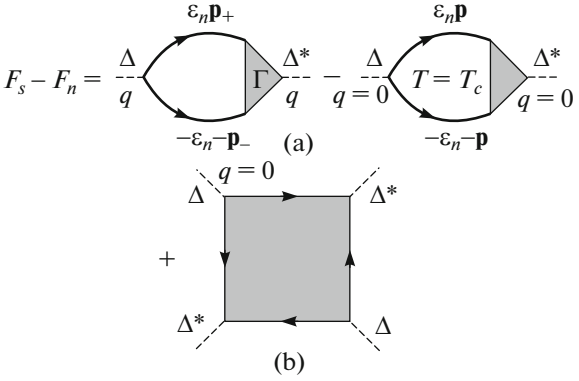

Fig. 1. Diagram representation of the Ginzburg–Landau expansion.

sion including the disorder dependence of the GL expansion coefficients.

We write the GL expansion for the difference of free energies of superconducting and normal phases in the standard form

$$F_s - F_n = A|\Delta_{\mathbf{q}}|^2 + q^2 C|\Delta_{\mathbf{q}}|^2 + \frac{B}{2}|\Delta_{\mathbf{q}}|^4, \qquad (7)$$

where $\Delta_{\mathbf{q}}$ is the spatial Fourier component of the amplitude of the superconducting order parameter. Microscopically, this expansion is determined by diagrams of the loop expansion for the free energy of an electron in the "external field" of (static) superconducting order parameter fluctuations with a small wave vector $\mathbf{q}$, shown in Fig. 1 (where fluctuations are represented by dashed lines) [25]. Below, we limit ourselves to the case of a homogeneous expansion with $\mathbf{q} = 0$ and calculations of its coefficients A and B, leaving the (much more complicated) analysis of the general inhomogeneous case of finite $\mathbf{q}$ and calculations of the coefficient C in (7) for the future work.

Within the Nozieres–Schmitt-Rink approach [2], we use the weak-coupling approximation to calculate loop diagrams with two and four Cooper vertices shown in Fig. 1, dropping all corrections due to the Hubbard U, while including "dressing" by disorder scattering.[2] However, the chemical potential, which essentially depends on the coupling strength U and determines the BEC condition in the strong-coupling region, is calculated via the full DMFT+Σ procedure.

The coefficient A before the square of the order parameter in the GL expansion is given by the diagrams in Fig. 1a with $q = 0$ [25]:

$$A(T) = \chi_0(q = 0, T) - \chi_0(q = 0, T_c), \qquad (8)$$

where

$$\chi_0(q = 0, T) = -T\sum_n \sum_{\mathbf{pp}'} \Phi_{\mathbf{pp}'}(\varepsilon_n) \qquad (9)$$

is the two-particle loop in the Cooper channel "dressed" only by disorder scattering, while $\Phi_{\mathbf{pp}'}(\varepsilon_n)$ is the disorder-averaged two-particle Green's function in the Cooper channel ($\varepsilon_n = \pi T(2n + 1)$ is the corresponding Matsubara frequency). Subtraction of the second diagram in Fig. 1a, i.e., that of $\chi_0(q = 0, T_c)$ in (8), guarantees the validity of $A(T = T_c) = 0$, which necessarily holds in any kind of Landau expansion [25].

To obtain $\sum_{\mathbf{pp}'} \Phi_{\mathbf{pp}'}(\varepsilon_n)$, we use the exact Ward identity derived in [19]:

$$G(\varepsilon_n, \mathbf{p}) - G(-\varepsilon_n, -\mathbf{p}) = -\sum_{\mathbf{p}'} \Phi_{\mathbf{pp}'}(\varepsilon_n) \times (G_0^{-1}(\varepsilon_n, \mathbf{p}') - G_0^{-1}(-\varepsilon_n, -\mathbf{p}')). \qquad (10)$$

Here, $G(\varepsilon_n, \mathbf{p})$ is the disorder-averaged single-particle Green's function (not "dressed" by Hubbard interaction!). With the symmetry $\varepsilon(\mathbf{p}) = \varepsilon(-\mathbf{p})$ and $G(\varepsilon_n, -\mathbf{p}) = G(\varepsilon_n, \mathbf{p})$, we use Ward identity (10) to obtain

$$\sum_{\mathbf{pp}'} \Phi_{\mathbf{pp}'}(\varepsilon_n) = -\frac{\sum_{\mathbf{p}} G(\varepsilon_n, \mathbf{p}) - \sum_{\mathbf{p}} G(-\varepsilon_n, \mathbf{p})}{2i\varepsilon_n}, \qquad (11)$$

whence we obtain Cooper susceptibility (9)

$$\chi_0(q = 0, T) = T\sum_n \frac{\sum_{\mathbf{p}} G(\varepsilon_n, \mathbf{p}) - \sum_{\mathbf{p}} G(-\varepsilon_n, \mathbf{p})}{2i\varepsilon_n} = T\sum_n \frac{\sum_{\mathbf{p}} G(\varepsilon_n, \mathbf{p})}{i\varepsilon_n}. \qquad (12)$$

Performing the standard summation over Matsubara frequencies [25], we now obtain

$$\chi_0(q = 0, T) = \frac{1}{4\pi i}\int_{-\infty}^{\infty} d\varepsilon \frac{\sum_{\mathbf{p}} G^R(\varepsilon, \mathbf{p}) - \sum_{\mathbf{p}} G^A(\varepsilon, \mathbf{p})}{\varepsilon} \tanh\frac{\varepsilon}{2T} = -\int_{-\infty}^{\infty} d\varepsilon \frac{\tilde{N}(\varepsilon)}{2\varepsilon} \tanh\frac{\varepsilon}{2T}, \qquad (13)$$

where $\tilde{N}(\varepsilon)$ is the "bare" ($U = 0$) density of states "dressed" by disorder scattering, which in the case of a semi-elliptic band takes the form (6). In Eq. (13), the origin of ε is at the chemical potential. Replacing $\varepsilon \to \varepsilon - \mu$ to shift the origin of energy to the center of conduction band, we finally write

[2] In the absence of disorder, this approach just coincides with that used in [22–24], involving the Hubbard–Stratonovich transformation in the functional integral over fluctuations of the superconducting order parameter.

$$\chi_0(q=0,T) = -\int_{-\infty}^{\infty} d\varepsilon \frac{\tilde{N}(\varepsilon)}{2(\varepsilon-\mu)} \tanh\frac{\varepsilon-\mu}{2T}. \quad (14)$$

The Cooper instability of the normal phase, determining the superconducting transition temperature T_c, is written as

$$1 = -U\chi_0(q=0,T_c). \quad (15)$$

We then obtain the following equation for the critical temperature:

$$1 = \frac{U}{2}\int_{-\infty}^{\infty} d\varepsilon \tilde{N}_0(\varepsilon)\frac{\tanh((\varepsilon-\mu)/2T_c)}{\varepsilon-\mu}. \quad (16)$$

Using (15) to determine $\chi_0(q=0,\ T_c)$ and (14) for $\chi_0(q=0,\ T)$, we obtain the coefficient A in (8):

$$A(T) = \frac{1}{U} - \int_{-\infty}^{\infty} d\varepsilon \tilde{N}_0(\varepsilon)\frac{\tanh((\varepsilon-\mu)/2T)}{2(\varepsilon-\mu)}. \quad (17)$$

The chemical potential for different values of U and Δ is to be determined here from direct DMFT+Σ calculations, i.e., from the standard equation for the total number of electrons (band filling), defined by the Green's function obtained in the DMFT+Σ approximation. This allows us to find both T_c and GL expansion coefficients in a wide range of parameters of the model, including the BCS–BEC crossover region and the limit of strong coupling, for different disorder levels. Actually, this is the essence of the Nozieres–Schmitt-Rink approximation in the weak-coupling region, transition temperature is controlled by the equation for Cooper instability, while in the strong-coupling limit, it is defined as the temperature of Bose condensation, which is controlled by the equation for the chemical potential. The joint solution of Eqs. (16) and (17) with the DMFT+Σ equation for the chemical potential provides the correct interpolation for T_c and GL coefficient A from the weak-coupling region via the BCS–BEC crossover towards the strong coupling.

For $T \to T_c$, the coefficient $A(T)$ is written as

$$A(T) \equiv a(T - T_c), \quad (18)$$

where in the case of a temperature independent chemical potential,

$$a = \frac{1}{4T_c^2}\int_{-\infty}^{\infty} d\varepsilon \tilde{N}_0(\varepsilon)\frac{1}{\cosh^2((\varepsilon-\mu)/2T_c)}. \quad (19)$$

In the BCS approximation with the conduction band of an infinite width with a constant density of states $\tilde{N}_0(0)$, we obtain the standard result $a = \tilde{N}_0(0)/T_c$ from (19) [25]. However, in the BCS–BEC crossover region, the temperature dependence of μ is essential and we have to use the general expression (17) in conjunction with the equation for μ to calculate a. At the same time, it is clear from Eq. (17) that disorder scattering influences a only through the changes of the density of states $\tilde{N}_0(\varepsilon)$ and the chemical potential μ, which is a typical single-particle property. Thus, in the case of a semi-elliptic "bare" conduction band, the dependence of a on disorder is due to only the band widening by disorder, with the replacement $D \to D_{\text{eff}}$. Therefore, in the presence of disorder, we expect the universal dependence of $a(2D_{\text{eff}})^2$ on $U/2D_{\text{eff}}$ (all energies are to be normalized by the effective bandwidth $2D_{\text{eff}}$), which is confirmed by the results of direct numerical computations in the next section (cf. Fig. 4a).

The coefficient B is determined by a "square" diagram with four Cooper vertices with $q = 0$, "dressed" in an arbitrary way by disorder scattering, which is shown in Fig. 1b [25]:

$$B = \frac{1}{2}T\sum_n \sum_{\mathbf{p}_1\mathbf{p}_2\mathbf{p}_3\mathbf{p}_4} \langle G(i\varepsilon_n;\mathbf{p}_1,\mathbf{p}_2)G(-i\varepsilon_n;-\mathbf{p}_2,-\mathbf{p}_3) \times G(i\varepsilon_n;\mathbf{p}_3,\mathbf{p}_4)G(-i\varepsilon_n;-\mathbf{p}_4,-\mathbf{p}_1)\rangle, \quad (20)$$

where $\langle ... \rangle$ denotes averaging over disorder, and $G(i\varepsilon_n;\ \mathbf{p}_1,\ \mathbf{p}_2)$ (and other similar expressions) represent exact single-particle Green's functions for a fixed configuration of the random potential. Performing standard summation over Matsubara frequencies, we obtain

$$B = \frac{1}{2}\int_{-\infty}^{\infty}\frac{d\varepsilon}{2\pi i}\tanh\frac{\varepsilon}{2T} \times \sum_{\mathbf{p}_1\mathbf{p}_2\mathbf{p}_3\mathbf{p}_4} \langle G^R(\varepsilon;\mathbf{p}_1,\mathbf{p}_2)G^A(\varepsilon\ ;-\mathbf{p}_2,-\mathbf{p}_3) \times G^R(\varepsilon;\mathbf{p}_3,\mathbf{p}_4)G^A(-\varepsilon;-\mathbf{p}_4,-\mathbf{p}_1)\rangle. \quad (21)$$

Due to the zero momentum $\mathbf{q} = 0$ in Cooper vertices and the static nature of disorder scattering, we can now use a certain generalization of Ward identity (10) to obtain (at $T = T_c$)

$$B = \int_{-\infty}^{\infty}\frac{d\varepsilon}{4\varepsilon^3}\left(\tanh\frac{\varepsilon}{2T_c} - \frac{\varepsilon/2T_c}{\cosh^2\varepsilon/2T_c}\right)\tilde{N}_0(\varepsilon). \quad (22)$$

A detailed derivation is presented in Appendix A. In the BCS approximation, using the conduction band of an infinite width with a constant density of states $\tilde{N}_0(0)$, we immediately obtain the standard result from Eq. (22): $B = (7\zeta(3)/8\pi^2T_c^2)\tilde{N}_0(0)$ [25].

Again, replacing here $\varepsilon \to \varepsilon - \mu$ to shift the origin of energy to the middle of the conduction band, we can write

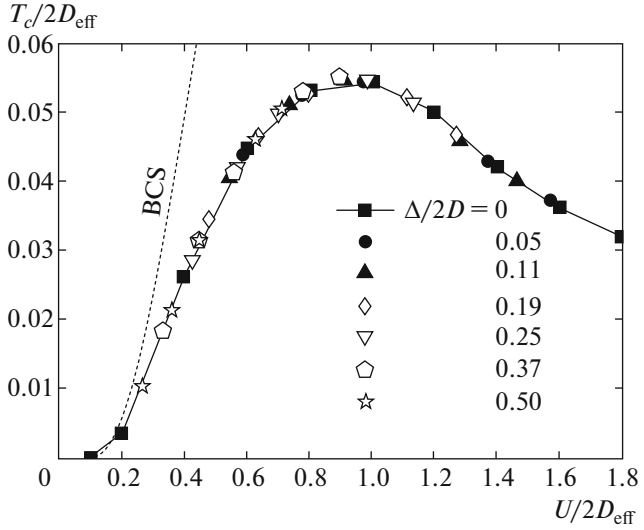

Fig. 2. Universal dependence of the superconducting critical temperature on disorder for different values of the Hubbard attraction.

$$B = \int_{-\infty}^{\infty} \frac{d\varepsilon}{4(\varepsilon-\mu)^3} \times \left(\tanh\frac{\varepsilon-\mu}{2T_c} - \frac{(\varepsilon-\mu)/2T_c}{\cosh^2\dfrac{\varepsilon-\mu}{2T_c}} \right) \tilde{N}_0(\varepsilon). \quad (23)$$

It follows that the disorder dependence of the coefficient B (similarly to A) is also determined only by the disorder-widened density of states $\tilde{N}_0(\varepsilon)$ and the chemical potential, and hence in the case of a semi-elliptic "bare" conduction band, it reduces to the simple replacement $D \to D_{\text{eff}}$, leading to a universal dependence of $B(2D_{\text{eff}})^3$ on $U/2D_{\text{eff}}$, which is confirmed by the results of direct numerical computations presented in the next section and shown in Fig. 4b.

We stress that Eqs. (17) and (23) for the GL coefficients A and B were obtained with the use of exact Ward identities, and are therefore valid also in the limit of strong disorder (beyond Anderson localization).

The universal dependence on disorder, related to the conduction band widening by disorder scattering, is also valid for the specific-heat discontinuity at T_c, because it is completely determined by the coefficients a and B:

$$C_s(T_c) - C_n(T_c) = T_c \frac{a^2}{B}. \quad (24)$$

Appropriate numerical results are also given in the next Section (cf. Fig. 5b).

The coefficient C before the gradient term of the GL expansion is determined essentially by two-particle characteristics (in particular, due to a nontrivial q-dependence of the vertex, which is obviously changed by disorder scattering). In particular, the behavior of C is significantly changed at the Anderson transition [27], and therefore no universality of the disorder dependence is expected in this case.

4. MAIN RESULTS

We now discuss the main results of our numerical calculations, directly demonstrating the universal dependences of the GL coefficients A and B and the specific heat discontinuity at T_c on disorder.

In Fig. 2, we show the universal dependence of the critical temperature T_c on the Hubbard attraction U for

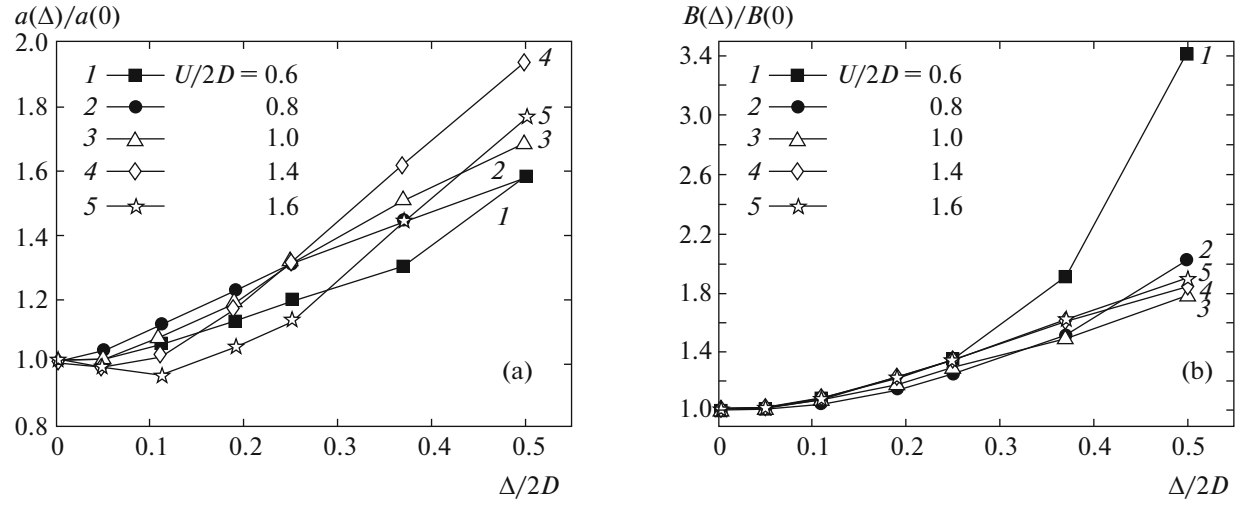

Fig. 3. Disorder dependence of the GL coefficients (a) a and (b) B, normalized by their values in the absence of disorder, for different values of the Hubbard attraction.

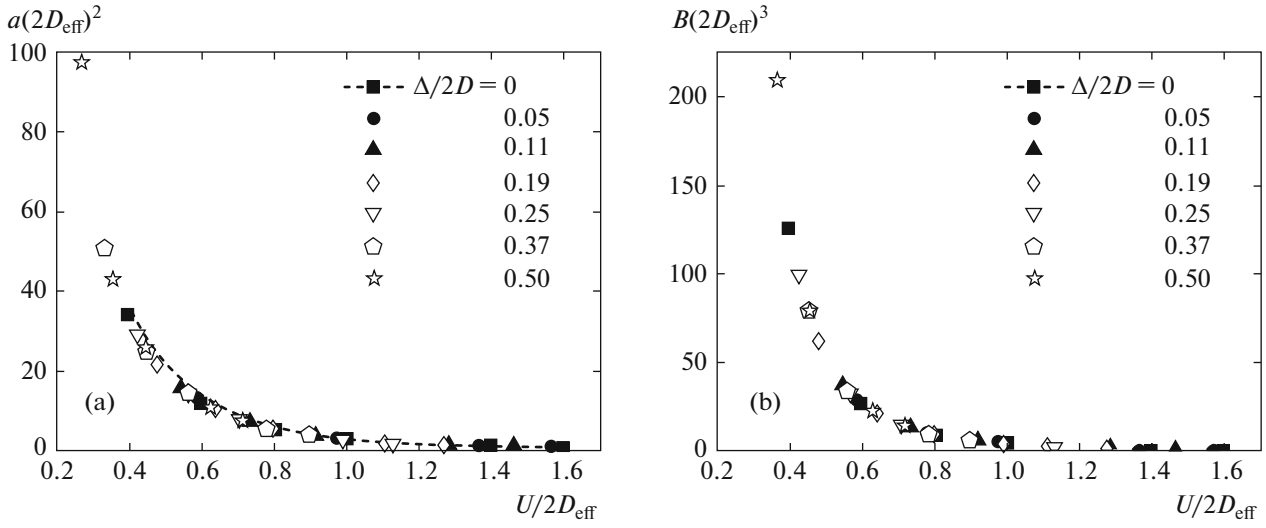

Fig. 4. Universal dependence of the GL coefficients (a) a and (b) B on the Hubbard attraction for different values of disorder.

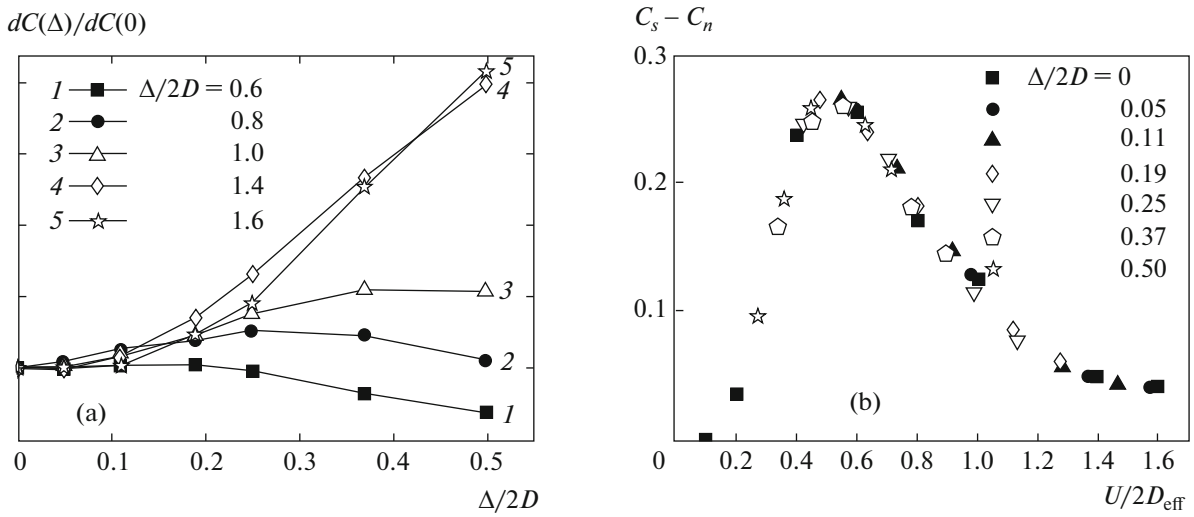

Fig. 5. (a) Dependence of the specific heat discontinuity at the critical temperature, $dC \equiv C_s - C_n$, on disorder for different values of the Hubbard attraction U and (b) universal dependence of this discontinuity on U for different values of disorder.

different levels of disorder, which was obtained and discussed in detail in [20, 21]. A typical maximum of T_c at $U/2D_{\text{eff}} \sim 1$ is characteristic of the BCS–BEC crossover region.

In Fig. 3, we present disorder dependences of the GL coefficients a (Fig. 3a) and B (Fig. 3b) for different values of the Hubbard attraction. We can see that a in general increases with an increase in disorder. Only in the limit of a strong enough coupling $U/2D > 1.4$ (curves *4* and *5*) in the region of weak disorder do we observe weak suppression of a by disorder scattering. The coefficient B grows sufficiently fast with disorder in the region of weak coupling (curve *1* in Fig. 3b), while in the region of strong coupling, this growth becomes more moderate (curves *4*, *5* in Fig. 3b), such that the dependence of B on disorder in this region becomes almost independent of the value of U (curves *4* and *5* practically coincide).

However, this rather complicated dependence of the coefficients a and B on disorder is determined solely by the growth of the effective conduction bandwidth with disorder, given by Eq. (5). In Fig. 4, we show the universal dependences of the GL coefficients a and B, normalized by appropriate powers of the effective bandwidth, on the strength of Hubbard attraction. In the absence of disorder (the dashed line

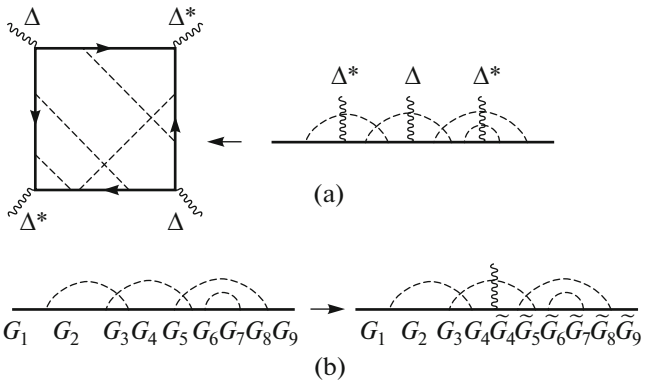

Fig. 6. Diagrams for the coefficient B and the derivation of a generalized Ward identity.

with squares), the coefficients a and B decrease fast as U increases. Other symbols in Fig. 4 show the results of our calculations for different levels of disorder. It is clearly seen that all the data ideally fit the universal curve obtained in the absence of disorder.

The coefficients a and B determine the specific heat discontinuity at the critical temperature, Eq. (24). Because these coefficients and T_c [20, 21] depend on disorder in a universal way due only to the growth of the effective bandwidth (5), the same type of universal dependence is also valid for the specific heat discontinuity. In Fig. 5a, we show the dependence of the specific heat discontinuity $dC \equiv C_s - C_n$ on disorder for different values of the Hubbard attraction U. It is seen that in the region of weak coupling (curve *1*), the specific heat discontinuity is suppressed by disorder; for intermediate couplings (curves *2* and *3*), weak disorder leads to an increase in the specific heat discontinuity, while further increasing the disorder suppresses this discontinuity. In the region of strong coupling (curves *4* and *5*), the increase in disorder leads to a significant increase in the specific heat discontinuity, which is mainly related to the similar increase in T_c (cf. [20, 21]). However, this complicated dependence of the specific heat discontinuity on disorder is again completely determined by the growth of effective bandwidth (5). In Fig. 5b, we show the universal dependence of the specific heat discontinuity on U, normalized by the bandwidth $2D_{\text{eff}}$. Black squares represent data in the absence of disorder. Other symbols in Fig. 5b show the data for different disorder levels. We see again that all the data precisely fit the universal dependence of the specific heat discontinuity obtained in the absence of disorder. The specific heat discontinuity increases with an increases in U in the region of weak coupling $U/2D_{\text{eff}} \ll 1$ and decreases with an increase in U in the limit of strong coupling $U/2D_{\text{eff}} \gg 1$. The maximum of the specific heat discontinuity is observed at $U/2D_{\text{eff}} \approx 0.55$. Actually, this dependence of the specific heat discontinuity qualitatively resembles a similar dependence of the critical temperature, although its maximum is attained at smaller values of the Hubbard attraction.

5. CONCLUSION

Using a combination of the Nozieres–Schmitt-Rink approximation with the generalized DMFT+Σ approach, we have studied disorder influence on the coefficients A and B determining the homogeneous Ginzburg–Landau expansion and specific heat discontinuity at the superconducting transition in the attractive Hubbard model.

We have demonstrated analytically that in the case of a "bare" conduction band with a semi-elliptic density of states, disorder influence on the GL coefficients A and B and the specific heat discontinuity is universal and is controlled only by the general conduction band (density of states) widening by disorder scattering; we illustrated this conclusion with explicit numerical calculations performed for a wide range of attractive potentials U, from the weak-coupling region, where $U/2D_{\text{eff}} \ll 1$ and the superconducting instability is described by the usual BCS approach, to the strong-coupling region, where $U/2D_{\text{eff}} \gg 1$ and the superconducting transition is determined by Bose–Einstein condensation of preformed Cooper pairs.

These results essentially prove the validity of the generalized Anderson theorem in the BCS–BEC crossover region and in the limit of strong coupling not only for T_c [20, 21] but also for the homogeneous Ginzburg–Landau expansion, determining appropriate thermodynamic effects like the specific heat discontinuity at the transition point.

ACKNOWLEDGMENTS

This work was supported by the Russian Science Foundation (project no. 14-12-00502).

APPENDIX

The Coefficient B in the Presence of Disorder

The coefficient B is determined by the "square" diagram with four Cooper vertices with $\mathbf{q} = 0$, "dressed" by disorder scattering, shown in Fig. 1b. The corresponding analytic expression is given in Eq. (20). After the standard summation over Matsubara frequencies, B is written as in (21), i.e., is determined by the following combination of four Green's functions with real frequencies:

$$\sum_{\mathbf{p}_1\mathbf{p}_2\mathbf{p}_3\mathbf{p}_4} \langle G^R(\varepsilon;\mathbf{p}_1,\mathbf{p}_2)G^A(-\varepsilon;-\mathbf{p}_2,-\mathbf{p}_3) \times G^R(\varepsilon;\mathbf{p}_3,\mathbf{p}_4)G^A(-\varepsilon;-\mathbf{p}_4,-\mathbf{p}_1)\rangle, \tag{A.1}$$

where $\langle ... \rangle$ denotes averaging over disorder and $G^{R(A)}(\varepsilon; \mathbf{p}_1, \mathbf{p}_2)$ are the exact retarded (advanced) single-particle Green's functions for a fixed configuration of disorder.

A typical diagram of the fourth order of disorder scattering (dashed lines) is shown in Fig. 6a. Arbitrary diagrams for such a four-particle Green's function can be obtained from diagrams for the single-particle Green's function of the same order of disorder scattering by arbitrarily inserting three Cooper vertices into the "bare" electron Green's functions, as shown in Fig. 6a. Taking the static nature of disorder scattering and the zero transferred momentum $\mathbf{q} = 0$ in Cooper vertices into account, we can evaluate (A.1) using a certain generalization of exact Ward identity (10), derived in [19].

We take the diagram for the single-particle Green' function, shown in the left part of Fig. 6b, and consider a certain configuration of momenta transferred by dashed lines. Here, we have nine "bare" electron Green's functions with momenta $\mathbf{p}_1$, ..., $\mathbf{p}_9$. In what follows, we use the short notation

$$G_i = G_0^R(\varepsilon; \mathbf{p}_i), \quad \tilde{G}_i = G_0^A(-\varepsilon; -\mathbf{p}_i), \tag{A.2}$$

where $G_0^{R(A)}(\varepsilon; \mathbf{p}) = 1/(\varepsilon - \varepsilon(\mathbf{p}) \pm i\delta)$ is the "bare" Green's function. Inserting a Cooper vertex leads to the sign change of momenta and frequencies (i.e., to the replacement $G_i \leftrightarrow \tilde{G}_i$) in all Green's functions standing to the right of the vertex. We assume that the central of the three Cooper vertices was inserted into the fourth Green's function, as shown in the right part of Fig. 6b. An arbitrary insertion of the first Cooper vertex into one of the first four of the Green's functions leads to the result

$$\begin{aligned} G_1G_2C_3G_4 \to G_1\tilde{G}_1\tilde{G}_2\tilde{G}_3\tilde{G}_4 + G_1G_2\tilde{G}_2\tilde{G}_3\tilde{G}_4 \\ + G_1G_2G_3\tilde{G}_3\tilde{G}_4 + G_1G_2G_3G_4\tilde{G}_4, \end{aligned} \tag{A.3}$$

whence, using the identify $G_i^{-1} - \tilde{G}_i^{-1} = 2\varepsilon$, we obtain

$$\begin{aligned} G_1\tilde{G}_1\tilde{G}_2\tilde{G}_3\tilde{G}_4 \frac{G_1^{-1} - \tilde{G}_1^{-1}}{2\varepsilon} + \ldots \\ + G_1G_2G_3G_4\tilde{G}_4 \frac{G_4^{-1} - \tilde{G}_4^{-1}}{2\varepsilon} = \frac{\tilde{G}_1\tilde{G}_2\tilde{G}_3\tilde{G}_4 - G_1G_2C_3G_4}{2\varepsilon}. \end{aligned} \tag{A.4}$$

Then $\tilde{G}_4\tilde{G}_5\tilde{G}_6\tilde{G}_7\tilde{G}_8\tilde{G}_9 \to G_4G_5G_6G_7G_8G_9$ and after all insertions of the last (third) Cooper vertex into one of the six Green's functions G_4, ..., G_9, we again obtain $(\tilde{G}_4\tilde{G}_5\tilde{G}_6\tilde{G}_7\tilde{G}_8\tilde{G}_9 - G_4G_5G_6G_7G_8G_9)/2\varepsilon$.

We thus obtain

$$\begin{aligned} &\langle G^R(\varepsilon)G^A(-\varepsilon)G^R(\varepsilon)G^A(-\varepsilon)\rangle \\ &= \left\langle \frac{G^A(-\varepsilon) - G^R(\varepsilon)}{2\varepsilon} \frac{G^A(-\varepsilon) - G^R(\varepsilon)}{2\varepsilon} \right\rangle \\ &= \frac{1}{4\varepsilon^2}(\langle G^A(-\varepsilon)G^A(-\varepsilon)\rangle + \langle G^R(\varepsilon)G^R(\varepsilon)\rangle \\ &- 2\langle G^R(\varepsilon)G^A(-\varepsilon)\rangle) = \frac{1}{4\varepsilon^2}\left\{\frac{d}{d\varepsilon}(\langle G^A(-\varepsilon)\rangle - \langle G^R(\varepsilon)\rangle) \right. \\ &\left. - \frac{\langle G^A(-\varepsilon)\rangle - \langle G^R(\varepsilon)\rangle}{\varepsilon}\right\}, \end{aligned} \tag{A.5}$$

where we can evaluate the two-particle Green's functions with $q = 0$ again using an analogue of Ward identity (10) for real frequencies. Using (A.5) in (21) and replacing $\varepsilon \to -\varepsilon$ in terms with $\langle G^A(-\varepsilon)\rangle$ in the integral over ε, we obtain

$$\begin{aligned} B &= \int_{-\infty}^{\infty} \frac{d\varepsilon}{2\pi i} \frac{\tanh(\varepsilon/2T)}{4\varepsilon^2}\left(\frac{d}{d\varepsilon} - \frac{1}{\varepsilon}\right) \\ &\times \left(\sum_{\mathbf{p}} G^A(\varepsilon, \mathbf{p}) - \sum_{\mathbf{p}} G^R(\varepsilon, \mathbf{p})\right) \\ &= \int_{-\infty}^{\infty} d\varepsilon \frac{\tanh(\varepsilon/2T)}{4\varepsilon^2}\left(\frac{d}{d\varepsilon} - \frac{1}{\varepsilon}\right)\tilde{N}_0(\varepsilon) \\ &= \int_{-\infty}^{\infty} \frac{d\varepsilon}{4\varepsilon^3}\left(\tanh\frac{\varepsilon}{2T} - \frac{\varepsilon/2T}{\cosh^2(\varepsilon/2T)}\right)\tilde{N}_0(\varepsilon). \end{aligned} \tag{A.6}$$

This expression was used in the main part of the paper.

REFERENCES

1. A. J. Leggett, in *Modern Trends in the Theory of Condensed Matter,* Ed. by A. Pekalski and J. Przystawa (Springer, Berlin, 1980).
2. P. Nozieres and S. Schmitt-Rink, J. Low Temp. Phys. **59**, 195 (1985).
3. Th. Pruschke, M. Jarrell, and J. K. Freericks, Adv. Phys. **44**, 187 (1995).
4. A. Georges, G. Kotliar, W. Krauth, and M. J. Rozenberg, Rev. Mod. Phys. **68**, 13 (1996).
5. D. Vollhardt, in *Lectures on the Physics of Strongly Correlated Systems XIV,* Ed. by A. Avella and F. Mancini, AIP Conf. Proc., Vol. 1297 (Amer. Inst. Physics, Melville, New York, 2010), p. 339; arXiv: 1004.5069.
6. M. Keller, W. Metzner, and U. Schollwock, Phys. Rev. Lett. **86**, 4612 (2001); arXiv: cond-mat/0101047.
7. A. Toschi, P. Barone, M. Capone, and C. Castellani, New J. Phys. **7**, 7 (2005); arXiv: cond-mat/0411637v1.
8. J. Bauer, A. C. Hewson, and N. Dupis, Phys. Rev. B **79**, 214518 (2009); arXiv: 0901.1760v2.
9. A. Koga and P. Werner, Phys. Rev. A **84**, 023638 (2011); arXiv: 1106.4559v1.

10. N. A. Kuleeva, E. Z. Kuchinskii, and M. V. Sadovskii, J. Exp. Theor. Phys. **119**, 264 (2014); arXiv: 1401.2295.
11. A. I. Posazhennikova and M. V. Sadovskii, JETP Lett. **65**, 270 (1997).
12. F. Palestini and G. C. Strinati, arXiv: 1311.2761.
13. E. Z. Kuchinskii, I. A. Nekrasov, and M. V. Sadovskii, JETP Lett. **82**, 198 (2005); arXiv: cond-mat/0506215.
14. M. V. Sadovskii, I. A. Nekrasov, E. Z. Kuchinskii, Th. Pruschke, and V. I. Anisimov, Phys. Rev. B **72**, 155105 (2005); arXiv: cond-mat/0508585.
15. E. Z. Kuchinskii, I. A. Nekrasov, and M. V. Sadovskii, J. Low Temp. Phys. **32**, 528 (2006); arXiv: cond-mat/0510376.
16. E. Z. Kuchinskii, I. A. Nekrasov, and M. V. Sadovskii, Phys. Usp. 55, 325 (2012); arXiv: 1109. 2305.
17. E. Z. Kuchinskii, I. A. Nekrasov, and M. V. Sadovskii, J. Exp. Theor. Phys. **106**, 581 (2008); arXiv: 0706.2618.
18. E. Z. Kuchinskii, N. A. Kuleeva, I. A. Nekrasov, and M. V. Sadovskii, J. Exp. Theor. Phys. **110**, 325 (2010); arXiv: 0908.3747.
19. E. Z. Kuchinskii, I. A. Nekrasov, and M. V. Sadovskii, Phys. Rev. B **75**, 115102 (2007); arXiv: cond-mat/0609404.
20. E. Z. Kuchinskii, N. A. Kuleeva, and M. V. Sadovskii, JETP Lett. **100**, 192 (2014); arXiv: 1406.5603.
21. E. Z. Kuchinskii, N. A. Kuleeva, and M. V. Sadovskii, J. Exp. Theor. Phys. **120**, 1055 (2015); arXiv: 1411.1547.
22. R. Micnas, Acta Phys. Pol. A **100** (s), 177 (2001); arXiv: cond-mat/0211561v2.
23. M. Drechsler and W. Zwerger, Ann. Phys. (Leipzig) **1**, 15 (1992).
24. S. Stintzing and W. Zwerger, Phys. Rev. B **56**, 9004 (1997); arXiv: cond-mat/9703129v2.
25. M. V. Sadovskii, *Diagrammatics* (World Scientific, Singapore, 2006).
26. R. Bulla, T. A. Costi, and T. Pruschke, Rev. Mod. Phys. **60**, 395 (2008).
27. M. V. Sadovskii, *Superconductivity and Localization* (World Scientific, Singapore, 2000).

ISSN 1063-7761, Journal of Experimental and Theoretical Physics, 2017, Vol. 125, No. 1, pp. 111–122. © Pleiades Publishing, Inc., 2017.
Published in Russian in Zhurnal Eksperimental'noi i Teoreticheskoi Fiziki, 2017, Vol. 152, No. 1, pp. 133–146.

ORDER, DISORDER, AND PHASE TRANSITION IN CONDENSED SYSTEM

Ginzburg–Landau Expansion in Strongly Disordered Attractive Anderson–Hubbard Model[1]

E. Z. Kuchinskii[a,*], N. A. Kuleeva[a], and M. V. Sadovskii[a,b,]**

[a] *Institute for Electrophysics, Ural Branch, Russian Academy of Sciences, Yekaterinburg, 620016 Russia*

[b] *Mikheev Institute for Metal Physics, Ural Branch, Russian Academy of Sciences, Yekaterinburg, 620990 Russia*

**e-mail: kuchinsk@iep.uran.ru*

***e-mail: sadovski@iep.uran.ru*

Received February 8, 2017

Abstract—We have studied disordering effects on the coefficients of Ginzburg–Landau expansion in powers of superconducting order parameter in the attractive Anderson–Hubbard model within the generalized DMFT+Σ approximation. We consider the wide region of attractive potentials U from the weak coupling region, where superconductivity is described by BCS model, to the strong coupling region, where the superconducting transition is related with Bose–Einstein condensation (BEC) of compact Cooper pairs formed at temperatures essentially larger than the temperature of superconducting transition, and a wide range of disorder—from weak to strong, where the system is in the vicinity of Anderson transition. In the case of semielliptic bare density of states, disorder's influence upon the coefficients A and B of the square and the fourth power of the order parameter is universal for any value of electron correlation and is related only to the general disorder widening of the bare band (generalized Anderson theorem). Such universality is absent for the gradient term expansion coefficient C. In the usual theory of "dirty" superconductors, the C coefficient drops with the growth of disorder. In the limit of strong disorder in BCS limit, the coefficient C is very sensitive to the effects of Anderson localization, which lead to its further drop with disorder growth up to the region of the Anderson insulator. In the region of BCS–BEC crossover and in BEC limit, the coefficient C and all related physical properties are weakly dependent on disorder. In particular, this leads to relatively weak disorder dependence of both penetration depth and coherence lengths, as well as of related slope of the upper critical magnetic field at superconducting transition, in the region of very strong coupling.

DOI: 10.1134/S1063776117060139

1. INTRODUCTION

The studies of disorder influence on superconductivity have a rather long history. The pioneer works by Abrikosov and Gor'kov [1–4] considered the limit of weak disorder ($p_F l \gg 1$, where p_F is the Fermi momentum and l is the mean free path) and weak coupling superconductivity well described by BCS theory. The notorious "Anderson theorem" on superconducting critical temperature T_c of superconductors with "normal" (nonmagnetic) disorder [5, 6] is usually also referred to these limits.

The generalization of the theory of "dirty" superconductors to the case of strong enough disorder ($p_F l \sim 1$) (and further up to the region of Anderson transition) was made in [7–9], where superconductivity was also considered in the weak coupling limit.

The problem of BCS theory generalization to the strong coupling region has also been studied for a long time. Significant progress in this direction was achieved by Nozieres and Schmitt-Rink [10], who proposed an effective method to study the crossover from BCS-type behavior in the weak coupling region to Bose–Einstein condensation (BEC) in the strong coupling region. At the same time, the problem of superconductivity of disordered systems in the limit of strong coupling and in the BCS–BEC crossover region remains relatively undeveloped.

One of the simplest models to study the BCS–BEC crossover is the attractive Hubbard model. The most successful approach to the studies of Hubbard model, both to describe strongly correlated systems in case of repulsive interactions and to study BCS–BEC crossover in case of attraction, is the dynamical mean-field theory (DMFT) [11–13].

In recent years, we have developed the generalized DMFT+Σ approach to the Hubbard model [14–19], which is very convenient to the description of different additional "external" (as compared to DMFT) inter-

[1] The article is published in the original.

actions. In particular, this approach is well suited to describe also the two-particle properties, such as optical (dynamic) conductivity [18, 20].

In [21], we have used this approach to analyze single-particle properties of the normal phase and optical conductivity in the attractive Hubbard model. Further on, we used the DMFT+Σ method in [22] to study disorder effects on superconducting critical temperature, which was calculated within the Nozieres–Schmitt-Rink approach. In particular, for the case of the semielliptic model of the bare density of states, which is adequate to describe three-dimensional systems, we have demonstrated numerically that disorder influence upon the critical temperature (for the whole range of interaction parameters) is related only to the general widening of the bare band (density of states) by disorder. In [23], we have presented an analytic derivation of such disorder influence (in DMFT+Σ approximation) on all single-particle properties and the temperature of superconducting transition for the case of the semielliptic band.

Starting with the classic paper by Gor'kov [3] it is well known that Ginzburg–Landau expansion plays the fundamental role in the theory of "dirty" superconductors, allowing the effective treatment of disorder dependence of different physical properties close to superconducting critical temperature [6]. The generalization of this theory to the region of strong disorder (up to Anderson metal–insulator transition) was also based upon microscopic derivation of the coefficients of this expansion [7–9]. However, as noted above, all these derivations were performed in the weak coupling limit of BCS theory.

In [24], we have combined the Nozieres–Schmitt-Rink and DMFT+Σ approximations within the attractive Hubbard model to derive coefficients of homogeneous Ginzburg–Landau expansion A and B before the square and the fourth power of superconducting order parameter, demonstrating the universal disorder influence on coefficients A and B and the related discontinuity of specific heat at the transition temperature. After that, in [25], we have studied the behavior of coefficient C before the gradient term of Ginzburg–Landau expansion, where such universality is absent. In this work, we have only considered this coefficient in the region of weak disorder ($p_F l \gg 1$) in the "ladder" approximation for impurity scattering, as it is usually done in the standard theory of "dirty" superconductors [3], though for the whole range of pairing interactions including the BCS–BEC crossover region and the limit of very strong coupling. In fact, here we have neglected the effects of Anderson localization, which can significantly change the behavior of the coefficient C in the limit of strong disorder ($p_F l \sim 1$) [7–9].

In this work, we shall concentrate mainly on the study of the coefficient C in the region of strong disorder, when Anderson localization effects become relevant.

2. HUBBARD MODEL WITHIN DMFT+Σ APPROACH AND THE NOZIERES–SCHMITT-RINK APPROXIMATION

We consider the disordered nonmagnetic attractive Anderson–Hubbard model, described by the Hamiltonian:

$$H = -t\sum_{\langle ij\rangle\sigma} a^{\dagger}_{i\sigma}a_{j\sigma} + \sum_{i\sigma}\epsilon_i n_{i\sigma} - U\sum_i n_{i\uparrow}n_{i\downarrow}, \qquad (1)$$

where $t > 0$ is transfer amplitude between nearest neighbors, U is the Hubbard-like onsite attraction, $n_{i\sigma} = a^{\dagger}_{i\sigma}a_{i\sigma}$ is electron number operator at a given site, $a_{i\sigma}$ ($a^{\dagger}_{i\sigma}$) is annihilation (creation) operator of an electron with spin σ, and local energies ϵ_i are assumed to be independent random variables at different lattice sites. For the validity of the standard "impurity" diagram technique [26, 27] we assume the Gaussian distribution for energy levels ϵ_i:

$$\mathcal{P}(\epsilon_i) = \frac{1}{\sqrt{2\pi}W}\exp\left(-\frac{\epsilon_i^2}{2W^2}\right). \qquad (2)$$

Distribution width W is the measure of disorder, while the Gaussian field of energy levels (independent on different sites—"white" noise correlation) induces the "impurity" scattering, which is described by the standard approach, based upon the calculation of the averaged Green's functions [27].

The generalized DMFT+Σ approach [14–17] extends the standard dynamical mean-field theory (DMFT) [11–13] introducing the additional "external" self-energy part (SEP) $\Sigma_{\mathbf{p}}(\varepsilon)$ (in general momentum dependent), which originates from any interaction outside the DMFT, and provides an effective procedure to calculate both single-particle and two-particle properties [18, 20]. The success of such a generalized approach is connected with the choice of single-particle Green's function in the following form:

$$G(\varepsilon,\mathbf{p}) = \frac{1}{\varepsilon + \mu - \varepsilon(\mathbf{p}) - \Sigma(\varepsilon) - \Sigma_{\mathbf{p}}(\varepsilon)}, \qquad (3)$$

where $\varepsilon(\mathbf{p})$ is the "bare" electronic dispersion, while the total SEP is an additive sum of Hubbard-like local SEP $\Sigma(\varepsilon)$ and "external" $\Sigma_{\mathbf{p}}(\varepsilon)$, neglecting the interference between Hubbard-like and "external" interactions. This allows us to conserve the system of self-consistent equations of the standard DMFT [11–13]. At the each step of DMFT iterations the "external" SEP $\Sigma_{\mathbf{p}}(\varepsilon)$ is recalculated with the use of some approximate scheme, corresponding to the form of additional interaction, while the local Green's function is also "dressed" by $\Sigma_{\mathbf{p}}(\varepsilon)$ at each step of the standard DMFT procedure.

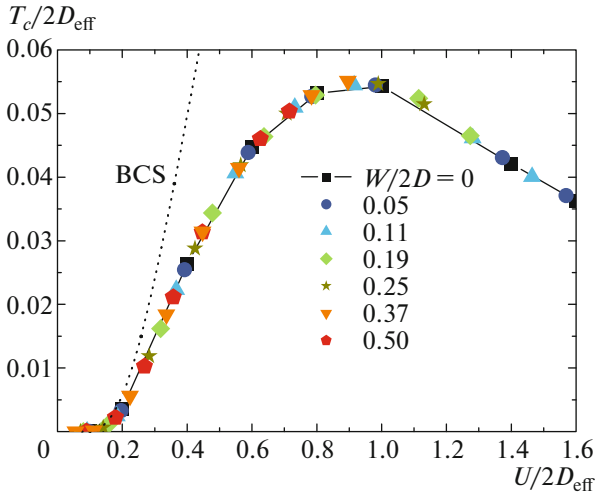

Fig. 1. (Color online) Universal dependence of the temperature of superconducting transition on the strength of Hubbard attraction for different levels of disorder.

The "external" SEP, entering DMFT+Σ cycle, in the problem of disorder scattering under consideration here [18, 19], is taken in the simplest (self-consistent Born) approximation, neglecting the "crossing" diagrams of impurity scattering, which gives:

$$\Sigma_{\mathbf{p}}(\varepsilon) \to \Sigma_{\text{imp}}(\varepsilon) = W^2 \sum_{\mathbf{p}} G(\varepsilon, \mathbf{p}). \tag{4}$$

To solve the effective single Anderson impurity problem of DMFT we use here, as in our previous papers, the quite efficient impurity solver using the numerical renormalization group (NRG) [28].

In the following, we are using the "bare" band with semielliptic density of states (per unit cell with lattice parameter a and single spin projection), which is a rather good approximation in the three-dimensional case:

$$N_0(\varepsilon) = \frac{2}{\pi D^2}\sqrt{D^2 - \varepsilon^2}, \tag{5}$$

where D defines the half–width of the conduction band.

In [23], we have shown that in the DMFT+Σ approach for the model with semi-elliptic density of states all effects of disorder upon single-particle properties reduce only to the band widening due to disorder, i.e., to the replacement $D \to D_{\text{eff}}$, where D_{eff} is the effective half-width of the "bare" band in the absence of electronic correlations ($U = 0$), widened by disorder:

$$D_{\text{eff}} = D\sqrt{1 + 4\frac{W^2}{D^2}}. \tag{6}$$

The "bare" density of states (in the absence of U) "dressed" by disorder:

$$\tilde{N}_0(\xi) = \frac{2}{\pi D_{\text{eff}}^2}\sqrt{D_{\text{eff}}^2 - \varepsilon^2}, \tag{7}$$

remains semielliptic also in the presence of disorder. It should be noted, that in other models of the "bare" band disorder effect is not reduced only to the widening of the band, changing also the form of the density of states, so that there is no complete universality of disorder influence on single-particle properties, reducing to a simple substitution $D \to D_{\text{eff}}$. However, in the limit of strong enough disorder of interest to us, the "bare" band becomes practically semielliptic, restoring such universality [23].

All calculations below, as in our previous works, were performed for the rather typical case of the quarter–filled band (the number of electrons per lattice site is $n = 0.5$).

To consider superconductivity for the wide range of pairing interaction U, following [21, 23], we use the Nozieres–Schmitt-Rink approximation [10], which allows qualitatively correct (though approximate) description of the BCS–BEC crossover region. In this approach, we determine the critical temperature T_c using the usual BCS-type equation [23]:

$$1 = \frac{U}{2}\int_{-\infty}^{\infty} d\varepsilon \tilde{N}_0(\varepsilon)\frac{\tanh[(\varepsilon - \mu)/2T_c]}{\varepsilon - \mu}, \tag{8}$$

with chemical potential μ determined via DMFT+Σ calculations for different values of U and W, i.e., from the standard equation for the number of electrons (band filling), determined by the Green's function given by Eq. (3), allowing us to find T_c for the wide range of the model parameters including the regions of BCS–BEC crossover and strong coupling, as well as for different levels of disorder. This reflects the physical meaning of the Nozieres–Schmitt-Rink approximation—in the weak coupling region, transition temperature is controlled by the equation for Cooper instability (8), while, in the strong coupling region, it is determined as BEC temperature controlled by chemical potential.

In [23], it was shown that disorder's influence on the critical temperature T_c and single-particle characteristics (e.g., density of states) in the model with semielliptic "bare" density of states is universal and reduces only to the change of the effective bandwidth. In Fig. 1, just for illustrative purposes, we show the universal dependence of the critical temperature T_c on Hubbard attraction for different levels of disorder [23]. In the weak coupling region, the temperature of superconducting transition is described well by the BCS model (for comparison, in Fig. 1, the dashed line represents the dependence obtained for T_c from Eq. (8) with chemical potential independent of U and determined by quarter filling of the "bare" band), while for the strong coupling region the critical temperature is mainly determined by the condition of Bose conden-

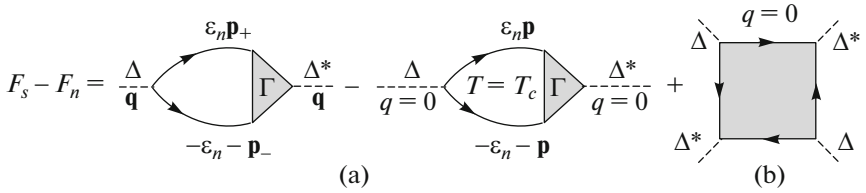

Fig. 2. Diagrammatic representation of Ginzburg–Landau expansion $\mathbf{p}_\pm = \mathbf{p} \pm \mathbf{q}/2$.

sation of Cooper pairs and drops with the growth of U as t^2/U, going through the maximum at $U/2D_{\text{eff}} \sim 1$.

The review of these and other results obtained for disordered Hubbard model in DMFT+Σ approximation can be found in [19].

3. GINZBURG–LANDAU EXPANSION

Ginzburg–Landau expansion for the difference of free-energy densities of superconducting and normal states is written in the standard form [27]:

$$F_s - F_n = A|\Delta_{\mathbf{q}}|^2 + q^2 C|\Delta_{\mathbf{q}}|^2 + \frac{B}{2}|\Delta_{\mathbf{q}}|^4, \qquad (9)$$

where $\Delta_{\mathbf{q}}$ is the Fourier component of the order parameter Δ.

This expansion (9) is determined by the loop–expansion diagrams for free-energy of an electron in the field of fluctuations of the order parameter (denoted by dashed lines) with small wavevector $\mathbf{q}$ [27], shown in Fig. 2 [27].

In the framework of the Nozieres–Schmitt-Rink approach [10], we use the weak coupling approximation to analyze Ginzburg–Landau coefficients, so that the "loops" with two and four Cooper vertices, shown in Fig. 2, do not contain contributions from Hubbard attraction and are "dressed" only by impurity scattering. However, like in the case of T_c calculation, the chemical potential, which is essentially dependent on the coupling strength and in the strong coupling limit actually controls the condition of Bose condensation of Cooper pairs, should be determined within full DMFT+Σ procedure.

In [24] it was shown that in this approach the coefficients A and B are determined by the following expressions:

$$A(T) = \frac{1}{U} - \int_{-\infty}^{\infty} d\varepsilon \tilde{N}_0(\varepsilon) \frac{\tanh[(\varepsilon-\mu)/2T]}{2(\varepsilon-\mu)}, \qquad (10)$$

$$B = \int_{-\infty}^{\infty} \frac{d\varepsilon}{2(\varepsilon-\mu)^3} \left(\tanh\frac{\varepsilon-\mu}{2T} - \frac{(\varepsilon-\mu)/2T}{\cosh^2[(\varepsilon-\mu)/2T]} \right) \tilde{N}_0(\varepsilon). \qquad (11)$$

For $T \to T_c$ the coefficient $A(T)$ takes the usual form:

$$A(T) \equiv \alpha(T - T_c). \qquad (12)$$

In BCS limit, where $T = T_c \to 0$, we obtain for coefficients α and B the standard result [27]:

$$\alpha_{BCS} = \frac{\tilde{N}_0(\mu)}{T_c}, \quad B_{BCS} = \frac{7\zeta(3)}{8\pi^2 T_c^2} \tilde{N}_0(\mu). \qquad (13)$$

In the general case, the coefficients A and B are determined only by the disorder widened density of states $\tilde{N}_0(\varepsilon)$ and chemical potential. Thus, in the case of semielliptic density of states the dependence of these coefficients on disorder is due only to the simple replacement $D \to D_{\text{eff}}$, leading to universal (independent of the level of disorder) curves for properly normalized dimensionless coefficients ($\alpha(2D_{\text{eff}})^2$ and $B(2D_{\text{eff}})^3$) on $U/2D_{\text{eff}}$) [24]. In fact, the coefficients α and B are rapidly suppressed with the growth of dimensionless coupling $U/2D_{\text{eff}}$.

It should be noted that Eqs. (10) and (11) for coefficients A and B were obtained in [24] using the exact Ward identities and remain valid also in the limit of arbitrarily large disorder (including the region of Anderson localization).

Universal dependence on disorder, related to widening of the band $D \to D_{\text{eff}}$, is observed, in particular, for specific heat discontinuity at the transition point, which is determined by coefficients α and B [24]:

$$C_s(T_c) - C_n(T_c) = T_c \frac{\alpha^2}{B}. \qquad (14)$$

From diagrammatic representation of Ginzburg–Landau expansion, shown in Fig. 2, it is clear that the coefficient C is determined by the coefficient before q^2 in a Cooper two-particle loop (first term in Fig. 2). Then we obtain the following expression:

$$C = -T \lim_{q\to 0} \sum_{n,\mathbf{p},\mathbf{p}'} \frac{\Psi_{\mathbf{pp}'}(\varepsilon_n, \mathbf{q}) - \Psi_{\mathbf{pp}'}(\varepsilon_n, 0)}{q^2}, \qquad (15)$$

where $\Psi_{\mathbf{p},\mathbf{p}'}(\varepsilon_n, \mathbf{q})$ is a two-particle Green's function in a Cooper channel (see Fig. 3), "dressed" in the Nozieres–Schmitt-Rink approximation only by impurity scattering. In case of time-reversal invari-

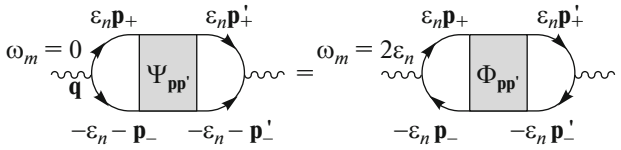

Fig. 3. The equality of loops in Cooper and diffusion channels under time-reversal invariance.

ance (in the absence of magnetic field and magnetic impurities) and because of the static nature of impurity scattering "dressing" two-particle Green's function $\Psi_{\mathbf{p},\mathbf{p}'}(\varepsilon_n, \mathbf{q})$, we can reverse here the direction of all lower electron lines with simultaneous change of the sign of all momenta (see Fig. 3). As a result, we obtain:

$$\Psi_{\mathbf{p},\mathbf{p}'}(\varepsilon_n, \mathbf{q}) = \Phi_{\mathbf{p},\mathbf{p}'}(\omega_m = 2\varepsilon_n, \mathbf{q}), \tag{16}$$

where ε_n are Fermionic Matsubara frequencies, $\mathbf{p}_\pm = \mathbf{p} \pm \frac{\mathbf{q}}{2}$, $\Phi_{\mathbf{p},\mathbf{p}'}(\omega_m = 2\varepsilon_n, \mathbf{q})$ is the two-particle Green's function in the diffusion channel, dressed by impurities. Then we obtain Cooper susceptibility as:

$$\begin{aligned}\chi(\mathbf{q}) &= -T\sum_{n,\mathbf{p},\mathbf{p}'} \Psi_{\mathbf{p},\mathbf{p}'}(\varepsilon_n, \mathbf{q}) \\ &= -T\sum_{n,\mathbf{p},\mathbf{p}'} \Phi_{\mathbf{p},\mathbf{p}'}(\omega_m = 2\varepsilon_n, \mathbf{q}).\end{aligned} \tag{17}$$

Performing the standard summation over Fermionic Matsubara frequencies [26, 27], we obtain:

$$\chi(\mathbf{q}) = -\frac{1}{2\pi}\int_{-\infty}^{\infty} d\varepsilon \,\mathrm{Im}\,\Phi^{RA}(\omega = 2\varepsilon, \mathbf{q}) \tanh\frac{\varepsilon}{2T}, \tag{18}$$

where $\Phi^{RA}(\omega, \mathbf{q}) = \sum_{\mathbf{p},\mathbf{p}'} \Phi^{RA}_{\mathbf{p},\mathbf{p}'}(\omega, \mathbf{q})$. To find the loop $\Phi^{RA}(\omega, \mathbf{q})$ in strongly disordered case (e.g., in the region of Anderson localization) we can use the approximate self-consistent theory of localization [27, 29–33]. Then this loop contains the diffusion pole of the following form [19]:

$$\Phi^{RA}(\omega = 2\varepsilon, \mathbf{q}) = -\frac{\sum_{\mathbf{p}} \Delta G_{\mathbf{p}}(\varepsilon)}{\omega + iD(\omega)q^2}, \tag{19}$$

where $\Delta G_{\mathbf{p}}(\varepsilon) = G^R(\varepsilon, \mathbf{p}) - G^A(-\varepsilon, \mathbf{p})$, G^R and G^A are the retarded and advanced Green's functions, and $D(\omega)$ is frequency dependent generalized diffusion coefficient. Then we obtain the coefficient C as:

$$\begin{aligned}C &= \lim_{q\to 0} \frac{\chi(\mathbf{q}) - \chi(\mathbf{q} = 0)}{q^2} \\ &= -\frac{1}{8\pi}\int_{-\infty}^{\infty} d\varepsilon \frac{\tanh\frac{\varepsilon}{2T}}{\varepsilon} \mathrm{Im}\left(\frac{iD(2\varepsilon)\sum_{\mathbf{p}} \Delta G_{\mathbf{p}}(\varepsilon)}{\varepsilon + i\delta}\right) \\ &= -\frac{1}{8\pi}\int_{-\infty}^{\infty} d\varepsilon \frac{\tanh\frac{\varepsilon}{2T}}{\varepsilon^2} \mathrm{Re}\left(D(2\varepsilon)\sum_{\mathbf{p}} \Delta G_{\mathbf{p}}(\varepsilon)\right) \\ &\quad -\frac{1}{16T}\mathrm{Im}\left(D(0)\sum_{\mathbf{p}} \Delta G_{\mathbf{p}}(0)\right).\end{aligned} \tag{20}$$

The generalized diffusion coefficient of the self-consistent theory of localization [27, 29–33] for our model can be found as the solution of the following self–consistency equation [18]:

$$\begin{aligned}D(\omega) = i\frac{\langle v\rangle^2}{d}\Bigg(&\omega - \Delta\Sigma^{RA}_{\mathrm{imp}}(\omega) + W^4\sum_{\mathbf{p}} (\Delta G_{\mathbf{p}}(\varepsilon))^2 \\ &\cdot \sum_{\mathbf{q}} \frac{1}{\omega + iD(\omega)q^2}\Bigg)^{-1},\end{aligned} \tag{21}$$

where $\omega = 2\varepsilon$, $\Delta\Sigma^{RA}_{\mathrm{imp}}(\omega) = \Sigma^R_{\mathrm{imp}}(\varepsilon) - \Sigma^A_{\mathrm{imp}}(-\varepsilon)$, d is space dimension, and velocity $\langle v\rangle$ is defined by the following expression:

$$\langle v\rangle = \frac{\sum_{\mathbf{p}} |\mathbf{v}_{\mathbf{p}}| \Delta G_{\mathbf{p}}(\varepsilon)}{\sum_{\mathbf{p}} \Delta G_{\mathbf{p}}(\varepsilon)}; \quad \mathbf{v}_{\mathbf{p}} = \frac{\partial\varepsilon(\mathbf{p})}{\partial\mathbf{p}}. \tag{22}$$

Due to the limits of diffusion approximation summation over q in Eq. (21) should be limited by the following cut-off [27, 32]:

$$q < k_0 = Min\{l^{-1}, p_{\mathrm{F}}\}, \tag{23}$$

where l is the mean free path due to elastic disorder scattering and p_{F} is Fermi momentum.

In the limit of weak disorder, when localization corrections are small, the Cooper susceptibility $\chi(\mathbf{q})$ and coefficient C related to it are determined by the "ladder" approximation. In this approximation coefficient C was studied by us in [25], where we obtained it in general analytic form. Let us now transform self-consistency Eq. (21) to make the obvious connection with exact "ladder" expression in the limit of weak disorder. In the "ladder" approximation, we just neglect the "maximally intersecting" diagrams entering the irreducible vertex. The second term in the r.h.s. of self-consistency Eq. (21) vanishes. Let us introduce the

frequency dependent generalized diffusion coefficient in "ladder" approximation as:

$$D_0(\omega) = \frac{\langle v\rangle^2}{d}\frac{i}{\omega - \Delta\Sigma^{RA}_{\rm imp}(\omega)}. \quad (24)$$

Then $\frac{\langle v\rangle^2}{d}$ entering the self-consistency Eq. (21) can be rewritten via this diffusion coefficient D_0 in "ladder" approximation, so that Eq. (21) takes the following form:

$$D(\omega = 2\varepsilon) = \frac{D_0(\omega = 2\varepsilon)}{1 + \dfrac{W^4}{2\varepsilon - \Delta\Sigma^{RA}_{\rm imp}(\omega = 2\varepsilon)}\sum_{\mathbf{p}}(\Delta G_{\mathbf{p}}(\varepsilon))^2\sum_{\mathbf{q}}\dfrac{1}{2\varepsilon + iD(\omega = 2\varepsilon)q^2}}. \quad (25)$$

Using the approach of [25], the diffusion coefficient $D_0(\omega = 2\varepsilon)$ in the "ladder" approximation can be derived analytically. In fact, in the "ladder" approximation the two-particle Green's function (19) takes the following form:

$$\Phi_0^{RA}(\omega = 2\varepsilon, \mathbf{q}) = -\frac{\sum_{\mathbf{p}}\Delta G_{\mathbf{p}}(\varepsilon)}{\omega + iD_0(\omega = 2\varepsilon)q^2}. \quad (26)$$

Then we obtain:

$$\varphi(\varepsilon, \mathbf{q} = 0) \equiv \lim_{q\to 0}\frac{\Phi_0^{RA}(\omega = 2\varepsilon, \mathbf{q}) - \Phi_0^{RA}(\omega = 2\varepsilon, \mathbf{q} = 0)}{q^2} = \frac{i\sum_{\mathbf{p}}\Delta G_{\mathbf{p}}(\varepsilon)}{\omega^2} D_0(\omega = 2\varepsilon). \quad (27)$$

Then the diffusion coefficient D_0 can be written as:

$$D_0 = \frac{\varphi(\varepsilon, \mathbf{q} = 0)(2\varepsilon)^2}{i\sum_{\mathbf{p}}\Delta G_{\mathbf{p}}(\varepsilon)}. \quad (28)$$

In [25] using the exact Ward identity we have shown, that in the "ladder" approximation $\varphi(\varepsilon, \mathbf{q} = 0)$ can be represented as:

$$\varphi(\varepsilon, \mathbf{q} = 0)(2\varepsilon)^2 = \sum_{\mathbf{p}} v_x^2 G^R(\varepsilon, \mathbf{p})G^A(-\varepsilon, \mathbf{p}) + \frac{1}{2}\sum_{\mathbf{p}}\frac{\partial^2\varepsilon(\mathbf{p})}{\partial p_x^2}(G^R(\varepsilon, \mathbf{p}) + G^A(-\varepsilon, \mathbf{p})), \quad (29)$$

where $v_x = \dfrac{\partial\varepsilon(\mathbf{p})}{\partial p_x}$.

Finally, using Eqs. (28), (29) we find the diffusion coefficient D_0 in the "ladder" approximation. Using self-consistency Eq. (25) we determine the generalized diffusion coefficient, and then using Eq. (20) we find the coefficient C. In the limit of weak disorder, when the "ladder" approximation works well and generalized diffusion coefficient just coincides with the diffusion coefficient in the "ladder" approximation, we obtain for coefficient C the result obtained in [25]:

$$C_0 = -\frac{1}{8\pi}\int_{-\infty}^{\infty} d\varepsilon\frac{\tanh\dfrac{\varepsilon}{2T}}{\varepsilon^2}\cdot\sum_{\mathbf{p}}\left(v_x^2\,\mathrm{Im}(G^R(\varepsilon, \mathbf{p})G^A(-\varepsilon, \mathbf{p})) + \frac{\partial^2\varepsilon_{\mathbf{p}}}{\partial p_x^2}\mathrm{Im}\,G^R(\varepsilon, \mathbf{p})\right) + \frac{1}{16T}\sum_{\mathbf{p}}\left(v_x^2\,\mathrm{Re}(G^R(0, \mathbf{p})G^A(0, \mathbf{p})) + \frac{\partial^2\varepsilon_{\mathbf{p}}}{\partial p_x^2}\mathrm{Re}\,G^R(0, \mathbf{p})\right). \quad (30)$$

Now we can use the iteration scheme to find the coefficient C, which in the limit of weak disorder reproduces the results of the "ladder" approximation, while in the limit of strong disorder takes into account the effects of Anderson localization (in the framework of the self-consistent theory of localization).

In numerical calculations using Eqs. (28) and (29) we first find the "ladder" diffusion coefficient D_0 for the given value of $\omega = 2\varepsilon$. Then, solving by iterations the transcendental self-consistency Eq. (25), we determine the generalized diffusion coefficient at this frequency. After that, using Eq. (20) we calculate the Ginzburg–Landau coefficient C.

In [18] it was shown, that in DMFT+Σ approximation for the Anderson–Hubbard model the critical disorder for Anderson metal–insulator transition $W/2D = 0.37$ and is independent of the value of the Hubbard interaction U. The approach developed here allows determination of the C coefficient also in the region of Anderson insulator at disorder levels $W/2D > 0.37$.

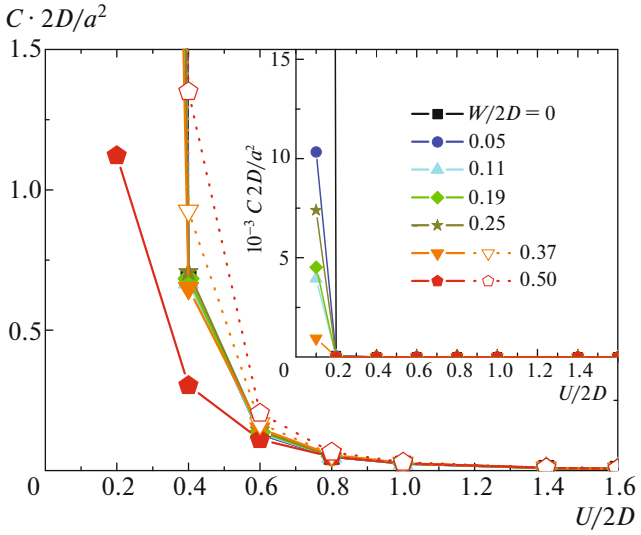

Fig. 4. (Color online) Dependence of C coefficient on the strength of Hubbard attraction for different levels of disorder (a is lattice parameter). Filled symbols and continuous lines correspond to calculations taking into account localization corrections. Unfilled symbols and dashed lines correspond to the "ladder" approximation.

4. MAIN RESULTS

The coherence length at given temperature $\xi(T)$ gives a characteristic scale of inhomogeneities of the order parameter Δ:

$$\xi^2(T) = -\frac{C}{A}. \tag{31}$$

Coefficient A changes its sign and becomes zero at a critical temperature: $A = \alpha(T - T_c)$, so that

$$\xi(T) = \frac{\xi}{\sqrt{1 - T/T_c}}, \tag{32}$$

where we have introduced the coherence length of a superconductor:

$$\xi = \sqrt{\frac{C}{\alpha T_c}}, \tag{33}$$

which reduces to a standard expression in the weak coupling region and in the absence of disorder [27]:

$$\xi_{BCS} = \sqrt{\frac{C_{BCS}}{\alpha_{BCS} T_c}} = \sqrt{\frac{7\zeta(3)}{16\pi^2 d}} \frac{v_F}{T_c}. \tag{34}$$

Penetration depth of magnetic field into superconductor is defined by:

$$\lambda^2(T) = -\frac{c^2}{32\pi e^2} \frac{B}{AC}. \tag{35}$$

Then:

$$\lambda(T) = \frac{\lambda}{\sqrt{1 - T/T_c}}, \tag{36}$$

where we have introduced:

$$\lambda^2 = \frac{c^2}{32\pi e^2} \frac{B}{\alpha C T_c}, \tag{37}$$

which in the absence of disorder has the form:

$$\lambda^2_{BCS} = \frac{c^2}{32\pi e^2} \frac{B_{BCS}}{\alpha_{BCS} C_{BCS} T_c} = \frac{c^2}{16\pi e^2} \frac{d}{N_0(\mu) v_F^2}. \tag{38}$$

As λ_{BCS} is independent of T_c, i.e., of coupling strength, it is convenient to use for normalization of penetration depth λ (37) at arbitrary U and W.

Close to T_c the upper critical magnetic field H_{c2} is determined by the Ginzburg–Landau coefficients as:

$$H_{c2} = \frac{\Phi_0}{2\pi\xi^2(T)} = -\frac{\Phi_0}{2\pi} \frac{A}{C}, \tag{39}$$

where $\Phi_0 = c\pi/e$ is a magnetic flux quantum. Then the slope of the upper critical filed close to T_c is given by:

$$\frac{dH_{c2}}{dT} = \frac{\Phi_0}{2\pi} \frac{\alpha}{C}. \tag{40}$$

In Fig. 4 we show the dependence of coefficient C on the strength of Hubbard attraction for different disorder levels. In this figure and in the following we use filled symbols and continuous lines corresponding to the results of calculations taking into account localization corrections, while unfilled symbols and dashed lines correspond to calculations in the "ladder" approximation. Coefficient C is essentially a two-particle characteristic and it does not follow universal behavior on disorder, as in case of coefficients A and B, and disorder dependence here is not reduced only to widening of effective bandwidth by disorder. Correspondingly, in the dependence of C on coupling strength, where all energies are normalized by effective bandwidth $2D_{\text{eff}}$, we do not observe a universal curve for different levels of disorder [25], in contrast to similar dependencies for coefficients α and B. In fact, coefficient C is rapidly suppressed with the growth of coupling strength. Especially strong suppression is observed in the weak coupling region (cf. insert in Fig. 4). Localization corrections become relevant in the limit of strong enough disorder ($W/2D > 0.25$). Under such strong disordering localization corrections significantly suppress coefficient C in weak coupling region (cf. dashed lines ("ladder" approximation) and continuous curves (with localization corrections) for $W/2D = 0.37$ and 0.5). In strong coupling region for $U/2D > 1$ localization corrections, in fact, do not change the value of coefficient C, as compared to the results of "ladder" approximation, even in the limit of strong disorder for $W/2D > 0.37$, where the system becomes an Anderson insulator.

In Fig. 5, we show the dependencies of coefficient C on disorder level for different values of coupling strength $U/2D$. In the limit of weak coupling ($U/2D = 0.1$), we

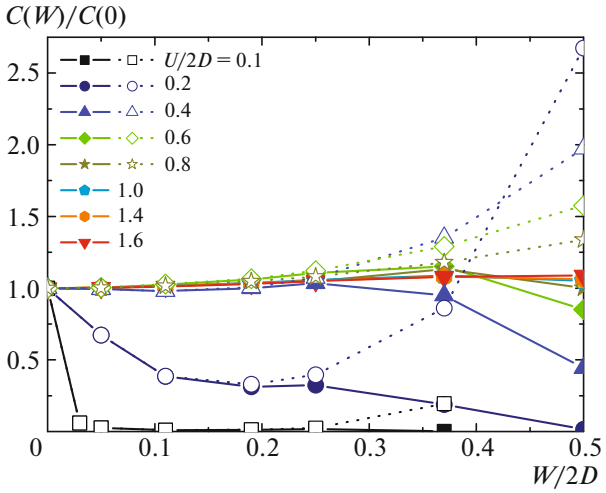

Fig. 5. (Color online) Dependence of coefficient C normalized by its value in the absence of disorder for different values of Hubbard attraction U. Dashed lines—"ladder" approximation, continuous curves—calculations with the account of localization corrections.

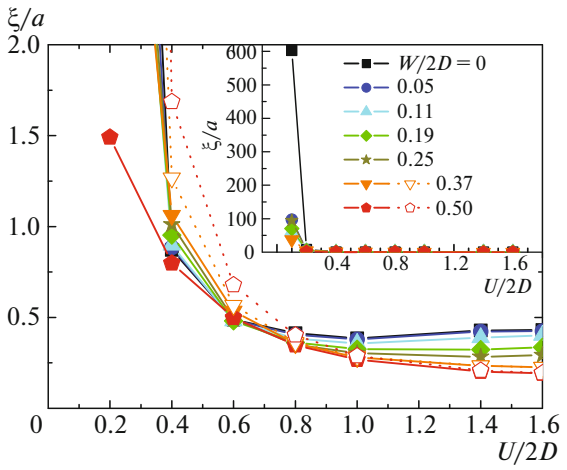

Fig. 6. (Color online) Dependence of coherence length on the strength of Hubbard attraction U for different disorder levels. Inset: the rapid growth of coherence length with diminishing coupling in BCS limit.

observe rather rapid suppression of coefficient C with the growth of disorder in case of weak enough impurity scattering. In the region of strong enough disorder in the "ladder" approximation, we can observe some growth of coefficient C with the increase of disorder, which is related mainly with significant widening of the band by such strong disorder and corresponding drop of the effective coupling $U/2D_{\text{eff}}$. However, localization corrections, which are significant at large disorder $W/2D > 0.25$, actually lead to suppression of coefficient C with the growth of disorder in the limit of strong impurity scattering. In the intermediate coupling region ($U/2D = 0.4$–0.6) coefficient C in the "ladder" approximation is only growing slightly with increasing disorder. In the BEC limit ($U/2D > 1$) coefficient C is practically independent of impurity scattering both in the "ladder" approximation and with the account of localization corrections. In the BEC limit the account of localization corrections in fact do not change the value of C in comparison with the "ladder" approximation.

As the Ginzburg–Landau expansion coefficient α and B demonstrate the universal dependence on disorder, Anderson localization in fact does not influence them at all, while coefficient C in the weak coupling region is strongly affected by localization corrections, being almost independent of them in the BEC limit, the physical properties depending on C will be also significantly changed by localization corrections in the weak coupling region, becoming practically independent of localization in the BEC limit.

Let us now discuss the behavior of physical properties. Dependence of coherence length on Hubbard attraction strength is shown in Fig. 6. We can see that in the weak coupling region (cf. insert at Fig. 6) coherence length rapidly drops with the growth of U for any disorder, reaching the value of the order of lattice parameter a in the intermediate coupling region of $U/2D \approx 0.4$–0.6. Further growth of coupling strength changes the coherence length only slightly. The account of localization corrections for coherence length is significant only at large disorder ($W/2D > 0.25$). We see that localization corrections lead to significant suppression of coherence length in the BCS limit of weak coupling and practically do not change the coherence length in the BEC limit.

In Fig. 7, we show the dependence of penetration depth, normalized by its BCS value in the absence of disorder (38), on the strength of Hubbard attraction U for different levels of disorder. In the absence of impurity scattering, penetration depth grows with the increase of the coupling strength. In BCS weak coupling limit disorder leads to a fast growth of penetration depth (for "dirty" BCS superconductors $\lambda \sim l^{-1/2}$, where l is the mean free path). In BEC strong coupling limit disorder only slightly diminish the penetration depth (cf. Fig. 10a). This leads to suppression of penetration depth with disorder with the growth of Hubbard attraction strength in the region of weak enough coupling and to the growth of λ with U in BEC strong coupling region. The account of localization corrections is significant only in the limit of strong disorder ($W/2D > 0.25$) and leads to noticeable growth of penetration depth as compared to the "ladder" approximation in the weak coupling region. In the BEC limit the influence of localization on penetration depth is just insignificant.

Dependence of the slope of the upper critical magnetic field on the strength of Hubbard attraction for different disorder levels is shown in Fig. 8. In the limit of weak enough impurity scattering, until Anderson

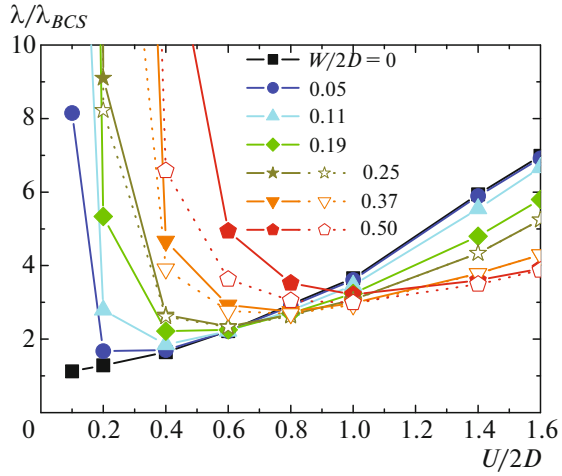

Fig. 7. (Color online) Dependence of penetration depth, normalized by its BCS value in the limit of weak coupling, on the strength of Hubbard attraction U for different levels of disorder.

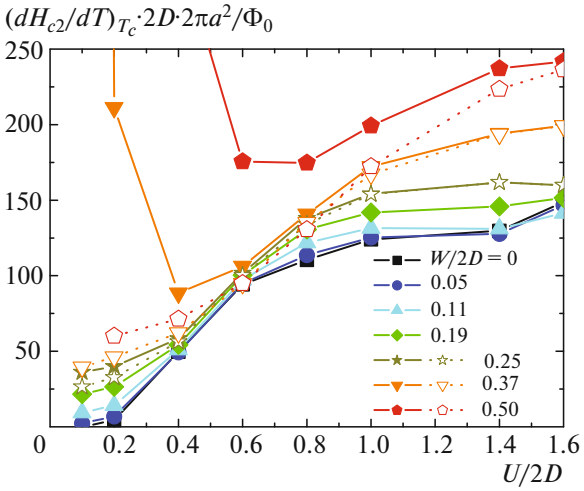

Fig. 8. (Color online) Dependence of the slope of the upper critical field on the strength of Hubbard attraction U for different level of disorder.

localization corrections remain unimportant, the slope of the upper critical field grows with the growth of the coupling strength. The fast growth of the slope is observed with the growth of U in the region of weak enough coupling, while in the limit of strong coupling the slope is rather weakly dependent on $U/2D$. In the region of strong enough disorder ($W/2D > 0.25$) the account of localization corrections becomes quite important—it qualitatively changes the behavior of the upper critical held. While the "ladder" approximation (dashed curves) conserves the behavior of the slope of the upper critical held typical for the region of weak disorder, where the slope grows with the growth of the coupling strength, the account of Anderson localization ($W/2D \geq 0.37$) leads to a strong increase of the slope of the upper critical held in the weak coupling limit. As a result, in Anderson insulator the slope of the upper critical hied rapidly drops with the growth of U in the weak coupling limit and just insignificantly grows with the growth of U in BEC limit. Note that the account of localization corrections is also unimportant for for the slope of the upper critical held in the strong coupling limit.

Let us consider now dependencies of physical properties on disorder. In Fig. 9 we show dependence of coherence length ξ on disorder for different values of coupling. In the BCS limit for weak coupling and for weak enough impurity scattering we observe the standard "dirty" superconductor dependence $\xi \propto l^{1/2}$, i.e., the coherence length rapidly drops with the growth of disorder (cf. insert in Fig. 9a). However, at strong enough disorder in "ladder" approximation (dashed lines) coherence length starts to grow with disorder (cf. Fig. 9b and insert in Fig. 9a), which is mainly related to the widening of the band by disorder and corresponding suppression of $U/2D_{\text{eff}}$. Taking into account localization corrections leads to noticeable suppression of coherence length in comparison with the "ladder" approximation in the limit of strong disorder, which leads to restoration of general suppression of ξ with the growth of disorder in this limit. In the standard BCS model with a bare band of infinite width coherence length drops with the growth of disorder $\xi \propto l^{1/2}$ and close to Anderson transition this suppression of ξ even accelerates, so that $\xi \propto l^{2/3}$ [7–9], which differs from the present model here, where close to Anderson coherence length is rather weakly dependent on disorder, which is related to significant widening of the band by disorder. With growth of coupling, for $U/2D > 0.4$–0.6 coherence length ξ becomes of the order of lattice parameter and is almost disorder independent, while in BEC limit of very strong coupling $U/2D = 1.4$, 1.6 the growth of disorder up to very strong values ($W/2D = 0.5$) leads to suppression of coherence length approximately by the factor of two (cf. Fig. 9b). Again we see, that in the limit of strong coupling the account of localization corrections is rather insignificant.

Dependence of penetration depth on disorder for different values of Hubbard attraction is shown in Fig. 10a. In weak coupling limit disorder in accordance with the theory of "dirty" superconductors leads to the growth of penetration depth ($\lambda \propto l^{-1/2}$). With increase of the coupling strength the growth of penetration depth slow down and in the limit of very strong coupling, for $U/2D = 1.4$, 1.6, penetration depth is even slightly suppressed by disorder. The account of localization corrections leads to some quantitative growth of penetration depth in comparison with the results of the "ladder" approximation in the weak coupling region. Qualitatively the dependence of penetration depth on disorder does not change. In BEC limit of strong coupling the account of localization corrections is rather irrelevant. In Fig. 10b we show the disorder dependence of dimensionless Ginzburg–Landau $\kappa = \lambda/\xi$.

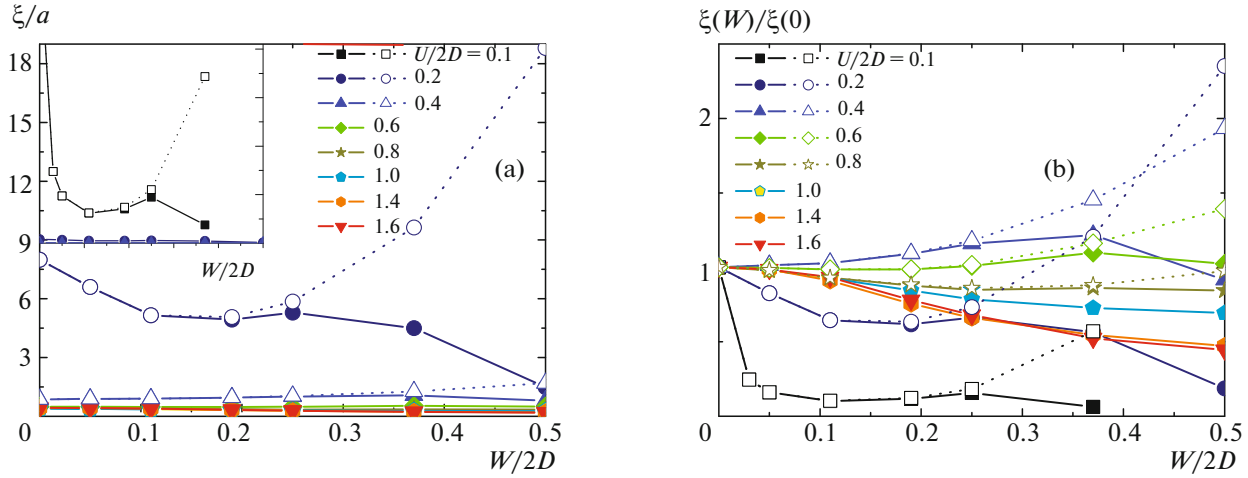

Fig. 9. (Color online) Dependence of coherence length on disorder for different values of Hubbard attraction, (a) coherence length normalized by lattice parameter a. Inset: dependence of coherence length on disorder in weak coupling limit, (b) coherence length normalized by its value in the absence of disorder.

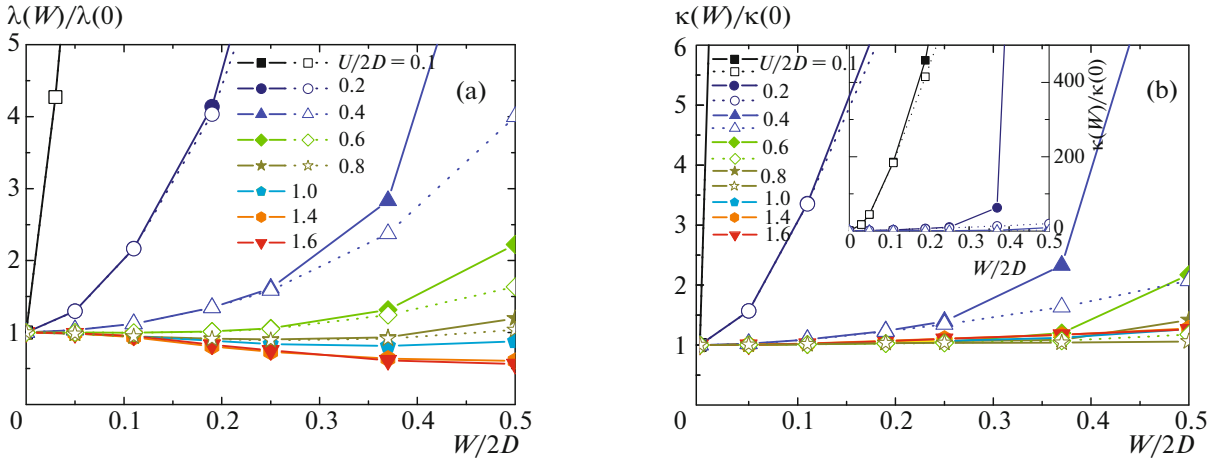

Fig. 10. (Color online) Dependence of penetration depth (a) and Ginzburg–Landau parameter (b) on disorder level for different values of Hubbard attraction. Inset shows the growth of the Ginzburg–Landau parameter with disorder in weak coupling limit.

We can see, that in the weak coupling limit Ginzburg–Landau parameter is rapidly growing with disorder (cf. insert in Fig. 10b) in accordance with the theory of "dirty" superconductors, where $\kappa \propto l^{-1}$. With the increase of coupling strength the growth of the Ginzburg–Landau parameter with disorder slows down and in the limit of strong coupling $U/2D > 1$ parameter κ is practically disorder independent. The account of localization corrections quantitatively increases Ginzburg–Landau parameter in Anderson insulator phase ($W/2D \geq 0.37$) in the strong coupling region. In the strong coupling region localization corrections are again irrelevant.

In Fig. 11 we show the disorder dependence of the slope of the upper critical field. In the weak coupling limit we again observe the behavior typical for "dirty" superconductors—the slope of the upper critical field grows with the growth of disorder (cf. Fig. 11a and the insert in Fig. 11b). The account of localization corrections in weak coupling limit sharply increases the slope of the upper critical field in comparison with the result of the "ladder" approximation in the region of Anderson insulator ($W/2D \geq 0.37$). As a result, in an Anderson insulator the slope of the upper critical field grows with the increase of impurity scattering much faster than in the "ladder" approximation. In intermediate coupling region ($U/2D = 0.4$–0.8) the slope of the upper critical field is practically independent of impurity scattering in the region of weak disorder. In the "ladder" approximation such behavior is conserved also in the region of strong disorder. However, the account of localization corrections leads to significant growth of the slope with disorder in Anderson insulator phase. In the limit of very strong coupling and weak disorder the slope of the upper critical field can even slightly diminish with disorder, but in the limit of

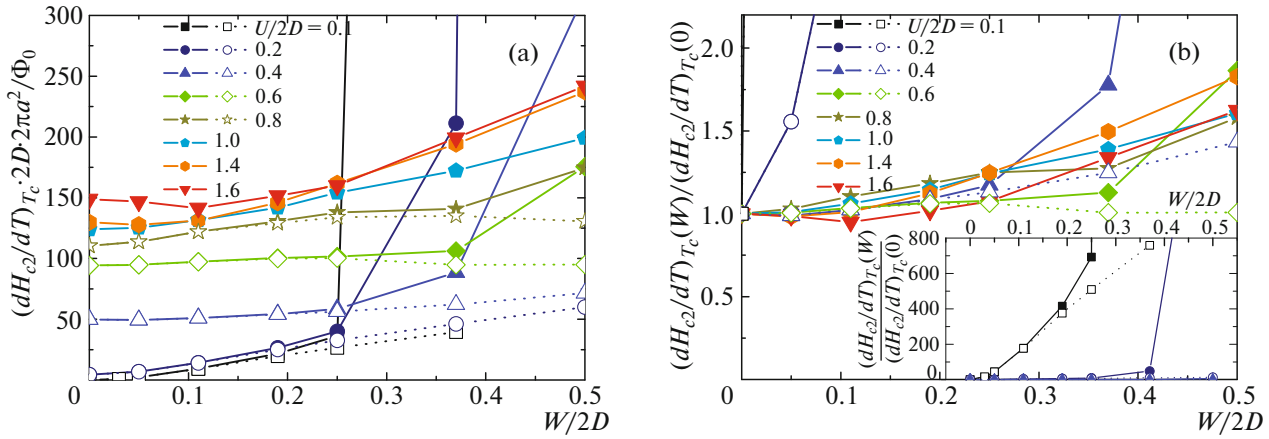

Fig. 11. (Color online) Dependence of the slope of the upper critical field (a) and this slope, normalized by its value in the absence of disorder (b), on disorder for different values of Hubbard attraction strength. In the inset we show the growth of the slope with disorder in weak coupling region.

strong disorder the slope grows with the growth of impurity scattering. In the BEC limit the account of localization corrections is irrelevant and only slightly changes the slope of the upper critical field as compared with the results of the "ladder" approximation.

5. CONCLUSIONS

In this paper in the framework of the Nozieres–Schmitt-Rink approximation and DMFT+Σ generalization of dynamical mean field theory we have studied the effects of disorder (including the strong disorder region of Anderson localization) on the Ginzburg–Landau coefficients and related physical properties close to T_c in disordered Anderson–Hubbard model with attraction. Calculations were done for the wide range of attractive potentials U, from weak coupling region $U/2D_{\text{eff}} \ll 1$, where instability of normal phase and superconductivity is well described by the BCS model, up to the strong coupling limit $U/2D_{\text{eff}} \gg 1$, where the transition into the superconducting state is due to Bose condensation of compact Cooper pairs, forming at a temperature much higher than the temperature of superconducting transition.

The growth of the coupling strength U leads to rapid suppression of all Ginzburg–Landau coefficients. The coherence length ξ rapidly drops with the growth of coupling and for $U/2D \approx 0.4$ becomes on the order of lattice spacing and only slightly changes with further increase of coupling. Penetration depth in "clean" superconductors grows with U, while in "dirty" superconductors it drops in the weak coupling and grows in BEC limit, passing through the minimum in the intermediate coupling region $U/2D \approx 0.4$–0.8. In the region of weak enough disorder ($W/2D < 0.37$), when Anderson localization effect are not very important, the slope of the upper critical field grows with the growth of U. However, in the limit of weak coupling in Anderson insulator phase localization effects sharply increase the slope of the upper critical field, while in BEC limit of strong coupling localization effects become unimportant. As a result, the slope of the upper critical field drops with the growth of U in BCS limit, passing through the minimum at $U/2D \approx 0.4$–0.8. The specific heat discontinuity grows with Hubbard attraction U in the weak coupling region and drops in the strong coupling limit, passing through the maximum at $U/2D_{\text{eff}} \approx 0.55$ [24].

Disorder influence (including the strong disorder in the region of Anderson localization) upon the critical temperature T_c and Ginzburg–Landau coefficients A and B and the related discontinuity of specific heat is universal and is completely determined only by disorder widening of the bare band, i.e., by the replacement $D \to D_{\text{eff}}$. Thus, even in the strong coupling region, the critical temperature and Ginzburg–Landau coefficients A and B satisfy the generalized Anderson theorem—all influence of disorder is related only to the change of the density of states. Disorder influence on coefficient C is not universal and is related not only to the bare band widening.

Coefficient C is sensitive to the effects of Anderson localization. We have studied this effect for a wide range of disorder, including the region of Anderson insulator. To compare and extract explicitly effects of Anderson localization we also studied coefficient C in the "ladder" approximation for disorder scattering. In the weak coupling limit $U/2D_{\text{eff}} \ll 1$ and weak disorder $W/2D < 0.37$ the behavior of coefficient C and related physical properties is well described by the theory of "dirty" superconductors—coefficient C and coherence length rapidly drop with the growth of disorder, while penetration depth and the slope of the upper critical field grow. In the region of strong disorder (in an Anderson insulator) in BCS limit the behavior of coefficient C is strongly affected by localization effects. In the "ladder" approximation the band widening effect leads to the growth of coefficient C with

the growth of W [25], however localization effects restore suppression of coefficient C by disorder and in Anderson insulator phase. Correspondingly, localization effects significantly change physical properties, related to coefficient C, so that for these properties qualitatively follow the dependencies characteristic for "dirty" superconductors—the coherence length is suppressed by disorder, while the penetration depth and the slope of the upper critical field grow with the growth of disorder. In the BCS–BEC crossover region and in the BEC limit coefficient C and all related physical properties are rather weakly dependent on disorder. In particular, in BEC limit both coherence length and penetration depth are slightly suppressed by disorder, so that their ratio (Ginzburg–Landau parameter) is practically disorder independent. In the BEC limit the effects of Anderson localization rather weakly affect the coefficient C and the related physical characteristics.

It should be noted that all results were derived here under implicit assumption of the self-averaging nature of superconducting order parameter entering the Ginzburg–Landau expansion, which is connected with our use of the standard "impurity" diagram technique [26, 27]. It is well known [9], that this assumption becomes, in the general case, inapplicable close to Anderson metal–insulator transition, due to strong fluctuations of the local density of states developing here [34] and inhomogeneous picture of superconducting transition [35]. This problem is very interesting in the context of the superconductivity in the BCS–BEC crossover region and in the region of strong coupling and deserves further studies.

ACKNOWLEDGMENTS

This work was supported by the Federal Agency for Scientific Organizations under the State contract no. 0389-2014-0001 and in part by the Russian Foundation for Basic Research (project no. 17-02-00015).

REFERENCES

1. A. A. Abrikosov and L. P. Gor'kov, Sov. Phys. JETP **9**, 220 (1959).
2. A. A. Abrikosov and L. P. Gor'kov, Sov. Phys. JETP **9**, 1090 (1959).
3. L. P. Gor'kov, Sov. Phys. JETP **36**, 1364 (1959).
4. A. A. Abrikosov and L. P. Gor'kov, Sov. Phys. JETP **12**, 1243 (1961).
5. P. W. Anderson, J. Phys. Chem. Solids **11**, 26 (1959).
6. P. G. de Gennes, *Superconductivity of Metals and Alloys* (W. A. Benjamin, New York, 1966).
7. L. N. Bulaevskii and M. V. Sadovskii, JETP Lett. **39**, 640 (1984).
8. L. N. Bulaevskii and M. V. Sadovskii, J. Low. Temp. Phys. **59**, 89 (1985).
9. M. V. Sadovskii, Phys. Rep. **282**, 226 (1997); arXiv:cond-mat/9308018, M. V. Sadovskii, *Superconductivity and Localization* (World Scientific, Singapore, 2000).
10. P. Nozieres and S. Schmitt-Rink, J. Low Temp. Phys. **59**, 195 (1985).
11. Th. Pruschke, M. Jarrell, and J. K. Freericks, Adv. Phys. **44**, 187 (1995).
12. A. Georges, G. Kotliar, W. Krauth, and M. J. Rozenberg, Rev. Mod. Phys. **68**, 13 (1996).
13. D. Vollhardt, in *Lectures on the Physics of Strongly Correlated Systems XIV,* Ed. by A. Avella and F. Mancini, AIP Conf. Proc. **1297**, 339 (2010); arXiv: 1004.5069.
14. N. A. Kuleeva, E. Z. Kuchinskii, and M. V. Sadovskii, J. Exp. Theor. Phys. **119**, 264 (2014); arXiv: 1401.2295.
15. E. Z. Kuchinskii, I. A. Nekrasov, and M. V. Sadovskii, JETP Lett. **82**, 198 (2005); arXiv: cond-mat/0506215.
16. M. V. Sadovskii, I. A. Nekrasov, E. Z. Kuchinskii, Th. Prushke, and V. I. Anisimov, Phys. Rev. B **72**, 155105 (2005); arXiv: cond-mat/0508585.
17. E. Z. Kuchinskii, I. A. Nekrasov, and M. V. Sadovskii, Low Temp. Phys. **32**, 398 (2006); arXiv: cond-mat/0510376.
18. E. Z. Kuchinskii, I. A. Nekrasov, and M. V. Sadovskii, Phys. Usp. **53**, 325 (2012); arXiv:1109.2305.
19. E. Z. Kuchinskii, I. A. Nekrasov, and M. V. Sadovskii, J. Exp. Theor. Phys. **106**, 581 (2008); arXiv: 0706.2618.
20. E. Z. Kuchinskii and M. V. Sadovskii, J. Exp. Theor. Phys. **122**, 509 (2016); arXiv:1507.07654.
21. E. Z. Kuchinskii, I. A. Nekrasov, and M. V. Sadovskii, Phys. Rev. B **75**, 115102 (2007); arXiv:cond-mat/0609404.
22. E. Z. Kuchinskii, N. A. Kuleeva, and M. V. Sadovskii, JETP Lett. **100**, 192 (2014); arXiv: 1406.5603.
23. E. Z. Kuchinskii, N. A. Kuleeva, and M. V. Sadovskii, J. Exp. Theor. Phys. **120**, 1055 (2015); arXiv:1411.1547.
24. E. Z. Kuchinskii, N. A. Kuleeva, and M. V. Sadovskii, J. Exp. Theor. Phys. **122**, 375 (2016); arXiv:1507.07649.
25. E. Z. Kuchinskii, N. A. Kuleeva, and M. V. Sadovskii, J. Low Temp. Phys. **43**, 17 (2017); arXiv: 1606.05125.
26. L. P. Gor'kov and I. E. Dzyaloshinskii, *Quantum Field Theoretical Methods in Statistical Physics* (Pergamon Press, Oxford, 1965).
27. M. V. Sadovskii, *Diagrammatics* (World Scientific, Singapore, 2006).
28. R. Bulla, T. A. Costi, and T. Pruschke, Rev. Mod. Phys. **60**, 395 (2008)
29. D. Vollhardt and P. Wölfle, Phys. Rev. B **22**, 4666 (1980); Phys. Rev. Lett. **48**, 699 (1982).
30. P. Wölfle and D. Vollhardt, in *Anderson Localization,* Ed. by Y. Nagaoka and H. Fukuyama, Springer Ser. Solid State Sci. **39**, 26 (1982).
31. A. V. Myasnikov and M. V. Sadovskii, Sov. Phys. Solid State **24**, 2033 (1982); E. A. Kotov and M. V. Sadovskii, Zs. Phys. B **51**, 17 (1983).
32. M. V. Sadovskii, in *Soviet Scientific Reviews – Physics Reviews*, Ed. I. M. Khalatnikov (Harwood Academic, New York, 1986), vol. 7, p. 1.
33. D. Vollhardt and P. Wölfle, in *Electronic Phase Transitions,* Ed. by W. Hanke and Yu. V. Kopaev (North–Holland, Amsterdam, 1992), vol. 32, p. 1.
34. L. N. Bulaevskii and M. V. Sadovskii, JETP Lett. **43**, 99 (1986).
35. L. N. Bulaevskii, S. V. Panyukov, and M. V. Sadovskii, Sov. Phys. JETP **65**, 380 (1987).

ISSN 1063-7761, Journal of Experimental and Theoretical Physics, 2017, Vol. 125, No. 6, pp. 1127–1136. © Pleiades Publishing, Inc., 2017.
Published in Russian in Zhurnal Eksperimental'noi i Teoreticheskoi Fiziki, 2017, Vol. 152, No. 6, pp. 1321–1332.

ORDER, DISORDER, AND PHASE TRANSITION IN CONDENSED SYSTEM

Temperature Dependence of the Upper Critical Field in Disordered Hubbard Model with Attraction[1]

E. Z. Kuchinskii[a,*], N. A. Kuleeva[a], and M. V. Sadovskii[a,b,]**

[a] *Institute for Electrophysics, Russian Academy of Sciences, Ural Branch, Yekaterinburg, 620016 Russia*
[b] *Mikheev Institute for Metal Physics, Russian Academy of Sciences, Ural Branch, Yekaterinburg, 620108 Russia*
** e-mail: kuchinsk@iep.uran.ru*
*** e-mail: sadovski@iep.uran.ru*

Received August 30, 2017

Abstract—We study disorder effects upon the temperature behavior of the upper critical magnetic field in an attractive Hubbard model within the generalized DMFT+Σ approach. We consider the wide range of attraction potentials U—from the weak coupling limit, where superconductivity is described by BCS model, up to the strong coupling limit, where superconducting transition is related to Bose–Einstein condensation (BEC) of compact Cooper pairs, formed at temperatures significantly higher than superconducting transition temperature, as well as the wide range of disorder—from weak to strong, when the system is in the vicinity of Anderson transition. The growth of coupling strength leads to the rapid growth of $H_{c2}(T)$, especially at low temperatures. In BEC limit and in the region of BCS–BEC crossover $H_{c2}(T)$, dependence becomes practically linear. Disordering also leads to the general growth of $H_{c2}(T)$. In BCS limit of weak coupling increasing disorder lead both to the growth of the slope of the upper critical field in the vicinity of the transition point and to the increase of $H_{c2}(T)$ in the low temperature region. In the limit of strong disorder in the vicinity of the Anderson transition localization corrections lead to the additional growth of $H_{c2}(T)$ at low temperatures, so that the $H_{c2}(T)$ dependence becomes concave. In BCS–BEC crossover region and in BEC limit disorder only slightly influences the slope of the upper critical field close to T_c. However, in the low temperature region $H_{c2}(T)$ may significantly grow with disorder in the vicinity of the Anderson transition, where localization corrections notably increase H_{c2} ($T = 0$) also making $H_{c2}(T)$ dependence concave.

DOI: 10.1134/S1063776117120159

INTRODUCTION

The studies of disorder influence on superconductivity have a rather long history. In pioneer papers by Abrikosov and Gor'kov [1–4] they analyzed the limit of weak disorder ($p_F l \gg 1$, where p_F is the Fermi momentum and l is the mean free path) and weak coupling superconductivity, which is well described by BCS theory. The well-known "Anderson theorem" on the critical temperature T_c of superconductors with "normal" (nonmagnetic) disorder [5, 6] is usually also attributed to this limit.

The generalization of the theory of "dirty" superconductors for the case of strong enough disorder ($p_F l \sim 1$) (and up to the region of Anderson transition) was done in [7–10], where superconductivity was also analyzed in the weak coupling limit.

Most dramatically, the effects of disordering are reflected in the behavior of the upper critical magnetic field. In the theory of "dirty" superconductors the growth of disorder leads to the increase both of the slope of the temperature dependence of the upper critical field at T_c [6] and of $H_{c2}(T)$ in the whole temperature region [11]. The effects of Anderson localization in the limit of strong enough disorder are also mostly reflected in the temperature dependence of the upper critical field. At the point of the Anderson metal–insulator transition itself, localization effects lead to a rather sharp increase of H_{c2} at low temperatures and temperature dependence of $H_{c2}(T)$ is qualitatively different from the dependence derived by Werthamer, Helfand and Hohenberg (WHH) [11], which is characteristic for the theory of "dirty" superconductors, and the $H_{c2}(T)$ dependence becomes concave, i.e., demonstrates positive curvature [7–9].

The problem of the generalization of BCS theory into the strong coupling region has been known for a pretty long time. Significant progress in this direction was achieved in a paper by Nozieres and Schmitt–Rink [12], who proposed an effective method to study the crossover from BCS–like behavior in the weak coupling region towards Bose–Einstein condensation (BEC) in the strong coupling region. At the same time, the problem of superconductivity of disordered

[1] The article was translated by the authors.

systems in the limit of strong coupling and in BCS–BEC crossover region is still rather poorly developed.

One of the simplest models to study BCS–BEC crossover is the Hubbard model with attractive interaction. The most successful approach to the Hubbard model, both to describe strongly correlated systems in the case of repulsive interaction, as well as to study the BCS–BEC crossover for the case of attraction, is the dynamical mean field theory (DMFT) [13–15].

In recent years, we have developed the generalized DMFT+Σ approach to the Hubbard model [16–21], which is very convenient for the studies of different external (with respect to those accounted by DMFT) interactions. In particular, this approach is well suited for the analysis of two-particle properties, such as optical (dynamic) conductivity [20, 22].

In [23] we have used this approach to analyze single-particle properties of the normal phase and optical conductivity in attractive Hubbard model. This was followed by our use of DMFT+Σ in [24] to study disorder influence on the temperature of superconducting transition, which was calculated within Nozieres–Schmitt-Rink approach. In particular, in this work for the case of semi-elliptic "bare" density of states (adequate for three-dimensional case) we have numerically demonstrated the validity of the generalized Anderson theorem, so that all effects of disordering on the critical temperature (for all values of interaction parameter) are related only to general widening of the "bare" band (density of states) by disorder.

An analytic proof of this universality of disorder influence on all single-particle properties in DMFT+Σ approximation and on superconducting critical temperature for the case of a semi-elliptic band was given in [25].

Starting with the classic work by Gor'kov [3], it is well known that the Ginzburg–Landau expansion is of fundamental importance for the theory of "dirty" superconductors, allowing the effective studies of the behavior of various physical parameters close to superconducting critical temperature for different disorder levels [6]. The generalization of this theory (for weak coupling superconductors) to the region of strong disorder (up to the Anderson metal–insulator transition) was done in [7–9].

In [26–28] combining Nozieres–Schmitt-Rink approximation with DMFT+Σ for attractive Hubbard models we provided microscopic derivation of the coefficients of Ginzburg–Landau expansion taking into account disordering, which allowed the generalization of Ginzburg–Landau theory to BCS–BEC crossover region and BEC limit of very strong coupling for different levels of disorder. In particular, in [28] using the generalization of self-consistent theory of localization this approach was extended to the case of strong disorder, where Anderson localization effects become important. It was shown, that in the weak coupling limit the slope of the $H_{c2}(T)$ dependence at $T = T_c$ increases with disordering in the region of weak disorder in accordance with the theory of "dirty" superconductors, while in the limit of strong disorder localization effects lead to the additional increase of the slope of the upper critical field. However, in the region of BCS–BEC crossover and in BEC limit the slope of $H_{c2}(T)$ close to T_c only slightly increases with the growth of disorder and the account of localization effects is more or less irrelevant.

In the present paper, using the combination of Nozieres–Schmitt-Rink and DMFT+Σ approximations for the attractive Hubbard model we shall analyze disorder effects on the complete temperature dependence of $H_{c2}(T)$ for the wide range of U interaction values, including the region of BCS–BEC crossover, and the wide range of disorder levels up to the vicinity of the Anderson transition.

HUBBARD MODEL WITHIN DMFT+Σ APPROACH IN NOZIERES–SCHMITT-RINK APPROXIMATION

We consider the disordered nonmagnetic Anderson–Hubbard model with attraction described by the Hamiltonian:

$$H = -t\sum_{\langle ij\rangle\sigma} a^{\dagger}_{i\sigma}a_{j\sigma} + \sum_{i\sigma}\epsilon_i n_{i\sigma} - U\sum_i n_{i\uparrow}n_{i\downarrow}, \qquad (1)$$

where $t > 0$ is a transfer integral between nearest neighbors, U is the Hubbard attraction on the lattice site, $n_{i\sigma} = a^{\dagger}_{i\sigma}a_{i\sigma}$—number of electrons operator on the site, $a_{i\sigma}$ ($a^{\dagger}_{i\sigma}$)—annihilation (creation) operator for an electron with spin σ, and local energies ϵ_i are assumed to be independent random variables on different lattice sites. For the validity of the standard "impurity" diagram technique [29, 30] we assume the Gaussian distribution for energy levels ϵ_i:

$$\mathcal{P}(\epsilon_i) = \frac{1}{\sqrt{2\pi}\Delta}\exp\left(-\frac{\epsilon_i^2}{2\Delta^2}\right) \qquad (2)$$

Distribution width Δ serves as a measure of disorder and the Gaussian random field of energy levels (independent on different lattice sites—"white noise" correlations) induces the "impurity" scattering, which is considered within the standard approach, based on calculations of the averaged Green's functions [30].

The generalized DMFT+Σ approach [16–19] extends the standard dynamical mean field theory (DMFT) [13–15] by addition of an "external" self-energy (SE) $\Sigma_{\mathbf{p}}(\varepsilon)$ (in general case momentum dependent), which is related to any interaction outside the limits of DMFT, and provides an effective method of calculations for both single-particle and two-particle properties [20, 22]. It completely conserves the standard self-consistent equations of DMFT [13–15], while at each step of DMFT iteration procedure the

external SE $\Sigma_{\mathbf{p}}(\varepsilon)$ is recalculated again using some approximate scheme, corresponding to the form of an external interaction and the local Green's function of DMFT is also "dressed" by $\Sigma_{\mathbf{p}}(\varepsilon)$ at each stage of the standard DMFT procedure.

In our problem of scattering by disorder [20, 21] for the "external" SE, entering the DMFT+Σ cycle, we use the simplest (self-consistent Born) approximation neglecting "crossing" diagrams for impurity scattering. This "external" SE remains momentum independent (local).

To solve the effective single-impurity Anderson model of DMFT in this paper, as in our previous works, we use the very efficient method of numerical renormalization group (NRG) [31].

In the following we assume the "bare" band with semi-elliptic density of states (per unit cell with lattice parameter a and for single spin projection), which is reasonable approximation for three-dimensional case:

$$N_0(\varepsilon) = \frac{2}{\pi D^2}\sqrt{D^2 - \varepsilon^2}, \tag{3}$$

where D defines conduction band half-width.

In [25] we have shown that in DMFT+Σ approach for the model with semi-elliptic density of states all the influence of disorder on single-particle properties reduces simply to disorder induced band widening, i.e., to the replacement $D \to D_{\text{eff}}$, where D_{eff} is the effective band half-width of conduction band in the absence of correlations ($U = 0$), widened by disorder:

$$D_{\text{eff}} = D\sqrt{1 + 4\frac{\Delta^2}{D^2}}. \tag{4}$$

The "bare" (in the absence of U) density of states, "dressed" by disorder,

$$\tilde{N}_0(\xi) = \frac{2}{\pi D_{\text{eff}}^2}\sqrt{D_{\text{eff}}^2 - \varepsilon^2}, \tag{5}$$

remains semi-elliptic also in the presence of disorder.

It should be noted that in other models of "bare" band disorder induces not only widening of the band, but also changes the form of the density of states. Thus, in the general case there will be no complete universality of disorder influence on single-particle properties, which are reduced to the simple replacement $D \to D_{\text{eff}}$. However, in the limit of strong disorder, which is of primary interest to us, the "bare" band always becomes, in practice, semi-elliptic and the universality is restored [25].

All calculations in this work, as in the previous, were done for rather typical case of a quarter-filled band (number of electrons per lattice site $n = 0.5$).

To analyze superconductivity for a wide range of pairing interaction U, following [23, 25], we use Nozieres–Schmitt-Rink approximation [12], which allows qualitatively correct (though approximate) description of BCS–BEC crossover region. In this approach, to determine the critical temperature T_c we use [25] the usual BCS-like equation:

$$1 = \frac{U}{2}\int_{-\infty}^{\infty} d\varepsilon \tilde{N}_0(\varepsilon)\frac{\tanh((\varepsilon - \mu)/2T_c)}{\varepsilon - \mu}, \tag{6}$$

where the chemical potential μ for different values of U and Δ is determined from DMFT+Σ-calculations, i.e., from the standard equation for the number of electrons (band filling), which allows us to find T_c for the wide interval of model parameters, including the BCS–BEC crossover region and the limit of strong coupling, as well as for different levels of disorder. This reflects the physical meaning of Nozieres–Schmitt-Rink approximation: in the weak coupling region transition temperature is controlled by the equation for Cooper instability (6), while in the limit of strong coupling it is determined as BEC temperature controlled by chemical potential.

It was shown in [25], that disorder influence on the critical temperature T_c and single-particle characteristics (e.g. density of states) in the model with semi-elliptic density of states is universal and reduces only to the change of the effective bandwidth. In the weak coupling region the temperature of superconducting transition is well described by the BCS model, while in the strong coupling region the critical temperature is mainly determined by the condition of Bose–Einstein condensation of Cooper pairs and decreases with the growth of U as t^2/U, passing through a maximum at $U/2D_{\text{eff}} \sim 1$.

The review of this and similar results obtained for disordered Hubbard model in DMFT+Σ approximation can be found in [21].

BASIC RELATIONS FOR THE UPPER CRITICAL FIELD

In Nozieres–Schmitt-Rink approach the critical temperature of superconducting transition is determined by combined solution of the weak coupling equation for Cooper instability in particle–particle (Cooper) channel and the equation for chemical potential for all values of Hubbard interaction within DMFT+Σ procedure. The usual condition for Cooper instability is written as:

$$1 = -U\chi(\mathbf{q}), \tag{7}$$

where $\chi(\mathbf{q})$ is Cooper susceptibility, determined by the loop diagram in Cooper channel, shown in Fig. 1. In the presence of an external magnetic field total momentum in Cooper channel $\mathbf{q}$ acquires contribution from the vector potential $\mathbf{A}$

$$\mathbf{q} \to \mathbf{q} - \frac{2e}{c}\mathbf{A}. \tag{8}$$

As we assume isotropic electron spectrum, Cooper susceptibility $\chi(\mathbf{q})$ depends on $\mathbf{q}$ only via q^2. The minimal eigenvalue of $(\mathbf{q} - 2e/c)\mathbf{A})^2$, determining

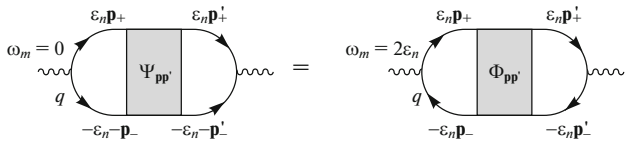

Fig. 1. Equivalence of loops in the Cooper and diffusion channels in the case of time inversion invariance.

(orbital)[2] upper critical magnetic field $H = H_{c2}$ is given by [30]

$$q_0^2 = 2\pi\frac{H}{\Phi_0}, \tag{9}$$

where $\Phi_0 = ch/2e = \pi\hbar/e$ is magnetic flux quantum. Then the equation for $T_c(H)$ or $H_{c2}(T)$ remains the same:

$$1 = -U\chi(q^2 = q_0^2). \tag{10}$$

In the following, we shall neglect relatively weak magnetic field influence on diffusion processes (broken time reversal invariance), which is reflected in non equality of loop diagrams in Cooper and diffusion channels. This influence was analyzed in [9, 10, 31, 32], where it was shown that the account of this broken symmetry only slightly decreases the value of $H_{c2}(T)$ at low temperatures, even close to the Anderson transition. In the case of time reversal invariance and due the static nature of impurity scattering "dressing" two-particle Green's function $\Psi_{\mathbf{p},\,\mathbf{p}'}(\varepsilon_n, \mathbf{q})$ we can change directions of all lower electronic lines in the loop with simultaneous sign change of all momenta on these lines (cf. Fig. 1). Then we obtain:

$$\Psi_{\mathbf{p},\mathbf{p}'}(\varepsilon_n, \mathbf{q}) = \Phi_{\mathbf{p},\mathbf{p}'}(\omega_m = 2\varepsilon_n, \mathbf{q}), \tag{11}$$

where ε_n are Fermionic Matsubara frequencies, $\mathbf{p}_\pm = \mathbf{p} \pm \mathbf{q}/2$, and $\Phi_{\mathbf{p},\,\mathbf{p}'}(\omega_m = 2\varepsilon_n, \mathbf{q})$ is the two-particle Green's function in diffusion channel, dressed by impurities. The we obtain the Cooper susceptibility as:

$$\begin{aligned}\chi(\mathbf{q}) &= -T\sum_{n,\mathbf{p},\mathbf{p}'}\Psi_{\mathbf{p},\mathbf{p}'}(\varepsilon_n, \mathbf{q}) \\ &= -T\sum_{n,\mathbf{p},\mathbf{p}'}\Phi_{\mathbf{p},\mathbf{p}'}(\omega_m = 2\varepsilon_n, \mathbf{q}).\end{aligned} \tag{12}$$

Performing the standard summation over Fermionic Matsubara frequencies [29, 30] we obtain for Cooper susceptibility entering Eq. (10):

$$\chi(q_0^2) = -\frac{1}{2\pi}\int_{-\infty}^{\infty} d\varepsilon\,\mathrm{Im}\,\Phi^{RA}(\omega = 2\varepsilon, q_0^2)\tanh\frac{\varepsilon}{2T}, \tag{13}$$

where $\Phi^{RA}(\omega, \mathbf{q}) = \sum_{\mathbf{p},\mathbf{p}'}\Phi^{RA}_{\mathbf{p},\mathbf{p}'}(\omega, \mathbf{q})$. To find the loop $\Phi^{RA}(\omega, \mathbf{q})$ in the case of strong disorder (including the region of Anderson localization) we use the approximate self-consistent theory of localization [30, 35–40]. Then this loop contains the diffusion pole contribution, which is written as [20]:

$$\Phi^{RA}(\omega = 2\varepsilon, q_0^2) = -\frac{\sum_{\mathbf{p}}\Delta G_{\mathbf{p}}(\varepsilon)}{\omega + iD(\omega)q_0^2}, \tag{14}$$

where $\Delta G_{\mathbf{p}}(\varepsilon) = G^R(\varepsilon, \mathbf{p}) - G^A(-\varepsilon, \mathbf{p})$, G^R and G^A are retarded and advanced Green's functions, while $D(\omega)$ is frequency dependent generalized diffusion coefficient. As a result, Eq. (10) for $H_{c2}(T)$ takes the form:

$$1 = -\frac{U}{2\pi}\int_{-\infty}^{\infty} d\varepsilon\,\mathrm{Im}\left(\frac{\sum_{\mathbf{p}}\Delta G_{\mathbf{p}}(\varepsilon)}{2\varepsilon + iD(2\varepsilon)2\pi H_{c2}/\Phi_0}\right)\tanh\frac{\varepsilon}{2T}. \tag{15}$$

The generalized diffusion coefficient in self-consistent theory of localization [30, 35–40] for the model under consideration is determined by the following self-consistence equation [20]:

$$\begin{aligned}D(\omega) = i\frac{\langle v\rangle^2}{d}\Bigg(&\omega - \Delta\Sigma^{RA}_{\mathrm{imp}}(\omega) + \Delta^4\sum_{\mathbf{p}}\Delta G^2_{\mathbf{p}}(\varepsilon) \\ &\cdot\sum_{\mathbf{q}}\frac{1}{\omega + iD(\omega)q^2}\Bigg)^{-1},\end{aligned} \tag{16}$$

where $\omega = 2\omega$, $\Delta\Sigma^{RA}_{\mathrm{imp}}(\omega) = \Sigma^R_{\mathrm{imp}}(\varepsilon) - \Sigma^A_{\mathrm{imp}}(-\varepsilon)$, d is space dimensionality, while the average velocity $\langle v\rangle$ is defined here as:

$$\langle v\rangle = \frac{\sum_{\mathbf{p}}|\mathbf{v}_{\mathbf{p}}|\Delta G_{\mathbf{p}}(\varepsilon)}{\sum_{\mathbf{p}}\Delta G_{\mathbf{p}}(\varepsilon)}, \quad \mathbf{v}_{\mathbf{p}} = \frac{\partial\varepsilon(\mathbf{p})}{\partial\mathbf{p}}. \tag{17}$$

Taking into account the limits of diffusion approximation summation over q in Eq. (16) should be limited by [30, 39]

$$q < k_0 = \min\{l^{-1}, p_{\mathrm{F}}\}, \tag{18}$$

where l is the mean-free path due to elastic scattering by disorder and p_{F} is the Fermi momentum.

In the limit of weak disorder, when localization corrections are small, Cooper susceptibility $\chi(\mathbf{q})$ is determined by ladder approximation. In this approximation Cooper susceptibility was studied by us in [27]. Let us now rewrite self-consistency Eq. (16) so that in the limit of weak disorder it explicitly reproduces the results of ladder approximation. In this approximation we neglect all contributions to irreducible vertex from "maximally crossed" diagrams and the last term in the r.h.s. of Eq. (16) just vanishes. Now we introduce the

[2] In this paper we do not consider paramagnetic effect due to electronic spin.

frequency dependent generalized diffusion coefficient in ladder approximation as:

$$D_0(\omega) = \frac{\langle v\rangle^2}{d}\frac{i}{\omega - \Delta\Sigma^{RA}_{\rm imp}(\omega)}. \quad (19)$$

The value of $\langle v\rangle^2/d$, entering the self-consistency Eq. (16), can now be expressed via this diffusion coefficient D_0 in ladder approximation. Then the self-consistency Eq. (16) takes the form:

$$D(\omega = 2\varepsilon) = D_0(\omega = 2\varepsilon)\left(1 + \frac{\Delta^4}{2\varepsilon - \Delta\Sigma^{RA}_{\rm imp}(\omega = 2\varepsilon)} \cdot \sum_{\mathbf{p}} \Delta G^2_{\mathbf{p}}(\varepsilon)\sum_{\mathbf{q}} \frac{1}{2\varepsilon + iD(\omega = 2\varepsilon)q^2}\right)^{-1}. \quad (20)$$

In the framework of the approach of [27] the diffusion coefficient D_0 ($\omega = 2\varepsilon$) in ladder approximation can be obtained in analytic form. In fact, in the ladder approximation, the two-particle Green's function (14) can be written as:

$$\Phi^{RA}_0(\omega = 2\varepsilon, \mathbf{q}) = -\frac{\sum_{\mathbf{p}} \Delta G_{\mathbf{p}}(\varepsilon)}{\omega + iD_0(\omega = 2\varepsilon)q^2}. \quad (21)$$

Let us introduce

$$\varphi(\varepsilon, \mathbf{q} = 0) \equiv \lim_{q\to 0}\frac{\Phi^{RA}_0(\omega = 2\varepsilon, \mathbf{q}) - \Phi^{RA}_0(\omega = 2\varepsilon, \mathbf{q} = 0)}{q^2} = \frac{i\sum_{\mathbf{p}} \Delta G_{\mathbf{p}}(\varepsilon)}{\omega^2} D_0(\omega = 2\varepsilon). \quad (22)$$

Then the diffusion coefficient D_0 can be written as:

$$D_0 = \frac{\varphi(\varepsilon, \mathbf{q} = 0)(2\varepsilon)^2}{i\sum_{\mathbf{p}} \Delta G_{\mathbf{p}}(\varepsilon)}. \quad (23)$$

In [27], using the exact Ward identity, written in ladder approximation, it was shown that $\varphi(\varepsilon, \mathbf{q} = 0)$ can be expressed as

$$\varphi(\varepsilon, \mathbf{q} = 0)(2\varepsilon)^2 = \sum_{\mathbf{p}} v_x^2 G^R(\varepsilon, \mathbf{p})G^A(-\varepsilon, \mathbf{p}) + \frac{1}{2}\sum_{\mathbf{p}} \frac{\partial^2\varepsilon(\mathbf{p})}{\partial p_x^2}(G^R(\varepsilon, \mathbf{p}) + G^A(-\varepsilon, \mathbf{p})), \quad (24)$$

where $v_x = \partial\varepsilon(\mathbf{p})/\partial p_x$.

The procedure for the numerical now looks as follows. First, using Eqs. (24), (23) we find the diffusion coefficient D_0 in the ladder approximation. Then using self-consistency Eq. (20) we find the generalized diffusion coefficient and solve Eq. (15) to determine $H_{c2}(T)$.

MAIN RESULTS

The chemical potential enters Eq. (15) defining $H_{c2}(T)$ as a parameter, which is to be determined from the condition of band (quarter) filling using the DMFT+Σ procedure. Chemical potential depends not only on the coupling strength, but also on the temperature, and this dependence is quite important in determining the value of $H_{c2}(T)$ in the limit of strong enough coupling. We use the NRG algorithm as an impurity solver of DMFT neglects electronic levels quantization in magnetic field, i.e., magnetic field influence on electron orbital motion and correspondingly on the chemical potential. In [23] we have shown that in an attractive Hubbard model our DMFT procedure becomes unstable for $T < T_c$, which is reflected in finite difference of even and odd iterations of DMFT. This instability is apparently related to instability of the normal state for $T < T_c$. In particular, it is most sharp in BEC strong coupling limit (for $U/2D \geq 1$), which makes it impossible to determine the chemical potential at $T < T_c$. In the weak coupling limit the difference between the results of even and odd DMFT iterations is very small, which allows us to find the values of $\mu(T)$ with high accuracy even for $T < T_c$. In Fig. 2, we show the temperature dependence of the chemical potential for different values of coupling strength. In the weak coupling limit ($U/2D = 0.4, 0.6$) in Fig. 2 we show data obtained from DMFT+Σ calculations, including the region of $T < T_c$. In the limit of strong coupling we can determine the chemical potential directly form DMFT+Σ procedure only at $T > T_c$ and appropriate data points are also shown in Fig. 2. From Fig. 2, we can see that in the presence of interactions the chemical potential acquires the linear temperature dependence, which is quite important for us. In the weak coupling limit the chemical potential does not have any singularities for $T < T_c$ and we can assume, that in the strong coupling region μ follows the same type of temperature dependence, which can be found from linear extrapolation (dashed lines for $U/2D = 1.0, 1.4$ in Fig. 2) from the region of $T > T_c$. This procedure was used in our calculations for the strong coupling region.

In the limit of weak disorder ($\Delta/2D = 0.05$ in Fig. 3a) and weak coupling ($U/2D = 0.2$) we observe the temperature dependence of the upper critical field similar to the standard WHH dependence [11] with negative curvature. The growth of the coupling strength in general leads to significant increase of the upper critical field up to extremely high values over $\Phi_0/2\pi a^2$ (a—lattice spacing) in the low temperature region. At intermediate couplings ($U/2D = 0.4, 0.6$) the temperature dependence of $H_{c2}(T)$ acquires weak maximum at $T/T_c \sim (0.2–0.4)$. Further increase of the

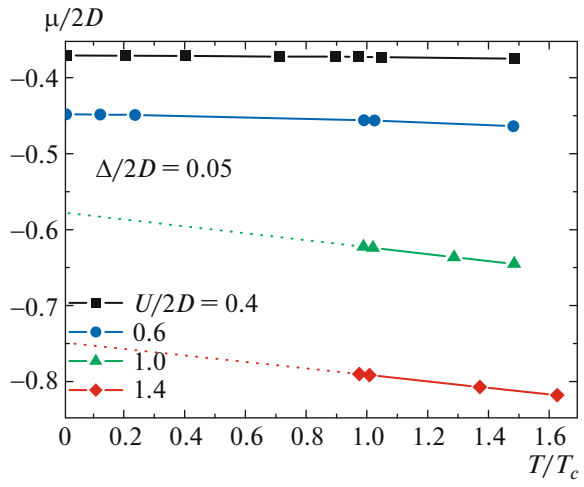

Fig. 2. (Color online) Temperature dependences of the chemical potential for $\Delta/2D = 0.05$ and different values of the interaction.

coupling strength leads to the growth of the upper critical field and for $U/2D = 1$ the temperature dependence $H_{c2}(T)$ becomes almost linear and for higher couplings the temperature dependence the value of the upper critical field remains practically the same for all temperatures. With the growth of disorder ($U/2D = 0.11$ in Fig. 3b), the situation remains qualitatively similar. The increase of the coupling strength leads at first to the growth of H_{c2} for all temperatures. The small maximum of $H_{c2}(T)$, observed at intermediate couplings ($U/2D = 0.4$, 0.6) and weak disorder ($\Delta/2D = 0.05$) vanishes. In the strong coupling region ($U/2D \geq 1$) $H_{c2}(T)$ is in fact linear and only weakly changes with coupling strength. At strong enough disorder ($\Delta/2D = 0.25$) with the growth of coupling strength the upper critical field also grows in the whole temperature region.

This growth continues up to BEC region of very strong coupling ($U/2D = 1.4$), after that $H_{c2}(T)$ dependence becomes linear and only weakly dependent on the coupling strength. For comparison on the left panel of Fig. 3c for $U/2D = 0.6$ we show both data obtained using a self-consistent theory of localization (filled triangles and continuous curve) and those calculated from ladder approximation for impurity scattering (unfilled triangles and dashed curve). Weak difference between these dependencies demonstrates that corrections from Anderson localization at this disorder level ($\Delta/2D = 0.25$) are rather weak.

In the model under consideration in DMFT+Σ approximation the Anderson metal–insulator transition occurs at $\Delta/2D = 0.37$ and this value of critical disorder is independent of the coupling strength (cf. [20]). Temperature behavior of the upper critical field precisely at the point of Anderson transition and in Anderson insulator phase for different values of coupling strength is shown in Fig. 4. In this figure filled symbols and continuous curves show results of calculations using the self-consistent theory of localization, while unfilled symbols and dashed curves correspond to the results of calculations using the ladder approximation for impurity scattering. At the point of Anderson transition ($\Delta/2D = 0.37$ in Fig. 4a) and in the limit of weak coupling localization effects strongly change the temperature dependence of $H_{c2}(T)$. In particular, these effects enhance $H_{c2}(T)$ in the whole temperature region. However, the greatest increase is observed at low temperatures, so that $H_{c2}(T)$ dependence acquires positive curvature, as was first shown in [7, 8]. The increase of the coupling strength leads to the growth of the upper critical field in the whole temperature interval. The curves of $H_{c2}(T)$ in the intermediate coupling region ($U/2D = 0.6$, 1) still have positive curvature. Further increase of the coupling up to $U/2D = 1.4$ also enhance Hc2 at all temperatures. However, the account of localization corrections at such a strong coupling is relevant only at low temperatures ($T/T_c < 0.1$). In this region, the $H_{c2}(T)$ dependence has positive curvature, while at other temperatures $H_{c2}(T)$ is, in fact, linear. With further increase of coupling strength ($U/2D = 1.6$) $H_{c2}(T)$ becomes practically linear and localization correction become irrelevant at all temperatures. Thus, in the BEC limit of very strong coupling, the influence of Anderson localization on the behavior of the upper critical field is rather weak. In Anderson insulator phase (Fig. 4b) and in BCS weak coupling limit ($U/2D = 0.2$) the account of localization effects leads to significant growth of $H_{c2}(T)$ (cf. insert in Fig. 4b). The increase of coupling strength leads to the growth of the upper critical field in the whole temperature region. At intermediate couplings ($U/2D = 0.6$, 1.0) the account of localization effects notably increases H_{c2} for all temperatures. However, the most significant increase is observed in the region of low temperatures, leading to the positive curvature of $H_{c2}(T)$ dependence and very sharp growth of $H_{c2}(T = 0)$. In BEC limit of very strong coupling ($U/2D = 1.4$, 1.6) the upper critical field almost does not grow with coupling strength. Contribution from localization effects for $T \sim T_c$ is irrelevant and $H_{c2}(T)$ dependence is practically linear. However, at low temperatures ($T \ll T_c$) contribution from Anderson localization still significantly enhances the upper critical field and $H_{c2}(T)$ curve has positive curvature. Thus, both in Anderson insulator phase and in BEC limit of very strong coupling the influence of Anderson localization on the behavior of the upper critical field is noticeably suppressed, though at low temperatures it still remains quite significant changing the value of $H_{c2}(T = 0)$.

In Fig. 5 we show temperature dependencies of the upper critical field for different levels of disorder in three characteristic regions of coupling strength: in

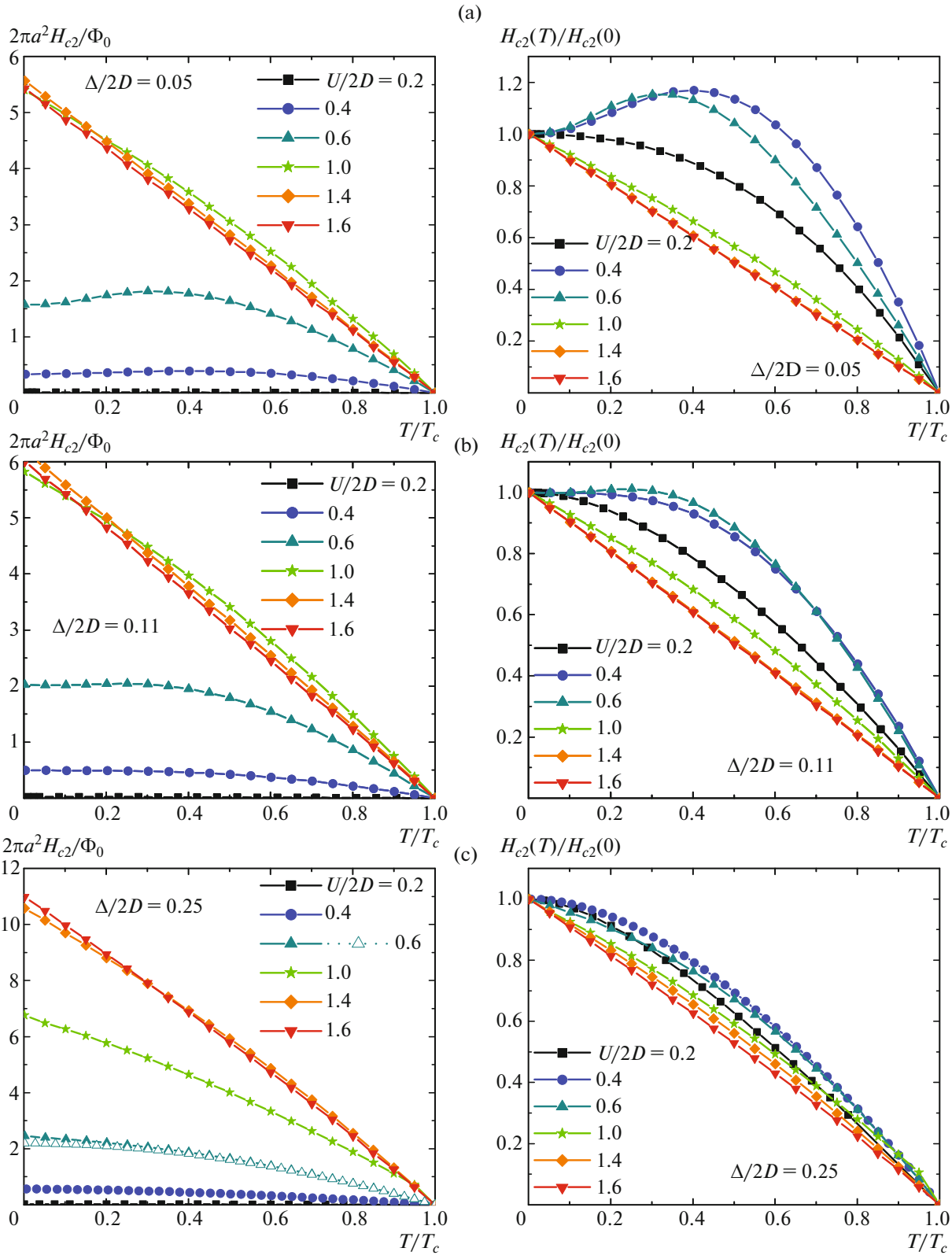

Fig. 3. (Color online) Temperature dependences of the upper critical field for different values of the coupling strength for different disorder levels. The upper critical field on the left panels is normalized to $\Phi_0/(2\pi a^2)$; on the right panels, the upper critical field is normalized to its value at $T = 0$.

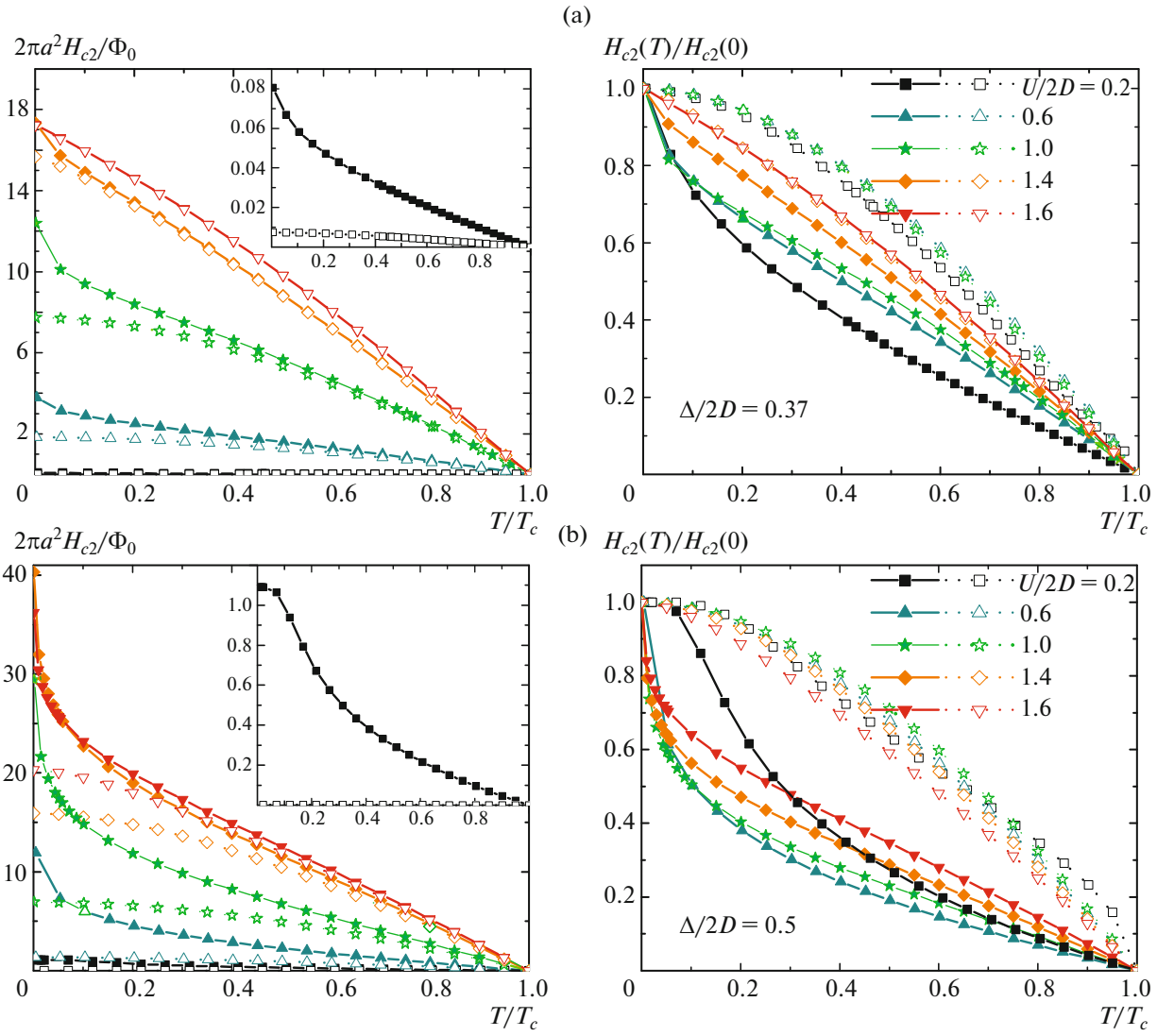

Fig. 4. (Color online) Temperature dependences of the upper critical field (a) on the Anderson metal–insulator transition and (b) in the Anderson insulator phase for different values of the coupling strength. On the left panels, H_{c2} is normalized to $\Phi_0/(2\pi a^2)$; the upper critical field on the right panels is normalized to its value at $T = 0$.

BCS weak coupling limit ($U/2D = 0.2$), in BCS–BEC crossover region (intermediate coupling $U/2D = 1.0$) and in BEC limit of strong coupling ($U/2D = 1.6$). In weak coupling limit (Fig. 5a) the growth of disorder leads to the increase of the upper critical field in the whole temperature region in the limit of weak disorder ($\Delta/2D < 0.19$), while the temperature dependence has the negative curvature and is close to the standard WHH dependence [11]. With further increase of disorder with no account for localization corrections, the upper critical field decreases for all temperatures. However, taking into account localization corrections in the weak coupling limit for the case of strong disorder ($\Delta/2D \geq 0.37$) significantly increases the upper critical field and qualitatively changes its temperature dependence, so that the curves of $H_{c2}(T)$ acquire positive curvature. The upper critical field rapidly grows with disorder at all temperatures. For intermediate coupling (Fig. 5b) in the limit of weak disorder the temperature dependence of the upper critical field becomes practically linear. The upper critical field grows with disorder at all temperatures. In the limit of strong disorder ($\Delta/2D \geq 0.37$) localization corrections, as in the weak coupling limit, increase the upper critical field at all temperatures and the curves of $H_{c2}(T)$ acquire positive curvature. However, in the intermediate coupling region the influence of localization corrections is much weaker, than in the weak coupling limit and is relevant only at low temperatures. In BEC limit of the strong coupling (Fig. 5c) and in the limit of weak disorder the curves of $H_{c2}(T)$ are in fact linear. The upper critical field grows with disorder at all tem-

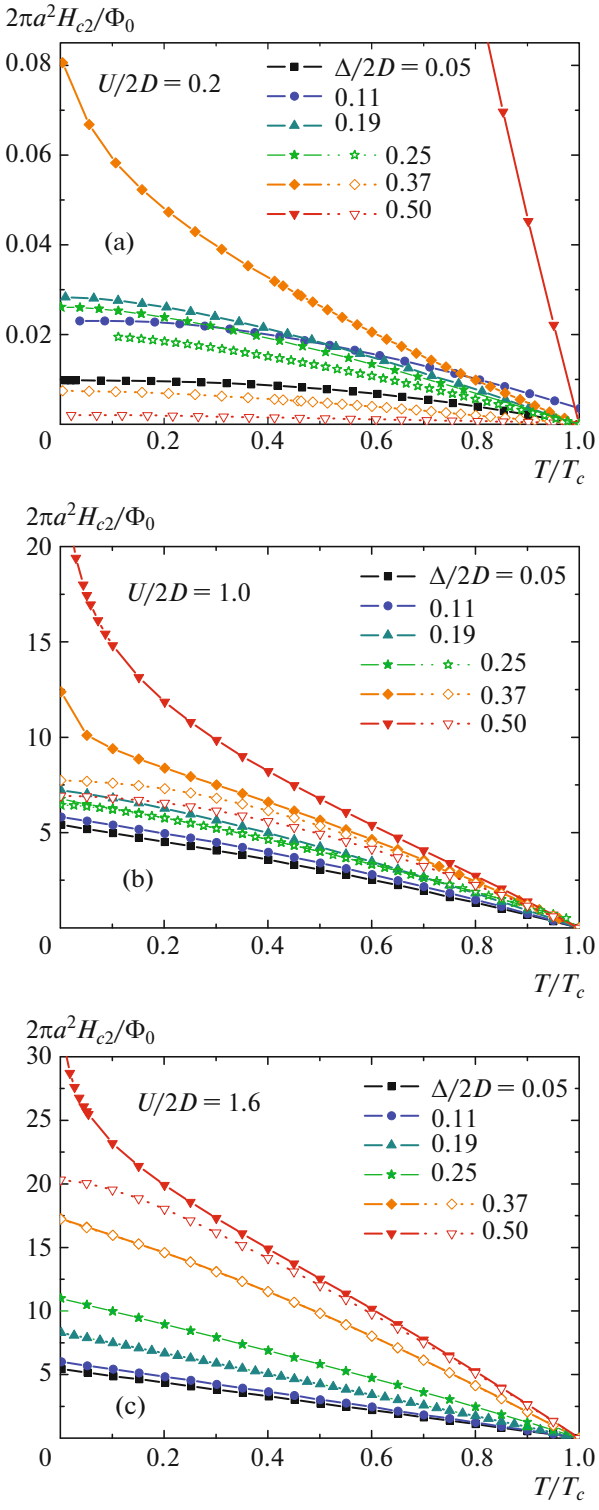

Fig. 5. (Color online) Temperature dependences of the upper critical field for different disorder levels: (a) BCS weak coupling limit, (b) BCS–BEC crossover region at intermediate coupling, (c) BEC strong coupling limit. Dark symbols and solid curves correspond to calculations taking localization corrections into account. Light symbols and dashed curves correspond to the ladder approximation for impurity scattering.

peratures. In the limit of strong disorder at the point of Anderson transition ($\Delta/2D = 0.37$) the $H_{c2}(T)$ dependence remains linear and the account of localization corrections in fact does not change the temperature dependence of the upper critical field. Further increase of disorder leads to the increase of $H_{c2}(T)$. Deeply in the Anderson insulator phase ($\Delta/2D = 0.5$) the $H_{c2}(T)$ dependence acquires the positive curvature and the account of localization effects enhances $H_{c2}(T)$ in the low temperature region, while close to T_c localization corrections are irrelevant even at such a strong disorder. Thus, the strong coupling significantly decreases the influence of localization effects of the temperature dependence of the upper critical field.

CONCLUSIONS

In this paper, within the combined Nozieres–Schmitt-Rink and DMFT+Σ generalization of the dynamical mean field theory we have investigated the influence of disordering, in particular the strong one (including the region of Anderson localization), and the growth of the strength of pairing interaction upon the temperature dependence of the upper critical field. Calculations were performed for the wide range of attractive potentials U, from the weak coupling limit of $U/2D \ll 1$, where instability of the normal phase and superconductivity is well described by BCS model, up to the strong coupling limit of $U/2D \gg 1$, where the superconducting transition is due to Bose–Einstein condensation of compact Cooper pairs, which are formed at temperatures much higher than the temperature of superconducting transition.

The growth of the coupling strength U leads to the fast increase of $H_{c2}(T)$, especially at low temperatures. In BEC limit and in the region of BCS–BEC crossover $H_{c2}(T)$ dependence becomes practically linear. Disordering also leads to the increase of $H_{c2}(T)$ at any coupling. In the weak coupling BCS limit the growth of disorder increases both the slope of the upper critical field close to $T = T_c$ and $H_{c2}(T)$ in low temperature region. In the limit of strong disorder in the vicinity of Anderson transition localization corrections lead to additional sharp increase of the upper critical field at low temperatures and $H_{c2}(T)$ dependence becomes concave, i.e., acquires positive curvature. In BCS–BEC crossover region and in BEC limit weak disorder is insignificant for the slope of the upper critical field at T_c, though the strong disorder in the vicinity of Anderson transition leads to noticeable increase of the slope of the upper critical field with the growth of disorder. In the low temperature region $H_{c2}(T)$ significantly grows with the growth of disorder, especially in the vicinity of Anderson transition, where localization corrections noticeably increase $H_{c2}(T = 0)$ and $H_{c2}(T)$ curve instead of linear temperature dependence, typical in the strong coupling limit at weak disorder, becomes concave.

In our model, the upper critical field at low temperatures may reach extremely large values significantly exceeding $\Phi_0/2\pi a^2$. This makes important the further analysis of the model, taking into account paramagnetic effect and inevitable role of electron spectrum quantization in magnetic field. Actually, we can hope that effects of quantization of the spectrum are irrelevant in the limit of the strong disorder, while paramagnetic effect is much weakened in the region of strong and very strong coupling. These questions will be the task of further studies.

ACKNOWLEDGMENTS

This work was performed within the State Contract (FASO) no. 0389-2014-0001 with partial support by RFBR grant no. 17-02-00015 and the Program of Fundamental Research of the RAS Presidium "Fundamental problems of high-temperature superconductivity."

REFERENCES

1. A. A. Abrikosov and L. P. Gor'kov, Sov. Phys. JETP **9**, 220 (1959).
2. A. A. Abrikosov and L. P. Gor'kov, Sov. Phys. JETP **9**, 1090 (1959).
3. L. P. Gor'kov, Sov. Phys. JETP **36**, 1364 (1959).
4. A. A. Abrikosov and L. P. Gor'kov, Sov. Phys. JETP **12**, 1243 (1961).
5. P. W. Anderson, J. Phys. Chem. Solids **11**, 26 (1959).
6. P. G. de Gennes, *Superconductivity of Metals and Alloy*s (W. A. Benjamin, New York, 1966).
7. L. N. Bulaevskii and M. V. Sadovskii, JETP Lett. **39**, 640 (1984).
8. L. N. Bulaevskii and M. V. Sadovskii, J. Low. Temp. Phys. **59**, 89 (1985).
9. M. V. Sadovskii, Phys. Rep. **282**, 226 (1997).
10. M. V. Sadovskii, *Superconductivity and Localizatio*n (World Scientific, Singapore, 2000).
11. N. R. Werthamer and E. Helfand, Phys. Rev. **147**, 288 (1966); N. R Werthamer, E. Helfand, and P. C. Hohenberg, Phys. Rev. **147**, 295 (1966).
12. P. Nozieres and S. Schmitt-Rink, J. Low Temp. Phys. **59**, 195 (1985).
13. Th. Pruschke, M. Jarrell, and J. K. Freericks, Adv. Phys. **44**, 187 (1995).
14. A. Georges, G. Kotliar, W. Krauth, and M. J. Rozenberg, Rev. Mod. Phys. **68**, 13 (1996).
15. D. Vollhardt, in *Lectures on the Physics of Strongly Correlated Systems XIV*, Ed. by A. Avella and F. Mancini, AIP Conf. Proc. **1297**, 339 (2010).
16. E. Z. Kuchinskii, I. A. Nekrasov, and M. V. Sadovskii, JETP Lett. **82**, 198 (2005).
17. M. V. Sadovskii, I. A. Nekrasov, E. Z. Kuchinskii, Th. Prushke, and V. I. Anisimov, Phys. Rev. B **72**, 155105 (2005).
18. E. Z. Kuchinskii, I. A. Nekrasov, and M. V. Sadovskii, Low Temp. Phys. **32**, 398 (2006); arXiv: cond-mat/0510376.
19. E. Z. Kuchinskii, I. A. Nekrasov, and M. V. Sadovskii, Phys. Usp. **53**, 325 (2012); arXiv:1109.2305.
20. E. Z. Kuchinskii, I. A. Nekrasov, and M. V. Sadovskii, J. Exp. Theor. Phys. **106**, 581 (2008); arXiv: 0706. 2618.
21. E. Z. Kuchinskii and M. V. Sadovskii, J. Exp. Theor. Phys. **122**, 509 (2016).
22. E. Z. Kuchinskii, I. A. Nekrasov, and M. V. Sadovskii, Phys. Rev. B **75**, 115102 (2007).
23. N. A. Kuleeva, E. Z. Kuchinskii, and M. V. Sadovskii, J. Exp. Theor. Phys. **119**, 264 (2014).
24. E. Z. Kuchinskii, N. A. Kuleeva, and M. V. Sadovskii, JETP Lett. **100**, 192 (2014).
25. E. Z. Kuchinskii, N. A. Kuleeva, and M. V. Sadovskii, J. Exp. Theor. Phys. **120**, 1055 (2015).
26. E. Z. Kuchinskii, N. A. Kuleeva, and M. V. Sadovskii, J. Exp. Theor. Phys. **122**, 375 (2016).
27. E. Z. Kuchinskii, N. A. Kuleeva, and M. V. Sadovskii, Low Temp. Phys. **42**, 17 (2017).
28. E. Z. Kuchinskii, N. A. Kuleeva, and M. V. Sadovskii, J. Exp. Theor. Phys. **125**, 111 (2017).
29. R. Bulla, T. A. Costi, and T. Pruschke, Rev. Mod. Phys. **60**, 395 (2008).
30. E. M. Lifshits and L. P. Pitaevski, *Course of Theoretical Physic*s, Vol. 9: *Statistical Physics, Part* 2 (Nauka, Moscow, 1978; Pergamon, New York, 1980), Chap. 5.
31. E. Z. Kuchinskii and M. V. Sadovskii, Sverkhprovodim.: Fiz., Khim., Tekh. **4**, 2278 (1991).
32. E. Z. Kuchinskii and M. V. Sadovskii, Physica C **185–189**, 1477 (1991)
33. A. A. Abrikosov, L. P. Gor'kov, and I. E. Dzyaloshinskii, *Quantum Field Theoretical Methods in Statistical Physic*s (Fizmatgiz, Moscow, 1963; Pergamon, Oxford, 1965).
34. M. V. Sadovskii, *Diagrammatic*s (Regulyar. Khaotich. Dinamika, Moscow, Izhevsk, 2010; World Scientific, Singapore, 2006).
35. D. Vollhardt and P. Wölfle, Phys. Rev. B **22**, 4666 (1980); Phys. Rev. Lett. **48**, 699 (1982).
36. P. Wölfle and D. Vollhardt, in *Anderson Localizatio*n, Ed. by Y. Nagaoka and H. Fukuyama, Vol. 39 of *Springer Series in Solid State Science*s (Springer, Berlin, 1982), p. 26.
37. A. V. Myasnikov and M. V. Sadovskii, Sov. Phys. Solid State **24**, 2033 (1982).
38. E. A. Kotov and M. V. Sadovskii, Z. Phys. B **51**, 17 (1983).
39. M. V. Sadovskii, in *Soviet Scientific Reviews – Physics Review*s, Ed. by I. M. Khalatnikov (Harwood Academic, New York, 1986), Vol. 7, p. 1.
40. D. Vollhardt and P. Wölfle, in *Electronic Phase Transition*s, Ed. by W. Hanke and Yu. V. Kopaev (North–Holland, Amsterdam, 1992), vol. 32, p. 1.

ISSN 1063-7761, Journal of Experimental and Theoretical Physics, 2018, Vol. 127, No. 4, pp. 753–760. © Pleiades Publishing, Inc., 2018.
Published in Russian in Zhurnal Eksperimental'noi i Teoreticheskoi Fiziki, 2018, Vol. 154, No. 4, pp. 881–889.

ELECTRONIC PROPERTIES OF SOLID

Temperature Dependence of Paramagnetic Critical Magnetic Field in Disordered Attractive Hubbard Model[1]

E. Z. Kuchinskii[a,*], N. A. Kuleeva[a], and M. V. Sadovskii[a,b,]**

[a] *Institute for Electrophysics, Ural Branch, Russian Academy of Sciences, Yekaterinburg, 620016 Russia*
[b] *Mikheev Institute for Metal Physics, Ural Branch, Russian Academy of Sciences, Yekaterinburg, 620108 Russia*
**e-mail: kuchinsk@iep.uran.ru*
***e-mail: sadovski@iep.uran.ru*

Received June 25, 2018

Abstract—Within the generalized DMFT+Σ approach, we study disorder effects in the temperature dependence of paramagnetic critical magnetic field $H_{cp}(T)$ for Hubbard model with attractive interaction. We consider the wide range of attraction potentials U—from the weak coupling limit, when superconductivity is described by BCS model, up to the limit of very strong coupling, when superconducting transition is related to Bose–Einstein condensation (BEC) of compact Cooper pairs. The growth of the coupling strength leads to the rapid growth of $H_{cp}(T)$ at all temperatures. However, at low temperatures, paramagnetic critical magnetic field H_{cp} grows with U much more slowly, than the orbital critical field, and in BCS limit, the main contribution to the upper critical magnetic filed is of paramagnetic origin. The growth of the coupling strength also leads to the disappearance of the low temperature region of instability towards type I phase transition and Fulde–Ferrell–Larkin–Ovchinnikov (FFLO) phase, characteristic of BCS weak coupling limit. Disordering leads to the rapid drop of $H_{cp}(T)$ in BCS weak coupling limit, while in BCS–BEC crossover region and BEC limit $H_{cp}(T \to 0)$ dependence on disorder is rather weak. Within DMFT+Σ approach, disorder influence on $H_{cp}(T)$ is of universal nature at any coupling strength and is related only to disorder widening of the conduction band. In particular, this leads to the drop of the effective coupling strength with disorder, so that disordering restores the region of type I transition in the intermediate coupling region.

DOI: 10.1134/S1063776118100047

1. INTRODUCTION

In the weak coupling region and for the weak disorder, the upper critical magnetic field of a superconductor is determined by orbital effects and usually is much lower than the paramagnetic limit. However, the growth of the coupling strength and disordering lead to the rapid growth of the orbital H_{c2} possibly overcoming the paramagnetic limit.

In this paper, we study the behavior of paramagnetic critical field in the region of very strong coupling of electrons of the Cooper pair and in the crossover region from BCS-like behavior for the weak coupling to Bose–Einstein condensation (BEC) in the strong coupling region [1], taking disorder into account (including the strong enough).

The simplest model to study the BCS–BEC crossover is Hubbard model with attractive interaction. Most successful approach to the studies of Hubbard model, both to describe the strongly correlated systems in the case of repulsive interactions and to study the BCS–BEC crossover for the case of attraction, is the dynamical mean - field theory (DMFT) [2–4].

In recent years, we have developed the generalized DMFT+Σ approach to Hubbard model [5–11], which is quite effective for the studies of the influence of different external (outside those taken into account by DMFT) interactions. This DMFT+Σ method was used by us in [12–14] to study the disorder influence on the temperature of superconducting transition. In particular, for the case of semi-elliptic initial density of states, adequate to describe three-dimensional systems, it was demonstrated that disorder influence on the critical temperature (in the whole region of interaction strengths) is related only to the general widening of the initial conduction band (density of states) by disorder (the generalized Anderson theorem). In [15], using the combination of the Nozieres–Schmitt-Rink approximation and DMFT+Σ in attractive Hubbard model we have analyzed the influence of disordering on the temperature dependence of the orbital upper critical field $H_{c2}(T)$ both for the wide region of coupling strengths U, including the BCS–BEC crossover region, and in the wide region of disorder up to the vicinity of Anderson transition. Both the growth of the coupling strength and disorder lead to the rapid growth of H_{c2}, leading in the BEC-limit to unrealisti-

[1] The article is published in the original.

cally high values of $H_{c2}(T \to 0)$, significantly overcoming the paramagnetic limit.

In this work we perform the detailed analysis of disorder influence on the temperature dependence of paramagnetic critical magnetic field of a superconductor for the wide range of coupling strengths U, including the BCS–BEC crossover region and the limit of very strong coupling.

It is well known, that in BCS weak coupling limit paramagnetic effects (spin splitting) lead to the existence of a low temperature region at the phase diagram of a superconductor in magnetic field, where paramagnetic critical field H_{cp} decreases with further lowering of the temperature. This behavior signifies the instability leading to the region of type I phase transition, where also the so called Fulde–Ferrell–Larkin–Ovchinnikov (FFLO) phase may appear [16–18] with Cooper pairs with finite momentum $\mathbf{q}$ and spatially periodic superconducting order parameter. In the following we limit ourselves to the analysis of type II transition and homogeneous superconducting order parameter, allowing us to determine the border of instability towards type I transition in BCS–BEC crossover and strong coupling regions at different disorder levels. The problem of stability of FFLO phase under these conditions is not analyzed here.

2. HUBBARD MODEL WITHIN DMFT+Σ APPROACH IN NOZIERES–SCHMITT-RINK APPROXIMATION

We are considering the disordered Hubbard model with attractive interaction, taking into account spin-splitting by external magnetic field H, and described by the Hamiltonian:

$$H = -t\sum_{\langle ij\rangle\sigma} a^{\dagger}_{i\sigma}a_{j\sigma} + \sum_{i\sigma}\epsilon_i n_{i\sigma} - U\sum_i n_{i\uparrow}n_{i\downarrow} - \mu_B H\sum_{i\sigma}\sigma n_{i\sigma}, \quad (1)$$

where $t > 0$ is transfer amplitude between nearest neighbors, U is the onsite Hubbard attraction, $n_{i\sigma} = a^{\dagger}_{i\sigma}a_{i\sigma}$ is electron number operator on a given site, $a_{i\sigma}$ ($a^{\dagger}_{i\sigma}$) is electron annihilation (creation) operator, $\sigma = \pm 1$, $\mu_B = \frac{e\hbar}{2mc}$ is the Bohr magneton, and local energies ϵ_i are assumed to be independent and random on different lattice sites. We assume Gaussian distribution for energy levels ϵ_i at a given site:

$$\mathcal{P}(\epsilon_i) = \frac{1}{\sqrt{2\pi}\Delta}\exp\left(-\frac{\epsilon_i^2}{2\Delta^2}\right). \quad (2)$$

Distribution width Δ represents the measure of disorder, and Gaussian random field of energy levels (independent on different lattice sites) produces "impurity" scattering, which is analyzed within the standard approach, based on calculations of the averaged Green's functions.

The generalized DMFT+Σ approach [5–9] extends the standard dynamical mean field theory (DMFT [2–4] by addition of an "external" self-energy $\Sigma_{\mathbf{p}}(\varepsilon)$ (in general case momentum dependent) due to any kind of interaction outside the DMFT, which gives an effective calculation method both for single-particle and two-particle properties [8, 10]. This approach conserves the standard system of self-consistent DMFT equations [2–4], with "external" self-energy $\Sigma_{\mathbf{p}}(\varepsilon)$ being recalculated at each iteration step using some approximate scheme, corresponding to the type of additional interaction, while the local Green's function of DMFT is "dressed" by $\Sigma_{\mathbf{p}}(\varepsilon)$ at each step of the standard DMFT procedure.

In the problem of disorder scattering under discussion here [10, 11] for "external" self-energy we are using the simplest (self - consistent Born) approximation, neglecting diagrams with "crossing" interaction lines due to impurity scattering. Such an "external" self-energy remains momentum independent (local).

To solve the single-impurity Anderson problem of DMFT in this paper, as in our previous works, we use quite efficient method of numerical renormalization group (NRG) [19].

In the following we assume the "bare" conduction band with semi-elliptic density of states (per unit cell with lattice parameter a and single spin projection), which gives a good approximation for three-dimensional case:

$$N_0(\varepsilon) = \frac{2}{\pi D^2}\sqrt{D^2 - \varepsilon^2}, \quad (3)$$

where D defines the half-width of the conduction band.

In [14] we have shown, that in DMFT+Σ approach in the model with semi-elliptic density of states all the effects of disorder on single-particle properties reduce only to widening of conduction band by disorder, i.e. to the replacement $D \to D_{\text{eff}}$, where D_{eff} is the effective "bare" band half-width in the absence of correlations ($U = 0$), widened by disorder:

$$D_{\text{eff}} = D\sqrt{1 + 4\frac{\Delta^2}{D^2}}. \quad (4)$$

The "bare" (in the absence of U) density of states, "dressed" by disorder

$$\tilde{N}_0(\xi) = \frac{2}{\pi D_{\text{eff}}^2}\sqrt{D_{\text{eff}}^2 - \varepsilon^2}, \quad (5)$$

remains semi-elliptic also in the presence of disorder.

It is necessary to note, that in other models of the "bare" band disorder not only widens the band, but also changes the form of the density of states. In general, there is no complete universality of disorder

influence on single-particle properties, which reduces to the replacement $D \to D_{\text{eff}}$. However, in the limit of strong enough disorder the "bare" band becomes almost semi-elliptic and this universality is restored [14].

All calculations in the present paper, as in our previous works, were performed for rather typical case of quarter-filled band (electron number per lattice site $n = 0.5$).

To analyze superconductivity for the wide range of pairing interactions U, following [14], we use Nozieres–Schmitt-Rink approximation [1], which allows qualitatively correct (though approximate) description of BCS–BEC crossover. In this approach, to determine the critical temperature T_c (in the absence of H) we use [14] the conventional BCS weak coupling equation, but the chemical potential of the system μ for different values of U and Δ is determined from DMFT+Σ calculations, i.e. from the standard equation for the number of electrons in conduction band, which allows us to find T_c for the wide range of model parameters, including the BCS–BEC crossover region, as well as for different levels of disorder. This reflects the physical meaning of Nozieres–Schmitt-Rink approximation: in the weak coupling region transition temperature is controlled by the equation for Cooper instability, while in the strong coupling limit it is determined as BEC temperature, which is controlled by chemical potential. It was demonstrated, that such an approach guarantees the correct interpolation between the limits of weak and strong couplings, including also the effects of disorder [1, 12, 14]. In particular, in [12, 14] it was shown, that disorder influence on critical temperature T_c and single-particle characteristics (e.g. density of states) in the model with semi-elliptic "bare" density of states is universal and is reduced only to the changes of the effective bandwidth.

3. MAIN RESULTS

In the framework of Nozieres–Schmitt-Rink approach the critical temperature in the presence of spin-splitting of electron level in external magnetic field (and neglecting the orbital effects) or paramagnetic critical magnetic field H_{cp} at temperatures $T < T_c$ is determined by the following BCS-like equation:

$$1 = \frac{U}{4}\int\limits_{-\infty}^{\infty} d\varepsilon \frac{\tilde{N}_0(\varepsilon)}{\varepsilon - \mu}\left(\tanh\frac{\varepsilon - \mu - \mu_B H_{cp}}{2T} + \tanh\frac{\varepsilon - \mu + \mu_B H_{cp}}{2T}\right), \quad (6)$$

where the chemical potential μ for different values of U and Δ is determined from DMFT+Σ calculations, i.e. from the standard equation for the number of electrons in conduction band. The general derivation of Eq. (6) in the presence of disorder is given in the Appendix. Note that Eq. (6) is derived from the exact Ward identity and remains valid even in the case of strong disorder, including the vicinity of Anderson transition. Equation (6) explicitly demonstrates, that all disorder effects on H_{cp} are reduced to the renormalization of the initial density of states by disorder, so that for the case of initial band with semi-elliptic density of states disorder influence on H_{cp} is universal and is only due to the band widening by disorder, i.e. to the replacement $D \to D_{\text{eff}}$.

In Fig. 1 we show the temperature dependence of paramagnetic critical magnetic field for different values of coupling strength. Chemical potential entering Eq. (6) is, in general, dependent not only on the coupling strength, but also on the values of magnetic filed and temperature. In Figs. 1a–1e, for the sake of comparison, dashed lines show the results of calculations with chemical potential taken at $H = 0$ and $T = T_c$ for the given value of $U/2D$, while continuous curves with symbols represent the results of full calculations with $\mu = \mu(H, T)$.

In the weak coupling limit ($U/2D = 0.2$) we obtain the standard behavior of temperature dependence of paramagnetic critical field of BCS theory [18]. At low temperatures we observe the region of decreasing H_{cp} as temperature diminishes, with maximum H_{cp} at finite temperature. It is well known, that in this region the system is unstable with respect to type I phase transition [18], where is also a possibility of transition to FFLO phase [16, 17] with Cooper pairs with finite momentum ($\mathbf{q} \neq 0$) and inhomogeneous superconducting order parameter. Critical field in BCS limit is relatively weakly dependent on the value of chemical potential, so that we can neglect weak field and dependence of μ on the magnetic field and temperature (dotted curve in Fig. 1a in fact coincides with the result of an exact calculation). With the growth of the coupling strength the region of instability towards type I transition shrinks (cf. Figs. 1a, 1b, 1c) and it completely disappears with further increase of coupling (Figs. 1d, 1e). With the increase of coupling strength the critical magnetic field becomes more and more dependent on the value of the chemical potential, so that the account of its temperature and magnetic field dependence $\mu(H, T)$ becomes very important (cf. Figs. 1c–1e).

At intermediate coupling ($U/2D = 0.6$) the account of temperature and magnetic field dependence of μ leads to small changes of the critical field, however we observe significant qualitative changes for $T \sim T_c$. The small growth of chemical potential with increase of H at weak fields leads to noticeable growth of T_c, which overcomes the decrease of T_c with the growth of magnetic field due to explicit H-dependence in Eq. (6), leading to some increase of $T_c(H)$ at small H.

In Fig. 1f we show temperature dependencies of the critical magnetic field for different values of U. It is known that the critical temperature T_{c0} grows with coupling strength in BCS limit and decreases in BEC

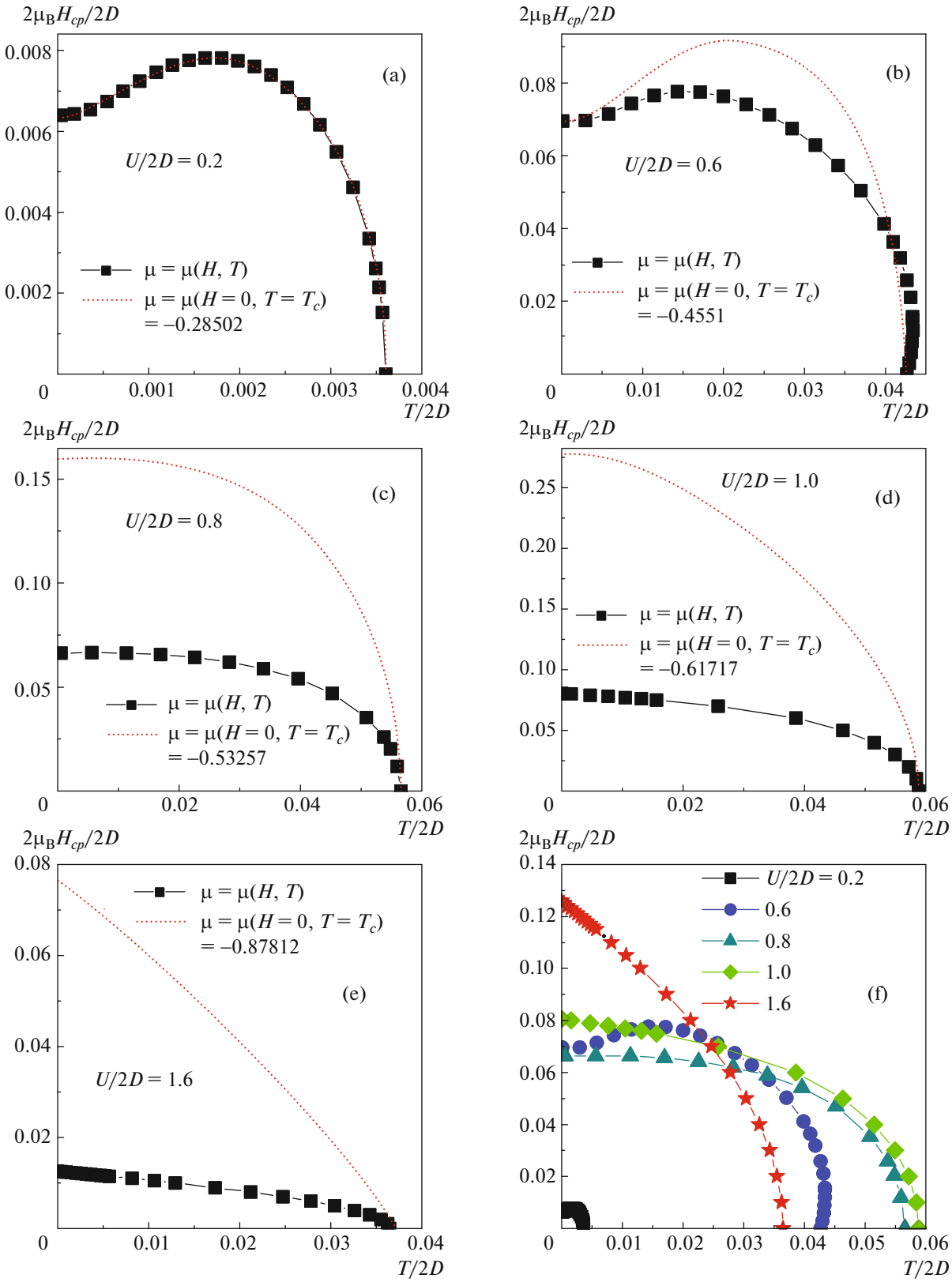

Fig. 1. (Color online) Dependence of paramagnetic critical magnetic field on temperature for different values of coupling strength. Dotted curves were obtained neglecting the dependence of chemical potential on temperature and magnetic field at given U.

strong coupling limit, passing through a maximum at $U/2D = 1$ [12–14]. The critical magnetic field at low temperatures grows with coupling strength both in BCS and BEC limits, though in BCS–BEC crossover region ($U/2D = 0.6$–1) we observe rather weak dependence of the critical magnetic field on coupling strength.

The physical reason of the growth of paramagnetic critical field with coupling strength is pretty obvious—it is more difficult for magnetic field to break the pairs of strongly coupled electrons.

In Fig. 2 we present our results on disorder influence on temperature dependence of paramagnetic critical magnetic field. In BCS weak coupling limit (Fig. 2) the increase of disorder leads both to decrease of the critical temperature in the absence of magnetic field T_{c0} (cf. [13, 14]) and to decrease of the critical magnetic field at all temperatures. The region of instability to type I transition is conserved also in the presence of disorder. In fact, as was noted above, disorder influence on $H_{cp}(T)$ is actually universal and related only to the replacement $D \to D_{\text{eff}}$. As a result, disorder growth leads to decrease of the effective coupling, which is defined by dimensionless parameter $U/2D_{\text{eff}}$. This leads to the increase of the relative width $T/T_c(H)$ of the temperature region of type I transition.

At intermediate coupling ($U/2D = 0.8$) in BCS–BEC transition region (Fig. 2b) disorder growth relatively weakly changes the critical temperature T_{c0} (cf. [13, 14]), leading to some increase of $H_{cp}(T)$. As all the effects of disordering are due to the replacement $D \to D_{\text{eff}}$, the increase of disorder again leads to the decrease of the effective coupling strength $U/2D_{\text{eff}}$ and restoration of the region of instability towards type I transition.

In BEC-limit of strong coupling the growth of disorder leads to significant increase of the critical temperature T_{c0} (cf. [13, 14]). At the same time, the critical magnetic field at low temperatures only weakly increases with increasing disorder. In BEC-limit instability to type I transition does not appear even in the presence of very strong disorder ($\Delta/2D = 0.5$). In fact, in BEC-limit disorder influence is again universal and related only to the replacement $D \to D_{\text{eff}}$. As a result, if we make the spin splitting and temperature dimensionless dividing both by the effective bandwidth $2D_{\text{eff}}$ and keep the effective coupling strength $U/2D_{\text{eff}}$ fixed, we obtain the universal temperature dependence of paramagnetic critical magnetic field. In Fig. 3 we show examples of such universal behavior for typical cases of weak and strong coupling an the absence and in the presence of disorder.

In the absence of disorder in BEC strong coupling limit with $U/2D = 1.6$ for $T \to 0$ we have (cf. Fig. 1) $2\mu_B H_{cp}/2D \approx 0.125$, so that for characteristic value of the bandwidth $2D \sim 1$ eV we get $H_{cp} \sim 10^7$ G. For orbital critical magnetic field (cf. [15]) in the same model and for the same coupling strength, for $T \to 0$ and typical value of lattice parameter $a = 3.3 \times 10^{-8}$ cm, we obtain

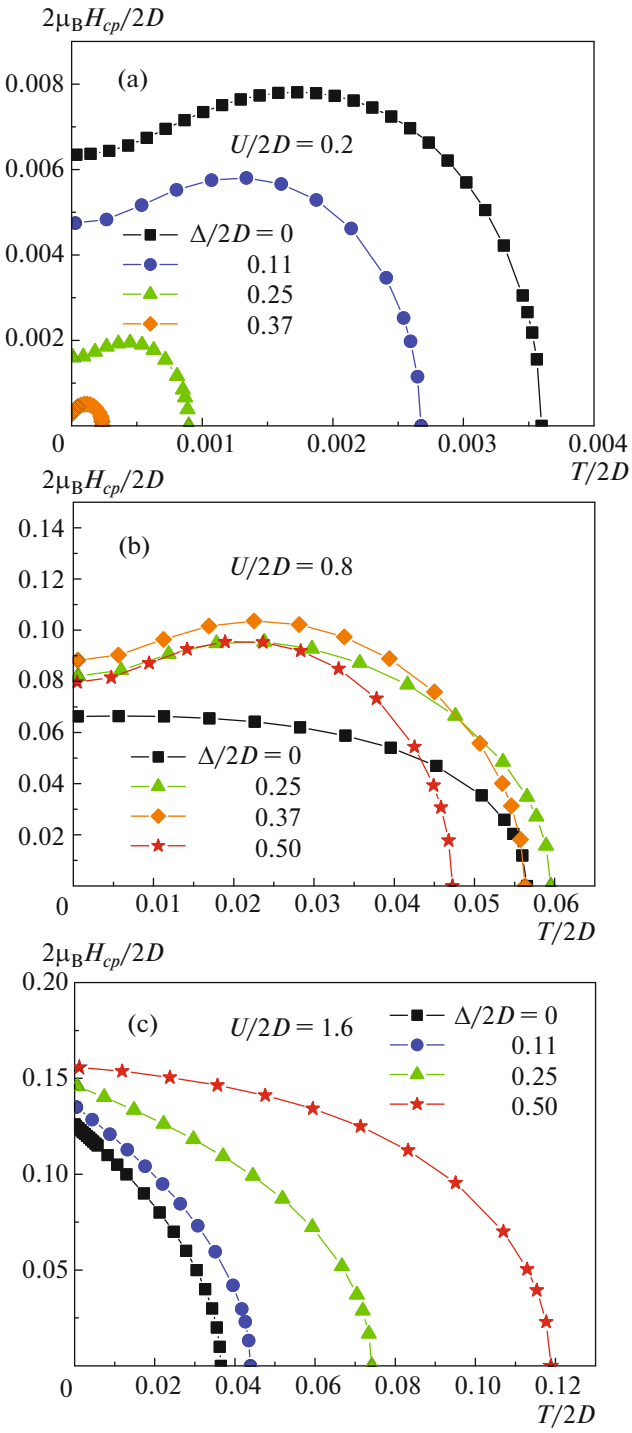

Fig. 2. (Color online) Temperature dependences of paramagnetic critical magnetic field for different levels of disorder: (a) BCS weak coupling limit ($U/2D = 0.2$); (b) BCS–BEC crossover region (intermediate coupling: $U/2D = 0.8$); (c) BEC strong coupling region ($U/2D = 1.6$).

$H_{cp} \approx 1.6 \times 10^8$ G. Thus, the orbital critical magnetic field at low temperatures grows with increase of the coupling strength much faster, than paramagnetic critical field, and in BEC strong coupling limit the main contribution to the upper critical field at low

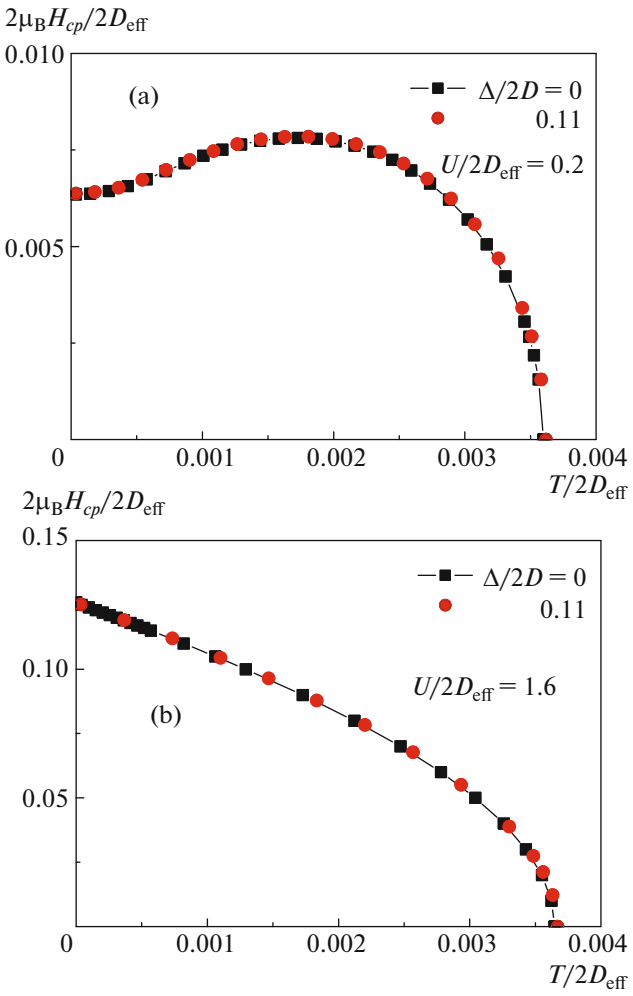

Fig. 3. (Color online) Universality of temperature dependence of paramagnetic critical magnetic field on disorder. (a) weak coupling $U/2D_{\text{eff}} = 0.2$, $\Delta = 0$, $\Delta = 0.11$, (b) strong coupling $U/2D_{\text{eff}} = 1.6$, $\Delta = 0$, $\Delta = 0.11$.

temperatures is actually due to the paramagnetic effect. The growth of disorder leads to significant growth of the orbital critical magnetic field [15], while H_{cp} ($T \to 0$) in the region of BCS–BEC crossover and in BEC limit is relatively weakly dependent on disorder. Thus, also in the presence of disorder in BEC limit the main contribution to the upper critical field at low temperatures comes from paramagnetic effect.

4. CONCLUSIONS

In this paper, within the combination of Nozieres–Schmitt-Rink and DMFT+Σ approximations, we have studied disorder influence on temperature behavior of paramagnetic critical magnetic field. Calculations were done for a wide range of the values of attractive potential U, from the weak coupling region $U/2D \ll 1$, where superconductivity is well described by BCS model, up to the limit of strong coupling $U/2D \gg 1$, where superconducting transition is due to Bose condensation of compact Cooper pairs, which are formed at temperatures much exceeding the temperature of superconducting transition.

The growth of coupling strength U leads to a fast increase of $H_{cp}(T)$ and disappearance, both in the region of BCS–BEC crossover and in BEC limit, of the region of instability, leading to type I transition, which appears at low temperatures in BCS weak coupling region. Physically this is due to the fact, that it becomes more and more difficult for magnetic field to break pairs of strongly coupled electrons.

The growth of disorder in BCS weal coupling limit leads both to decrease of critical temperature and decrease of $H_{cp}(T)$. The region of instability to type I transition at low temperatures remains also in the presence of disorder. In the intermediate coupling region ($U/2D = 0.8$) disorder only weakly affects both the critical temperature and $H_{cp}(T)$. However, the growth of disorder leads to restoration of the low temperature region of instability to type I transition, which is not observed in the absence of disorder. This, rather unexpected, conclusion is related to specifics of the attractive Hubbard model, which in disordered case is controlled by dimensionless coupling parameter $U/2D_{\text{eff}}$. As was shown in our previous works, in BEC strong coupling limit the growth of disorder leads to noticeable growth of the critical temperature in the absence of magnetic field. However, the value of H_{cp} ($T \to 0$) in this model is relatively weakly dependent on disorder. In BEC limit at low temperatures and for reasonable values of model parameters paramagnetic critical magnetic field is much smaller, than the orbital critical field, so that the upper critical field in this region is mainly determined by paramagnetic critical filed. In the presence of disorder this conclusion is even more valid, as the orbital critical field rapidly grows with increasing disorder, while paramagnetic critical field is weakly disorder dependent in this limit.

This work was performed under the State Contract no. 0389-2014-0001 with partial support of RFBR Grant no. 17-02-00015 and the Program of Fundamental Research of the RAS Presidium no. 12 "Fundamental problems of high-temperature superconductivity."

APPENDIX

EQUATION FOR PARAMAGNETIC CRITICAL MAGNETIC FIELD

In general case the Noziers–Schmitt-Rink approach [1] assumes, that corrections from strong pairing interaction significantly change the chemical potential of the system, but possible vertex corrections from this interaction in Cooper channel are irrelevant, so that to analyze Cooper instability we can use the weak coupling approximation (ladder approximation). In this approximation the condition of Cooper instability in disordered attractive Hubbard model is written as:

$$1 = U\chi_0(q = 0, \omega_m = 0), \quad (7)$$

where

$$\chi_0(q = 0, \omega_m = 0) = T\sum_n \sum_{\mathbf{pp'}} \Phi_{\mathbf{pp'}}(\varepsilon_n) \quad (8)$$

is two-particle loop in Cooper channel "dressed" only by impurity scattering, while $\Phi_{\mathbf{pp'}}(\varepsilon_n)$ is the averaged over impurities two-particle Green's function in Cooper channel at Matsubara frequencies $\varepsilon_n = \pi T(2n + 1)$.

To obtain $\sum_{\mathbf{pp'}} \Phi_{\mathbf{pp'}}(\varepsilon_n)$ we use an exact Ward identity, derived by us in [8]:

$$G_\uparrow(\varepsilon_n, \mathbf{p}) - G_\downarrow(-\varepsilon_n, -\mathbf{p}) = -\sum_{\mathbf{p}} \Phi_{\mathbf{pp'}}(\varepsilon_n)(G^{-1}_{0\uparrow}(\varepsilon_n, \mathbf{p'}) - G^{-1}_{0\downarrow}(-\varepsilon_n, -\mathbf{p})). \quad (9)$$

Here $G_{0\uparrow,\downarrow}(\varepsilon_n, \mathbf{p}) = (i\varepsilon_n + \mu - \varepsilon(\mathbf{p}) \pm \mu_B H)^{-1}$ is the "bare" Green's function and $G_{\uparrow,\downarrow}(\varepsilon_n, \mathbf{p})$ is averaged over impurities (but not "dressed" by Hubbard interaction!) single-particle Green's function. Using the symmetry $\varepsilon(\mathbf{p}) = \varepsilon(-\mathbf{p})$ we obtain from Ward identity (9):

$$\sum_{\mathbf{pp'}} \Phi_{\mathbf{pp'}}(\varepsilon_n) = -\frac{\sum_{\mathbf{p}} G_\uparrow(\varepsilon_n, \mathbf{p}) - \sum_{\mathbf{p}} G_\downarrow(-\varepsilon_n, \mathbf{p})}{2i\varepsilon_n + 2\mu_B H}, \quad (10)$$

so that for Cooper susceptibility (8) we get:

$$\chi_0(q = 0, \omega_m = 0) = -\frac{T}{2}\sum_n \frac{\sum_{\mathbf{p}} G_\uparrow(\varepsilon_n, \mathbf{p}) - \sum_{\mathbf{p}} G_\downarrow(-\varepsilon_n, \mathbf{p})}{i\varepsilon_n + \mu_B H} = -\frac{T}{2}\sum_n \left(\frac{\sum_{\mathbf{p}} G_\uparrow(\varepsilon_n, \mathbf{p})}{i\varepsilon_n + \mu_B H} + \frac{\sum_{\mathbf{p}} G_\downarrow(\varepsilon_n, \mathbf{p})}{i\varepsilon_n - \mu_B H} \right). \quad (11)$$

Performing the standard summation over Fermion Matsubara frequencies, we obtain:

$$\chi_0 = -\frac{1}{8\pi i}\int_{-\infty}^{\infty} d\varepsilon \left(\frac{\sum_{\mathbf{p}} G^R_\uparrow(\varepsilon, \mathbf{p}) - \sum_{\mathbf{p}} G^A_\downarrow(\varepsilon, \mathbf{p})}{\varepsilon + \mu_B H} + \frac{\sum_{\mathbf{p}} G^R_\downarrow(\varepsilon, \mathbf{p}) - \sum_{\mathbf{p}} G^A_\downarrow(\varepsilon, \mathbf{p})}{\varepsilon - \mu_B H} \right) \tanh\frac{\varepsilon}{2T} = \frac{1}{2}\int_{-\infty}^{\infty} d\varepsilon \left(\frac{\tilde{N}_{0\uparrow}(\varepsilon)}{\varepsilon + \mu_B H} + \frac{\tilde{N}_{0\downarrow}(\varepsilon)}{\varepsilon - \mu_B H} \right) \tanh\frac{\varepsilon}{2T}, \quad (12)$$

where $\tilde{N}_{0\uparrow,\downarrow}(\varepsilon)$ is the "bare" ($U = 0$) density of states for different spin projections, "dressed" by impurity scattering. Spin splitting can be considered as an addition to chemical potential, so that introducing the "bare" density of states "dressed" by disorder in the absence of external magnetic field $\tilde{N}_0(\varepsilon)$, we obtain the final result for Cooper susceptibility:

$$\chi_0 = \frac{1}{4}\int_{-\infty}^{\infty} d\varepsilon \frac{\tilde{N}_0(\varepsilon)}{\varepsilon}\left(\tanh\frac{\varepsilon + \mu_B H}{2T} + \tanh\frac{\varepsilon - \mu_B H}{2T} \right). \quad (13)$$

In Eq. (13) energy ε is counted from the chemical potential level. If we count it from the middle of the conduction band we have to replace $\varepsilon \to \varepsilon - \mu$ and the condition of Cooper instability (7) leads to the equation defining critical temperature depending on the external magnetic field, which gives the equation for paramagnetic critical magnetic filed (6). The chemical potential for different values of U and Δ should be determined from DMFT+Σ calculations, i.e. from the standard equation for electron number (band filling), which allows us to find H_{cp} for the wide range of model parameters, including the region of BCS–BEC crossover and the limit of strong coupling at different levels of disorder. This reflects the physical meaning of Nozieres–Scmitt-Rink approximation—in the weak coupling region the temperature of superconducting transition is controlled by the equation for Cooper instability (6), while in the strong coupling limit it is defined as the temperature of BEC, which is controlled by chemical potential. The joint solution of Eq. (6) and the equation for the chemical potential guarantees the correct interpolation for H_{cp} in the region of BCS–BEC crossover.

REFERENCES

1. P. Nozieres and S. Schmitt-Rink, J. Low Temp. Phys. **59**, 195 (1985).
2. Th. Pruschke, M. Jarrell, and J. K. Freericks, Adv. Phys. **44**, 187 (1995).
3. A. Georges, G. Kotliar, W. Krauth, and M. J. Rozenberg, Rev. Mod. Phys. **68**, 13 (1996).
4. D. Vollhardt, AIP Conf. Proc. **1297**, 339 (2010); arXiV: 1004.5069.
5. E. Z. Kuchinskii, I. A. Nekrasov, and M. V. Sadovskii, JETP Lett. **82**, 198 (2005); arXiv: cond-mat/0506215.
6. M. V. Sadovskii, I. A. Nekrasov, E. Z. Kuchinskii, Th. Prushke, and V. I. Anisimov, Phys. Rev. B **72**, 155105 (2005); arXiV: cond-mat/0508585.
7. E. Z. Kuchinskii, I. A. Nekrasov, and M. V. Sadovskii, Low Temp. Phys. **32**, 398 (2006); arXiv: cond-mat/0510376.
8. E. Z. Kuchinskii, I. A. Nekrasov, and M. V. Sadovskii, Phys. Rev. B **75**, 115102 (2007); arXiv: cond-mat/0609404.
9. E. Z. Kuchinskii, I. A. Nekrasov, and M. V. Sadovskii, Phys. Usp. **53**, 325 (2012); arXiv:1109.2305.

10. E. Z. Kuchinskii, I. A. Nekrasov, and M. V. Sadovskii, J. Exp. Theor. Phys. **106**, 581 (2008); arXiv: 0706.2618.
11. E. Z. Kuchinskii and M. V. Sadovskii, J. Exp. Theor. Phys. **122**, 509 (2016); arXiv:1507.07654
12. N. A. Kuleeva, E. Z. Kuchinskii, and M. V. Sadovskii, J. Exp. Theor. Phys. **119**, 264 (2014); arXiv: 1401.2295.
13. E. Z. Kuchinskii, N. A. Kuleeva, and M. V. Sadovskii, JETP Lett. **100**, 192 (2014); arXiv: 1406.5603.
14. E. Z. Kuchinskii, N. A. Kuleeva, and M. V. Sadovskii, J. Exp. Theor. Phys. **120**, 1055 (2015); arXiv:1411.1547.
15. E. Z. Kuchinskii, N. A. Kuleeva, and M. V. Sadovskii, J. Exp. Theor. Phys. **125**, 1127 (2017); arXiv:1709.03895
16. P. Fulde and R. A. Ferrell, Phys. Rev. A **135**, 550 (1964).
17. A. I. Larkin and Yu. N. Ovchinnikov, Sov. Phys. JETP **20**, 762 (1964).
18. D. Saint-James, G. Sarma, and E. J. Thomas, *Type II Superconductivity* (Pergamon, Oxford, 1969).
19. R. Bulla, T. A. Costi, and T. Pruschke, Rev. Mod. Phys. **60**, 395 (2008).

ISSN 1063-7761, Journal of Experimental and Theoretical Physics, 2019, Vol. 128, No. 3, pp. 455–463. © Pleiades Publishing, Inc., 2019.
Published in Russian in Zhurnal Eksperimental'noi i Teoreticheskoi Fiziki, 2019, Vol. 155, No. 3, pp. 527–537.

ORDER, DISORDER, AND PHASE TRANSITION IN CONDENSED SYSTEM

Electron–Phonon Coupling in Eliashberg–McMillan Theory Beyond Adiabatic Approximation[1]

M. V. Sadovskii[a,b]

[a] *Institute for Electrophysics, RAS Ural Branch, Yekaterinburg, 620016 Russia*
[b] *M. Mikheev Institute for Metal Physics, RAS Ural Branch, Yekaterinburg, 620108 Russia*
e-mail: sadovski@iep.uran.ru

Received August 14, 2018; revised August 14, 2018; accepted September 20, 2018

Abstract—Eliashberg–McMillan theory of superconductivity is essentially based on the adiabatic approximation. Small parameter of perturbation theory is given by $\lambda\frac{\Omega_0}{E_F} \ll 1$, where λ is the dimensionless electron–phonon coupling constant, Ω_0 is characteristic phonon frequency, while E_F is Fermi energy of electrons. Here we present an attempt to describe the electron–phonon interaction within Eliashberg–McMillan approach in situation, when characteristic phonon frequency Ω_0 becomes large enough (comparable to, or exceeding, the Fermi energy E_F). We consider the general definition of electron–phonon pairing coupling constant λ, taking into account the finite value of phonon frequency. Also, we obtain the simple expression for generalized coupling constant $\tilde{\lambda}$ that determines the mass renormalization, with the account of finite width of conduction band, which describes the smooth transition from the adiabatic regime to the region of strong nonadiabaticity. In the case of strong nonadiabaticity, when $\Omega_0 \gg E_F$, the new small parameter appears, $\lambda\frac{E_F}{\Omega_0} \sim \lambda\frac{D}{\Omega_0} \ll 1$ (D is conduction band half-width), and corrections to electronic spectrum become irrelevant. At the same time, the temperature of superconducting transition T_c in antiadiabatic limit is still determined by Eliashberg–McMillan coupling constant λ, while the preexponential factor in the expression for T_c, conserving the form typical of weak-coupling theory, is determined by the bandwidth (Fermi energy). For the case of interaction with a single optical phonon, we derive the single expression for T_c, valid both in adiabatic and antiadiabatic regimes and describing the continuous transition between these two limiting cases. The results obtained are discussed in the context of superconductivity in FeSe/STO.

DOI: 10.1134/S1063776119020122

1. INTRODUCTION

Eliashberg–McMillan superconductivity theory is the most successful approach to microscopic description of the properties of conventional superconductors with electron–phonon mechanism of Cooper pairing [1–3]. It basic principles can be directly generalized also for the description of non-phonon pairing mechanism in new high-temperature superconductors. Recently this theory was successfully applied to the description of record breaking superconductivity in hydrides at high pressures [4].

It is widely known that Eliashberg–McMillan theory is essentially based on the applicability of adiabatic approximation and Migdal's theorem [5], which allows the neglect of vertex corrections in calculations of electron–phonon coupling in typical metals. In this case the correct small parameter of perturbation theory is $\lambda\frac{\Omega_0}{E_F} \ll 1$, where λ is the dimensionless Eliashberg–McMillan electron–phonon coupling constant, Ω_0 is characteristic phonon frequency and E_F is Fermi energy of electrons. In particular, this leads to the common opinion, that vertex corrections in this theory can be neglected even for $\lambda > 1$, due to the validity of inequality $\frac{\Omega_0}{E_F} \ll 1$, characteristic for typical metals. This is certainly correct in continuous approximation, when we neglect the effects of lattice discreteness on electron spectrum.

The discreteness of the lattice leads to the breaking of Migdal's theorem for $\lambda \sim 1$ due to polaronic effects [6, 7]. At the same time, for the region of $\lambda < 1$ we can safely neglect these effects [7]. In the following we

[1] The article is published in the original.

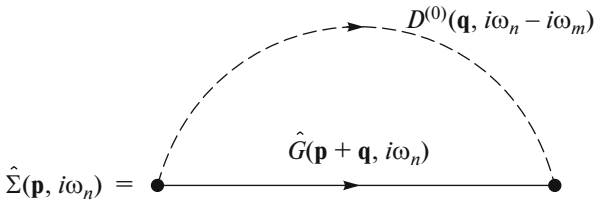

Fig. 1. Second-order diagram for self-energy. Dashed line—phonon Green's function $D^{(0)}$, continuous line—electron Green's function G in Matsubara representation.

shall consider only the continuous case, limiting our discussion to not so large values of electron–phonon coupling λ.

Recently a number of superconductors was discovered, where the adiabatic approximation can not be considered valid, and characteristic frequencies of phonons are of the order or even greater than Fermi energy. We bear in mind mainly superconductors based on FeSe monolayers, mostly the systems like single-atomic layer of FeSe on the $SrTiO_3$ substrate (FeSe/STO) [8]. For these systems this was first noted by Gor'kov [9, 10], while discussing the idea of possible T_c enhancement in FeSe/STO due to interaction with high-energy optical phonons in $SrTiO_3$ [8].

2. SELF-ENERGY AND ELECTRON–PHONON COUPLING CONSTANT

Consider the second-order (in electron–phonon coupling) diagram shown in Fig. 1. At first it is sufficient to consider a metal in normal (non superconducting) state.

We can perform our analysis either in Matsubara technique ($T \neq 0$) or in $T = 0$ technique. In particular, making all calculations in finite temperature technique, after the analytic continuation from Matsubara to real frequencies $i\omega_n \to \varepsilon \pm i\delta$ and in the limit of $T = 0$, the contribution of diagram Fig. 1 can be written in the standard form [1, 11]:

$$\Sigma(\varepsilon, \mathbf{p}) = \sum_{\mathbf{p}',\alpha} |g^{\alpha}_{\mathbf{pp}'}|^2 \left\{ \frac{f_{\mathbf{p}'}}{\varepsilon - \varepsilon_{\mathbf{p}'} + \Omega^{\alpha}_{\mathbf{p}-\mathbf{p}'} - i\delta} + \frac{1 - f_{\mathbf{p}'}}{\varepsilon - \varepsilon_{\mathbf{p}'} - \Omega^{\alpha}_{\mathbf{p}-\mathbf{p}'} + i\delta} \right\}, \quad (1)$$

where in notations of Fig. 1 we have $\mathbf{p}' = \mathbf{p} + \mathbf{q}$. Here, $g^{\alpha}_{\mathbf{p},\mathbf{p}'}$ is Fröhlich electron–phonon coupling constant, $\varepsilon_{\mathbf{p}}$ is electronic spectrum with energy zero taken at the Fermi level, $\Omega^{\alpha}_{\mathbf{q}}$ is phonon spectrum, and $f_{\mathbf{p}}$ is the (step-like) Fermi distribution.

In particular, for the imaginary part of self-energy at positive frequencies we have:

$$\mathrm{Im}\,\Sigma(\varepsilon > 0, \mathbf{p}) = -\pi \sum_{\mathbf{p}',\alpha} |g^{\alpha}_{\mathbf{pp}'}|^2 (1 - f_{\mathbf{p}'}) \delta(\varepsilon - \varepsilon_{\mathbf{p}'} - \Omega^{\alpha}_{\mathbf{p}-\mathbf{p}'}). \quad (2)$$

In these expressions index α enumerates the branches of phonon spectrum. In the following we just drop it for brevity.

Equation (1) can be identically written as:

$$\Sigma(\varepsilon, \mathbf{p}) = \int d\omega \sum_{\mathbf{p}'} |g_{\mathbf{pp}'}|^2 \delta(\omega - \Omega_{\mathbf{p}-\mathbf{p}'}) \left\{ \frac{f_{\mathbf{p}'}}{\varepsilon - \varepsilon_{\mathbf{p}'} + \omega - i\delta} + \frac{1 - f_{\mathbf{p}'}}{\varepsilon - \varepsilon_{\mathbf{p}'} - \omega + i\delta} \right\}. \quad (3)$$

In Eliashberg–McMillan approach we usually get rid of explicit momentum dependence here by averaging the matrix element of electron–phonon interaction over surfaces of constant energies, corresponding to initial and final momenta $\mathbf{p}$ and $\mathbf{p}'$, which usually reduces to the averaging over corresponding Fermi surfaces, as phonon scattering takes place only within the narrow energy interval close to the Fermi level, with effective width of the order of double Debye frequency $2\Omega_D$, and in typical metals we always have $\Omega_D \ll E_F$. This is achieved by the following replacement:

$$|g_{\mathbf{pp}'}|^2 \delta(\omega - \Omega_{\mathbf{p}-\mathbf{p}'}) \Rightarrow \frac{1}{N(0)} \sum_{\mathbf{p}} \frac{1}{N(0)} \sum_{\mathbf{p}'} |g_{\mathbf{pp}'}|^2 \delta(\omega - \Omega_{\mathbf{p}-\mathbf{p}'}) \delta(\varepsilon_{\mathbf{p}}) \delta(\varepsilon_{\mathbf{p}'}) \equiv \frac{1}{N(0)} \alpha^2(\omega) F(\omega), \quad (4)$$

where in the last expression we have introduced the *definition* of Eliashberg function $\alpha^2(\omega)$ and $F(\omega) = \sum_{\mathbf{q}} \delta(\omega - \Omega_{\mathbf{q}})$ is the phonon density of states.

In the case, when phonon energy becomes comparable with or even exceeds the Fermi energy, electron scattering is effective not in the narrow energy layer around the Fermi surface, but in a wider energy interval of the order of $\Omega_0 \sim E_F$, where Ω_0 is a characteristic phonon frequency (e.g. of an optical phonon). Then, for the case of initial $|\mathbf{p}| \sim p_F$ the averaging over $\mathbf{p}'$ in expression like (4) should be done over the surface of constant energy, corresponding to $E_F + \Omega_{\mathbf{p}-\mathbf{p}'}$, as is shown in Fig. 2. Then the Eq. (4) is directly generalized as:

$$|g_{\mathbf{pp}'}|^2 \delta(\omega - \Omega_{\mathbf{p}-\mathbf{p}'}) \Rightarrow \frac{1}{N(0)} \sum_{\mathbf{p}} \frac{1}{N(0)} \sum_{\mathbf{p}'} |g_{\mathbf{pp}'}|^2 \cdot \delta(\omega - \Omega_{\mathbf{p}-\mathbf{p}'}) \delta(\varepsilon_{\mathbf{p}}) \delta(\varepsilon_{\mathbf{p}'} - \Omega_{\mathbf{p}-\mathbf{p}'}) \equiv \frac{1}{N(0)} \alpha^2(\omega) F(\omega), \quad (5)$$

which in the last δ-function simply corresponds to transition from chemical potential μ to $\mu + \Omega_{\mathbf{p}-\mathbf{p}'}$. We remind that, as usual, the energy zero is taken at $\mu = 0$.

After the replacement like (4) or (5) the explicit momentum dependence of the self-energy disappears and in fact in the following we are dealing with Fermi surface average $\Sigma(\varepsilon) \equiv \frac{1}{N(0)}\sum_{\mathbf{p}} \delta(\varepsilon_{\mathbf{p}})\Sigma(\varepsilon, \mathbf{p})$, which is now written as:

$$\Sigma(\varepsilon) = \int d\varepsilon' \int d\omega \alpha^2(\omega) F(\omega) \cdot \left\{ \frac{f(\varepsilon')}{\varepsilon - \varepsilon' + \omega - i\delta} + \frac{1 - f(\varepsilon')}{\varepsilon - \varepsilon' + \omega - i\delta} \right\}. \quad (6)$$

This expression forms the basis of Eliashberg–McMillan theory and determines the structure of Eliashberg equations for the description of superconductivity.

3. MASS RENORMALIZATION AND ELECTRON–PHONON COUPLING CONSTANT

For the case of self-energy dependent only on frequency (and not on momentum) we have the following simple expressions, relating mass renormalization of an electron to the residue a the pole of the Green's function [12]:

$$Z^{-1} = 1 - \left.\frac{\partial \Sigma(\varepsilon)}{\partial \varepsilon}\right|_{\varepsilon=0}, \quad (7)$$

$$m^{\star} = \frac{m}{Z} = m\left(1 - \left.\frac{\partial \Sigma(\varepsilon)}{\partial \varepsilon}\right|_{\varepsilon=0}\right). \quad (8)$$

Then from Eq. (6) by direct calculations (all integrals here are in infinite limits) we obtain:

$$-\left.\frac{\partial \Sigma(\varepsilon)}{\partial \varepsilon}\right|_{\varepsilon=0} = \int d\varepsilon' \int d\omega \alpha^2(\omega) F(\omega) \left\{ \frac{f(\varepsilon')}{(\omega - \varepsilon' - i\delta)^2} + \frac{1 - f(\varepsilon')}{(\omega + \varepsilon' + i\delta)^2} \right\} = 2\int_0^{\infty} \frac{d\omega}{\omega} \alpha^2(\omega) F(\omega) \quad (9)$$

so that introducing the dimensionless Eliashberg–McMillan electron–phonon coupling constant as:

$$\lambda = 2\int_0^{\infty} \frac{d\omega}{\omega} \alpha^2(\omega) F(\omega), \quad (10)$$

we immediately obtain the standard expression for electron mass renormalization due to electron–phonon interaction:

$$m^{\star} = m(1 + \lambda). \quad (11)$$

The function $\alpha^2(\omega)F(\omega)$ in the expression for Eliashberg–McMillan electron–phonon coupling constant (10) should be calculated according to (4) or (5) depending on the relation between Fermi energy E_F and characteristic phonon frequency Ω (roughly estimated by Ω_D). As long as $\Omega \ll E_F$ we can use the standard expression (4), while in case of $\Omega \sim E_F$ we should use (5). In principle all these facts are known

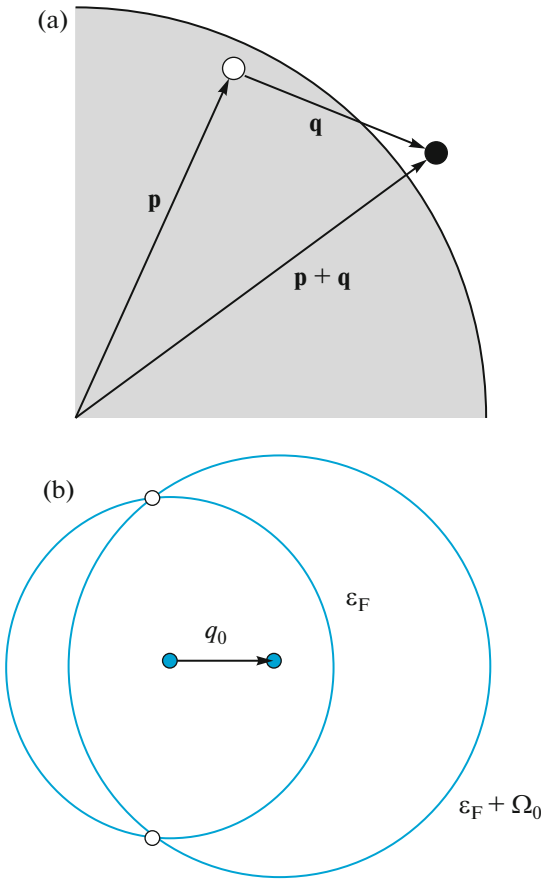

Fig. 2. (Color online) (a) Elementary act of electron–phonon scattering in the vicinity of the Fermi surface. (b) Surfaces of constant energy for initial and final states of an electron scattered by an optical phonon with energy comparable to Fermi energy. Averaging of the matrix element of interaction in (12) or (14) goes over the intersection region of these surfaces.

for a long time—implicitly these results were mentioned e.g. in Allen's paper [13], but misunderstandings still appear [14]. Using Eq. (5) we can rewrite (10) in the following form:

$$\lambda = \frac{2}{N(0)} \int \frac{d\omega}{\omega} \sum_{\mathbf{p}} \sum_{\mathbf{p}'} |g_{\mathbf{p}\mathbf{p}'}|^2 \cdot \delta(\omega - \Omega_{\mathbf{p}-\mathbf{p}'}) \delta(\varepsilon_{\mathbf{p}}) \delta(\varepsilon_{\mathbf{p}'} - \Omega_{\mathbf{p}-\mathbf{p}'}), \quad (12)$$

which gives the most general expression to calculate the electron–phonon constant λ, determining Cooper pairing in Eliashberg–McMillan theory.

4. ELECTRON INTERACTION WITH OPTICAL PHONONS WITH "FORWARD" SCATTERING

The discovery of high-temperature superconductivity in single—atomic layers of FeSe on $SrTiO_3$ (FeSe/STO) and similar substrates, with record—breaking, for iron—based superconductors, critical temperature T_c, nearly an order of magnitude higher

than in the bulk FeSe (see review in [8]), has sharpened the problem of search of microscopic mechanism of T_c enhancement. It was followed by the discovery in ARPES experiments on FeSe/STO of the so called "replicas" of conduction band [15], which lead to the idea of T_c enhancement due to interaction of conduction electrons with optical phonons of $SrTiO_3$, with rather high energies (frequencies) ~100 meV and "nearly forward" scattering (i.e. with small transferred momentum of the phonon) due to the peculiarities of interaction with optically active Ti–O dipoles at the interface with STO. The model of such scattering introduced in [15] has revived the interest to earlier model of T_c enhancement, proposed by Dolgov and Kulic, due to "forward" scattering [16, 17], which was further developed and applied to FeSe/STO in [18, 19]. In fact, this model explains the formation of the "replicas" of conduction band and the possibility to achieve high values of T_c, though its basic conclusions were criticized (from different points of view) in [20–22] and are still under discussion.

One of the major circumstances, which was not payed much attention in [15, 18, 19], was the nonadiabatic character, as noted by Gor'kov [9, 10], of FeSe electrons interaction with optical phonons of STO. The Fermi energy in conduction band of FeSe/STO is small, of the order of 50–60 meV [8, 15], which by itself is a serious problem for theoretical explanation [20, 21]. Correspondingly, the energy of optical phonons (~100 meV) exceeds is nearly twice, leading to strong enough breaking of adiabaticity. Let us see, first of all, the consequences of this fact for calculations of electron–phonon coupling constant in Eliashberg–McMillan approach.

Consider a particular example of electrons interacting with a single optical (Einstein-like) phonon mode with high-enough frequency Ω_0, which scatters essentially "forward". The general qualitative picture of such scattering is shown in Fig. 2. In this case in Eq. (12) the density of phonon states is simply $F(\omega) = \delta(\omega - \Omega_0)$, and for the momentum dependence of interaction with optical phonon at FeSe/STO interface we can assume the characteristic dependence, obtained in [15]:

$$g(\mathbf{q}) = g_0 \exp(-|\mathbf{q}|/q_0), \tag{13}$$

where the typical value of $q_0 \sim 0.1\frac{\pi}{a} \ll p_F$ (where a is the lattice constant and p_F is the Fermi momentum), leading to nearly "forward" scattering of electrons by optical phonons.

Then the dimensionless pairing constant of electron–phonon interaction in Eliashberg theory is written as:

$$\lambda = \frac{2}{N(0)\Omega_0}\sum_{\mathbf{p}}\sum_{\mathbf{q}}|g_{\mathbf{q}}|^2\delta(\varepsilon_{\mathbf{p}})\delta(\varepsilon_{\mathbf{p+q}} - \Omega_0). \tag{14}$$

As in FeSe/STO we have in fact $\Omega_0 > E_F$ the finite value in the second δ-function here should be taken into account.

For simple estimates let us assume the linearized form of electronic spectrum (v_F is Fermi velocity): $\varepsilon_{\mathbf{p}} \approx v_F(|\mathbf{p}| - p_F)$, which allows to perform all calculations analytically. Then, substituting (13) into (14) and considering two-dimensional case, after calculating all integrals here we obtain [21]:

$$\lambda = \frac{g_0^2 a^2}{\pi^2 v_F^2} K_1\left(\frac{2\Omega_0}{v_F q_0}\right), \tag{15}$$

where $K_1(x)$ is Bessel function of imaginary argument (McDonald function). Using the well-known asymptotic form of $K_1(x)$ and dropping a number of irrelevant constants, we have:

$$\lambda \sim \lambda_0 \frac{q_0}{4\pi p_F}, \tag{16}$$

for $\frac{\Omega_0}{v_F q_0} \ll 1$, and

$$\lambda \sim \lambda_0 \frac{\Omega_0}{\pi E_F}\sqrt{\frac{v_F q_0}{\Omega_0}}\exp\left(\frac{2\Omega_0}{v_F q_0}\right), \tag{17}$$

for $\frac{\Omega_0}{v_F q_0} \gg 1$.

Here we introduced the standard dimensionless electron–phonon coupling constant:

$$\lambda_0 = \frac{2g_0^2}{\Omega_0}N(0), \tag{18}$$

where $N(0)$ is the density of electronic states at the Fermi level per single spin projection.

The result (16) is known [18, 19] and by itself is rather unfavorable for significant T_c enhancement in model under discussion. Even worse is the situation if we take into account the large values of Ω_0, as pairing constant becomes exponentially suppressed for $\frac{\Omega_0}{v_F q_0} > 1$, which is typical for FeSe/STO interface, where $\Omega_0 > E_F \gg v_F q_0$ [8]. This makes the enhancement of T_c due to interaction of FeSe electrons with optical phonons of STO rather improbable. In fact, similar conclusions were made from first—principles calculations in [23], where the dependence of Eliashberg coupling constant on frequency of the optical phonon in STO was also taken into account. However, the effect of suppression of this constant was much smaller, which was probably due to unrealistically large values of the Fermi energy, obtained form LDA calculations of electronic spectrum of FeSe/STO, which does not account for the role of correlations [23]. Correspondingly, in [23] they always had $\Omega_0 \ll E_F$. The account of correlations within LDA+DMFT calculations, per-

formed in [20, 21], allowed to obtain the values of Fermi energy in conduction band of FeSe/STO in accordance with ARPES data, which show that in this system we meet with antiadiabatic situation with $\Omega_0 > E_F$.

Certainly, the results obtained above in the asymptotic of high frequencies Ω_0 depend on the form of momentum dependence in Eq. (13). For example, if we choose the Gaussian form of interaction fall with transferred momentum, we shall obtain more fast Gaussian suppression with frequency in the limit of Eq. (17). In general case, for fast enough fall of interaction in (13) on the scale of q_0 we shall always obtain rather fast suppression of coupling constant for $\Omega_0 \gg v_F q_0$.

For a more realistic case, when the optical phonon scatters electrons not only in "forward" direction, but in a wide interval of transferred momenta (as it follows e.g. from first - principles calculations of [23]), in the above expression we have simply to use large enough value of the parameter q_0. Choosing e.g. $q_0 \sim 4\pi p_F$ and using the low frequency limit (16) we immediately obtain $\lambda \approx \lambda_0$, i.e. the standard result. Similarly, parameter q_0 can be taken equal to an inverse lattice vector $2\pi/a$. Then for $q_0 \sim 2\pi/a$ from (16) we obtain:

$$\lambda \sim \lambda_0 \frac{1}{2p_F a} \sim \lambda_0 \tag{19}$$

for typical $p_F \sim 1/2a$. In general case there always remain the dependence on the value of Fermi momentum and cutoff parameter (cf. similar analysis in [12]).

In the limit of (17), assuming $q_0 \sim p_F$ we immediately obtain:

$$\lambda \sim \frac{\sqrt{2}}{\pi}\lambda_0\sqrt{\frac{\Omega_0}{E_F}}\exp\left(-\frac{\Omega_0}{E_F}\right), \tag{20}$$

which simply signifies the effective interaction cutoff for $\Omega_0 > E_F$ in antiadiabatic limit. This fact was stressed by Gor'kov in [9, 10].

5. EFFECTS OF FINITE BANDWIDTH AND ANTIADIABATIC LIMIT

As was already noted above, the usual Migdal–Eliashberg approach is totally justified in adiabatic approximation, related for usual electron–phonon systems (metals) with the presence of a small parameter $\Omega_D/E_F \ll 1$ (or $\Omega_0/E_F \ll 1$ for the case of a single optical phonon with frequency Ω_0). The true parameter of perturbation theory in this case is given by $\lambda(\Omega_0/E_F)$, which is small even for $\lambda \sim 1$. The presence of this small parameter allows us to limit ourselves to calculations of a simple diagram of the second order over electron–phonon interaction considered above, and neglect all vertex corrections (Migdal's theorem) [5]. These conditions are broken in FeSe/STO system, where $\Omega_0 \sim 2E_F$.

Our discussion up to now implicitly assumed the conduction band of an infinite width. It is clear that in case of large enough characteristic phonon frequency it may be comparable not only with Fermi energy, but also with conduction band width. Below we shall show that in the limit of strong nonadiabaticity, when $\Omega_0 \gg E_F \sim D$ (where D is the conduction band half-width), in fact, we are dealing with the situation, when a new small parameter of perturbation theory $\lambda D/\Omega_0 \sim \lambda E_F/\Omega_0$ appears in the theory.

Let us consider the case of conduction band of the finite width $2D$ with constant density of states (which formally corresponds formally to two-dimensional case). The Fermi level as above is considered as an origin of energy scale and we assume the typical case of half-filled band. Then (6) reduces to:

$$\begin{aligned}\Sigma(\varepsilon) &= \int_{-D}^{D} d\varepsilon' \int d\omega\alpha^2(\omega)F(\omega) \\ &\cdot \left\{\frac{f(\varepsilon')}{\varepsilon - \varepsilon' + \omega - i\delta} + \frac{1 - f(\varepsilon')}{\varepsilon - \varepsilon' - \omega + i\delta}\right\} \\ &= \int_{-D}^{D} d\varepsilon' \int d\omega\alpha^2(\omega)F(\omega) \\ &\cdot \left\{\frac{1}{\varepsilon + \varepsilon' + \omega - i\delta} + \frac{1}{\varepsilon - \varepsilon' - \omega + i\delta}\right\} \\ &= \int d\omega\alpha^2(\omega)F(\omega)\left\{\ln\frac{\varepsilon + D + \omega - i\delta}{\varepsilon - D - \omega + i\delta} - \ln\frac{\varepsilon + \omega - i\delta}{\varepsilon - \omega + i\delta}\right\}.\end{aligned} \tag{21}$$

For the model of a single optical phonon $F(\omega) = \delta(\omega - \Omega_0)$ and we immediately obtain:

$$\begin{aligned}\Sigma(\varepsilon) &= \alpha^2(\Omega_0)F(\Omega_0) \\ &\cdot \left\{\ln\frac{\varepsilon + D + \Omega_0 - i\delta}{\varepsilon - D - \Omega_0 + i\delta} - \ln\frac{\varepsilon + \Omega_0 - i\delta}{\varepsilon - \Omega_0 + i\delta}\right\} \\ &= \alpha^2(\Omega_0)F(\Omega_0)\ln\left\{\frac{\varepsilon + D + \Omega_0 - i\delta}{\varepsilon - D - \Omega_0 + i\delta}\frac{\varepsilon - \Omega_0 + i\delta}{\varepsilon + \Omega_0 - i\delta}\right\}.\end{aligned} \tag{22}$$

Correspondingly, form (21) we get:

$$\begin{aligned}-\left.\frac{\partial\Sigma(\varepsilon)}{\partial\varepsilon}\right|_{\varepsilon=0} &= 2\int_0^D d\varepsilon' \int_0^\infty d\omega\alpha^2(\omega)F(\omega)\frac{1}{(\omega + \varepsilon')^2} \\ &= 2\int_0^\infty d\omega\alpha^2(\omega)F(\omega)\frac{D}{\omega(\omega + D)}\end{aligned} \tag{23}$$

and we can define the generalized coupling constant as:

$$\tilde{\lambda} = 2\int_0^\infty \frac{d\omega}{\omega}\alpha^2(\omega)F(\omega)\frac{D}{\omega + D}, \tag{24}$$

which for $D \to \infty$ reduces to the usual Eliashberg–McMillan constant (10), while for $D \to 0$ is gives the "antiadiabatic" coupling constant:

$$\lambda_D = 2D\int \frac{d\omega}{\omega^2}\alpha^2(\omega)F(\omega). \tag{25}$$

Equation (24) describes the smooth transition between the limits of wide and narrow conduction bands. Mass renormalization in general case is determined by $\tilde{\lambda}$:

$$m^\star = m(1+\tilde{\lambda}). \tag{26}$$

In strong antiadiabatic limit of $D \ll \Omega_0$, after elementary calculations we obtain from (21):

$$\mathrm{Re}\,\Sigma(\varepsilon) = 2D\int d\omega\alpha^2(\omega)F(\omega)\frac{\varepsilon}{\varepsilon^2-\omega^2} \tag{27}$$

and from (22)

$$\mathrm{Re}\,\Sigma(\varepsilon) = \alpha^2(\Omega_0)\frac{2D\varepsilon}{\varepsilon^2-\Omega_0^2} = \lambda_\mathrm{D}\frac{\Omega_0^2\varepsilon}{\varepsilon^2-\Omega_0^2}. \tag{28}$$

For the model of a single optical phonon with frequency Ω_0 we have:

$$\tilde{\lambda} = \frac{2}{\Omega_0}\alpha^2(\Omega_0)\frac{D}{\Omega_0+D} = \lambda\frac{D}{\Omega_0+D} = \lambda_\mathrm{D}\frac{\Omega_0}{\Omega_0+D}, \tag{29}$$

where Eliashberg–McMillan constant is:

$$\lambda = 2\int_0^\infty\frac{d\omega}{\omega}\alpha^2(\omega)F(\omega) = \alpha^2(\Omega_0)\frac{2}{\Omega_0} \tag{30}$$

and λ_D reduces to:

$$\lambda_D = 2\alpha^2(\Omega_0)\frac{D}{\Omega_0^2} = 2\alpha^2(\Omega_0)\frac{1}{\Omega_0}\frac{D}{\Omega_0}, \tag{31}$$

where in the last expression we have introduced the new small parameter $D/\Omega_0 \ll 1$, appearing in strong antiadiabatic limit. Correspondingly, in this limit we always have:

$$\lambda_\mathrm{D} = \lambda\frac{D}{\Omega_0} \sim \lambda\frac{E_\mathrm{F}}{\Omega_0} \ll \lambda \tag{32}$$

so that for reasonable values of λ (even up to a strong coupling region of $\lambda \sim 1$) "antiadiabatic" coupling constant remains small. Obviously, all vertex corrections are also small in this limit, as was shown by direct calculations in [24], which went rather unnoticed. Thus we come to an unexpected conclusion—in the limit of strong nonadiabaticity the electron–phonon coupling becomes weak!

For imaginary part of self-energy in strong antiadiabatic limit we easily obtain:

$$\begin{aligned}\mathrm{Im}\,\Sigma(\varepsilon>0) &= -i2\pi D\varepsilon\int d\omega\alpha^2(\omega)F(\omega)\delta(\varepsilon^2-\omega^2)\\ &= -i2\pi D\varepsilon\int d\omega\alpha^2(\omega)F(\omega)\frac{1}{2\varepsilon}\{\delta(\varepsilon-\omega)+\delta(\varepsilon+\omega)\}\\ &= -i\pi D\alpha^2(\varepsilon)F(\varepsilon),\end{aligned} \tag{33}$$

which in a single phonon model reduces to:

$$\begin{aligned}\mathrm{Im}\,\Sigma(\varepsilon>0) &= -i\pi D\alpha^2(\Omega_0)\delta(\varepsilon-\Omega_0)\\ &= -\frac{i\pi}{2}\lambda_\mathrm{D}\Omega_0^2\delta(\varepsilon-\Omega_0).\end{aligned} \tag{34}$$

From these expressions it is clear that this imaginary part is not particularly important in this limit (being non zero only for $\varepsilon = \Omega_0$), and equation for the real part of electronic dispersion:

$$\varepsilon - \varepsilon_\mathbf{p} - \mathrm{Re}\,\Sigma(\varepsilon) = 0 \tag{35}$$

is now:

$$\varepsilon - \varepsilon_\mathbf{p} - \alpha^2(\Omega_0)\frac{2D\varepsilon}{\varepsilon^2-\Omega_0^2} = 0. \tag{36}$$

Correspondingly, for $\varepsilon \sim \varepsilon_\mathbf{p}$ we can write:

$$\varepsilon - \varepsilon_\mathbf{p} - \alpha^2(\Omega_0)\frac{2D\varepsilon_\mathbf{p}}{\varepsilon_\mathbf{p}^2-\Omega_0^2} = 0, \tag{37}$$

which for $\varepsilon_\mathbf{p} \to 0$ gives a small correction to the spectrum:

$$\varepsilon \approx \varepsilon_\mathbf{p} - \alpha^2(\Omega_0)\frac{2D}{\Omega_0^2}\varepsilon_\mathbf{p} = \varepsilon_\mathbf{p} - \lambda_D\varepsilon_\mathbf{p} = \varepsilon_\mathbf{p}(1-\lambda_D) \tag{38}$$

obviously reducing to a small ($\lambda_\mathrm{D} \ll 1$) renormalization of the effective mass (26).

Physically, the weakness of electron–phonon coupling in strong nonadiabatic limit is pretty clear—when ions move much faster than electrons, these have no time to "fit" the rapidly changing configuration of ions and, in these sense, only weakly react on their movement.

6. ELIASHBERG EQUATIONS AND THE TEMPERATURE OF SUPERCONDUCTING TRANSITION

All analysis above was performed for the normal state of a metal. The problem arises, to which extent the results obtained can be generalized for the case of a metal in superconducting state? In particular, what coupling constant (λ, $\tilde{\lambda}$, or λ_D) determines the temperature of superconducting transition T_c an antiadiabatic limit? Let us analyze the situation within appropriate generalization of Eliashberg equations.

Taking into account that in antiadiabatic approximation vertex corrections are irrelevant and neglecting the direct Coulomb interaction, Eliashberg equations can be derived by calculating the diagram of Fig. 1, where electronic Green's function in superconducting state is taken in Nambu's matrix representation. For real frequencies this is written in the following standard form [2]:

$$G(\varepsilon,\mathbf{p}) = \frac{Z(\varepsilon)\varepsilon\tau_0 + \varepsilon_\mathbf{p}\tau_3 + Z(\varepsilon)\Delta(\varepsilon)\tau_1}{Z^2(\varepsilon)\varepsilon^2 - Z^2(\varepsilon)\Delta^2(\varepsilon) - \varepsilon_\mathbf{p}^2}, \tag{39}$$

which corresponds to the matrix of self-energy:

$$\Sigma(\varepsilon,\mathbf{p}) = [1-Z(\varepsilon)]\varepsilon\tau_0 + Z(\varepsilon)\Delta(\varepsilon)\tau_1, \tag{40}$$

where τ_i are standard Pauli matrices, while functions of mass renormalization $Z(\varepsilon)$ and energy gap $\Delta(\varepsilon)$ are determined from solution of integral Eliashberg equa-

tions, which in representation of real frequencies are written as [2]:

$$[1 - Z(\varepsilon)]\varepsilon = -\int_{-D}^{D} d\varepsilon' K(\varepsilon', \varepsilon) \operatorname{Re} \frac{\varepsilon'}{\sqrt{\varepsilon'^2 - \Delta^2(\varepsilon')}} \operatorname{sign} \varepsilon, \quad (41)$$

$$Z(\varepsilon)\Delta(\varepsilon) = \int_{-D}^{D} K(\varepsilon', \varepsilon) \operatorname{Re} \frac{\Delta(\varepsilon')}{\sqrt{\varepsilon'^2 - \Delta^2(\varepsilon')}} \operatorname{sign} \varepsilon, \quad (42)$$

where integral equation kernel has the following form:

$$K(\varepsilon', \varepsilon) = \frac{1}{2}\int_0^\infty d\omega \alpha^2(\omega) F(\omega) \cdot \left\{ \frac{\tanh\frac{\varepsilon'}{2T} + \coth\frac{\omega}{2T}}{\varepsilon' + \omega - \varepsilon - i\delta} - \frac{\tanh\frac{\varepsilon'}{2T} - \coth\frac{\omega}{2T}}{\varepsilon' - \omega - \varepsilon - i\delta} \right\}. \quad (43)$$

The only difference here from the similar equations of [2] is the appearance of the finite integration limits, determined by the bandwidth, as well as the absence of the contribution of direct Coulomb repulsion, which will not be discussed here. In fact, Eqs. (41) and (42) are the direct analog of Eqs. (6) and (21) for normal metal and replace them after the transition into superconducting phase.

To determine the temperature of superconducting transition it is sufficient, as usual, to analyze the linearized Eliashberg equations, which are written as:

$$[1 - Z(\varepsilon)]\varepsilon = \int_0^D d\varepsilon' \int_0^\infty d\omega \alpha^2(\omega) F(\omega) f(-\varepsilon') \cdot \left(\frac{1}{\varepsilon' + \varepsilon + \omega + i\delta} - \frac{1}{\varepsilon' - \varepsilon + \omega - i\delta} \right), \quad (44)$$

$$Z(\varepsilon)\Delta(\varepsilon) = \int_0^D \frac{d\varepsilon'}{\varepsilon'} \tanh\frac{\varepsilon}{2T_c} \operatorname{Re} \Delta(\varepsilon') \cdot \int_0^\infty d\omega \alpha^2(\omega) F(\omega) \cdot \left(\frac{1}{\varepsilon' + \varepsilon + \omega + i\delta} + \frac{1}{\varepsilon' - \varepsilon + \omega - i\delta} \right). \quad (45)$$

For us it is sufficient to consider in these equations the limit of $\varepsilon \to 0$ and look for the solutions $Z(0) = Z$ and $\Delta(0) = \Delta$. Then from (44) we obtain:

$$[1 - Z]\varepsilon = -2\varepsilon \int_0^\infty d\omega \alpha^2(\omega) F(\omega) \int_0^D \frac{d\varepsilon'}{(\varepsilon' + \omega)^2} = -2\varepsilon \int_0^\infty d\omega \alpha^2(\omega) F(\omega) \frac{D}{\omega(\omega + D)} \quad (46)$$

or

$$Z = 1 + \tilde{\lambda}, \quad (47)$$

where the constant $\tilde{\lambda}$ was defined above in Eq. (24). Thus, precisely this effective constant determines mass renormalization both in normal and superconducting phases. As was shown above, in the limit of strong antiadiabaticity this renormalization is very small and determined by the limiting value of λ_D (31).

Situation is different in Eq. (45). In the limit of $\varepsilon \to 0$, using (47) we immediately obtain from (45) the following equation for T_c

$$1 + \tilde{\lambda} = 2\int_0^\infty d\omega \alpha^2(\omega) F(\omega) \int_0^D \frac{d\varepsilon'}{\varepsilon'(\varepsilon' + \omega)} \tanh\frac{\varepsilon'}{2T_c}. \quad (48)$$

In antiadiabatic limit, when characteristic frequencies of phonons exceed the width of the conduction band, we can neglect ε' as compared to ω in the denominator of the integrand in (48), so that the equation for T_c is rewritten as:

$$1 + \tilde{\lambda} \approx 2\int_0^\infty d\omega \frac{\alpha^2(\omega) F(\omega)}{\omega} \int_0^D \frac{d\varepsilon'}{\varepsilon'} \tanh\frac{\varepsilon'}{2T_c} = \lambda \int_0^D \frac{d\varepsilon'}{\varepsilon'} \tanh\frac{\varepsilon'}{2T_c}, \quad (49)$$

where λ is Eliashberg–McMillan coupling constant as defined above in Eq. (10). From here we immediately obtain the BCS-type result:

$$T_c \sim D \exp\left(-\frac{1 + \tilde{\lambda}}{\lambda} \right). \quad (50)$$

We have seen above, that in antiadiabatic limit we always have $\tilde{\lambda} \to \lambda_D \ll \lambda$, so that in the exponent in (50) we can neglect it, so that the expression for T_c is reduced simply to BCS *weak* coupling formula, with preexponential factor determined by the half-width of the band (Fermi energy), while the pairing coupling constant in the exponential is determined the general Eliashberg–McMillan expression (taking account the discussion above).

In the model with single optical phonon of frequency Ω_0 Eq. (49) has the form:

$$1 + \tilde{\lambda} = 2\alpha^2(\Omega_0) \int_0^D \frac{d\varepsilon'}{\varepsilon'(\varepsilon' + \Omega_0)} \tanh\frac{\varepsilon'}{2T_c}. \quad (51)$$

Equation (51) is easily solved (the integral here can be taken, as usual, by partial integration) and we obtain:

$$T_c \sim D \exp\left(-\frac{1 + \tilde{\lambda} + \lambda \ln\left(\frac{D}{\Omega_0} + 1\right)}{\lambda} \right) = \frac{D}{1 + \frac{D}{\Omega_0}} \exp\left(-\frac{1 - \tilde{\lambda}}{\lambda} \right), \quad (52)$$

where for λ is naturally defined by Eq. (30). We see, that in antiadiabatic regime, for $\frac{D}{\Omega_0} \ll 1$ this expression reduces to (50), while in adiabatic limit $\frac{D}{\Omega_0} \gg 1$ we obtain the usual expression for T_c of Eliashberg theory for the case of intermediate coupling:

$$T_c \sim \Omega_0 \exp\left(-\frac{1+\lambda}{\lambda}\right). \quad (53)$$

Thus, Eq. (51) gives the unified expression for T_c, which is valid both in adiabatic and antiadiabatic limits, smoothly interpolating between these two limits.

Finally, we come to rather unexpected conclusions—in the limit of strong nonadiabaticity T_c is determined by an expression like BCS weak coupling theory, with preexponential determined not by a characteristic phonon frequency, but by Fermi energy (the same conclusion was reached in a recent paper by Gor'kov [10]), while the pairing coupling constant conserves the standard form of Eliashberg–McMillan theory. The effective coupling constant $\tilde{\lambda}$, tending in antiadiabatic limit to λ_D, determines the mass renormalization, but not the temperature of superconducting transition.

7. CONCLUSIONS

In this work we have considered the electron–phonon coupling in Eliashberg–McMillan theory outside the limits of the standard adiabatic approximation. We have obtained some simple expressions for interaction parameters of electrons and phonons in the situation, when the characteristic frequency of phonons Ω_0 becomes large enough (comparable or even exceeding the Fermi energy E_F). In particular, we have analyzed the general definition of the pairing constant λ, taking into account the finite value of phonon frequency. It was shown, that in a popular model with dominating "forward" scattering it leads to exponential suppression of the coupling constant for the frequencies $\Omega_0 \gg v_F q_0$, where q_0 defines the characteristic size of the region of transferred momenta, where electrons interact with phonons. Similar situation appears also in the usual case, when q_0 is of the order of inverse lattice vector, and phonon frequency exceeds the Fermi energy E_F.

We have obtained a simple expression for electron–phonon coupling constant, $\tilde{\lambda}$, determining the mass renormalization in Eliashberg–McMillan theory, taking into account the finite width of conduction band, which describes the smooth transition from adiabatic regime to the region of strong nonadiabaticity. It was shown, that under the conditions of strong nonadiabaticity, when $\Omega_0 \gg E_F$, a new small parameter $\lambda\frac{E_F}{\Omega_0} \sim \lambda\frac{D}{\Omega_0} \ll 1$ (D is the half-width of conduction band) appears in the theory, and corrections to electron spectrum become, in fact, irrelevant, as well as all vertex corrections. In fact, this allows us to apply the general Eliashberg equations outside the limits of adiabatic approximation in strong antiadiabatic limit. Our results show, that outside the limits of adiabatic approximation, in the limit of strong nonadiabaticity, for superconductivity we have a weak coupling regime. Mass renormalization is small and determined by effective coupling constant λ_D, while the strength of the pairing interaction is determined by the standard Eliashberg–McMillan coupling constant $\lambda \gg \lambda_D$, appropriately generalized with the account of finiteness of phonon frequency (comparable or exceeding the Fermi energy). The cutoff of pairing interaction in Cooper channel in antiadiabatic limit, as we have seen above (cf. also Gor'kov's paper [10]), takes place at the energies $\sim E_F$, in weak approximation (supported by our estimates) possible vertex corrections are irrelevant and for T_c we can use the usual expression of BCS theory (50), which was also stressed in [10]. The small value of E_F in FeSe/STO system leads to the conclusion, that the only interaction with antiadiabatic phonons of STO is insufficient to explain the experimentally observed values of T_c, as far as we limit ourselves to weak coupling approximation ant the value of λ dies not exceed 0.25. In this case it is necessary to take into account two pairing mechanisms, those responsible for the formation of initial T_{c0} in the bulk FeSe (phonons or spin fluctuations in FeSe) and those enhancing the pairing due interaction with optical phonons of STO. Appropriate estimates of T_c, performed in [8, 10] are in reasonable agreement with experiments on FeSe/STO, with no use of the ideas on pairing mechanisms with "forward" scattering. At the same time, our analysis show, that the expression for T_c like Eq. (50), which formally has the form of weak coupling approximation of BCS theory, in reality "works" (in the limit of strong nonadiabaticity) also for large enough values of λ, at least up to $\lambda \sim 1$, when polaronic effects become relevant. Correspondingly, to explain the experimentally observed values of T_c in FeSe/STO it may be sufficient to deal only with electron interactions with optical phonons of STO, as far as the values of $\lambda \sim 0.5$ can be realized in this system. However, the realization of such large values of coupling constant here seems rather doubtful in the light of our discussion above (cf. also the results of first—principles calculations of λ in [23]).

The separate question, which remained outside our discussion, is the account of direst Coulomb repulsion. In standard Eliashberg–McMillan theory, in adiabatic approximation, when the frequency of phonons is orders of magnitude smaller, than Fermi energy, this repulsion enters via Coulomb pseudopo-

tential $\mu^\star$ which is significantly suppressed by Tolmachev logarithm [2]. In antiadiabatic situation this mechanism of suppression does not operate, which creates additional difficulties for realization of superconductivity. In general, the problem of the possible role of Coulomb repulsion in antiadiabatic regime of electron–phonon coupling deserves serious further studies.

This work was partially supported by RFBR grant no. 17-02-00015 and the Program of Fundamental Research of the Presidium of the Russian Academy of Sciences no. 12 "Fundamental problems of high-temperature superconductivity."

REFERENCES

1. D. J. Scalapino, in *Superconductivity*, Ed. by R. D. Parks (Marcel Dekker, New York, 1969), p. 449.
2. S. V. Vonsovsky, Yu. A. Izyumov, and E. Z. Kurmaev, *Superconductivity of Transition Metals, Their Alloys and Compounds* (Nauka, Moscow, 1977; Springer, Berlin, Heidelberg, 1982).
3. P. B. Allen and B. Mitrović, *Solid State Physics*, Ed. by F. Seitz, D. Turnbull, and H. Ehrenreich (Academic, New York, 1982), Vol. 37, p. 1
4. L. P. Gor'kov and V. Z. Kresin, Rev. Mod. Phys. **90**, 011001 (2018)
5. A. B. Migdal, Sov. Phys. JETP **7**, 996 (1958).
6. A. S. Alexandrov and A. B. Krebs, Phys. Usp. **35**, 345 (1992).
7. I. Esterlis, B. Nosarzewski, E. W. Huang, D. Moritz, T. P. Devereux, D. J. Scalapino, and S. A. Kivelson, Phys. Rev. B 97, 140501(R) (2018)
8. M. V. Sadovskii, Phys. Usp. **51**, 1243 (2008).
9. L. P. Gor'kov, Phys. Rev. B **93**, 054517 (2016)
10. L. P. Gor'kov, Phys. Rev. B **93**, 060507 (2016)
11. J. R. Schrieffer, *Theory of Superconductivity* (Fizmatlit, Moscow, 1968; W. A. Benjamin, New York, 1964).
12. M. V. Sadovskii, *Diagrammatics* (ICS, Moscow, Izhevsk, 2010; World Scientific, Singapore, 2006).
13. P. B. Allen, Phys. Rev. B **6**, 2577 (1972)
14. M. Kulić, AIP Conf. Proc. **715**, 75 (2004) arXiv:1712.06222
15. J. J. Lee, F. T. Schmitt, R. G. Moore, S. Johnston, Y. T. Cui, W. Li, Z. K. Liu, M. Hashimoto, Y. Zhang, D. H. Lu, T. P. Devereaux, D. H. Lee, and Z. X. Shen, Nature (London, U.K.) **515**, 245 (2014)
16. O. V. Danylenko, O. V. Dolgov, M. L. Kulic[acute], and V. Oudovenko, Eur. J. Phys. B **9**, 201 (1999)
17. M. L. Kulic[acute], AIP Conf. Proc. **715**, 75 (2004)
18. L. Rademaker, Y. Wang, T. Berlijn, and S. Johnston, New J. Phys. **18**, 022001 (2016)
19. Y. Wang, K. Nakatsukasa, L. Rademaker, T. Berlijn, and S. Johnston, Supercond. Sci. Technol. **29**, 054009 (2016)
20. I. A. Nekrasov, N. S. Pavlov, and V. V. Sadovskii, JETP Lett. **105**, 370 (2017).
21. I. A. Nekrasov, N. S. Pavlov, and M. V. Sadovskii, J. Exp. Theor. Phys. **126**, 485 (2018).
22. Fengmiao Li and G. A. Sawatzky, Phys. Rev. Lett. **120**, 237001 (2018)
23. Y. Wang, A. Linscheid, T. Berlijn, and S. Johnson, Phys. Rev. B **93**, 134513 (2016)
24. M. A. Ikeda, A. Ogasawara, and M. Sugihara, Phys. Lett. A **170**, 319 (1992)

ISSN 0021-3640, JETP Letters, 2019, Vol. 109, No. 3, pp. 166–170. © Pleiades Publishing, Inc., 2019.
Published in Russian in Pis'ma v Zhurnal Eksperimental'noi i Teoreticheskoi Fiziki, 2019, Vol. 109, No. 3, pp. 165–169.

CONDENSED MATTER

Antiadiabatic Phonons, Coulomb Pseudopotential, and Superconductivity in Eliashberg–McMillan Theory[1]

M. V. Sadovskii*

Institute for Electrophysics, Ural Branch, Russian Academy of Sciences, Yekaterinburg, 620016 Russia

**e-mail: sadovski@iep.uran.ru*

Received November 26, 2018; revised November 26, 2018; accepted November 28, 2018

The influence of antiadiabatic phonons on the superconducting transition temperature is considered within Eliashberg–McMillan approach in the model of discrete set of (optical) phonon frequencies. A general expression for superconducting transition temperature T_c is proposed, which is valid in situation, when one (or several) of such phonons becomes antiadiabatic. We study the contribution of such phonons into the Coulomb pseudopotential μ^*. It is shown that antiadiabatic phonons do not contribute to Tolmachev's logarithm and its value is determined by partial contributions from adiabatic phonons only. The results obtained are discussed in the context of the problem of an unusually high superconducting transition temperature of the FeSe monolayer on STO.

DOI: 10.1134/S0021364019030044

1. INTRODUCTION

The most developed approach to description of superconductivity in the system of electrons and phonons is Eliashberg–McMillan theory [1–4]. It is well known that this theory is completely based on the applicability of adiabatic approximation and Migdal theorem [5], which allows neglecting vertex corrections in calculations of the effects of electron–phonon interaction in typical metals. The real small parameter of perturbation theory is $\lambda\frac{\Omega_0}{E_F} \ll 1$, where λ is the dimensionless electron–phonon coupling constant, Ω_0 is the characteristic phonon frequency, and E_F is the Fermi energy of the electrons. In particular, this leads to a conclusion that vertex corrections in this theory can be neglected even for $\lambda > 1$, because of the validity of inequality $\frac{\Omega_0}{E_F} \ll 1$ characteristic of typical metals.

In a recent paper [6] we have shown that under the conditions of strong nonadiabaticity, when $\Omega_0 \gg E_F$, a new small parameter appears in the theory $\lambda_D \sim \lambda\frac{E_F}{\Omega_0} \sim \lambda\frac{D}{\Omega_0} \ll 1$ (D is the half-width of electron band), so that corrections to electronic spectrum become irrelevant and vertex correction can be similarly neglected [7]. In general case, the renormalization of electronic spectrum (effective mass of an electron) is determined by the new dimensionless constant $\tilde{\lambda}$, which reduces to the usual λ in adiabatic limit, while in the strong antiadiabatic limit it tends to λ_D. At the same time, the superconducting transition temperature T_c in antiadiabatic limit is determined by Eliashberg–McMillan pairing coupling constant λ, while the pre-exponential factor in the expression for T_c, which is of the typical weak-coupling form, is determined by band half-width (Fermi energy). For the case of the interaction with a single optical phonon in [6] we obtained the unified expression for T_c, valid both in adiabatic and antiadiabatic regimes, and producing a smooth interpolation in the intermediate region.

In [6] we also noted that the presence of high phonon frequencies of the order of or even exceeding the Fermi energy, leads to the obvious suppression of Tolmachev's logarithm in the expression for Coulomb pseudopotential μ^*, which creates additional difficulties for the realization of superconducting state in the system with antiadiabatic phonons.

The interest to this problem is stimulated by the discovery of a number superconductors, where adiabatic approximation is not valid, while characteristic phonon frequencies are of the order of or even higher than Fermi energy of electrons. Most typical in this sense are intercalated systems with monolayers of FeSe, as well as monolayers of FeSe on $Sr(Ba)TiO_3$ (and similar) substrates (FeSe/STO) [8]. For the first time, the nonadiabatic character of superconductivity in FeSe/STO was noted by Gor'kov [9, 10], while discussing the idea of possible mechanism of the

[1] The article is published in the original.

enhancement of superconducting transition temperature T_c in FeSe/STO system due to interaction with high-energy optical phonons of $SrTiO_3$ [8].

In this work, we consider the generalized model with discrete set of the frequencies of (optical) phonons, part of which may be andiabatic. We obtain the general expressions for T_c, valid both in adiabatic and antiadiabatic limits. We also present the general analysis of the problem of the Coulomb pseudopotential in such model. The results obtained are used for simple estimates of T_c in situation typical for FeSe/STO.

2. SUPERCONDUCTING TRANSITION TEMPERATURE

Linearized Eliashberg equations, determining superconducting transition temperature T_c, written in real frequencies representation, have the following form [2]:

$$[1 - Z(\varepsilon)]\varepsilon = \int_0^D d\varepsilon' \int_0^\infty d\omega \alpha^2(\omega) F(\omega) f(-\varepsilon') \cdot \left(\frac{1}{\varepsilon' + \varepsilon + \omega + i\delta} - \frac{1}{\varepsilon' - \varepsilon + \omega - i\delta} \right), \quad (1)$$

$$Z(\varepsilon)\Delta(\varepsilon) = \int_0^D \frac{d\varepsilon'}{\varepsilon'} \tanh \frac{\varepsilon'}{2T_c} \mathrm{Re}\Delta(\varepsilon') \cdot \int_0^\infty d\omega \alpha^2(\omega) F(\omega) \cdot \left(\frac{1}{\varepsilon' + \varepsilon + \omega + i\delta} + \frac{1}{\varepsilon' - \varepsilon + \omega - i\delta} \right). \quad (2)$$

Here, $\Delta(\omega)$ is the gap function of a superconductor, $Z(\omega)$ is the electron mass renormalization function, and $f(\varepsilon)$ is the Fermi distribution function. In difference with the standard approach [2], we have introduced the finite integration limits, determined by the (half)bandwidth D. In the following we assume the half–filled band of degenerate electrons in two dimensions, so that $D = E_F \gg T_c$, with constant density of states. For simplicity, we first neglect the contribution of direct Coulomb repulsion. In these (integral) equations $\alpha^2(\omega)$ represents Eliashberg–McMillan function, determining the strength electron–phonon interaction, and $F(\omega)$ is the phonon density of states. The Eliashberg–McMillan coupling constant is defined as:

$$\lambda = 2\int_0^\infty \frac{d\omega}{\omega} \alpha^2(\omega) F(\omega). \quad (3)$$

The details concerning its calculation for systems with nonadiabatic phonons were discussed in details in [6].

Situation is considerably simplified [6], if we consider these equations in the limit of $\varepsilon \to 0$ and look for the solutions $Z(0) = Z$ and $\Delta(0) = \Delta$. Then, from Eq. (1) we obtain:

$$[1 - Z]\varepsilon = -2\varepsilon \int_0^\infty d\omega \alpha^2(\omega) F(\omega) \frac{D}{\omega(\omega + D)} \quad (4)$$

or

$$Z = 1 + \tilde{\lambda} \quad (5)$$

where

$$\tilde{\lambda} = 2\int_0^\infty \frac{d\omega}{\omega} \alpha^2(\omega) F(\omega) \frac{D}{\omega + D}, \quad (6)$$

which for $D \to \infty$ reduces to the usual Eliasberg–McMillan constant (3), while for D significantly smaller than characteristic phonon frequencies it gives the "antiadiabatic" coupling constant:

$$\lambda_D = 2D\int \frac{d\omega}{\omega^2} \alpha^2(\omega) F(\omega). \quad (7)$$

Equation (6) describes smooth transition between the limits of wide and narrow conduction bands. Mass renormalization is, in general case, determined exclusively by constant $\tilde{\lambda}$:

$$m^\star = m(1 + \tilde{\lambda}). \quad (8)$$

In the limit of strong nonadiabaticity, this renormalization is quite small and determined by the limiting expression λ_D [6].

From Eq. (2) in the limit of $\varepsilon \to 0$ and using (5), we immediately obtain the following expression for T_c:

$$1 + \tilde{\lambda} = 2\int_0^\infty d\omega \alpha^2(\omega) F(\omega) \int_0^D \frac{d\varepsilon'}{\varepsilon'(\varepsilon' + \omega)} \tanh \frac{\varepsilon'}{2T_c}. \quad (9)$$

Consider now the situation with discrete set of phonon modes (dispersionless, Einstein phonons). In this case, the phonon density of states is written as:

$$F(\omega) = \sum_i \delta(\omega - \omega_i), \quad (10)$$

where ω_i are discrete frequencies modeling the optical branches of the phonon spectrum. Then, from Eqs. (3) and (6) we have:

$$\lambda = 2\sum_i \frac{\alpha^2(\omega_i)}{\omega_i} \equiv \sum_i \lambda_i, \quad (11)$$

$$\tilde{\lambda} = 2\sum_i \frac{\alpha^2(\omega_i) D}{\omega_i(\omega_i + D)} = 2\sum_i \lambda_i \frac{D}{\omega_i + D} \equiv \sum_i \tilde{\lambda}_i. \quad (12)$$

Correspondingly, in this case:

$$\alpha^2(\omega)F(\omega) = \sum_i \alpha^2(\omega_i)\delta(\omega - \omega_i) = \sum_i \frac{\lambda_i}{2}\omega_i\delta(\omega - \omega_i). \quad (13)$$

The standard Eliashberg equation (in adiabatic limit) for such model were consistently solved in [11]. For our purposes, it is sufficient to analyze only Eq. (9), which takes now the following form:

$$1 + \tilde{\lambda} = 2\sum_i \alpha^2(\omega_i)\int_0^D \frac{d\varepsilon'}{\varepsilon'(\varepsilon' + \omega_i)}\tanh\frac{\varepsilon'}{2T_c}. \quad (14)$$

Solving Eq. (14), we obtain:

$$T_c \sim \prod_i \left(\frac{D}{1 + \frac{D}{\omega_i}}\right)^{\frac{\lambda_i}{\lambda}} \exp\left(-\frac{1 + \tilde{\lambda}}{\lambda}\right). \quad (15)$$

For the case of two optical phonons with frequencies ω_1 and ω_2 we have:

$$T_c \sim \left(\frac{D}{1 + \frac{D}{\omega_1}}\right)^{\frac{\lambda_1}{\lambda}} \left(\frac{D}{1 + \frac{D}{\omega_2}}\right)^{\frac{\lambda_2}{\lambda}} \exp\left(-\frac{1 + \tilde{\lambda}}{\lambda}\right), \quad (16)$$

where $\tilde{\lambda} = \tilde{\lambda}_1 + \tilde{\lambda}_2$ and $\lambda = \lambda_1 + \lambda_2$. For the case of $\omega_1 \ll D$ (adiabatic phonon), and $\omega_2 \gg D$ (antiadiabatic phonon) Eq. (16) is immediately reduced to:

$$T_c \sim (\omega_1)^{\frac{\lambda_1}{\lambda}}(D)^{\frac{\lambda_2}{\lambda}} \exp\left(-\frac{1 + \tilde{\lambda}}{\lambda}\right). \quad (17)$$

Here, we can see that the frequency of antiadiabatic phonon in the pre-exponential factor is replaced by band half-width (Fermi energy), which plays a role of cutoff for logarithmic divergence in Cooper channel in antiadiabatic limit [6, 9, 10].

The general result (15) gives the unified expression for T_c for the discrete set of optical phonons, valid in both adiabatic and antiadiabatic regimes and interpolating between these limit in intermediate region.

3. COULOMB PSEUDOPOTENTIAL

Above, we had neglected the direct Coulomb repulsion of electrons, which in the standard approach [1–3] is described by the Coulomb pseudopotential μ^*, which is effectively suppressed by large Tolmachev's logarithm. As noted in [6] antiadiabatic phonons suppress Tolmachev's logarithm, which apparently leads to a sufficient suppression of the superconducting transition temperature. To clarify this situation let us consider the simplified version of integral equation for the gap (2), writing it as:

$$Z(\varepsilon)\Delta(\varepsilon) = \int_0^D d\varepsilon' K(\varepsilon, \varepsilon')\frac{1}{\varepsilon'}\tanh\frac{\varepsilon'}{2T_c}\Delta(\varepsilon'), \quad (18)$$

where the integral kernel we write as a combination of two-step functions:

$$K(\varepsilon, \varepsilon') = \lambda\theta(\tilde{D} - |\varepsilon|)\theta(\tilde{D} - |\varepsilon'|) - \mu\theta(D - |\varepsilon|)\theta(D - |\varepsilon'|), \quad (19)$$

where μ is the dimensionless (repulsive) Coulomb potential, while the parameter $\tilde{D}$, determining the energy width of attraction region due to phonons is determined by pre-exponential factor of Eq. (15):

$$\tilde{D} = \prod_i \left(\frac{D}{1 + \frac{D}{\omega_i}}\right)^{\frac{\lambda_i}{\lambda}}. \quad (20)$$

Note that we always have $\tilde{D} < D$. Equation (18) is now rewritten as:

$$Z(\varepsilon)\Delta(\varepsilon) = (\lambda - \mu)\int_0^{\tilde{D}} \frac{d\varepsilon'}{\varepsilon'}\tanh\frac{\varepsilon'}{2T_c}\Delta(\varepsilon') - \mu\int_{\tilde{D}}^D \frac{d\varepsilon'}{\varepsilon'}\Delta(\varepsilon'). \quad (21)$$

Writing the mass renormalization due to phonons as:

$$Z(\varepsilon) = \begin{cases} 1 + \tilde{\lambda} & \text{for} \quad \varepsilon < \tilde{D}, \\ 1 & \text{for} \quad \varepsilon > \tilde{D}, \end{cases} \quad (22)$$

we look for the solution of Eq. (18) for $\Delta(\varepsilon)$, as usual, also in the two-step form [1–3]:

$$\Delta(\varepsilon) = \begin{cases} \Delta_1 & \text{for} \quad \varepsilon < \tilde{D}, \\ \Delta_2 & \text{for} \quad \varepsilon > \tilde{D}. \end{cases} \quad (23)$$

Then, Eq. (21) transforms to the system of two homogeneous linear equations for constants Δ_1 and Δ_2:

$$(1 + \tilde{\lambda})\Delta_1 = (\lambda - \mu)\ln\frac{\tilde{D}}{T_c}\Delta_1 - \mu\ln\frac{D}{\tilde{D}}\Delta_2,$$
$$\Delta_2 = -\mu\ln\frac{\tilde{D}}{T_c}\Delta_1 - \mu\ln\frac{D}{\tilde{D}}\Delta_2 \quad (24)$$

with the condition for nontrivial solution taking the form:

$$1 + \tilde{\lambda} = \left(\lambda - \frac{\mu}{1 + \mu\ln\frac{D}{\tilde{D}}}\right)\ln\frac{\tilde{D}}{T_c}. \quad (25)$$

Correspondingly, for the transition temperature we get:

$$T_c = \tilde{D}\exp\left(-\frac{1 + \tilde{\lambda}}{\lambda - \mu^*}\right), \quad (26)$$

where the Coulomb pseudopotential is determined by the expression

$$\mu^* = \frac{\mu}{1 + \mu\ln\frac{D}{\tilde{D}}} = \frac{\mu}{1 + \mu\ln\prod_i\left(1 + \frac{D}{\omega_i}\right)^{\frac{\lambda_i}{\lambda}}}. \quad (27)$$

Thus, the phonon frequencies enter Tolmachev's logarithm as the product of partial contributions, with values determined also by corresponding coupling constants. Similar structure of Tolmachev's logarithm was first obtained (in somehow different model) in [12], where the case of frequencies going outside the limits of adiabatic approximation was not considered. In this sense, Eq. (27) has a wider region of applicability. In particular, for the model of two optical phonons with frequencies $\omega_1 \ll D$ (adiabatic phonon) and $\omega_2 \gg D$, from Eq. (27) we get:

$$\mu^* = \frac{\mu}{1+\mu\ln\left(\frac{D}{\omega_1}\right)^{\frac{\lambda_1}{\lambda}}} = \frac{\mu}{1+\mu\frac{\lambda_1}{\lambda}\ln\frac{D}{\omega_1}}. \qquad (28)$$

We can see that the contribution of antiadiabatic phonon drops out of Tolmachev's logarithm, while the logarithm itself remains, with its value determined by the ratio of the band half-width (Fermi energy) to the frequency of adiabatic (low frequency) phonon. The general effect of suppression of Coulomb repulsion also remains, though it becomes weaker proportionally to the partial interaction of electrons with corresponding phonon. This situation is conserved also in the general case, where Tolmachev's logarithm and corresponding Coulomb pseudopotential are determined by contributions of adiabatic phonons, while antiadiabatic phonons drops out. Thus, in general case, situation becomes more favorable for superconductivity, as compared to the case of a single antiadiabatic phonon, considered in [6].

4. CONCLUSIONS

To summarize, we have considered the electron–phonon coupling in Eliashberg–McMillan theory in situation, when antiadiabatic phonons with high enough frequency (comparable or exceeding the Fermi energy E_F) are present in the system. The value of mass renormalization, in general case, is determined by the coupling constant $\tilde{\lambda}$, while the value of the pairing interaction is always determined by the standard coupling constant λ of Eliashberg–McMillan theory, appropriately generalized by taking into account the finite value of phonon frequency [6]. Mass renormalization due to antiadiabatic phonons is small and determined by the coupling constant $\lambda_D \ll \lambda$. In this sense, in the limit of strong antiadiabaticity, the coupling of such phonons with electrons becomes weak and corresponding vertex correction are irrelevant [7], similarly to the case of adiabatic phonons [5]. Precisely this this fact allows us to use Eliashberg–McMillan approach in the limit of strong antiadiabaticity. In the intermediate region all expressions proposed above are of interpolating nature and for more deep understanding of this region we have to use other approaches (see, e.g., [13, 14]).

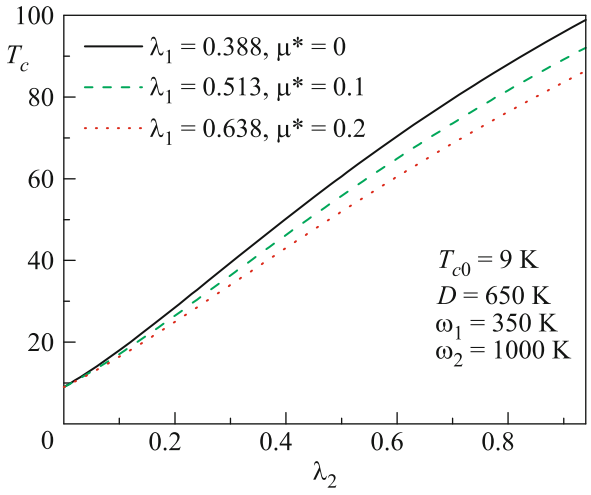

Fig. 1. (Color online) Superconducting transition temperature versus the coupling constant with a high-energy phonon for the typical parameters of the FeSe/STO system.

The cutoff of pairing interaction in Cooper channel in antiadiabatic limit takes place at energies $\sim E_F$, as was previously noted in [6, 9, 10]), so that corresponding phonons do not contribute to Tolmachev's logarithm in Coulomb pseudopotential, though large enough values of this logarithm (and corresponding smallness of μ^*) can be guaranteed due to contributions from adiabatic phonons.

Note that above we have used rather simplified analysis of Eliashberg equations. However, in our opinion, more elaborate approach, e.g., along the lines of [11], will not lead to qualitative change of our results.

In conclusion, let us discuss the current results in the context of possible explanation of high-temperature superconductivity in a monolayer of FeSe on Sr(Ba)TiO_3 (FeSe/STO) [8]. The presence in Sr(Ba)TiO_3 of high-energy optical phonons indicates the possibility of significant enhancement of T_c in this system due to interactions of FeSe electrons with these phonons on FeSe/STO interface [8, 15]. ARPES experiments [15] and LDA + DMFT calculations [16, 17] have shown that Fermi energy E_F in this system is significantly (practically two times) lower than the energy of the optical phonon, which unambiguously indicates the realization, in this case, of antiadiabatic situation [9, 10]. Let us look if we can explain the observed high values of T_c in this system using the expressions derived in this work. Assuming for FeSe on STO the characteristic value of phonon frequency $\omega_1 = 350$ K, Fermi energy $E_F = D = 650$ K, and the energy of the optical phonon in $SrTiO_3$ $\omega_2 = 1000$ K [8, 15], we calculate T_c using Eqs. (16), (26) (the case two phonon frequencies), considering μ^* as a free

model parameter. Let us choose the value of λ_1 to obtain, in the absence of interactions with high-energy phonon of STO, the value of $T_c = 9$ K, typical for the bulk FeSe, which gives $\lambda_1 > 0.4$. Results of our calculations are shown in Fig. 1. We can see that the experimentally observed [8] high values of $T_c \sim 60$–80 K can be obtained only for large enough values of the coupling constant of FeSe electrons with high-energy optical phonon of STO $\lambda_2 > 0.5$, so that the total pairing coupling constant $\lambda = \lambda_1 + \lambda_2 > 0.9$. Strictly speaking, such values of the coupling constants cannot be considered something unusual. However, the appearance of these large values in FeSe/STO system seems rather improbable in the light of qualitative estimates of λ for nonadiabatic case in [6], as well as the results of ab initio calculations of λ for this system [18]. Note also that the values of the parameters used here for FeSe/STO belong to the intermediate region between adiabatic or nonadiabatic regions, where our expressions, as was stressed above, are of interpolating nature. Variation of the values of these parameters in relatively wide range does not lead to the qualitative change of our results. Traditionally low values of μ^* used here, cannot be obtained for the assumed values of $D = E_F$, ω_l and coupling constants from expressions like (28) with usual values of μ, due to rather small values of corresponding Tolmachev's logarithm.

I am grateful to E.Z. Kuchinskii for discussions and help with numerical calculations. This work was partially supported by the Russian Foundation for Basic Research (project no. 17-02-00015) and by the Presidium of the Russian Academy of Sciences (program of basic research no. 12 "Fundamental Problems of High-Temperature Superconductivity").

REFERENCES

1. D. J. Scalapino, in *Superconductivity,* Ed. by R. D. Parks (Marcel Dekker, New York, 1969), p. 449.
2. S. V. Vonsovsky, Yu. A. Izyumov, and E. Z. Kurmaev, *Superconductivity of Transition Metals, Their Alloys and Compounds* (Nauka, Moscow, 1977; Springer, Berlin, Heidelberg, 1982).
3. P. B. Allen and B. Mitrović, *Solid State Physics,* Ed. by F. Seitz, D. Turnbull, and H. Ehrenreich (Academic, New York, 1982), p. 1.
4. L. P. Gor'kov and V. Z. Kresin, Rev. Mod. Phys. **90**, 011001 (2018).
5. A. B. Migdal, Sov. Phys. JETP **7**, 996 (1958).
6. M. V. Sadovskii, J. Exp. Theor. Phys. **128** (2019, in press); arXiv:1809.02531.
7. M. A. Ikeda, A. Ogasawara, and M. Sugihara, Phys. Lett. A **170**, 319 (1992).
8. M. V. Sadovskii, Phys. Usp. **51**, 1243 (2008).
9. L. P. Gor'kov, Phys. Rev. B **93**, 054517 (2016).
10. L. P. Gor'kov, Phys. Rev. B **93**, 060507 (2016).
11. A. E. Karakozov, E. G. Maksimov, and S. A. Mashkov, Sov. Phys. JETP **41**, 971 (1975).
12. D. A. Kirzhnits, E. G. Maksimov, and D. I. Khomskii, J. Low. Temp. Phys. **10**, 79 (1973).
13. L. Pietronero, S. Strässler, and C. Grimaldi, Phys. Rev. B **52**, 10516 (1995).
14. C. Grimaldi, L. Pietronero, and S. Strässler, Phys. Rev. B **52**, 10530 (1995).
15. J. J. Lee, F. T. Schmitt, R. G. Moore, S. Johnston, Y. T. Cui, W. Li, Z. K. Liu, M. Hashimoto, Y. Zhang, D. H. Lu, T. P. Devereaux, D. H. Lee, and Z. X. Shen, Nature (London, U. K.) **515**, 245 (2014).
16. I. A. Nekrasov, N. S. Pavlov, and M. V. Sadovskii, JETP Lett. **105**, 370 (2017).
17. I. A. Nekrasov, N. S. Pavlov, and M. V. Sadovskii, J. Exp. Theor. Phys. **126**, 485 (2018).
18. Y. Wang, A. Linscheid, T. Berlijn, and S. Johnson, Phys. Rev. B **93**, 134513 (2016).

ISSN 0021-3640, JETP Letters, 2020, Vol. 111, No. 3, pp. 188–192. © Pleiades Publishing, Inc., 2020.
Published in Russian in Pis'ma v Zhurnal Eksperimental'noi i Teoreticheskoi Fiziki, 2020, Vol. 111, No. 3, pp. 203–208.

CONDENSED MATTER

On the Planckian Limit for Inelastic Relaxation in Metals

M. V. Sadovskii*

Institute for Electrophysics, Ural Branch, Russian Academy of Sciences, Yekaterinburg, 620016 Russia
**e-mail: sadovski@iep.uran.ru*

Received January 5, 2020; revised January 5, 2020; accepted January 5, 2020

We consider the simplest model for temperature-linear growth of the resistivity in metals. It is shown that the so-called "Planckian" limit for the temperature dependent relaxation rate of electrons follows from a certain procedure for representation of experimental data on the resistivity and, in this sense, is a kind of delusion.

DOI: 10.1134/S0021364020030029

Linear with temperature growth of electrical resistivity in cuprates and some other correlated systems in a wide region from very low to pretty high temperatures for many years remains one of the major puzzles of the physics of high-temperature superconductors. In recent years, a number of interesting papers appeared [1, 2], where by the analysis of experiments on rather wide range of compounds, it was shown that in the T-linear region of resistivity growth, the scattering rate of electrons (inverse relaxation time) with rather high accuracy is described as $\Gamma = \frac{1}{\tau} = \alpha\frac{k_B T}{\hbar}$, where $\alpha \sim 1$ and is weakly depending on the choice of the material. In particular, for systems being close to a quantum critical point (on the phase diagram of cuprates and some other similar systems) α belongs to the interval 0.7–1.1. More so, a similar dependence describes rather well the data for a number of usual metals (Cu, Au, Al, Ag, Pb, Nb, etc.) in the region of T-linear growth of the resistivity (which is usually realized at temperatures $T > \Theta_D/5$, where Θ_D is the Debye temperature). In this case, α covers a significantly wider interval from 0.7 to 2.7 [1, 2]. In connection with these (and some similar) results the notion of the universal (independent of interaction strength) "Planckian" *upper* limit of scattering rate was introduced $\frac{1}{\tau_P} = \Gamma_P = \frac{k_B T}{\hbar}$ [3]. To explain this temperature behavior of the resistivity for such different systems, also starting from very low temperatures, up to now a number of relatively complicated theoretical models were proposed [4–7], including some rather exotic, based on the analogies taken from black hole physics, cosmology and superstring theory (e.g., see [8–11]). In usual metals, the temperature dependence of the resistivity (conductivity) is almost completely related to inelastic scattering of electrons by phonons. In usual metals at high enough temperatures $T > \Theta_D/5$, it dominates and leads to T-linear growth of the resistivity

$$\rho(T) - \rho_0 = AT, \tag{1}$$

where ρ_0 is the residual resistivity at $T = 0$ due to the scattering by random impurities.

In terms of the conductivity, we may write the simple Drude expression

$$\sigma(T) = \sigma_0 + \sigma(T), \tag{2}$$

where σ_0 is the residual conductivity at $T = 0$ and

$$\sigma(T) = \frac{ne^2}{m}\tau(T) = \frac{ne^2}{m}\Gamma^{-1}(T). \tag{3}$$

Here and below, m is understood to be the *band* effective mass, while $\Gamma(T) = \frac{1}{\tau(T)}$ is the temperature dependent relaxation (scattering) rate due to inelastic scattering of electrons by phonons, which grows linearly with temperature for $T > 0.2\Theta_D$. Correspondingly, we obtain the resistivity as

$$\rho(T) - \rho_0 = \frac{m}{ne^2}\Gamma(T). \tag{4}$$

The concept of the Planckian relaxation rate can be introduced via elementary estimates [9]. At $T > 0$, the processes of inelastic scattering appear due to different interactions (electron–phonon, spin fluctuations, quantum fluctuation of arbitrary origin). In particular, these processes are responsible for thermodynamic equilibrium of electronic subsystem leading to Fermi distribution. The conductivity of a metal (degenerate case) is determined by electrons distributed in a layer of the width $\sim k_B T$ around the Fermi level (chemical potential).

Let us perform elementary estimates using the energy–time uncertainty relation

$$\Delta E\tau > \hbar, \tag{5}$$

where τ is the lifetime of a quantum state and ΔE is its energy uncertainty. Naturally, in our case $\tau = \tau(T)$, while $\Delta E \sim k_B T$, which immediately leads to an estimate

$$\Gamma(T) = \frac{1}{\tau(T)} < \alpha\frac{k_B T}{\hbar} \equiv \alpha\Gamma_P = \frac{\alpha}{\tau_P}, \tag{6}$$

where $\alpha \sim 1$. We conclude that, according to such an elementary estimate, the Planckian relaxation rate determines precisely the *upper* limit for the resistivity due to inelastic scatterings:

$$\rho(T) - \rho_0 = \frac{m}{ne^2}\Gamma(T) < \frac{m}{ne^2}\alpha\frac{k_B T}{\hbar} \equiv \alpha\rho_P(T). \tag{7}$$

However, it is obvious that this estimate is of rather speculative nature for the system of many interacting particles.

Consider the following Hamiltonian for interaction of metallic electrons with arbitrary quantum Bose-type fluctuations:[1]

$$H_{\text{int}} = \frac{1}{N}\sum_{\mathbf{pq}} g_{\mathbf{q}} a^+_{\mathbf{p+q}} a_{\mathbf{p}} \rho_{\mathbf{q}}. \tag{8}$$

Here we use the standard notations for creation and annihilation operators of electrons, $\rho_{\mathbf{q}}$ is the quantum fluctuation operator of "any kind" (e.g., the ion density in a lattice), $g_{\mathbf{q}}$ is the appropriate coupling constant (matrix element of interaction potential) [12, 13]. Let us introduce the appropriate (Matsubara) Green's function as

$$F(\mathbf{q},\tau) = -\left\langle T_\tau \rho_{\mathbf{q}}(\tau)\rho^+_{\mathbf{q}}(0)\right\rangle. \tag{9}$$

For this function, we can write the standard (Bose) spectral representation [14]

$$F(\mathbf{q}, i\omega_m) = \int_{-\infty}^{\infty} d\omega \frac{A(\mathbf{q},\omega)}{i\omega_m - \omega}, \tag{10}$$

where $\omega_m = 2\pi m T$ and the spectral density is defined as

$$A(\mathbf{q},\omega) = Z^{-1}\sum_{mn} e^{-\frac{E_n}{T}} |(\rho_{\mathbf{q}})_{nm}|^2 (1 - e^{-\frac{\omega_{mn}}{T}})\delta(\omega - \omega_{mn}), \tag{11}$$

where $\omega_{mn} = E_m - E_n$, $(\rho_{\mathbf{q}})_{nm} = \langle n|\rho_{\mathbf{q}}|m\rangle = (\rho^+_{\mathbf{q}})_{mn}$.

The dynamic structure factor of fluctuations is defined as [12, 13]

$$S(\mathbf{q},\omega) = Z^{-1}\sum_{mn} e^{-\frac{E_n}{T}} |(\rho_{\mathbf{q}})_{nm}|^2 \delta(\omega - \omega_{mn}). \tag{12}$$

[1] Below, we assume that $\hbar = k_B = 1$.

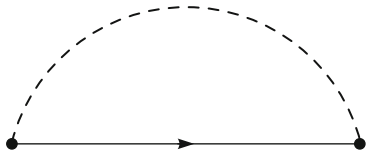

Fig. 1. Diagram of the second order for the electron self-energy, where the dashed line is the Green's function of quantum fluctuations F and the solid line is the electron Green's function G.

Comparing Eqs. (11) and (12), we obtain

$$A(\mathbf{q},\omega) = S(\mathbf{q},\omega)\left[1 - e^{-\frac{\omega}{T}}\right]. \tag{13}$$

Electronic Green's function in the Matsubara representation is written as

$$G(\varepsilon_n, \mathbf{p}) = \frac{1}{i\varepsilon_n - \xi_{\mathbf{p}} - \Sigma(\varepsilon_n, \mathbf{p})}, \tag{14}$$

where $\varepsilon_n = (2n+1)\pi T$ and $\xi_{\mathbf{p}}$ is the electronic spectrum measured from the chemical potential. Assuming the validity of Migdal's theorem [15] we can take the electron self-energy in the simplest approximation, shown in Fig. 1:

$$\begin{aligned}\Sigma(\varepsilon_n, \mathbf{p}) &= \frac{T}{N}\sum_{\mathbf{q}} g^2_{\mathbf{q}} \sum_m F(\mathbf{q}, i\omega_m) G(\varepsilon_n + \omega_m, \mathbf{p}+\mathbf{q}) \\ &= \frac{T}{N}\sum_{\mathbf{q}} g^2_{\mathbf{q}} \sum_m \int_{-\infty}^{\infty} d\omega \frac{S(\mathbf{q},\omega)}{i\omega_m - \omega}\left(1 - e^{-\frac{\omega}{T}}\right) \\ &\quad \cdot \frac{1}{i\varepsilon_n + i\omega_m - \xi_{\mathbf{p+q}}}.\end{aligned} \tag{15}$$

Consider now the case where the average frequency of fluctuations $\langle\Omega\rangle$ is significantly lower than the temperature T. Then in Eq. (15) we can limit ourselves only by term with $m = 0$ and thus to the picture of *quasielastic* scattering by fluctuations:

$$\begin{aligned}\Sigma(\varepsilon_n, \mathbf{p}) &= \frac{1}{N}\sum_{\mathbf{q}} g^2_{\mathbf{q}} \sum_m \int_{-\infty}^{\infty} d\omega \frac{S(\mathbf{q},\omega)}{i\varepsilon_n - \xi_{\mathbf{p+q}}} \\ &= \sum_{\mathbf{q}} g^2_{\mathbf{q}} S(\mathbf{q}) \frac{1}{i\varepsilon_n - \xi_{\mathbf{p+q}}},\end{aligned} \tag{16}$$

where we have introduced the structure factor of fluctuations as [13]

$$S(\mathbf{q}) = \frac{1}{N}\int_{-\infty}^{\infty} d\omega S(\mathbf{q},\omega). \tag{17}$$

In fact, this is a direct analog the well-known Ziman–Edwards approximation in the theory of liquid metals. The case of $S(\mathbf{q}) = \text{const}$ corresponds to chaotic distribution of static scattering centers [15].

Fluctuation operator $\rho_{\mathbf{q}}$ for the case of some collective mode can be expressed via (boson) annihilation and creation operators for corresponding quanta (e.g., phonons) [13]:

$$\rho_{\mathbf{q}} = \frac{1}{\sqrt{2}}\left(b_{\mathbf{q}}^{+} + b_{-\mathbf{q}}\right). \tag{18}$$

Then, we have

$$S(\mathbf{q},\omega) = Z^{-1}\sum_{m} e^{-\beta E_m}\left[\langle m|b_{\mathbf{q}}\, b_{\mathbf{q}}^{+}|m\rangle\delta(\omega-\omega_{\mathbf{q}}) + \langle m|b_{-\mathbf{q}}^{+}b_{-\mathbf{q}}|m\rangle\delta(\omega+\omega_{\mathbf{q}})\right], \tag{19}$$

where $\omega_{\mathbf{q}}$ is the spectrum of corresponding excitations. Introducing the usual Bose distribution

$$n_{\mathbf{q}} = Z^{-1}\sum_{m} e^{-\beta E_m}\langle m|b_{\mathbf{q}}^{+}b_{\mathbf{q}}|m\rangle = \frac{1}{e^{\beta\omega_{\mathbf{q}}}-1} \tag{20}$$

we get [13]

$$S(\mathbf{q},\omega) = \left[(n_{\mathbf{q}}+1)\delta(\omega-\omega_{\mathbf{q}}) + n_{\mathbf{q}}\delta(\omega+\omega_{\mathbf{q}})\right] = \delta(\omega-\omega_{\mathbf{q}}) + n_{\mathbf{q}}\left[\delta(\omega-\omega_{\mathbf{q}}) + \delta(\omega+\omega_{\mathbf{q}})\right]. \tag{21}$$

In case of $T \gg \omega_{\mathbf{q}}$, we have

$$n_{\mathbf{q}} = \frac{T}{\omega_{\mathbf{q}}} \tag{22}$$

and, correspondingly,

$$S(\mathbf{q}) = \frac{2T}{\omega_{\mathbf{q}}}; \tag{23}$$

i.e., we obtain the structure factor linear in T and its momentum dependence is determined simply by excitation spectrum of the appropriate collective mode (fluctuation). Then,

$$\Sigma(\varepsilon_n,\mathbf{p}) = T\sum_{\mathbf{q}}\frac{2g^2}{\omega_{\mathbf{q}}}\frac{1}{i\varepsilon_n - \xi_{\mathbf{p}+\mathbf{q}}}. \tag{24}$$

To simplify the model further let us assume the spectrum of fluctuations to be dispersionless (like Einstein phonon or optical phonon with weak dispersion) $\omega_{\mathbf{q}} = \Omega_0$. Then performing all calculations similarly to the problem of an electron in the field of random impurities [15], we get

$$\Sigma(\varepsilon_n,\mathbf{p}) = -i\pi\,\mathrm{sgn}\varepsilon_n\frac{2g_0^2}{\Omega_0}N(0)T, \tag{25}$$

where $N(0)$ is the density of states at the Fermi level. Correspondingly, the scattering rate (damping) is written as

$$\frac{\Gamma(T)}{2} = \pi\frac{2g_0^2}{\Omega_0}N(0)T = \pi\lambda_0 T, \tag{26}$$

where we introduced in a standard way the dimensionless coupling constant

$$\lambda_0 = \frac{2g_0^2 N(0)}{\Omega_0}. \tag{27}$$

Now, the electronic Green's function takes the usual form [15]

$$G(i\varepsilon_n,\mathbf{p}) = \frac{1}{i\varepsilon_n - \varepsilon_{\mathbf{p}} + \frac{i}{2}\Gamma(T)\mathrm{sgn}\varepsilon_n}, \tag{28}$$

where are no renormalization factors of any kind (the residue at the pole of the Green's function $Z = 1$), which is natural for temperatures much exceeding the frequencies of quantum fluctuations.

After the standard calculations [15], we obtain the resistivity as

$$\rho(T) = \frac{m}{ne^2}\Gamma(T) = 2\pi\lambda_0\rho_{\mathrm{P}}(T), \tag{29}$$

which in essence just coincide with high-temperature limit of Eliashberg–McMillan theory [16]. The constant α used in writing down the Planckian relaxation as (6) is expressed via the parameters of the theory as

$$\alpha = 2\pi\lambda_0. \tag{30}$$

Naturally, it is not universal and is just proportional to the coupling constant.

All this is known actually for a long time and trivially explains the T-linear growth of the resistivity in accordance with many experiments. To make such resistivity growth starting from low temperatures it is sufficient to demand that $\Omega_0 \ll T$. Near the quantum critical point (of any nature), we can expect the typical "softening" of fluctuation modes like [17]

$$\Omega_0 \sim |x - x_c|^{z\nu}, \tag{31}$$

where x, for example, may denote the carrier concentration close to the critical x_c, while ν and z are the standard critical exponents of the theory of quantum phase transitions, determining the critical behavior of characteristic lengths:

$$\xi \sim |x - x_c|^{-\nu}, \quad \xi_\tau \sim |x - x_c|^{-z\nu}, \tag{32}$$

where τ is the imaginary (Matsubara) time, so that above we may just assume $\Omega_0 \sim \xi_\tau^{-1}$. This may be responsible for T-linear behavior in systems like cuprates.

We can avoid the explicit introduction of phonons (or any other quasiparticles related to fluctuations). From Eq. (13) for $\omega \ll T$, we have

$$A(\mathbf{q},\omega) \approx \frac{\omega}{T}S(\mathbf{q},\omega) \tag{33}$$

or

$$S(\mathbf{q},\omega)\approx\frac{T}{\omega}A(\mathbf{q},\omega). \quad (34)$$

Substituting this expression into Eq. (16), we get the following expression for the self-energy:

$$\Sigma(\varepsilon_n,\mathbf{p})=\frac{T}{N}\sum_{\mathbf{p}'}g^2_{\mathbf{pp}'}\int_{-\infty}^{\infty}\frac{d\omega}{\omega}\frac{A(\mathbf{p}-\mathbf{p}',\omega)}{i\varepsilon_n-\xi_{\mathbf{p}'}}, \quad (35)$$

where everything is determined by the spectral density of fluctuations $A(\mathbf{q},\omega)$, which is not necessarily of a quasiparticle form. Obviously, for the simplest model with $A(\mathbf{q},\omega)=\delta(\omega-\Omega_0)$ (Einstein model of fluctuations) from Eq. (35) we immediately obtain the previous results of Eqs. (25)–(27).

Further, let us assume that fluctuations scatter electrons in some pretty narrow layer around the Fermi surface with width determined by their characteristic frequencies ($\langle\Omega\rangle\ll T$). Then, in the spirit of the Eliashberg–McMillan theory, we can introduce the self-energy averaged over momenta at the Fermi surface:

$$\Sigma(\varepsilon_n)=\frac{1}{N(0)}\sum_{\mathbf{p}}\delta(\xi_{\mathbf{p}})\Sigma(\varepsilon_n,\mathbf{p}), \quad (36)$$

and an effective interaction averaged over the initial and final momenta at the Fermi surface:

$$\begin{aligned}&g^2_{\mathbf{pp}'}A(\mathbf{p}-\mathbf{p}',\omega)\\ \Rightarrow\ &\frac{1}{N(0)}\sum_{\mathbf{p}}\frac{1}{N(0)}\sum_{\mathbf{p}'}g^2_{\mathbf{pp}'}A(\mathbf{p}-\mathbf{p}',\omega)\delta(\xi_{\mathbf{p}})\delta(\xi_{\mathbf{p}'})\\ &\equiv\frac{1}{N(0)}\alpha^2(\omega)F(\omega),\end{aligned} \quad (37)$$

where

$$F(\omega)=\sum_{\mathbf{q}}A(\mathbf{q},\omega) \quad (38)$$

is the density of states of fluctuations. Then, for (36) from (35) we get

$$\begin{aligned}\Sigma(\varepsilon_n)&=\frac{T}{N(0)}\\ &\cdot\int_{-\infty}^{\infty}\frac{d\omega}{\omega}\alpha^2(\omega)F(\omega)N(0)\int_{-\infty}^{\infty}d\xi\frac{1}{i\varepsilon_n-\xi}\\ &=-i\pi\mathrm{sgn}\varepsilon_n T\int_{-\infty}^{\infty}\frac{d\omega}{\omega}\alpha^2(\omega)F(\omega)\\ &=-i\pi\mathrm{sgn}\varepsilon_n\lambda T\equiv-i\frac{\Gamma(T)}{2}\mathrm{sgn}\varepsilon_n,\end{aligned} \quad (39)$$

where we introduced the dimensionless coupling costant similar to that in the Eliashberg–McMillan theory:

$$\lambda=2\int_0^{\infty}\frac{d\omega}{\omega}\alpha^2(\omega)F(\omega), \quad (40)$$

which is in fact determined by (averaged according to (37)) the spectral density of fluctuations $A(\mathbf{q},\omega)$.

Then, we obtain

$$\Gamma(T)=2\pi\lambda T, \quad (41)$$

which is formally of the same form as (26) and immediately leads to (29).

In [1, 2] experimental data on resistivity were fitted to standard Drude expression (4), where the effective mass was determined from low temperature measurements (electronic specific heat and oscillation effects in high magnetic fields) which is actually related to band structure effective mass by a simple replacement $m\to\tilde{m}=m(1+\lambda)$, which explicitly takes into account renormalization due to phonons. The deficiency of such approach was already noted in [18]. Let us show that precisely this kind of representation of data creates a *delusion* of universal Planckian relaxation. In fact, Eq. (29) for the *high-temperature* limit of the resistivity can be rewritten as

$$\rho(T)=\frac{m(1+\lambda)}{ne^2}\frac{\Gamma(T)}{1+\lambda}=\frac{\tilde{m}}{ne^2}\tilde{\Gamma}(T), \quad (42)$$

where

$$\tilde{\Gamma}(T)=2\pi\frac{\lambda}{1+\lambda}T, \quad (43)$$

which reduces at $\lambda\gg1$ to

$$\tilde{\Gamma}(T)=2\pi T \quad (44)$$

and simply imitates the universal Planckian behavior of relaxation rate (6) with $\alpha=2\pi$, which is independent of coupling constant of electrons with fluctuations (phonons). The replacement $m\to\tilde{m}=m(1+\lambda)$ in Eq. (42) is correct despite the fact, that here we are dealing with the high-temperature limit as fitting the experimental data in [1, 2] was performed using the effective mass $\tilde{m}$, obtained from *low temperature* measurements, which contains renormalization effects. For quantitative estimates, it is also quite important to take into account mass renormalization due to interelectron interactions. Correspondingly, Eq. (43) should be rewritten as

$$\tilde{\Gamma}(T)=2\pi\frac{\lambda}{1+\lambda+\lambda_{ee}}T, \quad (45)$$

where λ_{ee} is a dimensionless parameter, determining mass renormalization due to electron–electron interactions. In Landau–Silin theory of Fermi liquids $\lambda_{ee}=\frac{F_1^s}{3}$, where F_1^s is the appropriate coefficient in Landau function expansion [13]. Direct DMFT calculations for the Hubbard model produce the values of renormalization factor $Z=(1+\lambda_{ee})^{-1}$ in metallic phase monotonously changing with Hubbard interaction U in the interval between 1 and 0 [19]. Thus, for

rough estimates for typical metal we can safely take $\lambda_{ee} \sim 1$. Then,

$$\alpha = \frac{2\pi\lambda}{1+\lambda+\lambda_{ee}}. \quad (46)$$

Then the interval of $\alpha = 0.7$–2.7 [1, 2] for $\lambda_{ee} = 1$ corresponds to $\lambda = 0.25$–1.5, which seems quite reasonable. For example for Al we have the calculated value $\lambda = 0.44$ [16], which immediately gives $\alpha = 1.03$ in nice correspondence with "experimental" value $\alpha = 1$ from [1]. For Pb, taking $\lambda = 1.68$ [16] we get $\alpha \sim 2.86$ in reasonable agreement with $\alpha = 2.7$ [1]. Similarly, for Nb we have $\lambda = 1.26$ [16] and $\alpha \sim 2.42$, also in good agreement with $\alpha = 2.3$ of [1]. In general, taking into account the roughness of our estimate of $\lambda_{ee} \sim 1$ this agreement seems rather convincing.[2]

Thus, the "experimentally" observed universal Planckian relaxation rate in metals, independent of interaction strength, is nothing more than *delusion*, connected with the procedure used in [1, 2] to represent the experimental data. At low temperatures ($T < \langle\Omega\rangle$) Green's function takes the form

$$G(\varepsilon_n, \mathbf{p}) = \frac{Z}{i\varepsilon_n - Z\xi_{\mathbf{p}} + \frac{i}{2}Z\Gamma(T)\mathrm{sgn}\varepsilon_n}, \quad (47)$$

where the renormalization factor $Z < 1$ is assumed for simplicity a constant. The term $Z\Gamma(T) = \tilde{\Gamma}(T)$ in the denominator describes quasiparticle damping for which it may seem we have the "universal" high-temperature limit of Eq. (44). However, it is wrong: at high temperatures ($T > \langle\Omega\rangle$) the renormalization factor $Z \to 1$, as can be seen from our results above. Also for the low temperatures, when $Z < 1$, the term $Z\xi_{\mathbf{p}}$ in the denominator of (47) describes the renormalized spectrum of electrons with mass $\tilde{m} = m(1+\lambda)$, so that electron velocity at the Fermi surface $v_F = p_F/m \to \tilde{v}_F = p_F/\tilde{m} = v_F/(1+\lambda)$. Renormalization of damping corresponds to renormalization of mean free time $\tilde{\Gamma}^{-1} = \Gamma^{-1}(1+\lambda)$. Now we see that the mean free path is not renormalized: $l = \tilde{v}_F\tilde{\Gamma}^{-1} = v_F\Gamma^{-1}$ and renormalization due to many particle effects, important at low temperatures, actually do not affect conductivity (resistivity) at all [20]. In fact, this follows from the general Ward identity [21].

[2] We neglect rather insignificant [16] difference between λ and λ_{tr}.

ACKNOWLEDGMENTS

I am grateful to E.Z. Kuchinskii for numerous useful discussions.

FUNDING

This work was supported in part by the Russian Foundation for Basic Research, project no. 20-02-00011.

REFERENCES

1. J. A. N. Bruin, H. Sakai, R. S. Perry, and A. P. MacKenzie, Science (Washington, DC, U. S.) **339**, 804 (2013).
2. A. Legros, S. Benhabib, W. Tabis, et al., Nat. Phys. **15**, 142 (2019).
3. J. Zaanen, Nature (London, U.K.) **430**, 512 (2004).
4. V. R. Shaginyan, K. G. Popov, and V. A. Khodel, Phys. Rev. B **88**, 115103 (2013).
5. V. R. Shaginyan, M. Ya. Amusia, A. Z. Msezane, V. A. Stephanovich, G. S. Japaridze, and S. A. Artamonov, JETP Lett. **110**, 290 (2019).
6. A. A. Patel and S. Sachdev, Phys. Rev. Lett. **123**, 066601 (2019).
7. G. E. Volovik, JETP Lett. **110**, 352 (2019).
8. J. Zaanen, Nature (London, U.K.) **448**, 1000 (2007).
9. S. A. Hartnoll, Nat. Phys. **11**, 54 (2015).
10. C. P. Herzog, P. Kovtun, S. Sachdev, and D. T. Son, Phys. Rev. D **75**, 085020 (2007).
11. S. A. Hartnoll, P. K. Kovtun, M. Muller, and S. Sachdev, Phys. Rev. B **76**, 144502 (2007).
12. D. Pines, *The Many Body Problem* (W. A. Benjamin, New York, 1961).
13. D. Pines and P. Nozieres, *The Theory of Quantum Liquids* (W.A. Benjamin, New York, 1966), Vol. 1.
14. A. A. Abrikosov, L. P. Gorkov, and I. E. Dzyaloshinskii, *Methods of Quantum Field Theory in Statistical Physics* (Pergamon, Oxford, 1963; Fizmatgiz, Moscow, 1962).
15. M. V. Sadovskii, *Diagrammatics* (World Scientific, Singapore, 2019).
16. S. Y. Savrasov and D. Y. Savrasov, Phys. Rev. B **54**, 16487 (1996).
17. S. Sachdev, *Quantum Phase Transitions* (Cambridge Univ. Press, Cambridge, 1999).
18. C. M. Varma, arXiv:1908.05686.
19. A. Georges, G. Kotliar, W. Krauth, and M. J. Rozenberg, Rev. Mod. Phys. **68**, 13 (1996).
20. G. Grimvall, Phys. Scr. **14**, 63 (1978).
21. V. Heine, P. Nozieres, and J. W. Wilkins, Philos. Mag. **13**, 741 (1966).

ISSN 0021-3640, JETP Letters, 2021, Vol. 113, No. 9, pp. 581–585. © Pleiades Publishing, Inc., 2021.
Russian Text © The Author(s), 2021, published in Pis'ma v Zhurnal Eksperimental'noi i Teoreticheskoi Fiziki, 2021, Vol. 113, No. 9, pp. 600–604.

CONDENSED MATTER

Superconducting Transition Temperature for Very Strong Coupling in the Antiadiabatic Limit of Eliashberg Equations

M. V. Sadovskii*

Institute for Electrophysics, Ural Branch, Russian Academy of Sciences, Yekaterinburg, 620016 Russia

**e-mail: sadovski@iep.uran.ru*

Received March 31, 2021; revised March 31, 2021; accepted March 31, 2021

It is shown that the famous Allen–Dynes asymptotic limit for the superconducting transition temperature in the very strong coupling region $T_c > \frac{1}{2\pi}\sqrt{\lambda}\Omega_0$ (where $\lambda \gg 1$ is the Eliashberg–McMillan electron–phonon coupling constant and Ω_0 is the characteristic frequency of phonons) in the antiadiabatic limit of Eliashberg equations $\Omega_0/D \gg 1$ ($D \sim E_F$ is the half-width of the conduction band and E_F is the Fermi energy) is replaced by $T_c > (2\pi^4)^{-1/3}(\lambda D\Omega_0^2)^{1/3}$, with the upper limit $T_c < \frac{2}{\pi^2}\lambda D$.

DOI: 10.1134/S0021364021090034

1. INTRODUCTION

The discovery of superconductivity [1] with critical temperature up to $T_c = 203$ K in pressure interval of 100–250 GPa (in diamond anvils) in H_3S system initiated numerous experimental studies of high-temperature superconductivity of hydrides in megabar region (see reviews [2, 3]). Theoretical analysis immediately confirmed that these record-breaking T_c values are ensured by traditional electron–phonon interaction in the limit of strong enough electron–phonon coupling [4, 5]. More so, the detailed calculations performed for quite a number of hydrides of transition metals under pressure [4] lead to prediction of pretty large number of such systems with record T_c values. In some cases, these predictions were almost immediately confirmed by experiment, in particular the record values $T_c = 160$–260 K were achieved in LaH_{10} [6, 7], ThH_{10} [8], YH_6 [9], $(La,Y)H_{6,10}$ [10]. At last, some time ago the psychological barrier was overpassed, when in [11] superconductivity was obtained with $T_c = (287.7 \pm 1.2)$ K (i.e., near +15°C) in the C–H–S system at a pressure of (267 ± 10) GPa.

The principal achievement of these works was, before everything else, the demonstration of absence of any significant limitations for T_c, within the traditional picture of electron–phonon mechanism of Cooper pairing, contrary to a common opinion that T_c due to it cannot exceed 30–40 K. Correspondingly, even more demanding now is the problem of the upper limit of T_c values, which can be achieved with this mechanism of pairing.

Since BCS theory appeared, it became obvious that T_c can be increased either by an increase in the frequency of phonons responsible for Cooper pairing or by the enhancement of the effective interaction of these phonons with electrons. These problems were thoroughly studied by different authors. The most developed approach to description of superconductivity in electron–phonon system is Eliashberg–McMillan theory [5, 12, 13]. It is well known that this theory is entirely based on the applicability of adiabatic approximation and Migdal theorem [14], which allows to neglect vertex corrections while calculating the effects of electron–phonon interactions in typical metals. The actual small parameter of perturbation theory in these calculations is $\lambda\frac{\Omega_0}{E_F} \ll 1$, where λ is the dimensionless electron–phonon coupling constant, Ω_0 is characteristic frequency of phonons and E_F is the Fermi energy of electrons. In particular, this means that vertex corrections in this theory can be neglected even in the case of $\lambda > 1$, as we always have an inequality $\frac{\Omega_0}{E_F} \ll 1$ valid for typical metals.

In [15–17], we have recently shown that in the case of strong nonadiabaticity, when $\Omega_0 \gg E_F$, a new small parameter appears in the theory $\lambda_D \sim \lambda\frac{E_F}{\Omega_0} \sim \lambda\frac{D}{\Omega_0} \ll 1$ (D is the half-width of the electron band), so that corrections to the electronic spectrum become

irrelevant. Vertex corrections can also be neglected, as it was shown in [18]. In general case the renormalization of the electronic spectrum (effective mass of the electron) is determined by a new dimensionless constant $\tilde{\lambda}$, which reduces to the usual λ in the adiabatic limit, while in strong antiadiabatic limit it tends to λ_D. At the same time, the superconducting transition temperature T_c in the antiadiabatic limit is determined by Eliashberg–McMillan pairing constant λ, generalized by taking into account finite phonon frequencies.

For the case of interaction with a single optical (Einstein) phonon in [15] we have obtained the single expression for T_c, which is valid both in adiabatic and antiadiabatic regimes and smoothly interpolating in between:

$$T_c \sim \frac{D}{1+\frac{D}{\Omega_0}}\exp\left(-\frac{1+\tilde{\lambda}}{\lambda}\right), \tag{1}$$

where $\tilde{\lambda} = \lambda\dfrac{D}{\Omega_0 + D}$ is smoothly changing from λ for $\Omega_0 \ll D \sim E_F$ to λ_D in the limit $\Omega_0 \gg D \sim E_F$.

Besides the questions related to possible limits of T_c in hydrides, where possibly some small pockets of the Fermi surface with small Fermi energies exist [5], the interest to the problem of superconductivity in strongly antiadiabatic limit is stimulated by the discovery of a number of other superconductors, where adiabatic approximation cannot be considered valid and characteristic phonon frequencies is of the order or even exceed the Fermi energy of electrons. Typical in this respect are intercalated systems with monolayers of FeSe, and monolayers of FeSe on substrates like $Sr(Ba)TiO_3$ (FeSe/STO) [19]. With respect to FeSe/STO this was first noted by Gor'kov [20, 21], while discussing the idea of the possible mechanism of increasing the superconducting transition temperature T_c in FeSe/STO due to interactions with high-energy optical phonons of $SrTiO_3$ [19]. Similar situation appears also in an old problem of superconductivity in doped $SrTiO_3$ [22].

2. LIMITS FOR THE SUPERCONDUCTING TRANSITION TEMPERATURE IN THE CASE OF VERY STRONG ELECTRON–PHONON COUPLING

The general equations of the Eliashberg–McMillan theory determining the superconducting gap $\Delta(\omega_n)$ in the Matsubara representation ($\omega_n = (2n+1)\pi T$) can be written as [5, 12, 13]

$$\Delta(\omega_n)Z(\omega_n) = T\sum_{n'}\int_{-D}^{D} d\xi \int_0^\infty d\omega\alpha^2(\omega)F(\omega) \cdot D(\omega_n - \omega_{n'};\omega)\frac{\Delta(\omega_n')}{\omega_n^{2'} + \xi^2 + \Delta^2(\omega_{n'})}, \tag{2}$$

$$Z(\omega_n) = 1 + \frac{\pi T}{\omega_n}\sum_{n'}\int_{-D}^{D} d\xi \int_0^\infty d\omega\alpha^2(\omega)F(\omega) \cdot D(\omega_n - \omega_{n'};\omega)\frac{\omega_n'}{\omega_n^{2'} + \xi^2 + \Delta^2(\omega_{n'})}, \tag{3}$$

where

$$D(\omega_n - \omega_{n'};\omega) = \frac{2\omega}{(\omega_n - \omega_{n'})^2 + \omega^2}. \tag{4}$$

Here, $\alpha^2(\omega)F(\omega)$ is McMillan's function, $F(\omega)$ is the phonon density of states, and for simplicity we assume here the model of half-filled band of electrons with finite width $2D$ ($D \sim E_F$) with constant density of states (two-dimensional case).

We also neglect here the effects of Coulomb repulsion leading to the appearance of Coulomb pseudopotential μ^*, which is usually small and more or less irrelevant in the region of very strong electron–phonon attraction [5, 12, 13].

Then, taking into account

$$\int_{-D}^{D} d\xi \frac{1}{\omega_{n'}^2 + \xi^2 + \Delta^2(\omega_{n'})} = \frac{2}{\sqrt{\omega_{n'}^2 + \Delta^2(\omega_{n'})}}\arctan\frac{D}{\sqrt{\omega_{n'}^2 + \Delta^2(\omega_{n'})}} \to \frac{2}{|\omega_{n'}|}\arctan\frac{D}{|\omega_{n'}|} \quad \text{at} \quad \Delta(\omega_{n'}) \to 0, \tag{5}$$

the linearized Eliashberg equations acquire the general form

$$\Delta(\omega_n)Z(\omega_n) = T\sum_{n'}\int_0^\infty d\omega\alpha^2(\omega)F(\omega) \cdot D(\omega_n - \omega_{n'};\omega)\frac{2\Delta(\omega_{n'})}{|\omega_{n'}|}\arctan\frac{D}{|\omega_{n'}|}, \tag{6}$$

$$Z(\omega_n) = 1 + \frac{T}{\omega_n}\sum_{n'}\int_0^\infty d\omega\alpha^2(\omega)F(\omega) \cdot D(\omega_n - \omega_{n'};\omega)\frac{\omega_{n'}}{|\omega_{n'}|}2\arctan\frac{D}{|\omega_{n'}|}. \tag{7}$$

Consider the equation for $n = 0$ determining $\Delta(0) \equiv \Delta(\pi T) = \Delta(-\pi T)$, which follows directly from Eqs. (6), (7):

$$\Delta(0) = T\sum_{n'\neq 0}\int_0^\infty d\omega\alpha^2(\omega)F(\omega)\frac{2\omega}{(\pi T - \omega_{n'})^2 + \omega^2} \cdot \frac{2\Delta(\omega_{n'})}{|\omega_{n'}|}\arctan\frac{D}{|\omega_{n'}|}. \tag{8}$$

Leaving only the contribution from $n' = -1$, we immediately obtain the *inequality*

$$1 > \frac{2}{\pi}\int_0^\infty d\omega\alpha^2(\omega)F(\omega)\frac{2\omega}{(2\pi T)^2+\omega^2}\arctan\frac{D}{\pi T}, \quad (9)$$

which generalizes the similar inequality first obtained in [23] and determining the *lower* bound for T_c. For the Einstein model of the phonon spectrum, we have $F(\omega) = \delta(\omega - \Omega_0)$, so that Eq. (9) is reduced to:

$$1 > \frac{2}{\pi}\lambda\arctan\frac{D}{\pi T}\frac{\Omega_0^2}{(2\pi T)^2+\Omega_0^2}, \quad (10)$$

where $\lambda = 2\alpha^2(\Omega_0)/\Omega_0$ is the dimensionless pairing coupling constant. For $D \gg \pi T$, we immediately obtain the Allen–Dynes result [23]:

$$T_c > \frac{1}{2\pi}\sqrt{\lambda-1}\Omega_0 \to 0.16\sqrt{\lambda}\Omega_0 \quad \text{at} \quad \lambda \gg 1, \quad (11)$$

which in fact determines the asymptotic behavior of T_c in the region of very strong coupling $\lambda \gg 1$. The exact numerical solution of the Eliashberg equation [23] produces for T_c the result like (11) with the replacement of a numerical coefficient of 0.16 by 0.18. This asymptotic behavior rather satisfactory describes the T_c values already for $\lambda > 2$.

In the case of general phonon spectrum, it is sufficient to replace here $\Omega_0 \to \langle\Omega^2\rangle^{1/2}$, where

$$\langle\Omega^2\rangle = \frac{2}{\lambda}\int_0^\infty d\omega\alpha^2(\omega)F(\omega)\omega \quad (12)$$

is the average (over the spectrum) square frequency of phonons, and the general expression for the coupling constant is [5, 12, 13]:

$$\lambda = 2\int_0^\infty \frac{d\omega}{\omega}\alpha^2(\omega)F(\omega). \quad (13)$$

For $D \ll \pi T$ from Eq. (10), we obtain

$$T > \frac{1}{2\pi}\sqrt{\lambda^*(T)-1}\Omega_0, \quad (14)$$

where

$$\lambda^*(T) = \frac{2D}{\pi^2 T}\lambda, \quad (15)$$

so that in the strongly antiadiabatic limit, we get

$$T_c > (2\pi^4)^{-1/3}(\lambda D\Omega_0^2)^{1/3} \approx 0.17(\lambda D\Omega_0^2)^{1/3}. \quad (16)$$

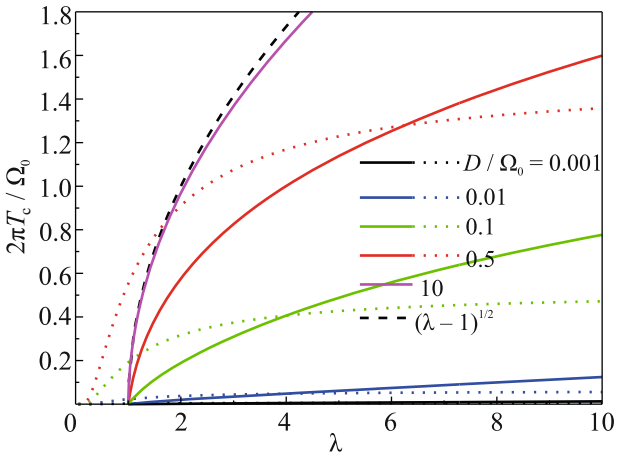

Fig. 1. (Color online) Superconducting transition temperature in the Einstein model of phonon spectrum in units of $2\pi T_c/\Omega_0$ versus the pairing constant λ for different values of the inverse adiabaticity parameter D/Ω_0. Dotted lines show the dependences for $2\pi T_c/\Omega_0$ in the region of weak and intermediate couplings (1) [15]. The black dashed line is the Allen–Dynes estimate valid in the adiabatic limit [23].

From the obvious requirement of $\lambda^*(T) > 0$, we obtain the condition:

$$T_c < \frac{2}{\pi^2}\lambda D, \quad (17)$$

which limits T_c from above.

Thus, we require the inequality

$$(2\pi^4)^{-1/3}(\lambda D\Omega_0^2)^{1/3} < T_c < \frac{2}{\pi^2}\lambda D, \quad (18)$$

which is reduced to:

$$\Omega_0 < \frac{4}{\pi}\lambda D \approx 1.27\lambda D \quad \text{or} \quad \frac{D}{\Omega_0} > \frac{0.78}{\lambda}, \quad (19)$$

so that for our analysis to be self-consistent it is required to have:

$$\lambda \gg \frac{\Omega_0}{D} \gg 1, \quad (20)$$

where the last inequality corresponds to strong antiadiabatic limit. Correspondingly, all the previous estimates are not valid for $\lambda \sim 1$ and can only describe the limit of very strong coupling.

In Figs. 1 and 2, we show the results of numerical comparison of the bounds for T_c, following from Eq. (10) with the values of transition temperature in the region of weak and intermediate coupling following from Eq. (1), for different values of adiabaticity parameter Ω_0/D. It is clear that in the vicinity of intersections of dotted and continuous lines on these

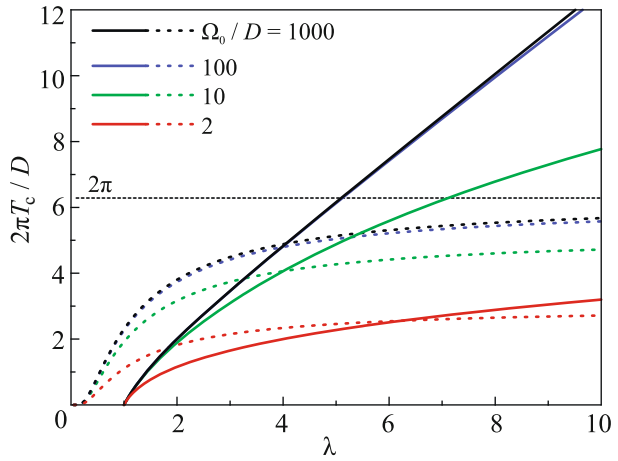

Fig. 2. (Color online) superconducting transition temperature in the Einstein model of the phonon spectrum in units of $2\pi T_c/D$ versus the pairing constant λ from different values of adiabaticity parameter $\frac{\Omega_0}{D}$. Dotted lines show the dependences for $2\pi T_c/D$ in the region of weak and intermediate couplings (1) [15].

graphs we actually have the smooth crossover from T_c behavior in the region of weak and intermediate coupling to its asymptotic behavior in the region of very strong coupling $\lambda \gg 1$. It is also seen that the increase in phonon frequencies and crossover to antiadiabatic limit does not lead, in general, to the increase in T_c as compared to adiabatic case.

3. CONCLUSIONS

In this work, we have considered the case of very strong electron–phonon coupling in Eliashberg–McMillan theory, including the antiadiabatic situation with phonons of very high frequency (exceeding the Fermi energy E_F). The value of mass renormalization is in general determined by the coupling constant $\tilde{\lambda}$ [15], which is small in antiadiabatic limit. At the same time, the pairing interaction is always determined by the standard coupling constant λ of Eliashberg–McMillan theory, appropriately generalized by taking into account the finite values of phonon frequencies [15]. However, the simplest estimates [15, 17] show, that in antiadiabatic situation this constant in general rather rapidly drops with the growth of phonon frequency Ω_0 for $\Omega_0 \gg E_F$. In this sense, the asymptotic behavior of T_c for very strong coupling discussed above can be possibly achieved only in some exceptional cases. Even in this case, as clear from our results, the transition into antiadiabatic region cannot increase T_c as compared to the standard adiabatic situation.

While the usual expression for T_c in terms of the pairing constant λ and characteristic phonon frequency $\Omega_0 \sim \langle\Omega^2\rangle^{1/2}$ are quite convenient and clear, it is to be taken into account that these parameters are in fact not independent. As seen from expressions like (12) and (13), these parameters are determined by the same Eliashberg–McMillan function $\alpha^2(\omega)F(\omega)$. Correspondingly, there are limitations for free changes of these parameters in estimates of optimal (maximum) values of T_c.

ACKNOWLEDGMENTS

I am grateful to E.Z. Kuchinskii for discussions and help with numerical computations.

FUNDING

This work is supported in part by the Russian Foundation for Basic Research, project no. 20-02-00011.

REFERENCES

1. A. P. Drozdov, M. I. Eremets, I. A. Troyan, V. Ksenofontov, and S. I. Shylin, Nature (London, U. K.) **525**, 73 (2015).
2. M. I. Eremets and A. P. Drozdov, Phys. Usp. **59**, 1154 (2016).
3. C. J. Pickard, I. Errea, and M. I. Eremets, Ann. Rev. Condens. Matter Phys. **11**, 57 (2020).
4. H. Liu, I. I. Naumov, R. Hoffman, N. W. Ashcroft, and R. J. Hemley, Proc. Natl. Acad. Sci. U. S. A. **114**, 6990 (2018).
5. L. P. Gor'kov and V. Z. Kresin, Rev. Mod. Phys. **90**, 01001 (2018).
6. A. P. Drozdov, P. P. Kong, V. S. Minkov, S. P. Besedin, M. A. Kuzovnikov, S. Mozaffari, L. Balicas, F. F. Balakirev, D. E. Graf, V. B. Prakapenka, E. Greenberg, D. A. Knyazev, M. Tkacz, and M. I. Eremets, Nature (London, U. K.) **569**, 528 (2019).
7. M. Somayazulu, M. Ahart, A. K. Mishra, Z. M. Geballe, M. Baldini, Y. Meng, V. V. Struzhkin, and R. J. Hemley, Phys. Rev. Lett. **122**, 027001 (2019).
8. D. V. Semenok, A. G. Kvashnin, A. G. Ivanova, V. Svitlyk, V. Y. Fominski, A. V. Sadakov, O. A. Sobolevskiy, V. M. Pudalov, I. A. Troyan, and A. R. Oganov, Mater. Today **33**, 36 (2020).
9. I. A. Troyan, D. V. Semenok, A. G. Kvashnin, et al., Adv. Mater. (2021, in press); arXiv: 1908.01534. https://doi.org/10.1002/adma.202006832
10. D. V. Semenok, I. A. Troyan, A. G. Kvashnin, et al., Mater. Today (2021, in press); arXiv: 2012.04787.

11. E. Snider, N. Dasenbrock-Gammon, R. McBride, M. Debessai, H. Vindana, K. Vencatasamy, K. V. Lawler, A. Salamat, and R. P. Dias, Nature (London, U. K.) **586**, 373 (2020).
12. D. J. Scalapino, in *Superconductivity,* Ed. by R. D. Parks (Marcel Dekker, New York, 1969), p. 449.
13. P. B. Allen and B. Mitrović, *Solid State Physics,* Ed. by F. Seitz, D. Turnbull, and H. Ehrenreich (Academic, New York, 1982), Vol. 37, p. 1.
14. A. B. Migdal, Sov. Phys. JETP **7**, 996 (1958).
15. M. V. Sadovskii, J. Exp. Theor. Phys. **128**, 455 (2019).
16. M. V. Sadovskii, JETP Lett. **109**, 166 (2019).
17. M. V. Sadovskii, J. Supercond. Novel Magn. **33**, 19 (2020).
18. M. A. Ikeda, A. Ogasawara, and M. Sugihara, Phys. Lett. A **170**, 319 (1992).
19. M. V. Sadovskii, Phys. Usp. **59**, 947 (2016).
20. L. P. Gor'kov, Phys. Rev. B **93**, 054517 (2016).
21. L. P. Gor'kov, Phys. Rev. B **93**, 060507 (2016).
22. L. P. Gor'kov, Proc. Natl. Acad. Sci. U. S. A. **113**, 4646 (2016).
23. P. B. Allen and R. C. Dynes, Phys. Rev. **12**, 905 (1975).

ISSN 1063-7761, Journal of Experimental and Theoretical Physics, 2023, Vol. 136, No. 3, pp. 368–377. © Pleiades Publishing, Inc., 2023.
Russian Text © The Author(s), 2023, published in Zhurnal Eksperimental'noi i Teoreticheskoi Fiziki, 2023, Vol. 163, No. 3, pp. 417–427.

ELECTRONIC PROPERTIES OF SOLID

Hall Effect in Doped Mott–Hubbard Insulator

E. Z. Kuchinskii[a],*, N. A. Kuleeva[a],, M. V. Sadovskii[a],***, and D. I. Khomskii[b],******

[a] *Institute for Electrophysics, Ural Branch, Russian Academy of Sciences, Yekaterinburg, 620016 Russia*
[b] *II Physikalisches Institut, Universität zu Koeln, Koeln, 50937 Germany*
**e-mail: kuchinsk@iep.uran.ru*
***e-mail: strigina@iep.uran.ru*
****e-mail: sadovski@iep.uran.ru*
*****e-mail: khomskii@ph2.uni-koeln.de*

Received October 4, 2022; revised October 4, 2022; accepted October 20, 2022

Abstract—We present theoretical analysis of Hall effect in doped Mott–Hubbard insulator, considered as a prototype of cuprate superconductor. We consider the standard Hubbard model within DMFT approximation. As a typical case we consider the partially filled (hole doping) lower Hubbard band. We calculate the doping dependence of both the Hall coefficient and Hall number and determine the value of carrier concentration, where Hall effect changes its sign. We obtain a significant dependence of Hall effect parameters on temperature. Disorder effects are taken into account in a qualitative way. We also perform a comparison of our theoretical results with some known experiments on doping dependence of Hall number in the normal state of YBCO and Nd-LSCO, demonstrating rather satisfactory agreement of theory and experiment. Thus the doping dependence of Hall effect parameters obtained within Hubbard model can be considered as an alternative to a popular model of the quantum critical point.

DOI: 10.1134/S1063776123030020

1. INTRODUCTION

The studies of Hall effect in high - temperature superconductors continues for a long time. The early experiments demonstrated the significant dependence of Hall effect parameters on temperature and doping, which are qualitatively different from the case of ordinary metals [1]. The complete understanding of Hall effects in cuprates at present is absent.

In recent years much interest was attracted to experimental studies of Hall effect at low temperatures in the normal state of high-temperature superconductors (cuprates), which is realized in very strong external magnetic fields [2–4]. The observed anomalies of Hall effect in these experiments are usually attributed to reconstruction of Fermi surface due to (antiferromagnetic) pseudogap formation and closeness to the corresponding quantum critical point [5].

Since the early days of theoretical studies of cuprates the leading point of view is, that these systems are strongly correlated and metallic (and superconducting) state is realized via doping of the initial Mott insulator phase, which in a simplest case can be described within Hubbard model. However, up to now there are only few papers where systematic studies of Hall effect dependence on doping and temperature were performed within this model [6].

Even the answer to a classical question on the doping level at which the Hall effect changes its sign is not perfectly clear. At small hole doping of an initial insulator, such as La_2CuO_4 or YBCO Hall effect is obviously determined by hole concentration δ. Then at what doping level Hall effect changes its sign and when the transition from hole – like Fermi surface to electron—like takes place? The answer to this question seems to be important also for the general theory of transport phenomena in strongly correlated systems. This paper is mainly devoted to the solution of this problem.

2. HALL CONDUCTIVITY AND HALL COEFFICIENT

One of the most general approaches to the studies of Hubbard model is the dynamical mean field theory (DMFT) [6–8], which gives an exact description of the system in the limit of infinite spatial dimensions (lattice with infinite number of nearest neighbors). General approaches allowing to overcome this rigid limitation are actively developed [9, 10], but as a rule these complicate the analysis very much. In this paper we limit ourselves to the analysis of Hall effect within the standard DMFT approximation. The aim of this work is systematic study of concentration and temperature dependence of Hall effect at different doping

levels of the lower Hubbard band and comparison of theoretical results with experiments on YBCO and Nd-LSCO [3, 4]. Preliminary results were published in [11].

In the standard DMFT [6–8] self-energy of a single-electron Green's function $G(\mathbf{p}\varepsilon)$ is local, i.e. independent of momentum. Due to this locality both the usual and Hall conductivities are completely determined by the spectral density of this Green's function

$$A(\mathbf{p}\varepsilon) = -\frac{1}{\pi}\operatorname{Im} G^R(\mathbf{p}\varepsilon). \quad (1)$$

In particular, the usual (diagonal) static conductivity is given by [6]:

$$\sigma_{xx} = \frac{\pi e^2}{2\hbar a}\int\limits_{-\infty}^{\infty} d\varepsilon\left(-\frac{df(\varepsilon)}{d\varepsilon}\right)\sum_{\mathbf{p}\sigma}\left(\frac{\partial\varepsilon(\mathbf{p})}{\partial p_x}\right)^2 A^2(\mathbf{p}\varepsilon), \quad (2)$$

while Hall (non-diagonal) conductivity is defined as:

$$\sigma_{xy}^H = \frac{2\pi^2 e^3 a H}{3\hbar^2}\int\limits_{-\infty}^{\infty} d\varepsilon\left(\frac{df(\varepsilon)}{d\varepsilon}\right) \times\sum_{\mathbf{p}\sigma}\left(\frac{\partial\varepsilon(\mathbf{p})}{\partial p_x}\right)^2\frac{\partial^2\varepsilon(\mathbf{p})}{\partial p_y^2}A^3(\mathbf{p}\varepsilon). \quad (3)$$

Here a is the lattice parameter, $\varepsilon(\mathbf{p})$ is electron dispersion, $f(\varepsilon)$ is Fermi distribution, and H is magnetic field along z axis. Then the Hall coefficient:

$$R_H = \frac{\sigma_{xy}^H}{H\sigma_{xx}^2} \quad (4)$$

is also completely determined by the spectral density $A(\mathbf{p}\varepsilon)$, which in the following will be calculated within the DMFT [6–8]. Effective Anderson single-impurity model of DMFT in this paper was solved with numerical renormalization group (NRG) [12].

In the following we consider two basic models of the bare electron band. The model with semi-elliptic density of states (DOS) (per elementary cell and single spin projection) is a reasonable approximation for three-dimensional case:

$$N_0(\varepsilon) = \frac{2}{\pi D^2}\sqrt{D^2-\varepsilon^2}, \quad (5)$$

where D is conduction band half-width. We assume that the bare electronic spectrum is isotropic. To find the momentum derivatives of the spectrum in this model, entering Eqs. (2) and (3), we follow the procedure proposed before in [13]. Appropriate technical details are presented in Appendix.

For two-dimensional systems, in anticipation of comparison with experimental data for cuprates, we limit ourselves to the usual tight-binding model of electronic spectrum:

$$\varepsilon(\mathbf{p}) = -2t(\cos(p_x a)+\cos(p_y a)) - 4t'\cos(p_x a)\cos(p_y a). \quad (6)$$

Within this two-dimensional model we consider a number of cases:

(1) spectrum with only nearest hoppings ($t' = 0$) and full electron-hole symmetry;

(2) spectrum with $t'/t = -0.25$, which qualitatively corresponds to electronic dispersion in systems like LSCO;

(3) spectrum with $t'/t = -0.4$, which qualitatively corresponds to situation observed in YBCO.

Below we present the results of detailed calculations of Hall coefficient for all these models.

3. HALL COEFFICIENT IN TWO-DIMENSIONAL MODEL OF TIGHT-BINDING SPECTRUM OF ELECTRONS

Let us start with simplest qualitative analysis. It is easy to understand that deep in Mott insulator state with well defined upper and lower Hubbard bands the Hall coefficient under hole doping is in fact determined by filling the lower Hubbard band (the upper band is significantly higher in energy and is practically unfilled). In this situation in the model with electron–hole symmetry (in two dimensions this corresponds to spectrum with $t' = 0$), an estimate of band filling corresponding to the sign change of the Hall coefficient can be obtained using very simple arguments. Let us consider the paramagnetic phase with $n_\uparrow = n_\downarrow = n$, so that in the following n denotes electron density per one spin projection, so the complete density of electrons is given by $2n$. Qualitatively the situation is illustrated in Fig. 1. In lower Hubbard band (in the vicinity of the Fermi level $E = 0$) $2n$ electrons occupy states below the Fermi energy E_F. An additional electron can go to the upper Hubbard band in the vicinity of $E \sim U$, where we also have $2n$ states. It also can go to the lower Hubbard band, where there still remain $2(1 - 2n)$ empty states in the region of $E > E_F$. Summing we obtain $2n + 2(1 - 2n) + 2n = 2$ as it should be. The sign of the Hall coefficient will change at the half filling of the lower band, when $2n = 2(1 - 2n)$. Now it is clear that the value of the critical concentration is $n_c = 1/3$.

The same result is easily obtained in Hubbard I approximation, where the Green's function spin-up electron takes the form [14]:

$$G_\uparrow^R(\mathbf{p}\varepsilon) = \frac{1-n_\downarrow}{\varepsilon-\varepsilon_-(\mathbf{p})+i\delta} + \frac{n_\downarrow}{\varepsilon-\varepsilon_+(\mathbf{p})+i\delta}, \quad (7)$$

where $\varepsilon_\pm(\mathbf{p})$ is quasiparticle spectrum in upper and lower Hubbard bands. We see that in this approximation the number of states with upper spin projection in the lower Hubbard band (first term in Eq. (7)) is in fact $1 - n_\downarrow$. During hole doping of Mott insulator

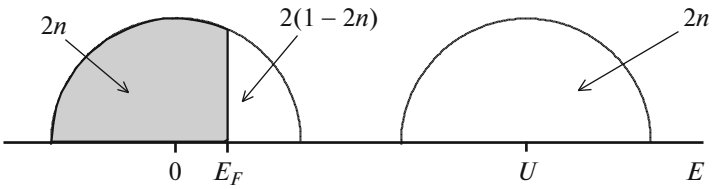

Fig. 1. Schematic picture of doping in Hubbard bands for the case of complete electron-hole symmetry.

practically all filling takes place in the lower Hubbard band, so that:

$$n = n_{\uparrow} \approx (1 - n_{\downarrow}) \int_{-\infty}^{\infty} d\varepsilon f(\varepsilon) \times \left(-\frac{1}{\pi} \mathrm{Im} \sum_{\mathbf{p}} \frac{1}{\varepsilon - \varepsilon_{-}(\mathbf{p}) + i\delta} \right) \equiv (1 - n) n_0. \quad (8)$$

Then at half-filling of the lower Hubbard band we have $n_0 = 1/2$ and the Hall coefficient (effective mass of the quasiparticles) changes its sign at $n = n_c = 1/3$, corresponding to our previous estimate.

In general case situation is obviously more complicated. In strongly correlated systems Hall coefficient (and other electronic properties) become significantly dependent on temperature. At low temperature in these systems DMFT approximation leads, besides the formation of lower and upper Hubbard bands, to the appearance of a narrow quasiparticle band, or quasiparticle peak in the density of states [6–8]. In hole doped Mott insulator (in the following we consider only hole doping) such a peak appears close to the upper edge of the lower Hubbard band (cf. Fig. 2). Thus at low temperatures the Hall coefficient is mainly determined by filling of this quasiparticle band. At high enough temperature (of the order or higher than quasiparticle peak width) quasiparticle peak is damped and the Hall coefficient is mainly determined by filling of the lower Hubbard band. Thus, in general case it is necessary to consider two different temperature regimes for Hall coefficient.

In low temperature regime both the width and the amplitude of quasiparticle peak depend on filling and temperature. Increasing temperature leads to widening of quasiparticle peak and some shift of the Fermi level below the maximum of this peak (cf. Fig. 2). This may lead to a significant drop of the Hall coefficient, though further increase of the temperature leading to the damping of the quasiparticle peak leads to the growth of this coefficient. Thus the relevant dependence of the quasiparticle peak on band filling in the low temperature regime leads to the regions of non-monotonous filling dependence of the Hall coefficient (cf. Fig. 3a).

From Fig. 3a it is easy to see that high-temperature behavior of the Hall coefficient in doped Mott insulator ($U/2D = 4$; 10) in a model with full electron-hole symmetry ($t' = 0$), completely confirms the qualitative estimate given above. However, this estimate becomes invalid in the case of noticeable breaking of electron-hole symmetry (cf. Fig. 3b).

It should be noted that damping and disappearance of quasiparticle peak can be not only due increasing temperature, but also due to disordering [9, 13] (cf. Fig. 4) or due to pseudogap fluctuations, which are entirely neglected within local DMFT [9, 15]. Thus, in reality the region of applicability of simplest estimates given above may be much wider.

In general case taking into account disorder scattering (more so pseudogap fluctuations) in calculations of the Hall effect is rather complicated problem. As a simple estimate we present below results of calculations using Eqs. (2)–(4), where we have used the values of the spectral density $A(\mathbf{p}\varepsilon)$ for disordered Hubbard model obtained within DMFT+Σ approach [9, 15]. Disorder parameter Δ denotes the effective scattering rate of electrons by random field (in self-consistent Born approximation). It is clear that this approach based only on the account of disorder in spectral density is oversimplified, but it seems reasonable for qualitative analysis.

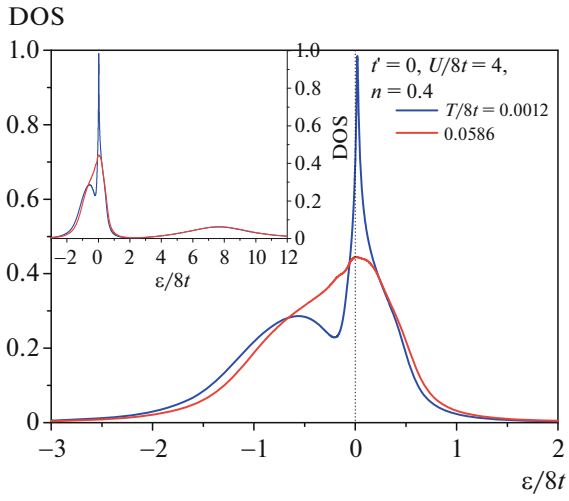

Fig. 2. Density of states (DOS) in doped Mott insulator at different temperatures. Parameters of the Hubbard model are shown in figure, $8t$ is the initial band-width. At the insert—the density of states in a wide energy interval including the upper Hubbard band.

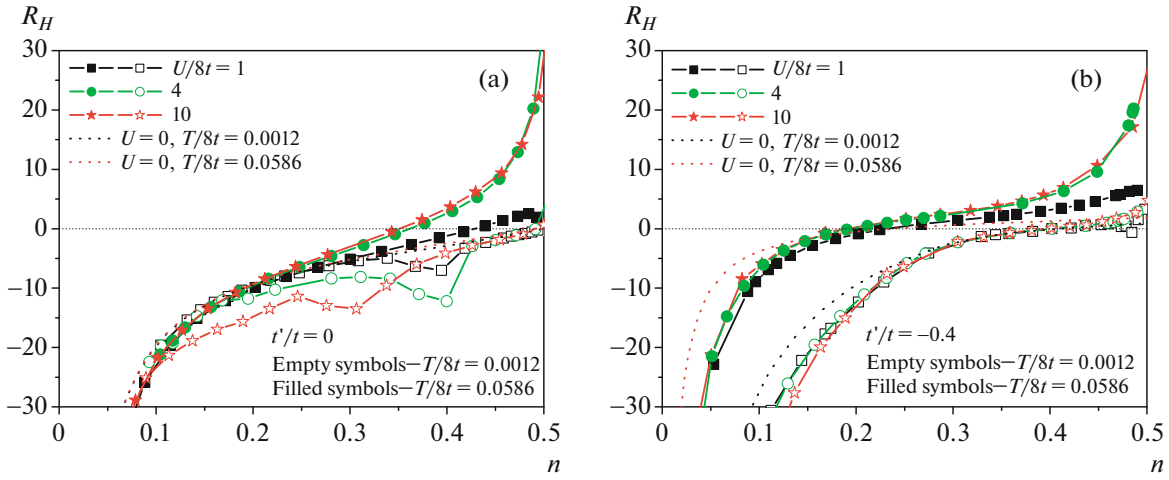

Fig. 3. Dependence of Hall coefficient on correlation strength U on band filling for $t' = 0$ (a) and $t'/t = -0.4$ (b) in low temperature regime (empty symbols) and in high temperature regime (filled symbols).

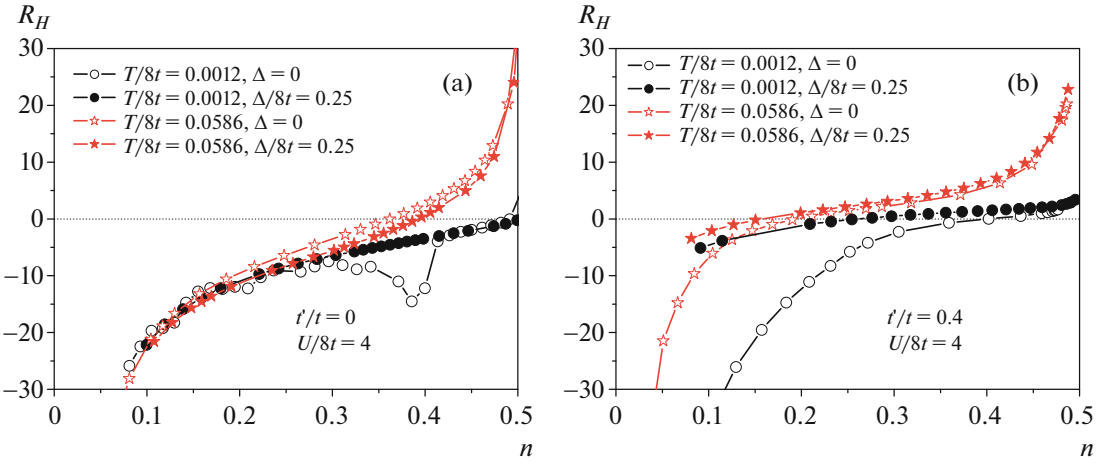

Fig. 4. Dependence of Hall coefficient on band filling in presence of impurity scattering ($\Delta/8t = 0.25$, filled symbols) and in its absence ($\Delta = 0$, empty symbols) for two models of two-dimensional electronic spectrum: (a) full electron-hole symmetry ($t' = 0$); (b) $t'/t = -0.4$.

In Fig. 4 we compare the dependencies of Hall coefficient on band filling in the absence of disorder and for the case of impurity scattering with $\Delta/8t = 0.25$ for Mott insulator with $U/8t = 4$. It is seen that for different values of t' in high temperature limit disorder only slightly affects the Hall coefficient by rather insignificant shift of the value of filling, where R_H changes its sign. In low temperature regime impurity scattering, damping the quasiparticle peak, lead to disappearance of the anomalies of R_H, connected with its existence (cf. Fig. 4a) and weakening differences between low temperature and high temperature regimes.

In Fig. 5 we show dependencies of Hall coefficient on band filling and temperature for the case of Mott insulator with $U/8t = 4$ for different models of electronic spectrum, both for the case of full electron-hole symmetry with $t' = 0$ and for $t'/t = -0.25$ and $t'/t = -0.4$, characteristic for cuprate systems LSCO and YBCO respectively. On the dependence of R_H on band filling with the growth of temperature we observe smooth evolution from low to high temperature regime with smooth weakening of the anomalies of Hall coefficient related to quasiparticle peak, which are most clearly seen in Figs. 3a and 5a. For all cases of electronic spectrum under consideration ($t'/t = 0$; -0.25; -0.4) increasing temperature leads to a shift of the value of filling corresponding to $R_H = 0$ into the region of larger hole dopings.

Also in the r.h.s. part of Figs. 5b, 5d, 5f we show the temperature dependencies of Hall coefficient for different band fillings. In all case we observe the signifi-

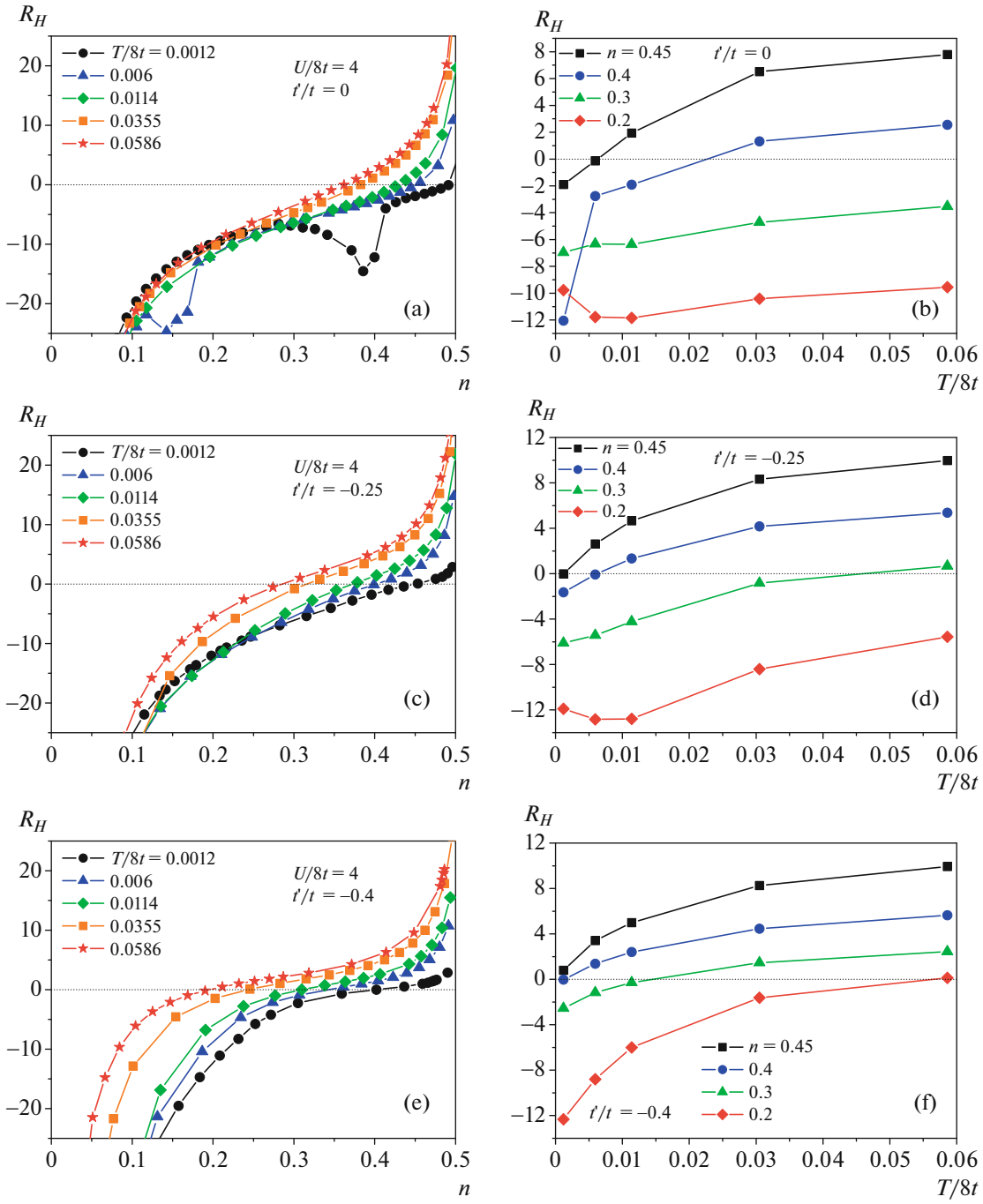

Fig. 5. Dependence of Hall coefficient on band filling for different values of temperature—left column (a, c, e) and temperature dependence of R_H for different band fillings—right column (b, d, f).

cant dependence of R_H on temperature and for small hole dopings ($n = 0.45$–0.3) R_H grows with increasing temperature and we obtain the sign change of R_H at larger hole dopings ($n = 0.3$–0.2). For small enough values of t' ($t'/t = 0$; -0.25) we can observe non monotonous dependence of Hall coefficient on temperature, when R_H decreases with increasing temperature, while it grows at high T.

The sign change of Hall coefficient is usually connected to a change of the type of charge carriers. Hall coefficient approaching zero corresponds to divergence of Hall number $n_H \sim 1/R_H$. At Fig. 6 we show temperature dependence of the band filling corresponding to the sign change of the Hall coefficient for all three values of t'/t considered here. We see that in all models the band filling at which R_H changes its sign

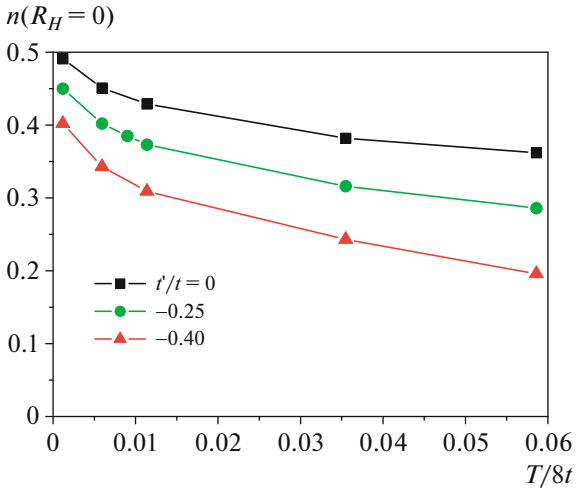

Fig. 6. Temperature dependence of band filling corresponding to a sign change of Hall coefficient in doped Mott insulator for three different values of t'/t.

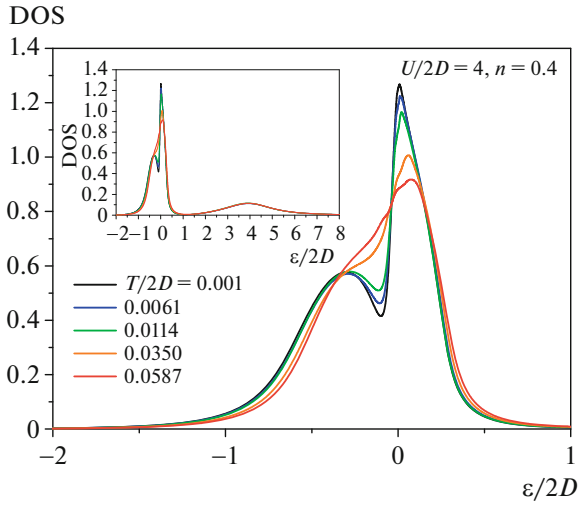

Fig. 7. Density of states (DOS) in doped Mott insulator with semi-elliptic band (three-dimensional case) for different temperatures.

decreases with temperature. In case of the full electron-hole symmetry $t' = 0$ we see, that in high temperature regime hole doping $\delta = 1 - 2n$ corresponding to the sign change of R_H really tends to 1/3. However, with increasing $|t'/t|$ we observe the significant decrease of the value of hole doping where R_H changes its sign.

4. HALL COEFFICIENT IN THE MODEL WITH SEMI-ELLIPTIC DENSITY OF STATES

Let us briefly discuss results obtained in the model of electronic band with semi-elliptic density of states, which has the full electron-hole symmetry. The main results are qualitatively similar to the case two-dimensional tight-binding electronic spectrum with $t' = 0$ also having the complete electron-hole symmetry. Similarly to two-dimensional case the Hall coefficient in three-dimensional strongly correlated system is significantly dependent on temperature and it is necessary to consider separately the low and high temperature regimes for R_H, as in the low temperature regime the Hall coefficient is mainly determined on filling the quasiparticle band (quasiparticle peak).

Increasing temperature leads to damping of quasiparticle peak (cf. Fig. 7) and in high temperature regime Hall coefficient is mainly determined by filling of the lower (for the case of hole doping considered here) Hubbard band.

In Fig. 8a we show the Hall coefficient dependence on electronic band filling if low temperature (unfilled symbols) and in high temperature (filled symbols) regimes, both for the case of strongly correlated metal ($U/2D = 1$) and for doped Mott insulator ($U/2D = 4$; 10). We can see that in the low temperature regime, as in two dimensional model with $t' = 0$ (R_H is negative practically at all band fillings) at small hole dopings there is a significant non monotonous dependence of R_H on doping.

In high temperature regime the Hall coefficient at small hole dopings is positive (hole-like), decreasing with increasing hole doping, while at larger dopings R_H becomes negative, changing its sign (in Mott insulator) at hole doping $\delta = 1 - 2n \approx 1/3$, which again confirms qualitative estimates given above. A smooth evolution of Hall coefficient dependence of filling as temperature increases from low temperature to high temperature regime in Mott insulator ($U/2D = 4$) is shown in Fig. 8b.

In Fig. 9 we demonstrate disorder influence on Hall coefficient in Mott insulator. In high temperature limit impurity scattering practically does not influence R_H at all, while in low temperature limit damping the quasiparticle peak by disorder removes the anomalous non monotonous behavior of R_H dependence on n.

5. COMPARISON WITH EXPERIMENTS

As we mentioned before in recent years the unique experimental studies were performed measuring Hall effect at low temperatures in the normal state of high-temperature superconductors (cuprates), which was achieved in very strong external magnetic fields [2–4]. These experiments revealed the dependence of Hall number $n_H = \dfrac{a^2}{|eR_H|}$ on doping with a smooth transition from linear dependence on hole concentration ~δ at small dopings to the values ~(1 + δ) for high enough concentrations of the order of critical hole concentration of vanishing (closing) pseudogap. These data are usually interpreted within the picture of Fermi surface

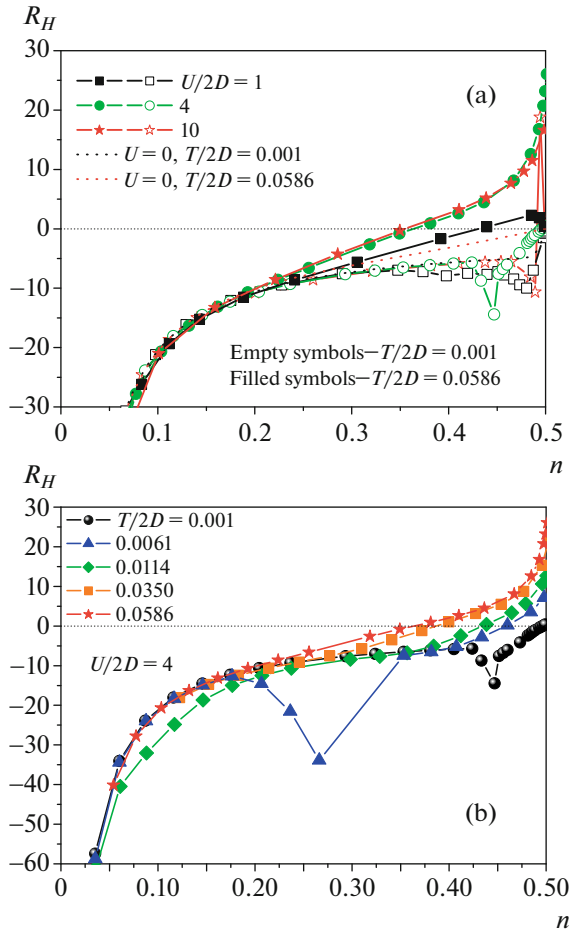

Fig. 8. Dependence of Hall coefficient on band filling for semi-elliptic density of states: (a) for different values of U in low temperature (empty symbols) and high temperature (filled symbols) regimes; (b) for different temperatures at fixed $U/2D = 4$.

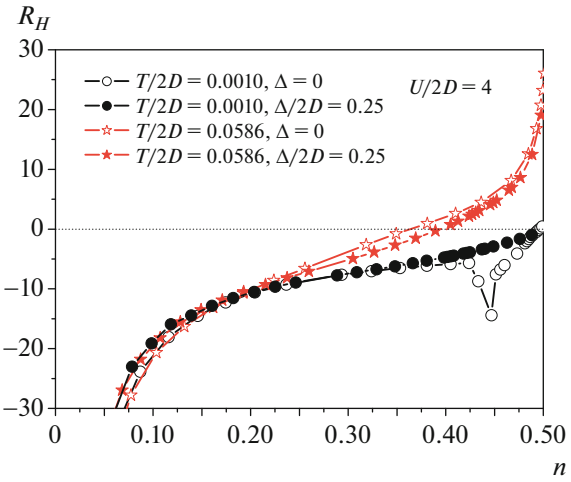

Fig. 9. Dependence of Hall coefficient on band filling in low temperature regime (black curves) and high temperature regime (red curves) in the absence of disorder $\Delta = 0$ (empty symbols) and for $\Delta/2D = 0.25$ (filled symbols).

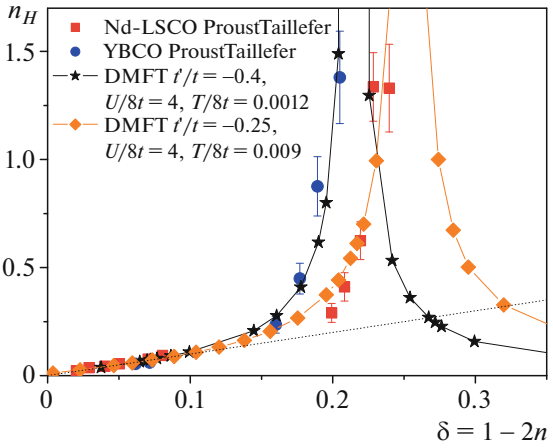

Fig. 10. Dependence of Hall number n_H on doping—comparison with experiments [3, 4] on YBCO and Nd-LSCO, $\delta = 1 - 2n$—hole concentration. Stars and diamonds—results of our calculations, blue circles and red squares—experiment.

reconstruction in the vicinity of the expected quantum critical point in the framework of rather specific model of cuprates with inhomogeneous localization of carriers [5, 16]. It should be noted, that in none of papers known to us were in fact presented experimental points reliably demonstrating the dependence $\sim(1 + \delta)$, and clearly established experimental fact is only the observed growth of the Hall number.

Below we propose an alternative interpretation of the growth of Hall number in these experiments as reflecting the approach of the system to critical concentration of carriers at which Hall effect just changes its sign (Hall coefficient R_H becomes zero) [11].

In Fig. 10 we show the comparison of the results of our calculations for Hall number (Hall concentration) $n_H = \dfrac{a^2}{|eR_H|}$ for typical parameters of the model with experimental data for YBCO and Nd-LSCO from [3, 4]. We can see that even for this, rather arbitrary, choice of parameters we can obtain almost quantitative agreement with experiment, with no assumptions about the connection of Hall effect with reconstruction of Fermi surface by pseudogap and closeness to corresponding quantum critical point, which were used in [3–5, 16]. Thus it seems reasonable to interpret Hall effect in cuprates within picture of lower Hubbard model doping in Mott insulator, as an alternative to the scenario based upon closeness to a quantum critical point.

In this respect it seems to be quite important to try to perform more detailed studies of the Hall effect in the vicinity of a critical concentration corresponding to sign change of the Hall effect (divergence of the

Hall number). It requires the studies of systems (cuprates) where such sign change can be achieved under doping.

6. CONCLUSIONS

We have studied Hall effect in metallic state appearing while doping Mott insulator. Main attention was to the case of hole doping, characteristic for a major part of cuprates. We considered a number of two-dimensional tight-binding models of electronic spectrum appropriate for description of electronic structure of cuprates, as well as three-dimensional model with semi-elliptic bare density of states. In all models the Hall coefficient R_H in doped Mott insulator is significantly dependent on temperature. In low temperature limit R_H is mainly determined by the filling of quasiparticle peak, which may lead to non monotonous dependence of Hall coefficient on doping. In high temperature limit, when quasiparticle peak is essentially damped, R_H is mainly determined by filling of the lower (for hole doping) Hubbard band. In this limit the sign change of the Hall coefficient and corresponding divergence of the Hall number takes place, in the simplest (symmetric) case close to the band filling $n = 1/3$ per single spin projection or 2/3 for total density of electrons, which corresponds to hole doping $\delta = 1 - 2n = 1/3$, though in general case this filling may strongly depend on the choice of parameters of the model. This concentration follows from simple qualitative estimates and not related with more complicated factors like changing the topology of Fermi surface or the presence of quantum critical points.

Rather satisfactory agreement of obtained concentration dependencies of Hall number with experiments on YBCO and Nd-LS CO [3, 4] shows, that our model may serve as a reasonable alternative to a picture of Hall effect in the vicinity of quantum critical point related to closing the pseudogap [5, 16].

The work of EZK, NAK, and MVS was supported in part by RFBR grant no. 20-02-00011. DIK work was partly supported by DFG project. no. 277146847-CRC 1238.

APPENDIX

"BARE" ELECTRONIC DISPERSION AND ITS DERIVATIVES FOR BAND WITH SEMIELLIPTIC DENSITY OF STATES

Let us assume that electronic spectrum corresponding to density of states (5) is isotropic $\varepsilon(\mathbf{p}) = \varepsilon(|\mathbf{p}|) \equiv \varepsilon(p)$. To calculate derivatives in (2) and (3) it is necessary to perform "angle" averaging of these derivatives by momentum components

$$\left\langle \left(\frac{\partial \varepsilon(\mathbf{p})}{\partial p_x} \right)^2 \right\rangle_\Omega = \varepsilon'^2(p) \left\langle \frac{p_x^2}{p^2} \right\rangle_\Omega = \frac{1}{d} \varepsilon'^2(p) = \frac{1}{3} \varepsilon'^2(p), \quad (9)$$

where $\langle ... \rangle_\Omega = \int \frac{d\Omega}{4\pi} ...$ is solid angle averaging in three-dimensional system ($d = 3$) and $\varepsilon'(p) = \frac{d\varepsilon(p)}{dp}$ is derivative over the absolute value of momentum.

$$\left(\frac{\partial \varepsilon(\mathbf{p})}{\partial p_x} \right)^2 \frac{\partial^2 \varepsilon(\mathbf{p})}{\partial p_y^2} = \varepsilon'^2(p) \left[\varepsilon''(p) \frac{p_x^2 p_y^2}{p^4} + \frac{\varepsilon'(p)}{p} \frac{p_x^2 p^2 - p_x^2 p_y^2}{p^4} \right], \quad (10)$$

where $\varepsilon''(p) = \frac{d^2 \varepsilon(p)}{dp^2}$. Thus we have a problem of finding the angle average $\left\langle \frac{p_x^2 p_y^2}{p^4} \right\rangle_\Omega$. Let us introduce notations: $\left\langle \frac{p_x^4}{p^4} \right\rangle_\Omega \equiv a$ and $\left\langle \frac{p_x^2 p_y^2}{p^4} \right\rangle_\Omega \equiv b$. First of all we have:

$$\left\langle \frac{(p_x^2 + p_y^2 + p_z^2)^2}{p^4} \right\rangle_\Omega = \left\langle \frac{(p_x^4 + p_y^4 + p_z^4)^2 + 2p_x^2 p_y^2 + 2p_x^2 p_z^2 + 2p_y^2 p_z^2}{p^4} \right\rangle_\Omega = d \left\langle \frac{p_x^4}{p^4} \right\rangle_\Omega + d(d-1) \left\langle \frac{p_x^2 p_y^2}{p^4} \right\rangle_\Omega = 3a + 6b = 1. \quad (11)$$

Similarly:

$$\left\langle \frac{(p_x^2 + p_y^2)^2}{p^4} \right\rangle_\Omega = \left\langle \frac{p_x^4 + p_y^4 + 2p_x^2 p_y^2}{p^4} \right\rangle_\Omega = 2a + 2b = \frac{8}{15}. \quad (12)$$

As

$$\left\langle \frac{(p_x^2 + p_y^2)^2}{p^4} \right\rangle = \langle \sin^4 \theta \rangle_\Omega = \frac{1}{2} \int_0^\pi \sin\theta \sin^4 \theta d\theta = \frac{1}{2} \int_{-1}^1 (1 - \tau^2)^2 d\tau = \frac{8}{15}, \quad (13)$$

where θ is an angle between vector **p** and z-axis, Then from Eqs. (11), (12) we immediately obtain $a = \left\langle \frac{p_x^4}{p^4} \right\rangle_\Omega = 1/5$ and $b = \left\langle \frac{p_x^2 p_y^2}{p^4} \right\rangle_\Omega = 1/15$, so that we have:

$$\left\langle \left(\frac{\partial \varepsilon(\mathbf{p})}{\partial p_x} \right)^2 \frac{\partial^2 \varepsilon(\mathbf{p})}{\partial p_y^2} \right\rangle_\Omega = \frac{\varepsilon'^2(p)}{15} [\varepsilon''(p) + 4\varepsilon'(p)/p]. \quad (14)$$

To find derivatives $\varepsilon'(p)$, $\varepsilon''(p)$ for the spectrum determined by semi-elliptic density of states (5) we can use the approach developed in [13]. Equating the number of states in a phase volume element d^3p and the number of states in an energy interval $[\varepsilon, \varepsilon + d\varepsilon]$, we obtain differential equation determining $\varepsilon(p)$:

$$\frac{4\pi p^2 dp}{(2\pi)^3} = N_0(\varepsilon) d\varepsilon. \quad (15)$$

Assuming the quadratic dispersion of $\varepsilon(p)$ close to lower band edge we obtain the initial condition for (15): $p \to 0$ for $\varepsilon \to -D$. As a result:

$$p = \left[6\pi \left(\pi - \varphi + \frac{1}{2} \sin(2\varphi) \right) \right]^{\frac{1}{3}}, \quad (16)$$

where $\varphi = \arccos\left(\frac{\varepsilon}{D}\right)$ and momentum is given in units of inverse lattice parameter. This expression implicitly defines the dispersion law $\varepsilon(p)$ on electronic branch of the spectrum $\varepsilon \in [-D, 0]$.

We can determine characteristic momentum p_0 corresponding to $\varepsilon = 0$:

$$p_0 = p(\varepsilon = 0) = (3\pi^2)^{\frac{1}{3}}. \quad (17)$$

We are interested in calculating two derivatives of this spectrum over the momentum. From (15) we get:

$$\varepsilon'(p) = \frac{d\varepsilon}{dp} = \frac{p^2}{2\pi^2} \frac{1}{N_0(\varepsilon)}, \quad (18)$$

where p is defined by (16).

$$\varepsilon''(p) = \frac{d}{dp}\frac{d\varepsilon}{dp} = \frac{1}{2\pi^2} \frac{2pN_0(\varepsilon) - p^2 \frac{dN_0(\varepsilon)}{d\varepsilon}\frac{d\varepsilon}{dp}}{N_0^2(\varepsilon)} = \frac{1}{N_0(\varepsilon)} \left[\frac{p}{\pi^2} - \varepsilon'^2 \frac{dN_0(\varepsilon)}{d\varepsilon} \right], \quad (19)$$

where $\frac{dN_0(\varepsilon)}{d\varepsilon} = -\frac{2}{\pi D^2} \frac{\varepsilon}{\sqrt{D^2 - \varepsilon^2}}$, $\varepsilon'(p)$ is determined from (18), while p is defined by (16).

On the hole branch of the spectrum ($\varepsilon \in [0, D]$), to obtain quadratic dispersion law close to the upper edge of the band ($\varepsilon \to D$) we introduce a hole momentum $\tilde{p} = 2p_0 - p$ and equate the number of states in a phase volume element $d^3\tilde{p}$ and in energy interval $[\varepsilon, \varepsilon + d\varepsilon]$:

$$\frac{4\pi \tilde{p}^2 d\tilde{p}}{(2\pi)^3} = -N_0(\varepsilon) d\varepsilon. \quad (20)$$

Demanding $\tilde{p} \to 0$ at the upper band edge $\varepsilon \to 0$, we obtain:

$$\tilde{p} = \left[6\pi \left(\varphi - \frac{1}{2} \sin(2\varphi) \right) \right]^{\frac{1}{3}}. \quad (21)$$

For the velocity on the hole branch of the spectrum we get:

$$\varepsilon'(p) = -\frac{d\varepsilon}{d\tilde{p}} = \frac{\tilde{p}^2}{2\pi^2} \frac{1}{N_0(\varepsilon)}. \quad (22)$$

Equations (18), (22) determine the dependence of velocity $\varepsilon'(p)$ on energy. One is easily convinced that velocity is even in energy and goes to zero at band edges. The second derivative over momentum in this approach is explicitly defined on electronic branch of the spectrum ($\varepsilon \in [-D, 0]$), but on the hole branch it is more difficult to do. However, we can require full electron-hole symmetry of the model, which reduces to demanding the square of velocity, entering Eq. (2), being even in $\varepsilon(p)$, while Eq. (14) entering Eq. (3) for Hall conductivity being odd (sign change under change of the type of charge carriers).With the account of such symmetry the results obtained in this Appendix allow to replace summation over momenta in Eqs. (2), (3) by integration over energy.

CONFLICT OF INTEREST

The authors declare that they have no conflicts of interest.

REFERENCES

1. Y. Iye, J. Phys. Chem. Solids **53**, 1561 (1992).
2. F. F. Balakirev, J. B. Betts, A. Migliori, I. Tsukada, Y. Ando, and G. S. Boebinger, Phys. Rev. Lett. **101**, 017004 (2009).
3. S. Badoux, W. Tabis, F. Laliberte, B. Vignolle, D. Vignolles, J. Beard, D. A. Bonn, W. N. Hardy, R. Liang, N. Doiron-Leyraud, L. Taillefer, and C. Proust, Nature (London, U.K.) **531**, 210 (2016).
4. C. Collignon, S. Badoux, S. A. A. Afshar, B. Michon, F. Laliberte, O. Cyr-Choiniere, J.-S. Zhou, S. Licciardello, S. Wiedmann, N. Doiron-Leyraud, and L. Taillefer, Phys. Rev. B **95**, 224517 (2017).
5. C. Proust and L. Taillefer, Ann. Rev. Condens. Matter Phys. **10**, 409 (2019).

6. Th. Pruschke, M. Jarrell, and J. K. Freericks, Adv. Phys. **44**, 187 (1995).
7. A. Georges, G. Kotliar, W. Krauth, and M. J. Rozenberg, Rev. Mod. Phys. **68**, 13 (1996).
8. D. Vollhardt, in *Lectures on the Physics of Strongly Correlated Systems XIV,* Ed. by A. Avella and F. Mancini, AIP Conf. Proc. **1297**, 339 (2010); arXiV: 1004.5069.
9. E. Z. Kuchinskii, I. A. Nekrasov, and M. V. Sadovskii, Phys. Usp. **55**, 325 (2010).
10. G. Rohringer, H. Hafermann, A. Toschi, A. A. Katanin, A. E. Antipov, M. I. Katsnelson, A. I. Lichtenstein, A. N. Rubtsov, and K. Held, Rev. Mod. Phys. **90**, 025003 (2018).
11. E. Z. Kuchinskii, N. A. Kuleeva, D. I. Khomskii, and M. V. Sadovskii, JETP Lett. **115**, 402 (2022).
12. R. Bulla, T. A. Costi, and T. Pruschke, Rev. Mod. Phys. **60**, 395 (2008).
13. E. Z. Kuchinskii, I. A. Nekrasov, and M. V. Sadovskii, J. Exp. Theor. Phys. **106**, 581 (2008).
14. D. I. Khomskii, *Basic Aspects of the Quantum Theory of Solids* (Cambridge Univ. Press, New York, 2010).
15. M. V. Sadovskii, I. A. Nekrasov, E. Z. Kuchinskii, Th. Pruschke, and V. I. Anisimov, Phys. Rev. B **72**, 155105 (2005).
16. D. Pelc, P. Popčević, M. Požek, M. Greven, and N. Barišić, Sci. Adv. **5**, eaau4538 (2019).

GENERALIZED DYNAMICAL KELDYSH MODEL

E.Z. Kuchinskii, M.V. Sadovskii

Institute for Electrophysics, Russian Academy of Scieneces, Ural Branch, Amundsen str. 106, Ekaterinburg 620016, Russia

We consider a certain class of exactly solvable models, describing spectral properties an electron moving in random in time external field with different statistical characteristics. This electron can be band – like or belong to a quantum well. The known dynamical Keldysh model is generalized for the case of fields with finite correlation time of fluctuations and for finite transfer frequencies of these fluctuations. In all cases we are able to perform the complete summation of all Feynman diagrams of corresponding perturbation series for the Green's function. This can be done either by the reduction of this series to some continuous fraction or by the use of the generalized Ward identity from which we can derive recurrence relations for the Green's function. In the case of a random field with finite transferred frequency there appear the interesting effects of modulation of spectral density and density of states.

Dedicated to 130-th anniversary of Pyotr Leonidovich Kapitza

1. INTRODUCTION

While being an outstanding experimentalist, P.L. Kapitza sometimes addressed also some purely theoretical problems. Well known is his elegant solution of a problem of the motion of a classical particle in fast oscillating field [1], where he essentially described this motion as a particle in a random field with appropriate time averaging. Such fields and processes appear in many problems of statistical radiophysics and radiotechnics, where a vast literature exists [2, 3]. In quantum theory there is also multitude problems of this kind.

In this work we shall consider a certain class of exactly solvable quantum mechanical problems, related in general to the theory of electrons in disordered systems and quantum structures, which is a dynamical generalization of the so called Keldysh model.

The initial model was introduced by L.V. Keldysh in his unpublished thesis in 1965 [4]. Some of his results were used by A.L Efros in Ref. [5], devoted to doped semiconductors. The detailed presentation of different aspects of this model in the general context of electron theory of disordered systems was given in [6], where the notion of "Keldysh model" was introduced for the first time.

In the following, the number of similar models were proposed, e.g. for the description of the pseudogap appearing due to electron scattering by fluctuations of short – range order in one – dimensional systems [6–12], which were later generalized for two – dimensional case to describe pseudogap in high – temperature superconductors [13–17].

dynamical generalization of the initial Keldysh model for the case of electron scattering by random in *time* fluctuations of external field was proposed by Kikoin and Kiselev [18], who considered electrons in quantum dots. Detailed presentation of different results obtained for this and similar models was given in Ref. [19]. The present paper is devoted to further development and generalization of this type of models both for the case of electrons in quantum dots and band – like electrons in conductors of different dimensionalities under the influence of dynamic random fields.

2. DYNAMICAL KELDYSH MODEL

The model under consideration was proposed by Keldysh in 1965 [4] as some limiting case of problem of electron scattering by the random field of static impurities in a disordered system [6, 20]. Keldysh has shown that the single – particle Green's function in

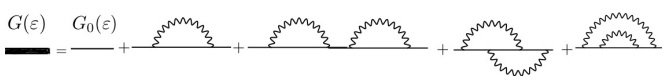

Рис. 1. Diagrammatic expansion for the Green's function. Double line corresponds to "dressed" Green's function, wavy line corresponds to correlator of Gaussian random field.

Gaussian random field $V(r)$ with "forward" scattering (i.e. with zero transferred momentum, corresponding to the limit of infinite spatial range of fluctuations of the random potential) described by correlator (d is spatial dimensionality):

$$D(\mathbf{r}-\mathbf{r}') = \langle V(\mathbf{r})V(\mathbf{r}')\rangle = \Delta^2 \to D(\mathbf{q}) = (2\pi)^d\Delta^2\delta(\mathbf{q}), \tag{1}$$

can be found by complete summation of all Feynman diagrams of perturbation series. In fact, according to the usual diagram rules for the problem of scattering by static random disorder [6, 20], diagram of N - th order contains N interaction line with Gaussian random field (denoted by by wavy lines), $2N+1$ solid lines, corresponding to Green's functions and $2N$ vertices. The total number of diagrams in the given order of perturbation theory A_N corresponds to the total number of ways to connect $2N$ vertices by N interaction lines, which is equal to [6, 21]:

$$A_N = (2N-1)!! = \frac{(2N-1)!}{2^{N-1}(N-1)!}. \tag{2}$$

Diagrammatic contributions of the lowest orders in the series for single – electron Green's function are shown in Fig. 1. In this model all Feynman diagrams of the given order N give the same contributions to Green's function, so that the full series for it is of the following form:

$$G(E) = G_0(E)\left\{1+\sum_{N=1}^{\infty}(2N-1)!!G_0^{2N}(E)\Delta^{2N}\right\}. \tag{3}$$

Further, to shorten notations we define $E = \epsilon - \epsilon_{\mathbf{p}}$, where $\epsilon_{\mathbf{p}}$ is free the electron spectrum, so that the "bare" Green's function is written as $G_0(E) = 1/E$. Using integral representation of Γ – function, we can use:

$$(2N-1)!! = \frac{1}{\sqrt{2\pi}}\int_{-\infty}^{\infty} dt t^{2N-2}e^{-t^2/2} \tag{4}$$

so that the retarded Green's function (after the summation of geometric series) can be written as:

$$G^R(E) = \frac{1}{\sqrt{2\pi\Delta^2}}\int_{-\infty}^{\infty} dV \frac{e^{-V^2/2\Delta^2}}{E-V+i\delta} \tag{5}$$

This equation has an obvious meaning [6] — electron propagates in spatially homogeneous Gaussian random field. There is also another way to obtain this elegant result, which was also proposed by Keldysh [4] and later by Efros [5], and is based on the use of an exact Ward identity, which allows the derivation of differential equation for the Green's function. This equation has the following form:

$$\Delta^2\frac{dG(E)}{dE} + E\cdot G(E) = 1. \tag{6}$$

Solving this equation with boundary condition $G(E\to\infty) = 1/E$ immediately leads to Eq. (5) [6].

Direct consequence of the obtained solution is the appearance of the Gaussian "tail" in the density of states of an electron in energy region $\epsilon < 0$ [6].

In Refs. [18, 19] Keldysh model was reformulated for the case of electron scattered by very slow *temporal* fluctuations of the random potential. Appropriate dynamical Keldysh model can also be generalized for the case of scattering by multiple component Gaussian non – Markovian random fields [19].

As an example, following Refs. [18, 19] we may consider an electron in a single quantum well (dot), which is formed by appropriate confining potential, as shown in Fig. 2. The gate creates external noise slowly changing confining potential of the well.

Single – particle Hamiltonian for this problem has the following form:

$$H = [\epsilon_0 + V(t)]\, n. \tag{7}$$

where $n = c^\dagger c$, and $c^\dagger$, c are creation and annihilation operators of an electron at the level within well. For simplicity we consider spinless (spinpolarized) electrons. Classical potential random (Gaussian) in time $V(t)$ is determined by its average value and pair correlation function:

$$\langle V(t)\rangle = 0, \quad \langle V(t)V(t')\rangle = D(t-t'). \tag{8}$$

For this function we assume the following form:

$$D(t-t') = \Delta^2 e^{-\gamma|t-t'|}, \tag{9}$$

where $\gamma = 1/\tau$, with τ determining characteristic correlation time of potential fluctuations, while Δ is the

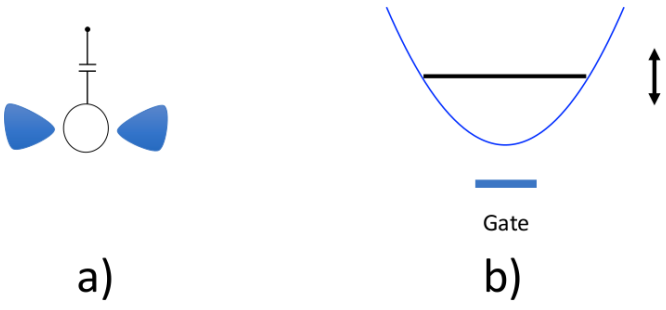

Рис. 2. (a) single quantum dot, with noise applied by external electrodes (gate), (b) corresponding quantum well with fluctuating level.

amplitude of the noise. We may consider two limiting cases:

$$\gamma \to \infty : \quad D(t-t') \to \Delta^2 \delta(t-t'), \tag{10}$$

$$\gamma \to 0 : \quad D(\omega) \to 2\pi\Delta^2 \delta(\omega). \tag{11}$$

Here $D(\omega)$ is the Fourier – transform of $D(t-t')$. The first case corresponds to "fastest" possible noise ("white" noise) and Markovian random process. The second case corresponds to slow noise, with Keldysh model giving its slowest possible realization with (infinitely) large relaxation time of fluctuations (infinite memory, of non – Markovian process).

Single – electron (retarded) Green's function of electron in a well for the given realization of the potential is:

$$G^R(\epsilon) = \frac{1}{\epsilon - \epsilon_0 - V + i\delta} \tag{12}$$

where ϵ_0 is energy level in a well, while time – averaging is again reduced to Gaussian integration of this expression with distribution function $P(V) = 1/\sqrt{2\pi\Delta^2}\exp(-V^2/(2\Delta^2))$:

$$G^R(\epsilon) = \frac{1}{\sqrt{2\pi\Delta^2}} \int_{-\infty}^{\infty} dV \frac{e^{-V^2/2\Delta^2}}{\epsilon - \epsilon_0 - V + i\delta} \tag{13}$$

Similarly we can consider an electron not within the well, but within energy band of a system (placed between capacitor plates, on which a random noise is generated) of any dimensionality. In this case it is just sufficient to make a replacement $\epsilon_0 \to \epsilon_{\mathbf{p}}$, where $\epsilon_{\mathbf{p}}$ is band spectrum of an electron with quasimomentum $\mathbf{p}$.

The single – well model is easily generalized also for the case of several wells [18, 19], which leads to Keldysh model with multicomponent noise. Particularly interesting is the model of two quantum wells, which (in its band – like variant) is deeply related to an exactly solvable model of the pseudogap state [7–12]. However, below we shall only consider the single – well model, leaving the two – well case (pseudogap fluctuations) for the separate work.

3. KELDYSH MODEL AND FLUCTUATIONS WITH FINITE CORRELATION TIME

Below we show that an exact solution for the single – particle Green's function can also be obtained for Keldysh model with finite correlation time of fluctuations $\tau = \gamma^{-1}$. This solution is easily found using the method proposed by one of the authors in Ref. [11], devoted to the model of pseudogap in one – dimensional systems.

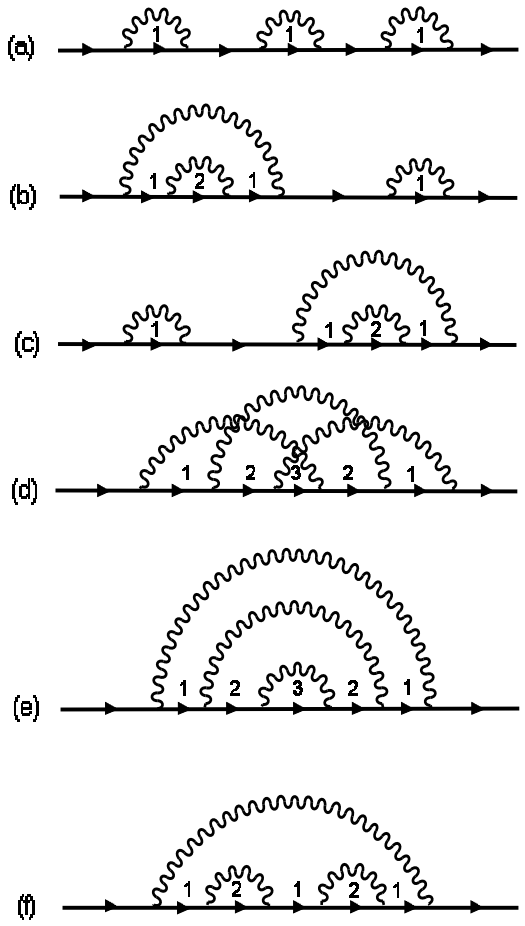

Рис. 3. Typical diagrams of the third order.

Fourier – transform of Eq. (9), which is associated with interaction lines in diagrams, can be written as:

$$D(\omega) = 2\pi\Delta^2 \frac{1}{\pi}\frac{\gamma}{\omega^2+\gamma^2} = 2\pi\Delta^2 \frac{1}{\pi}\frac{\gamma}{(\omega+i\gamma)(\omega-i\gamma)} \tag{14}$$

For $\gamma \to 0$ this is naturally reduced to the second expression in (11). Let us clarify the calculations of a diagram of an an arbitrary order. In fact this can be done exactly. As an example let us consider some typical diagrams of third order shown in Fig. 3. We can easily calculate the contribution of an arbitrary diagram as we can actually guarantee that nonzero contribution to integrals (over transferred frequencies) appear only from the poles of Lorentzians[1)] $D(\omega)$.

[1)] In the problem analyzed in Ref. [11] this statement is only approximate [21]. Here all calculations (frequency integrations) are performed exactly.

For example, elementary calculations show, that contribution of diagram in Fig. 3 (d) to the retarded Green's function has the following form:

$$\Delta^6 \frac{1}{\epsilon-\epsilon_0}\frac{1}{\epsilon-\epsilon_0+i\gamma}\frac{1}{\epsilon-\epsilon_0+2i\gamma}\frac{1}{\epsilon-\epsilon_0+3i\gamma}\times \\ \times\frac{1}{\epsilon-\epsilon_0+2i\gamma}\frac{1}{\epsilon-\epsilon_0+i\gamma}\frac{1}{\epsilon-\epsilon_0} \tag{15}$$

Contributions of arbitrary diagrams are quite similar: integers k, written above electronic lines Fig. 3, show have many times the term $i\gamma$ enters corresponding denominator. Note that contribution of diagram with crossing interaction lines in Fig. 3 (d) are just equal to the contribution of diagram with no intersections of interaction lines shown in Fig. 3 (e). This is a manifestation of the general property – contribution of any diagram with crossing interaction lines is equal to the contribution of some diagram with no intersections [11]. Precisely because of this property we can introduce an exact algorithm of complete summation of Feynman series.

Details of combinatorics and rules to reduce diagrams with crossing interaction lines to those without intersections were considered in Ref. [11] (see also Ref. [6])[2)]. One can easily convince himself that the number of irreducible diagrams for self – energy which are equal to the given diagram with no intersections of interaction lines is equal to the product of certain combinatorial factors $v(k)$ (k is the number of $i\gamma$ contributions in the denominator of the Green's function in diagram without intersections, standing below k interaction lines) which are associated with consequent interaction lines of this diagram. Correspondingly in the following we can use just the diagrams with no intersections of interaction lines associating extra combinatorial factors $v(k)$ to interaction lines of such diagrams. In our case $v(k) = k$ [11].

Then we can easily obtain the recursion relation determining the irreducible self – energy, which includes *all* diagrams of corresponding Feynman series [6, 11]:

$$\Sigma_k(\epsilon,\epsilon_0) = \frac{\Delta^2 v(k)}{\epsilon-\epsilon_0+ik\gamma-\Sigma_{k+1}(\epsilon,\epsilon_0)};\ v(k)=k \tag{16}$$

[2)] In the problem under consideration here combinatorics of diagrams is reduced to commensurate case of Ref. [11].

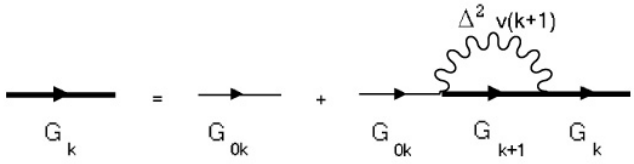

Рис. 4. "Dyson equation" representation of recurrence equation for the Green's function. Here we introduced $G_{0k} = [\epsilon-\epsilon_0+ik\gamma]^{-1}$.

Then we immediately get the recursion relation for Green' function itself:

$$G_k(\epsilon,\epsilon_0) = \{\epsilon-\epsilon_0+ik\gamma-\Delta^2 v(k+1)G_{k+1}(\epsilon,\epsilon_0)\}^{-1}, \tag{17}$$

and the *physical* Green's function is defined as $G(\epsilon,\epsilon_0) \equiv G_{k=0}(\epsilon,\epsilon_0)$, which is equivalent the complete sum of Feynman series for our model. In fact these relations give the following *continuous – fraction* representation of single – electron Green's function:

$$G(\epsilon,\epsilon_0) = \\ = \cfrac{1}{\epsilon-\epsilon_0-\cfrac{\Delta^2}{\epsilon-\epsilon_0+i\gamma-\cfrac{2\Delta^2}{\epsilon-\epsilon_0+2i\gamma-\cfrac{3\Delta^2}{\epsilon-\epsilon_0+3i\gamma-\ldots}}}} \tag{18}$$

Symbolically our recursion relation can be represented as a kind of "Dyson equation", shown in Fig. 4.

For $\gamma = 0$ we can use the following continuous – fraction representation of incomplete (upper) Γ – function:

$$\Gamma(\alpha,x) = \int_x^\infty dt e^{-t}t^{\alpha-1} = \cfrac{x^\alpha}{x+\cfrac{1-\alpha}{1+\cfrac{1}{x+\cfrac{2-\alpha}{1+\ldots}}}} \tag{19}$$

to convince ourselves that Eq. (18) reproduces an exact result of (13) obtained by direct summation of all diagrams.

4. FLUCTUATIONS WITH FINITE TRANSFERRED FREQUENCY AND FINITE CORRELATION TIME

Let us consider now more general case of fluctuations with finite characteristic frequency ω_0. We shall again consider classical potential random in time $V(t)$ (8) with pair correlation function:

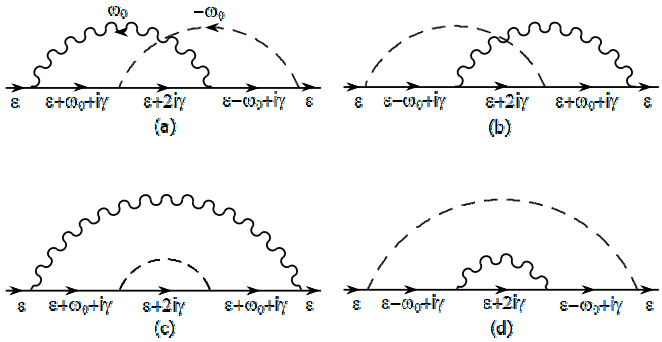

Рис. 5. Typical diagrams of second order.

$$D(t-t') = \Delta^2 e^{-\gamma|t-t'|}\cos[\omega_0(t-t')] = \\ = \frac{\Delta^2}{2} e^{-\gamma|t-t'|}\left[e^{i\omega_0(t-t')} + e^{-i\omega_0(t-t')}\right]. \qquad (20)$$

For $\omega_0 = 0$ we obtain again correlator (9) and the model with zero transferred frequency considered above.

Fourier – transform of correlator (20) has the form:

$$D(\omega) = 2\pi\frac{\Delta^2}{2}\left[\frac{1}{\pi}\frac{\gamma}{(\omega-\omega_0)^2+\gamma^2} + \frac{1}{\pi}\frac{\gamma}{(\omega+\omega_0)^2+\gamma^2}\right]. \qquad (21)$$

Thus in corresponding diagram technique we have two sorts of interaction lines – wavy and dashed, transferring frequencies $+\omega_0$ and $-\omega_0$ correspondingly. Both interaction lines lead to addition of $i\gamma$ term to energy ϵ in each electron Green's function, which is below corresponding interaction line. In Fig. 5 we show typical second order diagrams. It is easy to see that in current model the contribution of diagrams with intersecting interaction lines does not necessarily coincide with some diagram without such intersections. However, we still can obtain an exact solution for the single – electron Green's function using the generalized Ward identity.

4.1. Generalized Ward identity and recurrence equations for the Green's function

Single – electron Green's function G can be easily determined via the full two – particle function Φ:

$$G(\epsilon) = G_0(\epsilon) + G_0(\epsilon)\frac{\Delta^2}{2}\left\{\sum_{\epsilon'}\Phi_{\epsilon\epsilon'}(\omega_0) + \sum_{\epsilon'}\Phi_{\epsilon\epsilon'}(-\omega_0)\right\}. \qquad (22)$$

Here Φ is the full two – particle Green's function, including four external electronic lines and contribution corresponding to the product of two "dressed" single – particle Green's functions G. To shorten expressions in our analysis we make a replacement $\epsilon - \epsilon_0 \to \epsilon$, i.e. count energies from energy level in the well ϵ_0, then

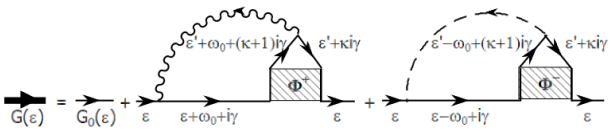

Рис. 6. Diagrammatic representation of equation for the Green's function

$G_0(\epsilon) = 1/\epsilon$. Diagrammatic representation of Eq. (22) for the Green's function is shown in Fig. 6. To find two – particle Green's functions Φ entering Eq. (22) we shall use the generalized Ward identity [22], which in this purely dynamical model takes the following form:

$$G(\epsilon+\omega) - G(\epsilon) = -\sum_{\epsilon'}\Phi_{\epsilon\epsilon'}(\omega)\left\{G_0^{-1}(\epsilon'+\omega) - G_0^{-1}(\epsilon')\right\}. \qquad (23)$$

Here the expression in figure brackets in the r.h.s. $G_0^{-1}(\epsilon'+\omega) - G_0^{-1}(\epsilon') = \epsilon' + \omega - \epsilon' = \omega$ is independent of ϵ', so that we immediately obtain:

$$\sum_{\epsilon'}\Phi_{\epsilon\epsilon'}(\omega) = -\frac{G(\epsilon+\omega) - G(\epsilon)}{\omega}. \qquad (24)$$

In the current problem any interaction line again adds $i\gamma$ term to energy of electronic lines below it, i.e. effectively our interaction lines transfer a complex frequency $\pm\omega_0 + i\gamma$. Then Ward identity (23) for the vertex with $+\omega_0$ takes the form:

$$G(\epsilon+\omega_0+i\gamma) - G(\epsilon) = \\ = -\sum_{\epsilon'}\Phi_{\epsilon\epsilon'}(\omega_0)(\epsilon'+\omega_0+(k+1)i\gamma - (\epsilon'+ki\gamma)) = \\ = -(\omega_0+i\gamma)\sum_{\epsilon'}\Phi_{\epsilon\epsilon'}(\omega_0). \qquad (25)$$

As a result for the two – particle Green's function with $+\omega_0$ vertex we obtain:

$$\sum_{\epsilon'}\Phi_{\epsilon\epsilon'}(\omega_0) = -\frac{G(\epsilon+\omega_0+i\gamma) - G(\epsilon)}{\omega_0+i\gamma}. \qquad (26)$$

Similarly for Φ with $-\omega_0$ vertex we get:

$$\sum_{\epsilon'}\Phi_{\epsilon\epsilon'}(-\omega_0) = -\frac{G(\epsilon-\omega_0+i\gamma) - G(\epsilon)}{-\omega_0+i\gamma}. \qquad (27)$$

Substituting these two – particle functions (26) and (27) into Eq. (22), we obtain the functional equation for the Green's function:

$$G(\epsilon) = G_0(\epsilon) - G_0(\epsilon)\frac{\Delta^2}{2} \times$$
$$\times \left\{ \frac{G(\epsilon+\omega_0+i\gamma) - G(\epsilon)}{\omega_0+i\gamma} + \frac{G(\epsilon-\omega_0+i\gamma) - G(\epsilon)}{-\omega_0+i\gamma} \right\} \quad (28)$$

so that:

$$G(\epsilon) = \frac{1 - \frac{\Delta^2}{2}\left[\frac{G(\epsilon+\omega_0+i\gamma)}{\omega_0+i\gamma} + \frac{G(\epsilon-\omega_0+i\gamma)}{-\omega_0+i\gamma}\right]}{G_0^{-1}(\epsilon) + \Delta^2\frac{i\gamma}{\omega_0^2+\gamma^2}}. \quad (29)$$

It should be noted that the use of the generalized Ward identity (23) allows also an exact solution (reducing to the integral equation) of the problem of finding the single – particle Green's function $G(\epsilon)$ of an electron in random *Gaussian* potential with arbitrary correlator $D(\omega)$. Equation for the Green's function in this case has the following form:

$$G(\epsilon) = G_0(\epsilon) + G_0(\epsilon)\int_{-\infty}^{+\infty}\frac{d\omega}{2\pi}D(\omega)\sum_{\epsilon'}\Phi_{\epsilon\epsilon'}(\omega). \quad (30)$$

Using Ward identity (23) we immediately obtain (24) and the integral equation for the Green's function:

$$G(\epsilon) = G_0(\epsilon) - G_0(\epsilon)\int_{-\infty}^{+\infty}\frac{d\omega}{2\pi}D(\omega)\frac{G(\epsilon+\omega) - G(\epsilon)}{\omega}. \quad (31)$$

If we use $D(\omega)$ in the form given by Eq. (21) the frequency integral here is easily calculated. The second factor in the integrand does not contain pole at $\omega = 0$ and is analytic in the upper half – plane of complex ω, so that closing the integration contour above, we obtain the contribution to integral only from the poles at $\omega = \pm\omega_0 + i\gamma$ of two Lorentzians in (21) immediately getting (28), and functional equation (29).

Solving Eq. (29) by iterations, starting from initial the approximation

$$\widetilde{G}_0(\epsilon) = \frac{1}{G_0^{-1}(\epsilon) + \Delta^2\frac{i\gamma}{\omega_0^2+\gamma^2}}, \quad (32)$$

one can easily see that each iteration adds to energy (besides $\pm\omega_0$) additional $i\gamma$ term. Thus we can introduce the following notations:

$$G_n(\epsilon) \equiv G(\epsilon+ni\gamma) \qquad G_{0n}(\epsilon) \equiv G_0(\epsilon+ni\gamma) = \frac{1}{\epsilon+ni\gamma}, \quad (33)$$

where $n = 0, 1, 2\ldots$ and apply Eq. (29) for energy $\epsilon + ni\gamma$, making replacement $\epsilon \to \epsilon + ni\gamma$. Then in notations of (33) equation (29) takes the form[3)]:

$$G_n(\epsilon) = \frac{1 - \frac{\Delta^2}{2}\left[\frac{G_{n+1}(\epsilon+\omega_0)}{\omega_0+i\gamma} + \frac{G_{n+1}(\epsilon-\omega_0)}{-\omega_0+i\gamma}\right]}{G_{0n}^{-1}(\epsilon) + \Delta^2\frac{i\gamma}{\omega_0^2+\gamma^2}}. \quad (34)$$

[3)] Naturally, Eq. (34) can be also obtained directly using the generalized Ward identity applying it for energy $\epsilon + ni\gamma$.

As a result we obtain the recursion procedure where at each "storey" n G_n depends only on real energy. Numerical realization of such procedure is rather simple. At some high "storey" $n = N \gg 1$ we define a set of $G_N(\epsilon)$, e.g. $G_N(\epsilon) = 0$. Then, withe the help of (34) and interpolation we find the set $G_{N-1}(\epsilon)$ etc., until we reach the physical $G(\epsilon) = G_{n=0}(\epsilon)$.

For $\omega_0 = 0$ we return to the model with zero transferred frequency and finite correlation time described above. In this limit the recursion equation (34) takes the form:

$$G_n(\epsilon) = \frac{1 + i\frac{\Delta^2}{\gamma}G_{n+1}(\epsilon)}{G_{0n}^{-1}(\epsilon) + i\frac{\Delta^2}{\gamma}}. \quad (35)$$

Visually the recursion procedure (35) has nothing in common with procedure (17), leading to continuous – fraction representation of G given by Eq. (18). However, direct numerical calculations show that both produce absolutely same results for the physical Green's function $G_{n=0}(\epsilon)$ (in the limit of initial "storey" $N \to \infty$).

For $\gamma = 0$ in the limit of $\omega_0 \to 0$ Eq. (28) immediately reduces to differential equation (6) for the Green's function in the usual Keldysh model, as $\lim\limits_{\omega_0\to 0}\frac{G(\epsilon+\omega_0)-G(\epsilon)}{\omega_0} = \lim\limits_{\omega_0\to 0}\frac{G(\epsilon-\omega_0)-G(\epsilon)}{-\omega_0} = \frac{dG(\epsilon)}{d\epsilon}$. Green's function $G(\epsilon)$ is analytic in the upper half – plane of complex energy ϵ and the derivative $\frac{dG(\epsilon)}{d\epsilon}$ gives the same result along different directions of $d\epsilon$ in this half – plane. Thus for other order of limits $\omega_0 = 0$, $\gamma \to 0$ from Eq. (28) we again obtain the differential equation (6). Analyticity of the Green's function allows to write it (in the upper half – plane of ϵ) as:

$$G(\epsilon) = \int_{-\infty}^{\infty} d\epsilon' \frac{\rho(\epsilon')}{\epsilon - \epsilon'}, \quad (36)$$

where $\rho(\epsilon) = -\frac{1}{\pi}ImG(\epsilon)$ is the spectral density (density of states for the quantum dot). Then in this limit in Eq. (28) we get:

$$\lim_{\gamma\to 0}\frac{G(\epsilon+i\gamma) - G(\epsilon)}{i\gamma} =$$
$$= \lim_{\gamma\to 0}\frac{1}{i\gamma}\int_{-\infty}^{\infty} d\epsilon'\rho(\epsilon')\left[\frac{1}{\epsilon+i\gamma-\epsilon'} - \frac{1}{\epsilon-\epsilon'}\right] =$$
$$= -\int_{-\infty}^{\infty} d\epsilon'\frac{\rho(\epsilon')}{(\epsilon-\epsilon')^2} = \frac{dG(\epsilon)}{d\epsilon} \quad (37)$$

Analytic properties of Green's function (36) allow to reduce the functional equation (29) to integral equation for spectral density $\rho(\epsilon)$. Let us rewrite functional equation (29) as:

$$G(\epsilon) = \widetilde{G}_0(\epsilon) - \widetilde{G}_0(\epsilon)\frac{\Delta^2}{2} \times \times \left[\frac{G(\epsilon+\omega_0+i\gamma)}{\omega_0+i\gamma} + \frac{G(\epsilon-\omega_0+i\gamma)}{-\omega_0+i\gamma}\right], \quad (38)$$

where $\widetilde{G}_0(\epsilon)$, defined in (32), can be written as:

$$\widetilde{G}_0(\epsilon) = \frac{1}{\epsilon+i\Gamma}. \quad (39)$$

Here

$$\Gamma = \frac{\Delta^2\gamma}{\omega_0^2+\gamma^2} \quad (40)$$

is an effective non – perturbative damping due to the random field. Then for the spectral density we immediately obtain:

$$\rho(\epsilon) = \widetilde{\rho}_0(\epsilon) + \frac{\Delta^2}{2\pi} \times \times Im\left\{\widetilde{G}_0(\epsilon)\left[\frac{G(\epsilon+\omega_0+i\gamma)}{\omega_0+i\gamma} + \frac{G(\epsilon-\omega_0+i\gamma)}{-\omega_0+i\gamma}\right]\right\} \quad (41)$$

where $\widetilde{\rho}_0(\epsilon) = -\frac{1}{\pi}Im\widetilde{G}_0(\epsilon) = \frac{1}{\pi}\frac{\Gamma}{\epsilon^2+\Gamma^2}$ is an effective "bare" spectral density (density of states). Eq. (41) is easily solved numerically by iterations, starting from initial approximation $\rho(\epsilon) = \widetilde{\rho}_0(\epsilon)$.

4.2. Exact solution for the Green's function in the form of infinite series

Eq. (38) can be solved by iterations starting from $\widetilde{G}_0(\epsilon)$. If we represent the result of each iteration as simple fractions (so that there are no ϵ in the coefficients), one can easily convince himself, that the Green's function G becomes the sum of $\widetilde{G}_0(\epsilon + (n-m)\omega_0 + (n+m)i\gamma)$, where n and m are integers, with coefficients independent of ϵ. Thus we look for the solution for the Green's function in the following form:

$$G(\epsilon) = \sum_{n,m=0}^{\infty} A_{nm}\frac{1}{\epsilon+(n-m)\omega_0+(n+m)i\gamma+i\Gamma}, \quad (42)$$

where coefficients A_{nm} are independent of ϵ and can be found substituting (42) into (38). Then we have:

$$\widetilde{G}_0(\epsilon)G(\epsilon+\omega_0+i\gamma) = = \sum_{n,m=0}^{\infty} A_{nm}\frac{1}{\epsilon+i\Gamma}\frac{1}{\epsilon+i\Gamma+(n+1-m)\omega_0+(n+1+m)i\gamma} = = \sum_{n,m=0}^{\infty} A_{nm}\frac{1}{(n+1)(\omega_0+i\gamma)+m(-\omega_0+i\gamma)} \times \times \left[\frac{1}{\epsilon+i\Gamma} - \frac{1}{\epsilon+i\Gamma+(n+1)(\omega_0+i\gamma)+m(-\omega_0+i\gamma)}\right] \quad (43)$$

$$\widetilde{G}_0(\epsilon)G(\epsilon-\omega_0+i\gamma) = = \sum_{n,m=0}^{\infty} A_{nm}\frac{1}{n(\omega_0+i\gamma)+(m+1)(-\omega_0+i\gamma)} \times \times \left[\frac{1}{\epsilon+i\Gamma} - \frac{1}{\epsilon+i\Gamma+n(\omega_0+i\gamma)+(m+1)(-\omega_0+i\gamma)}\right] \quad (44)$$

Substituting (43), (44) into (38) we find the coefficient A_{00} before $\frac{1}{\epsilon+i\Gamma}$ as:

$$A_{00} = 1 - \frac{\Delta^2}{2} \times \times \left[\frac{1}{\omega_0+i\gamma}\sum_{n,m=0}^{\infty} A_{nm}\frac{1}{(n+1)(\omega_0+i\gamma)+m(-\omega_0+i\gamma)} + + \frac{1}{-\omega_0+i\gamma}\sum_{n,m=0}^{\infty} A_{nm}\frac{1}{n(\omega_0+i\gamma)+(m+1)(-\omega_0+i\gamma)}\right]. \quad (45)$$

For other coefficients:

$$A_{nm} = \frac{\Delta^2}{2}\frac{1}{n(\omega_0+i\gamma)+m(-\omega_0+i\gamma)} \times \times \left[\frac{A_{n-1m}}{\omega_0+i\gamma} + \frac{A_{nm-1}}{-\omega_0+i\gamma}\right]. \quad (46)$$

Naturally we have $A_{-1m} = A_{n-1} = 0$.

Eq. (46) allows to obtain the whole set of coefficients at $n_f = n+m$ "storey" from the values of coefficients at $n_f - 1$ "storey", and finally to express all coefficients via A_{00}. Coefficients obtained for several lower "storeys" allow us to guess, that the general form of the coefficients can be written as:

$$A_{nm} = \frac{A_{00}}{n!m!}\left(\frac{\Delta^2}{2}\right)^{n+m}\frac{1}{(\omega_0+i\gamma)^{2n}(-\omega_0+i\gamma)^{2m}}. \quad (47)$$

Substitution of A_{nm} from (47) into Eq. (46) confirms this guess.

Now using Eq. (45) we can find A_{00}:

$$A_{00} = 1 - \frac{\Delta^2}{2} \times \times \left[\frac{1}{\omega_0+i\gamma}\sum_{n=1,m=0}^{\infty} A_{n-1m}\frac{1}{n(\omega_0+i\gamma)+m(-\omega_0+i\gamma)} + + \frac{1}{-\omega_0+i\gamma}\sum_{n=0,m=1}^{\infty} A_{nm-1}\frac{1}{n(\omega_0+i\gamma)+m(-\omega_0+i\gamma)}\right]. \quad (48)$$

Using (46) in (47) we get:

$$A_{00} = 1 - \sum_{\substack{n,m \\ n+m\neq 0}} A_{nm} = = 1 - \sum_{\substack{n,m \\ n+m\neq 0}} \frac{A_{00}}{n!m!}\left(\frac{\Delta^2}{2}\right)^{n+m}\frac{1}{(\omega_0+i\gamma)^{2n}(-\omega_0+i\gamma)^{2m}}. \quad (49)$$

Finally A_{00} takes the form:

$$A_{00} = \frac{1}{\sum\limits_{n=0}^{\infty} \frac{1}{n!}\left(\frac{\Delta^2}{2}\right)^n \frac{1}{(\omega_0+i\gamma)^{2n}} \sum\limits_{m=0}^{\infty} \frac{1}{m!}\left(\frac{\Delta^2}{2}\right)^m \frac{1}{(-\omega_0+i\gamma)^{2m}}} =$$
$$= e^{-\frac{\Delta^2}{2(\omega_0+i\gamma)^2}} e^{-\frac{\Delta^2}{2(\omega_0+i\gamma)^2}} = e^{-\frac{\Delta^2(\omega_0^2-\gamma^2)}{(\omega_0^2+\gamma^2)^2}} \quad (50)$$

As a result we obtain the following expression for the Green's function (42):

$$G(\epsilon) = e^{-\frac{\Delta^2(\omega_0^2-\gamma^2)}{(\omega_0^2+\gamma^2)^2}} \sum_{n,m=0}^{\infty} \frac{1}{n!}\frac{1}{m!} \frac{1}{(\omega_0+i\gamma)^{2n}(-\omega_0+i\gamma)^{2m}}$$
$$\left(\frac{\Delta^2}{2}\right)^{n+m} \frac{1}{\epsilon+(n-m)\omega_0+(n+m)i\gamma+i\Gamma} \quad (51)$$

Let us briefly analyze the limiting behavior of the Green's function and corresponding spectral density $\rho(\epsilon) = -\frac{1}{\pi} ImG(\epsilon)$ following from (51).

In the limit of $\gamma \to 0$ we get:

$$G(\epsilon) = e^{-\frac{\Delta^2}{\omega_0^2}} \sum_{n,m=0}^{\infty} \frac{1}{n!}\frac{1}{m!}\left(\frac{\Delta^2}{2\omega_0^2}\right)^{n+m} \frac{1}{\epsilon+(n-m)\omega_0+i\delta}, \quad (52)$$

and spectral density has the form:

$$\rho(\epsilon) = e^{-\frac{\Delta^2}{\omega_0^2}} \sum_{n,m=0}^{\infty} \frac{1}{n!}\frac{1}{m!}\left(\frac{\Delta^2}{2\omega_0^2}\right)^{n+m} \delta(\epsilon+(n-m)\omega_0) \quad (53)$$

which is the set of δ peaks at $\epsilon = \pm k\omega_0$. The weights of these peaks (coefficients before corresponding δ – functions) are:

$$S^{(+k)} = S^{(-k)} = e^{-\frac{\Delta^2}{\omega_0^2}} \sum_{n=0}^{\infty} \frac{1}{n!(n+k)!}\left(\frac{\Delta^2}{2\omega_0^2}\right)^{2n+k} =$$
$$= e^{-\frac{\Delta^2}{\omega_0^2}} I_k\left(\frac{\Delta^2}{\omega_0^2}\right), \quad (54)$$

where I_k – is the modified Bessel function of imaginary argument. The total area of all these peaks is:

$$S = \sum_{k=-\infty}^{\infty} S^{(k)} = e^{-\frac{\Delta^2}{\omega_0^2}} \sum_{n,m=0}^{\infty} \frac{1}{n!}\frac{1}{m!}\left(\frac{\Delta^2}{2\omega_0^2}\right)^{n+m} =$$
$$= e^{-\frac{\Delta^2}{\omega_0^2}} \sum_{n=0}^{\infty} \frac{1}{n!}\left(\frac{\Delta^2}{2\omega_0^2}\right)^n \sum_{m=0}^{\infty} \frac{1}{m!}\left(\frac{\Delta^2}{2\omega_0^2}\right)^m = 1, \quad (55)$$

as it should be.

In the limit of $\omega_0 \to 0$ we return to the model of fluctuations with finite correlation time and from Eq. (51) we obtain:

$$G(\epsilon) = e^{\frac{\Delta^2}{\gamma^2}} \sum_{n,m=0}^{\infty} \frac{1}{n!}\frac{1}{m!}\left(-\frac{\Delta^2}{2\gamma^2}\right)^{n+m} \frac{1}{\epsilon+(n+m)i\gamma+i\frac{\Delta^2}{\gamma}} =$$
$$= e^{\frac{\Delta^2}{\gamma^2}} \sum_{k=0}^{\infty} \left[\sum_{n=0}^{k} \frac{1}{n!(k-n)!}\right]\left(-\frac{\Delta^2}{2\gamma^2}\right)^k \frac{1}{\epsilon+ki\gamma+i\frac{\Delta^2}{\gamma}}. \quad (56)$$

As $\sum\limits_{n=0}^{k} \frac{k!}{n!(k-n)!} = 2^k$ we get for the Green's function:

$$G(\epsilon) = e^{\frac{\Delta^2}{\gamma^2}} \sum_{k=0}^{\infty} \frac{1}{k!}\left(-\frac{\Delta^2}{\gamma^2}\right)^k \frac{1}{\epsilon+ki\gamma+i\frac{\Delta^2}{\gamma}} = \quad (57)$$

$$= e^{\frac{\Delta^2}{\gamma^2}} \frac{1}{i\gamma}\left(\frac{\Delta^2}{\gamma^2}\right)^{-\left(\frac{\epsilon}{i\gamma}+\frac{\Delta^2}{\gamma^2}\right)} \gamma\left(\frac{\epsilon}{i\gamma}+\frac{\Delta^2}{\gamma^2}, \frac{\Delta^2}{\gamma^2}\right), \quad (58)$$

where

$$\gamma(\alpha, x) = \int_0^x dt e^{-t} t^{\alpha-1} \quad (59)$$

is incomplete (lower) Γ – function. Eqs. (57) and (58) can be considered as series and integral representations for continuous fraction of (18).

The problem of an electron in Gaussian field of dynamic fluctuations with finite correlation time has much in common with the problem of Holstein polaron in semiconductors with low mobility, i.e. with the problem of finding the single electron Green's function in Holstein model [23] of an electron interacting with optical phonon mode with frequency Ω in the limit of transfer integral between nearest neighbors $t \to 0$ ($t \ll \Omega$). Usually such problem is analyzed by making Lang – Firsov canonical transformation [24] in Holstein Hamiltonian [23] However, the diagram technique for electron – phonon interaction in this model is completely equivalent to diagram technique in our model of dynamical fluctuations with finite correlation time after the replacement:

$$\Delta \to g \qquad i\gamma \to -\Omega \quad (60)$$

where g is electron – phonon coupling constant. We only have to take into account that in this diagram technique in the denominators of electron Green's functions we have continuous addition $-\Omega$ terms instead of $i\gamma$, because of two terms in phonon propagator:

$$D(\omega) = \frac{1}{\omega-\Omega+i\delta} - \frac{1}{\omega+\Omega-i\delta} \quad (61)$$

only the first term contribute to frequency integrals due to the fact that all electronic Green's functions in this problem are retarded.

Thus the Green's function of Holstein polaron (for $t \to 0$) is determined by continuous fraction (18) with

replacement (60). For the first time Holstein polaron Green's function of this form was derived in Ref. [25]. Our series expression for the Green's function (57) in the model of dynamical fluctuations with finite correlation time immediately allows us to get (after the replacement (60)) the well known exact result for the Green's function of Holstein polaron as [24, 25]:

$$G(\epsilon) = e^{-\frac{g^2}{\Omega^2}} \sum_{k=0}^{\infty} \frac{1}{k!} \left(\frac{g^2}{\Omega^2}\right)^k \frac{1}{\epsilon - k\Omega + \frac{g^2}{\Omega} + i\delta} = \quad (62)$$

Note that our use of the Ward identity is in some sense equivalent to Lang – Firsov transformation in Holstein polaron problem. An effective "bare" Green's function (39)with non – perturbative damping (40), appearing due to the use of the Ward identity, in the model with $\omega_0 = 0$ is:

$$\widetilde{G}_0(\epsilon) = \frac{1}{\epsilon + i\frac{\Delta^2}{\gamma}}. \quad (63)$$

which in the Holstein polaron problem, after the replacement (60), takes the form:

$$\widetilde{G}_0(\epsilon) = \frac{1}{\epsilon + \frac{g^2}{\Omega} + i\delta}, \quad (64)$$

appearing after Lang – Firsov transformation of an effective "bare" Green's function of polaron with non – perturbative shift of the ground state $\epsilon_0 = -\frac{g^2}{\Omega}$ [24,25].

5. NUMERICAL RESULTS

Now for the most general model of fluctuations with finite frequency and correlation time we actually have three exact numerical procedures to find the Green's function:

1. recursive procedure (34),
2. integral equation for spectral density (41),
3. series representation (51).

For the wide range of parameters (Δ, γ, ω_0) of the model our numerical calculations showed that all three procedures lead to absolutely same results for spectral density (density of states). Of these, the recursion procedure (34) is most fast for numerics, though for small values of $\gamma \ll \Delta, \omega_0$ and $\omega_0 < 0.3\Delta$ it requires significant increase of the number of energies in corresponding array and the number of an initial "storey" to start, while series representation (51) in this range of parameters is well convergent. However, the series representation is inappropriate for direct numerical analysis in the region of $\Delta \gg \gamma > \omega_0$, which is connected both with large values of the exponent before the series and with the large number of terms in the series to be taken into account to compensate this exponent.

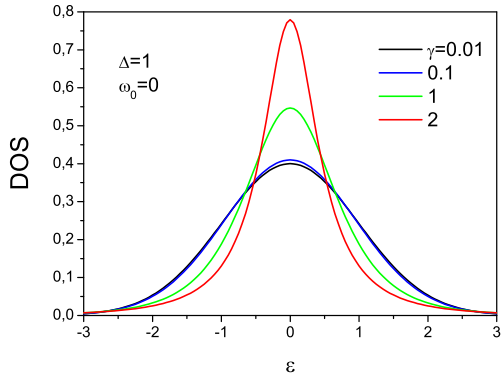

Рис. 7. Spectral density (density of states in quantum dot) in the model with finite correlation time ($\omega_0 = 0$) for different values of γ.

Now let us discuss our numerical results. In Fig.7 we demonstrate evolution of the spectral density with increasing γ (i.e. with decreasing correlation time of fluctuations) for the model with $\omega_0 = 0$. For $\gamma = 0$ (in the usual Keldysh model) spectral density is Gaussian with the width Δ (dispersion – Δ^2). The growth of γ leads to decrease of characteristic width of the spectral density with appropriate growth of $\rho(0)$.

In Fig. 8 we show spectral densities (densities of states in quantum dot) in the model with finite transferred frequency for $\Delta = 1$ and different values of ω_0 and γ. We can see that in all cases for small γ significant modulations of the spectral density appear with frequency ω_0 with peaks of spectral density appearing at energies $\epsilon = \pm n\omega_0$, where n is integer. The height of these peaks decreases with increasing n and for $\epsilon > 3\Delta$ peaks are practically invisible. Increasing γ leads to decreasing peak heights and starting from some values of γ modulations with frequency ω_0 become unobservable. Further increase of γ only somehow narrows Gaussian – like spectral density, as it was observed in Fig.7 for the model with $\omega_0 = 0$. At large enough values of γ, when no modulations of spectral density with frequency ω_0 are observed, the growth of ω_0 only weakly changes the spectral density (see Fig.8f) and we can use more simple model with $\omega_0 = 0$. Note that the values of γ, for which modulations of spectral

density are observable depends on ω_0. In particular, for $\omega_0 = 0.1$ (Fig.8a) modulations are observed only for $\gamma = 0.0001$, while for $\omega_0 = 0.5$ (Fig.8c) modulations are observable already for $\gamma = 0.05$.

As was already noted above it is not difficult to generalize our model to consider not a single quantum well in dynamical random fields, but electron in crystal lattice of d dimensions (in the following we take lattice parameter $a \equiv 1$) with transfer integral between nearest neighbors t, which is placed in a capacitor, with noise created at its plates, the same for all lattice sites. This field is thus constant in space and the electron momentum is not changed during scattering, so that the account of electron hops between lattice sites is taken into account by a simple replacement $\epsilon \to \epsilon - \epsilon_{\mathbf{p}}$, where $\epsilon_{\mathbf{p}}$ is band – like spectrum of electrons with quasimomentum $\mathbf{p}$. In such a model the Green's function is given by:

$$G(\epsilon, \mathbf{p}) = \int_{-\infty}^{\infty} d\epsilon' \frac{\rho(\epsilon')}{\epsilon - \epsilon_{\mathbf{p}} - \epsilon' + i\delta}, \tag{65}$$

where $\rho(\epsilon)$ is the spectral density (density od states) obtained above for the problem of a single quantum dot. Then for the density of states of our lattice model in d dimensions in dynamical random field we obtain:

$$N_d(\epsilon) = -\frac{1}{\pi} Im \sum_{\mathbf{p}} G(\epsilon, \mathbf{p}) = \int_{-\infty}^{\infty} d\xi N_{0d}(\xi)\rho(\epsilon - \xi), \tag{66}$$

where $N_{0d}(\xi) = \sum_{\mathbf{p}} \delta(\xi - \epsilon_{\mathbf{p}})$ is the "bare" density of states of d dimensional system in the absence of random field.

For one – dimensional chain:

$$\epsilon_p = -2t\cos(p) \tag{67}$$

"Bare" density of states in this case is:

$$N_{0d1}(\epsilon) = \frac{1}{\pi} \frac{1}{\sqrt{4t^2 - \epsilon^2}} \tag{68}$$

and diverges at the band edges. Full densities of states for this model for initial band of the width $W = 4t = 1$ and different values of random field parameters are shown in Fig. 9.

For two – dimensional lattice:

$$\epsilon_{\mathbf{p}} = -2t(\cos(p_x) + \cos(p_y)). \tag{69}$$

"Bare" density of states in this case has step – like behavior at the band edges and logarithmic Van-Hove singularity at the band center. Full densities of states obtained in this model for the band with initial width $W = 8t = 1$ and different values of random field parameters are shown in Fig.10.

To analyze three – dimensional case we use as the "bare" the model semi – elliptic density of states:

$$N_{0d3}(\epsilon) = \frac{2}{\pi D^2}\sqrt{D^2 - \epsilon^2}, \tag{70}$$

where D is the band half – width. This model guarantees the valid $\sim \epsilon^{1/2}$ "bare" density of states behavior near the band edges for $d = 3$. Full densities of states in this model for initial bandwidth $W = 2D = 1$ and different values of random field parameters are shown in Fig.11.

Thus in all these models for small values of γ we can observe modulations of the density of states with frequency ω_0. Increasing γ leads to sharp weakening of these modulations. The growth of random field amplitude Δ (Figs.9,10,11a,b,c) leads to some increase of modulations amplitude and weakening of singularities (Van - Hove, at band edges etc..), related to the "bare" density of states. For $\Delta = W$ (Figs.9,10,11c) density of states practically "forgets" the bare one. Increase of spatial dimensionality d leads to weakening of the modulations.

In one – dimensional chain (Fig.9) for $\omega_0 = 0.5$ peaks at $\epsilon = \pm\omega_0$ coincide with band – edges, where the bare density of states (68) diverges, while the peak at $\epsilon = 0$ appears at the minimum of the bare density of states. Thus the peaks at $\epsilon = \pm\omega_0$ are effectively increased and can can become larger than the weakened peak at $\epsilon = 0$ (Fig.9a,b,e). This mutual influence of divergence in the bare density of states at the bad edges in one dimension and modulations with frequency ω_0 leads to significant changes if the amplitude and shape of central peak (at $\epsilon = 0$) with small changes of ω_0 close to $\omega_0 = 0.5$ (Fig.9d,e,f).

For two – dimensional lattice Van - Hove divergence is at the band center, and central peak of modulations is always significantly larger than peaks at $\epsilon = \pm\omega_0$ and its shape is only weakly changes with small variations of ω_0 close to $\omega_0 = 0.5$ (Fig.10d,e,f).

For three – dimensional model modulations in the density of states with frequency ω_0 are weak enough and for $\omega_0 = 0.5$ even a small dip is observed in the density of states in the middle of the band (at $\epsilon = 0$) (Fig.11a,b,c,e). Small variations of ω_0 close to $\omega_0 = 0.5$ significantly change the shape of this weak feature at the band center (Fig.11d,e,f).

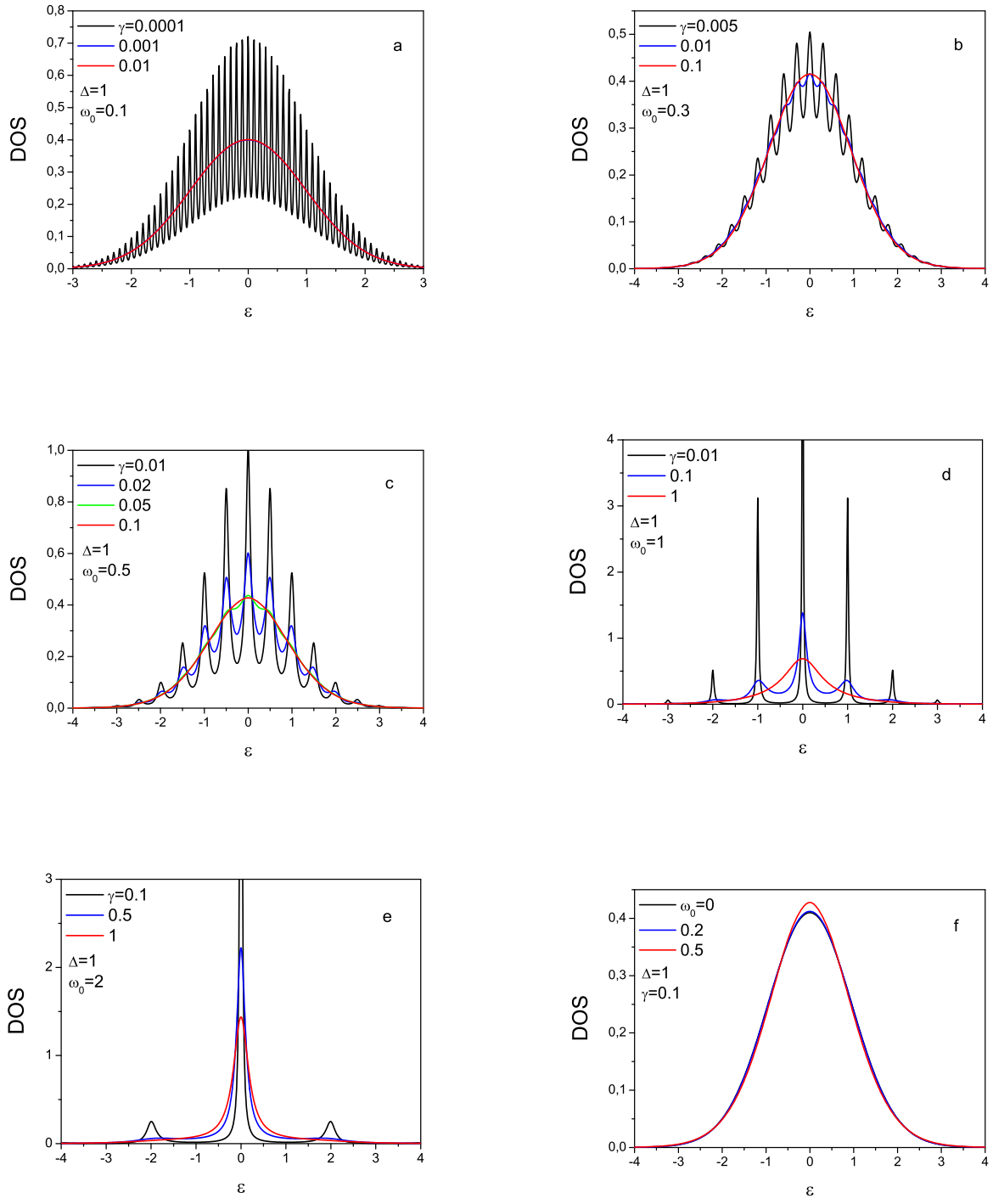

Рис. 8. Spectral density (density of states) of the quantum dot in the model with finite transfer frequency and relaxation time for $\Delta = 1$ and different values of ω_0 and γ.

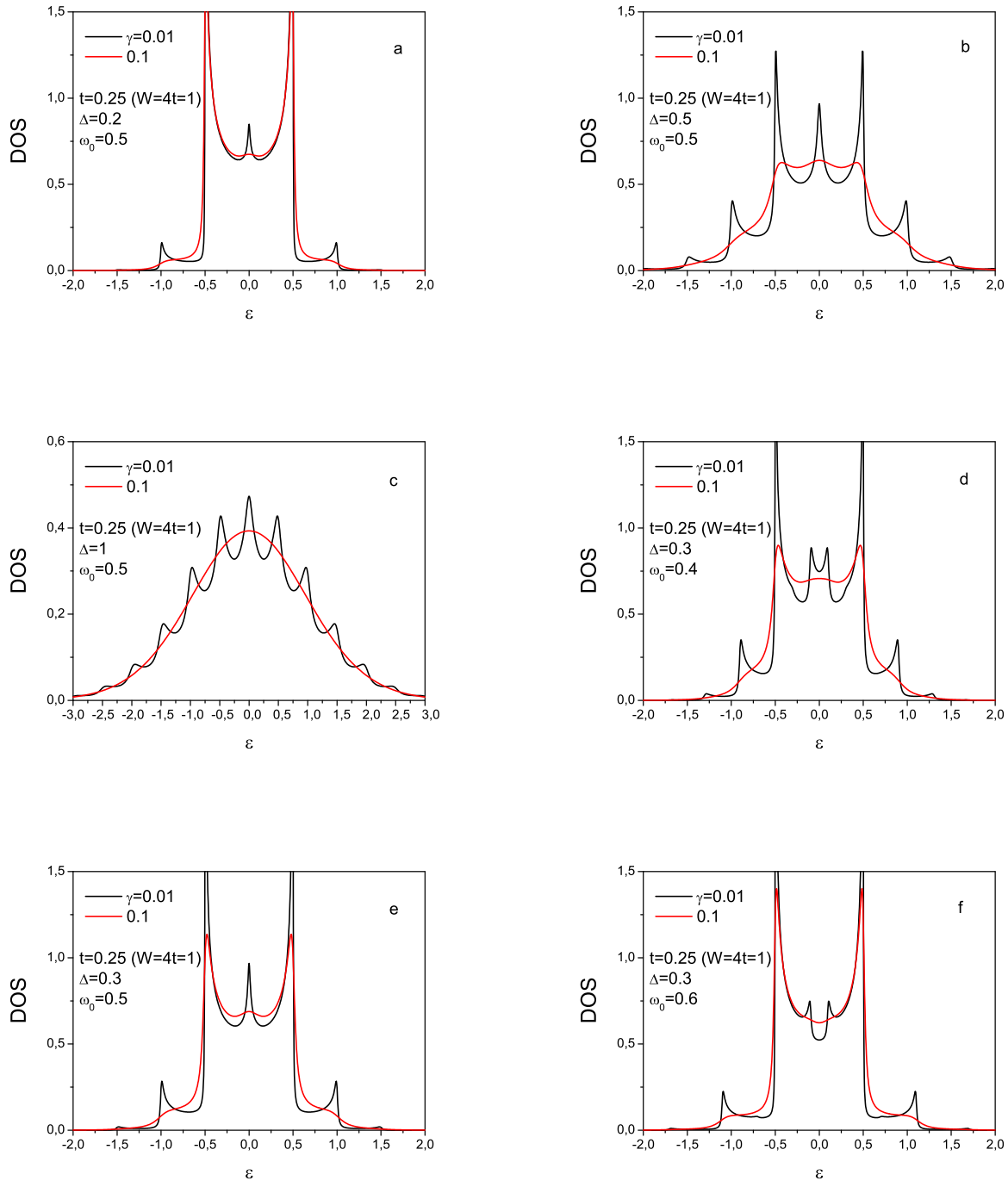

Рис. 9. Density of states for one – dimensional chain with initial bandwidth $W = 4t = 1$ for different Δ, ω_0 and γ.

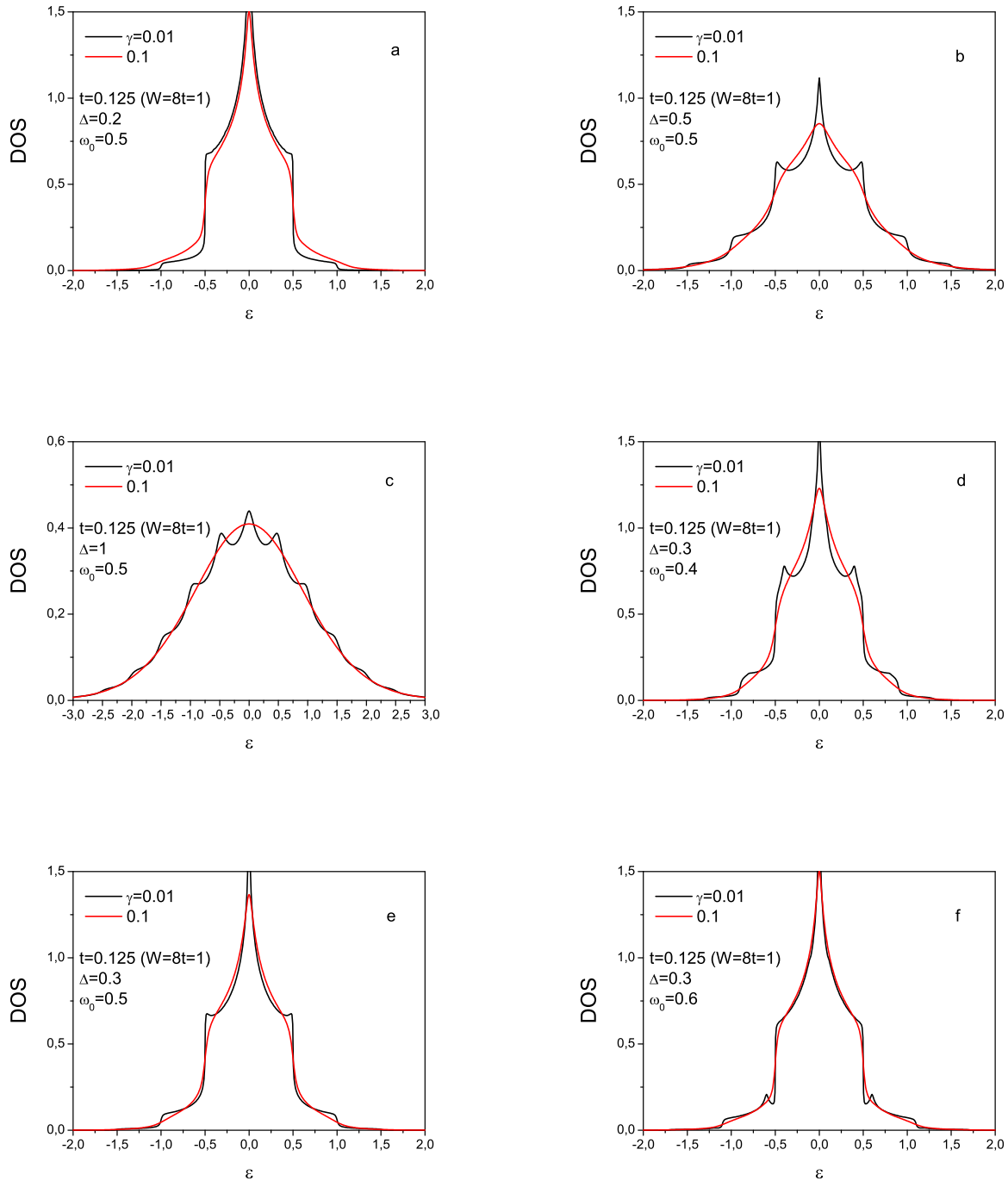

Рис. 10. Density of states in two – dimensional lattice with initial bandwidth $W = 8t = 1$ for different Δ, ω_0 and γ.

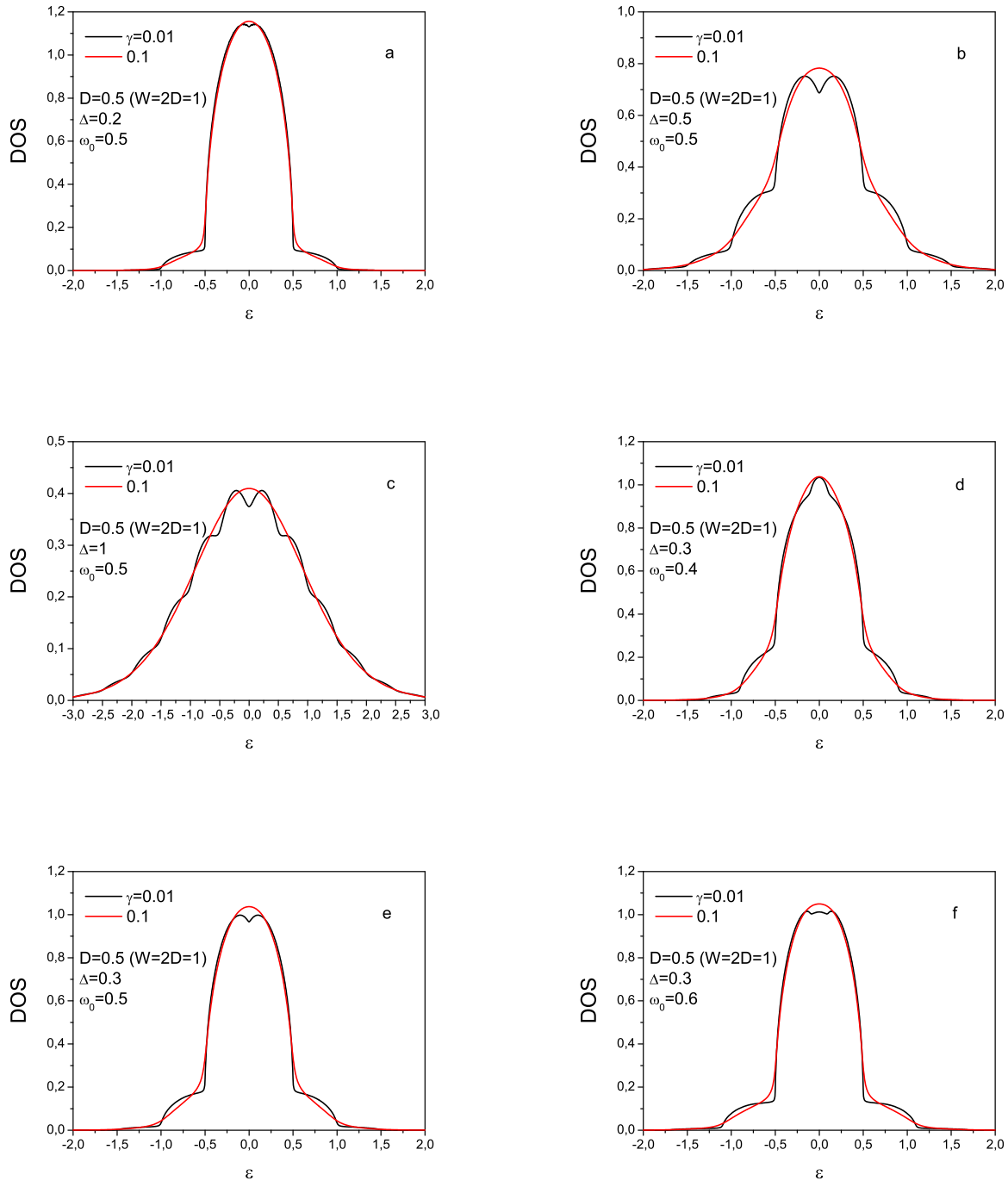

Рис. 11. Density of states of three – dimensional system with initial semi – elliptic density of states with bandwidth $W = 2D = 1$ for different Δ, ω_0 and γ.

6. CONCLUSIONS

Our analysis shows a plenty of new and interesting results, which can be derived even for this simple enough version of the generalized dynamical Keldysh model for the case of random fields with finite transferred frequency. It seems obvious that this model can have a direct relation to situations realized in real systems with quantum dots, which are used in different microelectronic devices, while the frequency ω_0 can be related to the clock frequency of these devices. Of course, the current simplest model is oversimplified, but one can hope that the results obtained can be useful also for the analysis of processes in realistic devices.

The question of experimental realization of our model remains open. In principle, the studies of quantum dots in the specially created (e.g. by electrotechnical means) random field seems quite feasible, though parameters of interaction with this are to be specially chosen to make the results discussed above observable. All this is also directly related to electronic systems (lattices) of different dimensionalities placed in a random field created on "capacitor" plates.

In real physical systems dynamical random fields can be created e.g. by phonons in the classical limit, when the temperature is much larger than the characteristic frequency of these phonons ω_0. For example, we can consider electron smattering at the interface of metallic film and dielectric substrate. It is well known that scattering with small transferred momenta (almost "forward" scattering) can appear at the interface of metallic monolayer of FeSe on the substrate made of ionic $SrTiO_3$ insulator [26], which leads to interesting models of superconductivity enhancement in this system [27]. Unfortunately we can not apply the analysis given above to this system, because the frequency of optical phonon in $SrTiO_3$ is pretty high and it can not be considered as classical (external random field). However, we can not exclude the existence of similar systems (structures) with "soft" enough optical phonons.

As was already noted above, the model with a single quantum well is directly generalized to the case of several wells [18, 19], leading to Keldysh model with multicomponent noise. In particular, the model with two wells is closely related (in the variant with band electrons) to the exactly solvable model of pseudogap state [7–12]. Different models of this kind were actively used to describe the pseudogap, appearing due to electron scattering by fluctuations of short – range order in one – dimensional models [6–12], which were also generalized for two – dimensional case to describe pseudogap in high – temperature superconductors [13–17]. In most of these papers only scattering by quasi static fluctuations was considered. It is of great interest to generalize these models for the case of dynamical fluctuations with finite transferred frequency, created by appropriate "soft" modes. However, it is clear that the analysis of such models requires significant development of the methods used in this paper. We hope to perform such studies in some future.

ЛИТЕРАТУРА

1. L.D. Landau, E.M. Lifshitz. Mechanics. Pergamon Press, Ozford, 1976

2. S.M. Rytov. Introduction to Statistical Radiophysics. "Nauka", Moscow , 1966 (in Russian)

3. B.R. Levin. Theoretical Foundations of Statistical Radio Engineering. "Sovetskoe Radio", Moscow, 1969 (in Russian)

4. L. V. Keldysh, *Semiconductors in strong electric field*, Dr. Sci. Thesis, Lebedev Institute, Moscow, 1965

5. A. L. Efros, *Theory of the electron states in heavily doped semiconductors*, Zh. Eksp. Teor. Fiz. **59**, 880 (1970) Sov. Phys. – JETP **32**, 479 (1971); [Zh. Eksp. Teor. Fiz. **59**, 880 (1970)]

6. M. V. Sadovskii. *'Diagrammatics*, World Scientific, Singapore, 2nd ed., 2019

7. M.V. Sadovskii. *A model of a disordered system (A contribution to the theory of "liquid semiconductors").* Sov. Phys. – JETP **39**, 845 (1974); [Zh. Eksp. Teor. Fiz. **66**, 1720 (1974)]

8. M.V. Sadovskii. *Quasi-one-dimensional systems undergoing a Peierls transition.* Sov. Phys. – Solid State **16**, 1632 (1974); [Fizika Tverdogo Tela **16**, 2504 (1974)]

9. W. Wonneberger, R. Lautenschlager. *Theory of infrared absorption of linear conductors.* J. Phys. C: Solid State Phys. **9**, 2865 (1976)

10. W. Wonneberger. *Infrared absorption of incommensurate linear condictors.* J. Phys. C: Solid State Phys. **10**, 1073 (1977)

11. M.V. Sadovskii. *Exact solution for the density of electronic states in a model of a disordered system.* Sov. Phys. – JETP **50**, 989 (1979); [Zh. Eksp. Teor. Fiz. **77**, 2070 (1979)]

12. M.V. Sadovskii, A.A. Timofeev. *The two-particle Green function in a model of a one-dimensional disordered system: An exact solution?*. J. Moscow Phys. Soc. **1**, 391 (1991)

13. J. Schmalian, D. Pines, B. Stojkovic. *Weak pseudogap behavior in the underdoped cuprate superconductors*. Phys. Rev. Lett. **80**, 3839 (1998)

14. J. Schmalian, D. Pines, B. Stojkovic. *Microscopic theory of weak pseudogap behavior in the underdoped cuprate superconductors: General theory and quasiparticle properties*. Phys. Rev. B **60**, 667 (1999)

15. E.Z. Kuchinskii, M.V. Sadovskii. *Models of the pseudogap state of two-dimensional systems*. JETP **88**, 968 (1999); [Zh. Ekap. Teor. Fiz. **115**, 1765 (1999)]

16. M.V. Sadovskii. *Pseudogap in high-temperature superconductors*. Physics – Uspekhi **44**, 515 (2001); [Usp. Fiz. Nauk **171**, 5 39 (2001)]

17. M.V. Sadovskii. *Models of the pseudogap state in high-temperature superconductors*. In *"Strings, Branes, Lattices, Networks, Pseudogaps Dust*. "Scientific World", Moscow, 2007 (in Russian); ArXiv:cond-mat/0408489

18. M.N. Kiselev, K.Kikoin, *Scalar and vector Keldysh models in the time domain*, JETP Letters, **89** (3), 133 (2009).

19. D.V. Efremov, M.N. Kiselev. *Seven Études on Dynamical Keldysh model*. SciPost Phys. Lect. Notes 65, doi:10.21468/SciPostPhysLectNotes65

20. A. A. Abrikosov, L. P. Gorkov, and I. E. Dzyaloshinski, *Methods of Quantum Field Theory in Statistical Physics*, Prentice-Hall, Englewood Cliffs, NJ, 1963.

21. E.Z. Kuchinskii, M.V. Sadovskii, *Combinatorics of Feynman diagrams for the problems with Gaussian random field*, JETP **113**, 664 (1999); [Zh. Eksp. Teor. Fiz. **113**, 664 (1998)]

22. E.Z. Kuchinskii, I.A. Nekrasov, M.V. Sadovskii. *Pseudogaps in Strongly Correlated Metals: Optical Conductivity within the Generalized Dynamical Mean-Field Theory Approach*, Phys. Rev. B **75**, 115102-115112 (2007)

23. T. Holstein. *Studies of polaron motion*, Ann. Phys. **8**, 325, 343 (1959)

24. I. G. Lang and Y. A. Firsov, *Kinetic Theory of Semiconductors with Low Mobility*, Sov. Phys. JETP **16**, №5, 1301 (1963) [Zh. Eksp. Teor. Fiz **43**, 1843 (1963)].

25. Glen L. Goodvin, Mona Berciu, George A. Sawatzky. *The Green's Function of the Holstein Polaron*, Phys. Rev. B **74**, 245104 (2006);

26. Lee J J, Schmitt F T, Moore R G, Johnston S, Cui Y T, Li W, Liu Z K, Hashimoto M, Zhang Y, Lu D H, Devereaux T P, Lee D H, Shen Z X. *Interfacial mode coupling as the origin of the enhancement of Tc in FeSe films on $SrTiO_3$*, Nature **515**, 245 (2014)

27. M.V. Sadovskii. *High – temperature superconductivity in FeSe monolayers*, Physics – Uspekhi **59**, 947 (2016); [Usp. Fiz. Nauk **186**, 1035 (2016)]

ISSN 0021-3640, JETP Letters, 2024, Vol. 120, No. 3, pp. 205–207. © The Author(s), 2024. This article is an open access publication.
ISSN 0021-3640, JETP Letters, 2024. © The Author(s), 2024. This article is an open access publication.
Russian Text © The Author(s), 2024, published in Pis'ma v Zhurnal Eksperimental'noi i Teoreticheskoi Fiziki, 2024, Vol. 120, No. 3, pp. 214–216.

CONDENSED MATTER

Upper Limit for the Superconducting Transition Temperature in Eliashberg–McMillan Theory

M. V. Sadovskii*

Institute for Electrophysics, Russian Academy of Sciences, Ural Branch, Yekaterinburg, 620016 Russia

**e-mail: sadovski@iep.uran.ru*

Received July 3, 2024; revised July 3, 2024; accepted July 3, 2024

We present simple qualitative estimates for the maximal superconducting transition temperature, which may be achieved due to electron–phonon coupling in Eliashberg–McMillan theory. It is shown that in the limit of very strong coupling the upper limit for transition temperature is determined in fact by a combination of atomic constants and density of conduction electrons.

DOI: 10.1134/S0021364024602409

Experimental discovery of high-temperature superconductivity in hydrides under high (megabar) pressures [1, 2] stimulated the search for the ways to achieve superconductivity at room temperature [3]. At the moment the common view [4, 5] is that the high-temperature superconductivity in hydrides can be described in the framework of the standard Eliashberg–McMillan theory [6–8]. Within this theory many attempts were undertaken to estimate the maximal achievable superconducting transition temperature and the discussion of some of these attempts can be found in the reviews [4, 5, 9]. In the recent paper [10] a new upper limit for T_c was proposed, expressed as some combination of fundamental constants. Below we shall show that with minor modifications such T_c limit follows directly from Eliashberg–McMillan theory.

Traditionally, after the appearance of BCS theory, in most papers devoted to possible ways of increasing T_c, discussion develops in terms of dimensionless constant of electron–phonon coupling λ and characteristic (average) frequency $\langle\Omega\rangle$ of phonons, responsible for Cooper pairing. In their fundamental paper [11] Allen and Dynes obtained in the limit of very strong coupling $\lambda > 10$ the following expression for T_c:[1]

$$T_c = 0.18\sqrt{\lambda\langle\Omega^2\rangle}. \tag{1}$$

Then it seems that limitations for the value of T_c are just absent, so that quite high values of T_c can be obtained with electron–phonon pairing mechanism. In reality the situation is more complicated. Actually parameters λ and $\langle\Omega^2\rangle$ in Eliashberg–McMillan theory are not independent, which is well known for quite a time [4, 5, 9, 12].

The relation of λ and $\langle\Omega^2\rangle$ is clearly expressed by McMillan's formula for λ, first derived in [8]:

$$\lambda = \frac{N(0)\langle I^2\rangle}{M\langle\Omega^2\rangle}, \tag{2}$$

where M is an ion mass, $N(0)$ is electronic density of states at the Fermi level and we introduced the matrix element of the gradient of electron–ion potential, averaged over the Fermi surface:

$$\langle I^2\rangle = \frac{1}{[N(0)]^2}\sum_{\mathbf{p}}\sum_{\mathbf{p}'}\left|\langle\mathbf{p}|\nabla V_{ei}(\mathbf{r})|\mathbf{p}'\rangle\right|^2\delta(\varepsilon_{\mathbf{p}})\delta(\varepsilon_{\mathbf{p}'}) = \left\langle\left|\langle\mathbf{p}|\nabla V_{ei}(\mathbf{r})|p'\rangle\right|^2\right\rangle_{FS}. \tag{3}$$

Here, $\varepsilon_{\mathbf{p}}$ is the spectrum of free electrons, with energy zero chosen at the Fermi surface. Equation (2) gives very useful representation for the coupling constant λ, which is routinely used in the literature and in practical (ab initio) calculations [5].

Using Eq. (2) in Eq. (1) we immediately obtain:

$$T_c^{\star} = 0.18\sqrt{\frac{N(0)\langle I^2\rangle}{M}} \tag{4}$$

so that both λ and $\langle\Omega^2\rangle$ just drop out from the expression for $T_c^{\star}$, which is now expressed via Fermi surface averaged matrix element of electron–ion potential, ion mass and electron density of states at the Fermi level. The only deficiency of this expression is the loss of intuitive understanding due to the absence of parameters in terms of which T_c is usually treated.

[1] In fact this asymptotic behavior works rather satisfactorily already for $\lambda > 2$.

As was already noted, all parameters entering this expression can be rather simply obtained during the ab initio calculations of T_c for specific materials (compounds) [5]. Let us also stress that the value of $T_c^\star$ defined in Eq. (4), calculated for any specific material does not have any direct relation to real value of T_c, but just defines precisely the upper limit of T_c, which "would be achieved" in the limit of strong enough electron–phonon coupling. Below we shall present some elementary qualitative estimates of its value.

In the following we shall assume to be dealing with three-dimensional metal with cubic symmetry with an elementary cell with lattice constant a and just one conduction electron per atom. Then we have:

$$N(0) = \frac{mp_F}{2\pi^2\hbar^3}a^3, \tag{5}$$

where $p_F \sim \hbar/a$ is the Fermi momentum, m is the mass of free (band) electron. Electron–ion potential (single-charged ion, e is electron charge) can be estimated as:

$$V_{ei} \sim \frac{e^2}{a} \sim e^2 p_F/\hbar \tag{6}$$

so that its gradient is:

$$\nabla V_{ei} \sim \frac{e^2}{a^2} \sim e^2 p_F^2/\hbar^2. \tag{7}$$

Then we easily obtain the estimate of (3):

$$I^2 \sim \left(\frac{e^2}{a^2}\right)^2 \sim (e^2 p_F^2/\hbar^2)^2. \tag{8}$$

Here, we have dropped different numerical factors of the order of unity. Collecting them back in the model of free electrons we get an estimate for $T_c^\star$ from Eq. (4) as:

$$T_c^\star \sim 0.2\sqrt{\frac{m}{M}}\frac{e^2}{\hbar v_F}E_F, \tag{9}$$

where $E_F = p_F^2/2m$ is the Fermi energy, $v_F = p_F/m$ is the electron velocity at the Fermi surface. The value of $\frac{e^2}{\hbar v_F}$, as is well known, represents the dimensionless coupling for Couloumb interaction and for typical metals it is of the order of or greater than unity. The factor of $\sqrt{\frac{m}{M}}$ determines isotopic effect.

Let us measure length in units of the Bohr radius a_B introducing the standard dimensionless parameter r_s by relation $a^3 = \frac{4\pi}{3}(r_s a_B)^3$. Then we have:

$$a \sim r_s a_B = r_s\frac{\hbar^2}{me^2} = r_s\frac{\hbar}{mc\alpha}, \tag{10}$$

where we have introduced the fine structure constant $\alpha = \frac{e^2}{\hbar c}$. Correspondingly the Fermi momentum is given by:

$$p_F \sim \frac{\hbar}{r_s a_B} = \frac{me^2}{\hbar r_s} = \frac{mc}{\hbar r_s}\alpha. \tag{11}$$

Then $T_c^\star$ (4) can be rewritten as:

$$\begin{aligned} T_c^\star &\sim \frac{0.2}{r_s}\sqrt{\frac{m}{M}}\alpha^2 mc^2 = \frac{0.2}{r_s}\sqrt{\frac{m}{M}}\frac{me^4}{\hbar^2} \\ &= \frac{0.2}{r_s}\sqrt{\frac{m}{M}}\,\mathrm{Ry}, \end{aligned} \tag{12}$$

where $\mathrm{Ry} = me^4/\hbar^2 \approx 13.6$ eV is the Rydberg constant. Here we have obtained the same combination of fundamental (atomic) constants, which was suggested in [10], by some quite different reasoning, as determining the upper limit of superconducting critical temperature. However, our expression contains an extra factor of r_s^{-1}, which necessarily reflects the specifics of a material under consideration (density of conduction electrons), so that the value of $T_c^\star$ is in no sense universal.

As was already noted above the value of $T_c^\star$ strictly speaking has no relation at all to the real superconducting transition temperature T_c. However, expressions (9) and (12) may be useful to estimate "potential perspectives" of some material in the sense of achieving high values of transition temperatures under the conditions of strong electron–phonon coupling. For example in metallic hydrogen M is equal to proton mass and we have $\sqrt{\frac{m}{m_p}} \sim 0.02$, so that for $r_s = 1$ we get an estimate of $T_c^\star \sim 650$ K. This is in nice agreement with the result of $T_c = 600$ K, obtained in [12] solving Eliashberg equations for FCC lattice of metallic hydrogen with $r_s = 1$, taking into account the calculated softening of the phonon spectrum, leading to realizations of very strong coupling ($\lambda = 6.1$). At the same time in the recent paper [13] an elegant numerical study of superconductivity of metallic hydrogen within jellium model has shown, that the maximal value of T_c can be achieved at $r_s \sim 3$, not exceeding 30 K. This is obviously related to the fact that in the "jellium" model the weak coupling is realized and there is no softening of the phonon spectrum. Finally we hope that Eqs. (9) and (12) can be relevant for preliminary estimates of T_c in some of the metallic hydrides, which are currently under intensive study in the search for room-temperature superconductivity.

FUNDING

This work was supported by ongoing institutional funding. No additional grants to carry out or direct this particular research were obtained.

CONFLICT OF INTEREST

The author of this work declares that he has no conflicts of interest.

REFERENCES

1. A. P. Drozdov, M. I. Eremets, I. A. Troyan, V. Ksenofontov, and S. I. Shylin, Nature (London, U. K.) **525**, 73 (2015).
2. J. A. Flores-Livas, L. Boeri, A. Sanna, G. Pinofeta, R. Arita, and M. Eremets, Phys. Rep. **856**, 1 (2020).
3. I. A. Troyan, D. V. Semenok, A. V. Sadakov, I. S. Lyubutin, and V. M. Pudalov, J. Exp. Theor. Phys. **139**, (2024, in press); arXiv: 2406.11344.
4. L. P. Gor'kov and V. Z. Kresin, Rev. Mod. Phys. **90**, 01001 (2018).
5. W. E. Pickett, Rev. Mod. Phys. **95**, 021001 (2023).
6. G. M. Eliashberg, Sov. Phys. JETP **11**, 696 (1960).
7. G. M. Eliashberg, Sov. Phys. JETP **12**, 1000 (1961).
8. W. L. McMillan, Phys. Rev. **167**, 331 (1968).
9. M. V. Sadovskii, Phys. Usp. **65**, 724 (2022).
10. K. Trachenko, D. Montserrat, M. Hutcheon, and C. J. Pickard, arXiv: 2406.08129.
11. P. B. Allen and R. C. Dynes, Phys. Rev. **12**, 905 (1975).
12. E. G. Maksimov, Phys. Usp. **51**, 567 (2008).
13. D. van der Marel and C. Berthod, arXiv: 2404.05554.

Translated by the author

LIST OF SCIENTIFIC PUBLICATIONS BY M.V. SADOVSKII

Books and Reviews:

1. M.V. Sadovskii. Superconductivity and Localization. World Scientific, 2000
2. M.V. Sadovskii. Lectures on Statistical Physics. "ICS", Moscow-Izhevsk, 2003 (in Russian)
3. M.V. Sadovskii. Lectures on Quantum Field Theory. "ICS", Moscow-Izhevsk, 2003 (in Russian)
4. M.V. Sadovskii. Diagrammatics. "ICS", Moscow-Izhevsk, 2004 (in Russian)
5. M.V. Sadovskii. Diagrammatics. World Scientific, 2006
6. M.V. Sadovskii. Diagrammatics, 2 ed. "ICS", Moscow-Izhevsk, 2010 (in Russian)
7. M.V. Sadovskii. Statistical Physics. Walter de Gruyter, Berlin/Boston, 2012
8. M.V. Sadovskii. Quantum Field Theory. Walter de Gruyter, Berlin/Boston, 2013
9. M.V. Sadovskii. Diagrammatics, 3 ed. "ICS", Moscow-Izhevsk, 2019 (in Russian)
10. M.V. Sadovskii. Diagrammatics, 2nd Edition. World Scientific, 2019
11. M.V. Sadovskii. Statistical Physics, 2nd Edition. De Gruyter, 2019
12. M.V. Sadovskii. Quantum Field Theory, 2nd Edition. De Gruyter, 2019
13. V.A. Alekseev, A.A. Andreev, M.V. Sadovskii. Semiconductor–Metal Transition in Liquid Semiconductors. Sov. Phys. – Uspekhi, v. 23, No. 9, 551–575 (1980)
14. M.V. Sadovskii. Electron Localization in Disordered Systems: Critical Behavior and Macroscopic Manifestations. Sov. Phys. – Uspekhi, v. 24, No. 2, 96–115 (1981)
15. M.V. Sadovskii. Theory of Electron Localization in Disordered Systems. Sov. Sci. Rev. A. Physics Reviews, Ed. by I.M. Khalatnikov, v. 7, 1–130, Harwood Academic Publishers, NY, 1986
16. B.N. Goshchitskii, V.L. Kozhevnikov, M.V. Sadovskii. High-T_c Studies in Sverdlovsk. Int. J. Mod. Phys. B, v. 2, No. 6, 1331–1379 (1988)
17. M.V. Sadovskii. Superconductivity in Strongly Disordered Systems. In "Studies of High-Temperature Superconductors", Ed. by A.V. Narlikar, v. 11, 131–223, Nova Science Publishers, NY, 1993
18. M.V. Sadovskii. Superconductivity and Localization. Superconductivity, Physics, Chemistry, Technology, v. 8, No. 3, 337–442 (1995) (in Russian)
19. M.V. Sadovskii. Superconductivity and Localization. Physics Reports, v. 282, No. 5&6, 225–348 (1997)

20. M.V. Sadovskii. Pseudogap in High-Temperature Superconductors. Physics Uspekhi, v. 44, No. 5, 515–540 (2001)
21. M.V. Sadovskii. Models of the Pseudogap State in High-Temperature Superconductors. In "Strings, branes, lattices, networks, pseudogaps and dust" (Proceedings of I.E. Tamm Seminar), 357–441, "Scientific World", Moscow, 2007 (in Russian); ArXiv: cond-mat/0408489
22. E.Z. Kuchinskii, I.A. Nekrasov, M.V. Sadovskii. Pseudogaps: Introducing the Length Scale into DMFT. Low Temp. Phys. v. 32, No. 4/5, 398–405 (2006)
23. M.V. Sadovskii. High-Temperature Superconductivity in Iron Based Layered Compounds. Physics Uspekhi, v. 51, No. 12, 1201–1227 (2008)
24. E.Z. Kuchinskii, I.A. Nekrasov, M.V. Sadovskii. Generalized Dynamical Mean Field Theory in the Physics of Strongly Correlated Systems. Physics Uspekhi, v. 55, No. 4, 325–355 (2012)
25. I.A. Nekrasov, M.V. Sadovskii. Electronic Structure of New Iron-Based Superconductors: From Pnictides to Chalcogenides and Other Similar Systems. JETP Letters, v. 99, No. 10, 598–612 (2014)
26. E.Z. Kuchinskii, M.V. Sadovskii. DMFT+Σ Approach to Disordered Hubbard Model. JETP, v. 122, No. 3, 510–525 (2016)
27. M.V. Sadovskii. High-Temperature Superconductivity in FeSe Monolayers. Physics Uspekhi, v. 59, No. 10, 947–967 (2016)
28. N.A. Kuleeva, E.Z. Kuchinskii, M.V. Sadovskii. Ginzburg–Landau Expansion and the Upper Critical Field in Disordered Attractive Hubbard Model. JETP Letters, v. 112, No. 9, 555–567 (2020)
29. M.V. Sadovskii. Planckian Relaxation Delusion in Metals. Physics Uspekhi, v. 64, No. 2, 157–190 (2021)
30. M.V. Sadovskii. Limits of Eliashberg Theory and Bounds for Superconducting Transition Temperature. Physics Uspekhi, v. 65, No. 7 , 724-739 (2022)

Selected papers:

1. M.V. Sadovskii. On the Theory of Conductivity of Metals with Non-Magnetic Impurities in Quantizing Magnetic Field. Phys. Metals and Phys. Metallography, v. 29, No. 6, 1160–1168 (1970)
2. P.S. Zyryanov, M.V. Sadovskii. On the Influence of Electron Scattering on Damping of Quantum Waves in the Fermi–Liquid of Metals. Phys. Metals and Phys. Metallography, v. 30, No. 5, 1099–1102 (1970)
3. L.N. Bulaevskii, M.V. Sadovskii. On the Influence of Crystal Lattice Disordering on Peierls Transition. Sov. Phys. – Solid State, v. 16, No. 4, 743 (1974)
4. M.V. Sadovskii. A Model of a Disordered System (A Contribution to the Theory of "Liquid Semiconductors"). Sov. Phys. – JETP, v. 39, No. 5, 845–850 (1974)
5. M.V. Sadovskii. Theory of Quasi-one-dimensional Systems Undergoing Peierls Transition. Sov. Phys. – Solid State, v. 16, No. 9, 1632 (1974)

6. M.V. Sadovskii. Localization of Electrons in Disordered Systems. The Mobility Edge and Theory of Critical Phenomena. Sov. Phys. – JETP, v. 43, No. 5, 1008–1010 (1976)

7. V.A. Alekseev, V.G. Ovcharenko, Yu.F. Ryzhkov, M.V. Sadovskii. Experimental Evidence of Anderson Localization in Liquid Selenium. JETP Letters, v. 24, No. 4, 189 (1976)

8. M.V. Sadovskii. Collective Excitations of Charge Density Waves in Quasi-one-dimensional Structures. Sov. Phys. – Solid State, v. 19, No. 4, 607 (1977)

9. M.V. Sadovskii. Electron in a Random Field in a Space of $d = 4 - \varepsilon$ Dimensions. Sov. Phys. – Solid State, v. 19, No. 8, 1366–1368 (1977)

10. V.A. Alekseev, V.G. Ovcharenko, Ju.F. Ryzhkov, M.V. Sadovskii. Possibility of Anderson Transition in Liquid Se and As in the Region of High Temperatures and Pressures. Phys. Lett., v. 65A, No. 2, 173–174 (1978)

11. M.V. Sadovskii. Electron in a Random Field, Theory of Phase Transitions, and Finite-Action Nonlinear Solutions. Sov. Phys. – Solid State, v. 21, No. 3, 435–439 (1979)

12. M.V. Sadovskii, Yu.N. Skryabin. Superconductivity in Spin-Glasses. Phys. Stat. Sol. (b), v. 95, No. 1, 59–64 (1979)

13. M.V. Sadovskii. Exact Solution for the Density of Electronic States in a Model of a Disordered System. Sov. Phys. – JETP, v. 50, No. 5, 989–994 (1979)

14. M.V. Sadovskii. Electron Localization in the Random-Phase Model and in Magnetic Field. Sov. Phys. – JETP, v. 53, No. 3, 581–587 (1981)

15. M.V. Medvedev, M.V. Sadovskii. Localization of One-Particle Spin Excitations in a Ferromagnet with a Random Easy-Axis Anisotropy. Sov. Phys. – Solid State, v. 23, No. 7, 1135–1137 (1981)

16. M.V. Sadovskii. Localization of Electrons in Disordered Systems and Critical Behavior at the Mobility Edge. In "Electronic Structure and Properties of Solids", Sverdlovsk, 1982, 36–41 (in Russian)

17. M.V. Medvedev, M.V. Sadovskii. Random Bond Ising Model in Self-Avoiding Walk Approximation. Phys. Stat. Sol. (b), v. 109, 49–57 (1982)

18. M.V. Medvedev, M.V. Sadovskii. Random Site Ising Model in Self-Avoiding Walk Approximation. Phys. Stat. Sol. (b), v. 109, 449–456 (1982)

19. M.V. Sadovskii. Localization Criterion in the Field Theory of an Electron in a Random Field. Sov. Phys. – JETP, v. 56, No. 4, 816–822 (1982)

20. A.V. Myasnikov, M.V. Sadovskii. Self-Consistent Theory of Localization in Spaces with $2 < d < 4$ Dimensions. Sov. Phys. – Solid State, v. 24, No. 12, 2033 (1982)

21. E.A. Kotov, M.V. Sadovskii. Self-Consistent Theory of Localization for the Anderson Model. Zs. Phys., v. 51, No. 1, 17–23 (1983)

22. M.I. Katsnelson, M.V. Sadovskii. Electron Interaction in Self-Consistent Theory of Localization. Sov. Phys. – Solid State, v. 25, No. 11, 1942 (1983)

23. M.I. Katsnelson, M.V. Sadovskii. Density of States and Screening near the Mobility Edge. Sov. Phys. – JETP, v. 60, No. 2, 300–306 (1984)

24. L.N. Bulaevskii, M.V. Sadovskii. Localization and Superconductivity. JETP Letters, v. 39, No. 11, 640–643 (1984)

25. L.N. Bulaevskii, M.V. Sadovskii. Anderson Localization and Superconductivity. J. Low-Temp. Phys., v. 59, No. 1/2, 89–113 (1985)

26. E.A. Kotov, M.V. Sadovskii. Hall Effect in Self-Consistent Theory of Localization. Phys. Metals and Phys. Metallography, v. 60, No. 1, 22–30 (1985)

27. L.N. Bulaevskii, A.A. Varlamov, M.V. Sadovskii. Fluctuations of Conductivity and Diamagnetic Susceptibility in Dirty Superconductors Close to the Edge of Anderson Localization. Sov. Phys. – Solid State, v. 28, No. 6, 1799 (1986)

28. L.N. Bulaevskii, M.V. Sadovskii. Increase of Spatial Fluctuations in Superconductors near the Anderson Transition. JETP Letters, v. 43, No. 2, 99–103 (1986)

29. S.A. Davydov, V.E. Arkhipov, B.N. Goshchitskii, M.V. Sadovskii. Metal Insulator Transition and Superconductivity in Mo_6Se_8 under Disordering. Phys. Metals and Phys. Metallography, v. 62, No. 6, 1130–1135 (1986)

30. L.N. Bulaevskii, S.V. Panyukov, M.V. Sadovskii. Inhomogeneous Superconductivity in Disordered Metals. Sov. Phys. – JETP, v. 65, No. 2, 380–388 (1987)

31. V.R. Galakhov et al. Electron and Phonon Properties of $La_{2-x}Sr_xCuO_{4-y}$. Phys. Metals and Phys. Metallography, v. 63, No. 4, 829–830 (1987)

32. V.L. Kozhevnikov et al. Galvanomagnetic Phenomena in La-Sr-Cu-O. Phys. Metals and Phys. Metallography, v. 64, No. 1, 184–186 (1987)

33. I.F. Berger et al. Structure, Magnetic Properties and Specific Heat of Superconductors $RBa_2Cu_3O_7$(R = Er, Ho). Phys. Metals and Phys. Metallography, v. 64, No. 2, 394–396 (1987)

34. A.V. Zaborov, M.V. Sadovskii. Nearest Neigbour Pairing in Hubbard Model. Series of preprints: "Problems of High-Temperature Superconductivity", No. 5, Ural Branch of the USSR Academy of Sciences, Syktyvkar, 1988

35. L.N. Bulaevskii, S.V. Panyukov, M.V. Sadovskii. Superconductivity in Metals with Strong Disorder. In "Problems of Theoretical Physics and Astrophysics", Nauka, Moscow, 1989, 120–137 (in Russian)

36. S.A. Davydov, B.N. Goshchitskii et al. Effects of Localization in Atomic-Disordered High-T_c Superconductots. Int. J. Mod. Phys. B, v. 3, No. 1, 87–92 (1989)

37. S.A. Davydov, B.N. Goshchitskii et al. Effects of Localization in Atomic-Disordered High-T_c Superconductots. In "Advances in Superconductivity", Kitazawa, Ishiguro (Eds.), Springer-Verlag, Tokyo, 1989, 463–468

38. E.Z. Kuchinskii, N.A. Kuleeva, M.V. Sadovskii. Ginzburg–Landau Expansion in Strongly Disordered Attractive Hubbard Model. JETP, v. 125, No. 1, 111–122 (2017)

39. B.N. Goshchitskii, S.A. Davydov, A.E. Karkin, A.V. Mirmelstein, M.V. Sadovskii, V.I. Voronin. Localization Effects in Disordered High-T_c Superconductors. Physica C, v. 162–164, 1019–1020 (1989)

40. B.N. Goshchitskii, S.A. Davydov, A.E. Karkin, A.V. Mirmelstein, M.V. Sadovskii, V.I. Voronin. Localization Effects in Atomic-Disordered High-T_c Superconductors. In "Progress in High Temperature Superconductivity", v. 11, World Scientific Singapore, 270–280 (1989)

41. B.A. Aleksashin, V.P. Voronin, S.V. Verkhovskii, B.N. Goshchitskii, S.A. Davydov, Yu.I. Zhdanov, A.E. Karkin, V.L. Kozhevnikov, A.V. Mirmelshtein, K.N. Mikhalev, M.V. Sadovskii, V.V. Serikov, S.M. Cheshnitskii. Localization Effects in Atomically Disordered High-Temperature Superconductors. Sov. Phys. – JETP, v. 68, No. 2, 382–394 (1989)

42. B.N. Goshchitskii, S.A. Davydov, A.E. Karkin, A.V. Mirmelstein, M.V. Sadovskii, V.I. Voronin, S.V. Verkhovskii, V.V. Serikov, B.A. Aleksashin, Yu.I. Zhdanov. Radiation Effects in High-T_c Superconductors. In "Progress in High Temperature Superconductors", v. 21, World Scientific, Singapore, 1990, 104–115

43. B.N. Goshchitskii, S.A. Davydov, A.E. Karkin, A.V. Mirmelstein, M.V. Sadovskii. Localization Effects in Radiationally Disordered High-Temperature Superconductors: Theoretical Interpretation. In "Progress in High Temperature Superconductors", v. 22, World Scientific, Singapore, 1990, 474–476

44. M.V. Sadovskii. Localization Effects in High-Temperature Superconductors. AIP Conf. Proc., v. 213, 207–216 (1990); Ann. NY Ac. Sci., v. 581, 207–216 (1990)

45. E.Z. Kuchinskii, M.V. Sadovskii. Energy Level Fluctuations in Finite Systems near the Metal–Insulator Transition. Sov. Phys. – JETP, v. 71, No. 2, 354–359 (1990)

46. M.V. Sadovskii, A.A. Timofeev. Optical Conductivity of High-Temperature Superconductors in "Spin-Bag" Model: Exact Solution? Superconductivity: Physics, Chemistry, Technology, v. 4, No. 1, 11–23 (1991)

47. E.Z. Kuchinskii, M.V. Sadovskii. Upper Critical Field of a Superconductor near Anderson Metal–Insulator Transition. Superconductivity: Physics, Chemistry, Technology, v. 4, No. 12, 2278–2292 (1991)

48. M.V. Sadovskii, A.A. Timofeev. Optical Conductivity of High-Temperature Superconductors: Exact Solution for a "Spin-Bag" Model. Physica C, v. 185–189, 1431–1432 (1991)

49. E.Z. Kuchinskii, M.V. Sadovskii. Upper Critical Field of a Superconductor near Anderson Transition. Physica C, v. 185–189, 1477–1478 (1991)

50. M.V. Sadovskii, A.A. Timofeev. The Two-Particle Green Function in a Model of a One-Dimensional Disordered System: An Exact Solution? J. Moscow Phys. Soc., v. 1, 391–406 (1991)

51. M.V. Medvedev, D.R. Plotitsin, M.V. Sadovskii. Critical State of High-Temperature Superconductor with Paramagnetic Ions. Superconductivity: Physics, Chemistry, Technology, v. 5, No. 11, 1999–2011 (1992)

52. M.A. Erkabaev, M.V. Sadovskii. Self-Consistent Localization Theory in the Two-Band Model. J. Moscow Phys. Soc., v. 2, 233–241 (1992)

53. S.V. Verkhovskii, Yu.I. Zhdanov, A.M. Bogdanovitch, K.N. Mikhalyov, B.A. Aleksashin, V.V. Serikov, V.V. Lavrentjev, M.V. Sadovskii. NMR and Spin-Lattice Relaxation Rate of ^{89}Y, ^{63}Cu in Radiation Disordered $YBa_2Cu_3O_{6.9}$. Appl. Magn. Reson., v. 3, 649–663 (1992)

54. E.Z. Kuchinskii, M.V. Sadovskii. Upper Critical Field of Two-Dimensional and Quasi-Two-Dimensional Superconductors near Anderson Metal–Insulator Transition. Superconductivity: Physics, Chemistry, Technology, v. 6, No. 6, 1119–1137 (1993)

55. E.Z. Kuchinskii, M.V. Sadovskii. Normal Impurities in Superconductors with an "Odd" Pairing. JETP Letters, v. 57, No. 8, 515–518 (1993)

56. E.Z. Kuchinskii, M.V. Sadovskii. Temperature Dependence of the Upper Critical Field in High-Temperature Superconductors: Localization Effects. JETP Letters, v. 58, No. 11, 819–823 (1993)

57. Yu.I. Zhdanov, A.M. Bogdanovitch, B.A. Aleksashin, K.N. Mikhalyov, V.V. Lavrentjev, S.V. Verkhovskii, V.V. Serikov, M.V. Sadovskii. Changes in Electron Spectrum of $YBa_2Cu_3O_{6.9}$ under Radiation Disordering: the ^{89}Y, ^{63}Cu NMR Data. JETP, v. 76, No. 5, 868–879 (1993)

58. E.Z. Kuchinskii, M.V. Sadovskii, M.A. Erkabaev. On the Theory of Superconductors with "Odd" Pairing. JETP, v. 77, No. 4, 692–699 (1993)

59. M.V. Sadovskii, E.Z. Kuchinskii, M.A. Erkabaev. On the Theory of "Odd-Pairing" Superconductors. Superconductors. Physica C, v. 235–240, 2403–2404 (1994)

60. E.Z. Kuchinskii, M.V. Sadovskii. Temperature Dependence of the Upper Critical Field in High-Temperature Superconductors: Localization Effects. Physica C, v. 235–240, 2621–2622 (1994)

61. E.Z. Kuchinskii, A.I. Posazhennikova, M.V. Sadovskii. The Ginzburg–Landau Expansion and the Physical Properties of Superconductors with Odd Pairing. JETP, v. 80, No. 2, 324–333 (1995)

62. E.Z. Kuchinskii, M.V. Sadovskii, V.G. Suvorov, M.A. Erkabaev. Self-Consistent Theory of Metal–Insulator Transitions in Disordered Systems. JETP, v. 107, No. 6, 2027–2047 (1995)

63. M.V. Sadovskii. Josephson Effect in Superconductors with Odd-Gap Pairing. JETP Letters, v. 61, No. 2, 129–130 (1995)

64. A.I. Posazhennikova. M.V. Sadovskii. Ginzburg–Landau Expansion and the Slope of the Upper Critical Field in Disordered Superconductors with Anisotropic Pairing. JETP Letters, v. 63, No. 5, 358–364 (1996)

65. E.Z. Kuchinskii, M.V. Sadovskii. M.A. Erkabaev. Superconductivity Suppression Close to the Metal–Insulator Transition in Strongly Disordered Systems. JETP, v. 85, No. 1, 104–108 (1997)

66. A.I. Posazhennikova. M.V. Sadovskii. Disorder Effects in Superconductors with Anisotropic Pairing: From Cooper Pairs to Compact Bosons. JETP Letters, v. 65, No. 3, 270–275 (1997)

67. A.I. Posazhennikova. M.V. Sadovskii. Ginzburg–Landau Expansion and the Slope of the Upper Critical Field in Superconductors with Anisotropic Normal Impurity Scattering. JETP, v. 85, No. 6, 1162–1167 (1997)

68. A.I. Posazhennikova. M.V. Sadovskii. Ginzburg–Landau Expansion and the Slope of the Upper Critical Field in Disordered Superconductors with Anisotropic Pairing. Physica C, v. 282–287, 1847–1848 (1997)

69. A.I. Posazhennikova. M.V. Sadovskii. Disorder Effects in Superconductors with Anisotropic Pairing: From Cooper Pairs to Compact Bosons. Physica C, v. 282–287, 1849–1850 (1997)

70. E.Z. Kuchinskii, M.V. Sadovskii. Combinatorics of Feynman Diagrams for the Problems with Gaussian Random Field. JETP, v. 86, No. 2, 367–374 (1998)

71. A.I. Posazhennikova, M.V. Sadovskii. Ginzburg–Landau Expansion in a Toy Model of Superconductor with Pseudogap. JETP, v. 88, No. 2, 347–355 (1999)

72. E.Z. Kuchinskii, M.V. Sadovskii. Models of the Pseudogap State of Two-Dimensional Systems. JETP, v. 88, No. 5, 968–979 (1999)

73. M.V. Sadovskii. Optical Conductivity in a Simple Model of Pseudogap State in Two-Dimensional System. JETP Letters, v. 69, No. 6, 483–489 (1999)

74. E.Z. Kuchinskii, M.V. Sadovskii. Superconductivity in a Toy Model of the Pseudogap State. JETP, v. 90, No. 3, 613–623 (2000)

75. M.V. Sadovskii. Models of the Pseudogap State in Cuprates. Physica C, v. 341–348, 811–814 (2000)

76. E.Z. Kuchinskii, M.V. Sadovskii. Superconductivity in a Toy Model of the Pseudogap State. Physica C, v. 341–348, 879–882 (2000)

77. M.V. Sadovskii. Optical Conductivity in a Simple Model of the Pseudogap State. Physica C, v. 341–348, 939–940 (2000)

78. E.Z. Kuchinskii, M.V. Sadovskii. Superconductivity in the Pseudogap State due to Fluctuations of Short-Range Order. JETP, v. 92, No. 3, 480–492 (2001)

79. A.E. Karkin, V.I. Voronin, T.V. Dyachkova, N.I. Kadirova, A.P. Tyutyunik, V.G. Zubkov, Yu.G. Zainulin, M.V. Sadovskii, B.N. Goshchitskii. Superconducting Properties of the Atomically Disordered MgB_2 Compound. JETP Letters, v. 73, No. 10, 570–572 (2001)

80. E.Z. Kuchinskii, M.V. Sadovskii. Superconductivity in an Exactly Solvable Model of the Pseudogap State: Absence of Self-Averaging. JETP, v. 94, No. 3, 654–769 (2002)

81. N.A. Strigina, M.V. Sadovskii. Optical Conductivity in a Two-Dimensional Model of the Pseudogap State. JETP, v. 95, No. 3, 526–537 (2002)

82. E.Z. Kuchinskii, M.V. Sadovskii, N.A. Strigina. Superconductivity in the Pseudogap State in "Hot-Spots" Model: Ginzburg–Landau Expansion. JETP, v. 98, No. 4, 748–759 (2004)

83. N.A. Strigina, M.V. Sadovskii. Optical Conductivity in the "Hot Spots" Model of the Pseudogap State. Physica C, v. 408–410, 418–419 (2004)

84. N.A. Kuleeva, E.Z. Kuchinskii, M.V. Sadovskii. Superconductivity in the "Hot-Spots" Model of the Pseudogap State: Impurity Scattering and Phase Diagram. JETP, v. 99, No. 6, 1264–1278 (2004)

85. E.Z. Kuchinskii, I.A. Nekrasov, M.V. Sadovskii. "Destruction" of the Fermi Surface due to Pseudogap Fluctuations in Strongly Correlated Systems. JETP Letters, v. 82, No. 4, 198–203 (2005)

86. M.V. Sadovskii, I.A. Nekrasov, E.Z. Kuchinskii, Th. Pruschke, V.I. Anisimov. Pseudogaps in Strongly Correlated Metals: A Generalized Dynamical Mean-Field Theory Approach. Phys. Rev. B, v. 72, No. 15, 155105 (2005)

87. E.Z. Kuchinskii, M.V. Sadovskii. Non-Fermi Liquid Behavior in Fluctuating Gap Model: From Pole to Zero of the Green's Function. JETP, v. 103, No. 3, 415–427 (2006)

88. E.Z. Kuchinskii, I.A. Nekrasov, M.V. Sadovskii. Pseudogaps in Strongly Correlated Metals: Optical Conductivity within the Generalized Dynamical Mean-Field Theory Approach. Phys. Rev. B, v. 75, No. 11, 115102 (2007)

89. E.Z. Kuchinskii, I.A. Nekrasov, Z.I. Pchelkina, M.V. Sadovskii. Pseudogap Behavior in $Bi_2Ca_2SrCu_2O_8$: Results of the Generalized Dynamical Mean-Field Approach. JETP, v. 104, No. 5, 792–804 (2007)

90. I.A. Nekrasov, E.Z. Kuchinskii, Z.V. Pchelkina, M.V. Sadovskii. Pseudogap in Normal Underdoped Phase of $Bi_2Ca_2SrCu_2O_8$: LDA+DMFT+Σ_k. Physica C, v. 460–462, 997–999 (2007)

91. M.V. Sadovskii, E.Z. Kuchinskii, I.A. Nekrasov. Destruction of the Fermi Surface due to Pseudogap Fluctuations in Correlated Systems. Physica C, v. 460–462, 1084–1085 (2007)

92. E.Z. Kuchinskii, I.A. Nekrasov, M.V. Sadovskii. Mott–Hubbard Transition and Anderson Localization: Generalized Dynamical Mean-Field Theory Approach. JETP, v. 106, No. 3, 581–596 (2008)

93. E.Z. Kuchinskii, N.A. Kuleeva, I.A. Nekrasov, M.V. Sadovskii. Optical Sum Rule in Strongly Correlated Systems. JETP, v. 107, No. 2, 281–287 (2008)

94. I.A. Nekrasov, E.E. Kokorina, E.Z. Kuchinskii, Z.V. Pchelkina, M.V. Sadovskii. Comparative Study of Electron and Hole Doped High-T_c Compounds in Pseudogap Regime: LDA+DMFT+Σ_k Approach. J. Phys. Chem. Solids, v. 69, No. 12, 3269–3273 (2008)

95. E.E. Kokorina, E.Z. Kuchinskii, I.A. Nekrasov, Z.V. Pchelkina, M.V. Sadovskii, A. Sekiyama, S. Suga, M. Tsunekawa. Origin of "Hot-Spots" in the Pseudogap Regime of $Nd_{1.85}Ce_{0.15}CuO_4$: LDA+DMFT+Σ_k Study. JETP, v. 107, No. 5, 828–838 (2008)

96. I.A. Nekrasov, Z.V. Pchelkina, M.V. Sadovskii. High Temperature Superconductivity in Transition Metal Oxypnictides: a Rare-Earth Puzzle? JETP Letters, v. 87, No. 10, 560–564 (2008)

97. I.A. Nekrasov, Z.V. Pchelkina, M.V. Sadovskii. Electronic Structure of Prototype AFe_2As_2 and ReOFeAs High-Temperature Superconductors: a Comparison. JETP Letters, v. 88, No. 2, 144–149 (2008)

98. I.A. Nekrasov, Z.V. Pchelkina, M.V. Sadovskii. Electronic Structure of New LiFeAs High-T_c Superconductor. JETP Letters, v. 88, No. 8, 543–545 (2008)

99. I.A. Nekrasov, Z.V. Pchelkina, M.V. Sadovskii. Electronic Structure of New AFFeAs Prototype of Iron Arsenide Superconductors. JETP Letters, v. 88, No. 10, 679–682 (2008)

100. E.Z. Kuchinskii, M.V. Sadovskii. Reconstruction of the Fermi Surface in the Pseudogap State of Cuprates. JETP Letters, v. 88, No. 3, 192–196 (2008)

101. E.Z. Kuchinskii, M.V. Sadovskii. Multiple Bands – a Key to High-Temperature Superconductivity in Iron Arsenides. JETP Letters, v. 89, No. 3, 156–160 (2009)

102. E.Z. Kuchinskii, I.A. Nekrasov, M.V. Sadovskii. Interplay of Electron–Phonon Interaction and Strong Correlations: LDA+DMFT+Σ_k Study. Phys. Rev. B, v. 80, 115124 (2009)

103. I.A. Nekrasov, N.S. Pavlov, E.Z. Kuchinskii, M.V. Sadovskii, Z.V. Pchelkina, V.B. Zabolotnyy, J. Geck, B. Buchner, S.V. Borisenko, D.S. Inosov, A.A. Kordyuk, M. Lambacher, A. Erb. Electronic Structure of $Pr_{2-x}Ce_xCuO_4$ studied via ARPES and LDA+DMFT+Σ_k. Phys. Rev. B, v. 80, 140510 (2009)

104. E.Z. Kuchinskii, M.V. Sadovskii. Multiple Bands – a Key to High-Temperature Superconductivity in Iron Arsenides. Physica C, v. 470, S418–S419 (2009)

105. E.Z. Kuchinskii, N.A. Kuleeva, I.A. Nekrasov, M.V. Sadovskii. Two-Dimensional Anderson–Hubbard Model in DMFT+Σ_k Approximation. JETP, v. 110, No. 2, 325–335 (2010)

106. E.Z. Kuchinskii, I.A. Nekrasov, M.V. Sadovskii. Anion Height Dependence of T_c and Density of States in Iron Based Superconductors. JEPT Letters, v. 91, No. 10, 518–522 (2010)

107. E.Z. Kuchinskii, M.V. Sadovskii. Electronic Structure and Possible Pseudogap Behavior in Iron Based Superconductors. JETP Letters, v. 91, No. 12, 660–664 (2010)

108. I.A. Nekrasov, E.E. Kokorina, E.Z. Kuchinskii, M.V. Sadovskii, S. Kasai, A. Sekiyama, S. Suga. ARPES Spectral Functions and Fermi Surface for $La_{1.86}Sr_{0.14}CuO_4$ Compared with LDA+DMFT+Σ_k Calculations. JETP, v. 110, No. 6 (2010)

109. I.A. Nekrasov, M.V. Sadovskii. Electronic Structure of Novel Multiple-Band Superconductor $SrPt_2As_2$. JETP Letters, v. 92, No. 11, 751 (2010)

110. I.A. Nekrasov, M.V. Sadovskii. Electronic Structure, Topological Phase Transitions and Superconductivity in $(K,Cs)_xFe_2Se_2$. JETP Letters, v. 93, No. 3, 166–169 (2011)

111. M.V. Sadovskii, E.Z. Kuchinskii, I.A. Nekrasov. Interplay of Electron–Phonon Interaction and Strong Correlations: DMFT+Σ Approach. J. Phys. Chem. Solids, v. 72, 366–370 (2011)

112. I.A. Nekrasov, E.Z. Kuchinskii, M.V. Sadovskii. Pseudogap Phase of High-T_c Compounds Described within the LDA+DMFT+Σ_k Approach. J. Phys. Chem. Solids, v. 72, 371–375 (2011)

113. M.V. Medvedev, I.A. Nekrasov, M.V. Sadovskii. Electronic and Magnetic Structure of Possible Iron Based Superconductor $BaFe_2Se_3$. JETP Letters, v. 95, No. 1, 33–37 (2012)

114. E.Z. Kuchinskii, I.A. Nekrasov, M.V. Sadovskii. Electronic Structure of Two-Dimensional Hexagonal Diselenides: Charge Density Waves and Pseudogap Behavior. JETP, v. 114, No. 4, 671–680 (2012)

115. I.A. Nekrasov, N.S. Pavlov, M.V. Sadovskii. Consistent LDA'+DMFT – an unambiguous way to avoid double counting problem: NiO test. JETP Letters, v. 95, No. 11, 581–585 (2012)

116. I.A. Nekrasov, M.V. Sadovskii. Electronic Structure of New Multiple Band Pt-Pnictide Superconductor APt_3P. JETP Letters, v. 96, No. 4, 227–230 (2012)

117. M.V. Sadovskii, E.Z. Kuchinskii, I.A. Nekrasov. Iron Based Superconductors: Pnictides versus Chalcogenides. JMMM, v. 324, 3481–3486 (2012)

118. I.A. Nekrasov, N.S. Pavlov, M.V. Sadovskii. Consistent LDA'+DMFT Approach to Electronic Structure of Transition Metal Oxides: Charge Transfer Insulators and Correlated Metals. JETP, v. 116, No. 4, 620–634 (2013)

119. I.A. Nekrasov, N.S. Pavlov, M.V. Sadovskii. LDA'+DMFT Investigation of Electronic Structure of $K_{1-x}Fe_{2-y}Se_2$ Superconductor. JETP Letters, v. 97, No. 1, 15–19 (2013)

120. I.A. Nekrasov, N.S. Pavlov, M.V. Sadovskii. Doping Dependence of Correlation Effects in of $K_{1-x}Fe_{2-y}Se_2$ Superconductor: LDA'+DMFT Insvestigation. JETP, v. 117, No. 5, 926–932 (2013)

121. I.A. Nekrasov, M.V. Sadovskii. Comparative Study of Electronic Structure of New Superconductors (Sr, Ca)Pd_2As_2 and Related Compound $BaPd_2As_2$. JETP Letters, v. 98, No. 1, 24–27 (2013)

122. N.A. Kuleeva, E.Z. Kuchinskii, M.V. Sadovskii. Normal Phase and Superconducting Instability in Attractive Hubbard Model: the DMFT (NRG) Study. JETP, v. 119, No. 2, 264–271 (2014)

123. I.A. Nekrasov, M.V. Sadovskii. Electronic Structure of New Iron-Based Superconductors: From Pnictides to Chalcogenides and Other Similar Systems. JETP Letters, v. 99, No. 10, 598–612 (2014)

124. E.Z. Kuchinskii, N.A. Kuleeva, M.V. Sadovskii. Disorder Effects in BCS–BEC Crossover Region of Attractive Hubbard Model. JETP Letters, v. 100, No. 3, 192–196 (2014)

125. E.Z. Kuchinskii, N.A. Kuleeva, M.V. Sadovskii. Attractive Hubbard Model with Disorder and the Generalized Anderson Theorem. JETP, v. 120, No. 6, 1055–1063 (2015)

126. I.A. Nekrasov, M.V. Sadovskii. Electronic and Magnetic Properties of the New Iron-Based Superconductor $[Li_{1-x}Fe_xOH]FeSe$. JETP Letters, v. 101, No. 1, 47–50 (2015)

127. I.A. Nekrasov, N.S. Pavlov, M.V. Sadovskii. Electronic Structure of NaFeAs Superconductor: LDA+DMFT calculations compared with ARPES experiments. JETP Letters, v. 102, No. 1, 26–31 (2015)

128. E.Z. Kuchinskii, N.A. Kuleeva, M.V. Sadovskii. Attractive Hubbard Model: Homogeneous Ginzburg–Landau Expansion and Disorder. JETP, v. 122, No. 2, 375–383 (2016)

129. E.Z. Kuchinskii, M.V. Sadovskii. DMFT+Σ Approach to Disordered Hubbard Model. JETP, v. 122, No. 3, 510–525 (2016)

130. E.Z. Kuchinskii, N.A. Kuleeva, M.V. Sadovskii. Attractive Hubbard Model within the Generalized DMFT: Normal State Properties, Disorder Effects and Superconductivity. Journal of Superconductivity and Novel Magnetism, v. 29, 1097 (2016)

131. I.A. Nekrasov, N.S. Pavlov, M.V. Sadovskii. Electronic Structure of NaFeAs Superconductor: LDA+DMFT calculation compared with ARPES experiment. Journal of Superconductivity and Novel Magnetism, v. 29, 1117 (2016)

132. I.A. Nekrasov, N.S. Pavlov, M.V. Sadovskii. A.A. Slobodchikov. Electronic Structure of FeSe Monolayer Superconductors. Low Temperature Physics, v. 42, No. 10, 891–899 (2016)

133. E.Z. Kuchinskii, N.A. Kuleeva, M.V. Sadovskii. Ginzburg–Landau expansion in BCS–BEC crossover region of disordered attractive Hubbard model. Low Temperature Physics, v. 43, No. 1, 17–26 (2017)

134. I.A. Nekrasov, N.S. Pavlov, M.V. Sadovskii. On the origin of the shallow and "replica" bands in FeSe monolayer superconductors. JETP Letters, v. 105, No. 6, 370–374 (2017)

135. E.Z. Kuchinskii, N.A. Kuleeva, M.V. Sadovskii. Ginzburg–Landau Expansion in Strongly Disordered Attractive Hubbard Model. JETP, v. 125, No. 1, 111–122 (2017)

136. E.Z. Kuchinskii, N.A. Kuleeva, M.V. Sadovskii. Temperature Dependence of the Upper Critical Field in Disordered Hubbard Model with Attraction. JETP, v. 125, No. 6, 1127–1136 (2017)

137. I.A. Nekrasov, N.S. Pavlov, M.V. Sadovskii. Electronic Structure of FeSe Monolayer Superconductors: Shallow Bands and Correlations. JETP, v. 126, No. 4, 485–496 (2018)

138. E.Z. Kuchinskii, N.A. Kuleeva, M.V. Sadovskii. Temperature Dependence of Paramagnetic Critical Magnetic Field of Disordered Attarctive Hubbard Model. JETP, v. 127, No. 4, 753–760 (2018)

139. M.V. Sadovskii. Electron–Phonon Coupling in Eliashberg–McMillan Theory Beyond Adiabatic Approximation. JETP, v. 128, No. 3, 455–463 (2019)

140. M.V. Sadovskii. Antiadiabatic Phonons, Coulomb Pseudopotential and Superconductivity in Eliashberg–McMillan Theory. JETP Letters, v. 109, No. 3, 166–170 (2019)

141. M.V. Sadovskii. Antiadiabatic Phonons and Superconductivity in Eliashberg–McMillan Theory. J. Superconductivity and Novel Magnetism, v. 33, No. 1, 19–26 (2020)

142. M.V. Sadovskii. On Planckian Limit for Inelastic Relaxation in Metals. JETP Letters, v. 111, No. 3, 188–192 (2020)

143. M.V. Sadovskii. Superconducting Transition Temperature for Very Strong Coupling in the Antiadiabatic Limit of Eliashberg Equations. JETP Letters, v. 113, No. 9, 581–585 (2021)

144. E.Z. Kuchinskii, N.A. Kuleeva, D.I. Khomskii, M.V. Sadovskii. Hall Effect in Doped Mott Insulator: DMFT Approximation. JETP Letters, v. 115, No. 7, 444–447 (2022)

145. E.Z. Kuchinskii, N.A. Kuleeva, D.I. Khomskii, M.V. Sadovskii. Hall Effect in Doped Mott Insulator.

JETP, v.136, No. 3, 368–377(2023)

146. E.Z. Kuchinskii, N.A. Kuleeva, M.V. Sadovskii. Thermoelectric Power and Hall Effect in Correlated

Metals and Doped Mott - Hubbard Dielectrics: DMFT Approximation. JETP v.137, No.6 (2023)

147. E.Z. Kuchinskii, M.V. Sadovskii. Generalized Dynamical Keldysh Model. JETP, v. 166, No. 1(7), (2024)

148. M.V. Sadovskii. Upper Limit for the Superconducting Transition Temperature in Eliashberg-McMillan Theory. JETP Letters v. 120, No. 3, 205-207 (2024)

Graduated in 1971 the Physical Department of the Ural State University (Sverdlovsk).

Ph.D. – 1975, Dr.Sci. – 1986.

1971–1974 – Ph.D work – theoretical department of P.N. Lebedev Physical Institute, USSR Academy of Sicences, Moscow.

1974–1986 – researcher at the Institute for Metal Physics USSR Academy of Sciences, Ural Scientific Centre (Sverdlovsk).

In 1987–2017 head of theoretical physics laboratory of the Institute for Electrophysics, Russian Academy of Sciences, Ural Branch (Ekaterinburg), at present the chief researcher in this laboratory. During 1993–2002 – deputy director of the Institute. In 2011–2013 also headed the laboratory of quantum theory of condensed matter, Institute for Metal Physics, Russian Academy of Sciences, Ural Branch, in 2013–2018 chief researcher of this laboratory and scientific supervisor of the Department of Theoretical Physics of the Institute for Metal Physics.

Professor of the Ural State University (Theoretical Physics), 1991–2010.

Author of more than 150 papers on condensed matter theory. Main interests – electronic theory of disordered systems (Anderson localization, pseudogap), superconductivity (disordered superconductors, high-temperature superconductivity). Developed the field theory approach to Anderson localization, self-consistent theory of localization, theory of superconductors close to the Anderson transition. Formulated exactly solvable models of the pseudogap state, models of disorder effects in the theory of Peierls transition. Recent interests were connected with extensions of dynamical mean field theory approach to the theory of electrons in strongly correlated systems and theoretical studies of iron based superconductors.

Corresponding member of the Russian Academy of Sciences (1994), Full Member (2003), member of the Presidium of the Ural Branch of RAS, member of the Bureau of the Physics Division of RAS and the RAS Comission on pseudoscience, member of American Physical Society, Fellow of the Institute of Physics (UK) – 2002. Member of editorial boards of JETP and Physics Uspekhi. Member of the "July 1st Club" opposing 2013 governmental reform of the Russian Academy of Sciences.

A.G. Stoletov Prize in Physics of the Russian Academy of Sciences (2002)
V.L. Ginzburg Gold Medal of the Russian Academy of Sciences (2016)
M.N. Mikheev Silver Medal of the Institute for Metal Physics (2017)
S.V. Vonsovsky Gold Medal of the Ural Branch of the Russian Academy of Sciences (2018)